PHYSICAL ACOUSTICS SUMMER SCHOOL

PASS 98

ASILOMAR CONFERENCE CENTER

VOLUME II: TRANSPARENCIES

1998 PHYSICAL ACOUSTICS SUMMER SCHOOL

VOLUME II: TRANSPARENCIES

This work relates to Department of Navy Grant N00014-98-1-0044 issued by the Office of Naval Research. The United States Government has a royalty-free license throughout the world in all copyrightable material contained herein.

Copies of this three-volume proceedings can be obtained by contacting: Libby Furr, NCPA, University of Mississippi, University, MS 38677; voice: 662-915-5808; fax: 662-915-7494; e-mail: libby@olemiss.edu

TABLE OF CONTENTS

[TR-1]

Physical Acoustics Summer School
1998

Sonoluminescence

Anthony A. Atchley
Graduate Program in Acoustics
The Pennsylvania State University

PENNSTATE
1855

[TR-2]

Outline

- Acoustic Levitation
- Bubble Dynamics
- Oversimplified (Unbelievable) Predictions
  - To Set the Stage
- Early SBSL
- Exploring Parameter Space
- Theories

ELSEVIER

PHYSICS REPORTS

Physics Reports 281 (1997) 65–143

[TR-3]

Defining the unknowns of sonoluminescence

Bradley P. Barber[a], Robert A. Hiller[b], Ritva Löfstedt[c], Seth J. Putterman[b], Keith R. Weninger[b]

[a] *Lucent Technologies, Murray Hill, NJ 07974, USA*
[b] *Physics Department, University of California, Los Angeles, CA 90095, USA*
[c] *Institute for Theoretical Physics, University of California, Santa Barbara, CA 93106, USA*

Received November 1996; editor: A.A. Maradudin

Contents

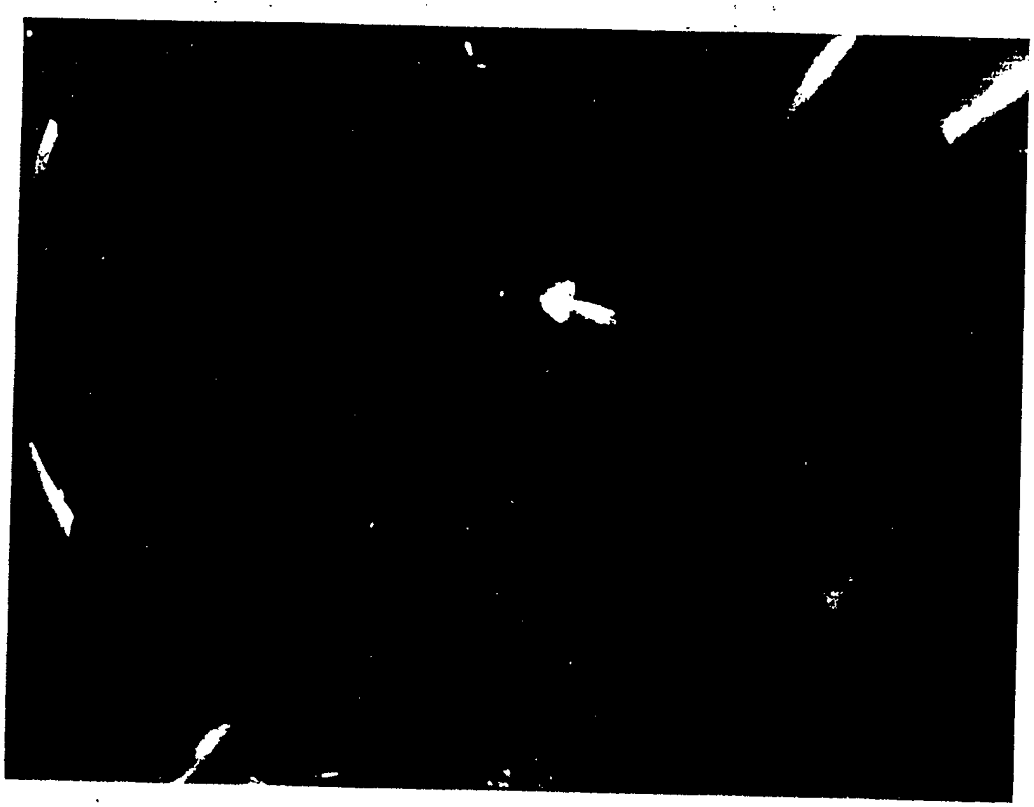

[TR-4]

Simplified Acoustic Levitation

Assume only two forces act on a gas bubble:
1) an acoustic force
2) buoyancy force

Also assume that any difficult problems can be ignored.

At equilibrium:

(1) $<F_{acoustic}>_t = - <F_{buoyancy}>_t$

(2) $F_{acoustic} = -V(z,t)\nabla P(z,t)$

(3) $F_{buoyancy} = \rho_L V(z,t)\, g \qquad (\rho_L \neq \rho_L(t))$

(4) $P(z,t) = P_m + P_A\cos(kz)\cos(\omega t)$

(5) $V(z,t) = V_m - V_A(P_A,\omega)\cos(kz)\cos(\omega t)$

(6) $F_{acoustic} = -[V_m - V_A(P_A,\omega)\cos(kz)\cos(\omega t)]$
$\quad \times[-kP_A\sin(kz)\cos(\omega t)]$

(7) $<F_{acoustic}>_t = -(1/2)\, kP_AV_A\sin(kz)\cos(kz)$
$\quad = -(1/4)\, kP_AV_A\sin(2kz)$

(8) $F_{buoyancy} = \rho_L[V_m - V_A(P_A,\omega)\cos(kz)\cos(\omega t)]g$

(9) $<F_{buoyancy}>_t = \rho_L V_m g$ (for linear oscillations)

(10) $(1/4)\, kP_AV_A\sin(2kz) = \rho_L V_m g$

(11) $\sin(2kz) = 4\rho_L V_m g/[kP_A V_A(P_A,\omega)]$

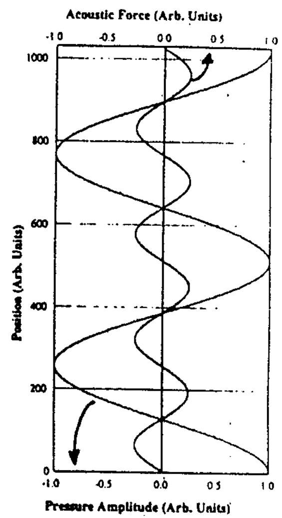

Bubble driven
below resonance.

Simplified Bubble Dynamics

Rayleigh - Plesset Equation

Bubble of instantaneous radius R
in an incompressible fluid.

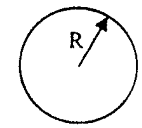

Find the Kinetic and Potential Energies and Apply
Conservation of Energy or Lagrange's Equations of Motion.

$KE + PE = constant$

$KE = -PE$

$L = KE - PE$

$\frac{\partial L}{\partial R} - \frac{d}{dt}\frac{\partial L}{\partial \dot{R}} = 0$

Kinetic Energy

(1) $$KE = \int_R^{\infty} \tfrac{1}{2}\rho_L u^2 dV$$

Consider the mass flux through a spherical surface centered on the bubble.
If the fluid is incompressible, then

$$4\pi r^2 u(r) = 4\pi R^2 u(R).$$

So,

$$u(r) = \frac{u(R)R^2}{r^2} = \frac{\dot{R}R^2}{r^2}$$

[TR-7]

Rayleigh Plesset Equation

$$KE = \int_R^{\infty} \tfrac{1}{2}\rho_L \left[\frac{\dot{R}R^2}{r^2}\right]^2 4\pi r^2 dr$$
$$= 2\pi\rho_L \dot{R}^2 R^4 \int_R^{\infty} \frac{dr}{r^2}$$
$$= 2\pi\rho_L R^3 \dot{R}^2$$
$$= \tfrac{1}{2} 3\left(\tfrac{4}{3}\pi R^3 \rho_L\right)\dot{R}^2$$

Recall that the effective mass of a small (kR <<1) bubble is

$$m_{eff} = 3\left(\tfrac{4}{3}\pi R^3 \rho_L\right)$$

So,

$$KE = \tfrac{1}{2} m_{eff} \dot{R}^2.$$

Taking the time derivative of the kinetic energy gives

$$\dot{KE} = 2\pi\rho_L \left[R^3 \dot{R}^2\right]^{\cdot}$$
$$= 2\pi\rho_L \left[3R^2\dot{R}^3 + 2R^3\dot{R}\ddot{R}\right]$$

[TR-8]

Rayleigh - Plesset Equation

Potential Energy

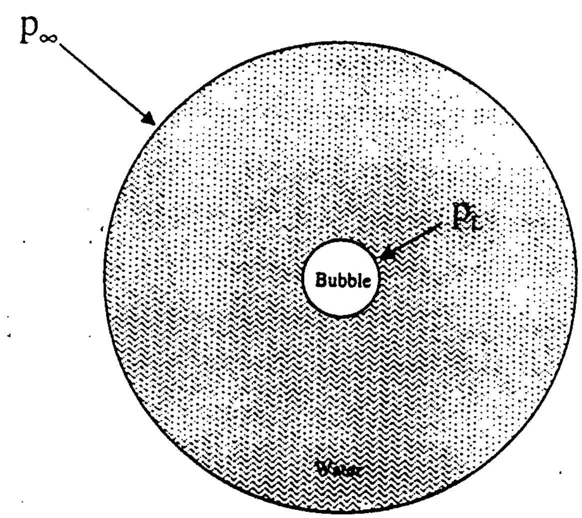

p_∞ = pressure in the water far from the bubble

p_L = pressure on the "wet" side of the bubble wall

If $p_\infty \neq p_L$, the bubble will change volume.

The time rate of change of the potential energy is

$$\dot{PE} = -(p_L - p_\infty)\frac{dV}{dt}$$
$$= -(p_L - p_\infty)4\pi R^2 \dot{R}.$$

[TR-9]

Rayleigh - Plesset Equation

Using

$$KE = -PE$$

gives the Rayleigh - Plesset equation

$$\boxed{R\ddot{R} + \frac{3}{2}\dot{R}^2 = \frac{p_L - p_\infty}{\rho_L}} \qquad (1)$$

where

$$p_L = p_G + p_V - \frac{2\sigma}{R} - 4\mu\frac{\dot{R}}{R}$$

$$p_\infty = p_0 + p_{acoustic}$$

Refinements - Keller Equation

Adding the effects of compressibility leads to the Keller Equation

$$\boxed{\left(1-\frac{\dot{R}}{c}\right)R\ddot{R} + \frac{3}{2}\left(1-\frac{1}{3}\frac{\dot{R}}{c}\right)\dot{R}^2 = \left(1+\frac{\dot{R}}{c}\right)\frac{p_L - p_s - p_0}{\rho_L} + \frac{R}{\rho_L c}\frac{dp_L}{dt}} \qquad (2)$$

[TR-10]

Predicted Bubble Response

$R_0 = 5\ \mu m$ $P_A = 0.05, 0.5, 1.25$ atm $f = 25$ kHz

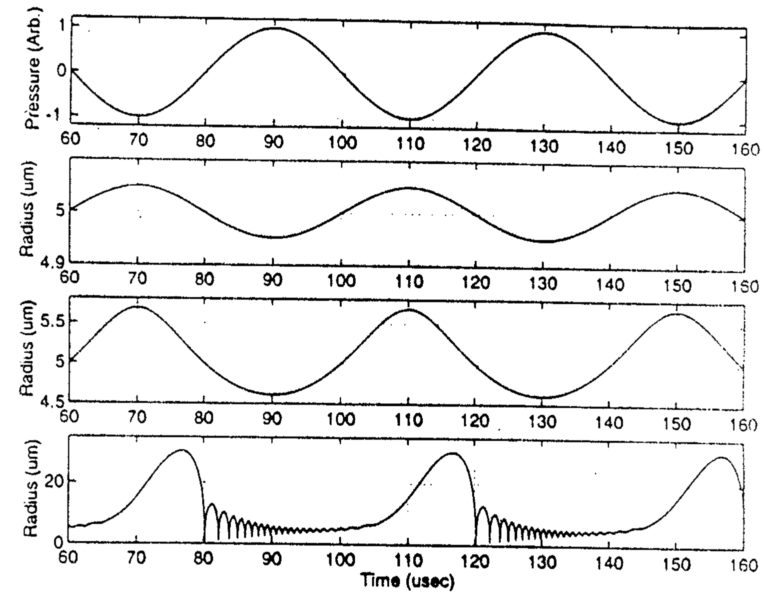

[TR-11]

A Closer Look Inside

$R_o = 5\ \mu m \quad P_A = 1.25$ atm $\quad f = 25$ kHz

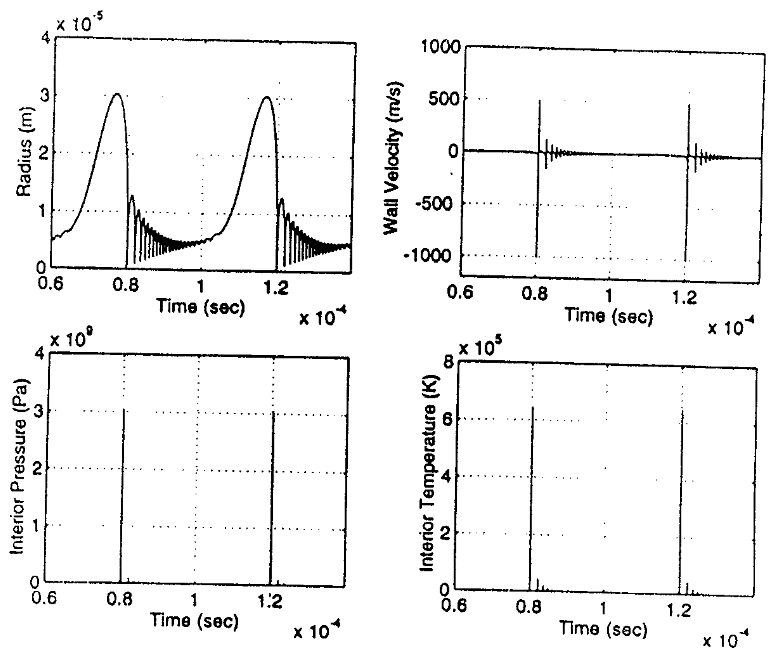

[TR-12]

Frontiers of Nonlinear Acoustics: Proceedings of 12th ISNA
edited by M.F. Hamilton and D.T. Blackstock
Elsevier Science Publishers Ltd, London, 1990

OBSERVATION OF SONOLUMINESCENCE FROM A SINGLE, STABLE CAVITATION BUBBLE IN A WATER/GLYCERINE MIXTURE

D. FELIPE GAITAN AND LAWRENCE A. CRUM
National Center for Physical Acoustics
The University of Mississippi
Oxford, Mississippi 38677 USA

ABSTRACT

High amplitude pulsations of a single gas bubble in a glycerine and water mixture have been attained in an acoustic stationary wave system at an acoustic pressure amplitude as high as 0.15 MPa. Cavitation streamers were uncharacteristically absent and no surface waves were detectable. Simultaneously, sonoluminescence with sufficient intensity to be seen with the unaided eye in a darkened room has been observed to originate at the geometric center of the bubble. Experimental radius-time curves have been obtained by a light scattering technique which show the pulsations of the bubble to be periodic in time with a frequency equal to that of the driving pressure. The phase of the sonoluminescence flashes has also been measured and the simultaneity of sonoluminescence emissions and bubble collapse has been established. The implications of these observations on the present understanding of acoustic cavitation will be discussed.

INTRODUCTION

Nonlinear radial pulsations of gas bubbles have been studied extensively both experimentally and theoretically [1-6]. However, because the threshold acoustic pressure amplitude for the presence of surface waves [7] is relatively small (a few tenths of a bar), experiments in the past have been restricted to small amplitude pulsations – normally less than 20% deviation from equilibrium. In this experiment, large amplitude radial pulsations of a single bubble with expansion ratios (Rmax/Ro) as large as 7 have been observed in a levitation chamber that incorporates a stationary wave to acoustically levitate the bubble. Even with driving pressure amplitudes as high as 0.15 MPa, no observable bubble break-up was observed for measurement periods of thousands of acoustic cycles. For these parameters, we have also calculated collapse ratios (Rmin/Ro) of 0.05 to 0.1 based on the recent theory of Prosperetti *et al.* [5]. Because of these relatively low values of the collapse ratio, and because our calculated values of the radius-time curve are quite similar to the measured ones, we are reasonably confident that we are truly observing sonoluminescence from a single, stable (as opposed to transient) cavitation bubble.

Because of the deterministic character of a pulsating bubble, this system offers a unique opportunity to study simultaneously both nonlinear bubble pulsations and the relatively little understood phenomenon of sonoluminescence.

[TR-13]

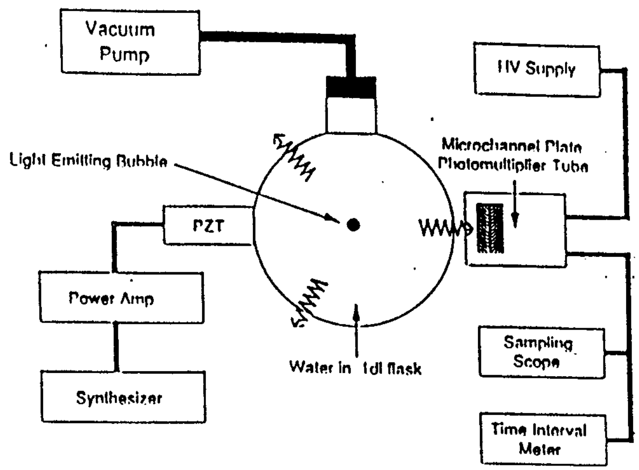

FIG. 2. Block diagram of the apparatus used to generate and observe SL. The sound field is driven with a piezoelectric transducer (PZT) and the emitted light is detected with a PMT biased by the high-voltage (HV) supply.

B. P. Barber, et. al., J. Acoust. Soc. Am. 91, 3061-3063 (1992).

[TR-14]

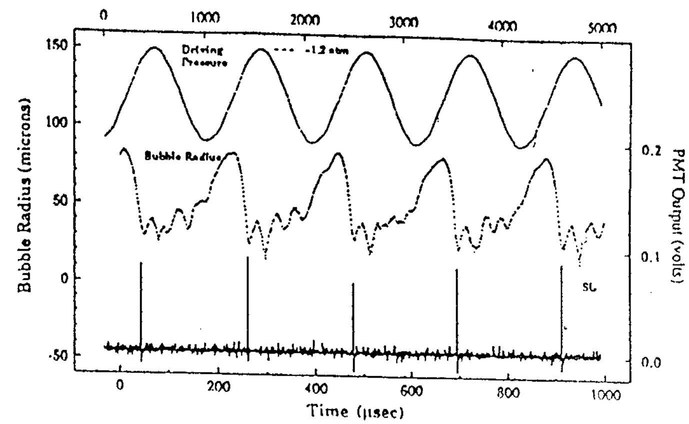

FIG. 18. Simultaneous plots of the sound field (top), bubble radius (middle) and sonoluminescence (bottom) in GLY21 at $P_A = 1.2$ atm and $f = 22.3$ kHz.

D. F. Gaitan, et. al., J. Acoust. Soc. Am. 91, 3166-3183 (1992).

[TR-15]

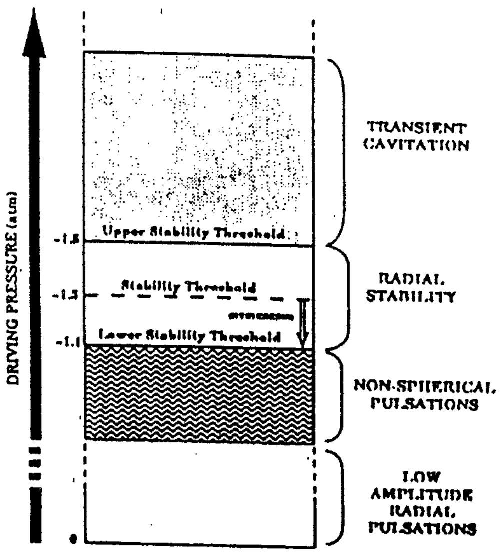

FIG. 10. Diagram of the observed radial stability thresholds for 15- to 20-mm bubbles in water/glycerine mixtures in an acoustic levitation system at $f = 21$–25 kHz.

D. F. Gaitan, et. al., J. Acoust. Soc. Am. 91, 3166-3183 (1992).

[TR-16]

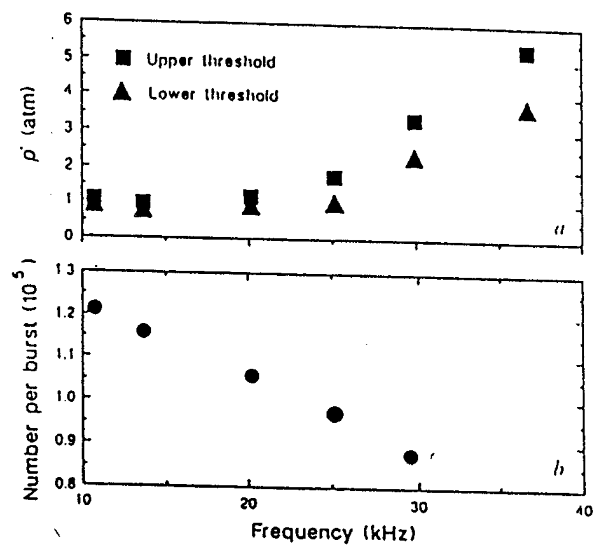

FIG. 1 *a*, Phase plane for continuous single-bubble sonoluminescence. The 20-kHz data point agrees with the measurement of Gaitan. *b*, Photons per burst as a function of acoustic frequency; p' has been chosen to maximize the light output.

B. P. Barber and S. J. Putterman, Nature 352, 318-320 (1991).

[TR-17]

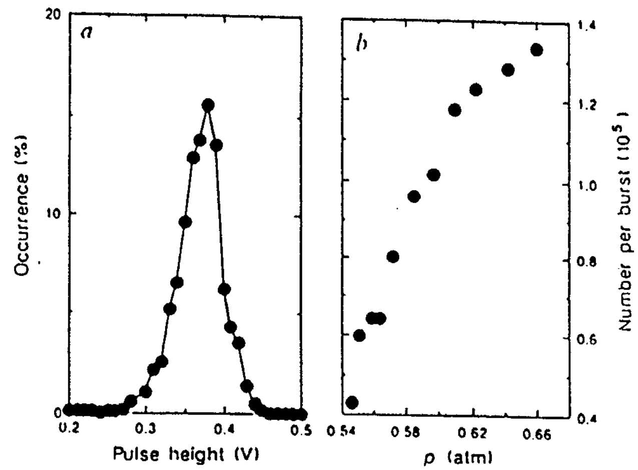

FIG. 3 *a*, Pulse height distribution. A pulse height of 0.1 V represents 1.1×10^4 photons emitted. $f_a = 20.193$ kHz. *b*, Photons per burst as a function of acoustic pressure amplitude. $f_a = 10.736$ kHz.

B. P. Barber and S. J. Putterman, Nature 352, 318-320 (1991).

[TR-18]

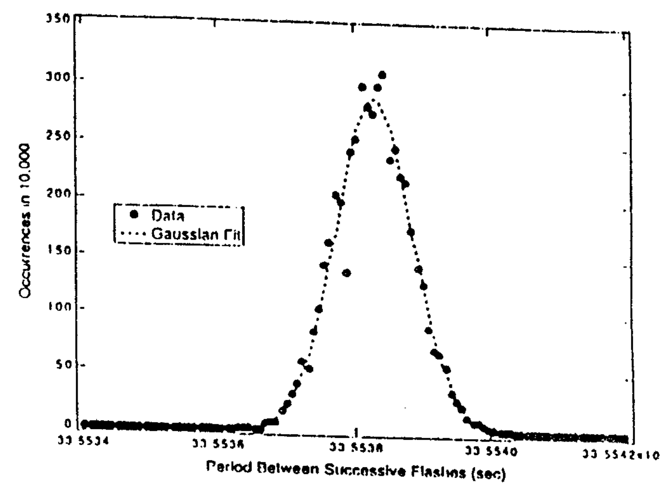

FIG. 3. Histogram of events versus period between flashes for sonoluminescence.

B. P. Barber, et. al., J. Acoust. Soc. Am. 91, 3061-3063 (1992).

[TR-19]

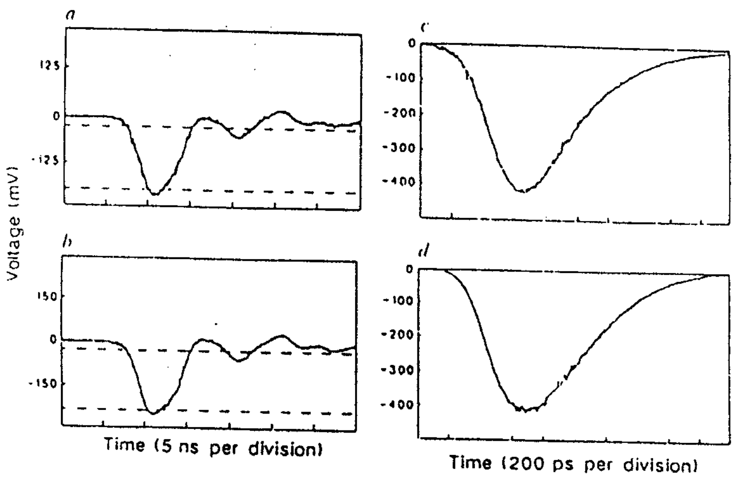

FIG. 2 The average of single-pulse outputs of the photomultiplier tube. *a*, SL data as recorded by a conventional (R928) PMT; *b*, same as *a*, but using a 34-ps laser pulser (Hamamatsu PLP-01) as the light source. *a* and *b* were obtained by running the PMT output into a digital sampling scope (HP 54201A). *c* and *d*, Data for a microchannel-plate PMT (Hamamatsu R1564U) running into a 20-GHz digital sampling scope (Tektronix 11802). *c* is for the SL source, and *d* for the 34-ps laser pulser.

B. P. Barber and S. J. Putterman, Nature 352, 318-320 (1991).

[TR-20]

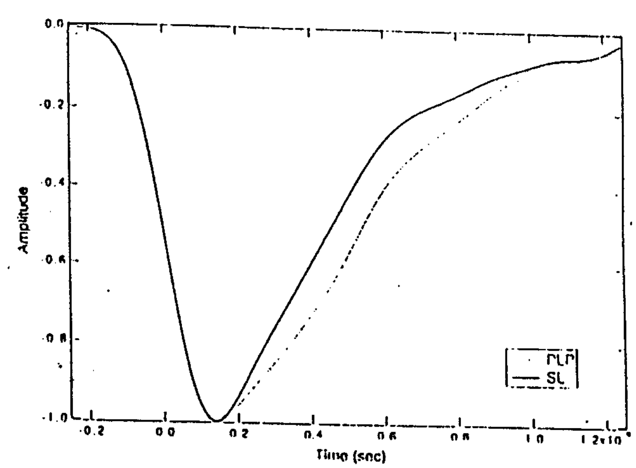

FIG. 1. Voltage versus time at the output of the PMT for SL and the PLP. The time scales are chosen so that the two curves pass through the 50% level at the same time. These curves correspond to the recording of about 25 photoelectrons. After passing through the delay line and 20-dB attenuator a single photoelectron corresponds to a peak amplitude of 2 mV.

B. P. Barber, et. al., J. Acoust. Soc. Am. 91, 3061-3063 (1992).

[TR-21]

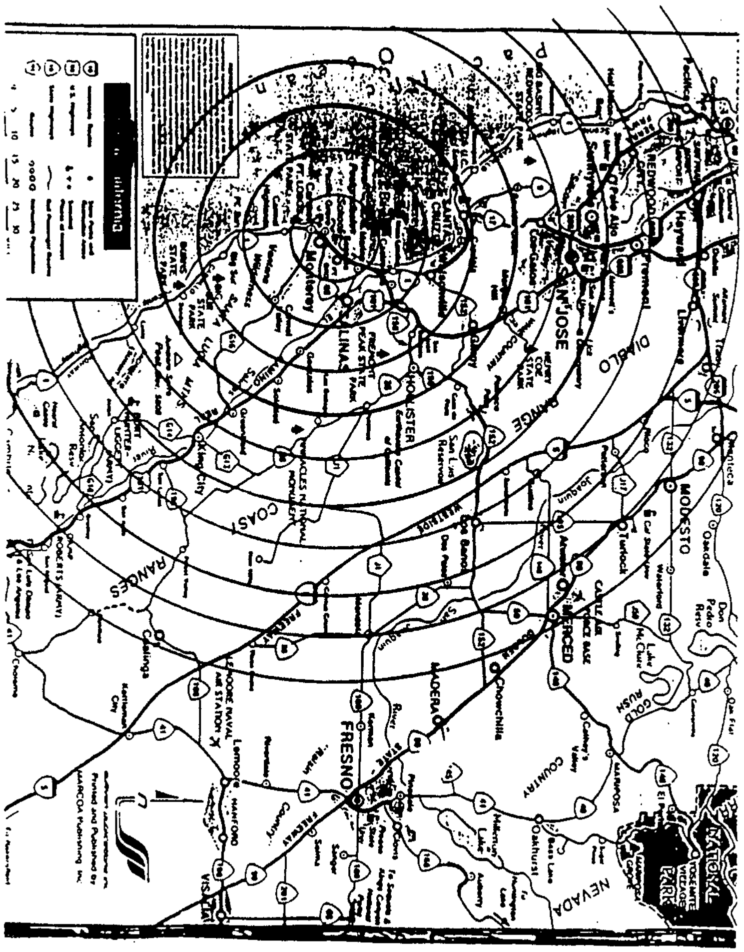

[TR-22]

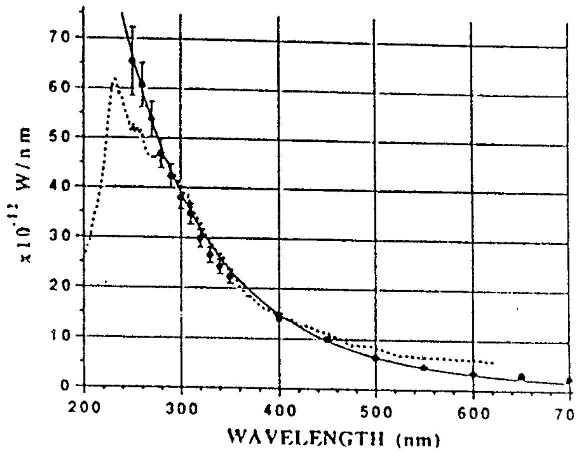

FIG. 1. Calibrated spectral density of the synchronous picosecond flashes of sonoluminescence at 22°C. The average spectral energy density of a single flash can be obtained by dividing by the acoustic frequency of 27 kHz. The dotted line was obtained via the D lamp calibration. The points with error bars were obtained by calibrating our apparatus with a QTH standard of spectral irradiance. The solid line is a 25000 K blackbody spectrum.

R. Hiller, et. al., Phys. Rev. Lett. 69, 1182-1184 (1992).

[TR-23]

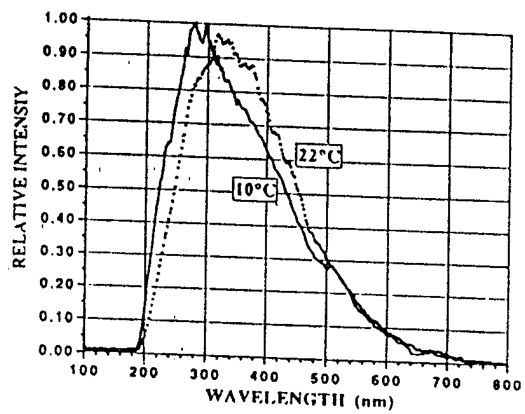

FIG. 4. Raw data for the spectral density of SL at 10 and 22°C. The peaks have been chosen so that the curves have equal area. These curves have not been corrected for the fiber grating, or PMT. The grating is blazed at 300 nm.

R. Hiller, et. al., Phys. Rev. Lett. 69, 1182-1184 (1992).

[TR-24]

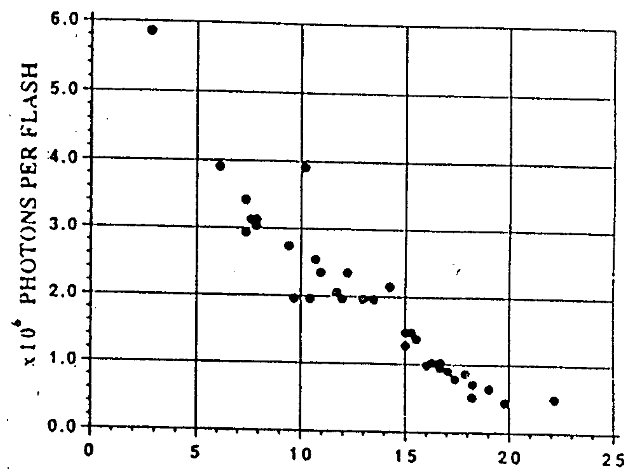

FIG. 3. Number of photons emitted per flash of SL as a function of temperature. At each temperature we recorded the output of the brightest bubble attainable.

R. Hiller, et. al., Phys. Rev. Lett. 69, 1182-1184 (1992).

[TR-26]

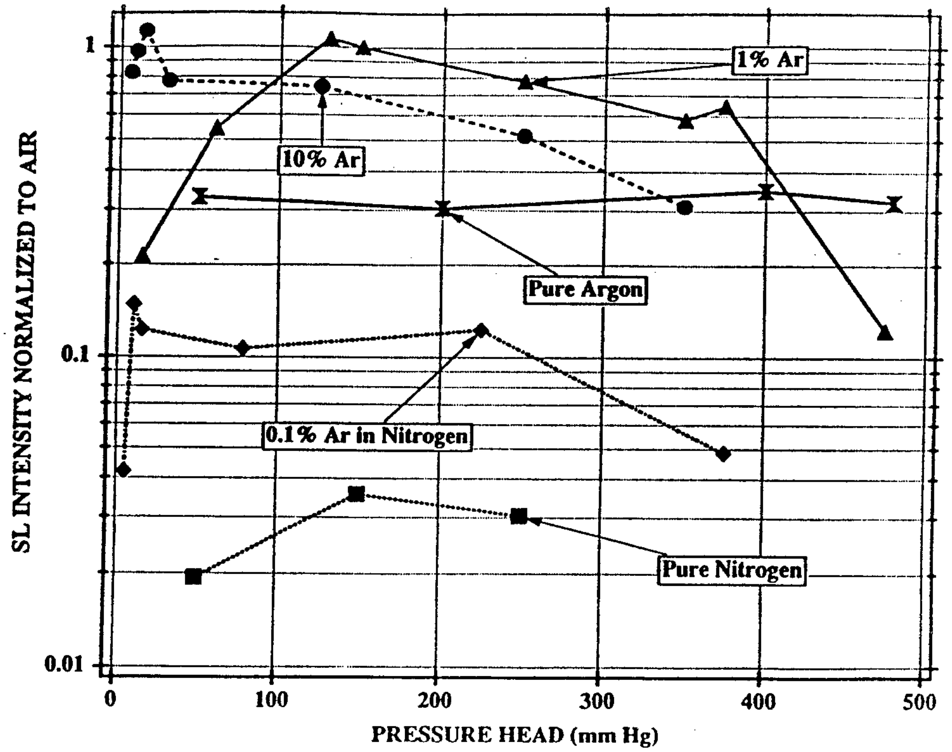

[TR-25]

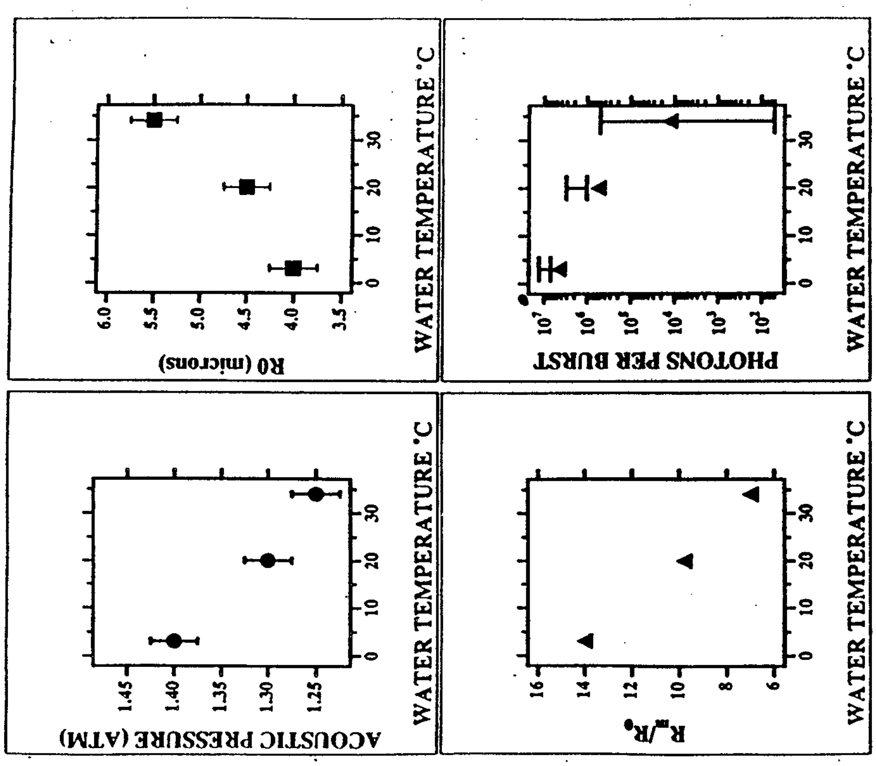

FIGURE 5: Values of the intensity of sonoluminescence, sound field level P_a, maximum bubble radius R_m and ambient radius R_0 as a function of water temperature for a trapped bubble of air. The number N of photons per burst (with wavelength greater than 200nm) is measured in each case near the maximum achievable value. The bars are the ranges of intensities calculated from the shock wave theory when the uncertainty in the experimental input parameters is allowed for.

[TR-27]

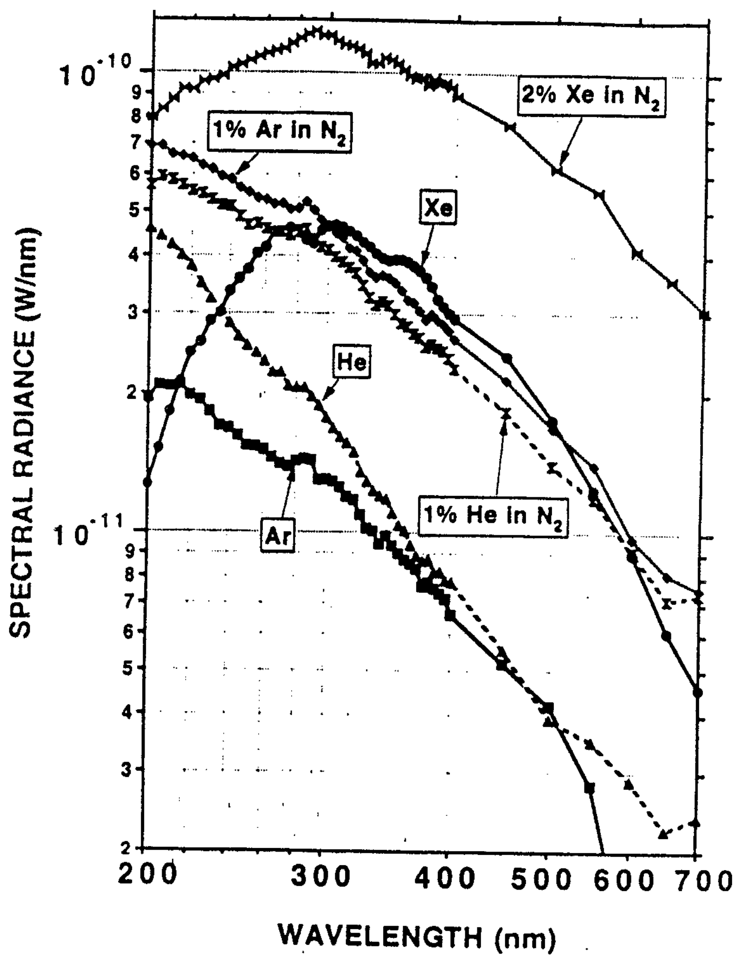

[TR-28]

B.P. Barber et al. / Physics Reports 281 (1997) 65–143

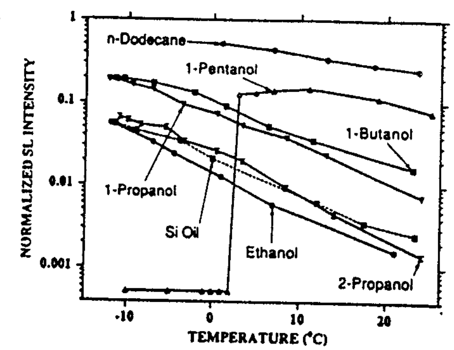

Fig. 44. Intensity of SL from a single xenon bubble trapped in various fluids as a function of temperature (normalized to 150 mm air in water at room temperature). These are the largest signals that can be observed for 30 s or longer. For 1-pentanol below 1°C non-light-emitting bubbles can be sustained. By sweeping the drive level a signal of 1–2 mV (0.1 normalized) can be attained for about 50 ms.

[TR-29]

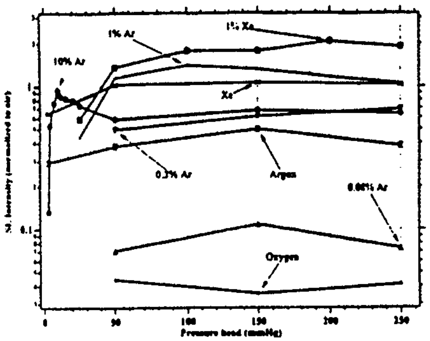

Fig. 24. Sonoluminescence from noble-gas doped-oxygen bubbles. The enhancement effect in oxygen is very similar to that which occurs in nitrogen.

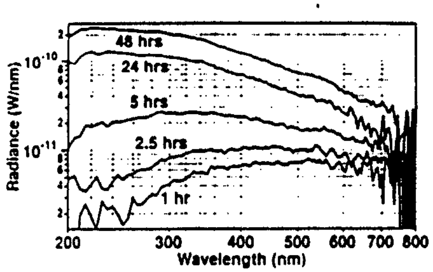

Fig. 71. Spectrum of a deuterium bubble in heavy water as a function of time from preparation of the 3 mm solution. The drift is due to an air leak either from the outside or outgassing from the RTV seals on the cylindrical resonator.

[TR-30]

VOLUME 75, NUMBER 13 PHYSICAL REVIEW LETTERS 25 SEPTEMBER 1995

Comparison of Multibubble and Single-Bubble Sonoluminescence Spectra

Thomas J. Matula, Ronald A. Roy, and Pierre D. Mourad
Applied Physics Laboratory, University of Washington, 1013 NE 40th Street, Seattle, Washington 98105

William B. McNamara III and Kenneth S. Suslick
School of Chemical Sciences, University of Illinois at Urbana-Champaign, Urbana, Illinois 61801
(Received 12 July 1995)

Comparisons of the spectral characteristics of sonoluminescence from cavitation in bubble fields (MBSL) versus cavitation of single bubbles (SBSL) have been made for aqueous solutions under similar experimental conditions. In particular, alkali metal chloride solutions exhibit sonoluminescence emission from excited state Na or K atoms in MBSL, while SBSL exhibits no such emission. Since the metal ions are not volatile, participation of the initially liquid phase must occur in MBSL. Surface wave and microjet formation in cavitating bubble fields versus the high spherical symmetry of collapse of an isolated bubble may account for the observed differences.

PACS numbers: 78.60.Mq, 43.25.+y, 47.40.Nm

It has long been known that under certain conditions acoustic irradiation of a liquid can result in light emission, a phenomenon called sonoluminescence (SL) [1,2]. The process typically involves the application of high intensity ultrasound to a liquid by an immersed acoustic horn driven with a piezoelectric transducer. The resulting cavitation-bubble field is made up of a complex distribution of gas and vapor-filled bubbles of various equilibrium sizes that pulsate at various phases relative to the driving acoustic pressure field. The bubble dynamics is further complicated by interactions with neighboring bubbles [3] as well as with the vessel walls. Depending on the location within the pressure field and these other influences, some of the bubbles may grow dramatically during the negative portion of the sound field, followed by a quasi-adiabatic collapse that results in the heating of the bubble interior and the subsequent emission of light [4].

In spite of the complexity of cavitating bubble fields, many studies have been made of multibubble sonoluminescence (MBSL) and the influences of fluid and gas properties. The optical spectra of MBSL typically contains distinct, pressure broadened molecular or atomic emission bands. Of particular significance here is the identification of individual transitions from excited states of diatomic carbon (C_2) that contribute to the optical spectrum of MBSL in nonaqueous liquids. The fitting of the measured spectrum of C_2 permitted the measurement of an effective rotational and vibrational temperature of the excited states of C_2 of 5100 K [5].

Recent experimental advances [6] have also made it possible to examine both the temporal and spectral nature of sonoluminescence from a single bubble (SBSL). Here a single bubble is acoustically levitated in an aqueous solution that has been partially degassed. The bubble can be made to undergo large-amplitude, nonlinear, presumably radial pulsations during which light emission can occur. Some properties of SBSL include [7] the synchronous emission of light with each and every acoustic cycle, temporal flash widths of less than 50 ps, and a continuous spectral energy density that increases from the visible into the UV, with eventual fall off due to UV absorption by the surrounding water. In addition, unlike in MBSL, there are little or no electronic or molecular bands associated with SBSL spectra. The shape of the spectrum of SBSL has led some researchers to suggest that SBSL is much "hotter" than MBSL, reaching temperatures as high as 50 000 K [8], and possibly much higher [9,10].

In order to probe the differences between MBSL and SBSL, we have explored emission from identical aqueous solutions containing potentially emissive, but nonvolatile, solutes using the same spectrometer for both systems. Nonvolatile solutes provide a test of the involvement of the initially liquid phase surrounding the cavitating bubble in the sonoluminescent event [11,12]. An observation of an SL emission peak from a nonvolatile solute requires either that a fluid shell surrounding the bubble be heated sufficiently [13], or that liquid droplets containing the nonvolatile species become entrained and heated within the bubble [4,14].

It was not possible to generate both MBSL and SBSL in a single apparatus, owing to the differences in techniques used to generate cavitation-bubble fields and isolated single bubbles. MBSL is generated using an ultrasonic horn, which produces large peak pressures within the liquid (around 10 bars), with high levels of gas saturation; while SBSL occurs with applied acoustic pressure amplitudes near 1 bar, and gas concentration levels that are a fraction of saturation. Nonetheless, comparison of the optical spectra can be made by using identical fluid preparation schemes under identical gases with a single calibrated spectrometer.

The SBSL apparatus consisted of a quartz cylindrical levitation cell (8 cm tall by 4.5 cm diameter), as shown in Fig. 1(a). The cell was closed on top with a glass plate. A hollow cylindrical PZT transducer, cemented to the glass, was used to drive the levitator in tandem with a power

[TR-31]

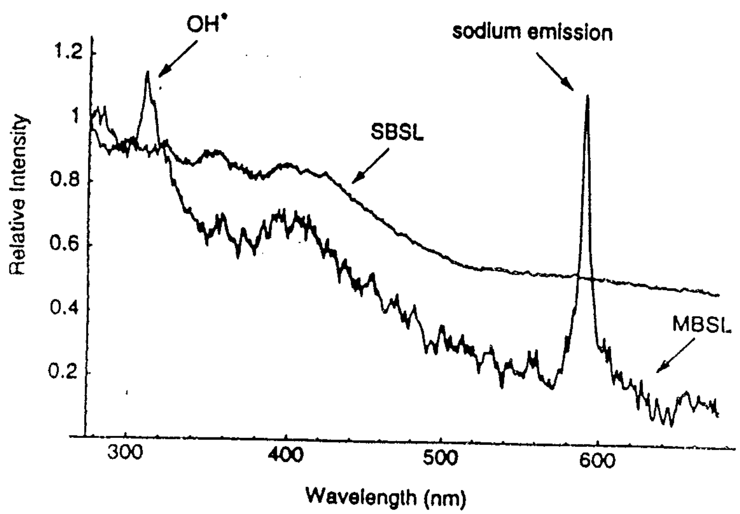

[TR-32]

VOLUME 74, NUMBER 26 PHYSICAL REVIEW LETTERS 26 JUNE 1995

Observation of a New Phase of Sonoluminescence at Low Partial Pressures

Bradley P. Barber, Keith Weninger, Ritva Löfstedt, and Seth Putterman
Physics Department, University of California, Los Angeles, California 90024
(Received 17 February 1995)

The acoustically driven pulsations of a gas bubble lead to 10^5-fold changes in its volume and the emission of a light flash upon collapse. Mass diffusion between the bubble and the gas dissolved in the surrounding fluid maintains this steady-state bubble motion only at low partial pressures, around 3 Torr. This diffusion-controlled regime is uniquely favorable to sonoluminescence (SL) from hydrogenic gases and polyatomic gases with low adiabatic heating. Our analysis indicates that the previously investigated SL from bubbles at 200 Torr requires a nondiffusive mass flow mechanism.

PACS numbers: 78.60.Mq

A gas bubble trapped in water can transduce the energy of a macroscopic sound field down to the microscopic level where it is emitted as picosecond flashes [1] of ultraviolet light [2]. This phenomenon, sonoluminescence (or SL), is particularly sensitive to the amplitude of the imposed sound field, the ambient temperature of the water [3], and the gas composition of the bubble [4]. This last parameter depends on the concentration of the gas dissolved in the water. In particular, the observation of SL from a single bubble of air requires that the water be somewhat degassed [5], whereas with pure argon the intensity of the light emission is relatively independent of the dissolved concentration [4].

Here we report the observation of a new phase of SL which makes this phenomenon accessible to hydrogenic and polyatomic gases. As shown in Fig. 1, this phase is characterized by very low concentrations of dissolved gas (about 10 ppb for deuterium) or, equivalently, low partial pressures of solution of the gas in the water. In this region of parameter space, the steady-state motion of every trapped bubble is accompanied by light emission, as in Fig. 2, which shows the stable dynamics of an ethane bubble as a function of the acoustic drive level. Below the lowest drive level, the bubble is unstable against dissolution in the water, and when driven at an amplitude above the upper threshold the bubble disappears. We have also found that the stability of light emission from pure noble gas bubbles dramatically improves as the partial pressure is reduced to the level where light emission from polyatomic and hydrogenic gases is optimized.

The investigation in this region of parameter space was motivated by considering the mass flow between the pulsating bubble and the gas dissolved in the surrounding fluid [6–8]. When the bubble expands in response to the rarefaction of the driving pressure, the pressure of the gas inside it decreases and mass diffuses into it from the fluid; when the bubble collapses, the gas pressure inside it causes mass to diffuse out. Requiring the net mass flow per acoustic cycle to vanish specifies the steady-state solution of mass diffusion and the bubble dynamics. For sufficiently nonlinear bubble motion, diffusive equilibrium requires that the partial pressure of gas dissolved in the fluid be given by [7,8]

$$P_\infty/P_0 = 3(R_0/R_m)^3. \tag{1}$$

where P_∞ is the partial pressure, P_0 is the ambient pressure (1 atm), R_0 is the ambient radius where the pressure of the gas inside the bubble is the ambient pressure, and R_m is the maximum radius to which the bubble expands in response to the drive. The relation (1) is derived from coupling the measured radius-versus-time curves, $R(t)$, for driven bubble to the diffusion equation for gas dissolved

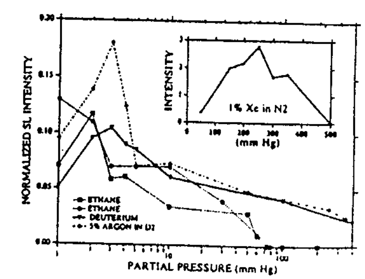

FIG. 1. Intensity of SL for ethane and deuterium as a function of partial pressure of the gas dissolved in the water. The intensities are normalized to air at 150 Torr. Air and xenon-doped nitrogen exhibit broad peaks centered near 200 mm. Inset: The intensities of D_2 and C_2H_6 peak at partial pressures of a few Torr. Between 50 and 150 mm of partial pressure, ethane gives intermittent light with an intensity of about 0.03 for a time scale of less than 25 s. These data points correspond to light-emitting states stable for over 1 min. The experiments were carried out in the acrylic resonators ($\omega_a \approx 35$ kHz) described elsewhere [4]. The saturated molar solubilities of D_2, C_2H_6, xenon, and nitrogen in water are about 15, 41, 88, and 13 ppm, respectively (at 1 atm). The two runs with ethane give a measure of the systematic variations.

 0031-9007/95/74(26)/5276(4)$06.00

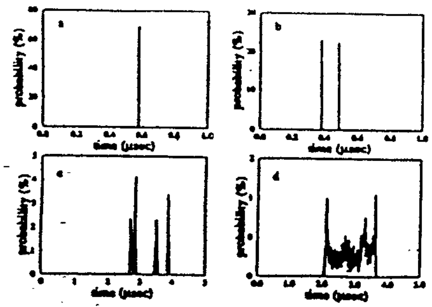

FIG. 2. Sequence of variation in time Δt between SL flashes from a single bubble. The data are histograms of the number of occurrences of a given Δt, measured sequentially during part of a bubble lifetime. The bin width is 0.25 nsec. Time zero is always defined as the time of the previous flash plus the ~36 μsec delay. The histograms show (a) a single maximum, (b) 2 maxima, (c) 4 maxima, and (d) a broad distribution. The frequency was slowly detuned about 0.01 kHz to initiate the bifurcation. $R_0 \sim 5$ μm, $P \sim 1.3$ atm, and $f_d = 27.0$ kHz.

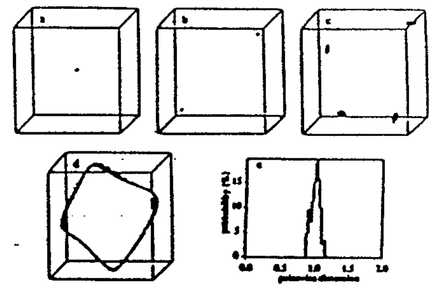

FIG. 3. Phase-space reconstruction of a typical bifurcation sequence of time series Δt. Each individual data point is a tuple of the form $(\Delta t_n, \Delta t_{n-1}, \Delta t_{n-2})$ generated using a single time series of flash data, where $3 \leq n \leq N$, and N is the number of data points (acoustic cycles) in each time series. Bifurcation of the variation Δt from period 1 (a) to 2 (b) to 4 (c) to a quasi-periodic state (d) is clearly shown. (a)–(d) are the attractors reconstructed from each of the Δt time series in Figs. 2(a)–2(d), respectively. (e) is the distribution of pointwise dimensions for (d).

Chaotic Sonoluminescence

R. Glynn Holt
Jet Propulsion Laboratory, MS 183-401, 4800 Oak Grove Drive, Pasadena, California 91109

D. Felipe Gaitan and Anthony A. Atchley
Department of Physics, Naval Postgraduate School, Monterey, California 93943

Joachim Holzfuss
Institut für Angewandte Physik, Technische Hochschule Darmstadt, Schlossgartenstrasse 7, D-64289 Darmstadt, Germany
(Received 12 November 1993)

[TR-34]

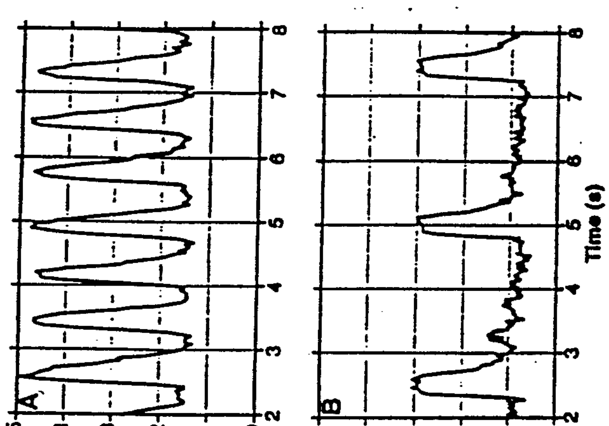

Fig. 5. Time dependence of SL from a pure N_2 bubble in water (with N_2 dissolved at 150 mmHg): (A) low drive, (B) high drive. The SL intensity has been normalized to the emission of an air bubble at the standard parameters delineated in Fig. 1. Uncertainty in the impurity concentration is about 0.05%. The long-term memory (over 100,000 cycles of sound) displayed in this data is indicative of an as yet unidentified physical process that is an essential aspect of the transition to SL. We were unable to observe steady SL from a single N_2 bubble. The average radius also drifts on the same time scales in these regimes. Because of this nonsteady motion and weak emission, we were unable to obtain a spectrum of a N_2 bubble.

[TR-33]

[TR-35]

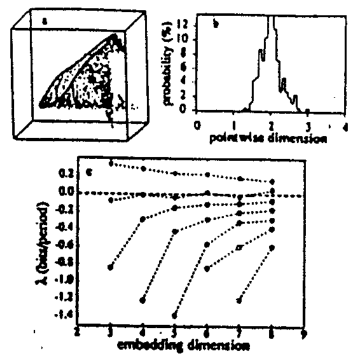

FIG. 4. Chaotic behavior in flash variation Δt. (a) is the attractor reconstructed from the flash time series. (b) is the distribution of pointwise dimensions for (a). (c) shows the results of calculation of the Lyapunov exponents for the attractor in (a).

VOLUME 72, NUMBER 9 PHYSICAL REVIEW LETTERS 28 FEBRUARY 1994

Chaotic Sonoluminescence

R. Glynn Holt

Jet Propulsion Laboratory, MS 183-401, 4800 Oak Grove Drive, Pasadena, California 91109

D. Felipe Gaitan and Anthony A. Atchley

Department of Physics, Naval Postgraduate School, Monterey, California 93943

Joachim Holzfuss

Institut für Angewandte Physik, Technische Hochschule Darmstadt, Schlossgartenstrasse 7, D-64289 Darmstadt, Germany

(Received 12 November 1993)

[TR-36]

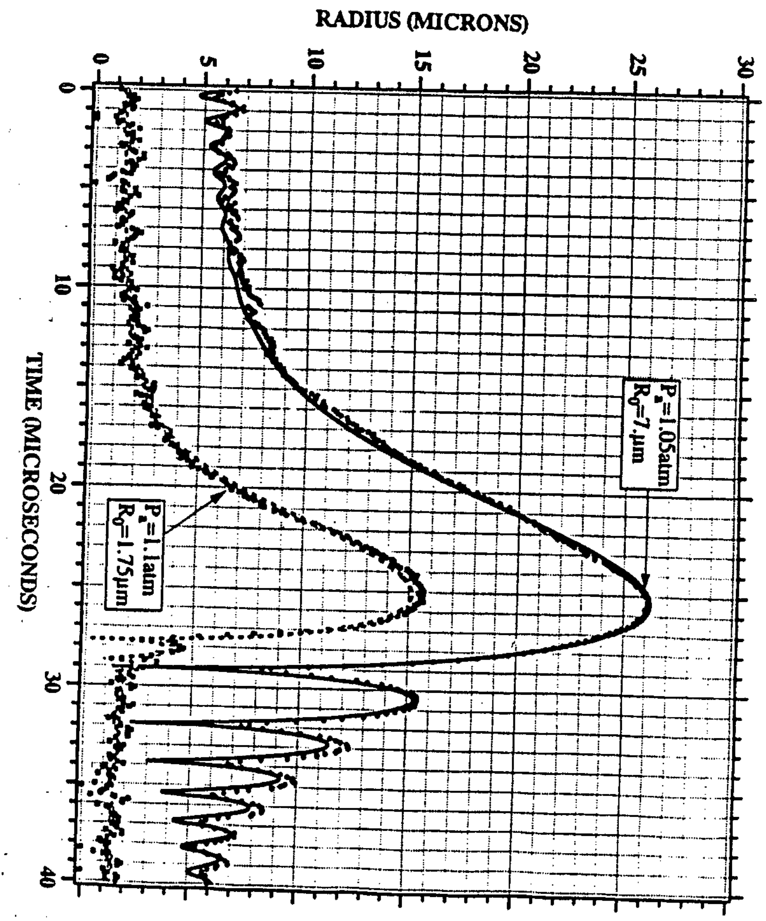

[TR-37]

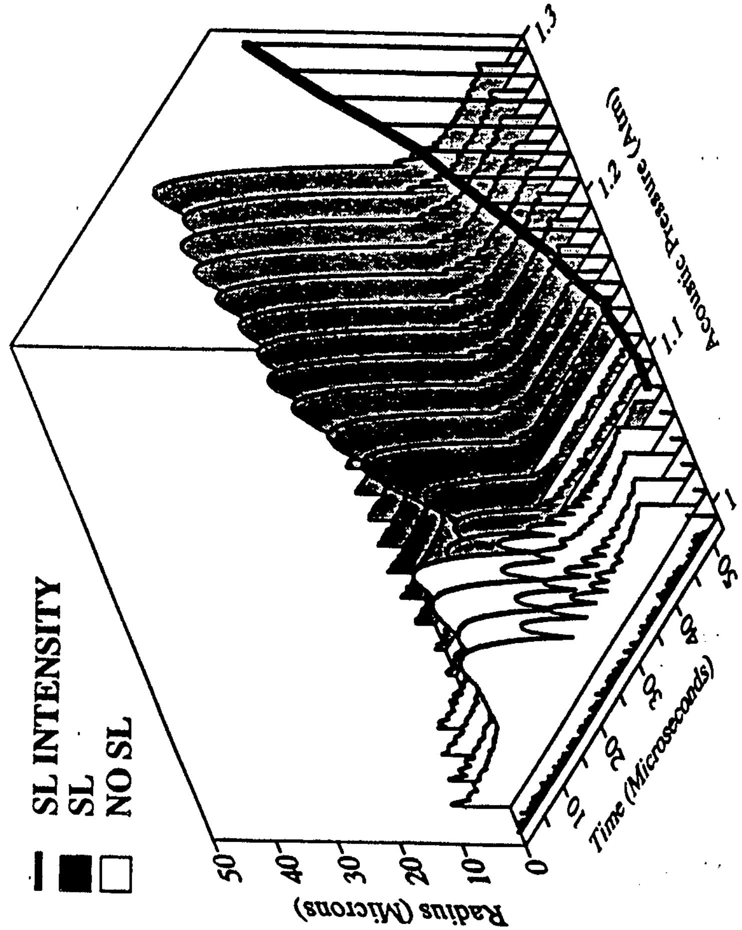

[TR-38]

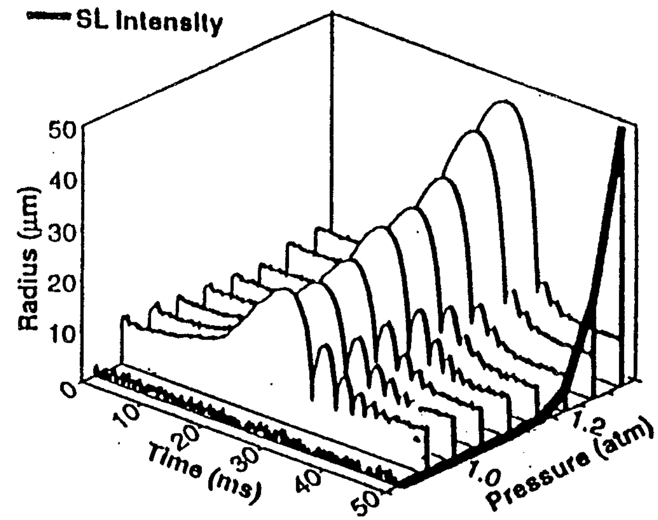

Fig. 4. Radius versus time curves for a pure Ar bubble in water (with Ar dissolved at 150 mmHg) as a function of increasing drive level for one cycle of the sound field. The ramp (labeled SL intensity) indicates the relative level of light emission. For a pure noble gas bubble, there is a smooth transition to the SL state.

Hiller, et al., Science, 266, 248-250 (1994).

[TR-39]

The effects of surfactant additives on the acoustic and light emissions from a single stable sonoluminescing bubble

Thomas R. Stottlemyer
Naval Undersea Warfare Center, Code 3111, Newport, Rhode Island 02841
Robert E. Apfel
Department of Mechanical Engineering, Yale University, New Haven, Connecticut 06520

J. Acoust. Soc. Am. 102 (3), September 1997

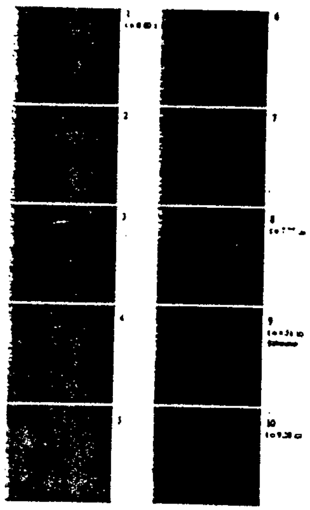

FIG. 9. The collapse of a sonoluminescing bubble in a solution of 1.0 CMC BSA in water.

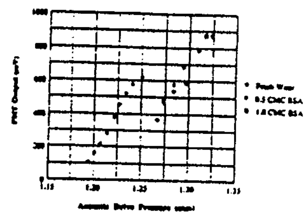

FIG. 8. The magnitude of the light pulses from a sonoluminescing bubble in water compared to solutions of BSA in water.

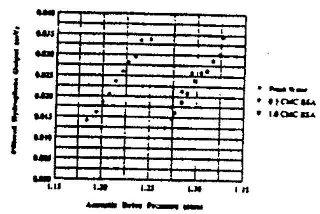

FIG. 7. The magnitude of the acoustic pulses from a sonoluminescing bubble in water compared to solutions of BSA in water.

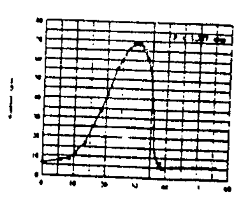

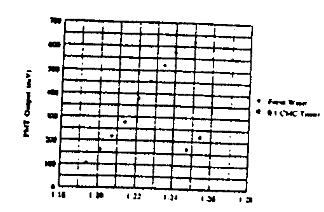

FIG. 3. The magnitude of the light pulses from a sonoluminescing bubble in water compared to a solution of 0.1 CMC Triton X-100 in water.

[TR-40]

VOLUME 77, NUMBER 23 PHYSICAL REVIEW LETTERS 2 DECEMBER 1996

Sonoluminescence in High Magnetic Fields

J. B. Young,[1] T. Schmiedel,[2] and Woowon Kang[1]
[1]The James Franck Institute and Department of Physics, University of Chicago, Chicago, Illinois 60637
[2]National High Magnetic Field Laboratory, Tallahassee, Florida 32310

(Received 15 July 1996)

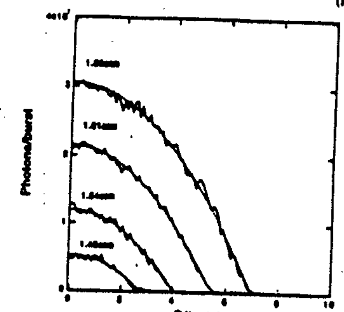

FIG. 1. Magnetic field dependence of SL intensity for various levels of applied forcing pressure at 15 °C. The dashed curves are a parabolic fit, $I_{SL} = a - bB^2$, to the field traces where the constant b is nearly identical for different pressures. The resonant frequency of the cavity was 43.1 kHz.

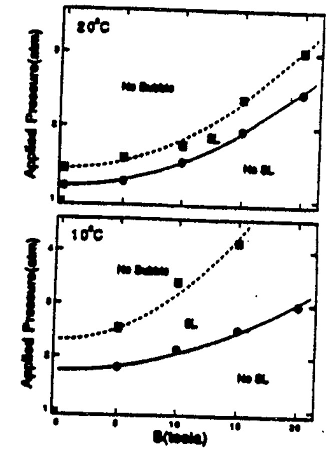

FIG. 3. The derived phase diagram from amplitude sweep data from Fig. 2 at 20 °C and 10 °C. The onset of SL is indicated as solid circles and the cut-off pressures as squares. The dotted (dashed) curve is a parabolic fit to the derived onset (cut-off) pressure points. Sonoluminescence is observed in the area between the two sets of curves. No luminescence occurs in the region below the onset points and bubbles disappear in the region above the cut-off points.

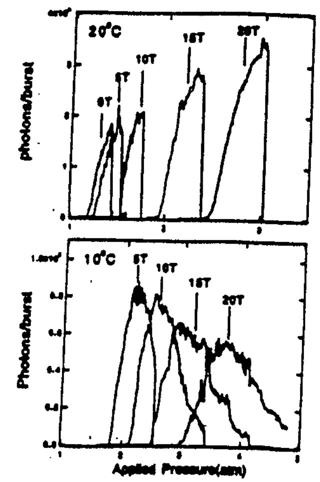

FIG. 2. Intensity of sonoluminescence as a function of applied drive amplitude at indicated values of magnetic field at 20 °C (upper) and 10 °C (lower). The resonant frequency of the cavity was 43.1 and 42.7 kHz at 20 and 10 °C, respectively.

[TR-41]

Observation of Stability Boundaries in the Parameter Space of Single Bubble Sonoluminescence

R. Glynn Holt and D. Felipe Gaitan
Jet Propulsion Laboratory, California Institute of Technology, Pasadena, California 91109
(Received 13 June 1996)

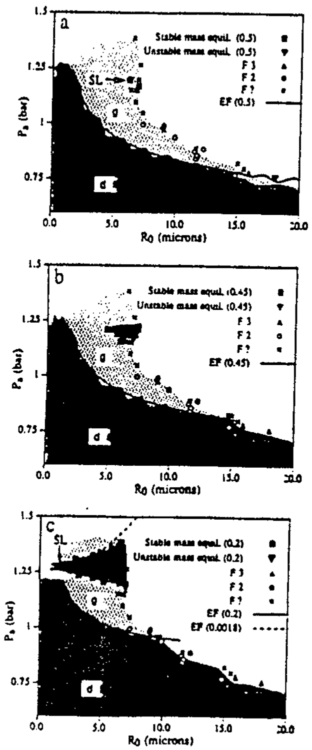

FIG. 1. Surfaces of constant dissolved air concentration from the 3D parameter space $(P_a, R_0, C_i/C_0)$ for acoustically levitated air bubbles in pure water. All bubbles are levitated in a cylindrical cell at 20.6 kHz. The symbols labeled "F n" are the measured values (P_a, R_0) at the onset of the Faraday instability for the nth mode ("?" indicates mode was undetermined). The line labeled "EF (C_i/C_0)" is the numerically generated diffusional equilibrium (1) for the experimentally measured C_i/C_{0L} using an RP equation [18]. The solid points are the measured mass flux equilibria at the given concentration: squares are stable, inverted triangles are unstable. Bubbles are observed to grow in regions labeled "g"; to dissolve in dark shaded regions labeled "d". (a) $C_i/C_{0L} = 0.5$; (b) $C_i/C_{0L} = 0.45$; (c) $C_i/C_{0L} = 0.2$; the arrow labeled "SL" indicates the minimum (P_a, R_0) where light is first emitted. (c) additionally displays the calculation of the Eller-Flynn equilibrium for $C_i/C_0 = 0.0018$ for comparison with the island boundary points on the upper segment.

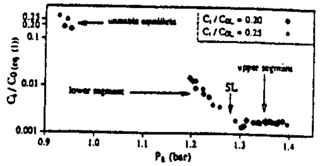

FIG. 2. Dissolved gas concentration $C_i/C_{0(eq(1))}$ calculated from (1) using the measured $R(t)$ for the stable and unstable mass flux equilibria vs acoustic pressure P_a for two data sets. The inferred C_i/C_{0L} from Henry's law is constant for each data set and drawn on the axis.

[TR-42]

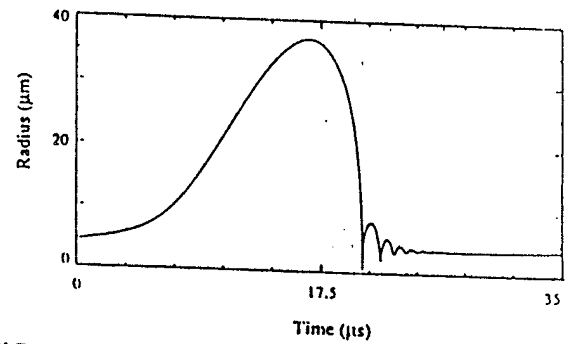

FIG. 1. Case (1): bubble radius vs time according to the adiabatic solution.

Wu and Roberts, Phys. Rev. Lett. 70, 3424-3427 (1993).

[TR-43]

Water Temperature Dependence of Single Bubble Sonoluminescence

Sascha Hilgenfeldt,[1] Detlef Lohse,[1] and William C. Moss[2]
[1]Fachbereich Physik der Universität Marburg, Renthof 6, D-35032 Marburg, Germany
[2]Lawrence Livermore National Laboratory, Livermore, California 94550

(Received 22 September 1997)

The strong dependence of the intensity of single bubble sonoluminescence (SBSL) on water temperature observed in experiment can be accounted for by the temperature dependence of the material constants of water, most essentially of the viscosity, of the argon solubility in water, and of the vapor pressure. The strong increase of light emission at low water temperatures is due to the possibility of applying higher driving pressures, caused by increased bubble stability. The presented calculations combine the Rayleigh-Plesset equation based hydrodynamical/chemical approach to SBSL and full gas dynamical calculations of the bubble's interior. [S0031-9007(98)05331-9]

PACS numbers: 78.60.Mq

One of the remarkable features of single bubble sonoluminescence (SBSL) [1,2] is the sensitivity of the light emission to the water temperature experimentally found by the UCLA group [2,3]; cf. Fig. 1. To obtain these results, Barber *et al.* proceeded as follows (Refs. [2,3,5]): Water was cooled to a temperature of 2.5 °C and completely degassed. An air pressure overhead of 150 Torr, corresponding to about 20% of gas saturation, was adjusted and sonoluminescence (SL) experiments were performed, still at 2.5 °C. Then the water was heated to 20 °C *without* readjusting the gas concentration, and the SL experiment was repeated. Finally, the same measurement was performed after heating the water to 32 °C. At all three temperatures, the forcing pressure amplitude P_a of the driving sound field was adjusted in order to give maximum light intensity, while maintaining bubble stability against fragmentation (*stable* SL). According to the "waterfall plots" shown e.g. in Ref. [5], a

strong bubble collapse results in a satisfactory fit with the physical values for σ and ν_l.

Because of the complications in the fits of Refs. [2,3], the resulting data should be read with some care. This is also reflected in Fig. 3, where we display the data from these two references for the expansion ratio (maximum radius R_{max} divided by R_0): they show large deviations at otherwise unchanged parameters. The expansion ratio is a quantity closely related to the violence of collapse and therefore, presumably, to the intensity of energy concentration and light emission [4]. It is therefore puzzling that the same light intensity has been observed in Refs. [2,3] in spite of the different expansion ratios reported in Fig. 3.

The central claim of this paper is that the observed dependence on water temperature T in Figs. 1–3 can be accounted for by the T dependence of the material

[TR-44]

The acoustic emissions from single-bubble sonoluminescence

Thomas J. Matula, Ibrahim M. Hallaj, Robin O. Cleveland, and Lawrence A. Crum
Applied Physics Laboratory, University of Washington, 1013 NE 40th Street, Seattle, Washington 98105

William C. Moss
Lawrence Livermore National Laboratory, P.O. Box 808, Livermore, California 94550

Ronald A. Roy
Department of Aerospace and Mechanical Engineering, Boston University, 110 Cummington Street, Boston, Massachusetts 02215

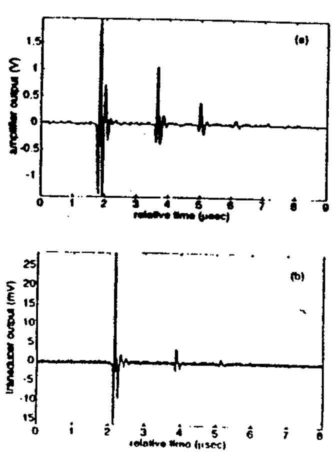

FIG. 2. Pressure pulses from an SBSL bubble measured with the focused transducer. The output from the transducer (a) with and (b) without a secondary 40 dB preamp. In (a) the first pulse amplitude causes distortion in the preamp, such that no amplitude comparisons can be made of that particular signal with the other pulses.

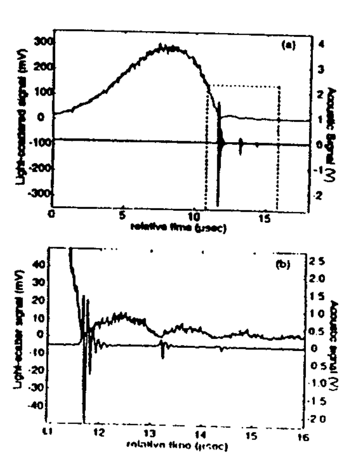

FIG. 3. (a) A single-shot $R(t)$ curve as measured using our light scattering system, with the corresponding acoustic signature. (b) A detailed view of the boxed area in (a). The acoustic data is shown here shifted in time equal to the time necessary for sound to travel from the bubble to the transducer, about 16.77 μs.

[TR-45]

VOLUME 79, NUMBER 7 PHYSICAL REVIEW LETTERS 18 AUGUST 1997

Resolving Sonoluminescence Pulse Width with Time-Correlated Single Photon Counting

B. Gompf,[1] R. Günther,[2] G. Nick,[1] R. Pecha,[1] and W. Eisenmenger[1]
[1]Physikalisches Institut, Universität Stuttgart, Pfaffenwaldring 57, D-70550 Stuttgart, Germany
[2]Natural and Medical Science Institute, Ebernardstrasse 29, D-72762 Reutlingen, Germany

(Received 17 April 1997)

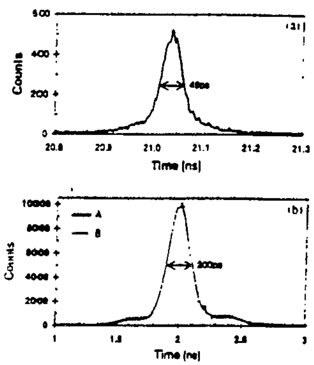

FIG. 2. (a) Response to a 300-fs 400-nm laser pulse. The response corresponds well with the convolution of the time transit spreads of the two multipliers. (b) curve A: SL pulse as measured with TC-SPC with a UV filter (300–400 nm). The two smaller peaks left and right of the main peak are due to reflections of the SL pulse at the glass flask. Curve B: Additionally to the measured SBSL signal the forward convolution of Fig. 3 is shown.

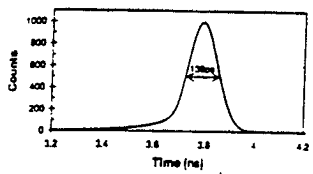

FIG. 3. SL pulse after subtraction of the reflections and deconvolution. The pulse shape is slightly asymmetric and its FWHM at 1.2 atm driving pressure and a gas concentration of 1.3 mg/l O_2 at 22 °C is 138 ps ($\pm$10 ps).

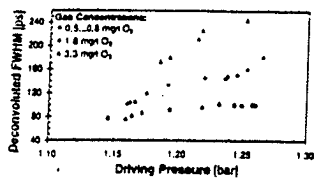

FIG. 4. Dependence of the FWHM of the SL pulse width on driving pressure and gas concentration at room temperature.

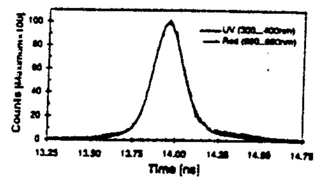

FIG. 5. SL pulse width measured at different parts of the spectrum. For the ease of comparison the pulses are not deconvoluted but without the glass wall reflections. (Red: 590–650 nm, UV: 300–400 nm).

[TR-46]

VOLUME 80, NUMBER 5 PHYSICAL REVIEW LETTERS 2 FEBRUARY 1998

Time-Resolved Spectra of Sonoluminescence

Robert A. Hiller, Seth J. Putterman, and Keith R. Weninger
Physics Department, University of California, Los Angeles, California 90095

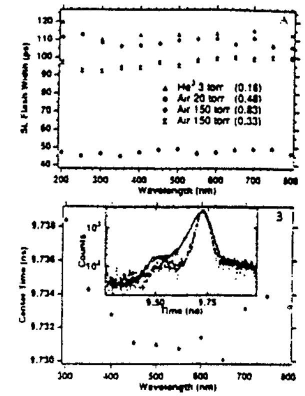

FIG. 1. Flash width (A) and relative emission time (B) of sonoluminescence as a function of wavelength, showing that these parameters are independent of the photon energy. The numbers in parentheses are intensity relative to the brightest SL from 150 torr air. (B) shows data for 20 torr air; the increase in emission time below 320 nm is due to variations in the index of refraction of water and the commercial quartz used for the acoustic resonator (the 200 nm data point lies at 9.766 ns). The inset to (B) contains instrument and SL response functions for this system (with the light sources attenuated so that each PMT operated at the single photon level). The intrinsic jitter is represented by the full width at half-maximum of 55 ps generated by the flashes of a 200 fs laser. The outer curve (FWHM = 78 ps) is generated by an air bubble in well-degassed water (about 20 torr partial pressure).

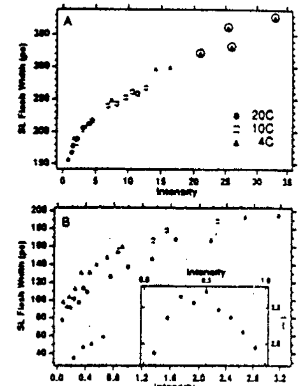

FIG. 2. Flash width at 500 nm as a function of integrated SL intensity (relative to the brightest SL from 150 torr air) for various bubbles: (A) shows data for 300 torr solution of a 1% xenon in oxygen mixture at 4, 10, 20 °C; (B) contains data for 3 torr xenon (●), 3 torr argon (▲), 3 torr helium (+), 20 torr air (◆), and 300 torr 1% xenon in oxygen (□), all at 20 °C. Note that for the same flash intensity, 3 torr helium and 3 torr xenon have the same flash width. The circled points indicate bubbles that could be as much as 1 cm off center in the flask (as tends to happen to the brightest bubbles). The inset to (B) shows the measurements for 3 torr argon scaled to a theoretical estimate based upon the shock-wave-plasma-bremsstrahlung model of SL [7]. The drift in gas content accounts for systematic variations in flash width that are observed when a region of parameter space is remeasured on the time scale of 1 hour. This variation of about 5–10 ps is readily apparent for the six helium data points. This variation is also the accuracy with which we claim that the dimmest xenon bubble has the same flash width (at the same intensity of SL) as the brightest helium bubble. We also note that, at a given SL intensity, air and pure noble gas bubbles have significantly different flash widths.

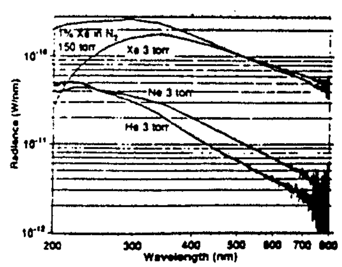

FIG. 4. High resolution (1 nm FWHM) spectra of SL from various gases in water, acquired using the optical arrangement of Fig. 3. The light is detected with a linear PMT (R2027) replacing the MCP (R3809) and the signal analyzed as in Refs. [1] and [8]. This data further restrict the presence of emission lines in single bubble sonoluminescence.

[TR-47]

Measurements of Sonoluminescence Temporal Pulse Shape

To Appear: June 1, 1998 Phys. Rev. Letters

M. J. Moran and D. Sweider, LLNL

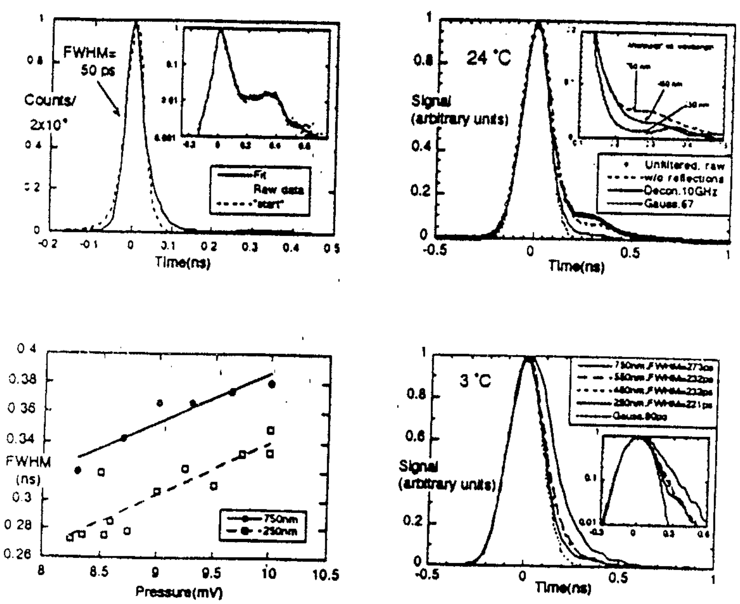

[TR-48]

VOLUME 78, NUMBER 7 PHYSICAL REVIEW LETTERS 17 FEBRUARY 1997

Sonoluminescing Air Bubbles Rectify Argon

Detlef Lohse,[1] Michael P. Brenner,[2] Todd F. Dupont,[3] Sascha Hilgenfeldt,[1] and Blaine Johnston[4]
[1]*Fachbereich Physik der Universität Marburg, Renthof 6, 35032 Marburg, Germany*
[2]*Department of Mathematics, Massachusetts Institute of Technology, Cambridge, Massachusetts 02139*
[3]*Department of Computer Science, University of Chicago, Chicago, Illinois 60637*
[4]*Department of Physics, University of Chicago, Chicago, Illinois 60637*
(Received 24 April 1996; revised manuscript received 8 October 1996)

The dynamics of single bubble sonoluminescence (SBSL) strongly depends on the percentage of inert gas within the bubble. We propose a theory for this dependence, based on a combination of principles from sonochemistry and hydrodynamic stability. The nitrogen and oxygen dissociation and subsequent reaction to water soluble gases implies that strongly forced air bubbles eventually consist of pure argon. Thus it is the partial argon (or any other inert gas) pressure which is relevant for stability. The theory provides quantitative explanations for many aspects of SBSL. [S0031-9007(97)02404-6]

PACS numbers: 78.60.Mq, 42.65.Re, 47.55.+y, 82.40.We

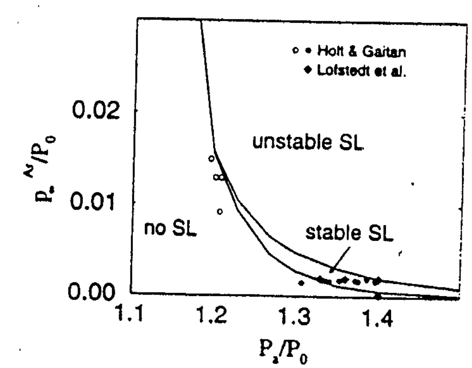

FIG. 1. Phase diagram for pure argon bubbles in the p_a^{Ar}/P_0 versus P_a/P_0 parameter space, from [5], but now with experimental data included. Stable SL is only possible in a very small window of argon concentration. The experimental data points refer to observed stable SL (filled symbols) or stable non-SL bubbles (open symbols) and are extracted (using the present theory) from Refs. [7] (diamonds) and [18] (circles) and show good agreement with the theory. This theoretical figure compares well with the experimental result: cf. Fig. 1(c) of [18].

[TR-49]

VOLUME 80, NUMBER 4 PHYSICAL REVIEW LETTERS 26 JANUARY 1998

Evidence for Gas Exchange in Single-Bubble Sonoluminescence

Thomas J. Matula and Lawrence A. Crum
Applied Physics Laboratory, University of Washington, 1013 NE 40th Street, Seattle, Washington 98105
(Received 6 August 1997)

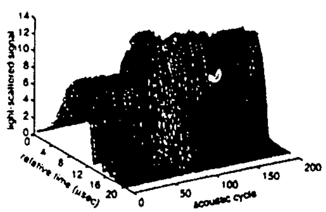

FIG. 1. The radius profile of a room-temperature air bubble as it transitions from a nonsonoluminescing state to a sonoluminescing state caused by an abrupt increase in the acoustic drive pressure. The increase occurs near acoustic cycle 60 in this figure. The bubble responds by collapsing at a later time, with a decrease in the rebound amplitude. The response time for the bubble (as well as the resonator) depends on the Q of the system; the pressure increase causes the bubble to overshoot initially before it settles down to a steady value after about 90 cycles. The highly irregular signal observed after the rapid increase in pressure is initiated is probably due in part to nonradial oscillations of the bubble.

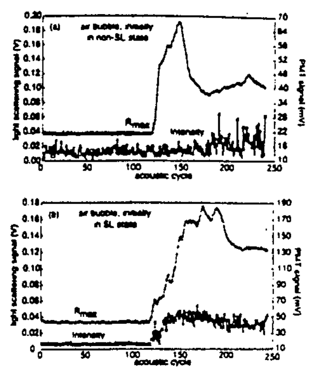

FIG. 2. The maximum radius (+) and sonoluminescence intensity (×) of an air bubble is plotted over approximately 240 consecutive acoustic cycles. The "radius" is actually a signal level, proportional to the square of maximum radius (assuming a geometrical optics limit for scattering from a sphere). (a) The bubble is initially below the light-emission threshold. The corresponding PMT signal level corresponds to noise. At approximately the 120th acoustic cycle, the drive pressure is rapidly increased to a value above the SBSL threshold. (b) For this case, the bubble is initially in a stable sonoluminescing state. The drive pressure is then rapidly reduced to a value below the light-emission threshold, and then quickly increased again after a time period of approximately 90 ms. In both (a) and (b), the drive amplitudes at the lower and upper values are the same.

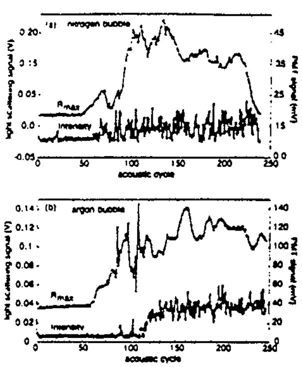

FIG. 3. The maximum radius (+) and sonoluminescence intensity (×) of (a) a nitrogen bubble and (b) an argon bubble are plotted over approximately 240 consecutive acoustic cycles. In both cases, the acoustic pressure has initially been below the light-emission threshold. The pressure is then rapidly increased to a value above the threshold (same values as in Fig. 2).

[TR-50]

PHYSICAL REVIEW E VOLUME 56, NUMBER 6 DECEMBER 1997

Sonoluminescence from an isolated bubble on a solid surface

K. R. Weninger, H. Cho, R. A. Hiller, S. J. Putterman, and G. A. Williams
Department of Physics and Astronomy, University of California, Los Angeles, California 90095
Received 23 June 1997)

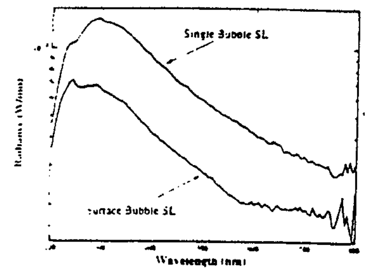

FIG. 2. Spectrum of 300-torr xenon in a water-surface-bubble and 150-torr 1% xenon in oxygen in a water-single-bubble SL generated in the same cell and acquired with the same equipment (10-nm full width at half maximum resolution). The dip at 240 nm and the falloff near 200 nm are attributed to absorption in the quartz wall of the resonator.

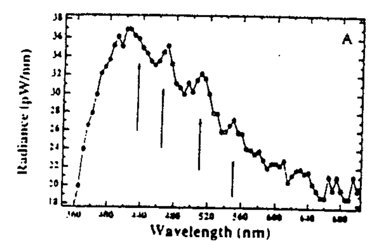

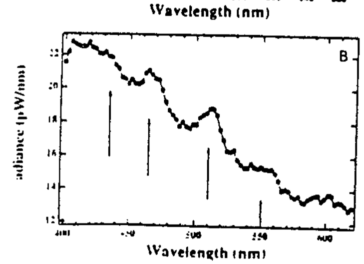

FIG. 6. Spectrum of 290-torr xenon in n-dodecane with 10-nm full width at half maximum resolution. The cutoff in blue is consistent with absorption in the liquid. Shown in (B) is a second scan of the Swan lines with the same resolution. The arrows indicate the expected location of Swan lines.

[TR-51]

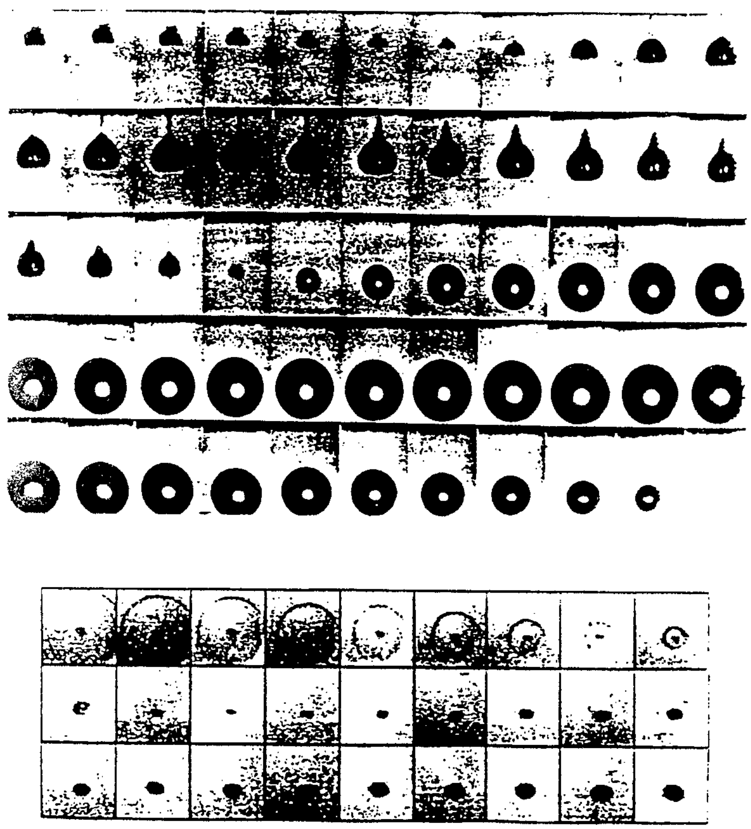

[TR-52]

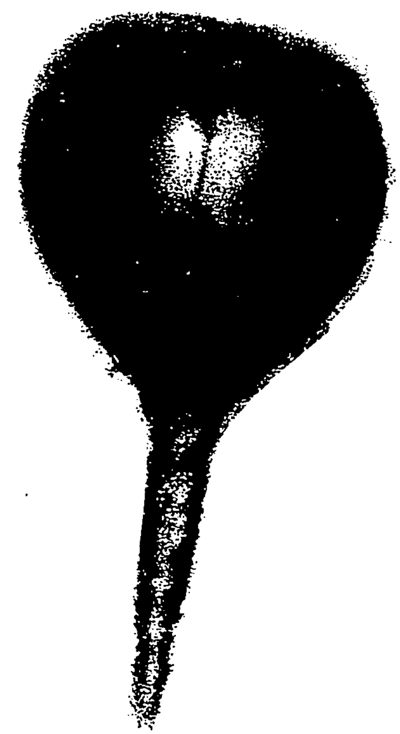

[TR-53]

Jets

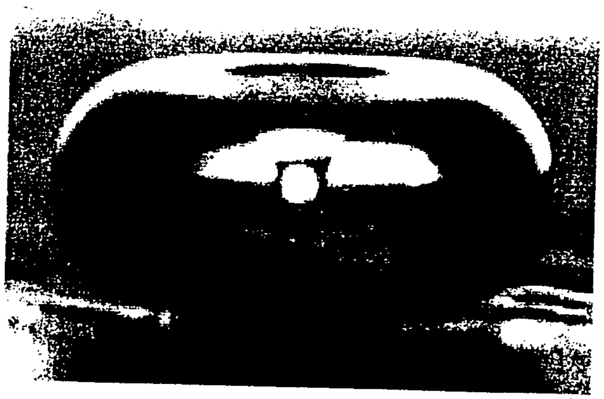

[TR-54]

Asymmetric Bubble Collapse

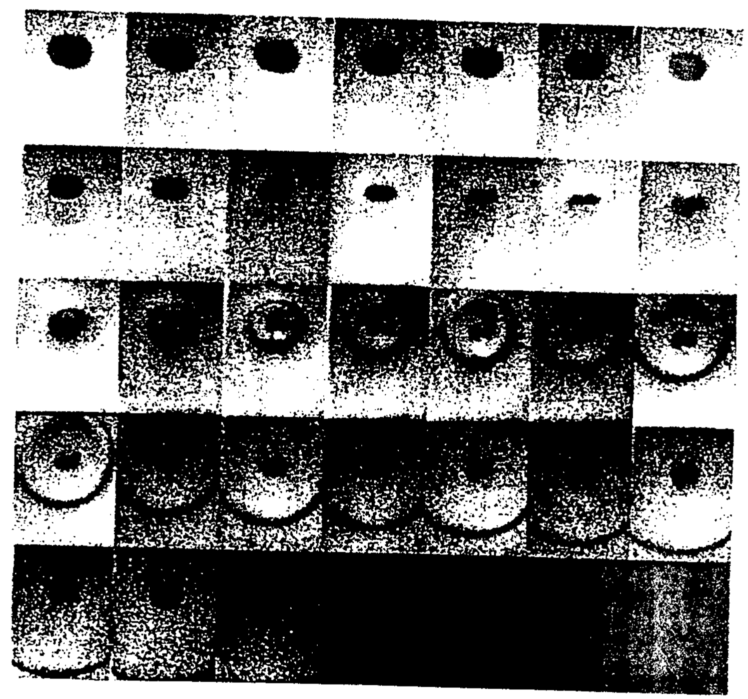

[TR-55]

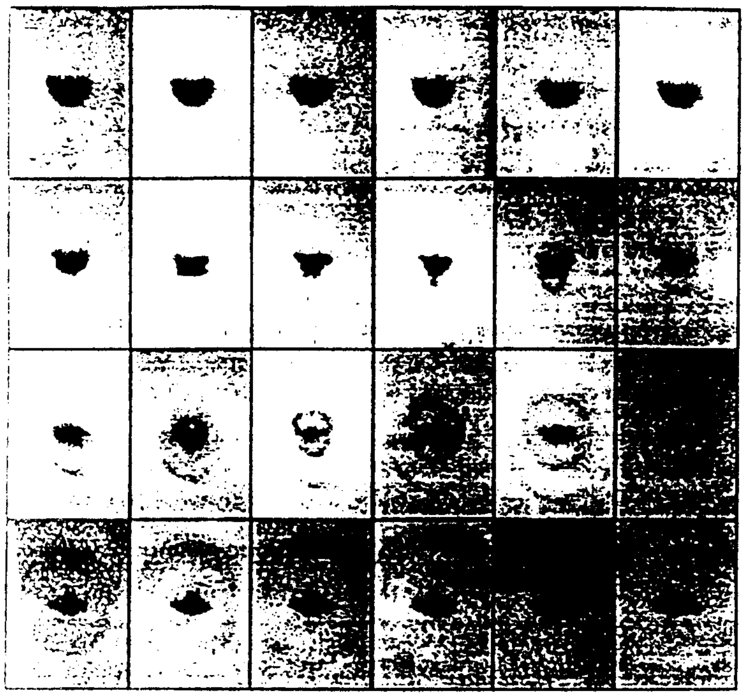

[TR-56]

Sonoluminescence: An alternative "electrohydrodynamic" hypothesis

Thierry Lepoint,[a)] Damien De Pauw, and Françoise Lepoint-Mullie
Laboratoire de Sonochimie et d'Etude de la Cavitation, Institut Meurice-CERIA 1, Avenue E. Gryson, 1070 Brussels, Belgium

Max Goldman and Alice Goldman
Laboratoire de Physique des Décharges, Ecole Supérieure d'Electricité, Plateau de Moulon, 91192 Gif-sur-Yvette Cedex, France

(Received 4 April 1996; accepted for publication 24 September 1996)

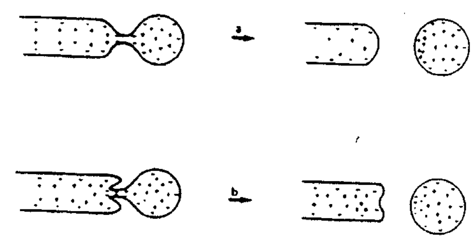

FIG. 5. Schematic representation of the two models of jet breakup: (a) breakup associated with the positive mode of charging ["positive" curvature of the neck according to the nomenclature by Iribarne and Klemes (1974)]; (b) negative mode of charging.

[TR-57]

J. Acoust. Soc. Am. 101 (4), April 1997

A new mechanism for sonoluminescence

A. Prosperetti[a)]
Department of Mechanical Engineering, The Johns Hopkins University, Baltimore, Maryland 21218

(Received 12 June 1996; accepted for publication 11 November 1996)

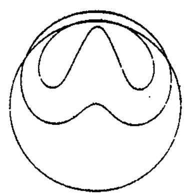

FIG. 1. Successive shapes of an axisymmetric translating and collapsing bubble in an unbounded, inviscid, incompressible liquid. The initial upward velocity of translation equals $0.6\times\sqrt{\Delta P/\rho}$, where ΔP is the difference (assumed constant) between the internal and external pressures and ρ is the liquid density. The successive shapes shown are at times 0, 0.6, and 0.86 in units of $R_0\sqrt{\rho/\Delta P}$. For $\Delta P=1$ bar and the density of water, with $R_0=10$ μm, this equals 1 μs. Surface tension is neglected. Note the jet directed in the same direction as the translational velocity. The jet becomes thinner with increasing translational velocity.

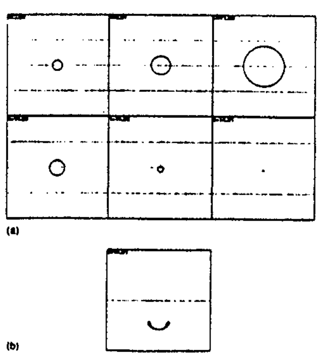

FIG. 2. Successive shapes of a 4.5-μm radius bubble in water placed in a pressure gradient in an unbounded liquid and subject to a pressure field oscillating at 26.5 kHz. The flow is assumed to be axisymmetric, irrotational, and incompressible, and the bubble initial velocity vanishes. Surface tension effects are accounted for. Times are in units of 1.1 μs. Figure (b) is an enlargement of the last frame of (a)

[TR-58]

VOLUME 80, NUMBER 2 PHYSICAL REVIEW LETTERS 12 JANUARY 1998

Luminescence from Spherically and Aspherically Collapsing Laser Induced Bubbles

C. D. Ohl, O. Lindau, and W. Lauterborn
Drittes Physikalisches Institut, Universität Göttingen, Bürgerstraße 42-44, D-37073 Göttingen, Federal Republic of Germany
(Received 15 August 1997)

Single cavitation bubble luminescence is investigated. The cavitation bubbles are produced by focused laser light and collapse under the action of the ambient pressure. Both spherical and aspherical collapse is studied. Luminescence is observed in both cases, but only up to a mildly aspherical collapse.
[S0031-9007(97)04982-X]

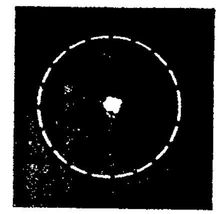

FIG. 2. ICCD image with a 5 μs shutter open time of a luminescing cavitation bubble with weak additional illumination from the front. The bubble appears dark on a bright background with the luminescence spot in the middle. During the shutter open time, the bubble wall collapses from the position marked with the dashed outline to a smaller bubble size, and therefore its shape becomes blurred. The size of the frame is 0.784 mm × 0.784 mm.

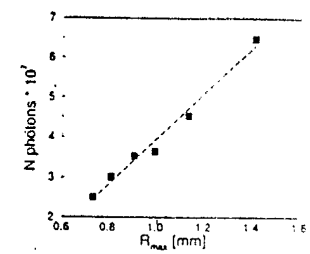

FIG. 3. Lower bound for the number of photons emitted during the primary bubble collapse for different maximum bubble radii.

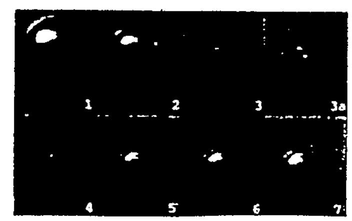

FIG. 4. Frames 1–7: bubble dynamics and light emission near a rigid boundary (not visible) placed $s = 4.9$ mm below the laser focus photographed with the image converter camera. The bubble reaches a maximum radius of $R_{max} = 0.83$ mm, leading to $\gamma = 5.9$. The frames have 4.4 μs interframe time. Frame 3a: Blended picture of frame 3 and photograph of the light emission with the ICCD for a bubble with the same experimental parameters. The size of all individual frames is 1.56 mm × 1.25 mm.

[TR-59]

Transition from *Normal* to *Fast* Sound in Liquid Water

F. Sette,[1] G. Ruocco,[2] M. Krisch,[1] C. Masciovecchio,[1] R. Verbeni,[1] and U. Bergmann[1]
[1]European Synchrotron Radiation Facility, B.P. 220, F-38043 Grenoble, Cedex France
[2]Universita di L'Aquila and Istituto Nazionale di Fisica della Materia, I-67100, L'Aquila, Italy
(Received 1 April 1996)

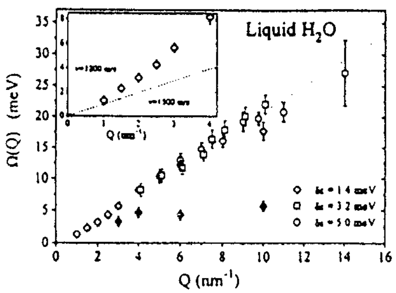

FIG. 2. Excitation energies, $\Omega(Q)$ from the DHO model, for the new high resolution data ($\diamond$, $\delta\epsilon = 1.4$ meV) and from previous IXS experiments ($\square$, $\delta\epsilon = 3.2$ meV [6]; $\circ$, $\delta\epsilon = 5.0$ meV, [5]). The open symbols refer to the dispersing excitation and the full diamond to the weakly dispersing ones. The dotted line, with a slope of 3200 m/s results from a fit for $Q \geq 4$ nm^{-1}. The inset shows an enlargement of the low Q region, where the transition from fast toward normal sound takes place, as emphasized by the two lines corresponding to the fast and normal sound branches.

[TR-60]

Sonoluminescence as Quantum Vacuum Radiation

Claudia Eberlein*
Department of Physics, University of Illinois at Urbana-Champaign, Urbana, Illinois 61801-3080
(Received 2 June 1995; revised manuscript received 11 December 1995)

Sonoluminescence is explained in terms of quantum vacuum radiation by moving interfaces between media of different polarizability. It can be considered as a dynamic Casimir effect, in the sense that it is a consequence of the imbalance of the zero-point fluctuations of the electromagnetic field during the noninertial motion of a boundary. The transition amplitude from the vacuum into a two-photon state is calculated in a Hamiltonian formalism and turns out to be governed by the transition matrix element of the radiation pressure. Expressions for the spectral density and the total radiated energy are given.
[S0031-9007(96)00240-2]

PACS numbers: 78.60.Mq, 03.70.+k, 42.50.Lc

Sonoluminescence is a phenomenon that has so far resisted all attempts of explanation. A short and intense flash of light is observed when ultrasound-driven air or other gas bubbles in water collapse. This process has been known for more than 60 years to occur randomly when degassed water is irradiated with ultrasound [1]. Recently interest has been revived by the contriving of stable sonoluminescence [2,3] where a bubble is trapped at the pressure antinode of a standing sound wave in a spherical or cylindrical container and collapses and reexpands with the periodicity of the sound. With a clock-like precision a light pulse is emitted during every cycle of the sound wave; the jitter in the sequence of pulses is almost unmeasurably small. Shining laser light upon the bubble and analyzing the scattered light on the basis of the Mie theory of scattering from spherical obstacles one has been able to record the time dependence of the bubble radius [4]; these experiments showed that the flash of light is emitted shortly after the bubble has collapsed, i.e., shortly after it has reached its minimum radius. This and the fact that the spectrum of the emitted light resembles radiation from a black body at several tens of thousands degree kelvin have led to the conjecture that the light could be thermal radiation from the highly compressed and heated gas contents of the bubble after the collapse [5]. It has also been argued that the experimentally observed spectrum would equally well be compatible with the idea of a plasma forming at the bubble center after the collapse and radiating by means of bremsstrahlung [6]. An alternative suggestion has tried to explain the sonoluminescence spectrum as pressure-broadened vibration-rotation lines [7], but although this theory has been very successful in the case of randomly excited (multibubble) sonoluminescence seen in silicone oil it has been inefficacious for sonoluminescence in water.

All of the above theories have serious flaws. Both blackbody radiation and bremsstrahlung would make a substantial part of the radiated energy appear below 200 nm where the surrounding water would absorb it. If one estimates the total amount of energy to be absorbed corresponding to the observed number of photons above the absorption edge, one quickly convinces oneself that this would be far too much to leave no macroscopically discernible traces in the water, as, for instance, dissociation [8]; however, nothing the like is observed. Another very strong argument against all three of the above theories is that the processes involved in each of them are far too slow to yield pulse lengths of 10 ps or less, but which are observed. Moreover, if a plasma were formed in the bubble, one should see at least remnants of slow recombination radiation from the plasma when the bubble reexpands. As to the theory involving vibration-rotation excitations, the line broadening required to model the observed spectrum seems rather unrealistic.

In its concept the theory to be presented here has been loosely inspired by Schwinger's idea [9] that sonoluminescence might be akin to the Casimir effect, in the sense that the zero-point fluctuations of the electromagnetic field might lie at the origin of the observed radiation. More closely related to this is the Unruh effect well known in field theory [10]; its original statement is that a uniformly accelerated mirror in vacuum emits photons with the spectral distribution of blackbody radiation. However, the phenomenon is far more general than that and in particular not restricted to perfect mirrors. This kind of quantum vacuum radiation has been shown to be generated also by moving dielectrics [11]. Whenever an interface between two dielectrics or a dielectric and the vacuum moves nonuniformly photons are created. In practice this effect is very feeble, so that it has up to now been far beyond any experimental verification. Sonoluminescence might be the first identifiable manifestation of quantum vacuum radiation.

The mechanism by which radiation from moving dielectrics and mirrors in vacuum is created is understood most easily by picturing the medium as an assembly of dipoles. The zero-point fluctuations of the electromagnetic field induce these dipoles and orient and excite them. However, as long as the dielectric stays stationary or uniformly moving such excitations remain virtual; real photons are created only when the dielectric or mirror moves

[TR-61]

Influence of Resonant rf Radiation on Gas/Liquid Interface: Can It Be a Quantum Vacuum Radiation?

Miroslav Colic[1,2,*] and Dwain Morse[1]
[1]R&D Division, ZPM Inc., 5770 Thornwood Drive, Suite C, Goleta, California 93117
[2]Materials Department, The University of California at Santa Barbara, Santa Barbara, California 93106
(Received 5 September 1997)

Sonoluminescence, a resonant cavitation of the gas/liquid interface with the kHz ultrasound, produces visible light and splitting of water. According to the quantum vacuum radiation model of sonoluminescence, high-Q resonant radio frequency (rf) or microwave cavity with movable walls should produce similar effects. The similarity of the effects of highly resonant nonthermal rf described in this Letter and sonoluminescence suggests that quantum vacuum radiation might indeed be the most feasible model to explain both phenomena. [S0031-9007(98)05506-9]

PACS numbers: 78.60.Ya

The concept of treating the gas/water interface with different stimuli to produce unusual effects has received considerable attention in recent years due to significant interest in the sonoluminescence phenomenon. Sonoluminescence [1-3] is an emission of light resulting from resonant ultrasonic treatment of water containing bubbles. The generation of visible light from 24 kHz ultrasound is an amazing amplification in frequency of 11 orders of magnitude. Interestingly, while the duration of ultrasound pulses is in microseconds, the emitted visible light pulses burst in picoseconds [1]. The mechanisms of the sonoluminescence phenomenon are still largely unknown. Eberlein recently proposed a quantum vacuum radiation theory of sonoluminescence [4] which predicts that an oscillating electromagnetic field (EMF) strongly influences the hydrophobic gas/water interface. In this model, the two interfaces with different polarizabilities (water and

and survived freezing, thawing cycles or boiling in a closed container. It was also realized that careful outgassing of the water solutions resulted in the lack of any measurable EMF effects. Atomic hydrogen seems to be stabilized in a hydrophobic hydration cage of argon or carbon dioxide. Sonoluminescence phenomena also cease to exist in the absence of noble gases or carbon dioxide [3]. Outgassed water has to be sparged with gases containing either a small amount of noble gases or carbon dioxide to produce sonoluminescence or EMF effects on the gas/liquid interface. Our preliminary experiments even identified delayed rf emissions upon cessation of primary rf treatment (unpublished data). The association of two hydrogen atoms into a hydrogen molecule radiates 20 cm wavelength rf's. This is the frequency that radio telescopes are programed to identify. Others have noticed that the presence of water

Sensor Physics: Signals and Noise

Thomas B. Gabrielson
Applied Research Laboratory
The Pennsylvania State University
P.O. Box 30
State College, PA 16804
(814) 865-1370
tbg3@psu.edu

Sensor Physics: Signals and Noise

Introduction

Equilibrium-Thermal Noise
- Relation of fluctuations to dissipation
- Total-energy methods; frequency distribution
- Examples

Shot and Nonequilibrium Noise
- Basic theory
- Molecular collisions
- Metals and semiconductors

Sensor Calibration
- Reciprocity calibration
- Bessel-null methods

Summary

Fluctuations and Noise in Thermal Equilibrium

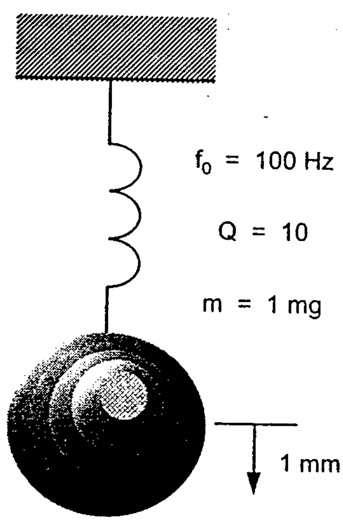

Given an initial displacement of 1mm, how long will it take for the amplitude to decay to 10^{-8} mm?

(A 10^{-8} mm amplitude is equivalent to an applied acceleration of 0.5 micro-g's.)

Resonant Systems: Q

(I-5)

(1) 2π times the number of cycles required for energy to decay by e^{-1}; π times the number of cycles for the amplitude to decay by e^{-1}. Alternately, $Q = \pi N / \ln(x)$ where N is the number of cycles for the amplitude to decay by a factor of x.

(2) Ratio of the resonance frequency to the width of the resonance peak. The width must be measured as the full width from one half-power point to the other.

(3) For series-connected elements: the ratio of mass reactance (or stiffness reactance) at resonance to the resistance. For parallel-connected elements: the reciprocal of that ratio.

(4) 2π times the energy stored in the system divided by the energy dissipated per cycle; 2π times the resonance frequency times the stored energy divided by the power dissipated.

(5) The reciprocal of 2 times the damping factor; the reciprocal of the loss tangent.

(6) If the damping is high (small Q), the resonance is isolated from other resonances, and there is no other mechanism to generate a changing phase, the Q can be determined from the rate-of-change of the phase (in radians per hertz) at the resonance frequency:

$$Q = \frac{f_0}{2}\left(\frac{d\phi}{df}\right)_{f_0}$$

Resonant Systems: Q

(I-6)

(7) From a curve-fit on an HP3562 dynamic signal analyzer: the curve-fit produces a conjugate set of poles, f_r +/- if_i, for a resonance peak. The resonance frequency, f_0, and the Q can be found as follows:

$$f_0 = \sqrt{f_r^2 + f_i^2} \approx f_i$$

$$Q = \frac{1}{2f_r}\sqrt{f_r^2 + f_i^2} \approx \frac{f_i}{2f_r}$$

where the approximations are valid for large Q.

(8) Drive the system with a square wave and observe the ringing at the edge transitions of the square wave. If the peak-to-peak amplitude of the first half-cycle of the ringing is a and the peak-to-peak amplitude of the second half-cycle is b, then the damping factor is:

$$\zeta = \frac{1}{2Q} = \frac{\ln(a/b)}{\sqrt{\ln^2(a/b) + \pi^2}}$$

Note: The equivalent noise bandwidth of a simple resonant system is:

$$\Delta f_{NB} = \frac{\pi f}{2Q}$$

Proper Dynamics for Damped Mass-Spring (I-7)

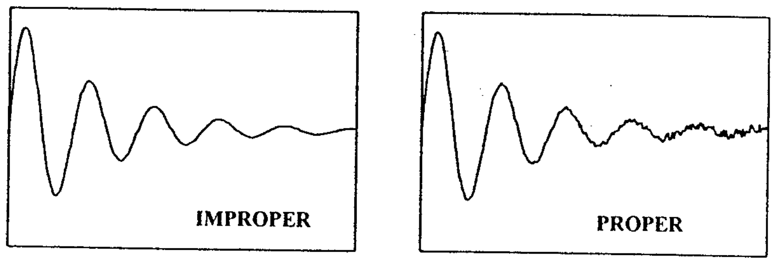

$$m\ddot{x} + R\dot{x} + kx = 0 \qquad\qquad m\ddot{x} + R\dot{x} + kx = f_n(R,t)$$

dmpdosc.ppt

Fluctuation-Dissipation Theorem: (I-8)

If there is a path along which energy can flow from a system to its environment, *then energy from the environment can flow back into the system*. Dissipation is a measure of the energy that leaves the system (either as ordered energy in the case of radiation or as disordered energy in the case of damping); thermal fluctuations are a measure of the disordered energy that enters the system from the environment. ***In thermal equilibrium, the presence of dissipation guarantees the presence of fluctuations.***

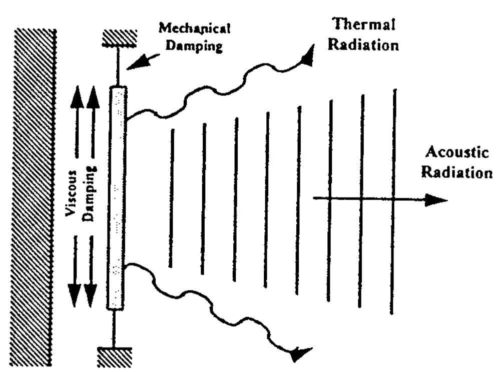

flucdiss.ppt

Equilibrium Thermal Fluctuations (I-9)

Total Energy

Each degree-of-freedom of a system has a "thermal" energy of $1/2\ k_BT$ where k_B is Boltzmann's constant (1.38×10^{-23} joules/kelvin) and T is the absolute temperature.

This thermal energy associated with each of the components of kinetic energy ($1/2\ mv_x^2$, $1/2\ mv_y^2$, $1/2\ mv_z^2$), spring-potential energy ($1/2\ kx^2$), rotational kinetic ($1/2\ I\omega^2$), capacitive ($1/2\ CV^2$), etc.

A molecule in a liquid has $\longrightarrow$ $\frac{1}{2} m v_x^2 = \frac{1}{2} k_B T$

A ball-bearing in a liquid has $\longrightarrow$ $\frac{1}{2} m v_x^2 = \frac{1}{2} k_B T$

An atom in a solid OR
A mass on a spring has $\longrightarrow$ $\frac{1}{2} k x^2 = \frac{1}{2} k_B T$

[The velocities and displacements indicated above are mean-square values; they represent an average of the actual fluctuating velocity or displacement.]

thermal.ppt

Energy Levels (I-10)

k_BT at room temperature:	0.025 eV
hf for visible light:	1.5 - 3 eV
acoustic wave (100 μPa in air):	0.4 eV/cm³
acoustic wave (100 μPa in water):	30 μeV/cm³
chemical bonds	
covalent:	4 eV
ionic:	2 eV
hydrogen:	0.2eV

(1 eV = 1.6×10^{-19} joules)

Sensing of Gravity by Protozoa (I-11)

Loxodes striatus

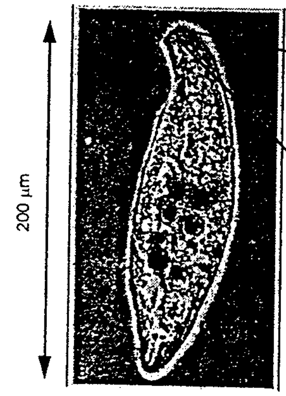

(reprinted with permission from Ref. 1)

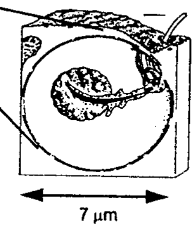

(reprinted with permission from Ref. 2)

proof mass, $m = 45$ picograms
range of mass motion, $L = 3\ \mu m$

sensor's potential energy = mgL
sensor's thermal energy = kT

$$mgL / kT = 330$$

If linear dimensions of sense organ were reduced by a factor of 4, then mgL/kT = 1 and the organism would be unable to distinguish up from down!

1. *Fenchel and Finlay*, "Geotaxis in the ciliated protozoon Loxodes," J. Exp. Biol. 110, 17-33 (1984)
2. *Fenchel and Finlay*, "The structure and function of Muller vesicles in Loxodid ciliates," J. Protozool. 33, 69-76 (1986)

Applied Research Laboratory - Penn State

protozoa.ppt

Sensing of Magnetic Fields by Bacteria (I-12)

magnetotactic bacterium

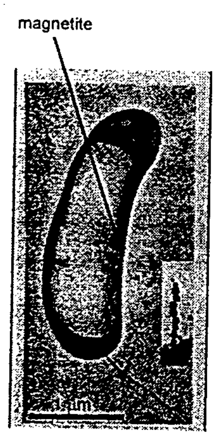

(reprinted with permission from Ref. 2)

magnetic dipole moment, $M = 1.3$ fA m^2
magnetic flux density, $B = 50\ \mu$tesla

sensor's potential energy = MB
sensor's thermal energy = kT

$$MB / kT = 16$$

1. *Frankel, Blakemore, and Wolfe*, "Magnetite in freshwater magnetotactic bacteria," Science 203, 1355 (1979)
2. *Blakemore, Frankel, and Kalmijn*, "South-seeking magnetotactic bacteria in the Southern Hemisphere," Nature 286, 384 (1980)

Applied Research Laboratory - Penn State

bacteria.ppt

Equilibrium Thermal Fluctuations (I-13)

Distribution of Energy

The distribution of thermal energy is given by Nyquist:

$$F_n^2 = 4\,k_B\,T\,R_{mechanical}\,df$$

$$V_n^2 = 4\,k_B\,T\,R_{electrical}\,df$$

R is resistance: force per velocity for mechanical resistance, volts per ampere for electrical resistance. In general, the real part of the relevant impedance is used for R (which may be a function of frequency). df is the increment of bandwidth.

Since the noise power is distributed over frequency, the noise is described by a power density (watts per hertz), or an amplitude-squared per hertz (newtons^2 per hertz, volts^2 per hertz), or an amplitude per root hertz (pascals per root hertz, meters per second per root hertz).

[The factor $4k_BT$ is about 4×10^{-21} at room temperature. These expressions are valid if $hf \ll k_BT$ where h is Plank's constant. At room temperature, this means that f must be much less than 10^{13} Hz.]

therm2.ppt

Noise Equivalent Signal (I-14)

What level of signal does the noise mimic?

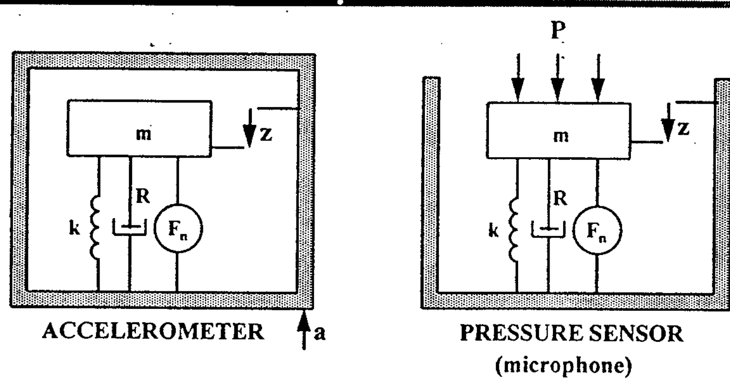

Set noise to zero and solve for signal response: $a = g(z)$

Set signal to zero and solve for output due to noise: $z_n = h(F_n)$

Calculate noise-equivalent signal: $a_n = g(z_n)$

nes2.ppt

Noise Equivalent Signal
(I-15)

Accelerometer

$$(ma_n)^2 = 4\,k_B\,T\,R\,df$$

$$a_n^2 / df = 4\,k_B\,T\frac{R}{m^2} = 4\,k_B\,T\left[\frac{\omega_0}{m\,Q}\right]$$

Pressure Sensor

$$(p_n A)^2 = 4\,k_B\,T\,R\,df$$

$$p_n^2 / df = 4\,k_B\,T\frac{R}{A^2} = 4\,k_B\,T\left[\frac{\omega_0\,m}{A^2\,Q}\right]$$

nea3.ppt

Frequency Distribution of Noise
(I-16)

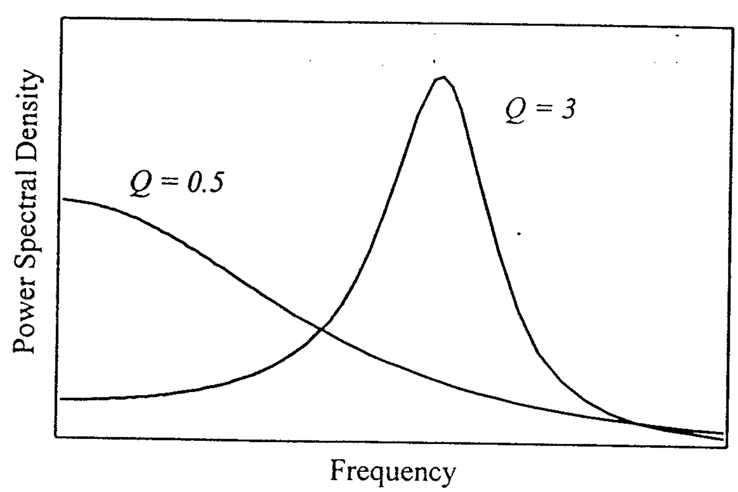

fdist.ppt

Noise Associated with Radiation (I-17)

Spherical wave (spherical source): $$p = \frac{A}{r} e^{i(kr-\omega t)}$$

Compute radial particle velocity from Newton's Law in fluid: $$-\nabla p = \rho \frac{\partial u}{\partial t} \quad \Rightarrow \quad u_r = \left(1 + \frac{i}{kr}\right)\frac{p}{\rho c}$$

Mechanical radiation resistance (ratio of force to velocity): $$Z = \frac{pA}{u_r} = \rho c A \left\{ \frac{(kr)^2}{1+(kr)^2} - i\frac{kr}{1+(kr)^2} \right\}$$

Radiation resistance for a point source ($A = 4\pi r^2$): $$\Re e\{Z\}\big|_{r \to 0} \rightarrow \rho c A (kr)^2 = \pi \frac{\rho f^2}{c} A^2$$

Pressure fluctuations associated with "loss" by radiation: $$\boxed{p_n^2 = 4 k_B T \frac{\Re e\{Z\}}{A^2} = 4 k_B T \pi \frac{\rho f^2}{c} df}$$

Noise Associated with Radiation (I-18)

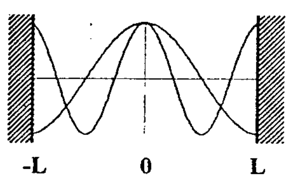

Start with a rigid-walled box, side = $2L$, sensor in the middle.

Modes have max pressure at walls and at center: $\cos(l\pi x/L)$, $\cos(m\pi y/L)$, $\cos(n\pi z/L)$

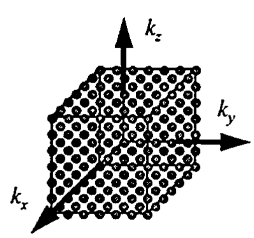

Wavenumbers are then:
$k_x = l\pi/L$, $k_y = m\pi/L$, $k_z = n\pi/L$
(spacing between k's = π/L)
and $k^2 = k_x^2 + k_y^2 + k_z^2$

Cell "volume" in k-space is $(\pi/L)^3$ with one k-point per cell.
Each mode gets $k_B T$ (1/2 for kinetic, 1/2 for potential) therefore,

k-space density of thermal energy $= k_B T (L/\pi)^3$

Noise Associated with Radiation (I-19)

Energy in dk is energy in a spherical shell between k and $k+dk$.

Volume of shell in k-space $= (4\pi/3)[(k + dk)^3 - k^3]$
$= 4\pi k^2\, dk$ for small dk.

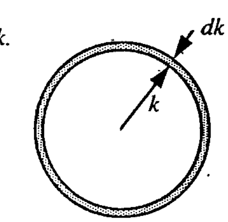

Therefore, $dE = k_B T\,(L/\pi)^3\, 4\pi k^2\, dk$, or, since $k = 2\pi f/c$,
$dE = 32\pi\, k_B T\, L^3 f^2\, df/c^3$

Divide by the spatial volume, $(2L)^3$, to get the true energy density:

$$\mathcal{E} = 4\pi\, k_B T\, f^2\, df/c^3$$

Another way to write the energy density is $\mathcal{E} = p^2/\rho c^2$
so the pressure fluctuations associated with the radiation are given by

$$\boxed{p_n^2 = 4\, k_B T\, \pi \frac{\rho f^2}{c}\, df}$$

Noise Associated with Radiation (I-20)

Spherical Source: $\mathscr{R}e\{Z_{rad}\} = \rho c A\left[\dfrac{(ka)^2}{1 + (ka)^2}\right]$

Circular Piston in Rigid Baffle: $\mathscr{R}e\{Z_{rad}\} = \rho c A\left[1 - \dfrac{J_1(2ka)}{ka}\right]$

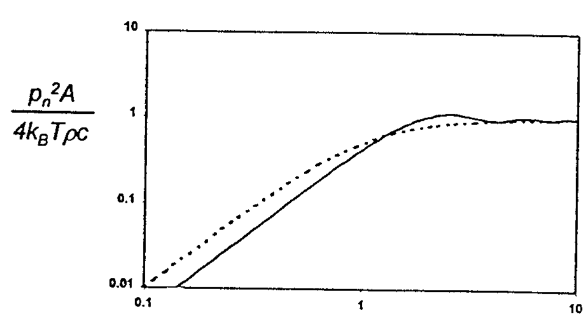

radrce4.ppt

The Simple Accelerometer

(I-21)

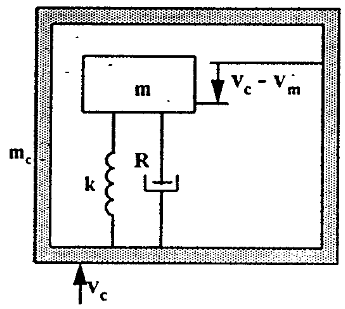

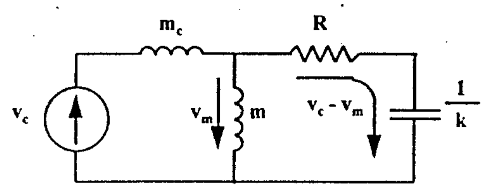

[Impedance Analogy]

SYSTEM RESPONSE

$$\frac{v_c - v_m}{v_c} = \frac{\left(\frac{\omega}{\omega_0}\right)^2}{\left(\frac{\omega}{\omega_0}\right)^2 - 1 - j\left(\frac{\omega}{\omega_0}\right)\left(\frac{1}{Q}\right)}$$

accel1.ppt

Equilibrium Noise in a Geophone

VELOCITY TRANSDUCER

(I-22)

$$a_n^2 = 4 k_B T \frac{\omega_0}{m Q} \quad \Rightarrow \quad v_n^2 = 4 k_B T \frac{\omega_0}{\omega^2 m Q}$$

$$e_{out} = const. * (v_c - v_m)$$

For the simple accelerometer, $(v_c - v_m)/v_c$ is proportional to ω^2 below ω_0 and is constant with frequency above ω_0. The noise velocity (referenced to the case) is proportional to ω^{-1}. Therefore, the output noise voltage (1) is proportional to ω below ω_0 and to ω^{-1} above ω_0.

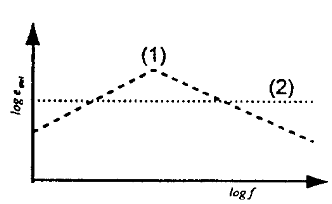

The equilibrium-thermal noise associated with the electrical resistance in the sense coil produces an output voltage noise (2) that is independent of frequency:

$$e_{out} = \sqrt{4 k_B T R_{coil}}$$

The total noise is the square root of the sum of the squares of the individual components.

therm3.ppt

Sensor Self-Noise Evaluation (I-23)

Ultra-Low Self-Noise Measurement

Measurement of molecular agitation of 32-gram proof mass in geophone. (Approx. 1 nano-g per root Hz)

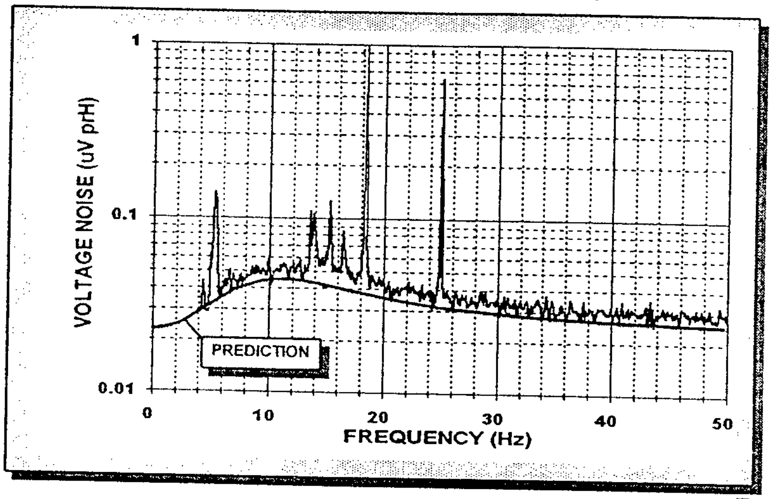

Equilibrium Noise in Fiber-Optic Sensors (I-24)

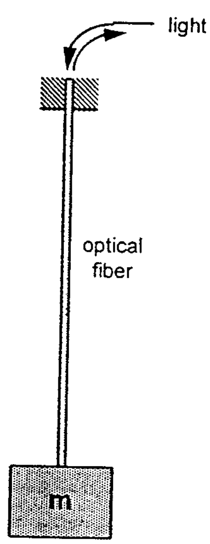

Noise associated with:

- *Damping* in spring-mass system formed by fiber and proof mass
- *Optical scattering* from thermally induced fluctuations in optical properties of fiber
- *Optical scattering* from impurities and density inhomogeneities frozen in during fiber manufacture

fiber1.ppt

Equilibrium Phase Fluctuations in Optical Fiber

(I-25)

$$\Phi^2 = 4k_B T\Delta f \, \frac{\pi T L}{2\kappa\lambda_0^2}\left(\frac{dn}{dT} + \frac{n}{L}\frac{dL}{dT}\right)^2 \ln\left[g(f)\right]$$

$$g(0) \longrightarrow \left(a_f / 1.2\, a_{mf}\right)^4$$

$$g(f_{high}) \longrightarrow 1 + 4\left(\delta_\kappa / a_{mf}\right)^4$$

L = fiber length
λ_0 = optical wavelength
n = index of refraction of fiber
a_f = fiber radius
a_{mf} = optical mode-field radius
δ_κ = thermal penetration depth in fiber
κ = thermal conductivity in fiber

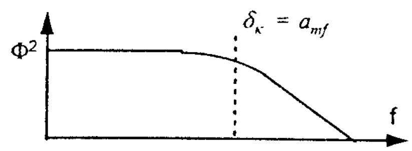

- Wanser, et al., Optical Fiber Sensors Conference, Paper W3.4, Florence, Italy, May 1993.
- Wanser, Electronics Letters, 28(1), 53, 1992.
- Glenn, IEEE J. Quantum Electronics 25(6), 1218, 1989.

fiber2.ppt

Signal-to-Noise Ratio: A Useful Theorem

(I-26)

The signal-to-noise ratio at the output of a linear circuit *does not depend on the value of the output load.*

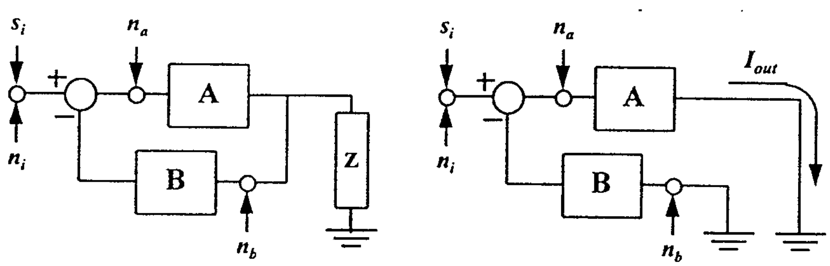

Analysis of complicated circuits can often be simplified by setting the output load to zero and calculating the ratio of signal *current* to noise *current.*

The effective Q of a system can be changed by adding feedback. Positive feedback increases the Q; negative feedback decreases the Q.

Can the noise of a system be reduced by adding feedback?

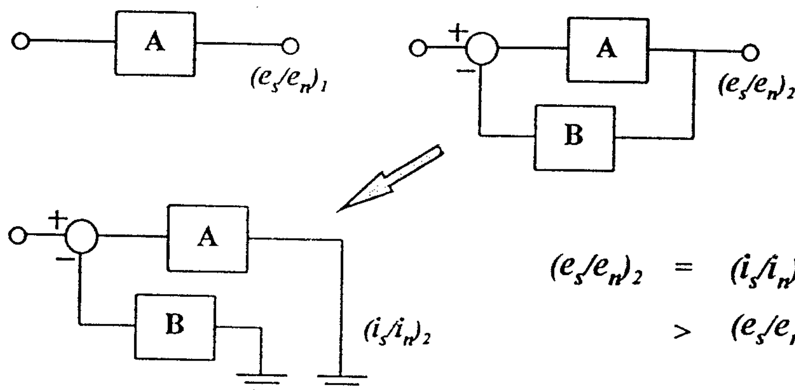

$$(e_s/e_n)_2 = (i_s/i_n)_2$$
$$> (e_s/e_n)_1$$

Not this way!

(II-1)

Shot Noise and Non-Equilibrium Noise

(II-2)

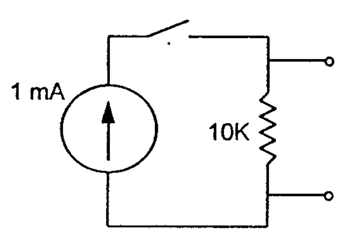

- Measure the spectral density of the voltage noise across a 10 K resistor.
- Put 1 mA DC current through the resistor.
- By what factor does the noise voltage increase? (Ignore 1/f noise.)

Shot Noise (II-3)

Given a current consisting of impulses:

$$I(t) = q\sum_{i=1}^{\infty}\delta(t-t_i)$$

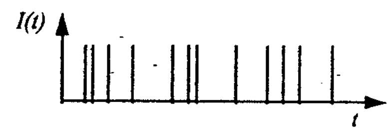

Expand current as a Fourier series:

$$I(t) = \sum_{k=0}^{\infty}\left[a_k\cos(2\pi f_k t) + b_k\sin(2\pi f_k t)\right]$$

$$\text{where} \quad a_k = \frac{2}{T}\int_0^T I(t)\cos(2\pi f_k t)\,dt = \frac{2q}{T}\sum_{i=1}^{N}\cos(2\pi f_k t_i)$$

(The period, T, is long enough to encompass many (N) events.)

One component of the expansion covers a band of $\Delta\phi$ ($= 1/T$). The mean-square value in that band is:

$$\overline{i_k^2} = a_k^2\,\overline{\cos^2(2\pi f_k t)} + b_k^2\,\overline{\sin^2(2\pi f_k t)} + a_k b_k\,\cancel{\overline{\cos()\sin()}} = \frac{1}{2}\left(a_k^2+b_k^2\right)$$

shot1.ppt

Shot Noise (II-4)

$$\frac{1}{2}\left(a_k^2+b_k^2\right) = \frac{2q^2}{T^2}\left\{\sum_{i=1}^{N}\left[\cos^2(2\pi f_k t_i) + \sin^2(2\pi f_k t_i)\right]\right\} +$$

$$\frac{2q^2}{T^2}\left\{\cancel{\sum_{i\neq j}\left[\cos(2\pi f_k t_i)\cos(2\pi f_k t_j) + \sin(2\pi f_k t_i)\sin(2\pi f_k t_j)\right]}\right\} = \frac{2q^2 N}{T^2}$$

The second summation is zero ***only if the impulses are statistically independent.*** If the events are not independent, then the cross-terms must be evaluated!

(For independent events, the mean-square value of b_k is identical to that of a_k.)

$$\text{Since} \quad I = \frac{qN}{T} \quad \text{and} \quad \Delta f = \frac{1}{T}$$

$$\boxed{\overline{i_k^2} = 2q\bar{I}\,\Delta f}$$

Applies to processes consisting of events that are:

(1) impulse-like
(2) independent

shot2.ppt

Circuit for Basic Shot-Noise Experiment (II-5)

Resistance bridge connected to gate permits noise measurement of input resistance with and without current. Bridge rejects noise introduced by the battery.

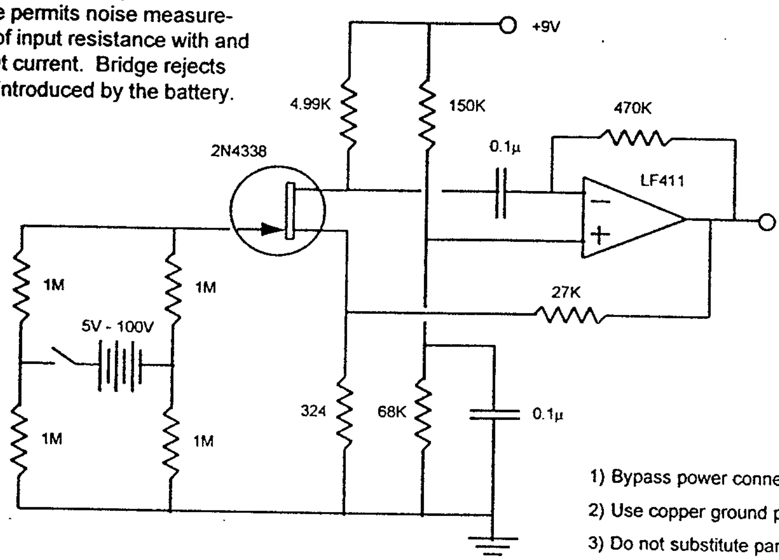

1) Bypass power connections
2) Use copper ground plane
3) Do not substitute parts

Resistor Noise with and without Current Flow (II-6)

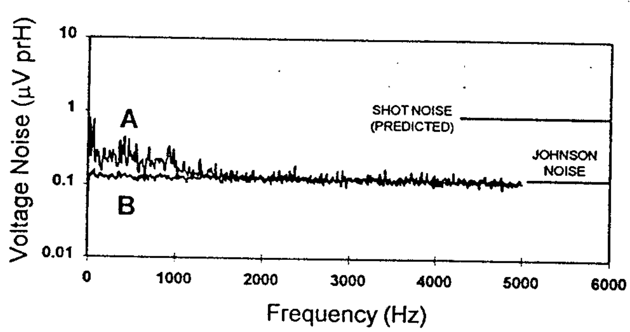

A: Current flow ($V_0 = 200 * k_B T/q$)

B: No current flow

Noise from Molecular Collisions — FREE-MOLECULAR FLOW (II-7)

$$\text{Force} = \sum_{\text{molecules}} \left\{ \begin{array}{c} \text{rate of change in momentum of a molecule} \\ \text{initially traveling to the right and hitting the} \\ \text{disk from behind} \end{array} \right\}$$

$$= \text{(molecular flux) (momentum change per collision)}$$

$$= \frac{n}{2} A\left(v_x - \dot{x}\right) \cdot 2m\left(v_x - \dot{x}\right)$$

$$= n m v_x^2 A - 2 n m v_x A \dot{x} + \cancel{n m \left(\dot{x}\right)^2 A}$$

$$= P_0 A - R_{mech}\, \dot{x}$$

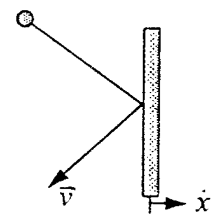

$$\boxed{R_{mech} = 2 n m v_x A}$$

Noise from Molecular Collisions — FREE-MOLECULAR FLOW (II-8)

$$p_n^2 = \frac{F_n^2}{A^2} = \frac{4 k_B T R_{mech}\, df}{A^2} = 8 n m k_B T v_x\, df / A$$

$$P_0 = n k_B T$$

$$\bar{v} = 2 \bar{v}_x$$

$$\boxed{p_n^2 = 2\left[2 m \bar{v}\right] \frac{P_0}{A} df}$$

Looks like a shot-noise expression!

Generalized Forms for Shot Noise (II-9)

$$\begin{bmatrix}\text{mean-square}\\\text{fluctuation in}\\\text{flux density}\end{bmatrix} = 2\begin{bmatrix}\text{quantity}\\\text{per}\\\text{carrier}\end{bmatrix}\begin{bmatrix}\text{average}\\\text{flux}\\\text{density}\end{bmatrix}\frac{[\text{bandwidth}]}{[\text{area}]}$$

electric-charge flux density: $j_n^2 = 2[q]\, J_0\, \Delta f / A$

photon flux density: $I_n^2 = 2[hf]\, I_0\, \Delta f / A$

momentum flux density: $p_n^2 = 2[2mv]\, P_0\, \Delta f / A$

> Pressure-fluctuation noise power is proportional to STATIC PRESSURE

Molecular-Impact Noise (II-10)

Equilibrium thermal fluctuations in force (Nyquist):

$$F_n^2 = 4\, k_B\, T R_{MECH}\, \Delta f$$

e.g., Stokes' flow (disk, radius a): $R_{MECH} = 16\,\eta\, a$

$$p_n^2 = 4\, k_B\, T\; 16\eta\, a / A^2$$

> Pressure-fluctuation noise power is almost INDEPENDENT of static pressure

Molecular-Impact Noise (II-11)

The shot-noise form requires that collisions be INDEPENDENT. As long as the mean-free-path is smaller than the disk radius, the molecular collisions are highly DEPENDENT.

Add some kinetic theory: $P_0 = n\, k_B T$

$$\eta = n\, mv\, (mfp) / 3$$

$$(p_{n1}^2) / (p_{n2}^2) = 3\pi / 8 \quad (radius) / (mean\text{-}free\text{-}path)$$

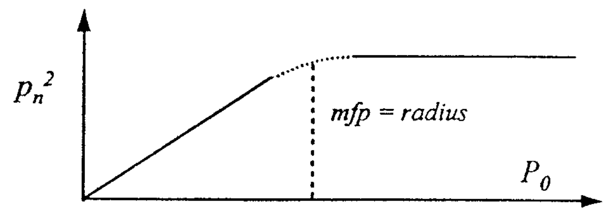

Noise in Metallic Conductors (II-12)

Carriers (electrons) are highly correlated

Noise is independent of flow volume (current)

$$i_n^2 = \left(4 k_B T / R\right) \Delta f$$

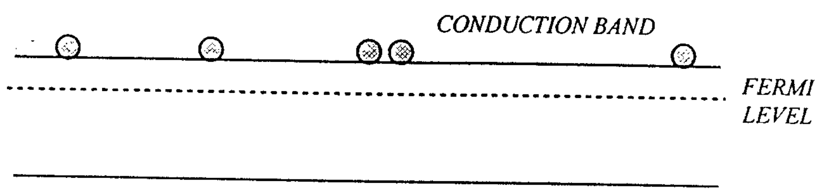

Carriers (holes or electrons) are independent

Noise is dependent on flow volume (current)

$$i_n^2 = 2qI_0\,\Delta f$$

(II-14)

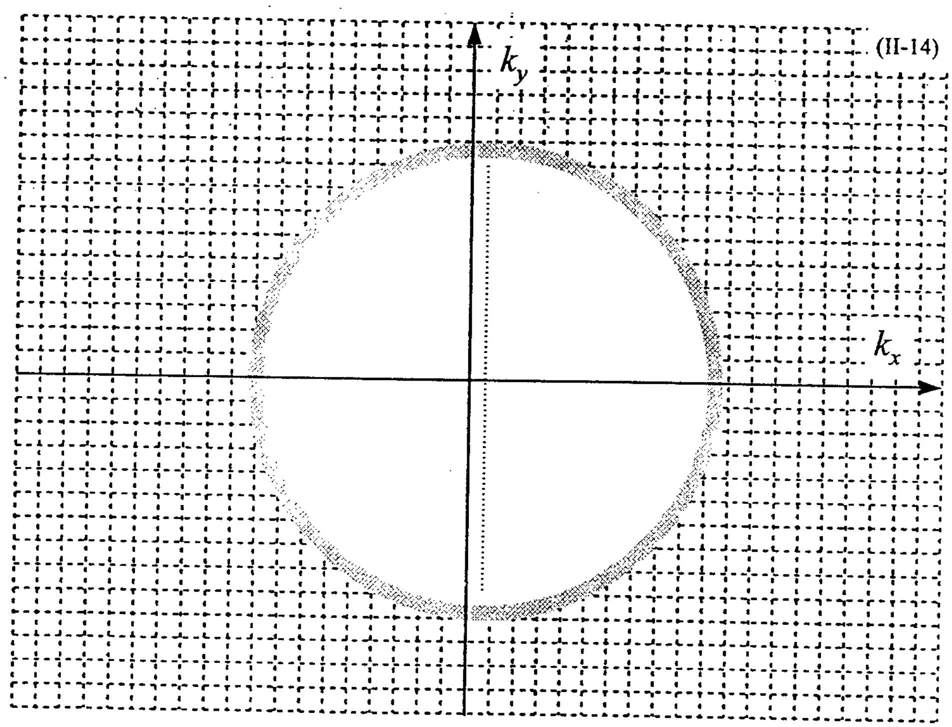

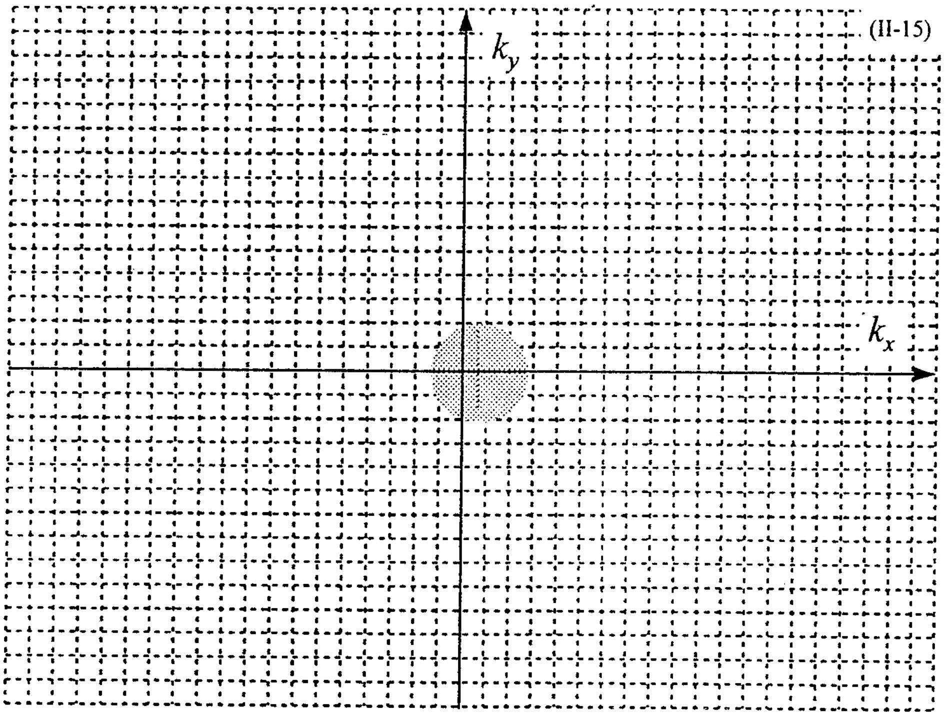

(II-15)

Occupation (f) and Fluctuation (df) (II-16)

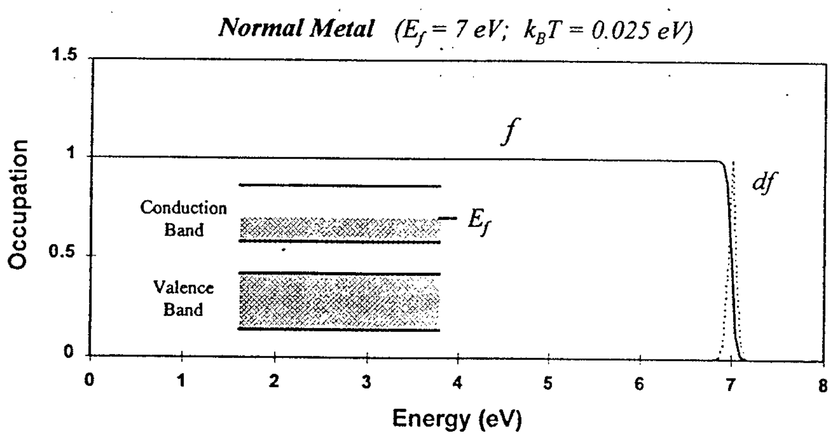

$$f = \frac{1}{1+e^{\frac{E-E_f}{k_BT}}} \qquad df = k_BT\frac{\partial f}{\partial E}$$

Occupation (f) and Fluctuation (df) (II-17)

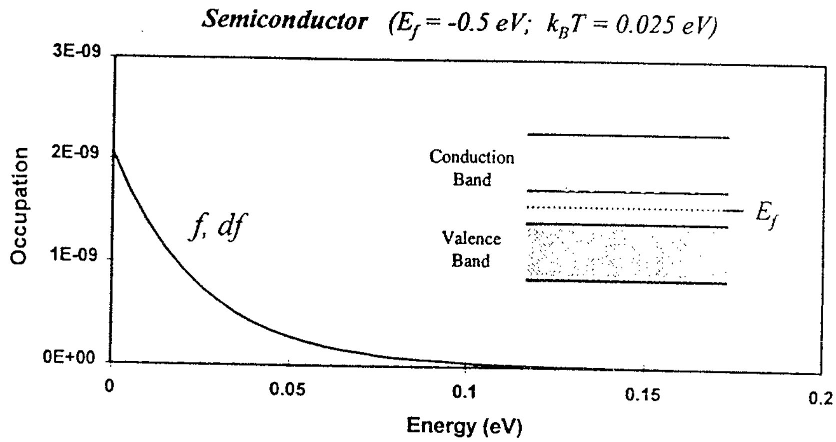

$$f \approx e^{\frac{-(E-E_f)}{k_B T}}$$

Noise as a Function of Applied Voltage (II-18)

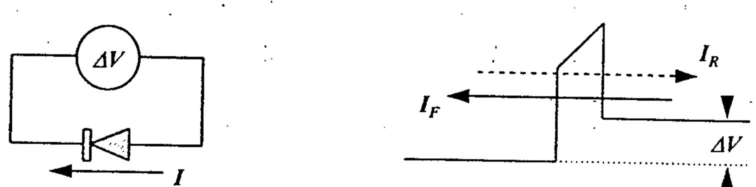

$$I_R = I_F\, e^{-\frac{q\Delta V}{k_B T}}$$

$$I = I_F - I_R = I_F\left[1 - e^{-\frac{q\Delta V}{k_B T}}\right] = \frac{\Delta V}{R}$$

$$i_n^2 = 2\,q\,I_R\,df + 2\,q\,I_F\,df = 2\,q\,I_F\left[1 - e^{-\frac{q\Delta V}{k_B T}}\right]$$

$$i_n^2 = 2\,\frac{q\,\Delta V}{R}\left(\frac{1 + e^{-\frac{q\Delta V}{k_B T}}}{1 - e^{-\frac{q\Delta V}{k_B T}}}\right) df$$

Noise as a Function of Applied Voltage (II-19)

For $q\Delta V \ll k_B T$ $\quad i_n^2 \rightarrow 2\dfrac{q\,\Delta V}{R}\left(\dfrac{2}{q\,\Delta V / k_B T}\right) df \;=\; 4 k_B T \dfrac{df}{R}$

For $q\Delta V \gg k_B T$ $\quad i_n^2 \rightarrow 2\dfrac{q\,\Delta V}{R}(1)\, df \;=\; 2 q I\, df$

Example from measurements in search of fractional quantum Hall effect

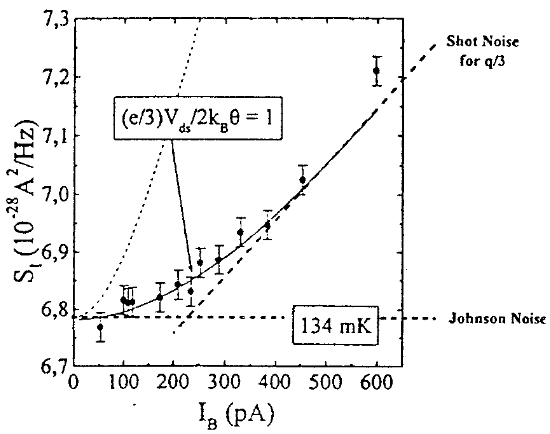

Saminadayar, Glattli, Jin, and Etienne, Phys. Rev. Lett. 79, 2526 (1997)

Shot Noise (II-20)

Suppose the current is a random sequence of non-impulsive responses:

$$I(t) = \sum_{i=1}^{\infty} h(t - t_i)$$

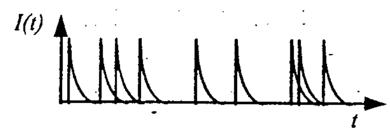

This current can be produced from a sequence of impulses:

$$\sum_{i=1}^{\infty} \delta(t - t_i) \longrightarrow \boxed{h(t)} \longrightarrow \sum_{i=1}^{\infty} h(t - t_i)$$

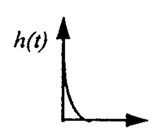

If the power spectral density of the sequence of impulses is $s_n^2(\omega)$, then the power spectral density for the current is:

$$i_n^2(\omega) = s_n^2(\omega)\left|H(j\omega)\right|^2$$

Shot Noise (Single Characteristic Process) (II-21)

For example, if the current is produced by random events and each event has an exponential decay (with time constant, t_0):

$$I(t) = \sum_{i=1}^{\infty} h(t - t_i) \quad ; \quad h(t) = e^{-t/t_0} U(t)$$

then the transfer function in the frequency domain, $H(j\omega)$, gives the spectral shape of the noise power:

$$|H(j\omega)|^2 = \frac{t_0^2}{1 + \omega^2 t_0^2}$$

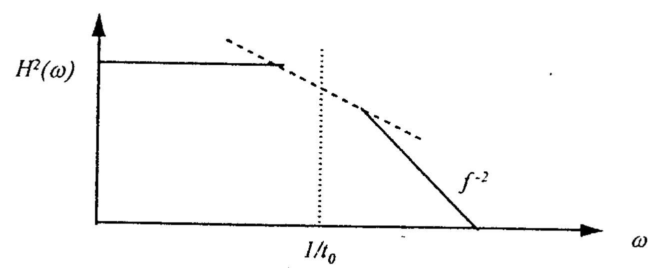

Shot Noise (Multiple Characteristic Processes) (II-22)

If there are many processes that can be triggered by the random impulses and each process is exponential with its own unique time constant, then the spectral distribution of the noise power can depart significantly from either white noise or a $1/f^2$ power distribution. This *may* be the way 1/f noise distributions are produced.

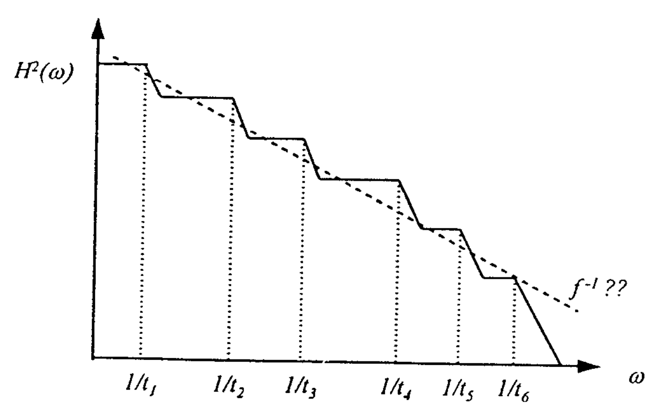

1/f Noise: A Brief and Inadequate Introduction

(II-23)

MANY physical processes produce fluctuations with a power spectrum that goes as 1/f.

The noise power in excess of the equilibrium-thermal fluctuations is associated with power input to the system that drives the system away from equilibrium.

Observed 1/f noise can extend over many decades in frequency. If the multiple-exponential-process model is correct, then there must a correspondingly large spread in process time constants.

The integral over all frequency of a 1/f power distribution is infinite so *there must actually be a lower limit to the 1/f behavior.* This means that there are at least two free parameters: the total fluctuation power and the lower frequency limit.

Sensor Calibration

$e^{j\omega t}$

Reciprocity

(III-2)

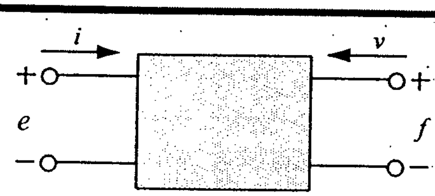

$$e = A\,i + B\,v$$
$$f = C\,i + D\,v$$

If $B = C$ then the device is *reciprocal*:

$$\left(\frac{e}{v}\right)_{i=0} = \left(\frac{f}{i}\right)_{v=0}$$

Reciprocal transducers:
- electrodynamic (moving-coil)
- piezoelectric
- capacitive (small-signal)

Nonreciprocal transducers:
- piezoresistive
- electron-tunneling

Reciprocity
(III-3)

If B = -C then interchange the roles of the variables on one side of the device.

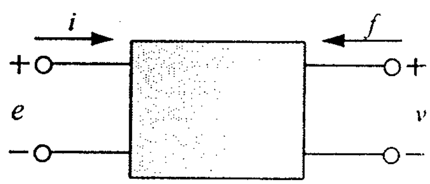

$$e = \mathbf{A}\, i + \mathbf{B} f$$
$$v = \mathbf{C}\, i + \mathbf{D} f$$

$\mathbf{A} = (AD - CB)/D$ $\quad \mathbf{B} = B/D$
$\mathbf{C} = -C/D$ $\quad \mathbf{D} = 1/D$

Therefore $\mathbf{B} = \mathbf{C}$

If B does not equal either C or -C, then the device is nonreciprocal.

Reciprocity
(III-4)

If a device is reciprocal, then the ratio of the output *potential* to the input *flow* is the same regardless of which port is taken to be the input.

For example:

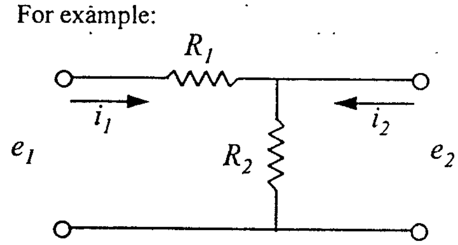

$$e_1 = (R_1 + R_2)\, i_1 + R_2\, i_2$$
$$e_2 = R_2\, i_1 + R_2\, i_2$$

$$\left.\frac{e_2}{i_1}\right|_{i_2=0} = \left.\frac{e_1}{i_2}\right|_{i_1=0} = R_2$$

(A transfer impedance in general.)

Reciprocity does *NOT* depend on the device being lossless.

Reciprocity does *NOT* mean that *voltage* ratios are identical.

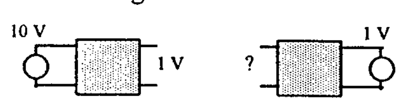

Reciprocity Calibration

(III-5)

Given a transducer (not necessarily reciprocal):

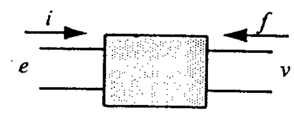

What is its response?

Receiving response: $\alpha = \left(\frac{e}{v}\right)_{i=0}$

Transmitting response: $\beta = \left(\frac{f}{i}\right)_{v=0}$

It is often inconvenient and inaccurate to directly measure forces and velocities.

Reciprocity Calibration

(III-6)

Use three transducers: a source (S), a receiver (R), and a reciprocal transducer (T). Altogether there are four unknowns: α_R, α_T, β_T, *and* β_S.

Connect the transducers *through a known transfer impedance* and make the following measurements:

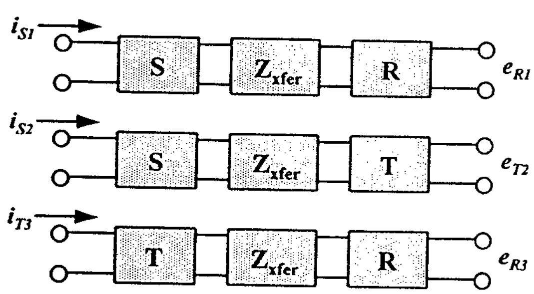

$[SR] = e_{R1}/i_{S1}$

$[ST] = e_{T2}/i_{S2}$

$[TR] = e_{R3}/i_{T3}$

This gives three equations for the four unknowns. Reciprocity provides the fourth equation and allows solving for all four responses.

Reciprocity Calibration (III-7)

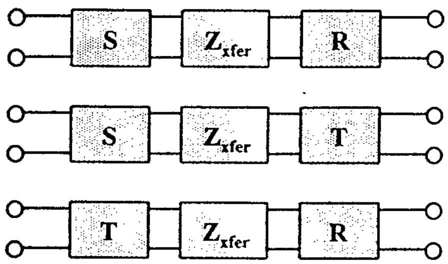

$$[SR] = \frac{1}{Z_{xfer}} \alpha_R \beta_S$$

$$[ST] = \frac{1}{Z_{xfer}} \alpha_T \beta_S$$

$$[TR] = \frac{1}{Z_{xfer}} \alpha_R \beta_T$$

Reciprocity gives the relationship between α_T and β_T:

$$\boxed{\frac{[SR][TR]}{[ST]} = \frac{1}{Z} \alpha_R^2 \frac{\beta_T}{\alpha_T}}$$

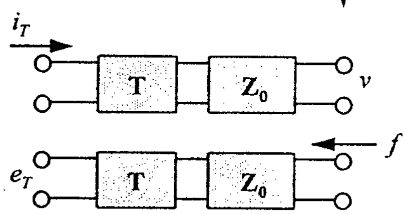

$$\frac{v}{i_T} = \beta_T \frac{1}{Z_0} = \frac{e_T}{f} = \alpha_T \frac{1}{Z_0}$$

$$\boxed{\alpha_T = \beta_T}$$

Reciprocity Calibration — VARIATIONS (III-8)

a) Measure currents by measuring voltage across a resistor. Resistance and voltage ratios are easier to measure accurately than absolute voltages.

b) Set $i_{S1} = i_{S2}$ and adjust i_{T3} so that $e_{R3} = e_{R1}$. This produces the same field at the receiver location for each measurement and also permits the use of source and receiver that are not linear.

c) If two reciprocal transducers are available, measure the reciprocity explicitly to check the transducers and apparatus.

d) If two "identical" reciprocal transducers are used, then only two measurements are required.

e) In some circumstances, only one transducer is required: (1) excite a lightly damped system and measure response during decay, (2) transmit a pulse and measure a reflection.

Reciprocity Calibration

EXAMPLES (III-9)

Free-Field

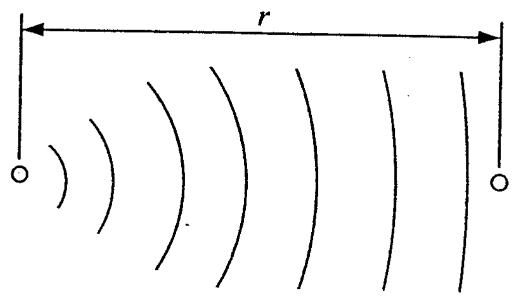

$$\alpha = \left(\frac{e}{p}\right)_{i=0}$$

$$Z_{xfer} = \frac{p_2}{U_1} = \frac{p_2}{4\pi a^2 u_1}$$

$$u_1 = \left(1 + \frac{1}{jka}\right)\frac{p_1}{\rho c} \approx \frac{p_1}{jka\,\rho c} \qquad \textit{(for ka << 1)}$$

Since

$$\frac{p_2}{p_1} = \frac{e^{-jkr}}{r}\,\frac{a}{e^{-jka}} \qquad \boxed{Z_{xfer} = j\,e^{-jk(r-a)}\,\frac{\rho f}{2r}}$$

Reciprocity Calibration

EXAMPLES (III-10)

Microphone Pressure Tube

$$\alpha = \left(\frac{e}{p}\right)_{i=0}$$

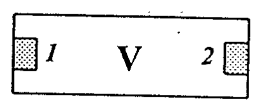

$$\boxed{Z_{xfer} = \frac{p_2}{U_1} = \frac{\gamma P_0}{j\omega V}}$$

Traveling-Wave Tube

$$\alpha = \left(\frac{e}{p}\right)_{i=0}$$

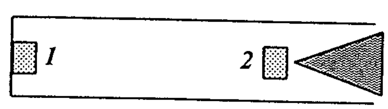

$$\boxed{Z_{xfer} = \frac{p_2}{U_1} = \frac{\rho c}{A}}$$

Reciprocity Calibration EXAMPLES (III-11)

Rigid-Walled Resonator

Energy stored in tube, E:

$$E = PE + KE = \int_0^L \left\{ \frac{1}{2}\rho v^2 + \frac{1}{2}\frac{p^2}{\rho c^2} \right\} A\,dx = \frac{p_0^2\, A\, L}{2\rho c^2}$$

Energy lost *per cycle*, ΔE = Energy supplied by driver per cycle:

$$\Delta E = \frac{\text{power}}{\text{frequency}} = \frac{F_1 v_1}{f_n} = \frac{p_1 A v_1}{f_n} = \frac{p_0 U_1}{f_n}$$

$$f_n = \frac{n\,c}{2\,L} \quad ; \quad Q_n = \frac{2\pi E}{\Delta E} = \frac{\pi\, n\, A\, p_0}{2\,\rho c\, U_1}$$

$$\boxed{Z_{xfer} = \frac{p_0}{U_1} = \frac{2\,\rho c\, Q_n}{\pi\, n\, A}}$$

Reciprocity Calibration EXAMPLES (III-12)

Linear Pendulum

$$\alpha = \left(\frac{e}{u}\right)_{i=0}$$

$$\boxed{Z_{xfer} = \frac{F_2}{u_1} = j\,\omega\, m}$$

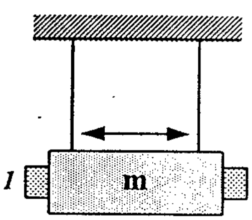

Torsional Pendulum

$$\alpha = \left(\frac{e}{\dot{\theta}}\right)_{i=0}$$

$$\boxed{Z_{xfer} = \frac{T_2}{\dot{\theta}_1} = j\,\Omega\, I}$$

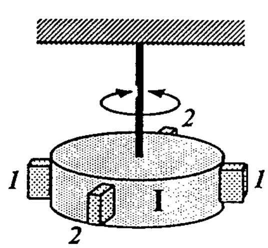

Reciprocity Calibration

EQUIPMENT (III-13)

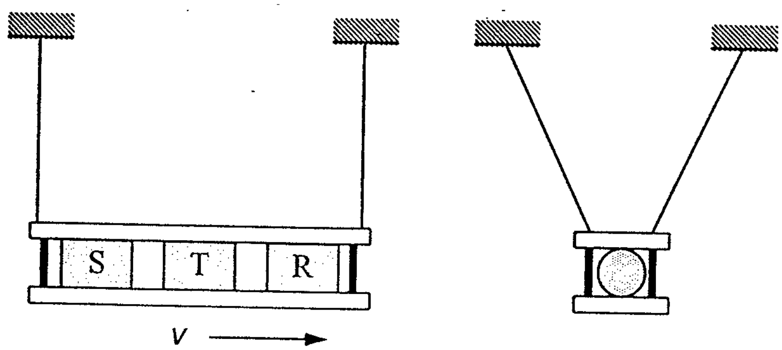

Reciprocity Calibration

Comparison calibration using reciprocity (III-14)

$$force = i\beta_T$$

$$acceleration = force/mass$$

$$e = acceleration * M$$

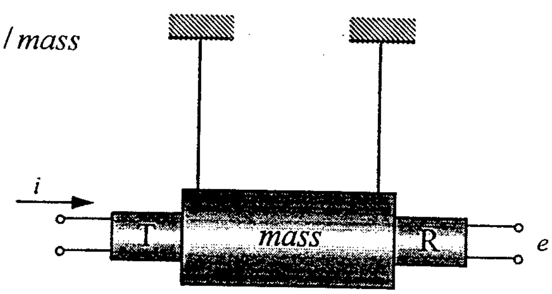

Since $\alpha_T = \beta_T$, $\qquad \alpha_T = \dfrac{e}{i}\dfrac{mass}{M}$

where M is reference accelerometer response (V/m/s²)

rcp_eqp3.ppt

Bessel-Null Calibration

(III-15)

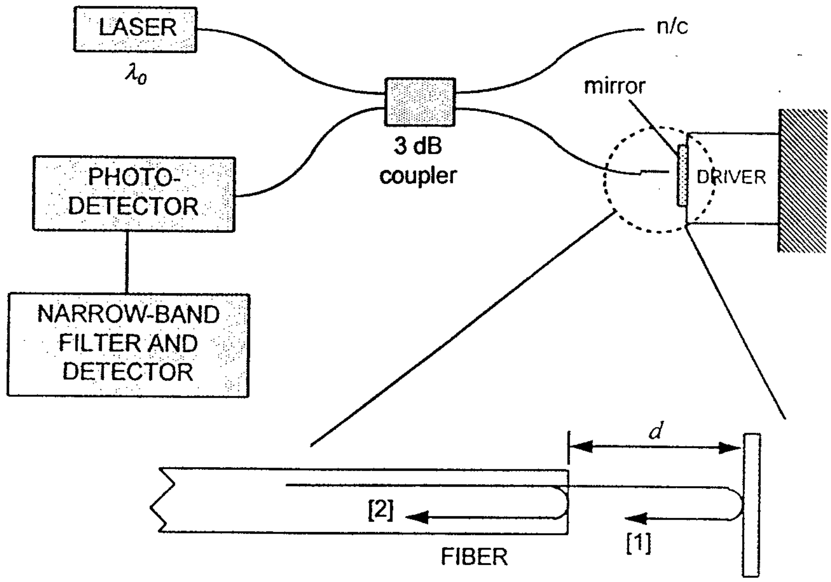

Bessel-Null Calibration

(III-16)

Component that reflects from moving mirror:

$$[1] \quad = \quad A\cos\left(\omega_0 t + 2k_0 d\right)$$

Component that reflects from cleaved end of fiber:

$$[2] \quad = \quad B\cos\left(\omega_0 t\right)$$

Photodetector output (square-law detector):

$$PD \quad = \quad \overline{\left([1]+[2]\right)^2}$$

$$\boxed{PD \quad \rightarrow \quad \cos\left(2k_0 d\right)}$$

Sinusoidal motion of mirror:

$$d \quad = \quad d_0 + d_1 \sin\left(\omega_1 t\right)$$

Interferometer Transfer Function

SMALL SIGNAL (III-17)

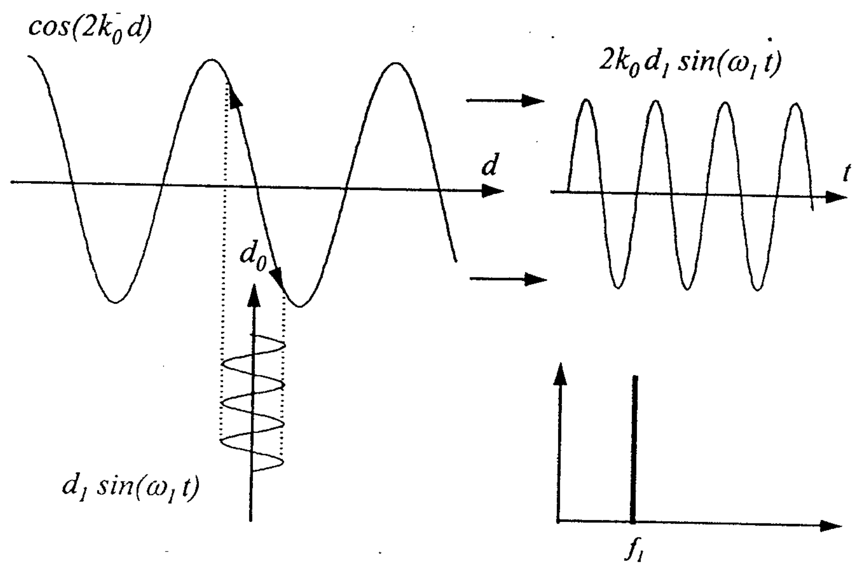

Interferometer Transfer Function

LARGE SIGNAL (III-18)

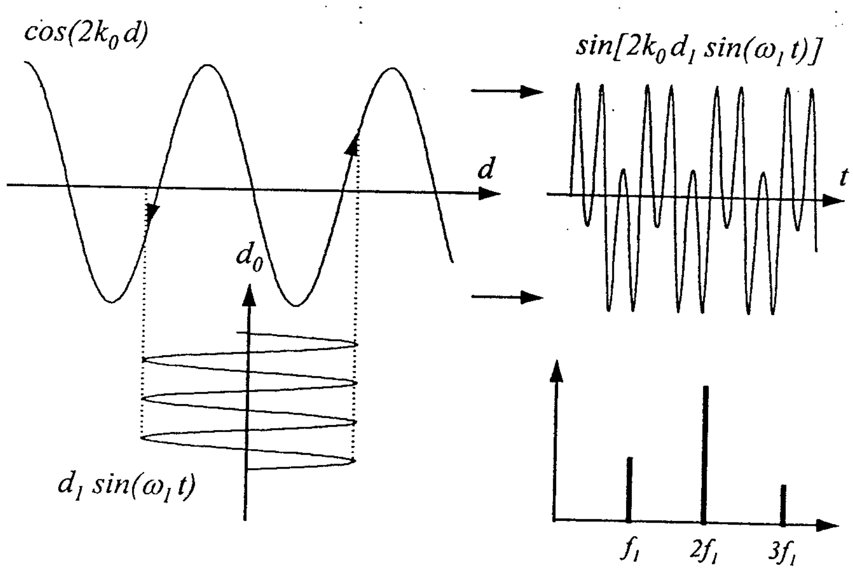

Large-Signal Photodetector Output (III-19)

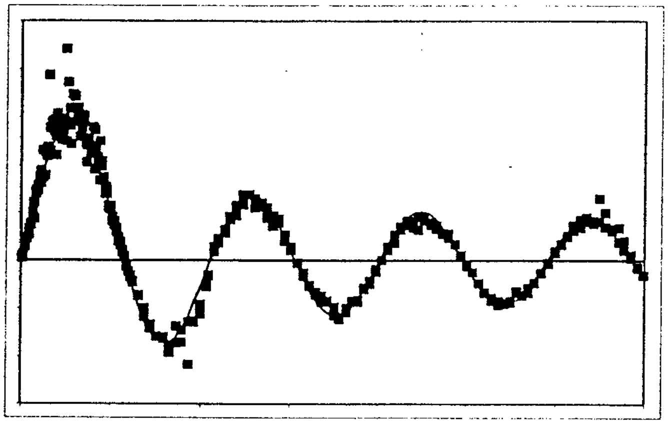

Bessel-Null Calibration (III-20)

For "large" signals then, the photodetector output *at the drive frequency* is:

$$PD\big|_{\omega_1} \rightarrow \sin(2k_0 d_0) J_1(2k_0 d_1)$$

Adjust the drive level to null the output of the photodetector at the drive frequency. These nulls correspond to the zeros, z_i, of the Bessel function, J_1. Consequently, the displacement amplitude, d_1, is only a function of the laser wavelength, λ_0:

$$d_1 = \frac{z_i}{2k_0} = \frac{\lambda_0 z_i}{4\pi}$$

(where z_i = 3.83171, 7.01559, 10.17347, 13.32369, ...)

Components of a Sensor System

(III-21)

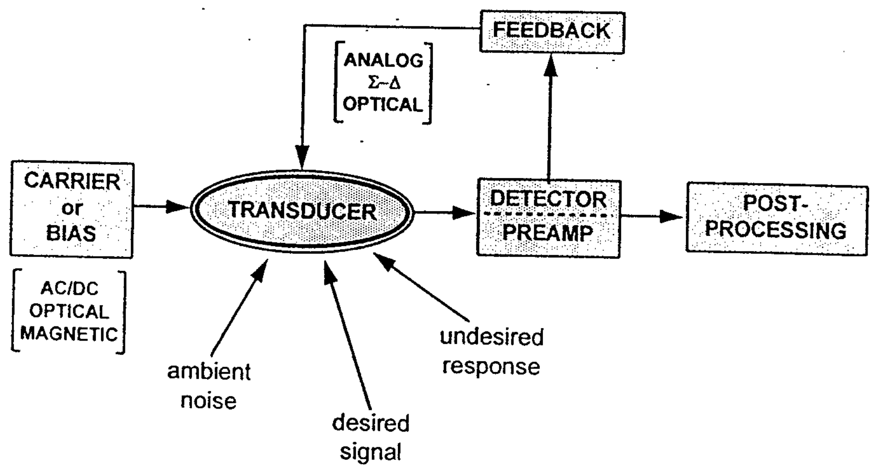

Sensor Electronics Supplement

Often, but certainly not always, the noise floor of a sensor system is set by the first stage of electronics connected to the transducer. In the design of high-performance sensors, it is important to understand the interaction between the sensor and the electronics.

Noise in Preamplifiers

OBSERVATIONS:

Noise at the output of a preamplifier depends on

(1) frequency
(2) impedance of the sensor
(3) gain of the preamplifier

SIMPLIFIED MODEL:

Eliminate (3) by referring noise to preamplifier input

Simplify dependence on (2) by using equivalent voltage and current sources

Applied Research Laboratory - Penn State

In order to understand this interaction, the characteristics of preamplifier must be examined. If a measurement of output noise from a preamplifier is made with various sensor elements connected to the input, the output noise is found to depend strongly on three factors: frequency, the impedance of the sensor connected to the input, and the gain of the amplifier.

In many cases, the output noise is directly proportional to amplifier gain (suggesting that the dominant noise-producing mechanisms in the amplifier are in the input stage) so, by referring the noise to the amplifier input, the effects of amplifier gain can be eliminated.

Also (in most cases) the noise can be divided into two components: one that is independent of the impedance of the attached sensor and one that depends linearly on the magnitude of that attached impedance. Consequently, the amplifier can be well represented by an equivalent voltage noise and an equivalent current noise (the current noise being the component that produces the noise proportional to the attached impedance).

Amplifier Performance

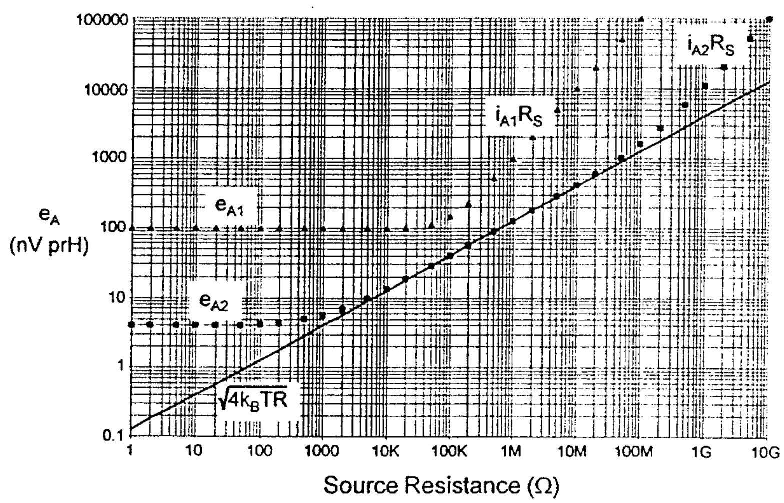

Applied Research Laboratory - Penn State

form10.ppt

If the noise of an amplifier is carefully measured with many different resistors connected to the input (to simulate a wide range of sensor impedance), the results appear as shown above. Below some value of resistance, the noise is constant. This value is selected for the value of the equivalent voltage noise component. Above some higher value of resistance, the noise increases linearly with resistance and the equivalent current noise value is obtained from the slope of that line.

The resistor produces noise of its own (from equilibrium thermal fluctuations in the material -- Johnson noise) and for a good low-noise amplifier (A2), that noise can be measured directly over some range of resistance. A poor amplifier (A1), on the other hand, shows no such region. The closest a poor amplifier comes to reaching the resistor's Johnson noise is for the value of resistance equal to the equivalent noise voltage, e_A, divided by the equivalent noise current, i_A. The region over which a good amplifier can measure resistor Johnson noise extends symmetrically about the value e_A / i_A.

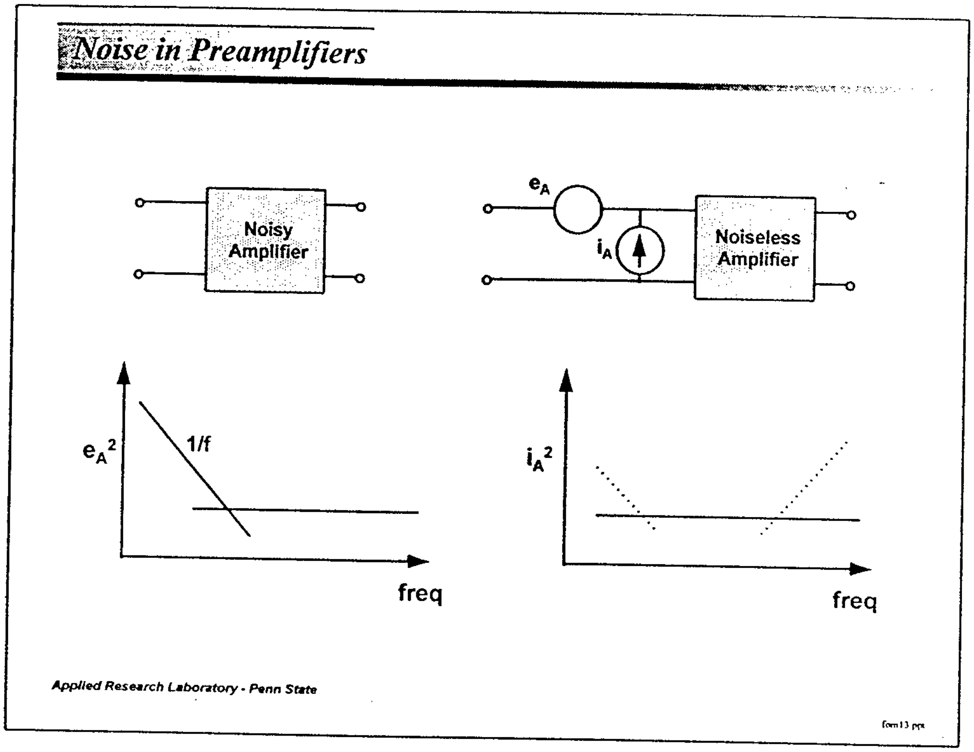

To analyze the noise performance of a sensor-amplifier combination, the noisy amplifier can be replaced by a noiseless amplifier with a noise-voltage source and a noise current source attached to the input. (The noiseless amplifier still has the same input and output impedances as the real amplifier, though.) For most purposes, it is acceptable to treat these two sources as completely uncorrelated even though there may be some correlation in reality. In the case of complete correlation, the maximum error that can be introduced is a factor of the square root of two in amplitude.

In general, there is some frequency dependence associated with these noise sources. Both the voltage noise and the current noise can have a low-frequency dependence of 1/f in power. In addition, the current noise often increases with frequency above some frequency. Components and amplifiers intended for low-noise applications will normally have voltage- and current-noise spectra provided by the manufacturer.

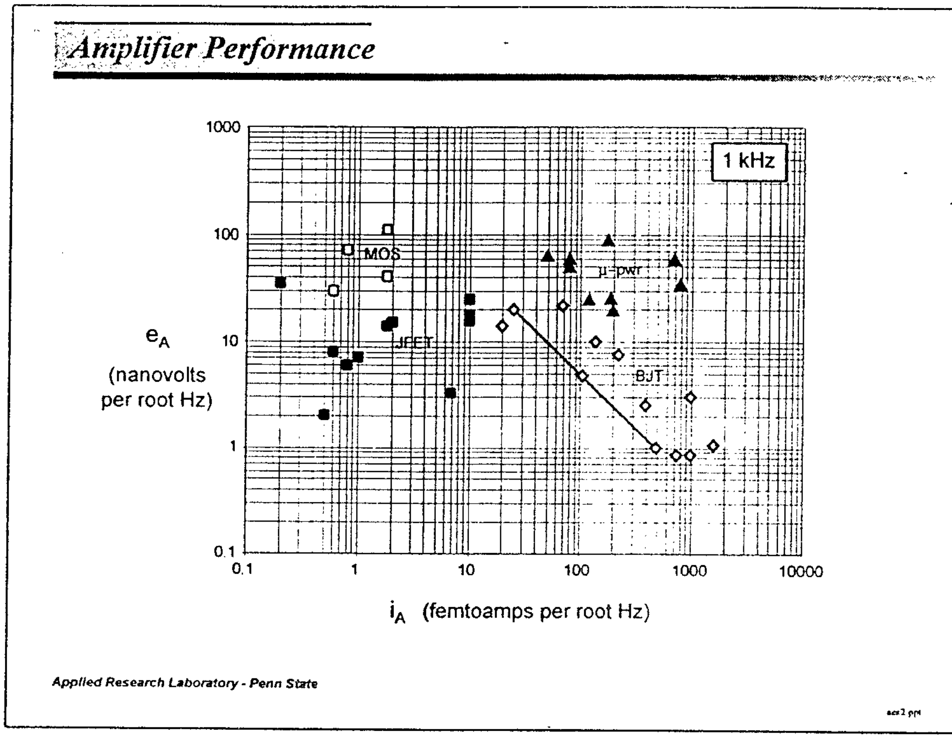

By selecting e_A and i_A, a two-dimensional space can be constructed on which various sensor materials and elements can be compared to various types of amplifiers. A number of off-the-shelf amplifiers and discrete transistors suitable for sensor preamplification are shown on this diagram (with the noise evaluated at 1 kHz).

JFET devices are especially suited to low-noise applications in which the current-noise component must be minimized; BJT devices are particularly suited when it is desireable to minimize the voltage-noise component. (The line connecting three of the symbols illustrates the performance of a single transistor under different conditions of collector current.) MOS devices are useful at ultrasonic frequencies and beyond but are plagued with high 1/f-noise powers that can dominate performance at low frequency. In addition, several micropower (μpwr) devices are included since overall power consumption is often a critical specification in a sensor system.

It is readily apparent that it is difficult to achieve much better than 1 nanovolt per root hertz or 0.5 femtoamp per root hertz regardless of device type. Of particular note is the fact that the space is not covered uniformly by devices. In general, cost and power consumption increase in the direction of decreasing voltage noise.

Noise in Preamplifiers

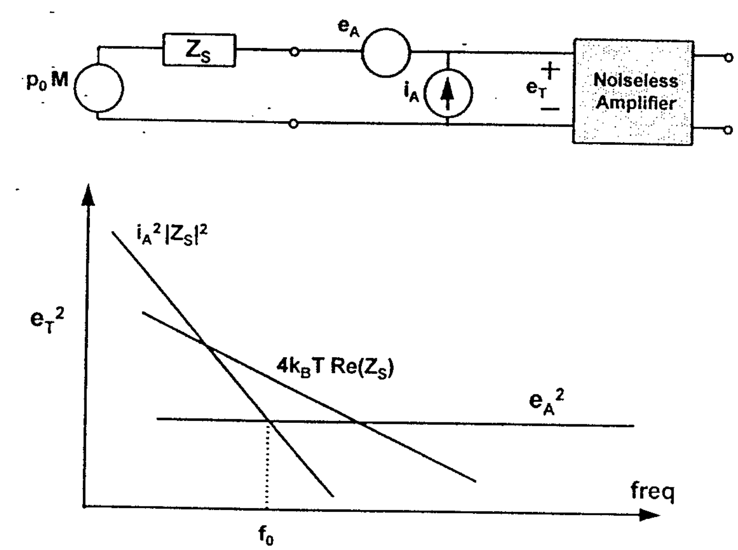

Applied Research Laboratory - Penn State

fom14.ppt

When connected to a sensor, the internally generated noise can be described by three components: (1) the amplifier voltage noise, (2) the amplifier noise current flowing through the sensor producing a noise voltage equal to that noise current times the magnitude of the sensor impedance, and (3) a thermal-equilibrium (Johnson) noise component associated with the real part of the sensor impedance. The plot shown above is representative of a piezoceramic sensor for which the sensor impedance is primarily capacitive and for which the real part of that impedance is dominated by dielectric loss. Not shown in this diagram are external resistors for bias and gain as would be used with an op amp. These resistors produce Johnson noise and also interact with the amplifier noise-current source but the accounting is straightforward. Each noise source is considered in isolation and the results are root-mean-square summed.

For any sensor, it is crucial to distinguish between the *magnitude* of the impedance and the *real part* of that impedance since the magnitude determines the effects of amplifier current noise (and so is a function of amplifier selection) while the real part produces a noise component unrelated to the amplifier.

Equivalent Pressure Noise

$$p_T^2 = p_{amb}^2 + \underbrace{4k_B T \frac{\mathrm{Re}[Z_S]}{M^2}}_{\text{irreducible component}} + \underbrace{\frac{e_A^2}{M^2} + \frac{i_A^2 |Z_S|^2}{M^2}}_{\text{amplifier component}}$$

The irreducible component is equilibrium-thermal noise internal to the sensor and depends on the resistive (real) part of the sensor impedance, Z_s .

M is the sensor response: volts per pascal in this example.

The amplifier contributes two terms, one of which depends on the sensor impedance.

Applied Research Laboratory - Penn State

fom24.ppt

A useful form in which to examine the various noise components is in terms of noise-equivalent pressure. If the voltage response (volts per pascal, for example) of a pressure sensor is *M*, then voltage-noise terms can be referred to equivalent pressure by dividing by *M*. To properly express the incoherent addition of noise terms, the expression above is written in mean-square pressures and voltages. There is an ambient noise term (p_{amb}), a term connected with the internal loss in the sensor (hence, "irreducible"), and two terms associated with the amplifier.

If the noise floor is dominated by the amplifier contribution, there are two terms to consider. In a particular situation, one of those terms may be considerably larger than the other. However, if it is not known which (if either) term dominates, then a compromise term can be introduced as the geometric mean of the two amplifier terms. Clearly, this is not a good strategy if one of the terms is much larger than the other. In the special case in which the two amplifier terms are of the same order, the geometric-mean term is useful.

Noise in Preamplifiers

Designing to a specification for noise floor

$$\overset{}{p_T^2} = \overset{1}{p_{amb}^2} + \overset{2}{4k_BT\frac{\mathrm{Re}[Z_S]}{M^2}} + \overset{3}{\frac{e_A^2}{M^2}} + \overset{4}{\frac{i_A^2|Z_S|^2}{M^2}}$$

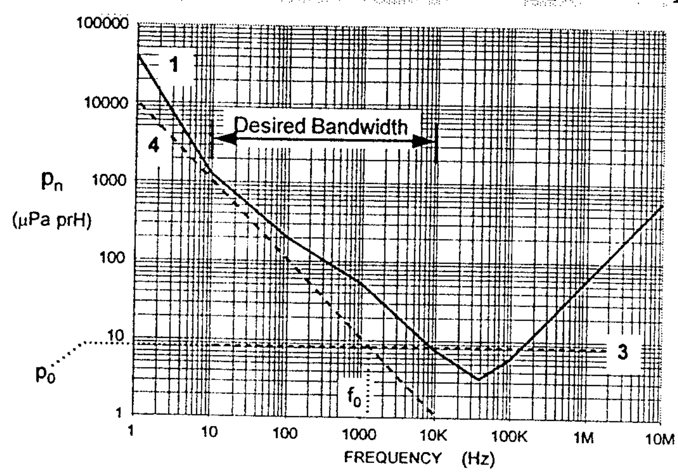

Applied Research Laboratory - Penn State

In designing a high-performance sensor, the desired noise floor, often determined by the ambient background, should be identified. When this is coupled with the design bandwidth of the sensor , the noise components can be individually assessed against this noise-floor specification. Ignoring for the time being the term resulting from dielectric loss (term 2), the design for a piezoceramic hydrophone with a self noise below quiet ocean ambient in the band 10 to 1000 Hz might appear as shown above. At the lower band edge, the desired background sets an upper limit on the allowable amplifier current noise, while at the upper band edge, the background sets an upper limit on the allowable amplifier voltage noise. The respective amplifier components can, of course, be lower than these limits. This limiting configuration can be specified in terms of the intersection between components 3 and 4 given by p_0 and f_0.

Noise in Preamplifiers *Designing to a specification for noise floor*

Ultrasonic Capacitive Sensor $$|Z_S| = \frac{1}{\omega C}$$

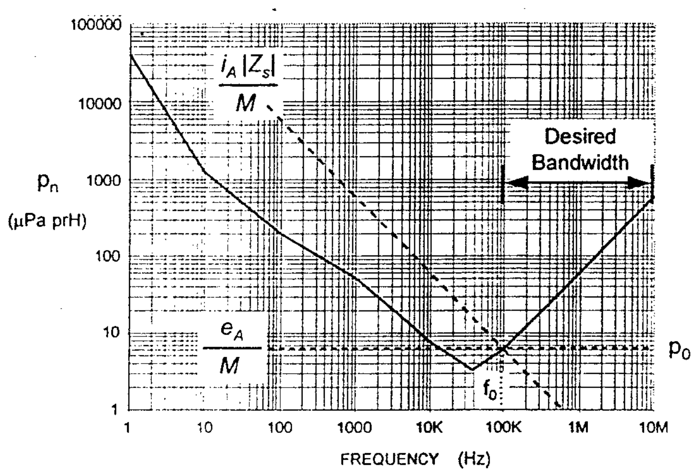

Applied Research Laboratory - Penn State

If a capacitive sensor were being designed for an ultrasonic band (100 kHz to 10 MHz), then the maximum permissible levels of voltage and current noise change as shown above. The principle is still the same. Identify the desired noise floor specification. Overlay the voltage and current components of amplifier noise adjusting e_A and i_A until the hypothetical amplifier is just adequate. A real, acceptable amplifier would then be one for which the voltage and current noise components would be equal to or less than these values.

Noise in Preamplifiers

Designing to a specification for noise floor

Moderate-Frequency Resistive Sensor $\qquad |Z_S| = R$

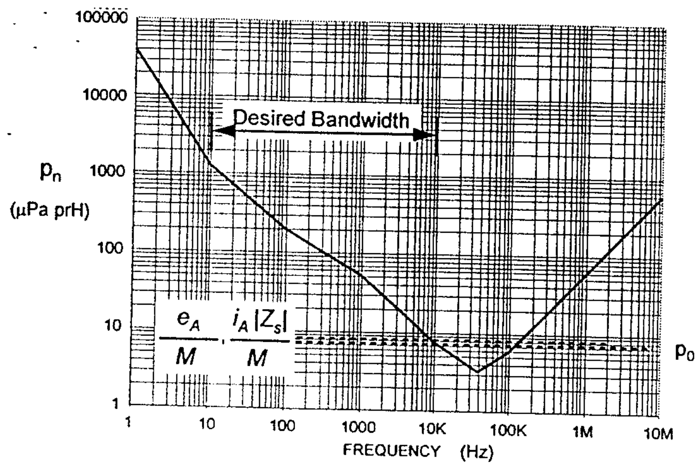

Applied Research Laboratory - Penn State

For a sensor having an impedance that is primarily resistive (a geophone or a piezoresistive pressure sensor, for example), the amplifier terms (to a first approximation) are constant with frequency. The same analysis applies: both amplifier terms must be at or below the desired noise floor over the design bandwidth.

Preamplifier Performance Measures

	Noise "resistance"	Noise Power Coefficient
	$R_A = \dfrac{e_A}{i_A}$	$\alpha_A = \dfrac{e_A i_A}{4 k_B T}$
JFET	1M - 100M	0.0001 - 0.001
BJT	1K - 1M	0. 01 - 0. 1

Applied Research Laboratory - Penn State

mcd1.ppt

There are two useful measures of amplifier noise performance. A commonly used parameter is the noise "resistance" given by the ratio of noise-voltage spectral density to noise-current spectral density. This is often cited as the value to which the resistive part of the sensor impedance should be matched for optimum noise performance. As discussed below, there is some truth to this statement but the merit of an amplifier is not determined by how close its noise resistance is to the source resistance.

Another important (but little used) measure is the noise power coefficient defined as the ratio of the product of the voltage- and current-noise densities to the thermal-noise power, $4k_BT$. This is a better measure of the performance of an amplifier than either the noise voltage or noise current alone. The smaller this ratio, the better the amplifier is. However, the noise power coefficient is not sufficient to determine the overall performance for a particular sensor. Both of the above measures are necessary. (The analysis of an amplifier/sensor combination can be performed perfectly well using both the current- and voltage-noise spectral densities without reference to these other measures but there are some conceptual advantages to the measures given above.)

Preamplifier Performance Measures

For purely resistive sensor, amplifier noise does not mask sensor noise if:

$$\alpha_A < 1 \quad \text{and} \quad \alpha_A < \frac{R_S}{R_A} < \frac{1}{\alpha_A}$$

For general sensor impedance, amplifier noise does not mask sensor noise if:

$$\alpha'_A < 1 \quad \text{and} \quad \alpha'_A < \frac{|Z_S|}{R_A} < \frac{1}{\alpha'_A}$$

$$\text{where} \quad \alpha'_A = \frac{e_A i_A}{4 k_B T} \frac{|Z_S|}{\mathrm{Re}[Z_S]}$$

Applied Research Laboratory - Penn State

imed2.ppt

In general, the noise floor should be controlled by elements close to the system input. For many designs, proper selection of the amplifier can result in the amplifier's noise floor being below the floor set by the sensor itself. The first condition above applies to the case of a purely resistive sensor. The smaller α is, the larger the range of source resistance is that can be accomodated without masking by a particular amplifier.

If the sensor impedance is not purely resistive, then the second condition above specifies the ranges of parameters for which the amplifier will not mask the sensor noise. This case is more complicated because the impedance is, in general, a function of frequency so the conditions may be satisfied over some regions of the spectrum and not satisfied over other regions. In a number of important cases, the ratio of the resistive part of the impedance to the magnitude of the impedance (the "loss tangent") is approximately constant over a range of frequency, which simplifies the determination somewhat.

In either case, if α (or α') is less than one, there is a region over which the sensor noise (the component from the real part of the impedance) MAY set the noise floor.

Preamplifier/Sensor Interaction — THE IRREDUCIBLE TERM

Real part of the sensor impedance:

1. Purely resistive sensor: $$\frac{|Z_S|}{\mathrm{Re}[Z_S]} = 1$$

2. Primarily reactive sensor (e.g. capacitive): $$\frac{|Z_S|}{\mathrm{Re}[Z_S]} = \frac{1}{\delta}$$

3. Typical sensor:

   - electrical loss (loss tangent, δ)
   - electrical loss (resistance, R_e)
   - mechanical loss (Q_m)
   - radiation resistance (R_{rad})

Applied Research Laboratory - Penn State

The ratio of impedance magnitude to real part is one for a purely resistive sensor and is equal to the reciprocal of the loss tangent for a reactive sensor. Since the electrical impedance of the sensor includes the electrical equivalent of the sensor's mechanical elements (by means of the transduction mechanism), the losses and, therefore, the noise may be caused by either electrical losses or mechanical losses.

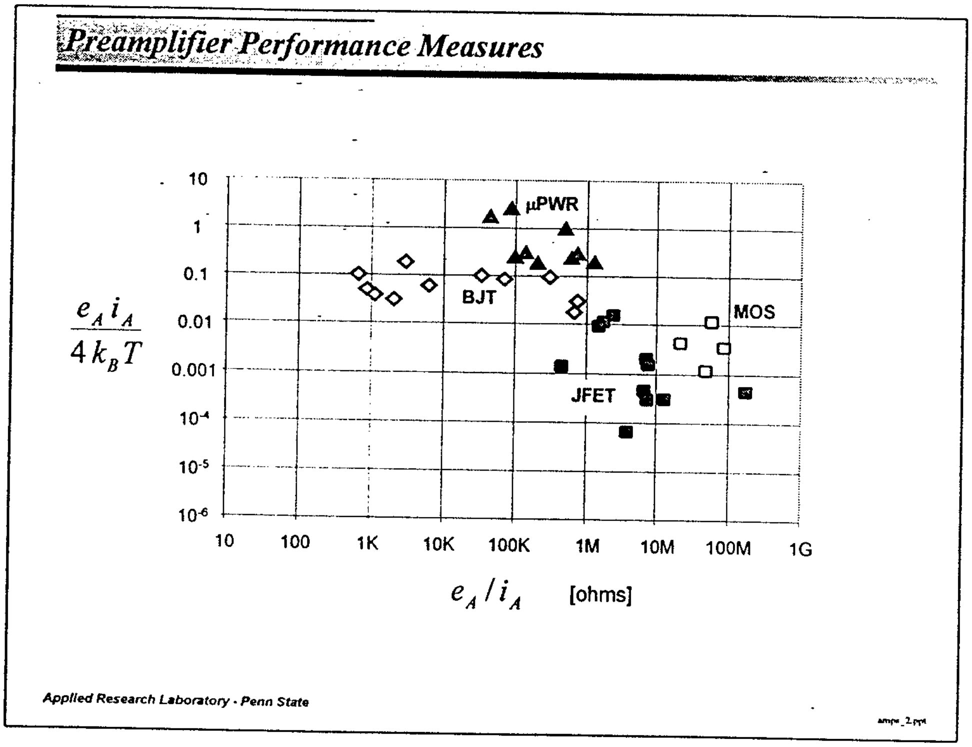

A number of various types of amplifiers (either op-amps or discrete transistors) are plotted above on the coordinates of noise power coefficient and noise resistance. This chart is useful for selecting an amplifier type once the sensor impedance, the operating bandwidth, and the desired noise floor are known.

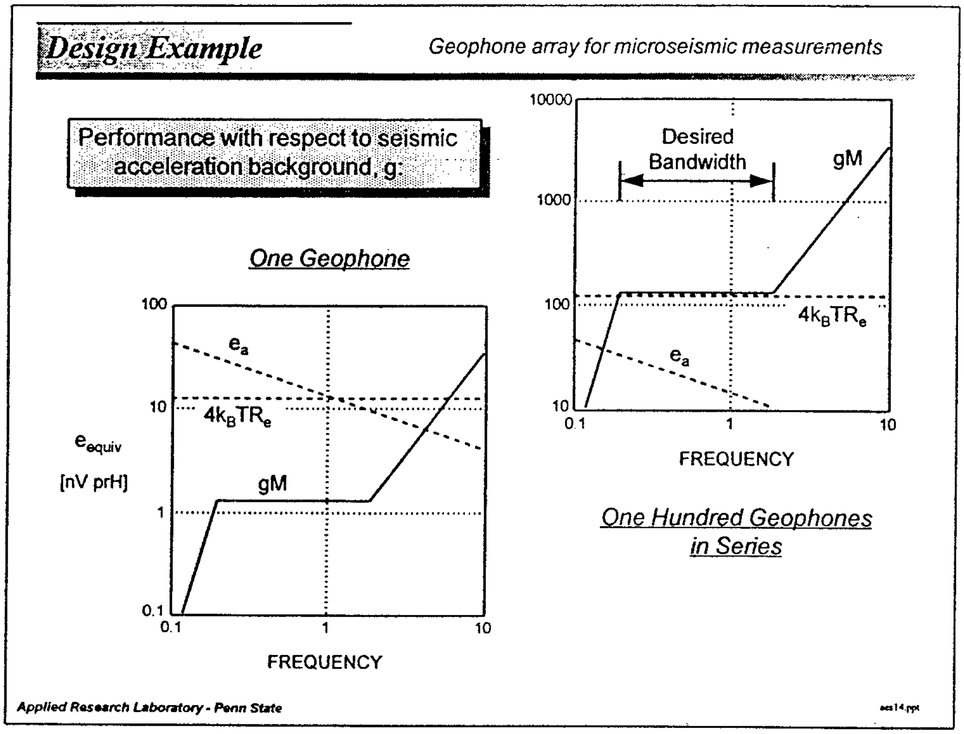

This is an illustration of the design of a geophone array for sensing microseismic disturbances. The frequency range of interest is 0.2 to 2 Hz. The curve labelled *gM* is the specification for self noise for this sensor. (This curve is produced by multiplying the noise-floor in seismic acceleration by the transfer function of the geophone or geophone array. This produces an equivalent voltage-noise noise floor.) For a single geophone, both the amplifier voltage noise and the irreducible noise associated with the electrical resistance of the geophone coil are well above the desired noise floor. By connecting 100 geophones in series, however, the desired noise floor is achieved. This may not be an elegant solution but the result is cheaper and more rugged than the closest commercial alternative.

Equivalent Voltage and Current Noise Values for Common Amplifiers

		eA	iA	eA/iA	eAiA/4kT
		nVprH	*fAprH*	*ohms*	-
BJT	LT1007	2.5	400	6250	0.0625
	LT1012	22	70	314286	0.0963
	LT1024	14	20	700000	0.0175
	LT1028	0.85	1000	850	0.0531
	OP05	10	140	71429	0.0875
	OP27	3	1000	3000	0.1875
	OPA77	7.5	220	34091	0.1031
	CLC425	1.05	1600	656	0.1050
(1mA)	*MAT02*	0.85	750	1133	0.0398
(1uA)	*MAT02*	20	25	800000	0.0313
(1mA)	*LM394*	1	500	2000	0.0313
(1uA)	*LM394*	20	25	800000	0.0313
JFET	LT1022	14	1.8	7777778	0.0016
	LT1055	15	2	7500000	0.0019
	LF353	16	10	1600000	0.0100
	LF411	25	10	2500000	0.0156
	AD743	3.2	6.9	463768	0.0014
	AD744	18	10	1800000	0.0113
	AD549	35	0.2	175000000	0.0004
	OPA111	8	0.6	13333333	0.0003
	U401	2	0.5	4000000	0.0001
	2N4338	6	0.8	7500000	0.0003
	2N6485	7	1	7000000	0.0004
uPwr	LM4250	50	80	625000	0.2500
	OP20	60	80	750000	0.3000
	OP21	20	200	100000	0.2500
	OP22	90	180	500000	1.0125
	OP90	60	700	85714	2.6250
	OP191	35	800	43750	1.7500
	OP193	65	50	1300000	0.2031
	OP196	26	190	136842	0.3088
	OPA1013	25	120	208333	0.1875
MOS	CA3440	110	1.8	61111111	0.0124
	CA3140	40	1.8	22222222	0.0045
	CA3160	72	0.8	90000000	0.0036
(chopper)	LTC1052	30	0.6	50000000	0.0011

Notes

1. eA and iA are the equivalent voltage and current noise components respectively.
   nVprh is nanovolts per root hertz; fAprh is femtoamps per root hertz.
2. All values are taken at 1 kHz from manufacturer's data sheets.

3. Devices shown in italics are discrete transistors; all other devices are integrated circuits.
4. uPwr stands for micropower (very low power consumption)
5. MOS devices have large 1/f-noise components in the voltage noise. The 1 kHz values cited are still on the 1/f portion of the curve. The 1/f portion of the voltage noise curves for the other devices are below (and, in some cases, well below) 1 kHz.
6. The LTC1052 (MOS) device is a chopper-stabilized amplifier (roughly speaking, the input is chopped at a high frequency, then amplified, then detected synchronously with the chopping frequency). It is representative of the best low-frequency performance obtainable with a MOS device. Essentially, there is no 1/f region in the voltage noise.
7. All of these devices require biasing and/or feedback resistors. The effects of these resistors must be considered when determining the overall amplifier noise. In most cases, low-current-noise amplifiers can be designed for minimal effect from biasing/feedback resistors; for very-low-voltage-noise amplifiers, the noise from those resistors can limit the achievable noise performance.
8. The two BJT discrete devices are shown for two operating points each. One of the advantages of using discrete devices is that the noise performance can be tuned by means of the collector (or drain) current. Throughout this adjustment range, the eAiA product is roughly constant.
9. Very low voltage noise is generally obtained by massively parallel emitter regions in BJT devices. This has two important consequences: (1) the input capacitance is large, and (2) the devices are *relatively* large. The second point is not important unless the amplifier must be integrated onto a chip with limited real estate: for example, a single MAT02 occupies 2x2 mm.
10. The "noise impedance" eA/iA is given for each device but should not be misinterpreted. This number is often cited as the resistance to which the source resistance must be matched for best noise performance. It is not, however, good practice to select an amplifier on the basis of the eA/iA-to-source-resistance match. *If the source* (transducer, for example) *is primarily resistive*, then the amplifier's noise contribution is negligible compared to the Johnson noise of the source *over a range of resistance* centered on the eA/iA value. The width of the region to either side of eA/iA is given (roughly) by the eAiA/4kT value. If eAiA/4kT is 0.01 and eA/iA is 100 000 ohms, then the amplifier's contribution is less than the source's Johnson noise for source resistances of 1000 ohms to 10 megohms. It is *never* appropriate to "match" amplifier noise resistance to the magnitude of a source's impedance if that impedance is primarily reactive.
11. The quantity eAiA/4kT is the product of noise voltage and noise current normalized by 4 times Boltzmann's constant times absolute temperature. The product 4kT is approximately 16 x 10^21 in SI units at room temperature.
12. Current noise is exponentially dependent on operating temperature in JFET devices. The values given are generally at 25 or 30 deg. C. Significant degradation in current-noise performance can be expected with operation at elevated temperatures.

Resources

Horowitz + Hill, The Art of Electronics, Cambridge U. Press (1989)

Pease, Troubleshooting Analog Circuits, Butterworth-Heinemann (1991)

www.analog.com (Analog Devices)

www.national.com (National Semiconductors)

www.linear-tech.com (Linear Technologies)

PHYSICAL ACOUSTICS SUMMER SCHOOL
Asilomar Conference Center
Pacific Grove, CA
19 June 1998

Thermoacoustics Made Simple

Steven Garrett
Penn State University
garrett@sabine.acs.psu.edu

PSU Thermoacoustic Web Page
www.acs.psu.edu/thermoacoustics.html

History

Enrico Fermi Summer Schools
Societa Italiana de Fisica
Villa Monastero - August 1974
Varenna sul Lago di Como

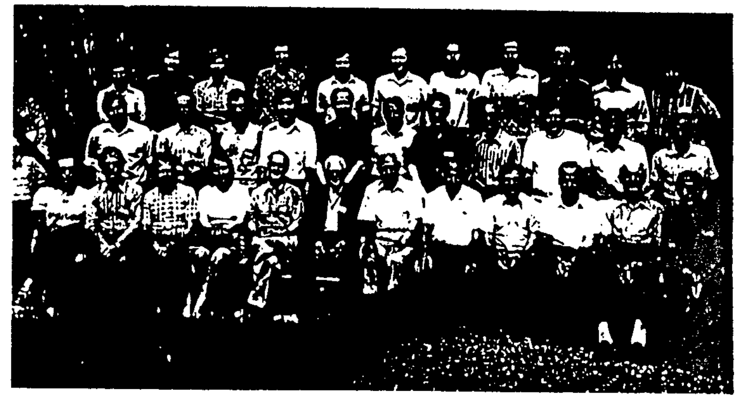

- The "Old Guys"

R. B. Lindsey, W. P. Mason, D. Sette,
K. Dransfield (?), R. K. Cook, E. F. Carome

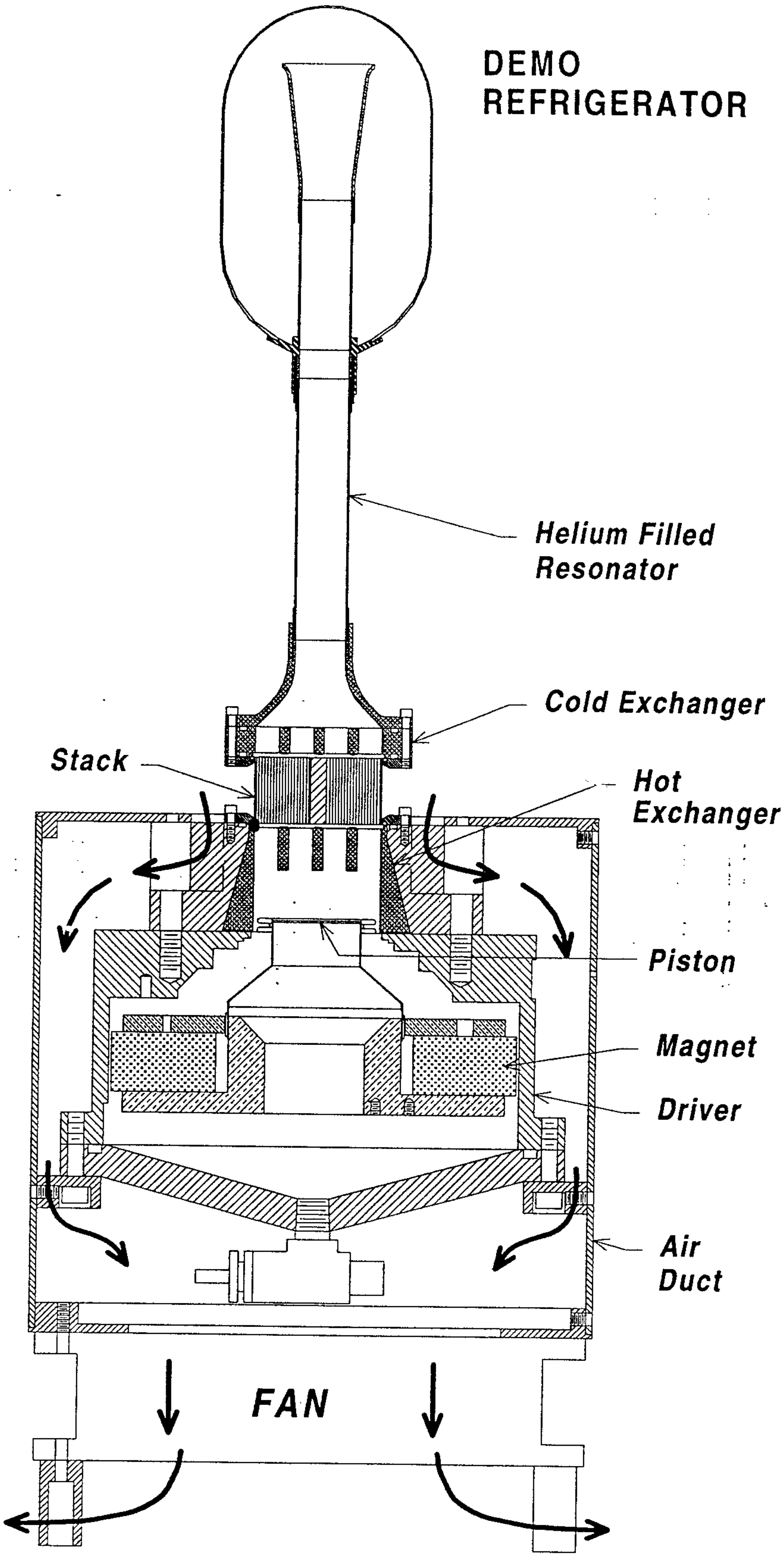
DEMO
REFRIGERATOR
Helium Filled
Resonator
Cold Exchanger
Stack
Hot
Exchanger
Piston
Magnet
Driver
Air
Duct
FAN

Slide H1

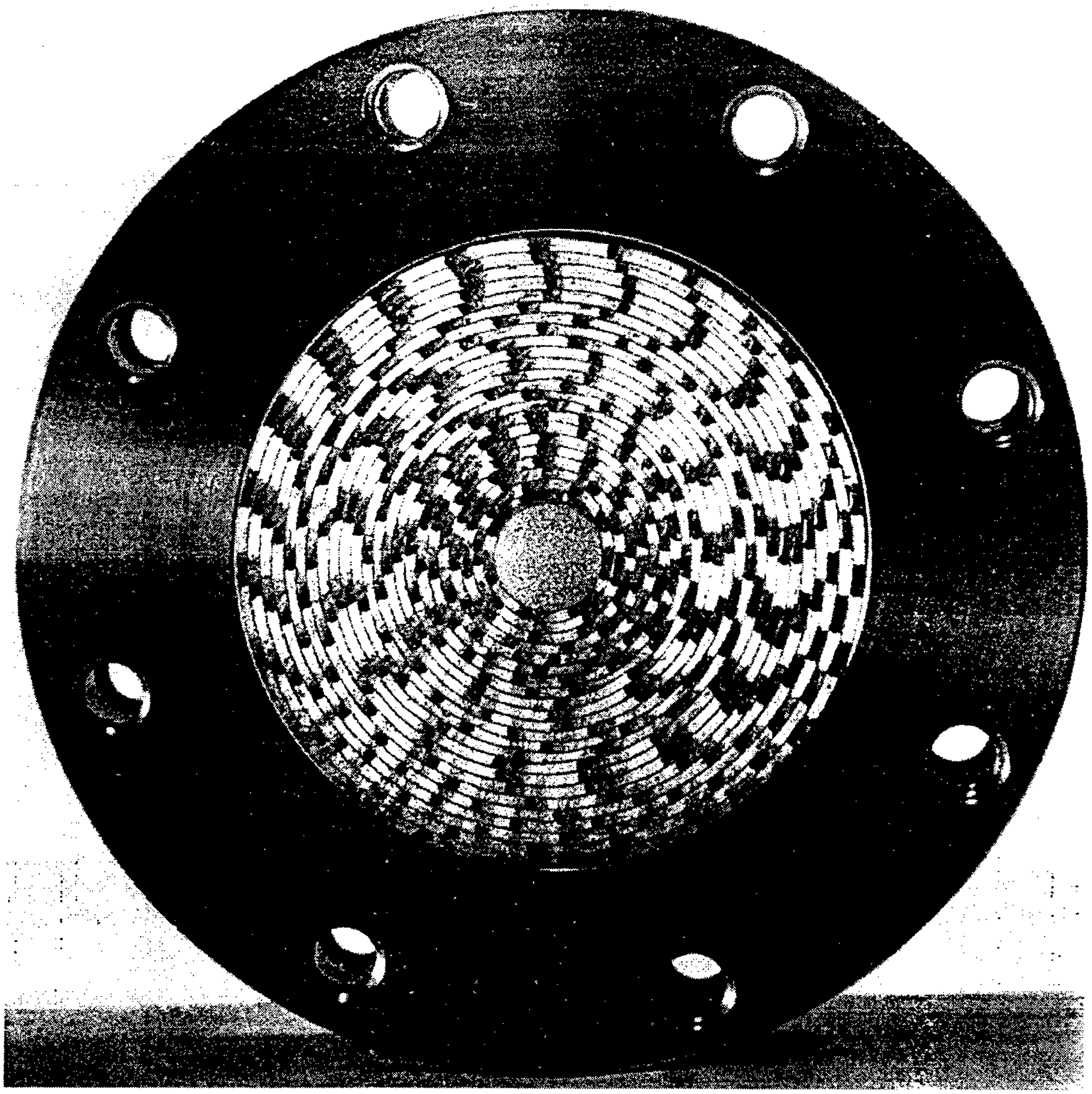

Slide H2

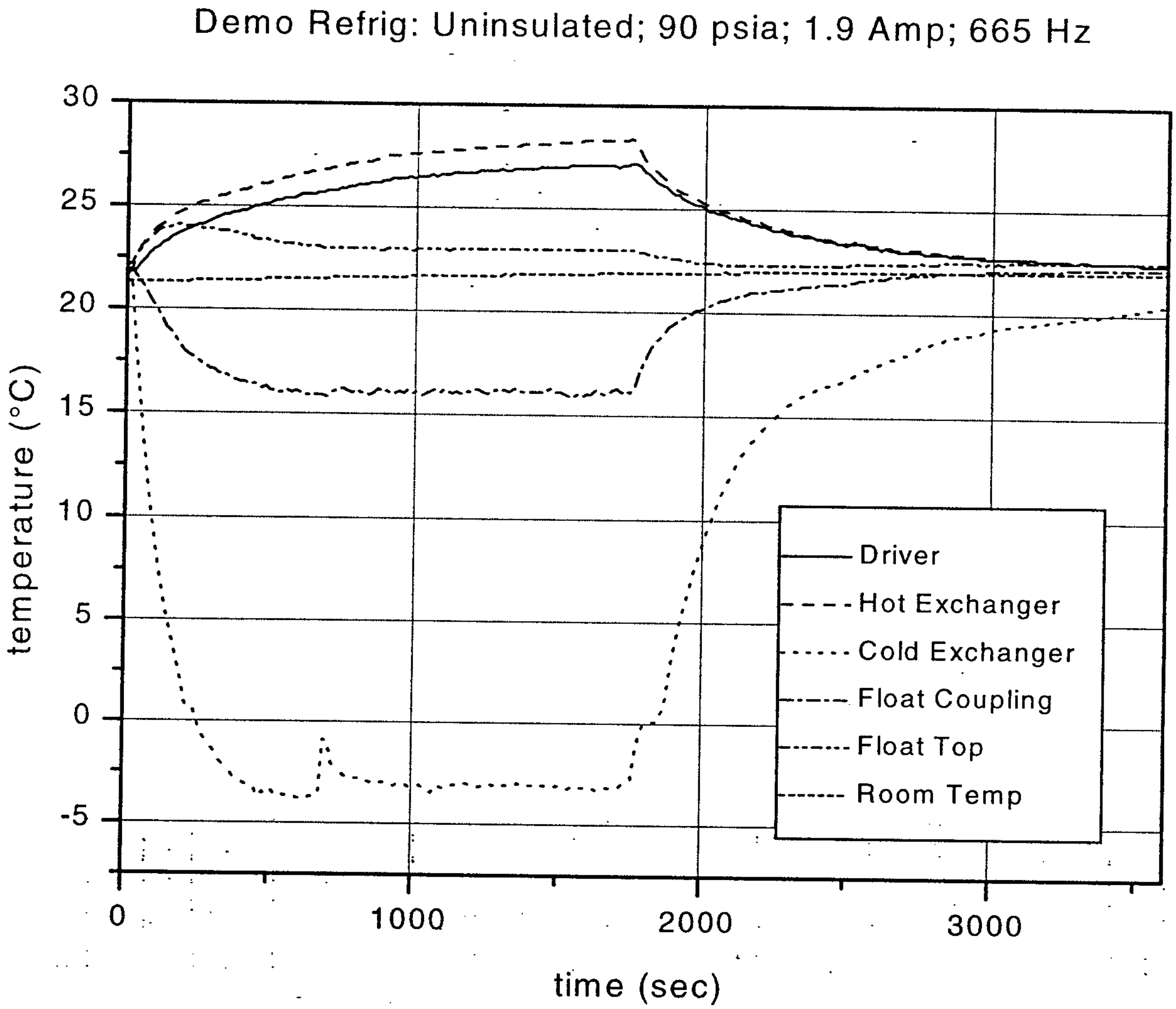

Demo Refrig: Uninsulated; 90 psia; 1.9 Amp; 665 Hz
30
25
20
15
10
5
0
-5
temperature (°C)
0
1000
2000
3000
time (sec)
Driver
Hot Exchanger
Cold Exchanger
Float Coupling
Float Top
Room Temp

Slide H3

Demo Refrig.: 90 psia He; po/pm = 5%; 665 Hz; 9/7/94

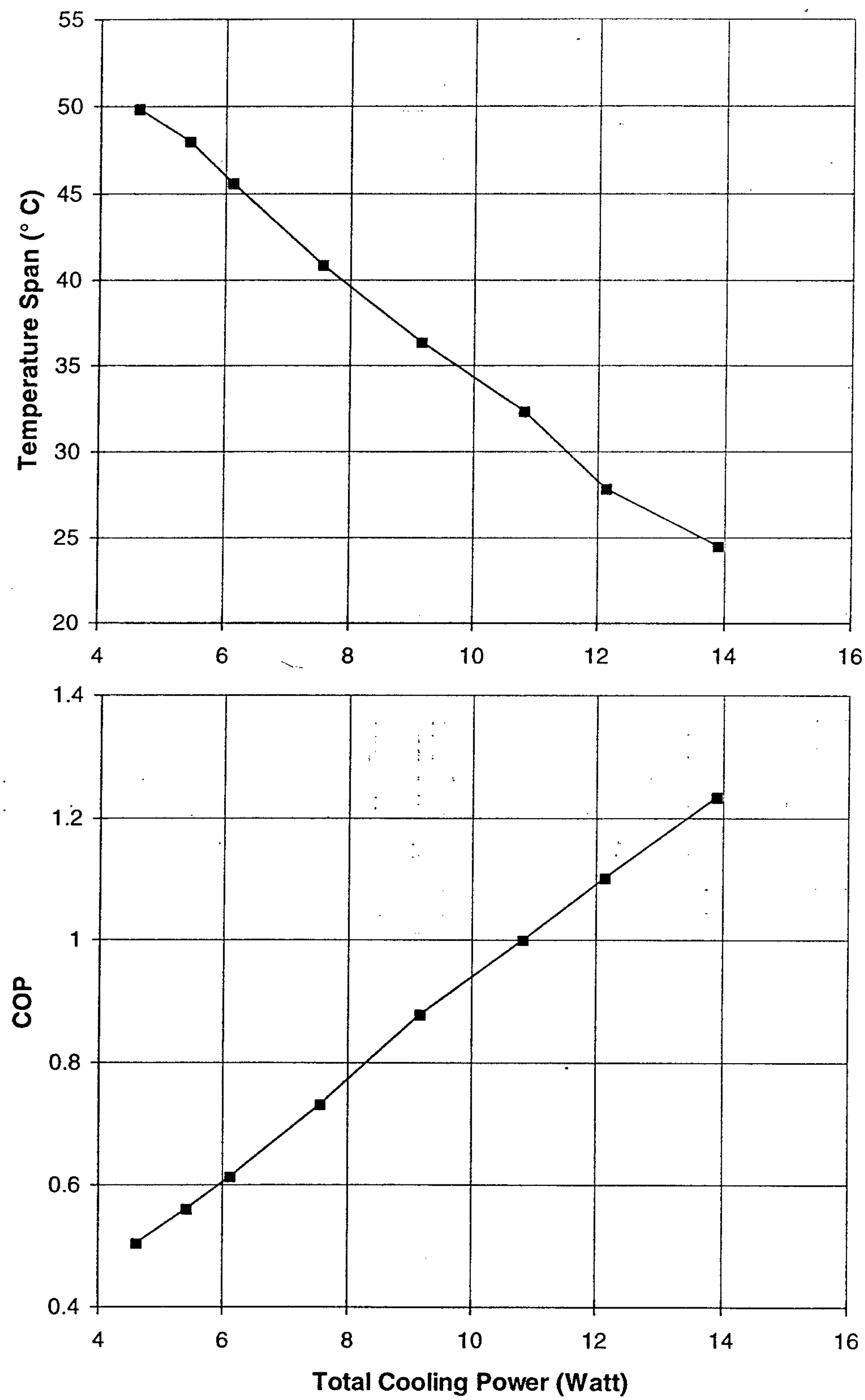

Slide H4

TITLE: Hofler Tube
DWG. No: HFLRTUBE
DATE: 1-25-95
SCALE: 1 = 1
MATERIAL: N/A

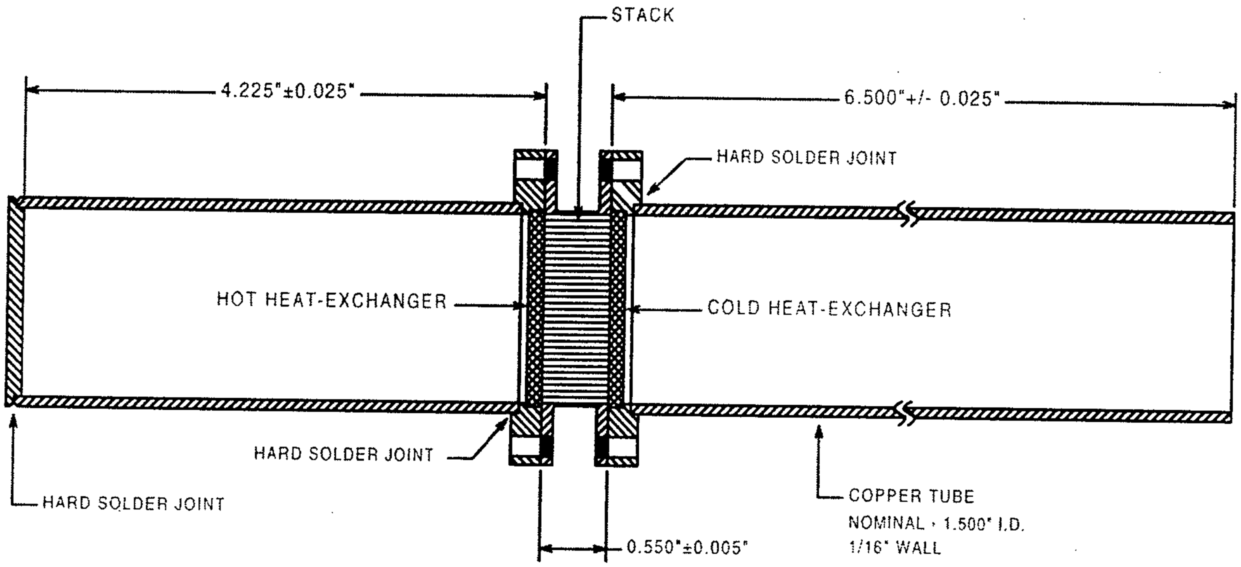

Slide H5

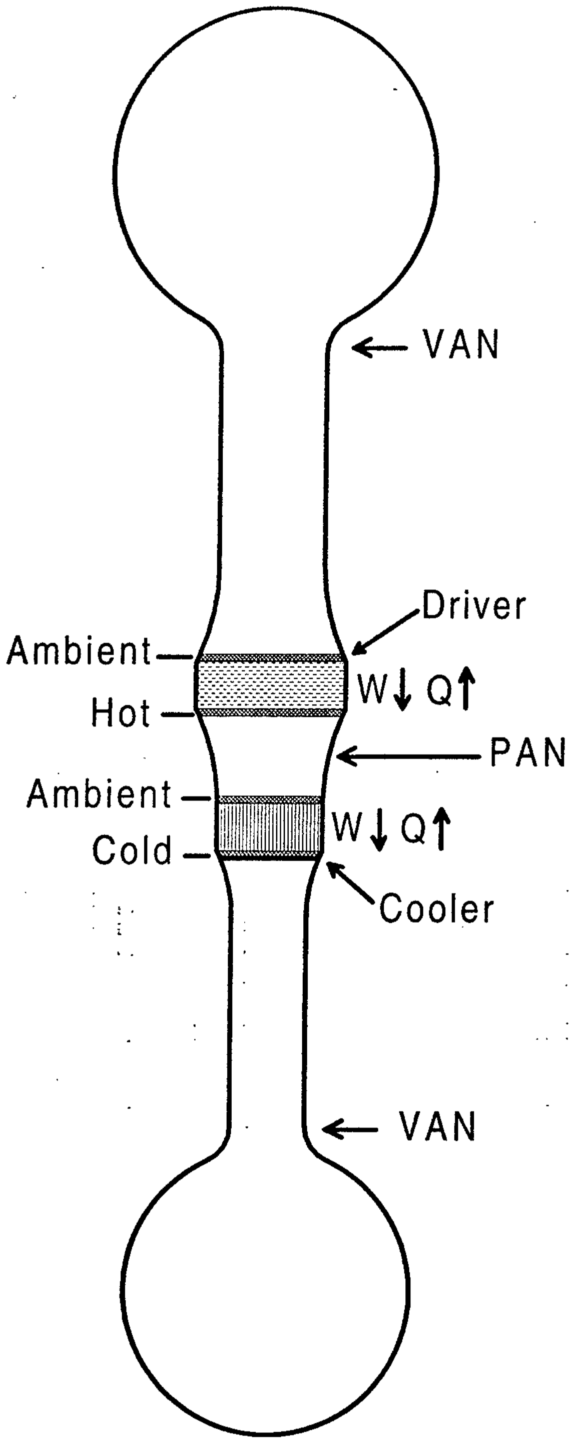

Slide H6

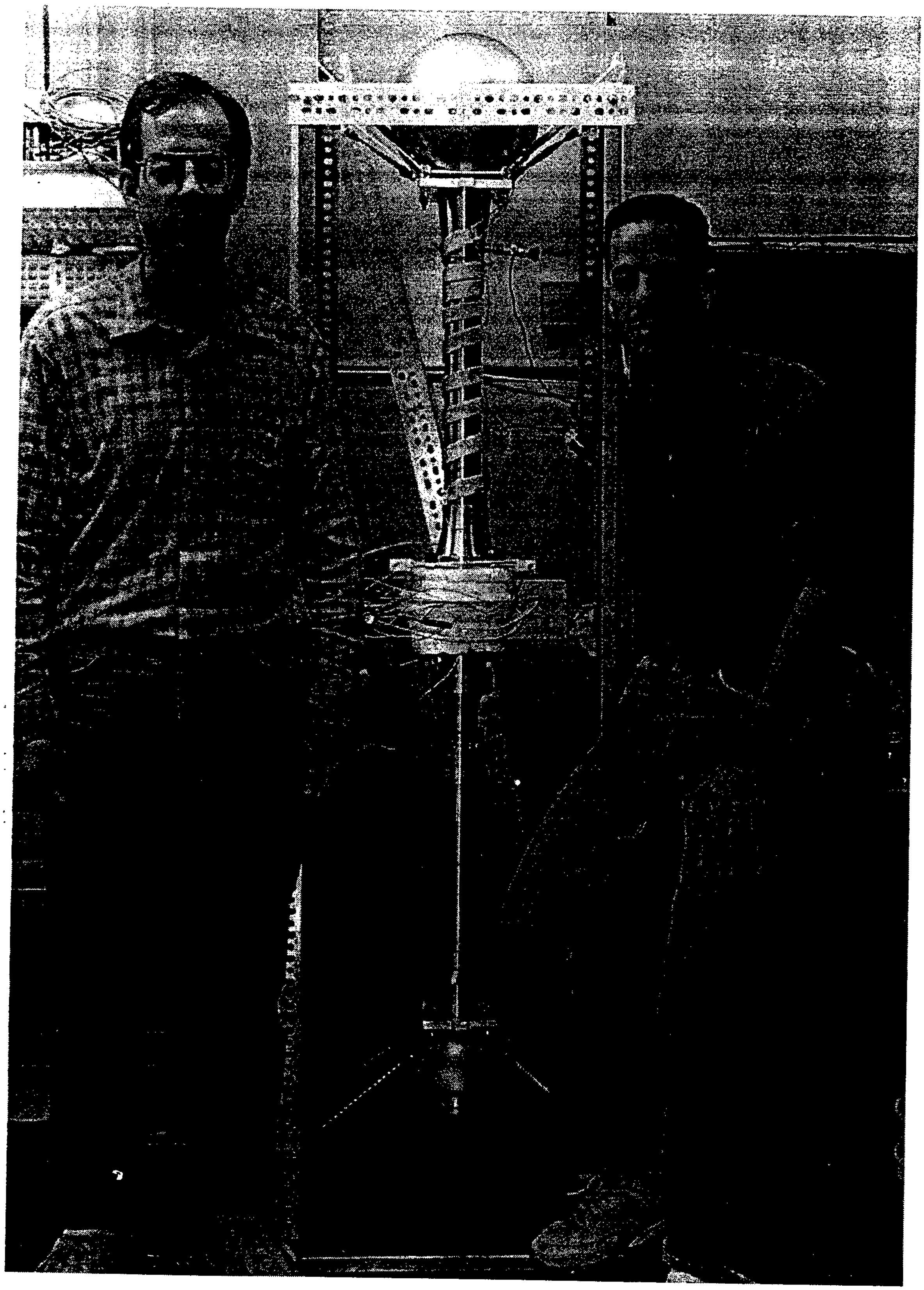

Slide H7

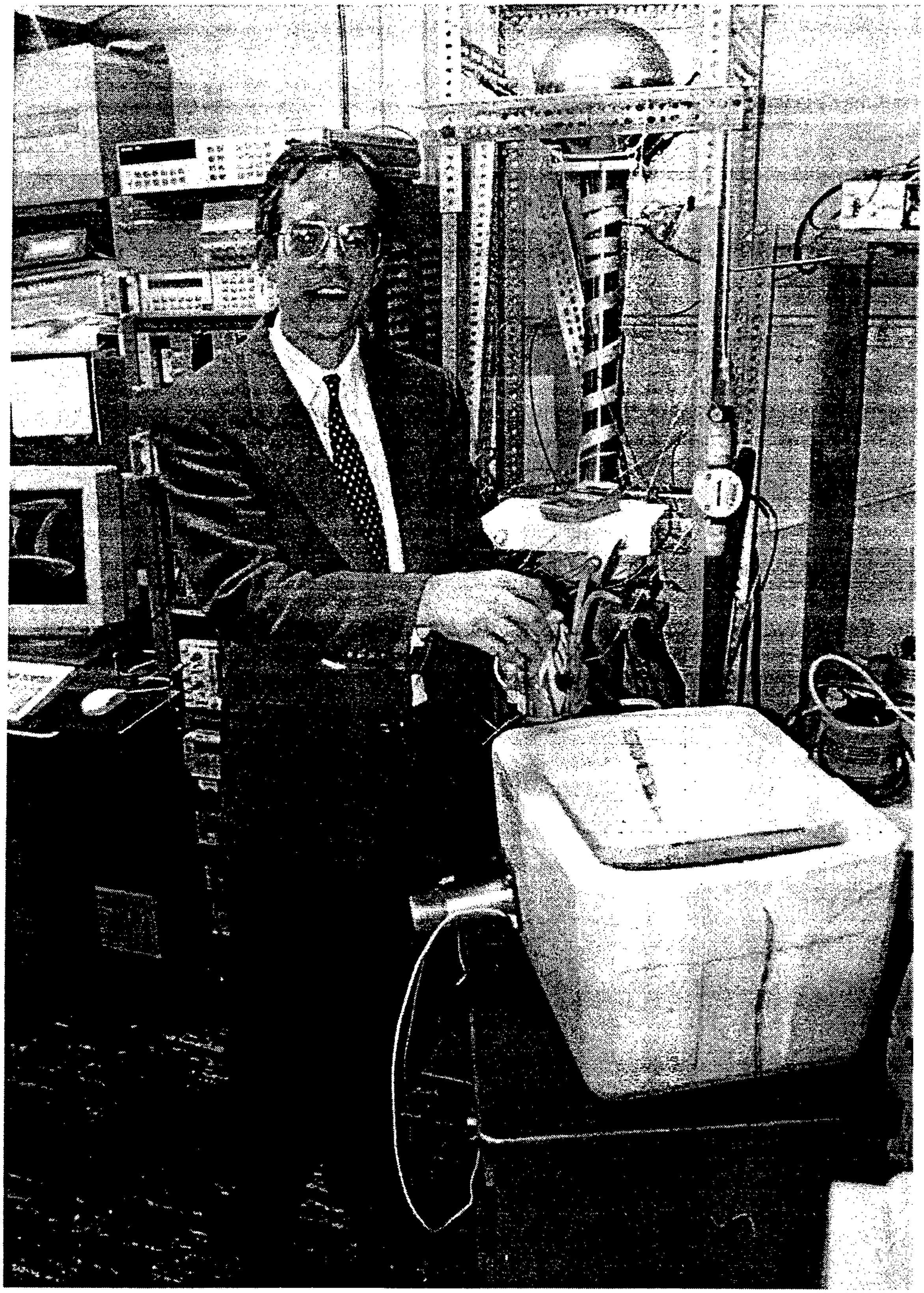

Slide H8

The Plan

- Motivation
  - New, simple, environmentally friendly
  - Good acoustics and engineering problem
    - Superfluids, superconductors, cavitation
- Fundamentals
  - Adiabatic and isothermal propagation
  - Thermal and viscous diffusion
  - Relation between temperature and pressure
- Standing Waves
  - The Lagrangian model
    - Critical temperature gradient
    - Crude calculation of heat transport
  - Thermoviscous surface dissipation
- Heat Engine Calculations
  - Thermoacoustic instability - prime movers
    - Limitation imposed by the 2nd Law
  - Thermoacoustic refrigeration
- Thermoacoustic Systems and Components
  - Electrodynamic loudspeakers
  - Anharmonic resonators
  - Heat exchangers

Sound Speed in an Ideal Gas

- Isothermal sound speed

  Ideal gas law

$$p = \frac{m}{V}\frac{RT}{M} = \rho\frac{RT}{M} \tag{1}$$

  Phase speed

$$c_{phase} = \frac{\omega}{|\vec{k}|} = \left(\frac{\partial p}{\partial \rho}\right)_T^{1/2} = a_N = \left(\frac{RT}{M}\right)^{1/2} \tag{2}$$

  Newtonian sound speed

$$a_N^2 = \frac{RT}{M} \tag{3}$$

  Principia, 2nd ed. (1713), a_N = 979 ft/sec
  Experimental value ≈ 1,130 ft/sec

- Adiabatic sound speed

  Define specific volume (per unit mass), $\rho = V^{-1}$

$$p\rho^{-\gamma} = const.' \tag{4}$$

  Take natural log and differentiate ($\int dx/x = \ln(x) + C$)

$$\frac{dp}{p_m} = \gamma\frac{d\rho}{\rho_m} \Rightarrow a^2 = \left(\frac{\partial p}{\partial \rho}\right)_S = \gamma\frac{p_m}{\rho_m} \tag{5}$$

  From the Ideal Gas Law, $p_m/\rho_m = RT/M$

$$a^2 = \gamma\frac{RT}{M} = \gamma a_N^2 \tag{6}$$

Thermal Conduction and Viscosity

- Newton's Law of Cooling

  Ohm's law for heat flow ($I = \Delta V/R$)

  $$\vec{\dot{q}} = -\kappa \vec{\nabla} T \tag{7}$$

  $\vec{\dot{q}}$ = Heat flux [Watts/m^2]

  κ = Thermal conductivity [W/m°K]

  One-dimensional thermal conductance

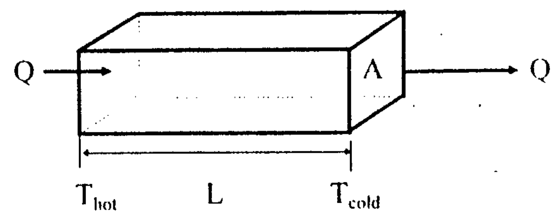

  $$\dot{Q} = -\kappa A \frac{(T_{hot} - T_{cold})}{L} = \frac{\kappa A}{L} \Delta T \tag{8}$$

  Ohm's Law: $I = G\,\Delta V$ or $\Delta V = R\,I$

  Electrical resistance: $R = L/\sigma A$

- Viscous shear stress

  Ohm's Law for one component of shear stress, P_{xy}

  $$P_{xy} = \mu \frac{\partial v_x}{\partial y} \tag{9}$$

  P_{xy} = Force per unit area in x-direction on a surface with its normal in the y-direction [Pa]

  μ = Shear viscosity [kg/m-sec]

Thermal (Fourier) Diffusion Equation

- Differential analysis

  Heat flow through a differential "slab"

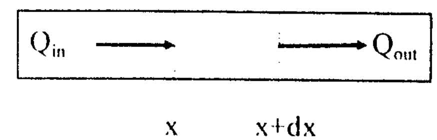

  Net heat is deposited in the slab of unit cross-section

  $$Q_{net} = Q_{in} - Q_{out} \tag{10}$$

  Temperature change rate depends on heat capacity

  $$\rho c_p \frac{\partial T}{\partial t} = \dot{Q}_{net} = -\kappa \left(\frac{\partial T}{\partial x}\right)_x + \kappa \left(\frac{\partial T}{\partial x}\right)_{x+dx} \tag{11}$$

  c_p = Specific heat at constant pressure [Joules/kg°K]

  Expand $(\partial T/dx)_{x+dx}$ about x in a Taylor series

  $$\left(\frac{\partial T}{\partial x}\right)_{x+dx} = \left(\frac{\partial T}{\partial x}\right)_x + \frac{\partial}{\partial x}\left(\frac{\partial T}{\partial x}\right)_x dx + \ldots \tag{12}$$

  Combine (44) and (45)

  $$\frac{\partial T}{\partial t} = \frac{\kappa}{\rho c_p} \nabla^2 T = \chi \nabla^2 T \tag{13}$$

  χ = Thermal diffusivity [m^2/sec]

Diffusion Equations

- Navier-Stokes Equation

  Diffusion of viscous shear stress (vorticity)

$$\frac{\partial \vec{v}}{\partial t} = \frac{\mu}{\rho}\nabla^2 \vec{v} - \frac{\vec{\nabla} p}{\rho} = \nu \nabla^2 \vec{v} - \frac{\vec{\nabla} p}{\rho} \quad (14)$$

  ν = Kinematic viscosity [m²/sec]

- Fick's Second Law of Diffusion

  Mass diffusion (random walk)

$$\frac{\partial C}{\partial t} = D \nabla^2 C \quad (15)$$

  C = Concentration [moles/m³]

  D = Mass diffusion constant [m²/sec]

- Maxwell's Equation in a Good Conductor

  Electromagnetic energy diffusion

$$\frac{\partial \vec{E}}{\partial t} = \frac{1}{\sigma \mu} \nabla^2 \vec{E} \quad (16)$$

  σ = Electrical conductivity [Siemens/m]

  μ = Magnetic permeability [N/Amp²]

  $(\sigma\mu)^{-1}$ = ??? [m²/sec]

Evanescent Wave

- Wavelike solutions to the diffusion equations

  We could choose any of the diffusion equations

  Solve Fourier Heat Equation, since it is scalar.

  Assume a plate with an oscillating temperature

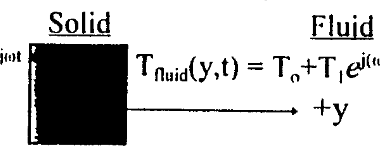

$T_{solid}(t) = T_o + T_s e^{j\omega t}$ $\quad$ $T_{fluid}(y,t) = T_o + T_1 e^{j(\omega t - ky)}$

  ω = "Driving" frequency [rad/sec]

  k = Complex wave number

  Substitute into the Fourier Equation

$$j\omega\, T_1 = -\chi\, k^2\, T_1 \quad (17)$$

  Solve for jk

$$jk = \left(\frac{j\omega}{\chi}\right)^{1/2} = \left(e^{j\frac{\pi}{2}}\right)^{1/2}\left(\frac{\omega}{\chi}\right)^{1/2} = \frac{1+j}{\sqrt{2}}\left(\frac{\rho c_p \omega}{\kappa}\right)^{1/2} \quad (18)$$

  Wavenumber has equal real and imaginary parts

- Thermal Penetration Depth

  Define a real length $\delta_\kappa = \Re e\,[k^{-1}]$

$$\delta_\kappa = \sqrt{\frac{2\chi}{\omega}} = \sqrt{\frac{2\kappa}{\rho c_p \omega}} \quad (19)$$

  Substitute into wavelike assumption

$$T_1(y,t) = T_1 e^{-y/\delta_\kappa}\left[\cos(y/\delta_\kappa) + j\sin(y/\delta_\kappa)\right] e^{j\omega t} \quad (20)$$

Thermal Boundary Layer

- Fluid over a plate with oscillating temperature

$$T_1(y,t) = T_1 e^{-(1+j)y/\delta_\kappa} e^{j\omega t} \qquad (21)$$

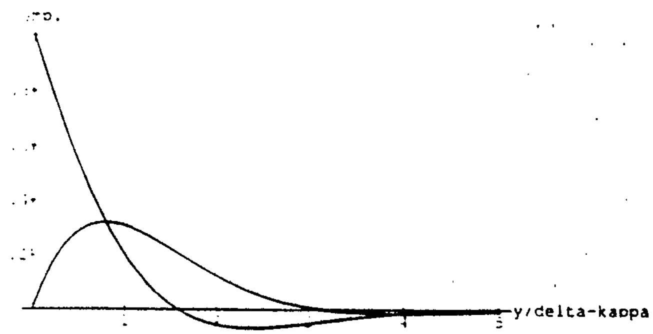

- Oscillating fluid temp. over an isothermal plate

$$T_1(y,t) = T_1\left[1 - e^{-(1+j)y/\delta_\kappa}\right] e^{j\omega t} \qquad (22)$$

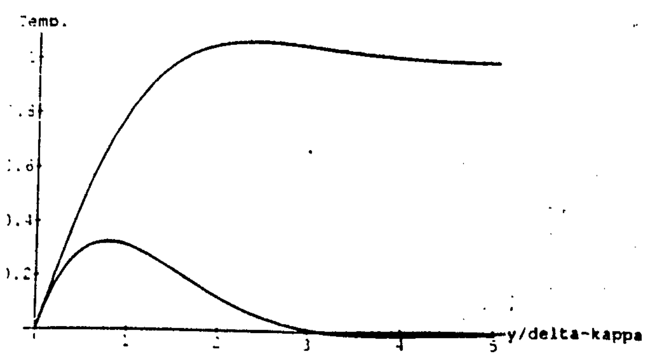

Analogous Boundary Layers

- Viscous boundary layer, δ_μ

  Exploit isomorphism with the Navier-Stokes equation

$$\delta_\mu = \sqrt{\frac{2\nu}{\omega}} = \sqrt{\frac{2\mu}{\rho\omega}} \qquad (23)$$

In air, $\delta_\mu = 0.21\ \mathrm{cm}/(f)^{1/2}$ or 100 μm @ 440 Hz

The quantification of the saying "still waters run deep"

- Electromagnetic skin depth

$$\delta = \sqrt{\frac{2}{\omega\sigma\mu}} \qquad (24)$$

In sea water δ = 30 m @ 60 Hz and 2 cm @ 1 MHz

In copper δ = 2.2 mm @ 1 kHz and 66 μm @ 1 MHz

- Mass diffusion length

$$\ell = \sqrt{\frac{2D}{\omega}} = \sqrt{2D\tau} \qquad (25)$$

τ = Diffusion time

For Argon in Helium, $\ell = 1.2\ \mathrm{cm}\ (\tau)^{1/2}$

Adiabatic Propagation

- Thermal diffusion

  What is the "speed of heat"?

  We could have solved for the thermal phase speed.

  Again, from the Fourier Eq'n: $j\omega = -\chi k^2$ (17)

$$c_{phase}^{THERMAL} = \left|\frac{\omega}{k}\right| = \left|\sqrt{j\chi\omega}\right| = \sqrt{\frac{\omega\kappa}{\rho c_p}} \qquad (26)$$

  Same result is obtained if we set $\delta_\kappa = \lambda\!\!\!^{-} = \lambda/2\pi = k^{-1}$

  Sound speed is non-dispersive (frequency independent).

  The thermal "wave" is **dispersive**, $c^{THERMAL} \propto \sqrt{\omega}$

  Critical frequency, ω_{crit}, when $c_{phase} = c^{THERMAL}$

$$\omega_{crit} = \frac{\rho c_{phase}^2 c_p}{\kappa} = \frac{\gamma p_o c_p}{\kappa} \qquad (27)$$

  In air, $f_{crit} = \omega_{crit}/2\pi \approx 860$ MHz $\Rightarrow \lambda/2\pi = \lambda\!\!\!^{-} \approx 0.065\ \mu$m.

  Adiabatic at $f < f_{crit}$ (heat moves too slow)

  Isothermal at $f > f_{crit}$ ($\Delta T = T(t) - T_o$ can't develop)

- Mean-free-path

  Phenomenology assumes the continuum hypothesis

  Many collisions are required in any "fluid volume" $<< \lambda\!\!\!^{-3}$

$$\langle \ell \rangle = \frac{1}{\sqrt{2}\,\pi d^2 n} \qquad (28)$$

  Ballistic propagation for $\lambda\!\!\!^{-} < \langle \ell \rangle$

  In air, $\langle \ell \rangle \approx 0.10\ \mu$m - **ITS NEVER ISOTHERMAL!**

Adiabatic Temperature Change

- Adiabatic compression

  Cannot have adiabatic and isothermal compression

  $5/3 \geq \gamma > 1$

  Adiabatic Equation of State

$$pV^\gamma = const. \qquad (4)$$

  Use the ideal gas law, PV=RT, to substitute for (pV)

$$pV^\gamma = (pV)^\gamma p^{1-\gamma} = (RT)^\gamma p^{1-\gamma} = const. \qquad (29)$$

  Explicit temperature dependence

$$p^{1-\gamma} T^\gamma = some\ other\ const. \qquad (30)$$

  Take the natural log and differentiate

$$(1-\gamma)\frac{p_1}{p_m} = -\gamma\frac{T_1}{T_m} \qquad (31)$$

  Adiabtic temperature change, T_1

$$T_1 = \frac{(\gamma-1)}{\gamma}\frac{p_1}{p_m}T_m = \frac{T_m\beta}{\rho_m c_p}p_1 \qquad (32)$$

- Typical values

  Normal speech in air (74 dB_{SPL} = 0.1 Pa_{rms})

  p_o = 101,325 Pa, γ = 1.4027, T = 293 °K (20 °C)

  T_1 = 83 μ°K_{rms}

  Thermoacoustic refrigerator (SETAC = 65 kPa_{rms})

  p_o = 2.1 MPa, γ = 5/3, T = 293 °K (20 °C)

  T_1 = 3.6 °K_{rms} = 18.5 °$F_{p\text{-}p}$

Acoustic Standing Wave

- Fundamental Plane Wave Mode

  One dimensional (below cut-off)

  Ideal boundary conditions, volume velocity source

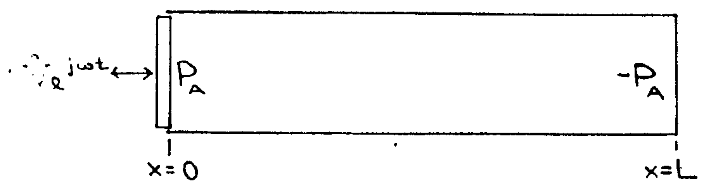

- Pressure distribution

$$p_1(x,t) = P_A \cos kx\, e^{j\omega t} \quad (33)$$

  Half-wavelength resonance (L = λ/2)

$$k = \frac{2\pi}{\lambda} = \frac{\omega}{a} = \frac{\pi}{L} \quad (34)$$

- Longitudinal particle velocity at resonance

  Euler's equation

$$\frac{\partial u_1}{\partial t} = j\omega u_1 = \frac{-1}{\rho_m}\frac{\partial p_1}{\partial x} = \frac{-P_A}{\rho_m} k \sin kx \quad (35)$$

  Particle velocity

$$u_1(x,t) = \frac{-j P_A}{\rho_m a} \sin kx\, e^{j\omega t} \quad (36)$$

  Note 90° phase shift between pressure and velocity

  Particle displacement is just the integral

$$x_1(x,t) = \frac{u_1(x,t)}{j\omega} = \frac{-\lambda}{2\pi}\frac{P_A}{\gamma p_m} \sin kx\, e^{j\omega t} \quad (37)$$

Critical Temperature Gradient

- Far from the resonator surface ($y \gg \delta_\kappa$)

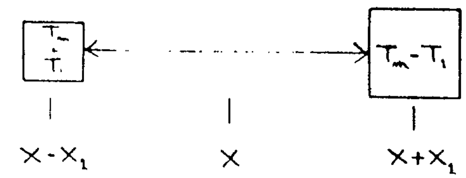

For now, let $\nabla T_m = 0$, $T(x) = T_m + T_1(x)$

$$T_1 = \frac{(\gamma-1)}{\gamma}\frac{p_1}{p_m} T_m = \frac{(\gamma-1)}{\gamma}\frac{T_m}{p_m} P_A \cos kx \quad (38)$$

Particle position, $x + x_1$

$$x_1(x) = \frac{-\lambda}{2\pi}\frac{P_A}{\gamma p_m} \sin kx \quad (39)$$

Their ratio is independent of pressure

$$\nabla T_{crit} = \frac{2T_1}{2x_1} = 2\pi(\gamma-1)\frac{T_m}{\lambda} \cot kx \quad (40)$$

This result diverges at the pressure anti-node!

Typical 'fridge, kx = 0.25 λ = 2.0 m, T_m = 270 °K

∇T_{crit} = 22 °C/cm

- At the resonator surface (y = 0), $T_1 = 0$

The Simple Lagrangian Model

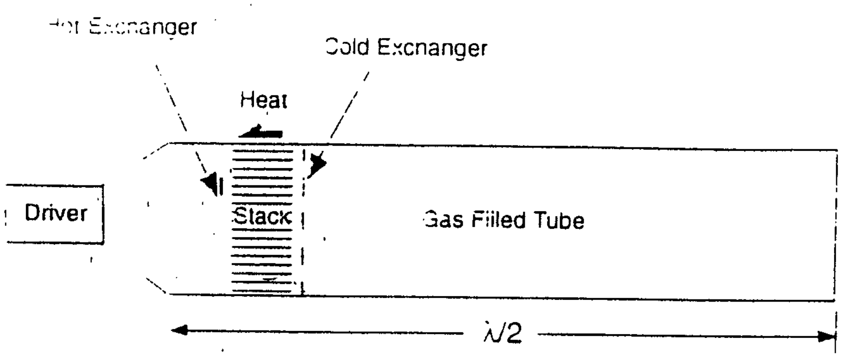

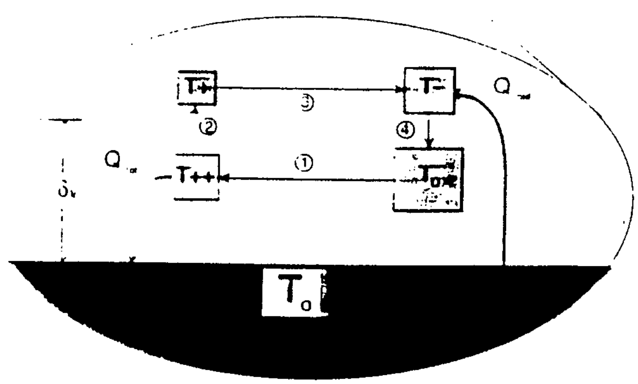

Heat Transfer

- A very crude heat transport model with $\nabla T_m = 0$

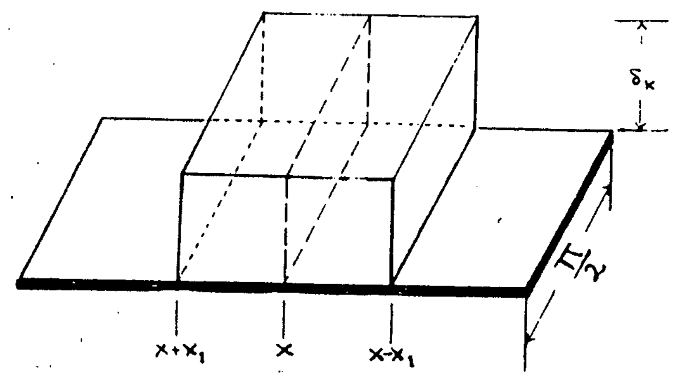

The gas between x and $x-x_1$ picks up heat, Q_{cold}

$$Q_{cold} = C_p \Delta T = \rho_m c_p \left(\frac{\Pi}{2}\frac{x_1}{2}\delta_\kappa\right)\left(T_m - \frac{T_1}{2}\right) \quad (41)$$

The gas between x and $x+x_1$ deposits Q_{hot}

$$Q_{hot} = C_p \Delta T = \rho_m c_p \left(\frac{\Pi}{2}\frac{x_1}{2}\delta_\kappa\right)\left(T_m + \frac{T_1}{2}\right) \quad (42)$$

Resulting in a net heat transfer, Q_{net}

$$Q_{net} = Q_{hot} - Q_{cold} = \rho_m c_p \left(\frac{\Pi \delta_\kappa}{4}\right) x_1 T_1 \quad (43)$$

Using $x_1 = u_1/\omega$ and $T_1 = (T_m \beta / \rho_m c_p)\, p_1$,

$$Q_{net} = T_m \beta \left(\frac{\Pi \delta_\kappa}{4}\right) p_1 \frac{u_1}{\omega} \quad (44)$$

Slide 17

Heat Transfer Rate

- Heat transfer rate

$$\dot{Q}_{net} = \omega\, Q_{net} = T_m \beta \left(\frac{\Pi \delta_\kappa}{4} \right) p_1 u_1 \quad (45)$$

It depends on the product, $p_1 u_1$, which is max at $x=\lambda/4$

∇T_{crit} is max at $x = 0$

- Stack temperature gradient, $\nabla T_m \neq 0$

$$\dot{Q}_{net} = T_m \beta \left(\frac{\Pi \delta_\kappa}{4} \right) p_1 u_1 (\Gamma - 1) \quad (46)$$

Where $\Gamma = \nabla T_m / \nabla T_{crit}$

- Enthalpy flux density

Include potential and thermal energy

$$\dot{H}_2 = \Pi \int_0^\infty \left[\rho_m c_p \langle T_1 u_1 \rangle + (1 - T_m \beta) \langle p_1 u_1 \rangle \right] dy \quad (47)$$

- Thermal back-flow

Both the stack and gas conduct heat

$$\dot{H}_2 = T_m \beta \left(\frac{\Pi \delta_\kappa}{4} \right) p_1 u_1 (\Gamma - 1) - \Pi (y_o K + \ell K_s) \frac{d T_m}{d x} \quad (48)$$

- Efficiency?

How much work must be done to move heat?

First we must calculate the dissipation.

Slide 18

Viscous Surface Losses

- Thermoviscous dissipation

Well-know (Stokes/Kirchhoff) surface losses

$$\dot{e} = \frac{\delta_\mu}{4} \rho_m u_1^2 \omega + \frac{\delta_\kappa}{4} \frac{(\gamma - 1)}{\gamma} \frac{p_1^2}{p_m} \omega \quad (49)$$

Viscous "scrubbing" (fluid friction)

Irreversible thermal conduction

Viscous is simple

Thermal is important!

- Viscous dissipation at a surface

Average dissipated power = <**F** • **v**> (50)

Time average power/unit area = $\dot{e}$

$$\dot{e}_\mu = \frac{\langle \vec{F}_\mu \bullet \vec{u} \rangle}{A} = \langle p_{xy} u_1 \rangle = \mu \left\langle \frac{\partial u_1}{\partial y} u_1 \right\rangle \quad (51)$$

Exponential length gives $\partial/\partial y = 1/\delta_\mu$

$$\dot{e}_\mu = \mu \frac{v_x^2}{2 \delta_\mu} \quad (52)$$

Stack surface area = $\Pi\, \Delta x$ and $\delta_\mu = (2\mu/\rho_m \omega)^{1/2}$

$$\dot{W}_2^{visc} = \frac{-\Pi \delta_\mu}{4} \Delta x\, \omega\, \rho_m u_1^2 \quad (53)$$

Dissipative volume = $\Pi\, \delta_\mu \Delta x$

Kinetic energy density = $(1/2)\, \rho_m u^2$

Positive-definite energy dissipation

Slide 19

Thermal Surface "Losses"

- Conduction "losses" will depend on phasing

  Calculate the rate of p dV work per unit volume

$$\dot{w} = \frac{p}{V}\frac{dV}{dt} = -\frac{p}{\rho}\frac{d\rho}{dt} \qquad (54)$$

  Expand the density total time derivative

$$\frac{d\rho}{dt} = \frac{\partial \rho}{\partial t} + u\frac{\partial \rho}{\partial x} = j\omega\rho_1 + u_1\frac{\partial \rho_m}{\partial x} \qquad (55)$$

  When multiplied by $p = p_m + p_1$, only one term survives the time averaging process

$$\dot{w} = -\left(\frac{\omega}{\rho_m}\right)\langle j\, p_1\, \rho_1\rangle = -\frac{1}{2}\omega\beta p_1 \,\mathrm{Im}[T_1] \qquad (56)$$

  Integrate density away from the plate surface

  For an ideal gas

$$\dot{W}_2^{therm} = \frac{\Pi\delta_\kappa}{4}\Delta x\,\omega\frac{(\gamma-1)}{\gamma\, p_m}p_1^2(\Gamma-1) \qquad (57)$$

- Thermal dissipation

  For $\nabla T_m = 0 \Rightarrow \Gamma = 0$, $W_2 < 0$, as in Kirchhoff

- Acoustic engine (Sondhauss Tube, 1850)

  For $\nabla T_m > \nabla T_{crit} \Rightarrow \Gamma > 1$, $W_2 > 0$!

  Compressed parcels get larger

  Expanded parcels get smaller

  Stack does work on the gas

Slide 20

Review of Fundamentals

- Sound in "bulk" is adiabatic ($\lambda/2\pi >> \delta_\kappa$)

  Pressure wave have associated temperature effects

$$T_1 = \frac{(\gamma-1)}{\gamma}\frac{p_1}{p_m}T_m = \frac{T_m\beta}{\rho_m c_p}p_1 \qquad (32)$$

  Standing wave exhibits critical temperature gradient

$$\nabla T_{crit} = 2\pi(\gamma-1)\frac{T_m}{\lambda}\cot kx \qquad (40)$$

  Heat transport characterized by a diffusion length

$$\delta_\kappa = \sqrt{\frac{2\chi}{\omega}} = \sqrt{\frac{2\kappa}{\rho c_p\,\omega}} \qquad (19)$$

- Short Stack Approximation ($\Delta x << \lambda/2\pi$)

  Energy is transported in standing waves near surfaces

$$\dot{H}_2 = -\left(\frac{\Pi\delta_\kappa}{4}\right)T_m\beta p_1 u_1(\Gamma-1) - \Pi(y_o K + \ell K_s)\frac{dT_m}{dx} \qquad (48)$$

  Where $\Gamma = \nabla T_m/\nabla T_{crit}$

  For $\Gamma < 1$, the sound wave opposes thermal conduction

  Energy is also absorbed and produced near surfaces

$$\dot{W}_2 = \frac{\Pi\delta_\kappa}{4}\Delta x\,\omega\frac{(\gamma-1)}{\gamma\, p_m}p_1^2(\Gamma-1) - \frac{\Pi\delta_\mu}{4}\Delta x\,\omega\,\rho_m u_1^2 \qquad (58)$$

  For $\Gamma > 1$, and instability is possible

- Thermoacoustics is superficial science

Prime Mover

- Acoustic instability ($R_m < 0$)

  Neglect other losses in the resonator

$$W_2 = \frac{\Pi\delta_\kappa}{4}\Delta x\,\omega\frac{(\gamma-1)}{\gamma p_m}p_1^2(\Gamma-1) - \frac{\Pi\delta_\mu}{4}\Delta x\,\omega\,\rho_m u_1^2 \quad (59)$$

  Set $W_2 = 0$ to determine onset of acoustic oscillations

$$(\Gamma-1)_{onset} = \frac{\delta_\mu \rho_m u_1^2(\gamma p_m)}{\delta_\kappa(\gamma-1)p_1^2} = \frac{\sqrt{\sigma}}{(\gamma-1)}\tan^2 kx \quad (60)$$

  Where the Prandtl Number, $\sigma = (\delta_\mu/\delta_\kappa)^2$

  Additional losses ($\approx p_1^2$, u_1^2) increase $(\Gamma-1)_{onset}$

- Acoustic power generation

  Above onset, heat is converted to work

  Assume $Q_{hot} >> W$, neglect conduction, ideal gas $T_m\beta=1$

$$\dot{Q}_{hot} - \dot{Q}_{onset} \cong \dot{H}_2 = \left(\frac{\Pi\delta_\kappa}{4}\right)p_1 u_1(\Gamma-1)_{onset} \quad (61)$$

  Solve for P_A^2

$$P_A^2 = \frac{4(\gamma-1)}{\Pi\delta_\kappa\sqrt{\sigma}}\frac{\tan kx}{\cos^2 kx}\rho_m a\left(\dot{Q}_{hot} - \dot{Q}_{onset}\right) \quad (62)$$

  Should give a straight line for P_A^2 vs. Q_{hot}

Solar Prime Mover

- Sunny Pennsylvania

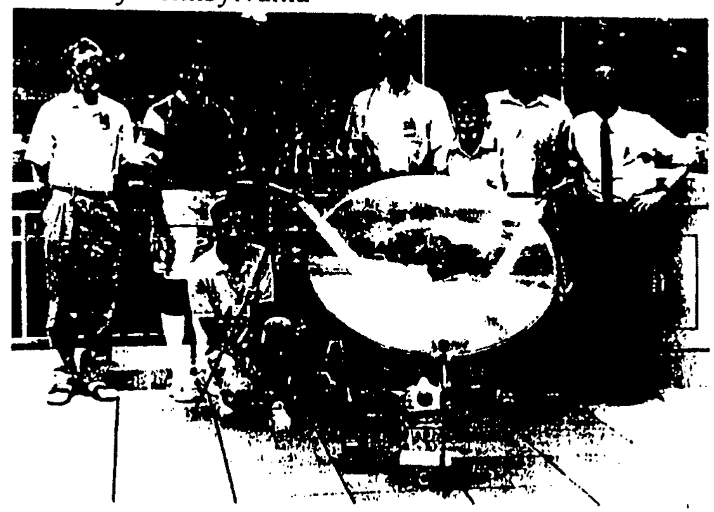

- Engine cross-section

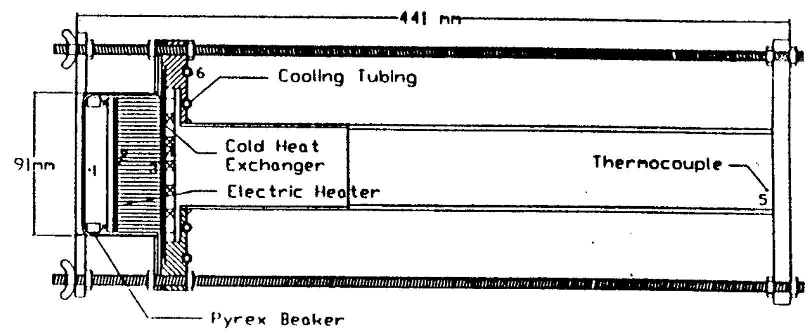

Prime Mover Performance

- Stack temperature difference

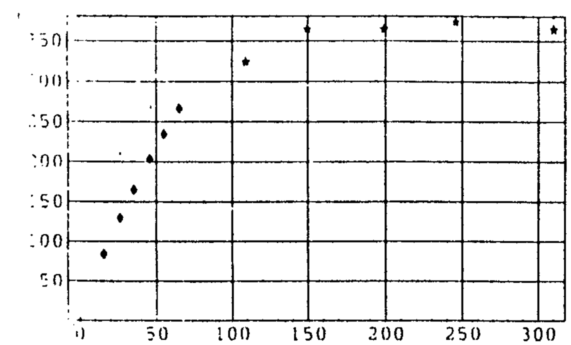

- Acoustic amplitude (P_A^2)

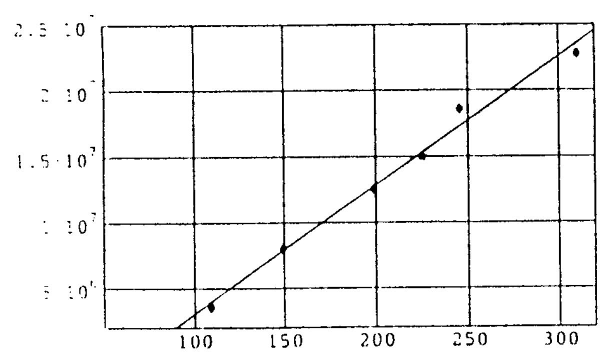

Solar Driven Ice Maker

- Engine cross-section

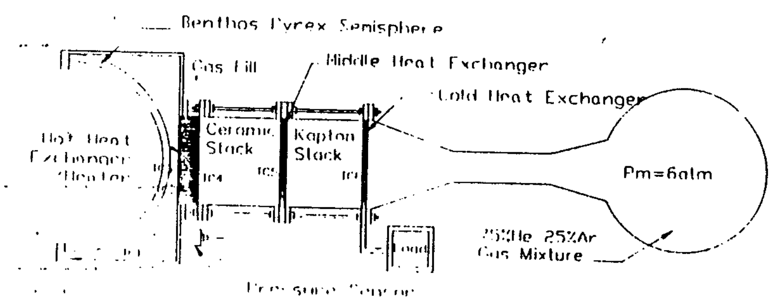

- Energy flow diagram

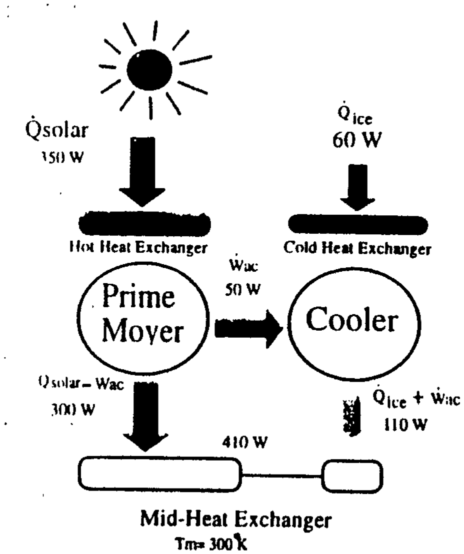

Thermodynamic Efficiency

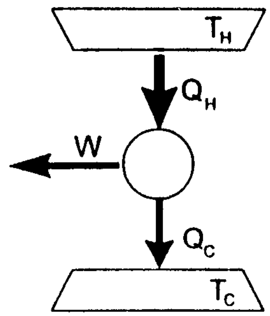

- Prime Movers

  The First Law, energy conservation

  $$Q_{hot} = W + Q_{cold} \quad (63)$$

  The Second Law, entropy does not decrease

  $$\frac{Q_{hot}}{T_{hot}} \geq \frac{Q_{cold}}{T_{cold}} \quad (64)$$

  Efficiency

  $$\eta = \frac{W}{Q_{hot}} \leq \frac{T_{hot} - T_{cold}}{T_{hot}} < 1 \quad (65)$$

- Solar Prime Mover

  Efficiency

  $$\eta = \frac{W}{Q_{hot}} = \frac{50\,W}{350\,W} = 0.14 < \frac{850 - 300}{850} = 0.65 \quad (66)$$

  22% of Carnot performance

  Reality will be more like 10-15% of Carnot

Coefficient-of-Performance

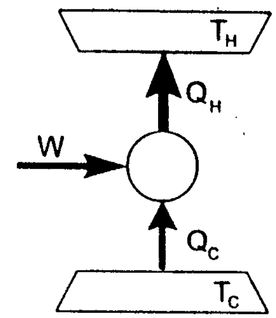

- Refrigerators

  Subject to the same two laws

  $$COP = \frac{Q_{cold}}{W} \leq \frac{T_{cold}}{T_{hot} - T_{cold}} = COP_{Carnot} \quad (67)$$

  The COP can be much greater than one!

  Coefficient-of-Performance relative to Carnot

  $$COPR = \frac{COP}{COP_{Carnot}} = \frac{Q_{cold}}{W}\frac{T_{hot} - T_{cold}}{T_{cold}} \leq 1 \quad (68)$$

- Solar Refrigerator

  Coefficient-of-Performance

  $$COP = \frac{60\,W}{50\,W} = 1.20 \leq \frac{263\,K}{50\,K} = 5.3 = COP_{Carnot}$$

  COPR = 23%

  Actual performance will be 15-20% of Carnot

Thermoacoustic Refrigerators

- Frankenfridge

  "I believe I can make a 'fridge from parts of others."

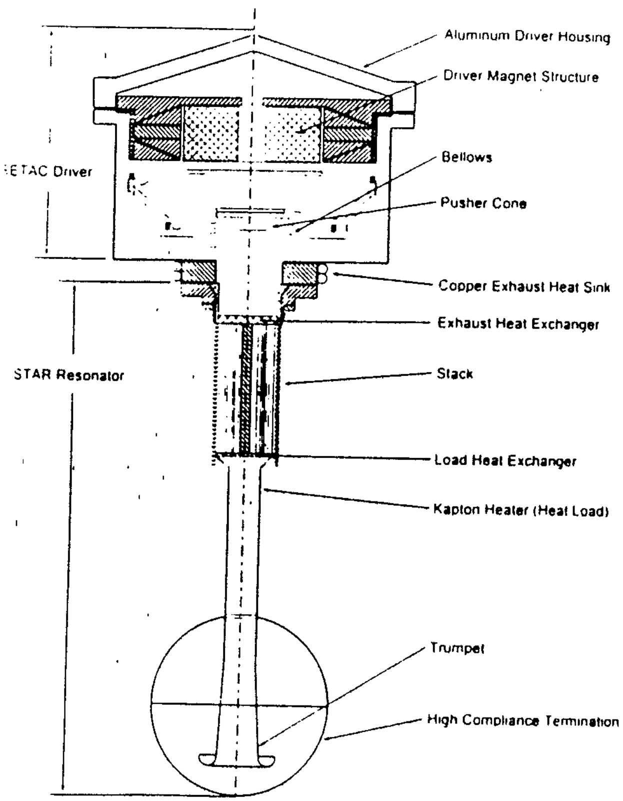

DELTAE Model

- Design Environment for Low-Amplitude ThermoAcoustic Engines (DELTAE)
  - G. Swift and W. Ward, Los Alamos Nat'l. Lab
    - <http://rott.esa.lanl.gov>
  - Solve the detailed equations in each segment
  - Match T and complex p and u between each segment
  - Solution vector of guesses and targets
  - Lots of useful elements
    - Transducers, different stack types
    - Gas and solid thermophysical properties
    - Free Targets
  - Designed by USERS for design and analysis
  - Excellent documentation!

- Modular
  - Frankenfridge

0	BEGIN - Globals: gas, pressure, frequency
1	ENDCAP - driver losses, volume velocity source
2-5	ISODUCT - bellows, flange, and tube
6	HXFRST - hot heat exchanger
7	STAKSLAB - roll-up stack
8	HXLAST - cold heat exchanger
9-11	INSCONE, INSDUCT - reducer, neck, and cone
12	COMPLIANEC - bulb
13	HARDEND - final boundary condition

DELTAE Model Agreement

- Frankenfridge heat pumping

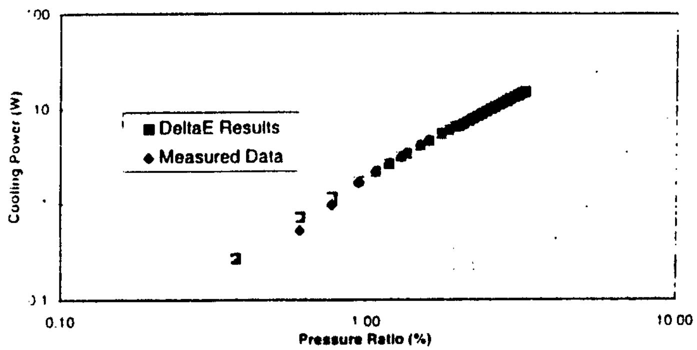

Excellent agreement at low amplitudes ($p_1/p_m < 3\%$)
Comparison under actual measurement conditions

- Systematic degreadation at high amplitudes

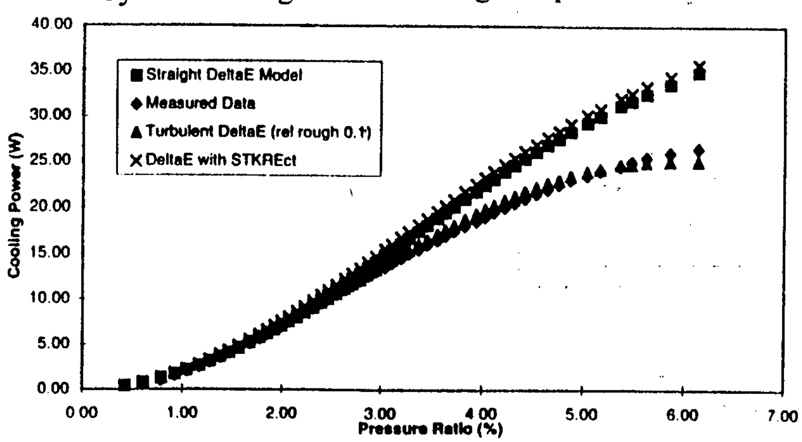

Thermoacoustic Refrigerators

- One design approach
  Specify requirements
  Heat pumping power, Q_s, and span $\Delta T = T_{hot} - T_{cold}$
  Cooling power

$$\dot{Q}_{cold} = \dot{H}_2 - \dot{W}_2 \qquad (69)$$

  Cooling power density

$$\frac{\dot{Q}_{cold}}{A} = \frac{p_m a}{F.O.D.}\left(\frac{p_1}{p_m}\right)^2 \qquad (70)$$

  For stack of cross-sectional area A
  Figure-of-Demerit depends upon design 40<F.O.D.<120

- Optimization choices
  What is your highest acceptable pressure?
  What limits your highest pressure ratio, P_A/p_m?
  Risk turbulence for reduced length?
  What is your minimum acceptable COPR?
  Trade sound speed for lower Prandtl number?
  Multiple stacks and heat exchangers?

Slide 31

Stack Position

- The trade-off: Efficiency *vs.* Power Density

Smaller kx: larger ∇T_{crit}

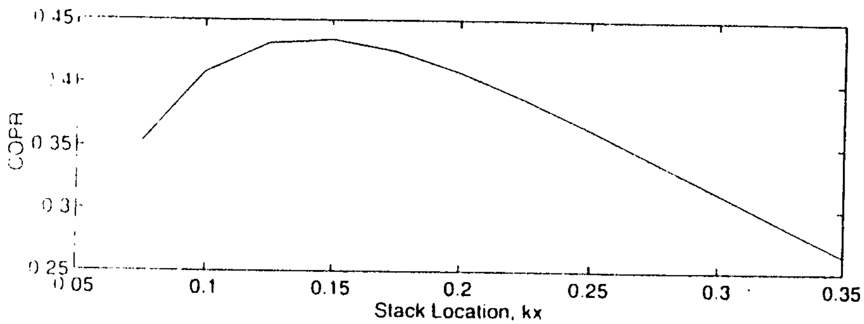

Shorter stack, higher COPR

Smaller kx: lower power density

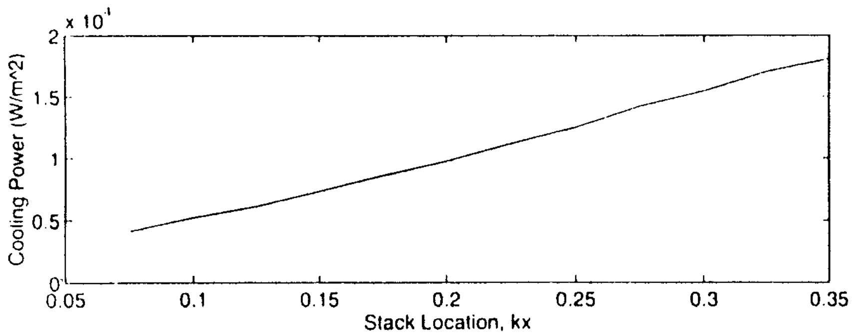

Requires larger stack diameter

Slide 32

Stack Performance

- Coefficient-of-Performance

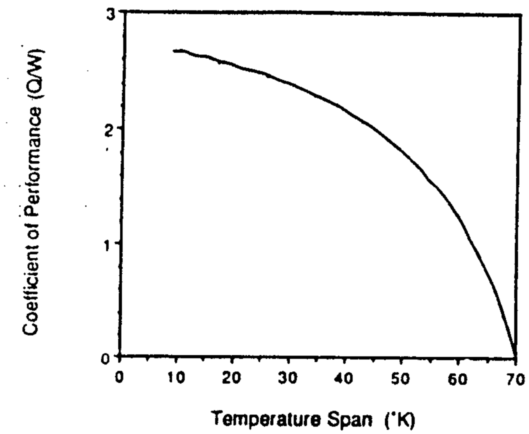

- Coefficient-of-Performance relative to Carnot

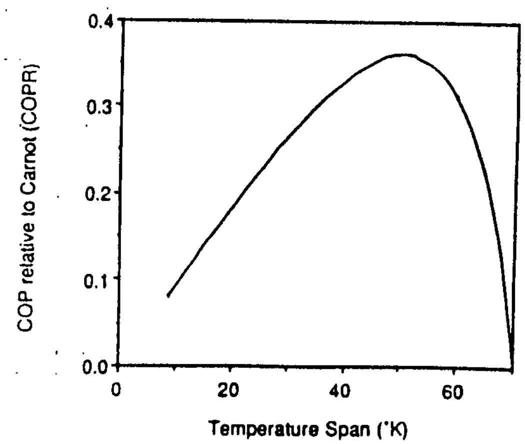

SETAC

- Shipboard Electronics ThermoAcoustic Cooler
  USS Deyo (DD-989) April, 1995
  It doesn't look like the moving parcel picture!

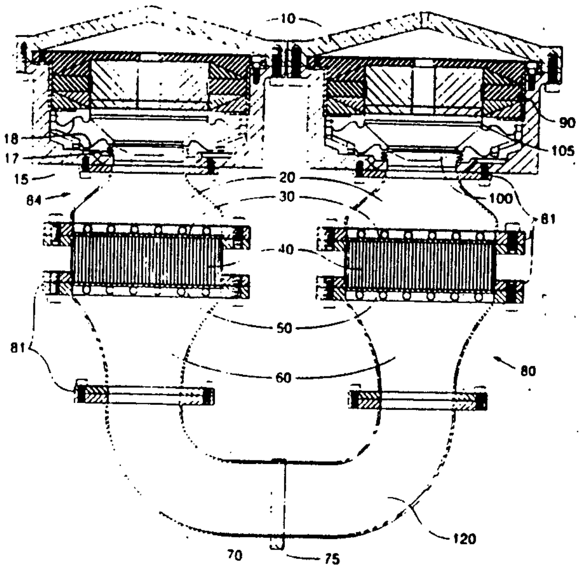

17	Metal bellows
18	Steel driver suspension
30	Hot heat exchangers
40	Stacks
50	Cold heat exchangers
90	Magnet structure
100	Piston
105	Voice coil

SETAC Operating Parameters

Fluid/Solid Thermophysical Parameters	Symbol	Value	Units
Mean pressure	p_m	2.07	MPa
Mean temperature in stack	T_m	290	K
Atomic mass (94.4%He/5.6%Ar)	m	6.014	a.m.u.
Gas mixture density	ρ_m	5.165	kg/m^3
Gas mixture sound speed	a	817.3	m/sec
Gas mixture isobaric specific heat	c_p	3.455	J/gK
Gas mixture polytropic coefficient (c_p/c_v)	γ	1.667	
Gas mixture Prandtl number	σ	0.524	
Gas mixture shear viscosity	μ	2.014x10^{-5}	Kg/sec-m
Gas mixture thermal conductivity	K	1.33	mW/cm-K
Stack thermal conductivity	K_s	1.89	mW/cm-K
Stack specific heat	c_s	1.056	J/gK
Stack mass density	ρ_s	1.42	g/cm^3

Stack Dimensions	Symbol	Value	Units
Stack plate thickness	$2l$	52	µm
Stack plate separation	$2y_0$	280	µm
Stack length	Δx	4.03	cm
Center position of the stack	x	6.06	cm
Stack diameter	$2R$	11.0	cm
Stack perimeter	$\Pi=\pi R^2/(y_0+l)$	57.3	m
Stack heat capacity correction factor	ϵ_s	0.092	
Normalized stack spacing	y_0/δ_κ	1.63	
	y_0/δ_ν	2.25	

Heat Exchanger Dimensions	Symbol	Value	Units
Heat exchanger length	Δx^{HX}	2.54	mm
Heat exchanger plate thickness	$2l^{HX}$	152	µm
Heat exchanger plate separation	$2y_0^{HX}$	380	µm

Calculated quantities	Symbol	Value	Units
Operating frequency	f	320	Hz
Operating radian frequency	$\omega = 2\pi f$	2011	rad/s
Thermal penetration depth	δ_κ	86.1	µm
Viscous penetration depth	δ_ν	62.3	µm
Resonator half-wavelength	$\lambda_{cold}/2$	1.23	m
Mean wavenumber in stack	$k = 2\pi/\lambda$	2.55	m^{-1}
Peak acoustic pressure amplitude	P_A	92.3	kPa
Peak acoustic velocity in stack	$\langle u_1^s \rangle$	3.8	m/s
Peak acoustic particle displacement	$d=\langle u_1^s \rangle/\omega$	1.9	mm

Slide 35

Anharmonic Resonator Shape

- Harmonic suppression

  Modes of a uniform cross-secton closed-closed tube

$$f_n = n f_1 = n\frac{a}{2L}; \quad n = 1,2,3,\ldots \qquad (71)$$

  The modal structure reinforces shock formation

- Simple incompressible inclusion

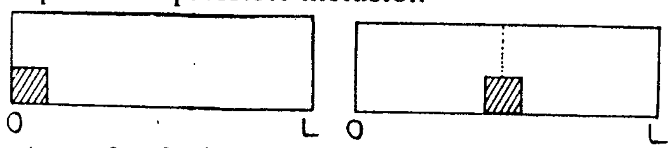

  At x = 0 or L, the effective length decreases

  The frequency of the perturbed mode increases, $f_1^* > f_1$

  At x = L/2, the effective length increases

  The frequency of the perturbed mode decreases, $f_1^* < f_1$

  The second perturbed mode frequency increases, $f_2^* > f_2$

  Shock formation is suppressed

  Macrosonix Corp takes this to the limit by "shaping"!

- SETAC quasi-Helmholtz shape

  Shorter length for the same frequency

  More space for stacks

  Hofler showed thermoviscous dissipation is reduced

  Non-linear effects may bite back at high amplitudes

Slide 36

Piston Area

- Simple driver electro-mechanical model

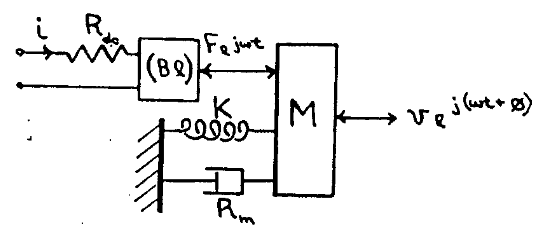

- Assume driver is located at pressure anti-node, P_A

  Driver delivers power, W_2, to the resonator

$$\dot W_2 = \frac{P_A \dot V}{2} = \frac{P_A v A}{2} = \frac{F v}{2} = \frac{B \ell i v}{2} \qquad (72)$$

  Joule heating due to voice coil resistance, R_{dc}

$$\dot W_{dc} = R_{dc}\frac{i^2}{2} = \frac{R_{dc}}{2}\left(\frac{P_A}{B\ell}\right)^2 A^2 \qquad (73)$$

  Increases like since force (current) increases with area

  Dissipation due to mechanical resistance, R_m

$$\dot W_m = R_m \frac{v^2}{2} = 2R_m\left(\frac{\dot W_2}{P_A}\right)^2 \frac{1}{A^2} \qquad (74)$$

  Decreases like A^{-2} since velocity depends on area

  Optimum piston area when losses are equal

$$A_{opt} = \left(\frac{4R_m}{R_{dc}}\right)^{1/4} \frac{(\dot W_2 B\ell)^{1/2}}{P_A} \qquad (75)$$

Slide 37

Voice Coil Efficiency

- Efficiency depends primarily the mass of copper

  Force on a current carrying conductor in mag. field

  $F = B\ell i$ (76)

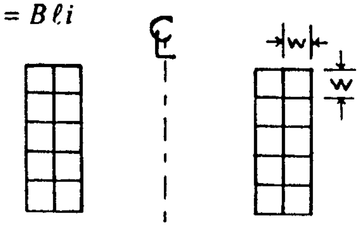

Voice coil resistance if conductor volume, $V_{Cu} = w^2 l$

$$R_{dc} = \rho_{Cu}\frac{\ell}{w^2} = \rho_{Cu}\frac{V_{Cu}}{w^4} \quad (77)$$

Voice coil dissipation, Π_{dc}

$$\Pi_{dc} = R_{dc}\frac{i^2}{2} = \frac{\rho_{Cu}V_{Cu}}{2w^4}i^2 \quad (78)$$

Given a required force and available magnetic field

$$i^2 = \left(\frac{F}{B}\right)^2\left(\frac{1}{\ell^2}\right) = \left(\frac{F}{B}\right)^2\frac{w^4}{V_{Cu}^2} \quad (79)$$

Π_{dc} depends only on the type and quantity of material

$$\Pi_{dc} = \frac{\rho_{Cu}}{2V_{Cu}}\left(\frac{F}{B}\right)^2$$

Slide 38

Moving Magnet Electrodynamic

- Efficiency depends primarily the mass of copper

  Put LOTS of copper in the stationary frame

- STAR Driver

  CFIC, Inc./Resonant Power Group, Troy, NY

  Electroacoustic efficiencies of 80-90%

  Power densities of ≈250 W/Kg

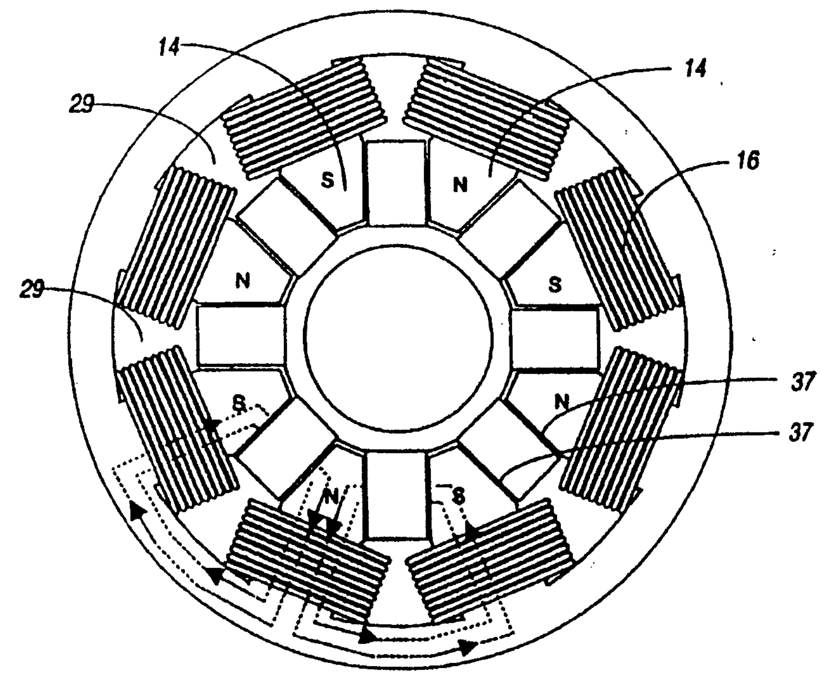

Slide

TRITON Resonator

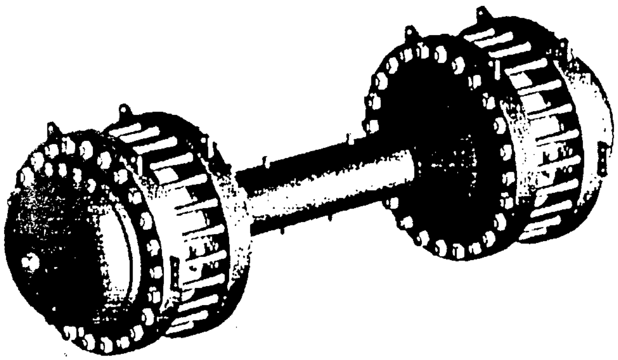

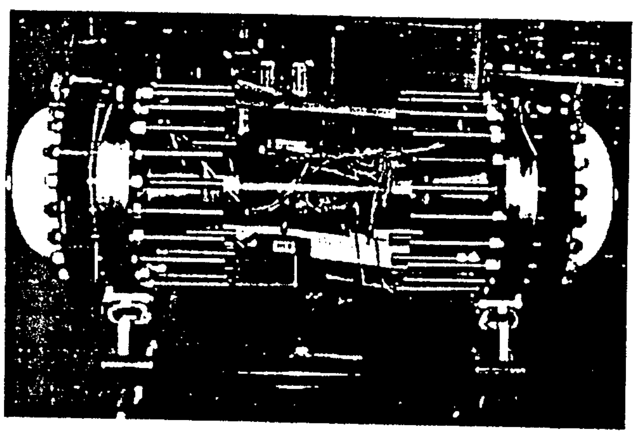

Slide 40

TRITON with Exposed Internals

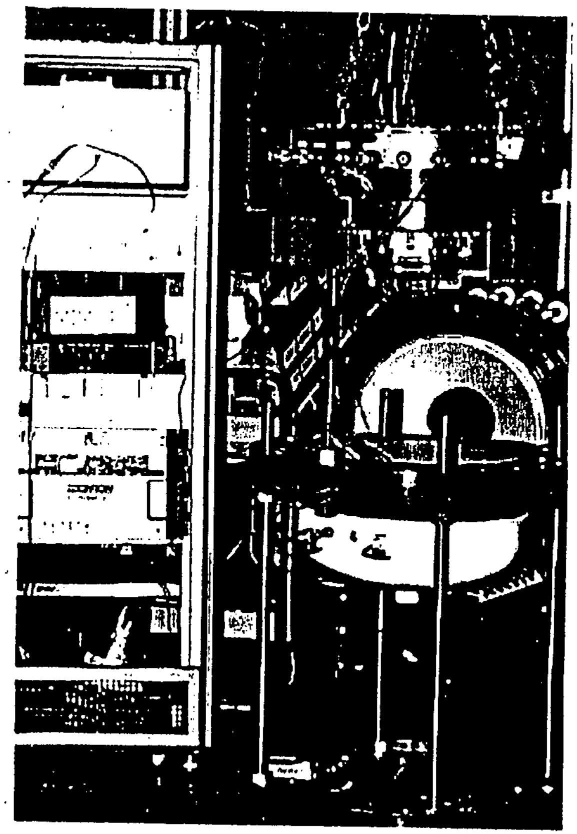

Slide 41

TRITON Hemielliptical Head Tests

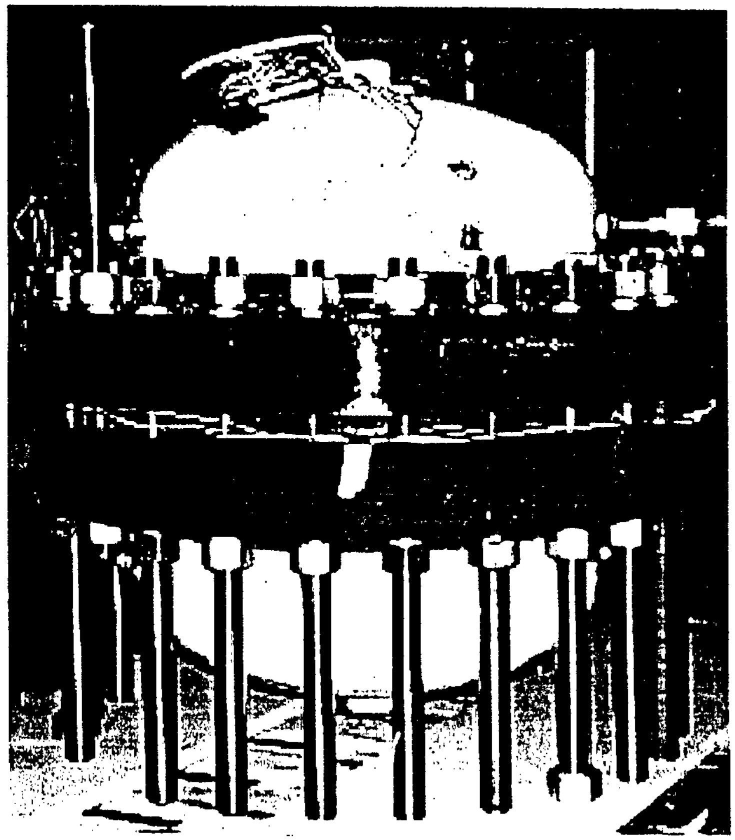

NONLINEAR ACOUSTICS

Mark F. Hamilton
Department of Mechanical Engineering
University of Texas

WHAT IS NONLINEAR ACOUSTICS?

Sources of nonlinearity in fluids:

1) Equation of state
2) Convection

Effects on plane waves:

- Propagation speed varies along waveform

Consequences:

- Wave distortion
- New frequencies
- Radiation pressures
- Acoustical streaming
- Shock waves

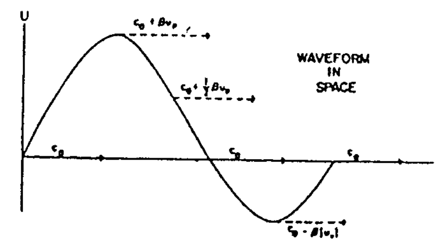

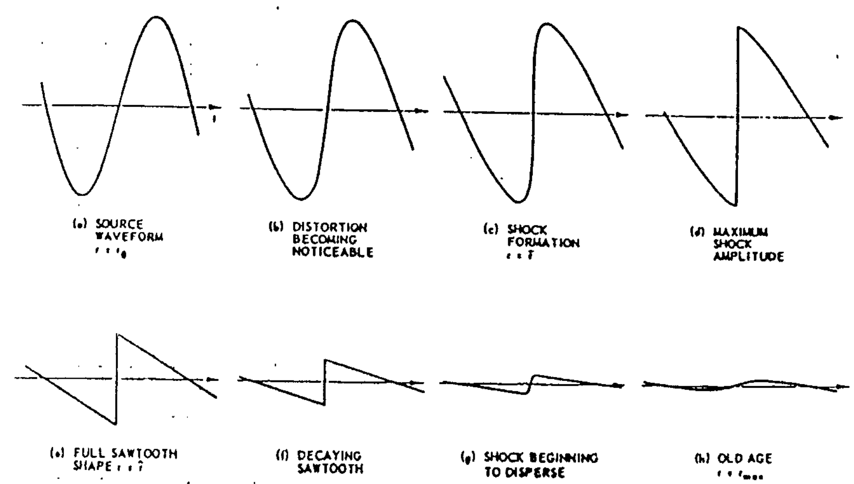

PROGRESSIVE PLANE WAVES

Exact equations for an isentropic gas:

Continuity: $\frac{\partial \rho}{\partial t} + u\frac{\partial \rho}{\partial x} + \rho\frac{\partial u}{\partial x} = 0$

Momentum: $\rho\frac{\partial u}{\partial t} + \rho u\frac{\partial u}{\partial x} + \frac{\partial p}{\partial x} = 0$

State: $\frac{p}{p_0} = \left(\frac{\rho}{\rho_0}\right)^\gamma$

Progressive waves (one direction):

$$\boxed{\frac{\partial u}{\partial t} + (c_0 + \beta u)\frac{\partial u}{\partial x} = 0}$$

where

$c_0 = \sqrt{\frac{\gamma p_0}{\rho_0}}$ = small signal sound speed

$\beta = \frac{\gamma+1}{2}$ = coefficient of nonlinearity

Exact solution:

$$\boxed{u = f\left(t - \frac{x}{c_0 + \beta u}\right)}$$ Poisson, 1808

Propagation speed:

$$\boxed{\frac{dx}{dt} = c_0 + \beta u}$$

PROPAGATION SPEED IN LIQUIDS

Expand general isentropic state equation $p = p(\rho)$

$$p = p_0 + \left(\frac{\partial p}{\partial \rho}\right)_{s,\rho_0}(\rho - \rho_0) + \frac{1}{2!}\left(\frac{\partial^2 p}{\partial \rho^2}\right)_{s,\rho_0}(\rho - \rho_0)^2 + \cdots$$

Let $p' = p - p_0$, $\rho' = \rho - \rho_0$:

$$p' = A\frac{\rho'}{\rho_0} + B\frac{1}{2!}\left(\frac{\rho'}{\rho_0}\right)^2 + C\frac{1}{3!}\left(\frac{\rho'}{\rho_0}\right)^3 + \cdots$$

where $\frac{B}{A} = \frac{\rho_0}{c_0^2}\left(\frac{\partial^2 p}{\partial \rho^2}\right)_{s,\rho_0}$ $\quad c_0^2 = \left(\frac{\partial p}{\partial \rho}\right)_{s,\rho_0}$

Liquids: $5 \lesssim \frac{B}{A} \lesssim 10$

Diatomic Gases: $\frac{B}{A} \simeq 0.4 \quad (= \gamma - 1)$

Propagation speed:

$$\frac{dx}{dt} = c_0 + \beta u$$

$$\beta = 1 + \frac{B}{2A}$$

$= 1.2$ in air

$= 3.5$ in water

R.T. Beyer
ASA 32
719 (1960)

[TR-4]

ALTERNATIVE FORMS OF B/A, C/A

Basic definitions:

$$A = \rho_0 \left(\frac{\partial P}{\partial \rho}\right)_{s,\rho_0} = \rho_0 c_0^2 , \quad B = \rho_0^2 \left(\frac{\partial^2 P}{\partial \rho^2}\right)_{s,\rho_0} , \quad C = \rho_0^3 \left(\frac{\partial^3 P}{\partial \rho^3}\right)_{s,\rho_0}$$

Alternative isentropic forms:

$$\frac{B}{A} = 2\rho_0 c_0 \left(\frac{\partial c}{\partial P}\right)_{s,\rho_0}$$

$$\frac{C}{A} = \frac{3}{2}\left(\frac{B}{A}\right)^2 + 2\rho_0^2 c_0^3 \left(\frac{\partial^2 c}{\partial P^2}\right)_{s,\rho_0}$$

- easier to measure change in sound speed as function of pressure
- sound waves can be used to produce the isentropic pressure variations ("finite amplitude method")

"Thermodynamic method":

$$\frac{B}{A} = 2\rho_0 c_0 \left(\frac{\partial c}{\partial P}\right)_{T,\rho_0} + \frac{2\alpha_T T_0 c_0}{c_p}\left(\frac{\partial c}{\partial T}\right)_{P,\rho_0}$$

- most accurate method of measurement

[Coppens et al., JASA 38, 797 (1965)]

[TR-5]

TABLE I

Values of B/A.
Except Where Indicated, All Values are at Atmospheric Pressure

Substance	T, °C	B/A
distilled water	0	4.2
	20	5.0
	40	5.4
	60	5.7
	80	6.1
	100	6.1
Pressure		
1 atm	30	5.2
200 kg/cm^2	30	6.2
4000	30	6.2
8000	30	5.9
sea water (3.5%)	20	5.25
methanol	20	9.6
thanol	0	10.4
	20	10.5
	40	10.6
n-propanol	20	10.7
N-butanol	20	10.7
acetone	20	9.2
beneze	20	9.0
chlorobenzene	30	9.3
liquid nitrogen	b.p.	6.6
benzyl alcohol	30	10.2
diethylamine	30	10.3
ethylene glycol	30	9.7
ethyl formate	30	9.8
heptane	30	10.0
hexane	30	9.9

Substance	T, °C	B/A
methyl acetate	30	9.7
cyclohexane	30	10.1
nitrobenzene	30	9.9
mercury	30	7.8
sodium	110	2.7
potassium	100	2.9
tin	240	4.4
indium	160	4.6
bismuth	318	7.1
monatomic gas	20	0.67
diatomic gas	20	0.40
methyl iodide	30	8.2
sulfur	121	9.5
glycerol (4% H_2O)	30	9.0
1,2 - dichloro-2 hexafluoro-cyclopentene (DHCP)	30	11.8

R.T. Beyer, *Nonlinear Acoustics* (1974)

[TR-6]

Characterization of biological media: L. Bjørnø

Table 1 Some B/A values for biological materials

	Biological material (and state)	Method*	B/A (and uncertainty)	Reference
1.	Bovine serum albumin (BSA) (20 g/100 cm³, 25°C)	Therm.	6.23 (± 0.25)	31
	BSA (22 g/100 cm³, 30°C)	F.A.	6.45 (± 0.30)	21
	BSA (38.9 g/100 cm³, 30°C)	F.A.	6.64	30
	BSA (38.9 g/100 cm³, 30°C)	Therm.	6.68 (± 0.2)	30
2.	Haemoglobin (50%, 30°C)	F.A.	7.6	22
3.	Whole porcine blood (12% haemoglobin, 7% plasma proteins, 30°C)	F.A.	6.2 (± 0.25)	22
4.	Beef liver (Whole, 23°C)	F.A.	7.75 (± 0.4)	22
	Beef liver (Homogenized, 23°C)	F.A.	6.8 (± 0.4)	22
	Beef liver (Whole, 30°C)	F.A.	6.42	30
	Beef liver (Whole, 30°C)	Therm.	6.88	30
	Beef liver (Whole, 30°C)	Therm.	6.54 (± 0.2)	32
	Dog liver (30°C)	F.A.	7.6 – 7.9 (± 0.8)	35
	Pig liver (25°C)	F.A.	6.7 (± 1.5)	36
	Human liver (Normal, 30°C)	F.A.	7.6 (± 0.8)	35
	Human liver (Congested, 30°C)	F.A.	7.2 (± 0.7)	35
5.	Pig fat	Therm.	10.9	27
	Pig fat	F.A.	11.0–11.3	27
	Human breast fat (22°C)	Therm.	9.21	32
	Human breast fat (30°C)	Therm.	9.91	32
	Human breast fat (37°C)	Therm.	9.63	32
6.	Canine spleen	F.A.	6.8	37
	Dog spleen	F.A.	6.8 (± 0.7)	35
	Human spleen (Congested)	F.A.	7.8	37
	Human spleen (Normal, 30°C)	F.A.	7.8 (± 0.8)	35
7.	Beef brain (30°C)	F.A.	7.6	27
8.	Beef heart (30°C)	F.A.	6.8–7.4	27
9.	Pig muscle (30°C)	F.A.	7.5–8.1	27
	Pig muscle (25°C)	F.A.	6.5 (± 1.5)	36
10.	Dog kidney (Normal, 30°C)	F.A.	7.2 (± 0.7)	35
	Canine kidney (30°C)	F.A.	7.2	37
11.	Human multiple myeloma (22°C)	F.A.	5.6	32
	Human multiple myeloma (30°C)	F.A.	5.8	32
	Human multiple myeloma (37°C)	F.A.	6.2	32

*Therm. = thermodynamic method; F.A. = finite amplitude method

the state of the tissue. Cancerous tissue normally shows a higher water fraction than normal tissue. The water fraction goes from 0.76 in normal liver tissue to 0.90 for multiple myeloma[32]. In general, water in tissue may be found as bound water and as free water in equilibrium with one another and expressed by

$$(H_2O)_n \rightleftharpoons n\,H_2O \tag{12}$$

where $(H_2O)_n$ is referred to as bound water while H_2O is generally referred to as free water. An increase in the bound state means that, on average, molecules have a greater degree of association with the neighbouring molecules which means that they are held more strongly together. This stronger binding also makes a larger ultrasonic pressure necessary in order to stretch the intermolecular bonds into their non-linear region, which microscopically is being felt as decreased non-linearity of the water according to Equation (3). This suggests that the magnitude of B/A in water-like media may be related to the relative amounts of bound and free water.

The equilibrium between these two water states, for instance expressed through the ratio of bound to free water, is closely related to the state and the nature of the tissue as shown by NMR studies[38]. Prospective relations between the ratio of bound to free water and the non-linear parameter B/A, have recently been suggested[39]. It was concluded by Yoshizumi *et al.*[39] that the temperature dependence of B/A, of water for instance, could be due to the change in the ratio of the bound to the free water with the change in temperature. Whether the estimates of the ratios of bound to free water determined from B/A measurements can be used for characterization of biological media such as human tissue is still an open question which has to be studied more closely.

The existence of several possible relationships between B/A of biological media and other physical qualities such as intermolecular potentials, macrostructure, water fraction and ratio of bound to free water of the biological media emphasize the need for further systematic studies. This will probably demand an internationally funded research programme where several qualified laboratories in various countries share a research programme over several years on advanced modelling of biological media.

In spite of the inhomogeneous character of biological materials such as tissues, where scattering, phase cancellations, dispersion, etc. influence the ultrasonic wave propagation, a reliable experimental procedure leading to reproducible B/A data should be developed to prove, *in vitro*, that B/A may be used for the characterization of biological media. If the uncertainties found in relation to the experimental data could be reduced for the thermodynamic or for the finite amplitude method – or maybe for both – an answer to the question of applicability of B/A for characterization of biological media may be found.

The prospective development of a clinically applicable

[TR-7]

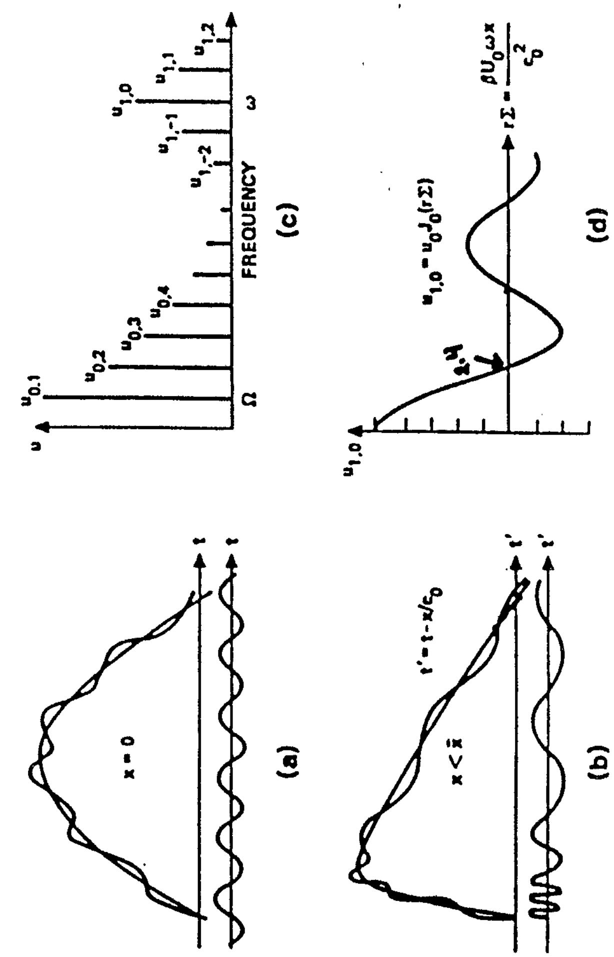

SUPPRESSION OF SOUND BY SOUND

TenCate, M.S. thesis, UT (1984)

[TR-8]

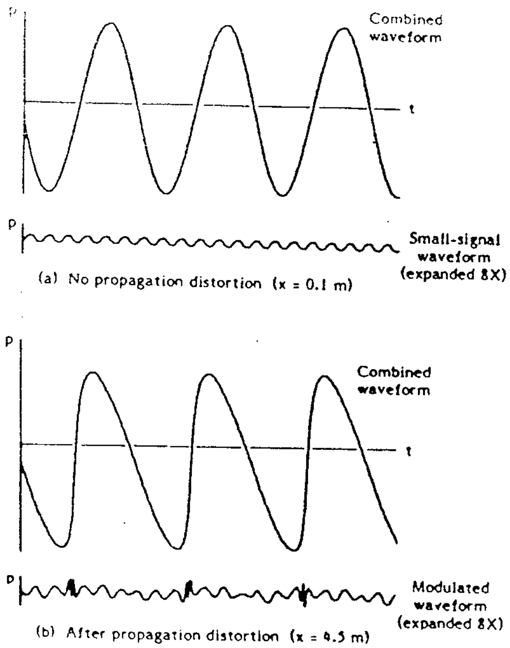

Figure 4.1
Demonstration of the collinear modulation of sound by sound

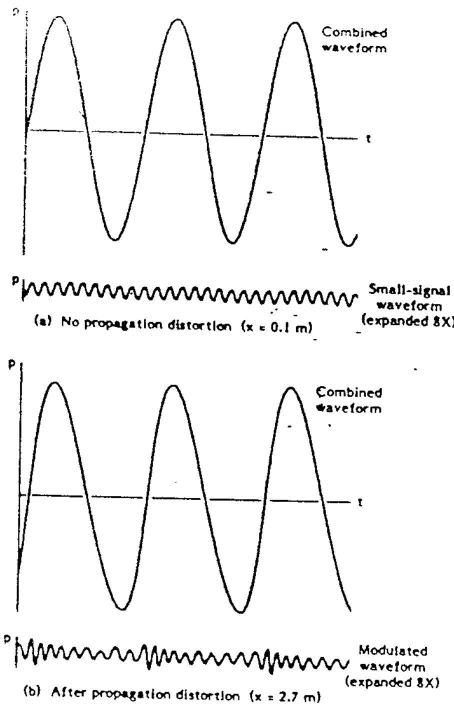

Figure 4.3
Demonstration of the noncollinear modulation of sound by sound

[TR-9]

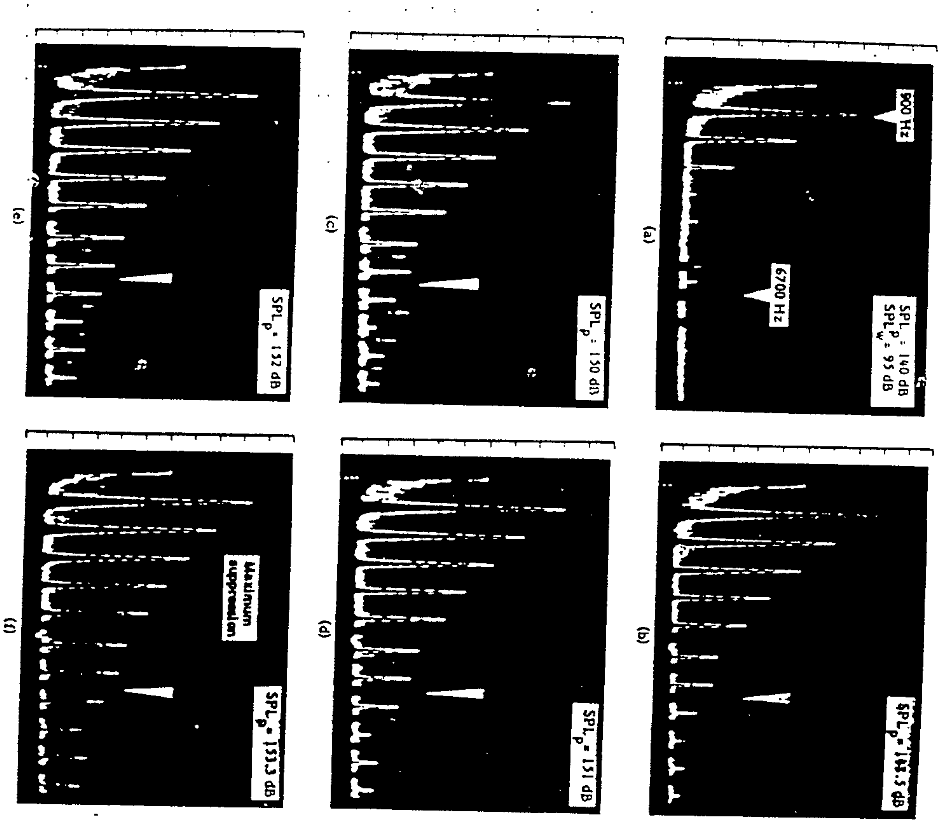

Figure 4.4
Observation of the modulation of sound by sound in the frequency domain

70

[TR-10]

Gong, Zhu, Du (1979)

有限振幅与小振幅平面声波的

非线性相互作用研究

(Nonlinear Interaction of a Finite-Amplitude Wave with a Small-Signal Wave in Air)

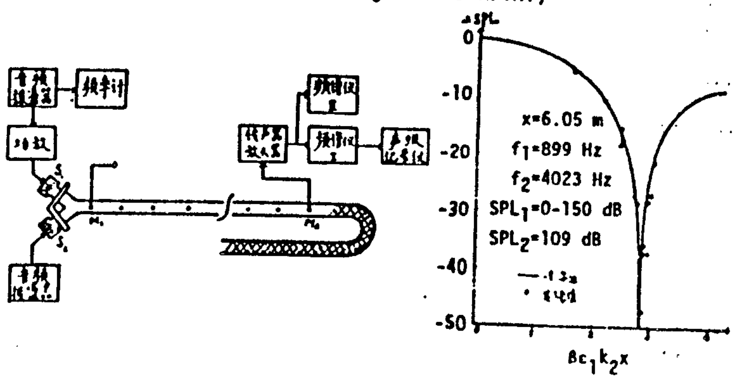

Ref. 59

[TR-11]

PERTURBATION

Differential Eqn.:

$$F\{u\} = G\{u^2\}$$

e.g., $F\{u\} = \frac{\partial u}{\partial t} + c_0 \frac{\partial u}{\partial x}$, $G\{u^2\} = -\frac{\beta}{2}\frac{\partial u^2}{\partial x}$

Expand:

$$u = \varepsilon u_1 + \varepsilon^2 u_2 + \varepsilon^3 u_3 + \cdots, \quad \varepsilon = \frac{u_0}{c_0} \ll 1$$

$O(\varepsilon)$: $F\{u_1\} = 0$

$O(\varepsilon^2)$: $F\{u_2\} = G\{u_1^2\}$

$O(\varepsilon^3)$: $F\{u_3\} = G\{u_1 u_2\}$

$\vdots$

ε	ε^2	ε^3
ω	2ω	$\omega, 3\omega$
ω_a, ω_b	$2\omega_a, 2\omega_b, \omega_a \pm \omega_b$	$\cdots$

PROCESSES IN A PARAMETRIC TRANSMITTING ARRAY

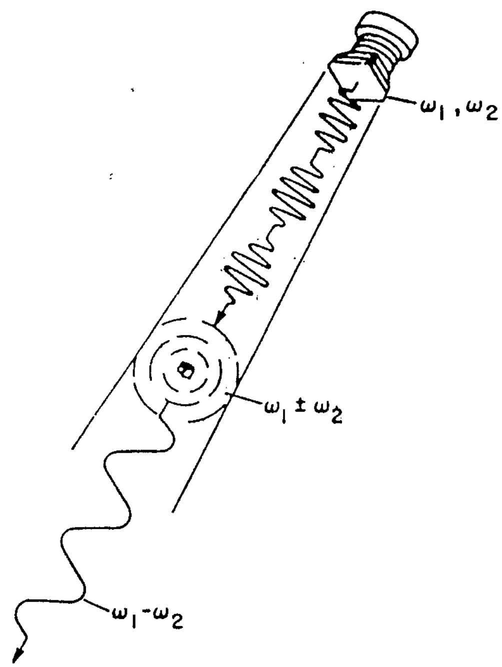

BIFREQUENCY SOURCES
$(\omega_1 \simeq \omega_2)$

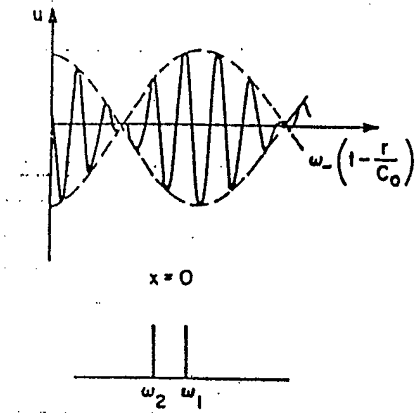

13a. SOURCE WAVEFORM

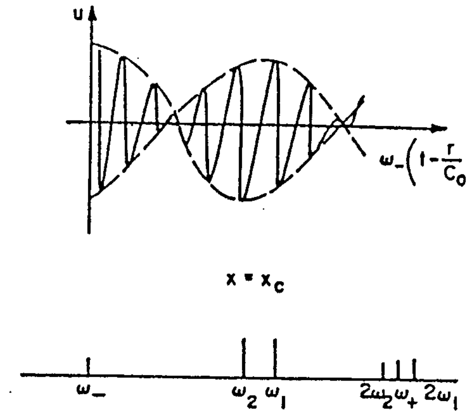

13b. WAVEFORM AT THE ONSET OF SHOCK FORMATION

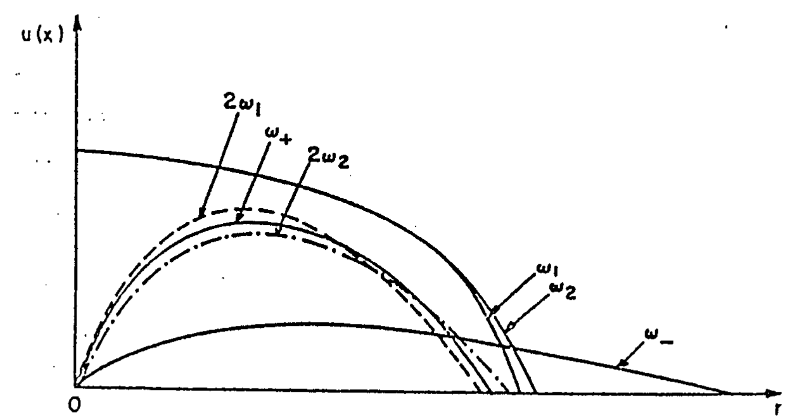

[TR-14]

WESTERVELT DIRECTIVITY

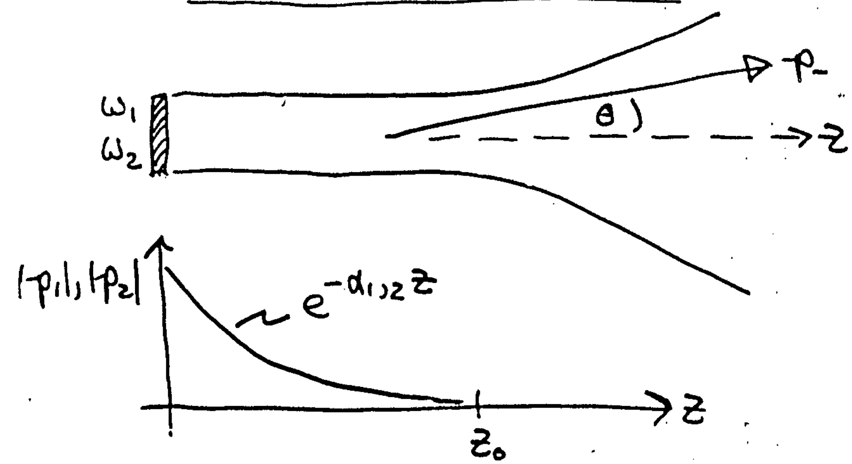

Collimated primary waves in nearfield:

$$p \simeq p_{01} e^{-\alpha_1 z} \sin(\omega_1 t - k_1 z) + p_{02} e^{-\alpha_2 z} \sin(\omega_2 t - k_2 z)$$

Difference frequency generation in nearfield behaves like exponentially tapered line array:

$$D_-(\theta) = \frac{1}{1 + j2(k_-/\alpha_T)\sin^2(\theta/2)}$$

$(\alpha_T = \alpha_1 + \alpha_2 - \alpha_-)$

Half-power angle:

$$\theta_{HP} \simeq \sqrt{\frac{2\alpha_T}{k_-}} \propto \sqrt{\frac{\lambda_-}{L_a}}$$

[TR-15]

$$\underbrace{D(\theta) \simeq \frac{1}{1 + j2(k_-/\alpha_T)\sin^2(\theta/2)}}$$

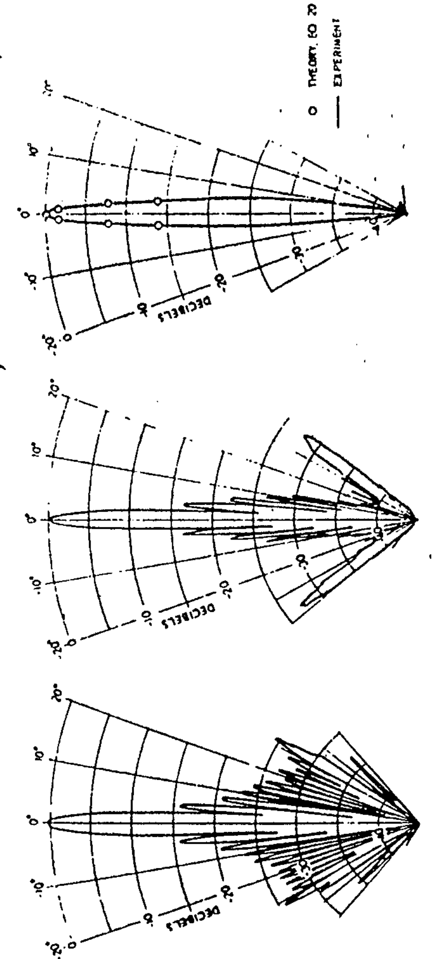

DIFFERENCE-FREQUENCY BEAM PATTERN

BEAM PATTERN OF THE 482 kHz CARRIER

BEAM PATTERN OF THE 418 kHz CARRIER

FIGURE 12
PARAMETRIC TRANSMITTING
ARRAY DIRECTIVITY PATTERNS

ARL-UT
AS-72-517

SELF-DEMODULATION (BERKTAY—1965)

Given the source pressure

$$P = E(t)\sin\omega_0 t$$

where

$E(t)$ = slowly varying modulation envelope

Berktay predicted that in the farfield ($\sigma \gg 1$) and for strong absorption ($A > 1$), the pressure on axis varies as

$$P \propto \frac{\partial^2 E^2(t)}{\partial t^2}$$

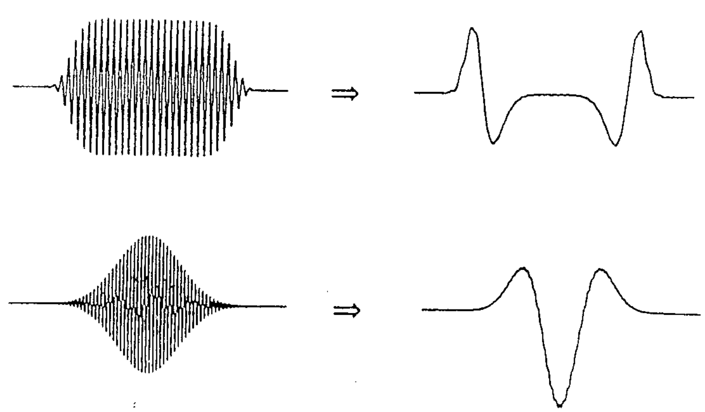

ABSORPTION IN AIR

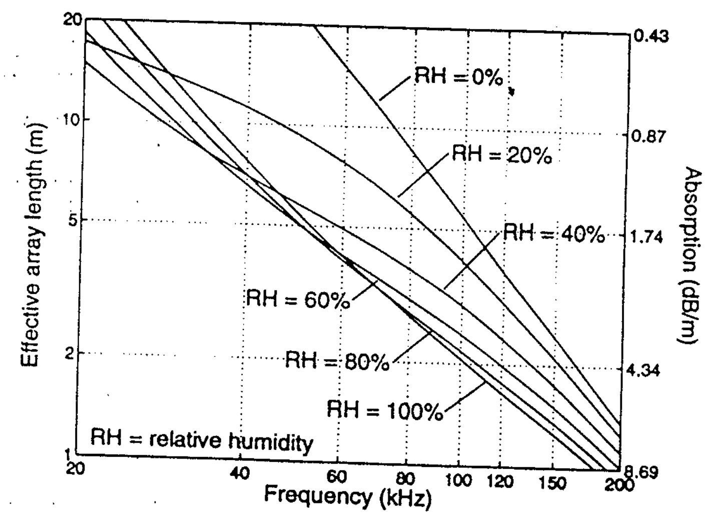

Thomas D. Kite, John T. Post, Mark F. Hamilton
Parametric Array in Air: Distortion Reduction by Preprocessing

4

[TR-19]

AUDIO SPOTLIGHT

American Technology Corp. device:

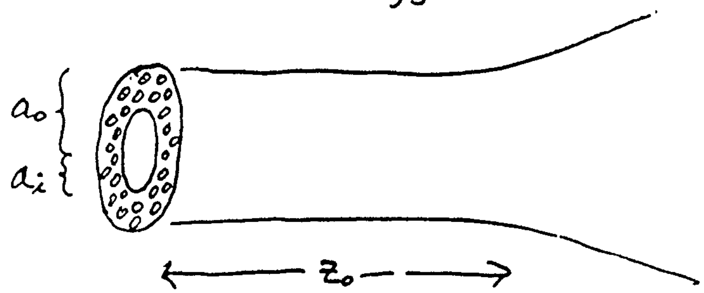

$a_o = 7$ cm
$a_i = 4$ cm

Primary frequency $f_o \sim 40$ kHz
Difference frequency $f_- \sim 1$ kHz

Absorption at f_o: $\alpha_o \simeq 1$ dB/m
Diffraction length: $z_o \simeq 1$ m $(a = a_o)$

Half-power angle at f_-: $2\theta_{HP} \simeq 17°$

* Since $k_- a_o \simeq 1$ direct radiation at f_- would produce very broad beam.

$L_p \sim 140$ dB at f_o
80 dB at f_-

[TR-20]

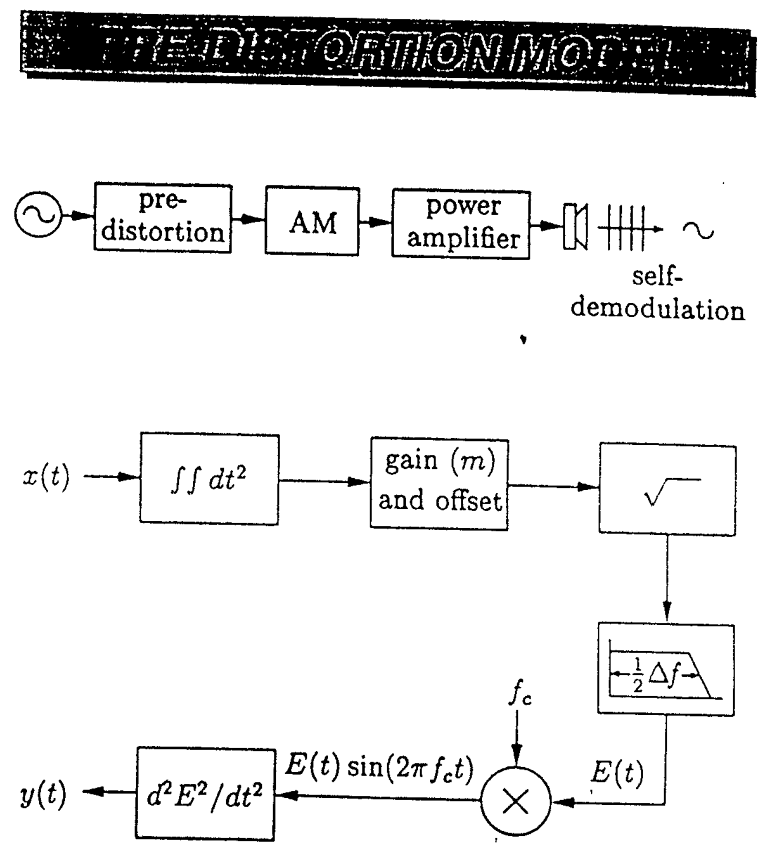

Thomas D. Kite, John T. Post, Mark F. Hamilton
Parametric Array in Air: Distortion Reduction by Preprocessing

5

IC DISTORTION

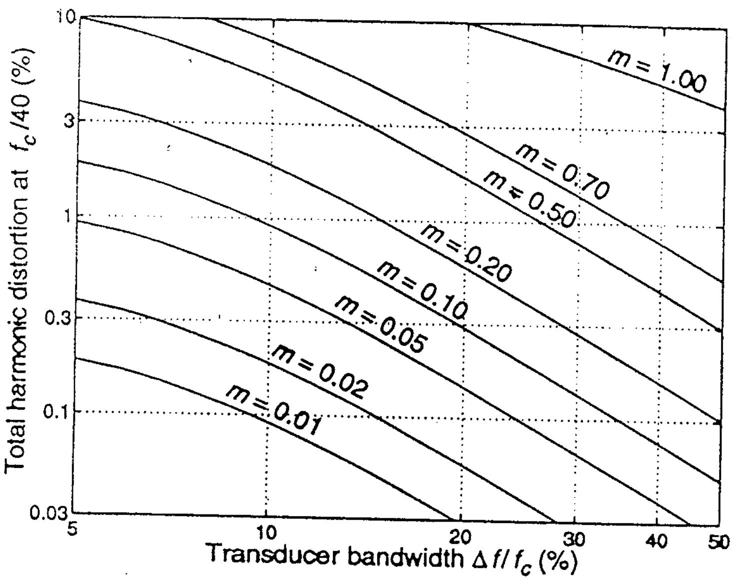

- Square root pre-distortion increases signal bandwidth
- THD: increases with m; decreases with Δf

Thomas D. Kite, John T. Post, Mark F. Hamilton
Parametric Array in Air: Distortion Reduction by Preprocessing

8

WEAK SHOCK THEORY

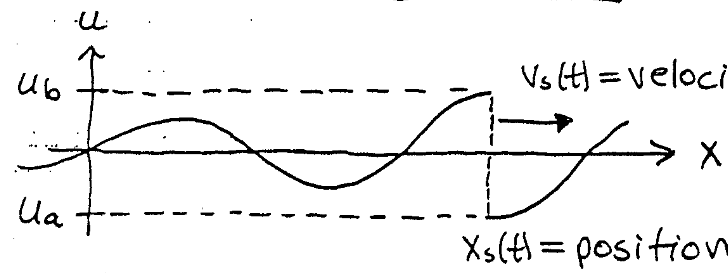

I. Weak Shock Limit of Rankine-Hugoniot Relations

$$V_s = c_0 + \frac{\beta}{2}(u_a + u_b)$$

step shock

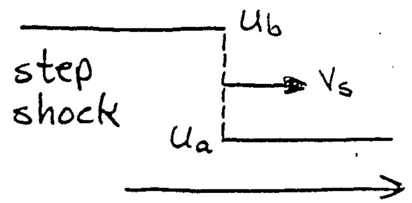

II. Landau's Equal Area Rule

Determine position X_s of shock by equating "areas"

$$A_1 \equiv A_2$$

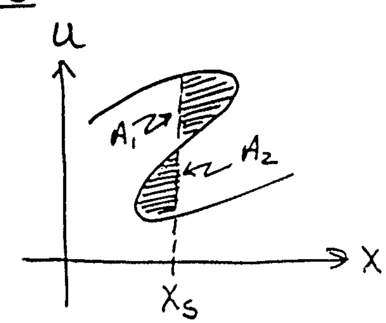

- Perfect discontinuities (jumps) assumed; shock structure (e.g., rise time) not described

[TR-25]

First-Generation Extracorporeal Shock Wave Lithotriptor

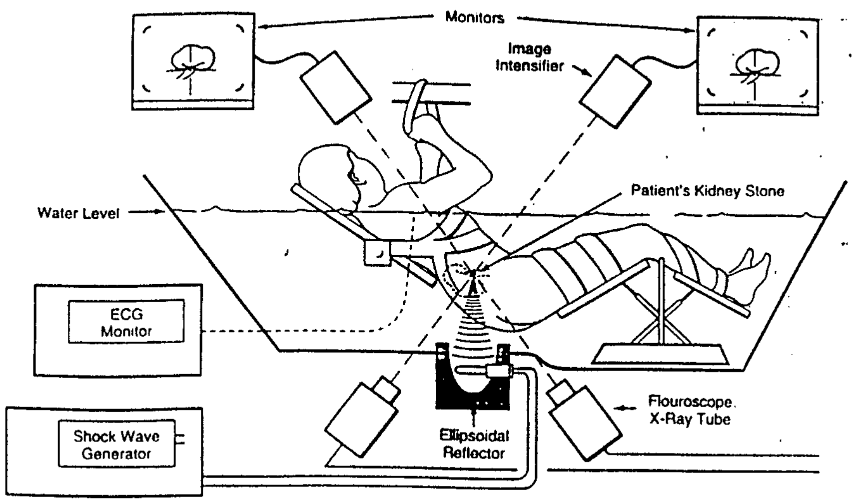

Second-Generation Extracorporeal Shock Wave Lithotriptor

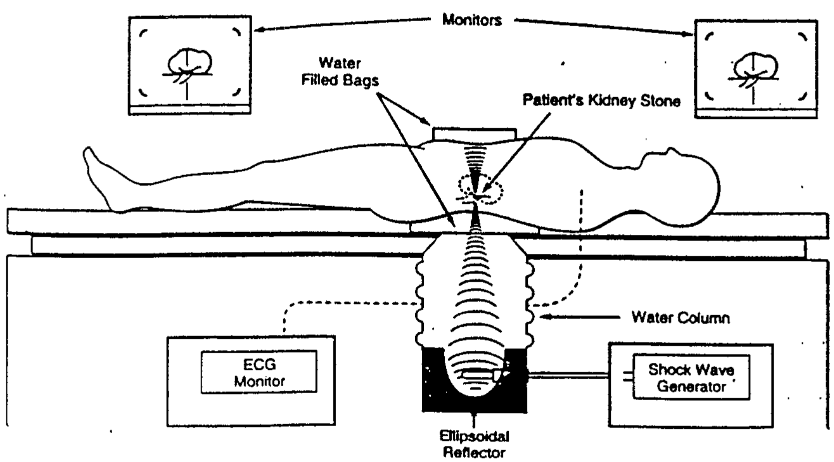

[TR-26]

THEORETICAL PREDICTIONS OF THE ACOUSTIC PRESSURE GENERATED BY A SHOCK WAVE LITHOTRIPTER

A. J. COLEMAN, M. J. CHOI and J. E. SAUNDERS
Medical Physics Department, St. Thomas' Hospital, London SE1 7EH, UK

(*Received 5 July 1990; in final form 1 October 1990*)

Ultrasound in Med. & Biol. Vol. 17, No. 3, pp. 245–255, 1991
Printed in the U.S.A.

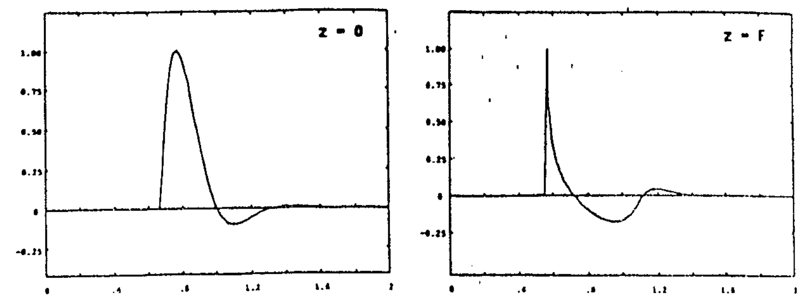

(c)

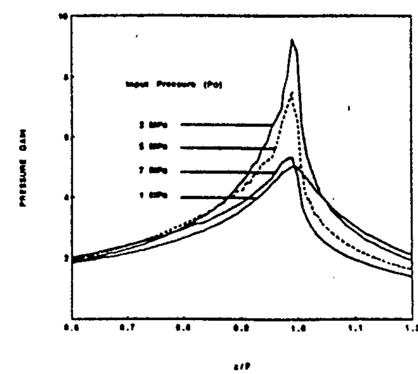

Fig. 4. Plots of the peak positive pressure gain ($p+/p_o$) along the beam axis, z/F, calculated for a pulsed (exponentially damped sinusoidal) aperture waveform with peak pressures, p_o, of 1, 3, 5 and 7 MPa ($n_{max} \geq 384$). The curve for 5 MPa is shown as a dotted line and corresponds to that predicted for the Dornier HM3 operated at around 20 kV

FOURIER ANALYSIS

Source Condition:

$$u(0,\tau) = u_0 \sin \omega\tau$$

Fourier Series Solution:

$$u(\sigma,\tau) = u_0 \sum_{n=1}^{\infty} B_n(\sigma) \sin n\omega\tau \quad , \quad \sigma = \frac{\beta \omega u_0 x}{c_0^2} = x/\bar{x}$$

$$B_n(\sigma) = \frac{2 J_n(n\sigma)}{n\sigma} \quad , \quad \sigma < 1 \text{ (Fubini)}$$

$$= \frac{2}{n(1+\sigma)} \quad , \quad \sigma \gtrsim 3 \text{ (sawtooth)}$$

$$\bar{x} = \frac{1}{\beta \varepsilon k} = \frac{c_0^2}{\beta u_0 \omega} = \frac{\rho_0 c_0^3}{\beta p_0 \omega}$$

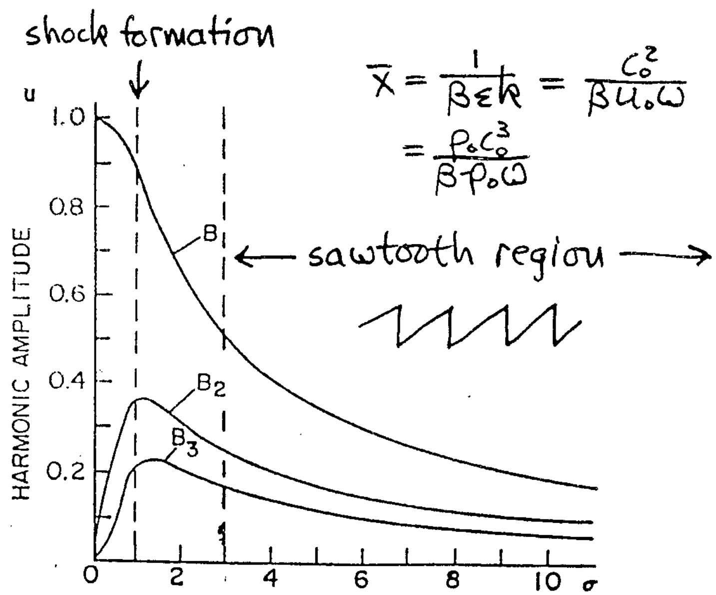

ACOUSTIC SATURATION

Use sawtooth solution ($\sigma \gtrsim 3$)

$$u = u_0 \sum_{n=1}^{\infty} \frac{2}{n(1+\sigma)} \sin n\omega\tau \quad , \quad \sigma = \frac{\beta \omega u_0 x}{c_0^2}$$

and let $\sigma \gg 1$:

$$u \sim u_0 \sum_{n=1}^{\infty} \frac{2}{n \beta \omega u_0 x / c_0^2} \sin n\omega\tau$$

$$= \frac{2 c_0^2}{\beta \omega x} \sum_{n=1}^{\infty} \frac{1}{n} \sin n\omega\tau$$

$\rightarrow$ No dependence on u_0 !

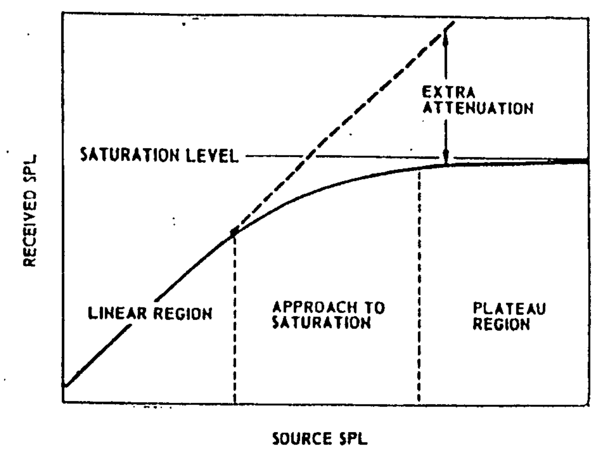

FIGURE 1-1
THE DEVELOPMENT OF SATURATION

[TR-29]

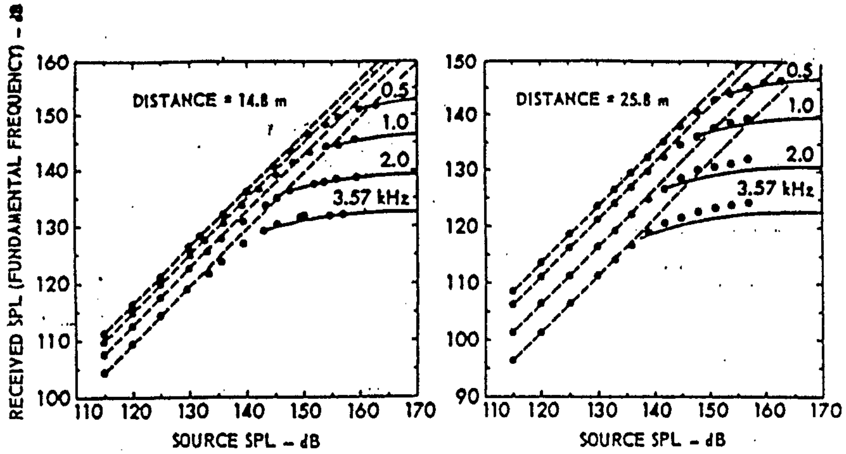

Webster
& Blackstock,
JASA 62,
518 (1977)

FIGURE 5-5
AMPLITUDE RESPONSE CURVES AT
FUNDAMENTAL FREQUENCY

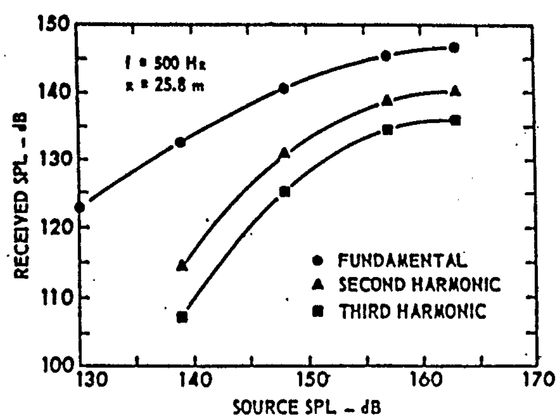

FIGURE 5-6
AMPLITUDE RESPONSE CURVES FOR
THE FIRST THREE HARMONICS OF
AN INITIALLY SINUSOIDAL WAVE

[TR-30]

NUMERICAL MODELING

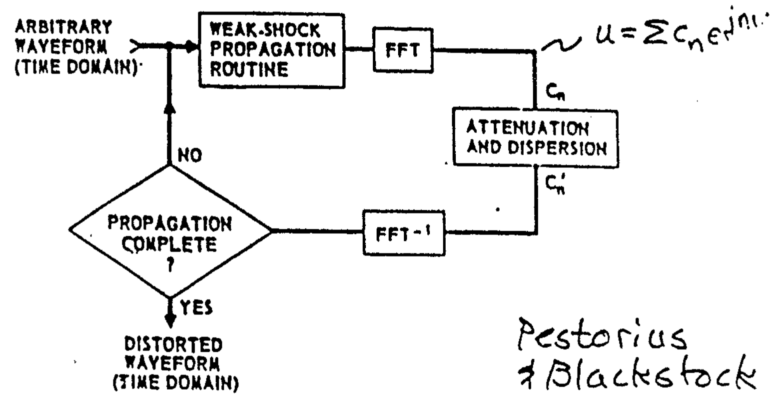

Pestorius
& Blackstock
1973

FIGURE 3-8
A SCHEMATIC DIAGRAM OF MODIFIED WEAK-SHOCK THEORY

Time Domain Steps:

$$\frac{dx}{dt} = c_0 + \beta u \quad \text{, continuous waves}$$

$$= c_0 + \frac{\beta}{2}(u_a + u_b) \quad \text{, shocks}$$

Frequency Domain steps:

$$c_n' = c_n e^{-(\alpha_n + j\delta_n)\Delta x}$$

α_n = attenuation coefficient

δ_n = dispersion coefficient

[TR-31 Unavaliable At Time Of Printing]

[TR-32]

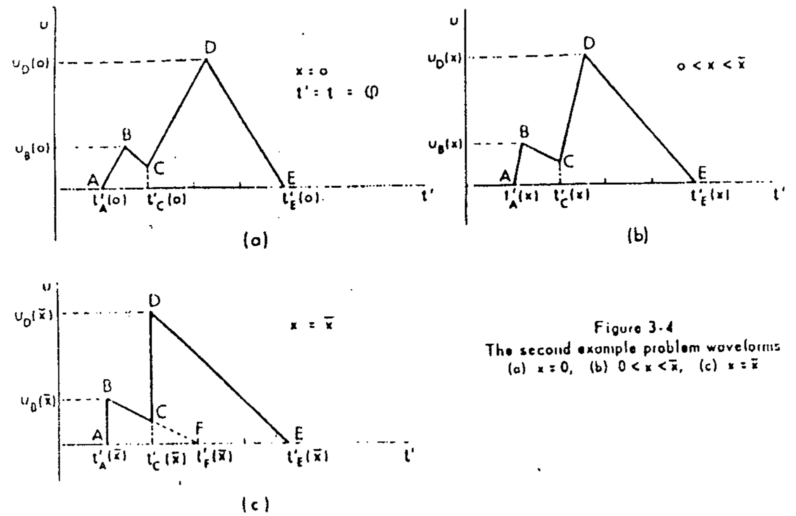

Figure 3-4
The second example problem waveforms
(a) $x = 0$, (b) $0 < x < \bar{x}$, (c) $x = \bar{x}$

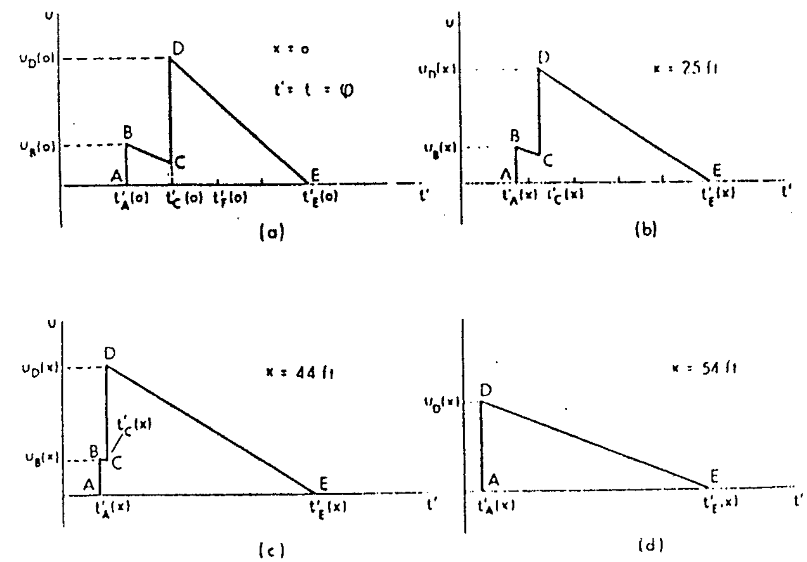

Figure 3-5
The second example problem (cont'd)
(a) The source waveform in the shifted coordinate system.
(b) The source waveform after propagating 25 ft.
(c) Just prior to shock merger.
(d) The simplified waveform after shock merger.

[TR-33]

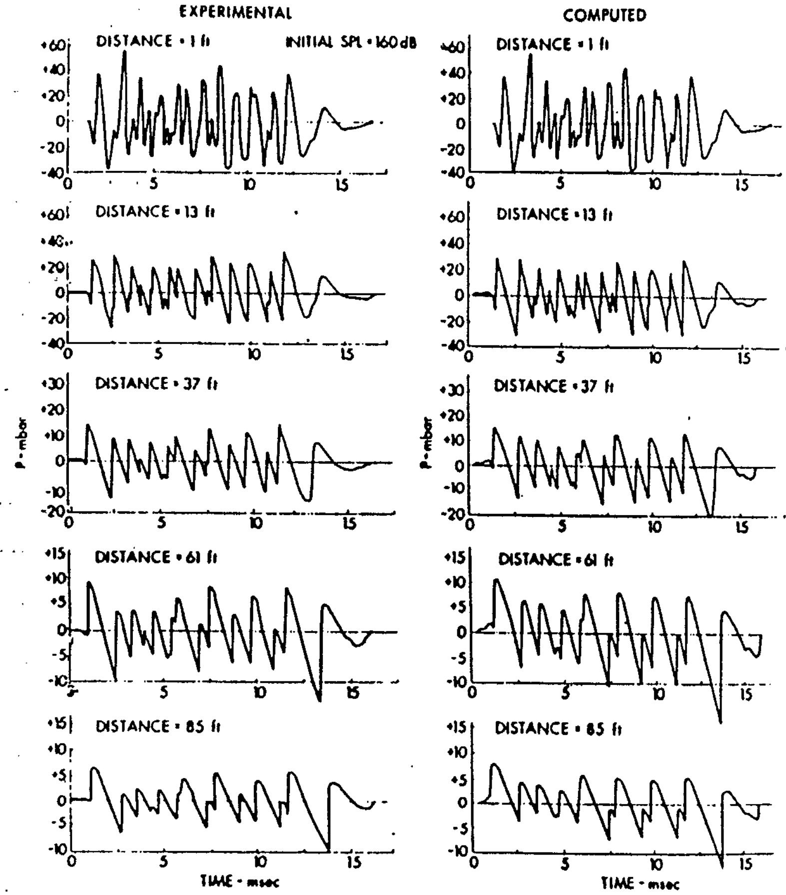

FIGURE 6-9
NOISE PULSE I AT VARIOUS DISTANCES

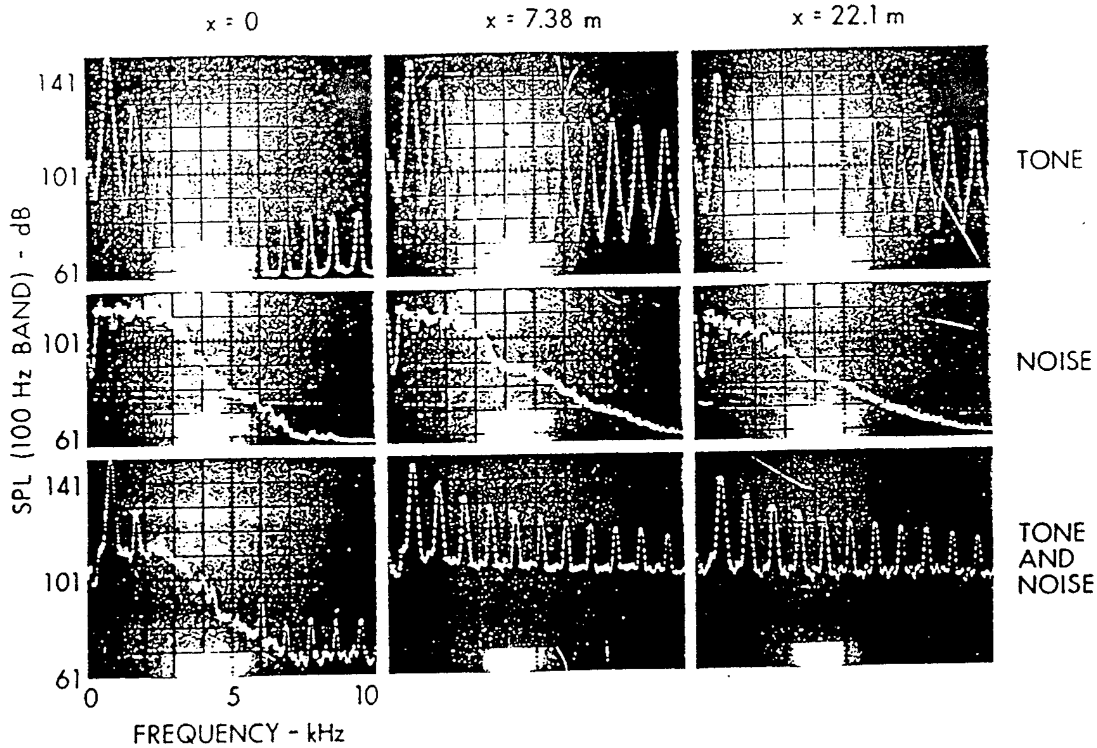

FIGURE 3

Interaction of tone with noise.
From Refs. 77-2, 77-6, and 78-1.

Webster & Blackstock
JASA, 62 (1977)

[TR-35]

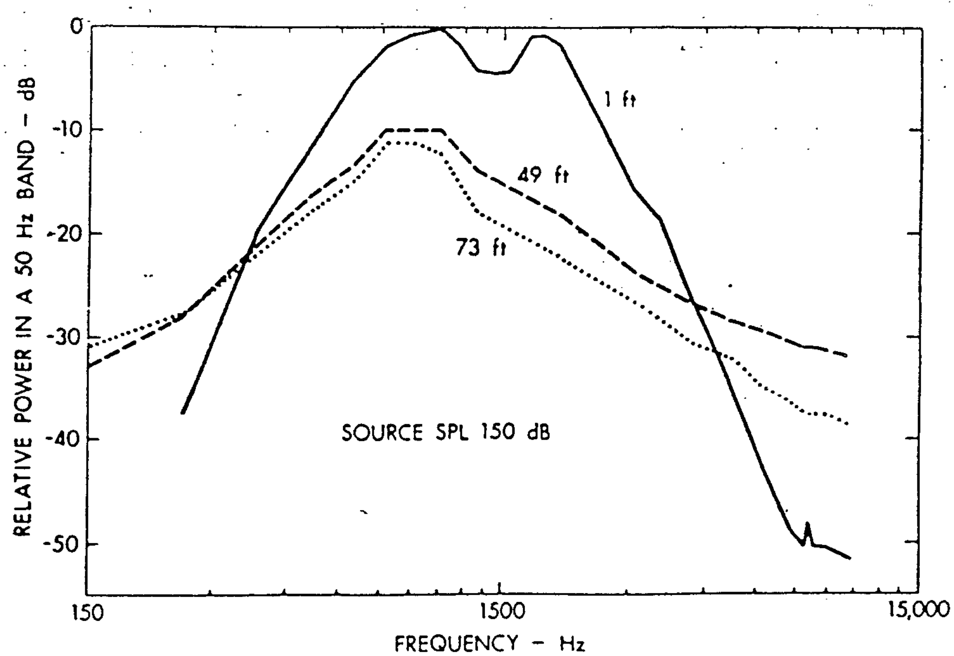

FIGURE 6-15
EXPERIMENTAL SPECTRUM AT VARIOUS DISTANCES

[TR-34]

156

D. A. Webster and D. T. Blackstock: Collinear interaction of noise with a tone

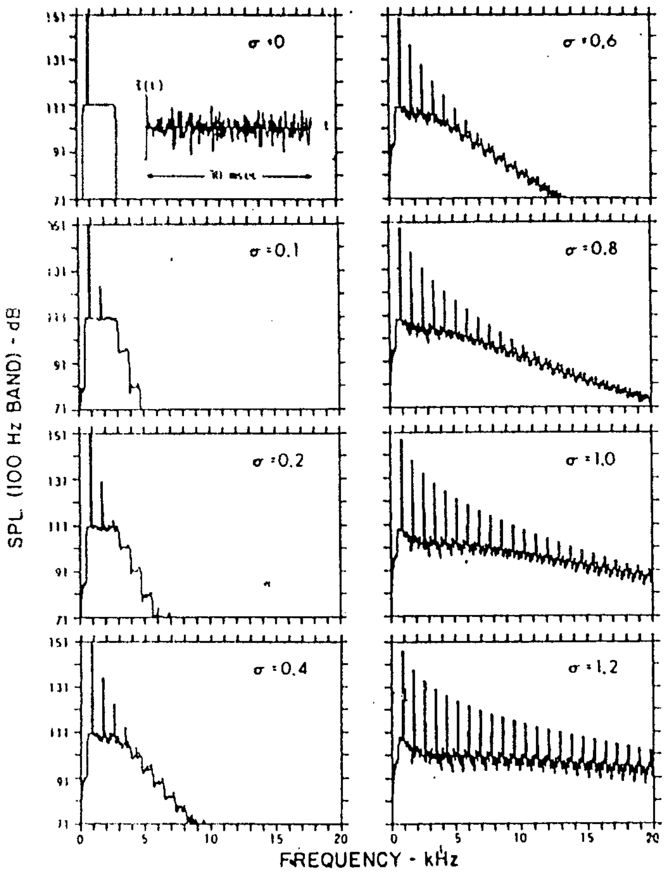

FIG. 8. Computed tone-noise interaction spectra. Symbols: $\sigma \equiv x/\bar{x}$, $\bar{x}=7.45$ m. The conditions are roughly those of experiment 1.

VISCOUS, HEAT CONDUCTING FLUIDS

Continuity:

$$\frac{D\rho}{Dt} + \rho\vec{\nabla}\cdot\vec{u} = 0 \qquad \left(\frac{D}{Dt} = \frac{\partial}{\partial t} + \vec{u}\cdot\vec{\nabla}\right)$$

Momentum:

$$\rho\frac{D\vec{u}}{Dt} + \vec{\nabla}P = \left(\zeta + \frac{4}{3}\eta\right)\nabla^2\vec{u} + \left(\zeta + \frac{\eta}{3}\right)\vec{\nabla}\times\vec{\nabla}\times\vec{u}$$

Entropy:

$$\rho T\frac{Ds}{Dt} = \kappa\nabla^2 T + \zeta(\vec{\nabla}\cdot\vec{u})^2 + \frac{\eta}{2}\left(\frac{\partial u_i}{\partial x_j} + \frac{\partial u_j}{\partial x_i} - \frac{2}{3}\delta_{ij}\frac{\partial u_k}{\partial x_k}\right)^2$$

State:

$$P = P(\rho, s)$$
$$= P_0\left(\frac{\rho}{\rho_0}\right)^\gamma \exp\left(\frac{s-s_0}{c_v}\right), \text{ perfect gas}$$

[See Landau & Lifshitz, Fluid Mechanics]

MODEL EQUATIONS OF NONLINEAR ACOUSTICS

- Exact equation for lossless ($\zeta, \eta, \kappa = 0$) perfect gas ($P \propto \rho^{\gamma}$) in terms of velocity potential ϕ:

$$c_0^2 \nabla^2 \phi - \phi_{tt} = \left(2\vec{\nabla}\phi_t + \frac{1}{2}\vec{\nabla}\,|\vec{\nabla}\phi|^2\right)\cdot\vec{\nabla}\phi + (\gamma-1)\left(\phi_t + \frac{1}{2}|\vec{\nabla}\phi|^2\right)\nabla^2\phi$$

- Common starting point in aeroelasticity, and for perturbation techniques used in nonlinear acoustics.

- ADVANTAGE: It's exact

- DISADVANTAGES:

  1) restricted to lossless gases

  2) no exact solutions known (except Poisson solution for progressive plane waves)

LIGHTHILL'S ORDERING SCHEME

All lossless linear terms (e.g., $\vec{\nabla}p$) are $O(\varepsilon)$, where

$$\varepsilon \sim \frac{u}{c_0} = \text{acoustic Mach number}$$

- All loss coefficients are $O(\mu)$:

$$\zeta, \eta, \kappa = O(\mu)$$

1) First-order terms:

$O(\varepsilon)$, lossless linear

2) Second-order terms:

$O(\varepsilon^2)$, lossless quadratic

$O(\mu\varepsilon)$, lossy linear

3) Higher-order terms:

$O(\varepsilon^3)$, $O(\mu\varepsilon^2)$, $O(\mu^2\varepsilon)$, etc.

- Discard <u>all</u> higher-order terms in derivations of all model equations

[TR-40]

SECOND-ORDER BASIC EQUATIONS

Let $p = P - P_0$, $\rho' = \rho - \rho_0$, etc., use first-order relations to simplify second-order terms, and ignore vorticity $(\vec{\nabla} \times \vec{u})$ to obtain:

Continuity

$$\frac{\partial \rho'}{\partial t} + \rho_0 \vec{\nabla} \cdot \vec{u} = \frac{1}{\rho_0 c_0^4} \frac{\partial p^2}{\partial t} + \frac{1}{c_0^2} \frac{\partial \mathcal{L}}{\partial t}$$

Momentum

$$\rho_0 \frac{\partial \vec{u}}{\partial t} + \vec{\nabla} p = -\frac{1}{\rho_0 c_0^2} \left(\zeta + \frac{4}{3} \eta \right) \vec{\nabla} \frac{\partial p}{\partial t} - \vec{\nabla} \mathcal{L}$$

Entropy & state

$$\rho' - \frac{p}{c_0^2} = -\frac{\kappa}{\rho_0 c_0^4} \left(\frac{1}{c_v} - \frac{1}{c_p} \right) \frac{\partial p}{\partial t} - \frac{1}{\rho_0 c_0^4} \frac{B}{2A} p^2$$

$$\mathcal{L} = \frac{\rho_0 u^2}{2} - \frac{p^2}{2 \rho_0 c_0^2} = \text{Lagrangian density}$$

Note: For progressive plane waves we have $p = \rho_0 c_0 u$ at first order and therefore $\mathcal{L} = 0$ at second order, in which case the momentum equation is linear!!

[TR-41]

- Full second-order wave equation

[Aanonsen et al., JASA 75, 749 (1984)]

$$\left(\nabla^2 - \frac{1}{c_0^2} \frac{\partial^2}{\partial t^2} \right) p + \frac{\delta}{c_0^4} \frac{\partial^3 p}{\partial t^3} = -\frac{\beta}{\rho_0 c_0^4} \frac{\partial^2 p^2}{\partial t^2} - \left(\nabla^2 + \frac{1}{c_0^2} \frac{\partial^2}{\partial t^2} \right) \mathcal{L}$$

- Westervelt equation

[Westervelt, JASA 35, 535 (1963)]

$$\left(\nabla^2 - \frac{1}{c_0^2} \frac{\partial^2}{\partial t^2} \right) p + \frac{\delta}{c_0^4} \frac{\partial^3 p}{\partial t^3} = -\frac{\beta}{\rho_0 c_0^4} \frac{\partial^2 p^2}{\partial t^2}$$

The appoximation $\mathcal{L} \approx 0$ to obtain Westervelt equation restricts it to quasiplane progressive waves.

$$\beta = 1 + \frac{B}{2A} = \text{coefficient of nonlinearity}$$

$$\delta = \frac{1}{\rho_0} \left(\frac{4}{3} \eta + \zeta \right) + \frac{\kappa}{\rho_0} \left(\frac{1}{c_v} - \frac{1}{c_p} \right)$$
$$= \text{sound diffusivity}$$

$$\alpha_\omega = \frac{\delta \omega^2}{2 c_0^3} = \text{thermoviscous attenuation}$$

- <u>Burgers Equation</u>

[Khokhlov et al., Acustica <u>14</u>, 248 (1964)]

Begin with Westervelt equation for 1-D:

$$\left(\frac{\partial^2}{\partial x^2}-\frac{1}{c_0^2}\frac{\partial^2}{\partial t^2}\right)p=-\frac{\delta}{c_0^4}\frac{\partial^3 p}{\partial t^3}-\frac{\beta}{\rho_0 c_0^4}\frac{\partial^2 p^2}{\partial t^2}$$

Two approximate sol'ns for limiting cases:

$$p\simeq \exp\left(-\frac{\omega^2}{2c_0^3}\delta z\right)\sin\omega t\ ,\quad \beta=0$$

$$\simeq \sin\left(\omega\tau+\frac{\beta k}{\rho_0 c_0^2}pz\right),\quad \delta=0\quad \text{(Poisson)}$$

Both solutions are of the form

$$p=p(x_1,\tau)$$

$$\tau=t-\frac{x}{c_0}=\text{retarded time}$$
$$x_1=\varepsilon x=\text{"slow" length scale}\ [\delta=O(\varepsilon)]$$

$$\Rightarrow\quad \frac{\partial^2}{\partial t^2}=\frac{\partial^2}{\partial\tau^2}$$

$$\frac{\partial^2}{\partial x^2}=\frac{1}{c_0^2}\frac{\partial^2}{\partial\tau^2}-\varepsilon\frac{2}{c_0}\frac{\partial^2}{\partial x_1\partial\tau}+\varepsilon^2\frac{\partial^2}{\partial x_1^2}$$

Keep only second-order terms on slow scale:

$$\frac{\partial p}{\partial x}=\frac{\delta}{2c_0^3}\frac{\partial^2 p}{\partial\tau^2}+\frac{\beta}{2\rho_0 c_0^3}\frac{\partial p^2}{\partial\tau}$$

<u>SPECTRAL NUMERICAL SOLUTION</u>

Dimensionless Burgers Equation:

$$\frac{\partial P}{\partial\sigma}=\frac{1}{\Gamma}\frac{\partial^2 P}{\partial\tau^2}+P\frac{\partial P}{\partial\tau}$$

$$P=\frac{p}{p_0},\quad \sigma=\frac{x}{\bar{x}},\quad \tau=\omega\left(t-\frac{x}{c_0}\right),\quad \Gamma=\frac{1}{\alpha\bar{x}}$$

Fourier Series Expansion:

$$P(\sigma,\tau)=\frac{1}{2}\sum_{n=-N}^{N}P_n(\sigma)e^{jn\tau}$$

Resulting Coupled First-Order ODE's:

$$\frac{dP_n}{d\sigma}=\underbrace{-\frac{n^2}{\Gamma}P_n}_{\text{absorption}}+\frac{jn}{4}\left(\underbrace{\sum_{m=1}^{n-1}P_mP_{n-m}}_{\text{sum freqs.}}+\underbrace{2\sum_{m=n+1}^{N}P_mP_{m-n}^*}_{\text{diff. freqs.}}\right)$$

Simple modification for arbitrary absorption and dispersion relations:

$$\frac{n^2}{\Gamma}\longrightarrow A_n+jD_n$$

Particle Displacement Wavefields

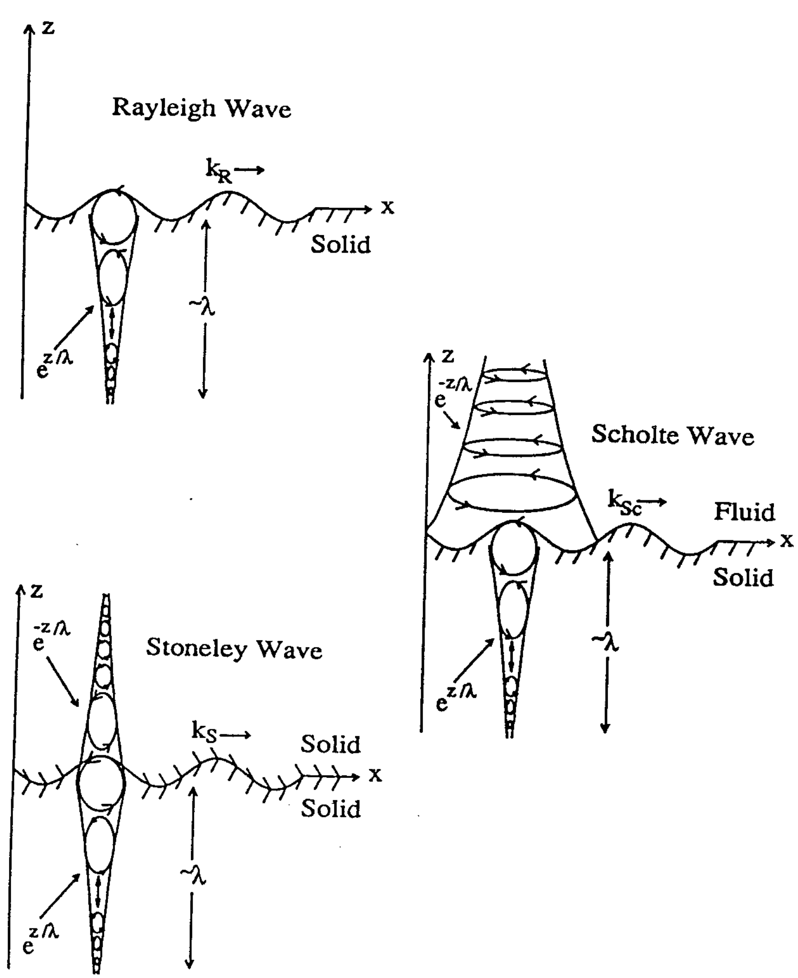

NORMAL MODE EXPANSION

- Fourier expansion of field vector components:

$$u_j(x,z,t) = \sum_{n=-\infty}^{\infty} a_n(t)\psi_{nj}(z)e^{inkx}, \qquad j = 1 \ldots M$$

where

$$\begin{aligned} M &= 2 \text{ for isotropic solids } (u_x, u_z) \\ &= 3 \text{ for crystals } (u_x, u_y, u_z) \\ &= 4 \text{ for piezoelectric materials } (u_x, u_y, u_z, \phi) \end{aligned}$$

- Eigenfunctions (depth dependence) from linear theory:

$$\psi_{nj}(z) = \sum_{s=1}^{M} \beta_j^{(s)} e^{ink_z^{(s)} z}$$

where

$$\begin{aligned} k_z^{(s)} &= \text{eigenvalues (vertical wavenumbers)} \\ \beta_j^{(s)} &= \text{eigenvectors} \end{aligned}$$

- Time dependence:

$$\begin{aligned} a_n(t) &\sim b_n(t)e^{\pm in\omega t} \\ b_n(t) &= \text{slowly varying function} \\ &= \text{constant in linear theory} \end{aligned}$$

HAMILTONIAN FORMALISM

Hamiltonian:

$$H = T + V$$

Kinetic energy:

$$T = \frac{\rho}{2}\iint \dot{u}_j^2\,dx\,dz$$
$$= \frac{\rho}{2k}\sum_n \frac{\dot{a}_n \dot{a}_{-n}}{|n|}$$

Define

$$a_n = \text{generalized displacements}$$
$$p_n = \text{generalized momenta}$$
$$= \frac{\partial T}{\partial \dot{a}_n} = \frac{\rho}{k}\frac{\dot{a}_{-n}}{|n|}$$

Canonical equations:

$$\dot{a}_n = \frac{\partial H}{\partial p_n} \qquad \dot{p}_n = -\frac{\partial H}{\partial a_n}$$

- Express potential energy V, and thus H, in terms of a_n
- Introduce slowly varying functions $b_n(t) = a_n(t)e^{in\omega t}$
- Derive temporal evolution equation for $\dot{b}_n$
- Transform to spatial evolution equation

POTENTIAL ENERGY

$$V = V_2 + V_3 + \cdots$$

where

$$V_n = \iint \mathcal{E}_n\,dx\,dz$$
$$\mathcal{E}_n = \text{elastic energy density at order } n$$

- Quadratic terms (linear effects):

$$\mathcal{E}_2 = \tfrac{1}{2}c_{ijkl}\frac{\partial u_i}{\partial x_j}\frac{\partial u_k}{\partial x_l} \qquad \text{(elastic)}$$
$$-\tfrac{1}{2}\epsilon_{ik}\frac{\partial \phi}{\partial x_i}\frac{\partial \phi}{\partial x_k} \qquad \text{(electric)}$$
$$+\,e_{ijk}\frac{\partial u_i}{\partial x_j}\frac{\partial \phi}{\partial x_k} \qquad \text{(piezoelectric)}$$

- Cubic terms (nonlinear effects):

$$\mathcal{E}_3 = \tfrac{1}{6}c'_{ijklmn}\frac{\partial u_i}{\partial x_j}\frac{\partial u_k}{\partial x_l}\frac{\partial u_m}{\partial x_n} \qquad \text{(elastic)}$$
$$+\tfrac{1}{6}\epsilon_{ikl}\frac{\partial \phi}{\partial x_i}\frac{\partial \phi}{\partial x_k}\frac{\partial \phi}{\partial x_l} \qquad \text{(electric)}$$
$$+\tfrac{1}{2}e'_{ijklm}\frac{\partial u_i}{\partial x_j}\frac{\partial u_k}{\partial x_l}\frac{\partial \phi}{\partial x_m} \qquad \text{(piezoelectric)}$$
$$-\tfrac{1}{2}d_{ijkl}\frac{\partial u_i}{\partial x_j}\frac{\partial \phi}{\partial x_k}\frac{\partial \phi}{\partial x_l} \qquad \text{(electrostrictive)}$$

[TR-48]

EVOLUTION EQUATION

- Fourier expansion of particle velocity components:

$$v_j(x,z,t) = \sum_{n=-\infty}^{\infty} v_n(x)\psi_{nj}(z)e^{in(kx-\omega t)}$$

- Coupled equations for spectral amplitudes:

$$\frac{dv_n}{dx} = \frac{n^2\omega}{2\rho c^4} \sum_{l+m=n} \frac{lm}{|lm|} S_{lm(-n)} v_l v_m$$

- Nonlinearity matrix:

$$S_{n_1 n_2 n_3} = \sum_{s_1,s_2,s_3=1}^{M} \frac{F_{s_1 s_2 s_3}}{n_j \operatorname{Re}\zeta_{s_j} - i|n_j| \operatorname{Im}\zeta_{s_j}}$$

where

$$\begin{aligned} F_{s_1 s_2 s_3} &= \text{material constants} \\ \zeta_{s_j} &= \text{eigenvalues} \\ M &= 2 \text{ for isotropic solids} \\ &= 3 \text{ for crystals} \\ &= 4 \text{ for piezoelectric materials} \end{aligned}$$

[TR-49]

RAYLEIGH WAVE EXPERIMENT

Lomonosov and Hess, University of Heidelberg

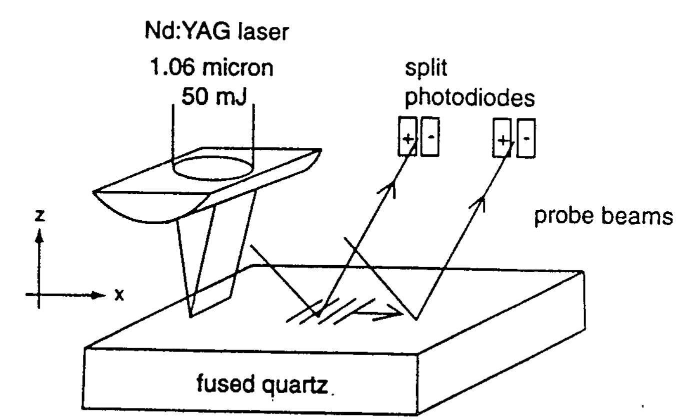

Laser excitation: x=0
1st probe beam: x=2.3 mm
2nd probe beam: x=18.3 mm

Theory based on 5 isotropic constants: μ, K, A, B, C

[TR-51]

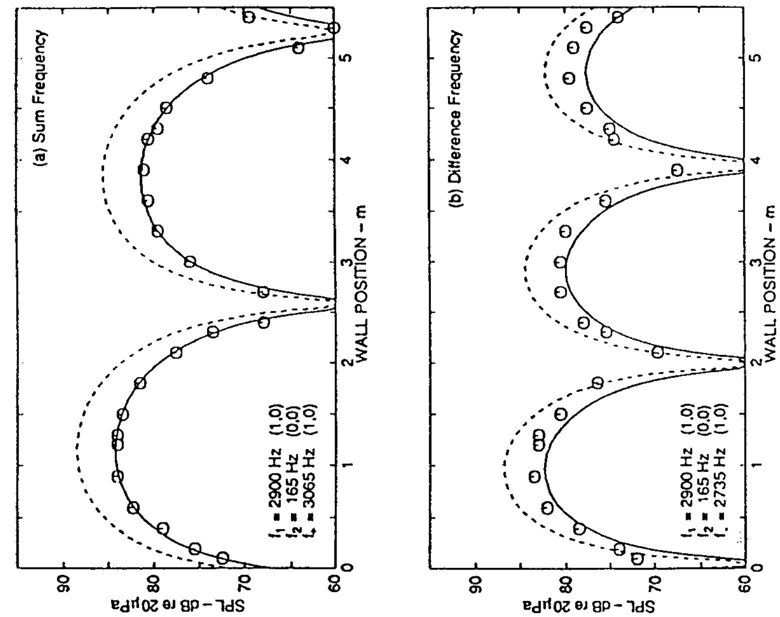

Figure 5.5

Hamilton & TenCate, JASA 81, 1703 (1987)

RESULTS

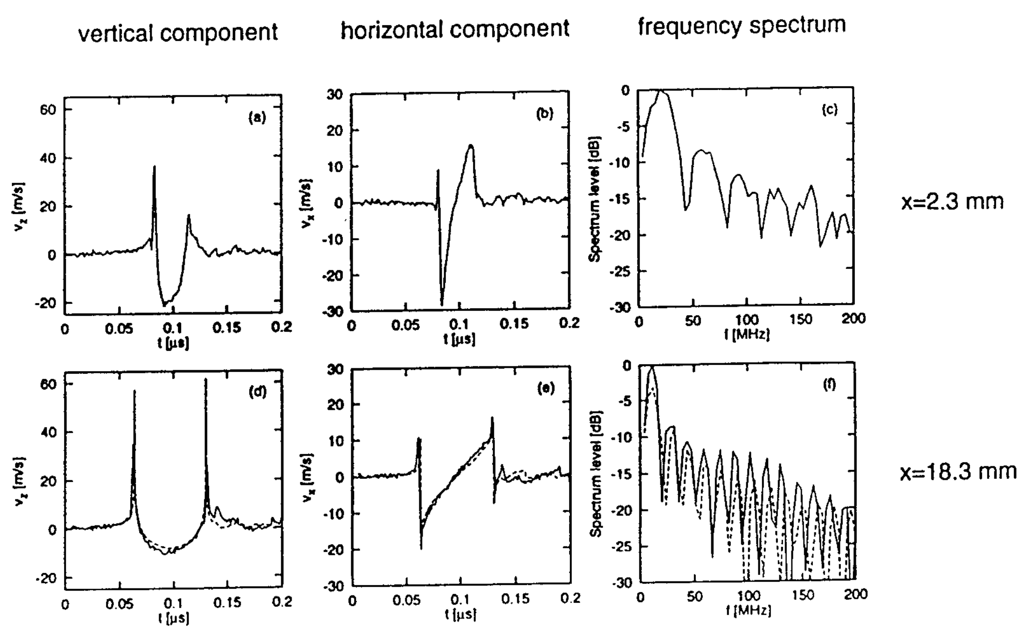

solid lines: experiment
dashed lines: theory

[TR-50]

ACOUSTIC PUMP
(MacroSonix)

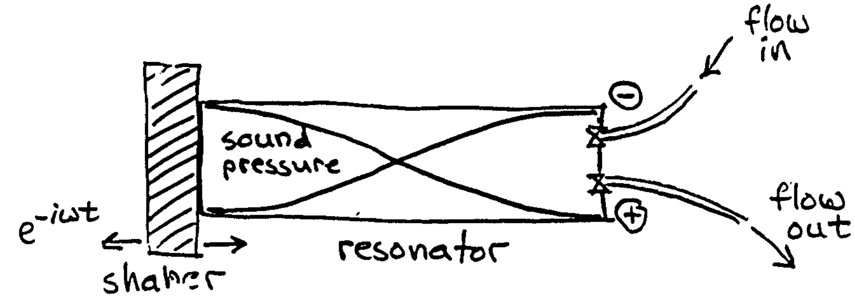

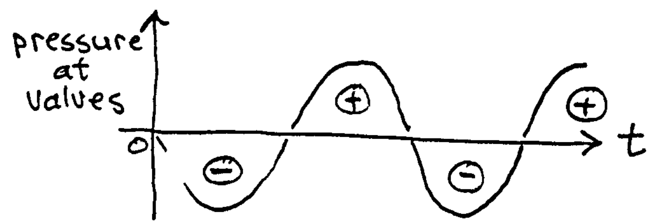

⊖ = upper valve open
⊕ = lower valve open

Problem: High SPL's needed for commercially viable compression produce shock waves → losses/saturation

Solution: Introduce dispersion to suppress shock formation

DISPERSION IN HORNS

Webster horn equation:

$$\frac{\partial^2 p}{\partial x^2} + \frac{1}{S}\frac{dS}{dx}\frac{\partial p}{\partial x} = \frac{1}{c_0^2}\frac{\partial^2 p}{\partial t^2}$$

$S(x)$ = cross sectional area

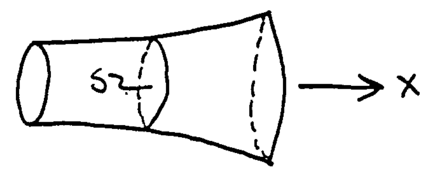

Exponential horn: $S(x) = S_0 e^{2x/h}$

Trial solution: $p(x,t) = p_0 \exp[i(\tilde{k}x - \omega t)]$

Dispersion relation: $\tilde{k}^2 - i\frac{2}{h}\tilde{k} - \frac{\omega^2}{c_0^2} = 0$

$$\Rightarrow \tilde{k} = i\frac{1}{h} \pm \frac{\omega}{c_0}\sqrt{1-(\omega_c/\omega)^2}$$

$\omega_c = \frac{c_0}{h}$ = cutoff frequency

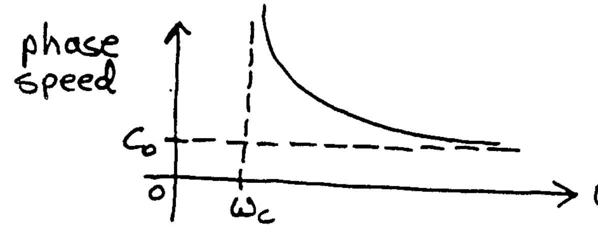

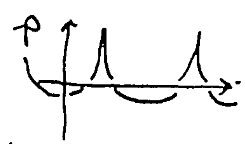

[TR-1]

CHAOS
AND
NONLINEAR BUBBLE DYNAMICS

Werner Lauterborn

Drittes Physikalisches Institut
Universität Göttingen

[TR-2]

Contents

[TR-3]

Philosophical Introduction

[TR-4]

Philosopher:

Ludwig Wittgenstein in his Tractatus logico-philosophicus (1921):

The world is
all that is the case

Original in German:

Die Welt ist alles, was der Fall ist.

[TR-5]

Physicist:

around 1900, in view of the unification of mechanics and thermodynamics

The world is statistical

around 1910, in view of Einstein's results

The world is relative

around 1930, in view of the achievements of quantum mechanics

The world is quantal

today, at the turn to the next century

The world is chaotic

[TR-6]

Determinism

does not imply

predictability

Example: Population of mosquitos

Laws:

Reproduction every year by a factor of 10

Population kept below 1 billion mosquitos = 1 mos

Start:	0.526 mos	5.26 mos
	0.26 mos	2.6? mos
	0.6? mos	6.?? mos
	?.?? mos	

[TR-7]

Historical

Notes

[TR-8]

Acoustics

Combination tones:

Sorge (1745), Romieu (1751), Tartini (1754)

Difference tone:

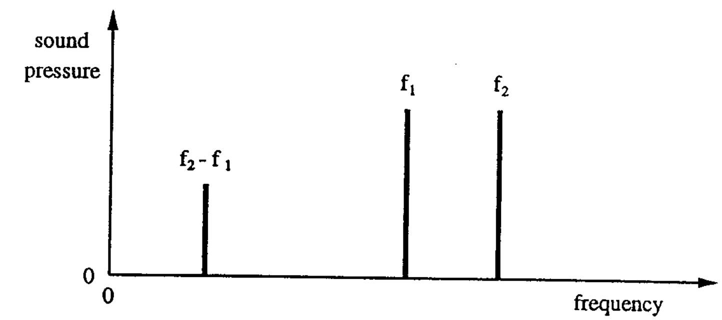

Cubic difference tone:

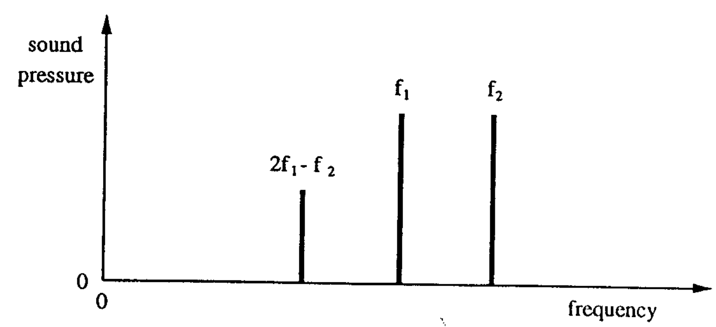

Acoustics

Vibrated liquid layer (Faraday 1831):

First subharmonic:

External vibration frequency: f
Vibration frequency of liquid layer: f/2

Experimentally obtained surface oscillations
Wright et al., PRL 76 (1996) 4528

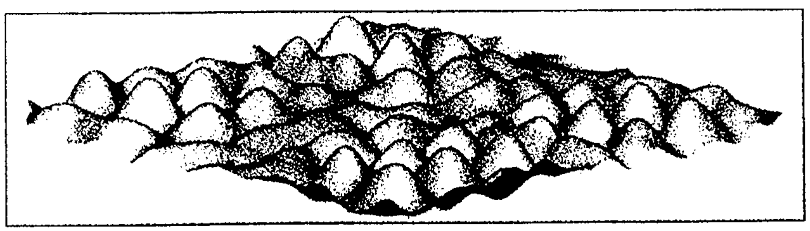

Vibrated liquid layer

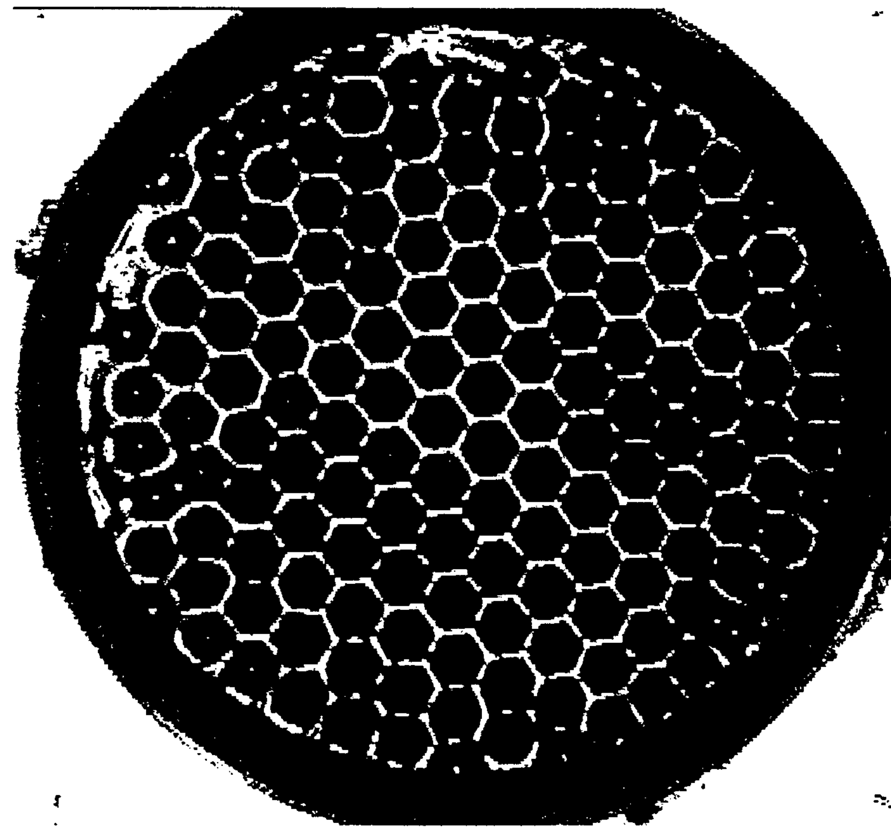

(after Ch. Merkwirth, Göttingen)

[TR-11]

Vibrated liquid layer

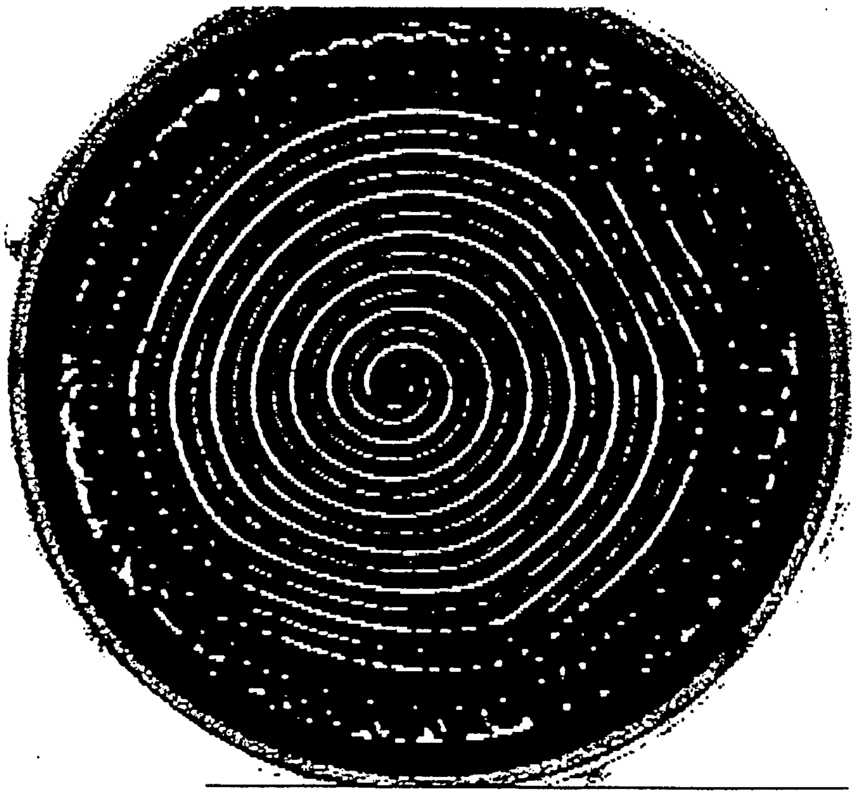

(after Ch. Merkwirth, Göttingen)

[TR-12]

Vibrated liquid layer

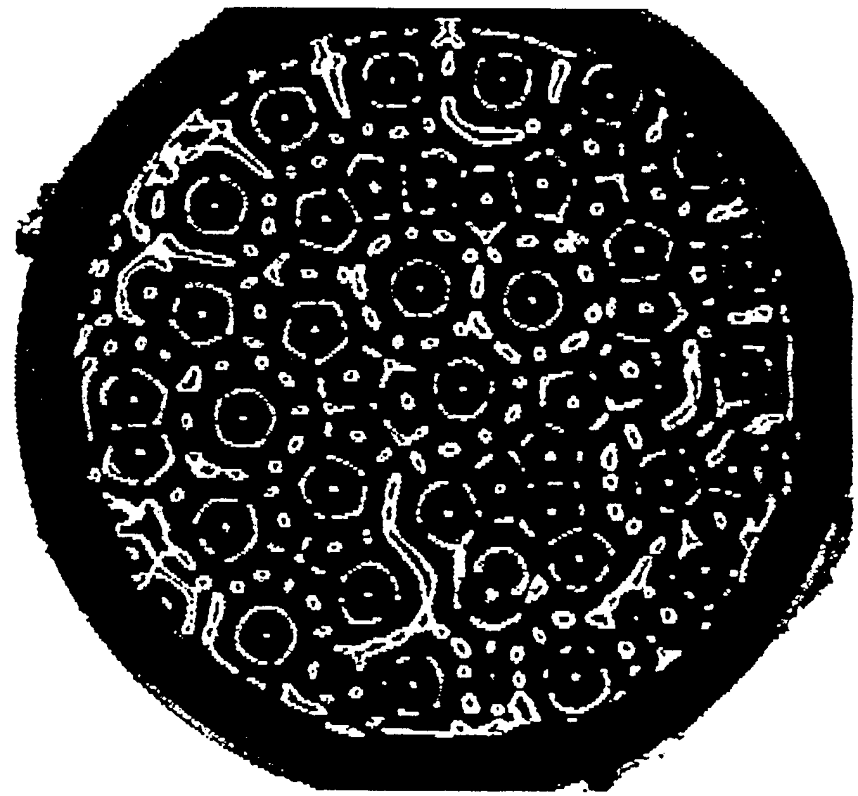

after Ch. Merkwirth, Göttingen

[TR-13]

Acoustics

Acoustic cavitation:

Esche, Acustica 2 (1952) AB208,
Lauterborn & Cramer, PRL 47 (1981)1445

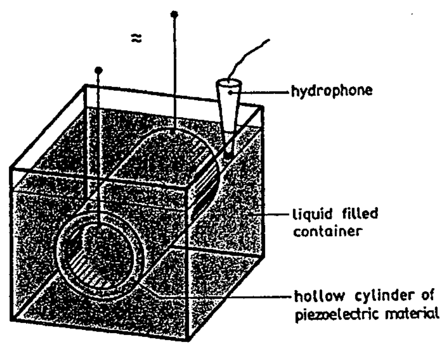

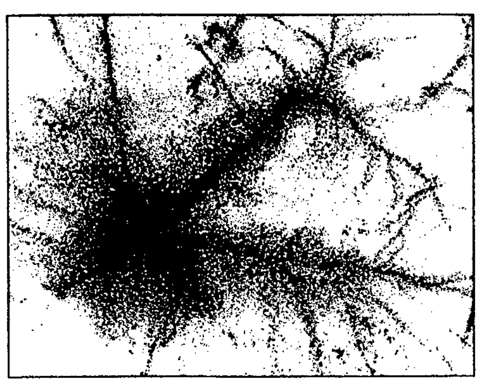

[TR-14]

Basic Notions in Nonlinear Dynamics

[TR-15]

Basic notions: state space

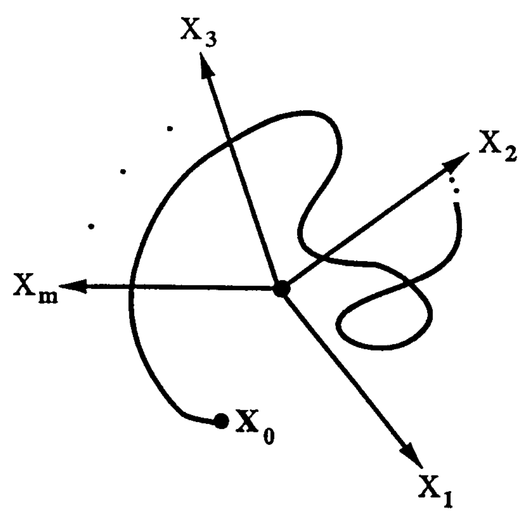

A state x_0 and a trajectory

Evolution equations:

$$\dot{\vec{x}} = \vec{f}(\vec{x};\vec{\mu}) \quad \vec{x} \in R^m,\ \vec{\mu} \in R^d$$

[TR-16]

Basic notions: attractors

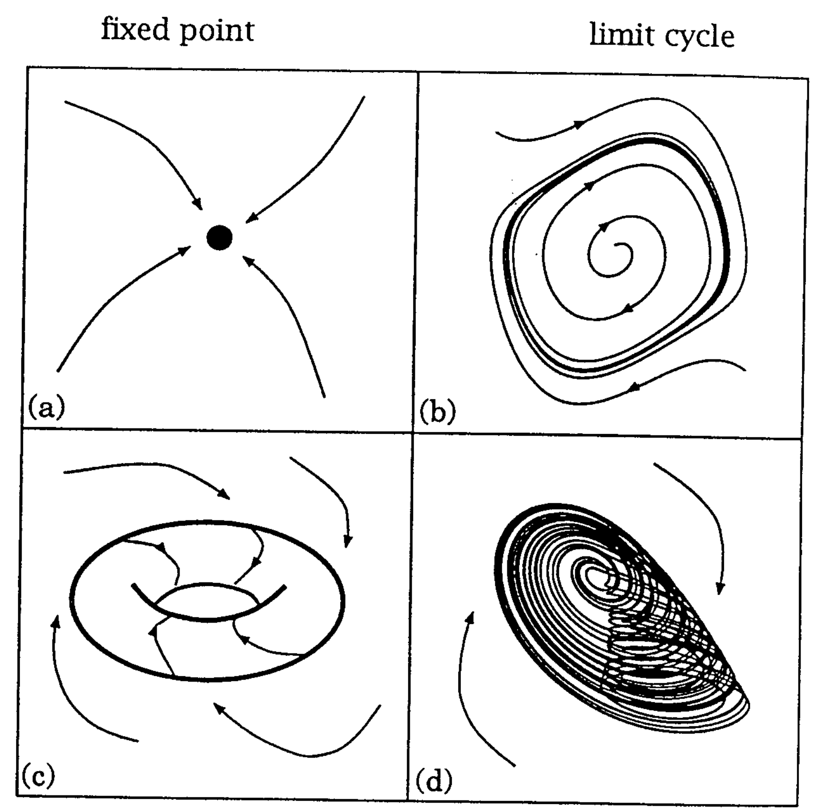

[TR-17]

Basic notions: Poincaré section

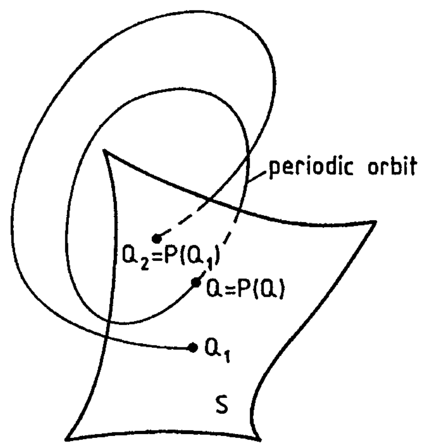

[TR-18]

Basic notions: strange attractor

Double-well Duffing oscillator

$$\ddot{x} + d\dot{x} - x + x^3 = a \sin \omega t$$
$$d = 0.2,\ a = 0.3,\ \omega = 1.24.$$

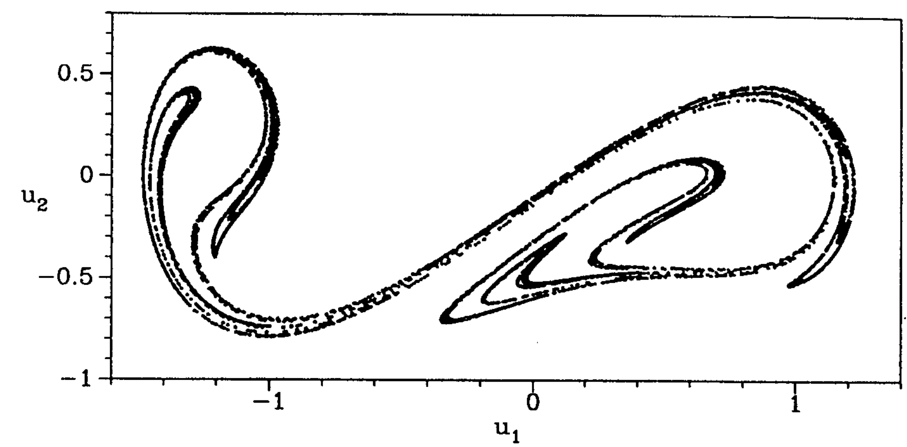

[TR-19]

Basic notions: strange attractor

Experimental driven pendulum

$$\ddot{\phi} + d\dot{\phi} + \sin\phi = a\sin\omega t$$

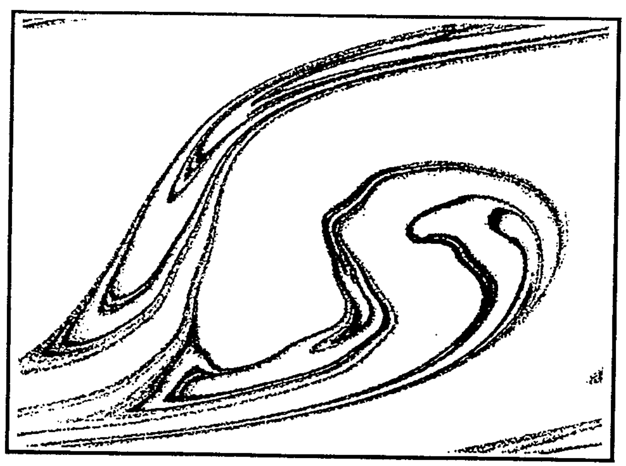

[TR-20]

Basic notions: Bifurcation

Bifurcation = Qualitative change of an attractor when a parameter is altered

There are four local bifurcations.

1. Hopf bifurcation:

Change of a fixed point to a limit cycle

Example: van der Pol oscillator, ...

2. Saddle-node or tangent bifurcation:

Sudden birth of a limit cycle

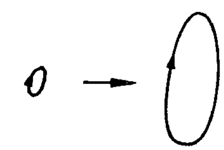

Example: resonance curves turning over, ...

Basic notions: Bifurcation

3. Period-doubling bifurcation:

Limit cycle changes to a limit cycle
of exactly double period

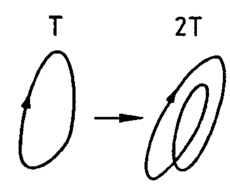

Example: driven oscillators, ...

4. Transcritical bifurcation:

Exchange of stability of two fixed points

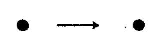

Example: laser rate equations, ...

Basic notions: Bifurcation diagram

Hopf bifurcation:

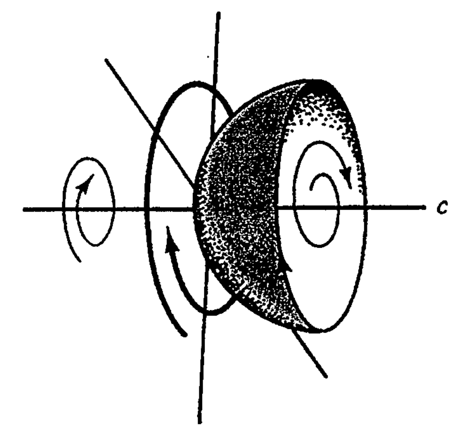

Saddle-node bifurcation:

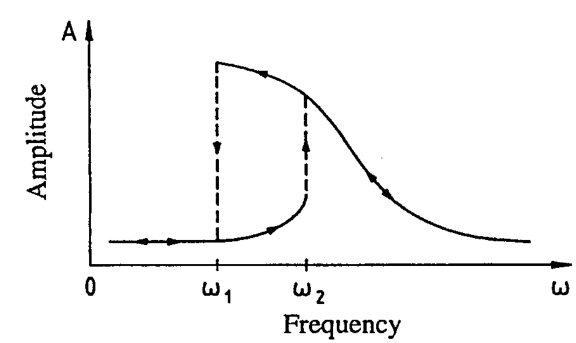

[TR-23]

Basic notions: Bifurcation diagram

Period-doubling bifurcation:

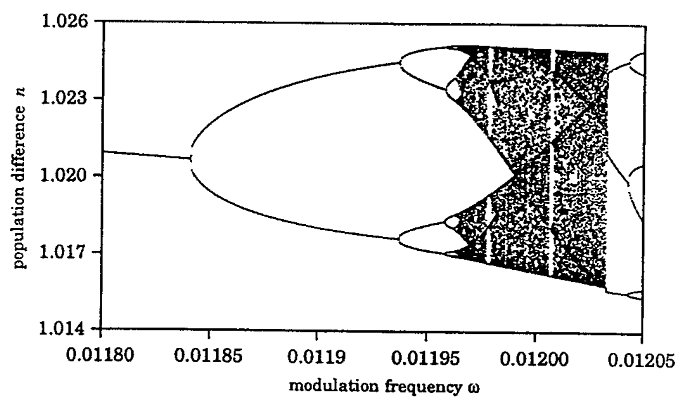

Transcritical bifurcation:

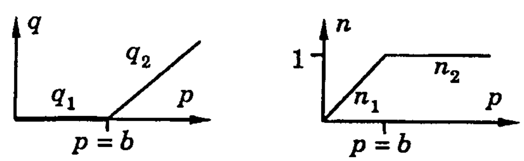

[TR-24]

Basic notions: Lyapunov Exponents

Stretching and folding:

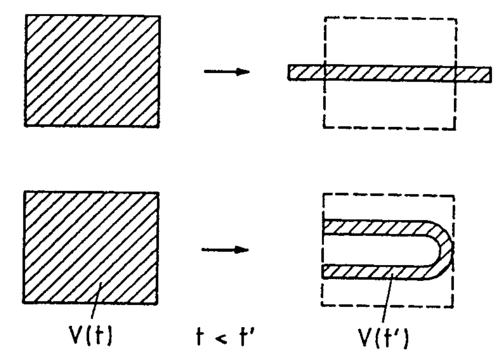

Experimental Pendulum Attractor:

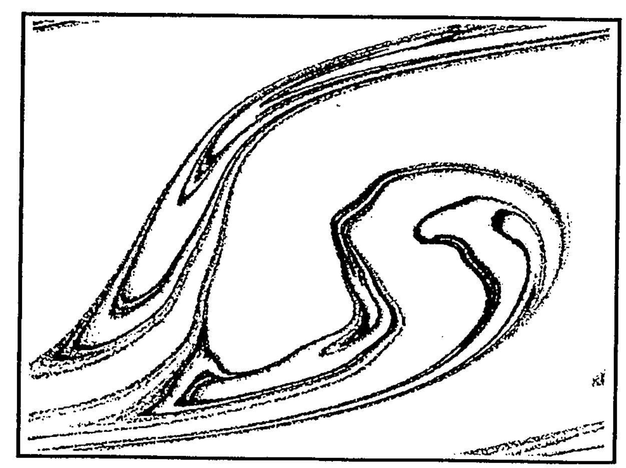

Basic notions: Lyapunov Exponents

Deformation of an infinitesimal ball:

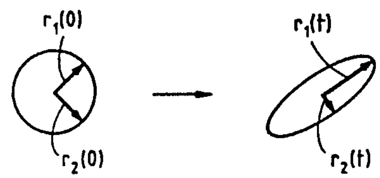

Definition of the Lyapunov exponent λ_i:

$$\lambda_i = \lim_{r_i(0)\to 0} \lim_{t\to\infty} \frac{1}{t} \log \frac{r_i(t)}{r_i(0)}$$

Lyapunov spectrum Λ:

$\Lambda = \{\lambda_i, i = 1, \ldots, m;\ \lambda_1 \geq \lambda_2 \geq \ldots \geq \lambda_m\}$

(m = dimension of the state space)

Basic notions: Lyapunov Exponents

The largest Lyapunov exponent characterizes the attractor.

For continuous systems we have:

λ_1	$<$	0	Fixed point
λ_1	$=$	0	Limit cycle ($\lambda_2 < 0$)
λ_1	$=$	0	Torus ($\lambda_2 = 0, \lambda_3 < 0$)
λ_1	$>$	0	Chaotic attractor

When $\lambda_1 > 0$ one says: The system shows sensitive dependence on initial conditions.

Practical predictability gets lost this way, because nonsignificant digits of the initial conditions get significant.

[TR-27]

Nonlinear Time Series Analysis

[TR-28]

Relation in physics

Theory	Experiment
trajectory in state space high-dimensional	time series one-dimensional

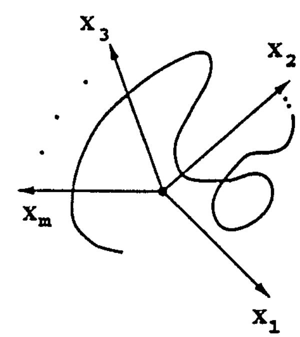

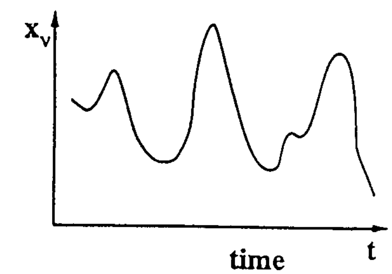

- Measurement yields a projection of a high-dimensional trajectory on one coordinate axis.

Question:

- Do experiments necessarily give underdetermined results?

[TR-29]

Nonlinear time series analysis

Embedding:

(Packard, Crutchfield, Farmer, Shaw 1980; Takens 1981)

Time series of sampled data:

$s_1, s_2, s_3, s_4, s_5, s_6, \ldots$

Embedding in a three-dimensional space:

$\mathbf{s}_1 = (s_1, s_2, s_3)$
$\mathbf{s}_2 = (s_3, s_4, s_5)$

•
•
•

Example:

Experimental data from a driven pendulum

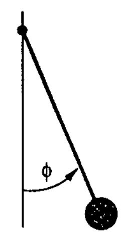

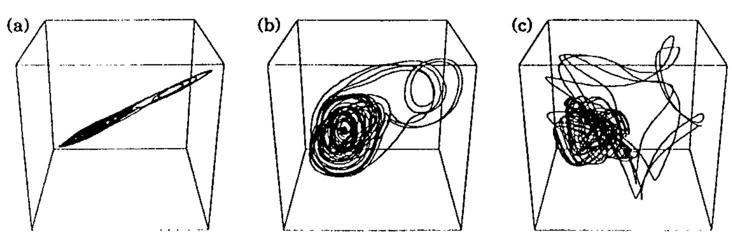

[TR-30]

Nonlinear time series analysis

General statement:

When the embedding of a time series into higher-dimensional spaces shows a structure, then some law is at work that generates it.

Task:

- Characterization of the structure (static)
  dimension estimation, etc
- Characterization of the structure (dynamic)
  expansion properties (Lyapunov spectrum), etc
- Find the laws behind the structure
  model building, parameter estimation, etc

[TR-31]

Nonlinear Time Series Analysis
Dimension Estimation

- pointwise dimension D of a point set M at a point P

$$N(r) \sim r^D, \; r \to 0$$

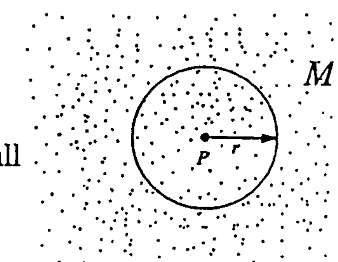

$N(r)$ = number of points of the set M inside the ball of radius r around P

Examples:

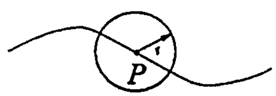

$$N(r) \sim r^1, \; r \to 0$$
$$D = 1$$

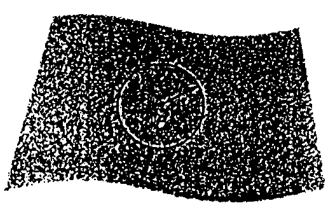

$$N(r) \sim r^2, \; r \to 0$$
$$D = 2$$

- Chaotic attractors usually have a fractal dimension, e. g. $D = 2.35$

[TR-32]

Nonlinear Time Series Analysis
Largest Lyapunov Exponent

Numerical determination from a time series:

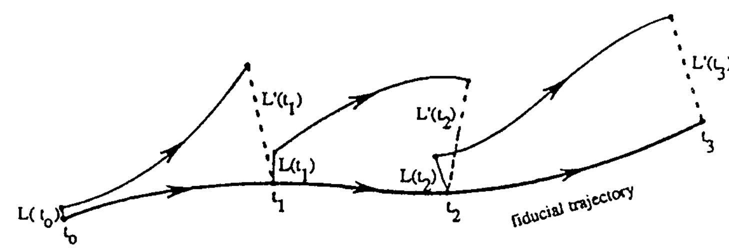

$$\lambda_{max} = \frac{1}{t_m - t_0} \sum_{k=1}^{m} \log_2 \frac{L'_k}{L_{k-1}} \left[\frac{bits}{s}\right]$$

- Method for determining the largest Lyapunov exponent

[TR-33]

Nonlinear time series analysis

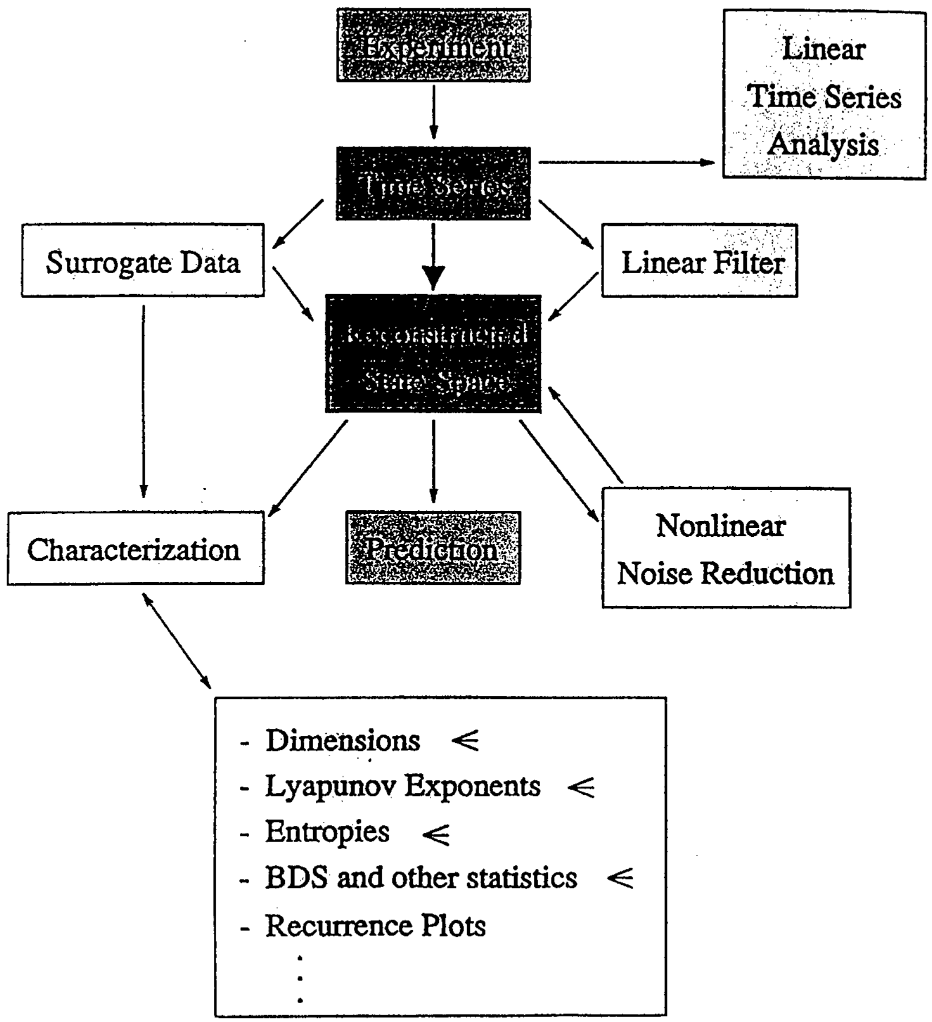

[TR-34]

Nonlinear Bubble Dynamics Theory

[TR-35]

Nonlinear Bubble Dynamics

Bubble Model Parameters

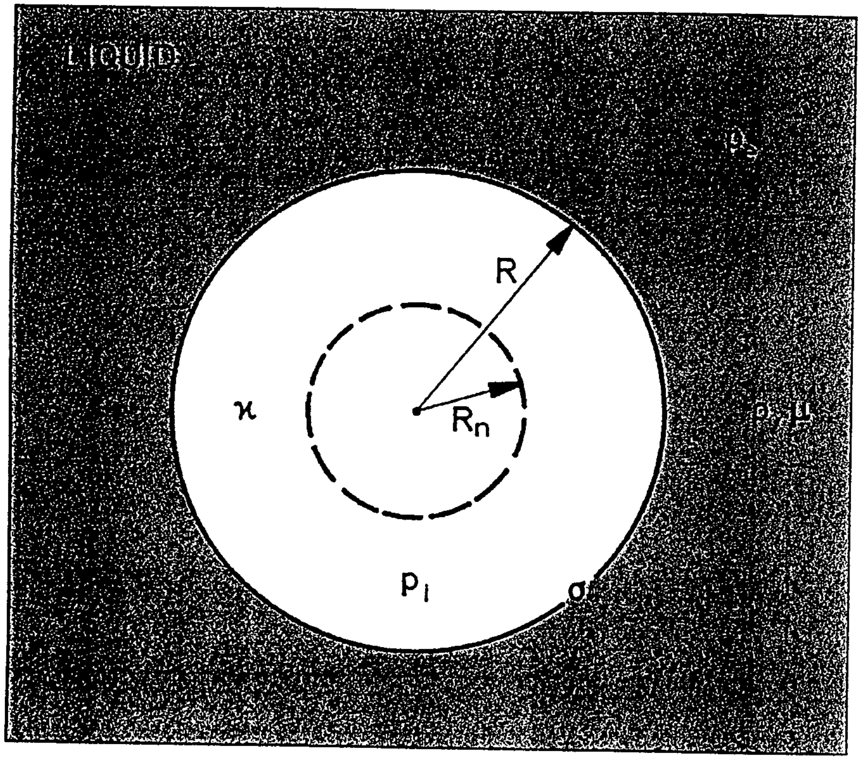

[TR-36]

Nonlinear Bubble Dynamics

Bubble Model

$$\left(1-\frac{\dot R}{C}\right)R\ddot R+\frac{3}{2}\left(1-\frac{\dot R}{3C}\right)\dot R^2=\left(1+\frac{\dot R}{C}\right)H+\frac{\dot R}{C}\left(1-\frac{\dot R}{C}\right)R\frac{dH}{dR}$$

$$H = \int_{p|_{r\to\infty}}^{p|_{r=R}} \frac{dp(\rho)}{\rho}$$

$$p(\rho) = A\left(\frac{\rho}{\rho_0}\right)^n - B$$

$$p|_{r=R} = \left(p_{stat}+\frac{2\sigma}{R_n}\right)\left(\frac{R_n^3-bR_n^3}{R^3-bR_n^3}\right)^\kappa - \frac{2\sigma}{R} - \frac{4\mu}{R}\dot R$$

$$p|_{r\to\infty} = p_{stat} + p(t)$$

$$C = \sqrt{c_0{}^2+(n-1)H}$$

R = bubble radius
R_n = bubble radius at rest
ρ = liquid density
ρ_0 = liquid density at normal conditions (998 kg/m^3)
p = pressure in the liquid
σ = surface tension (0.0725 N/m for water)
μ = viscosity of the liquid (0.001 Ns/m^2 for water)
c_0 = sound velocity in the liquid at normal conditions (1500 m/s)
C = sound velocity in the liquid at the wall of the bubble
p_{stat} = static ambient pressure (100 kPa)
κ = polytropic exponent (chosen as 5/3 for a monoatomic gas)
b = van der Waals constant (0.0016 to model some artificial gas)
A = 300.1 MPa, B = 300.0 MPa, n = 7
$p(t) = \hat p_a \sin 2\pi\nu t$

[TR-37]

Nonlinear Bubble Dynamics

Resonance Curves

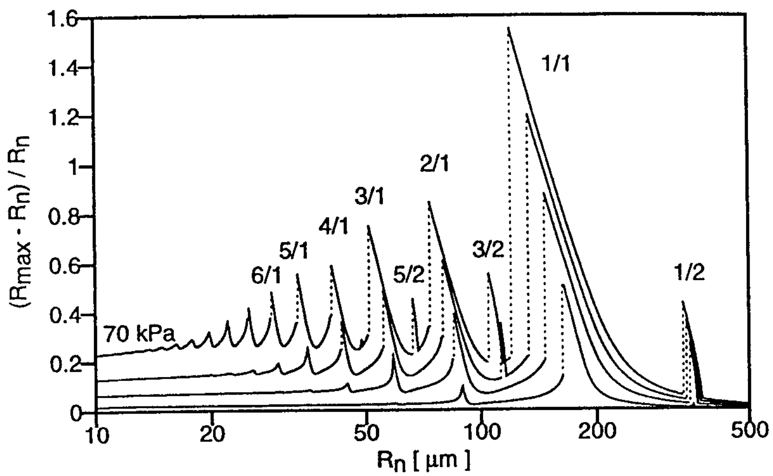

Driving Frequency: 20 kHz
Driving Amplitude: 10, 30, 50 and 70 kPa

[TR-38]

Nonlinear Bubble Dynamics
Radius - Time Curves

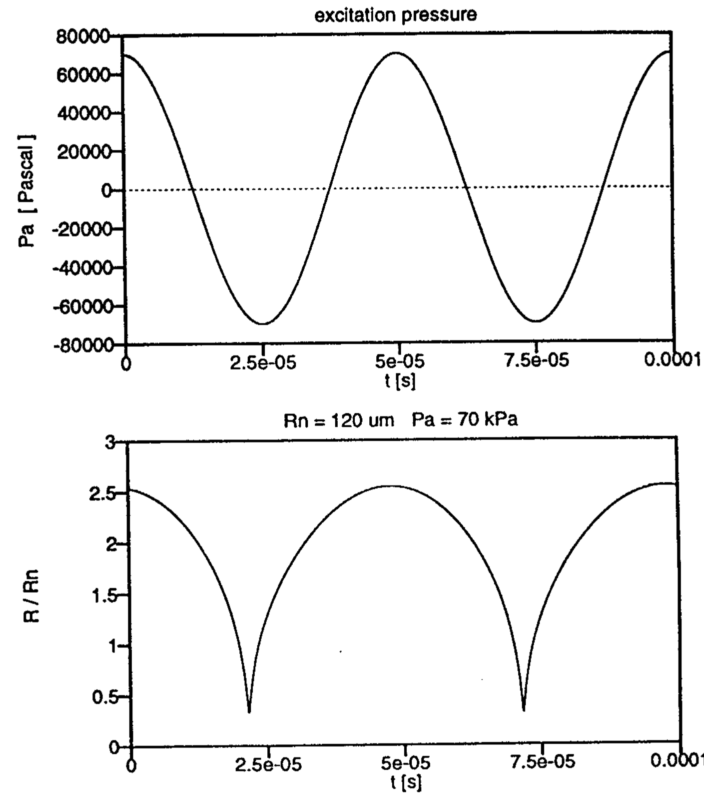

Driving Frequency: 20 kHz
Driving Amplitude: 70 kPa
Bubble Radius at Rest: 120 μm, main resonance

Period 1 Solution from Main Resonance

[TR-39]

Nonlinear Bubble Dynamics
Radius - Time Curves, 20 kHz, 70 kPa

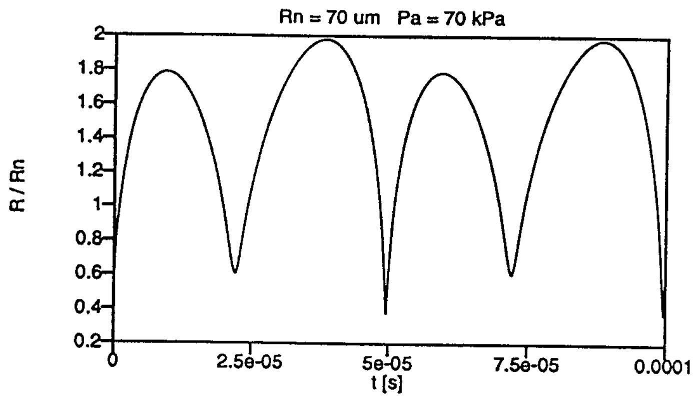

Bubble Radius at Rest: 70 μm, 2/1 resonance

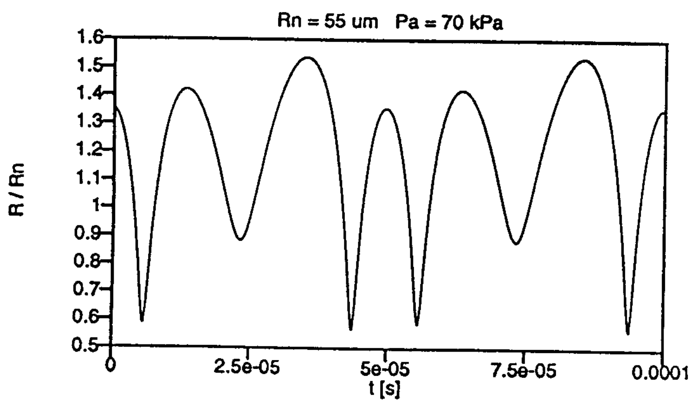

Bubble Radius at Rest: 55 μm, 3/1 resonance

Period 1 Solutions from 2/1 and 3/1 Resonance

[TR-40]

Nonlinear Bubble Dynamics
Radius - Time Curves, 20 kHz, 70 kPa

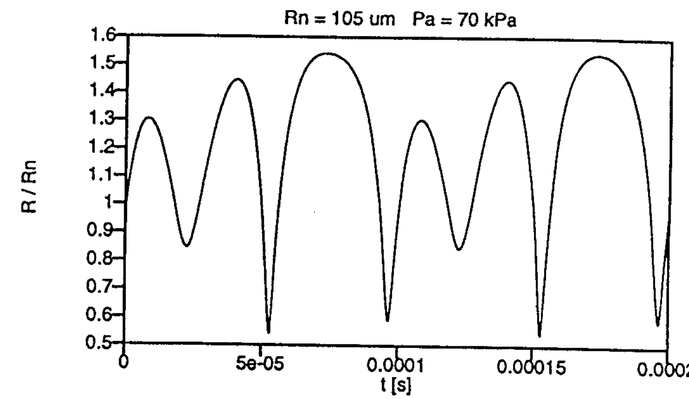

Bubble Radius at Rest: 105 μm, 3/2 resonance

Period 2 Solution from 3/2 Resonance

[TR-41]

Nonlinear Bubble Dynamics

Resonance Curves, 20 kHz, 80 kPa

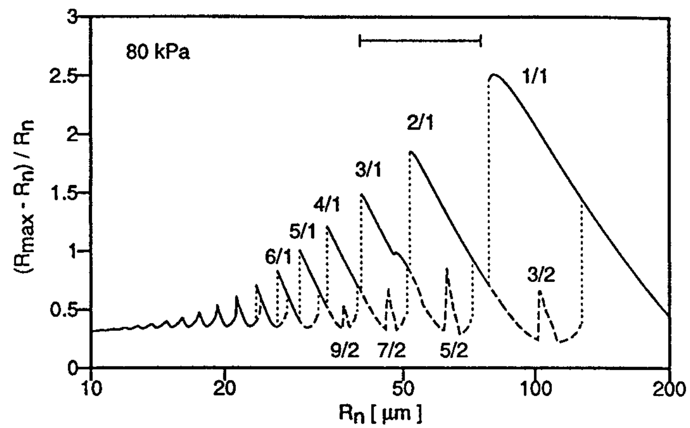

Bifurcation Diagram

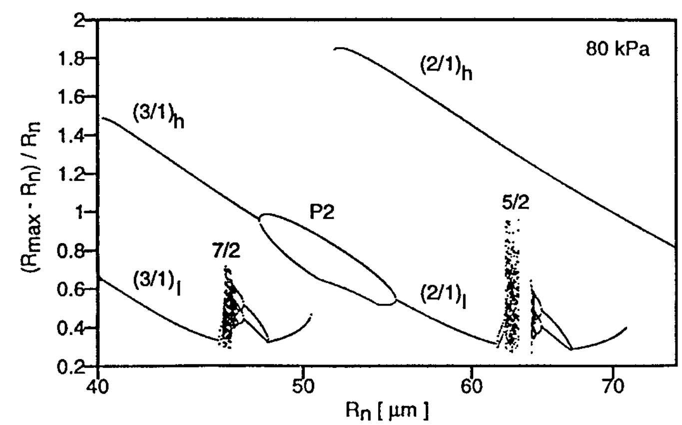

[TR-42]

Nonlinear Bubble Dynamics
Radius - Time Curves, 20 kHz, 80 kPa

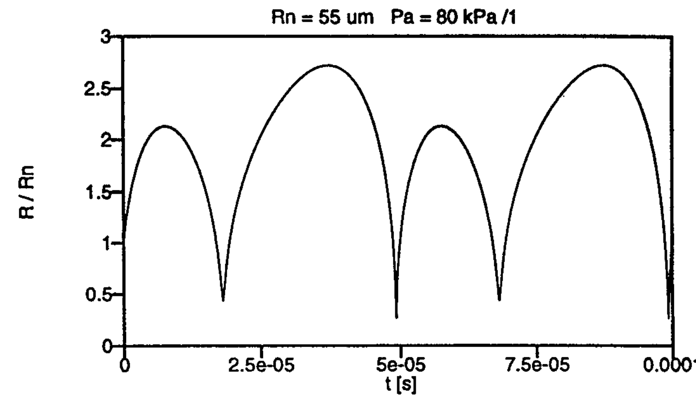

Bubble Radius at Rest: 55 μm, 2/1 resonance, upper branch

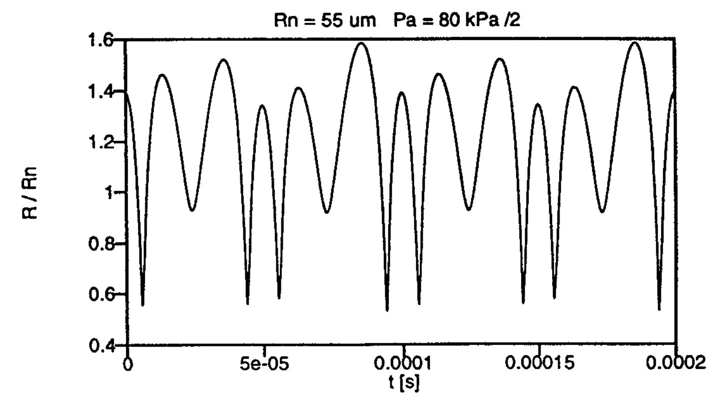

Bubble Radius at Rest: 55 μm, 3/1 resonance, upper branch, period doubled

Coexisting Solutions from 2/1 and 3/1 Resonance

[TR-43]

Nonlinear Bubble Dynamics
Radius - Time Curve, 20 kHz, 80 kPa

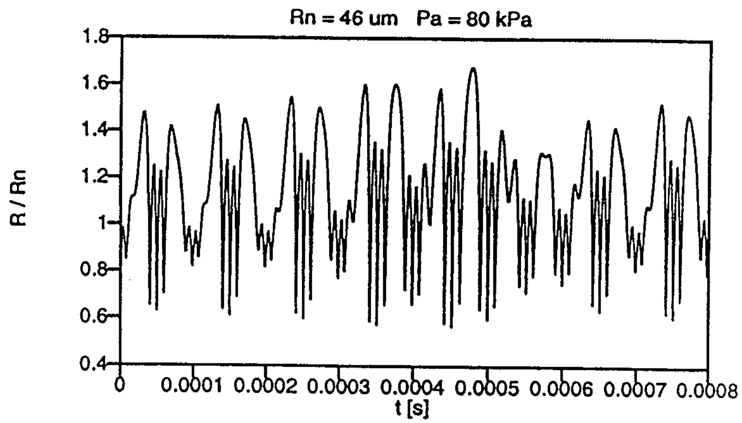

Bubble Radius at Rest: 46 μm, 7/2 resonance

Chaotic Solution from 7/2 Resonance

[TR-44]

Nonlinear Bubble Dynamics

Response Curves, 20 kHz, 90 - 110 kPa

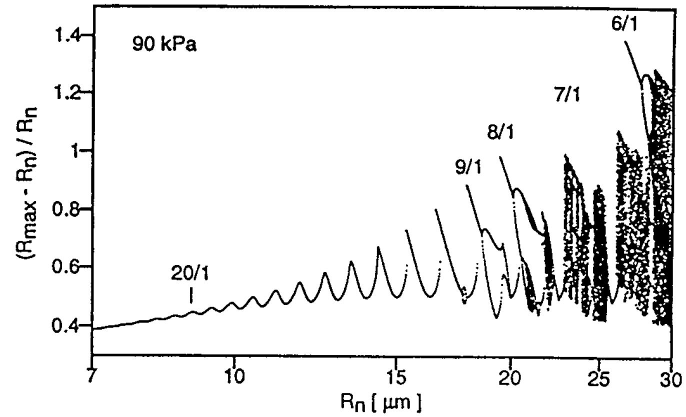

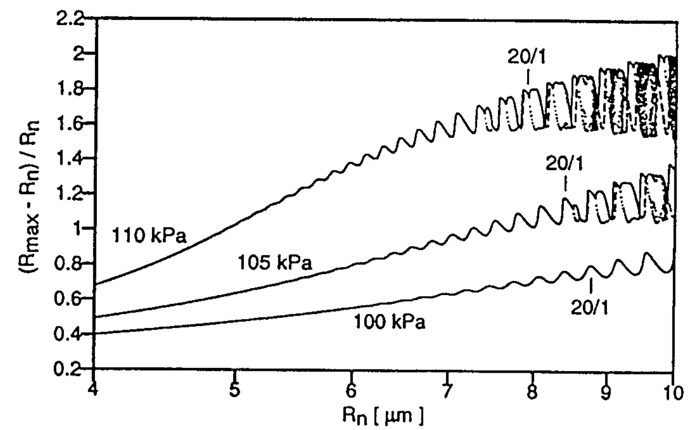

Intermediate High Driving
Small Bubbles

Nonlinear Bubble Dynamics

Radius - Time Curves, 20 kHz

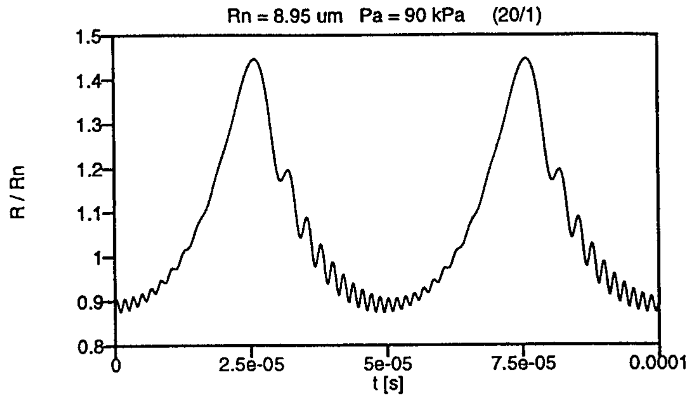

Bubble Radius at Rest: 8.95 μm, 90 kPa

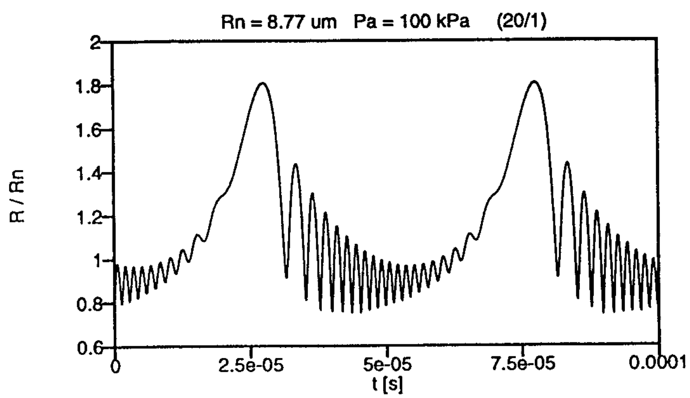

Bubble Radius at Rest: 8.77 μm, 100 kPa

Solutions from the 20/1 Resonance

Nonlinear Bubble Dynamics

Radius - Time Curves, 20 kHz

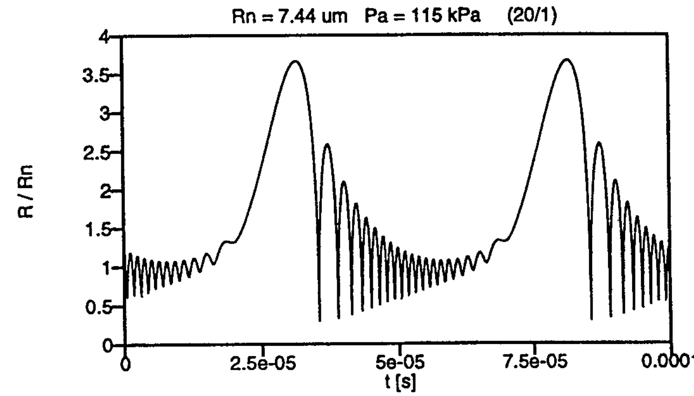

Bubble Radius at Rest: 7.44 μm, 115 kPa

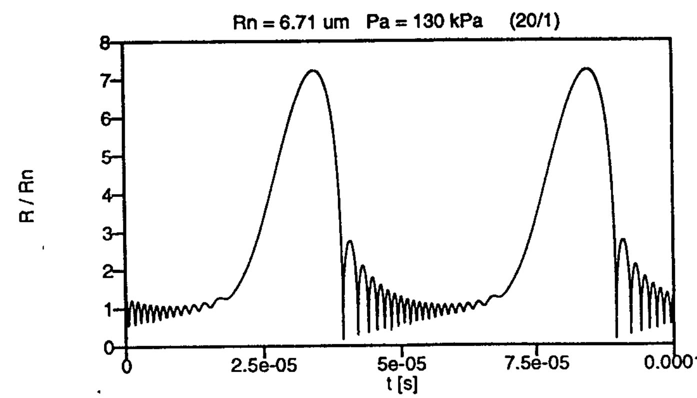

Bubble Radius at Rest: 6.71 μm, 130 kPa

Solutions from the 20/1 Resonance

[TR-47]

Nonlinear Bubble Dynamics

Response Curves, 20 kHz, 115 - 150 kPa

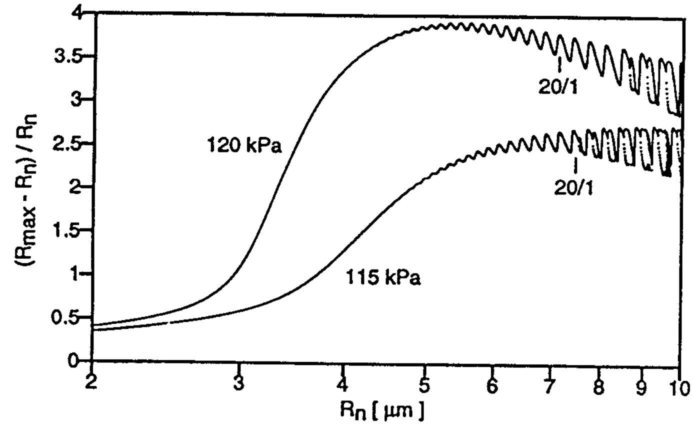

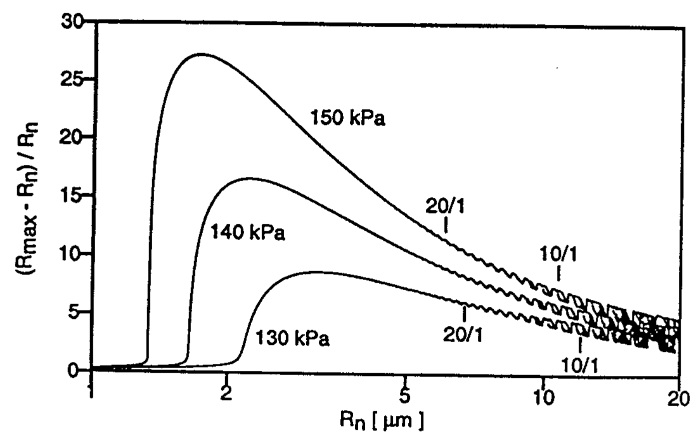

High Driving, Small Bubbles

[TR-48]

Nonlinear Bubble Dynamics

The Giant Response

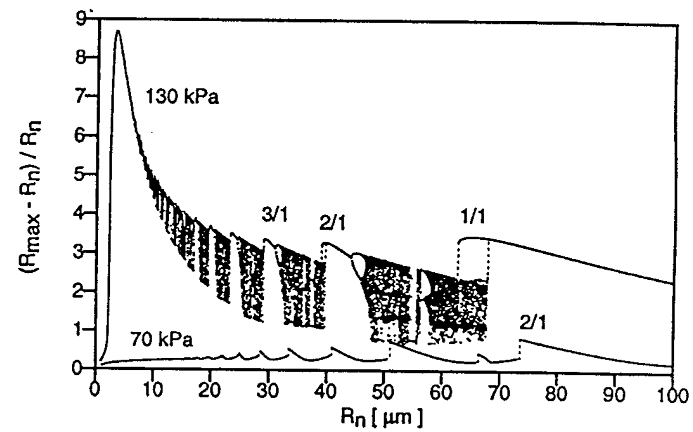

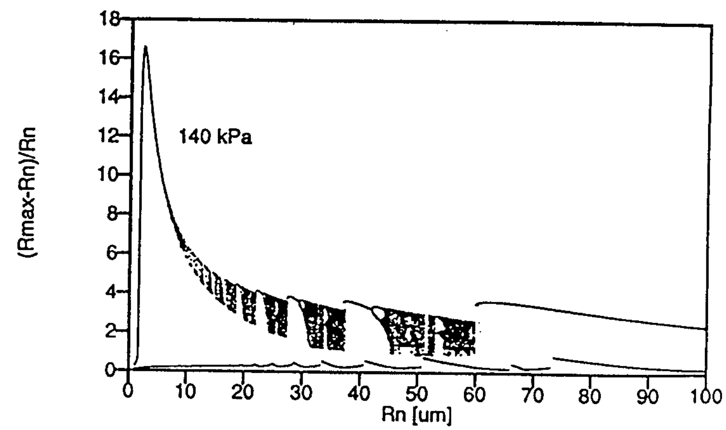

High Driving, Small Bubbles

Nonlinear Bubble Dynamics

The Giant Response

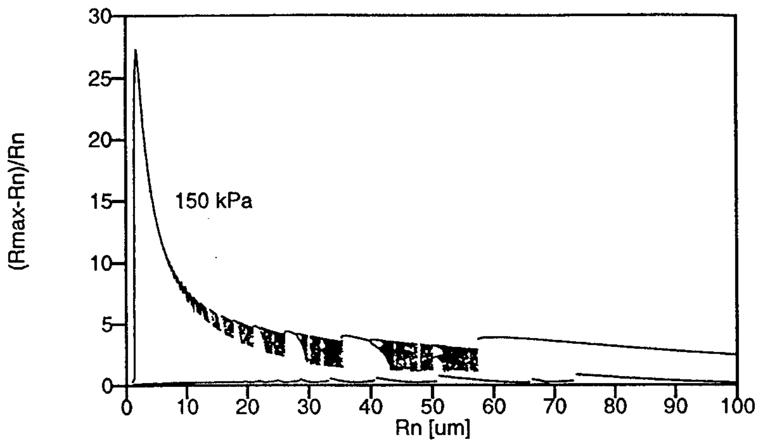

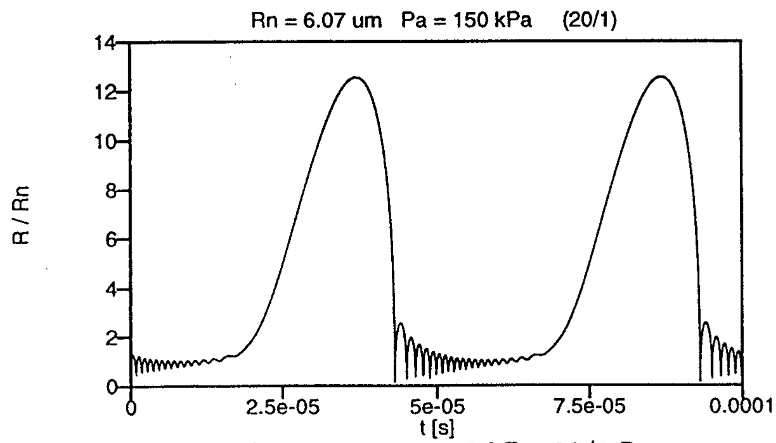

Bubble Radius at Rest: 6.07 μm, 150 kPa, 20/1 Resonance

High Driving, Small Bubbles

Radius-Time Curves

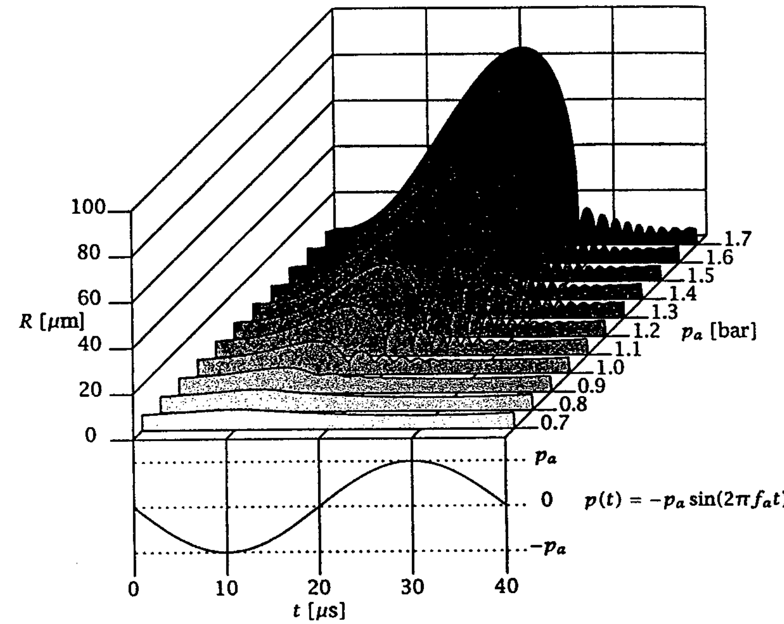

(Courtesy R. Geisler)

Driving frequency $f_a = 25$ kHz

Equilibrium radius $R_0 = 7\mu$m

[TR-51]

Nonlinear Bubble Dynamics

Frequency Dependence

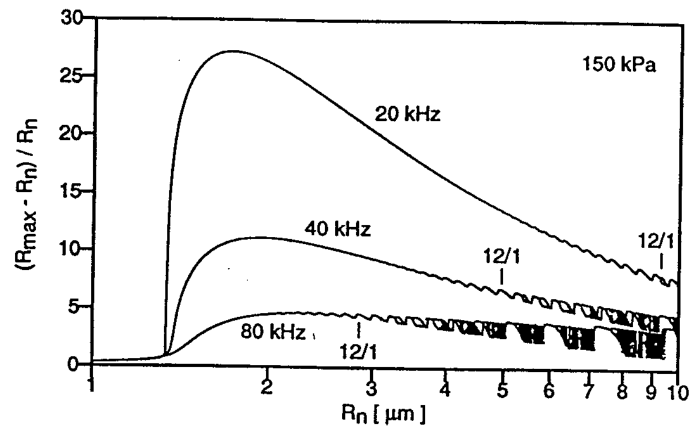

High Driving, Small Bubbles

[TR-52]

Nonlinear Bubble Dynamics Experiments

[TR-53]

Single bubble dynamics

Experimental arrangement

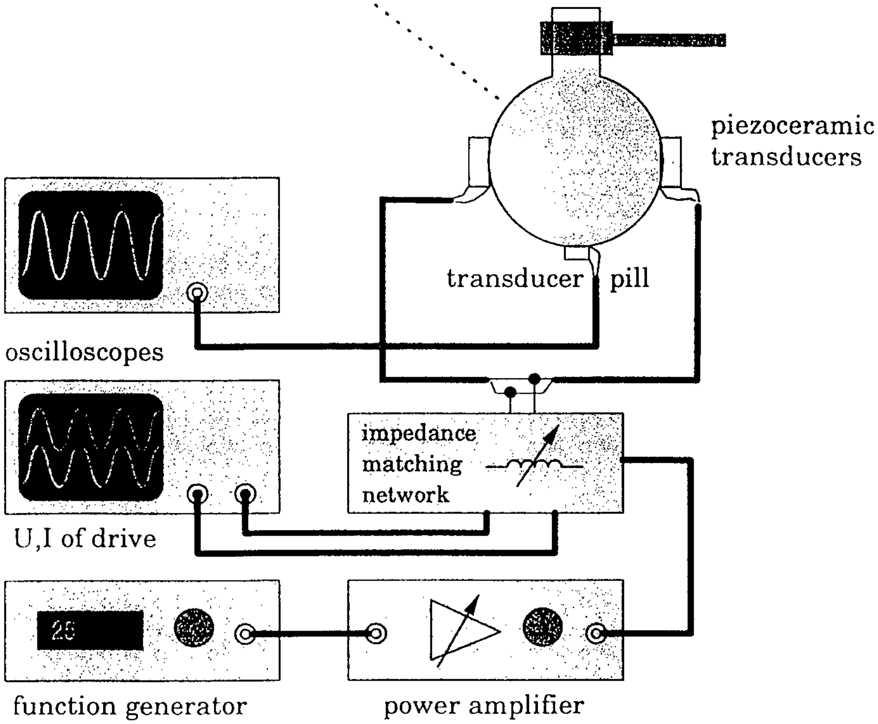

[TR-54]

Single Bubble Sonoluminescence

Spherical flask

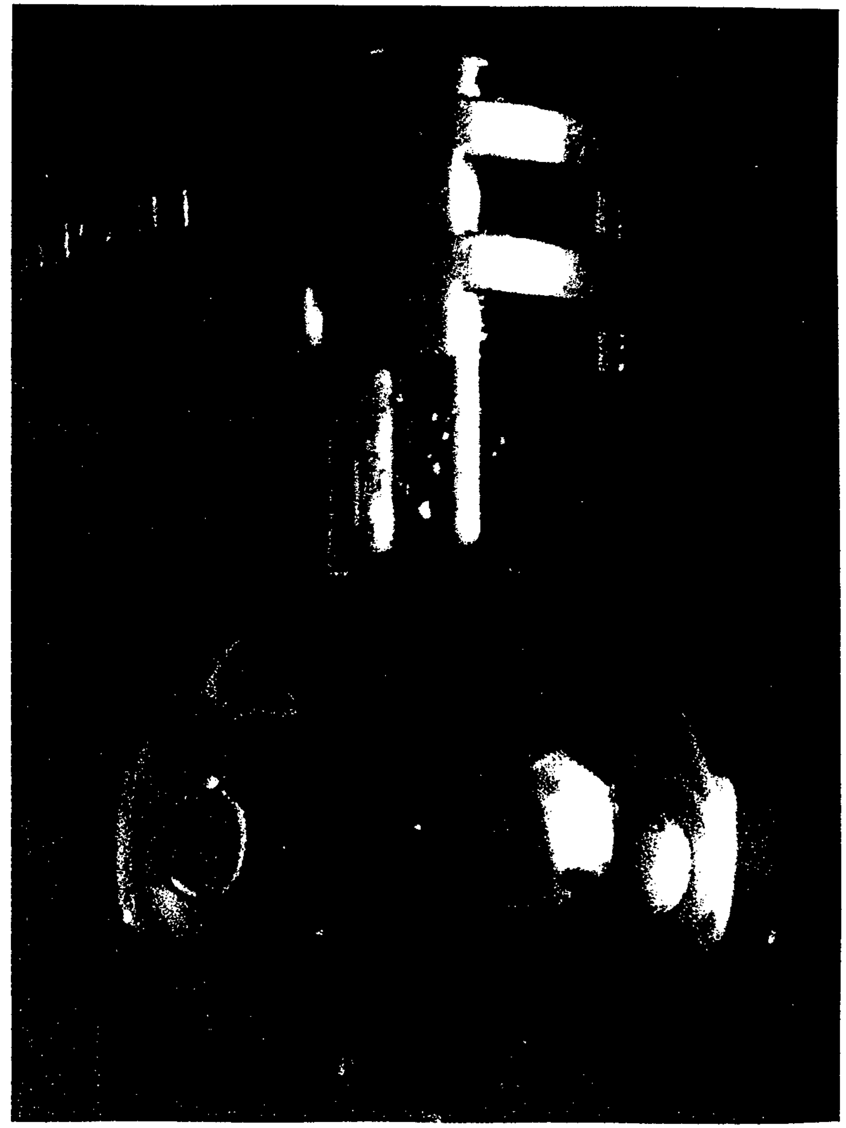

[TR-55]

Single Bubble Sonoluminescence

Square container

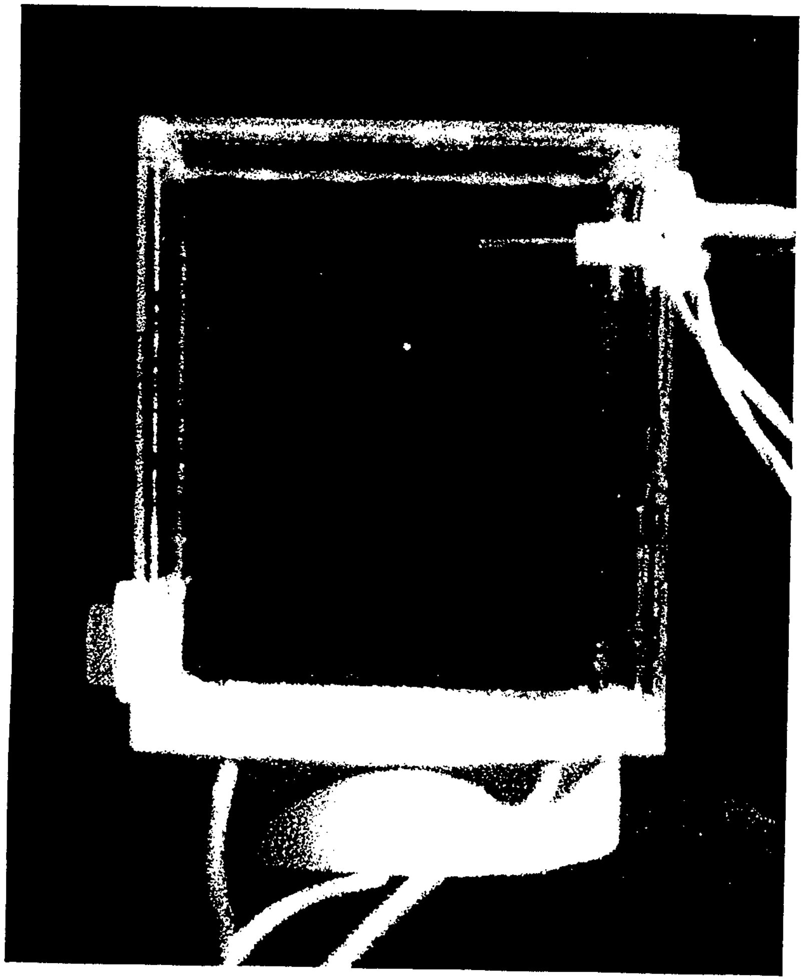

[TR-56]

Two Bubble Sonoluminescence

Cylindrical container

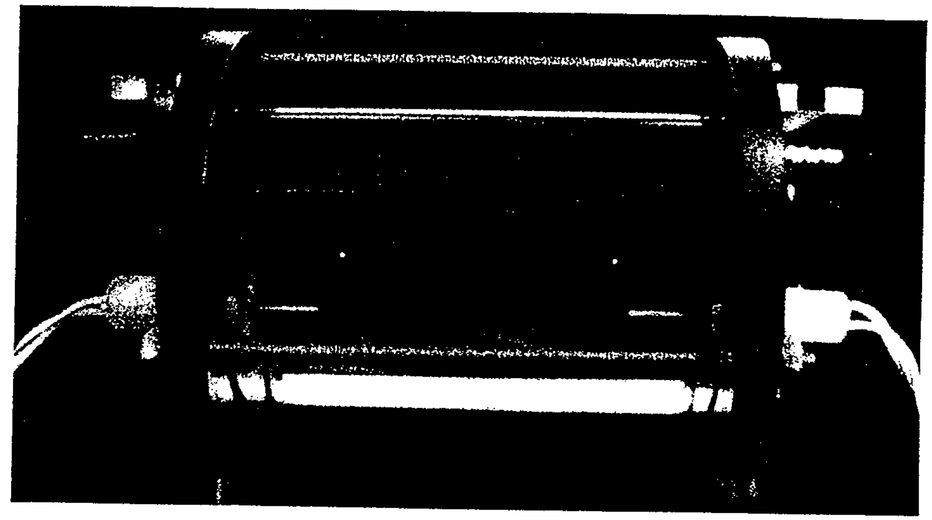

[TR-57]

Single-bubble Sonoluminescence

13h exposure time

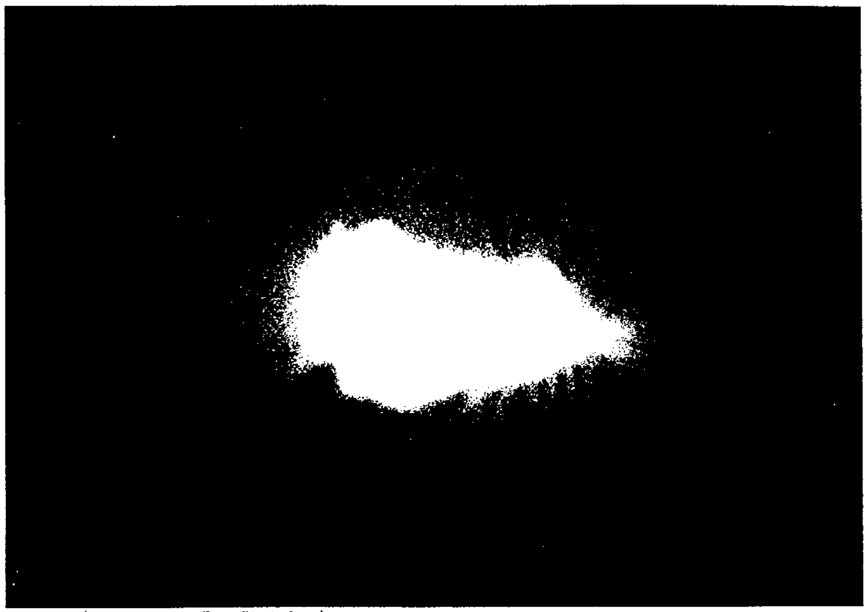

(courtesy R. Geisler)

[TR-58]

Single bubble dynamics

High speed photography

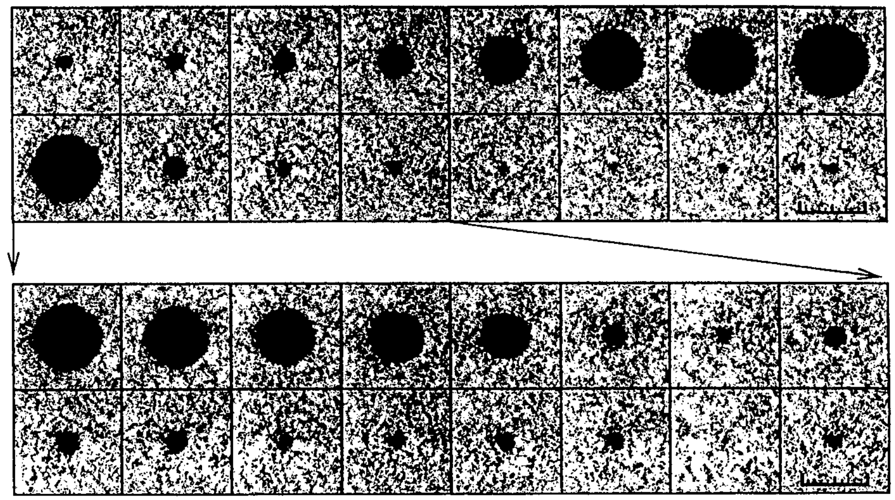

(Courtesy of R. Geisler)

Driving frequency: 21.4 kHz
Interframe time: 2.5 μs
Blow up interframe time: 500 ns
Ruler length: 100 μm

[TR-59]

Single bubble dynamics

Comparison experiment – theory

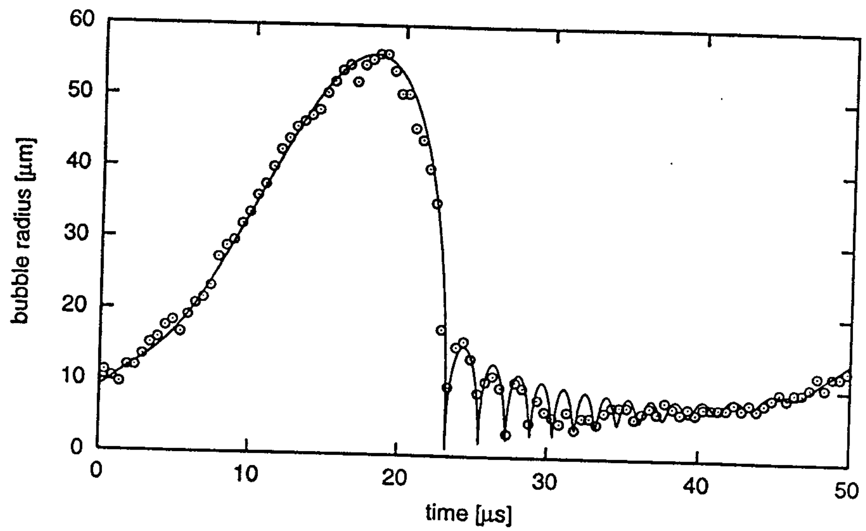

(Courtesy of R. Geisler and R. Mettin)

Driving frequency: 21.4 kHz
Driving amplitude: 132 kPa
Static pressure: 100 kPa
Bubble radius at rest: 8.1 μm
Surface tension: 0.0725 N/m
Viscosity: 0.0018 Ns/m^2
Density of liquid: 1000 kg/m^3
polytropic exponent: 1.2

[TR-60]

Single bubble dynamics

Shock wave at collapse

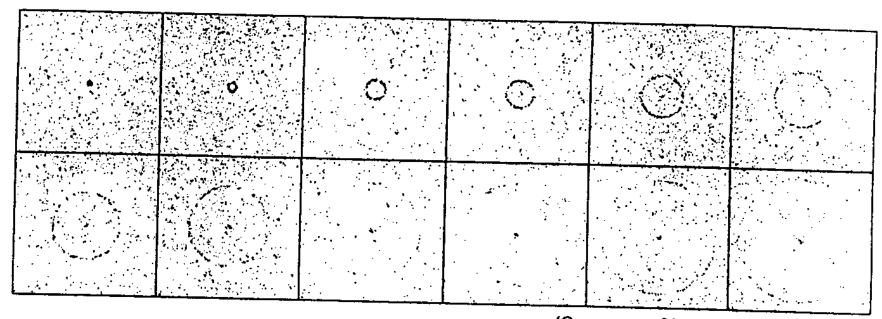

(Courtesy of R. Geisler)

Driving frequency: 21.4 kHz
Interframe time: 30 ns
Frame size: 1.6 mm × 1.6 mm

[TR-61]

Laser-produced bubble in water

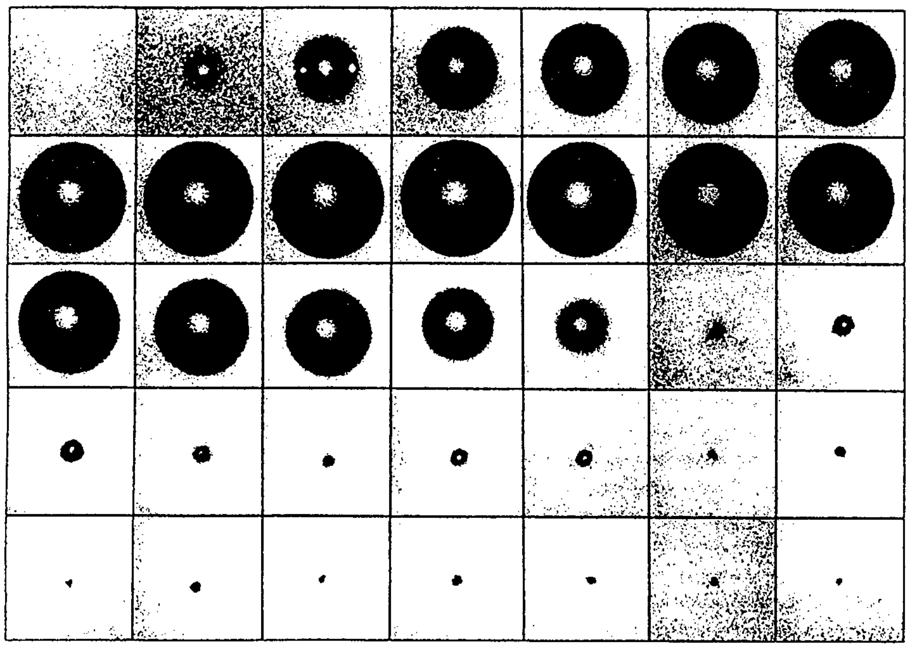

75,000 frames per second

$R_{max} = 1.3$ mm

[TR-62]

Acoustic cavitation

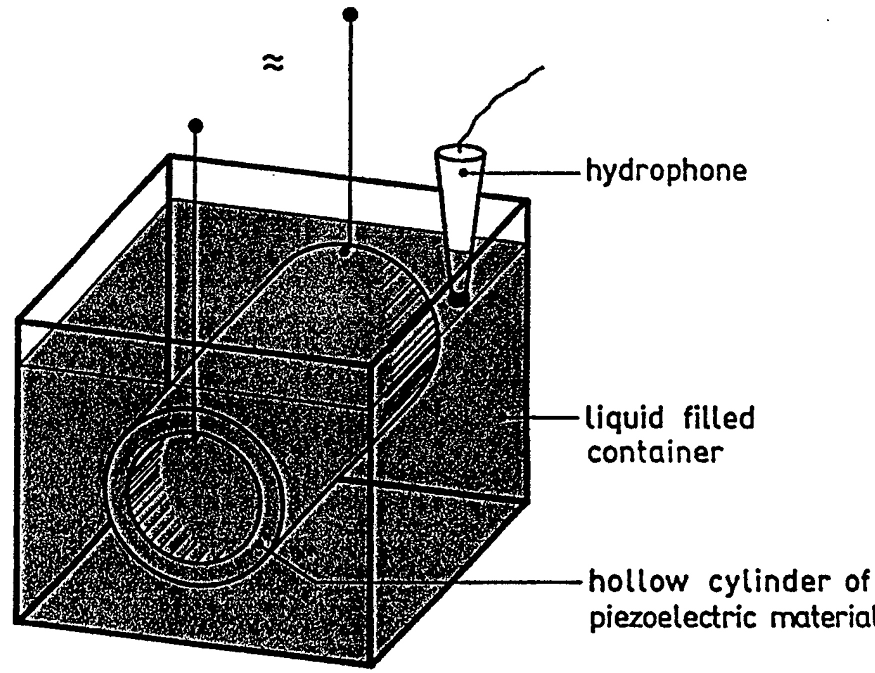

[TR-63]

Acoustic cavitation

Experimental arrangement

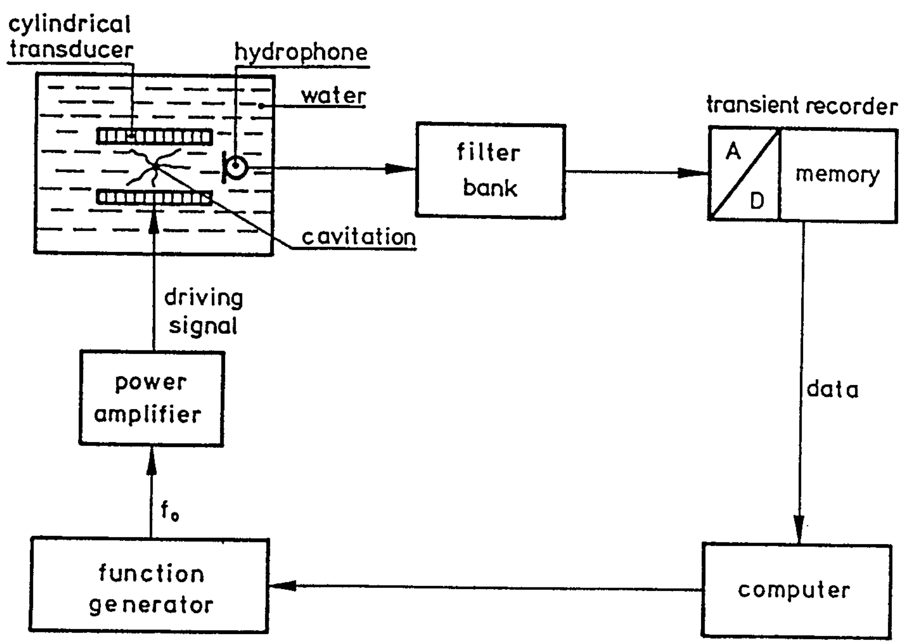

[TR-64]

Acoustic cavitation noise

Spectra of a period-doubling bifurcation cascade

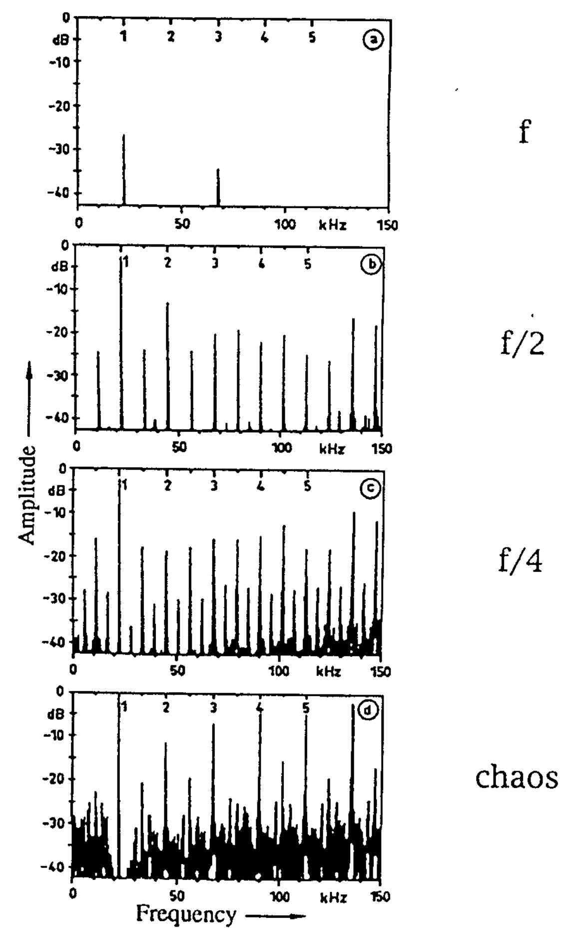

[TR-65]

Acoustic cavitation
Embedding of a chaotic attractor

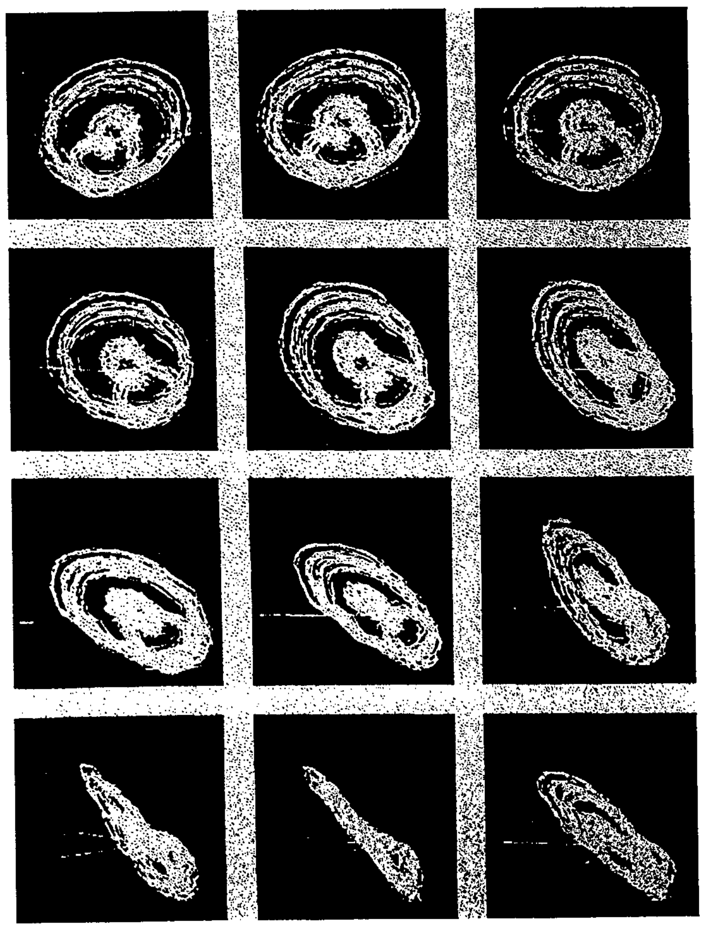

[TR-66]

Acoustic cavitation
Dimension estimation

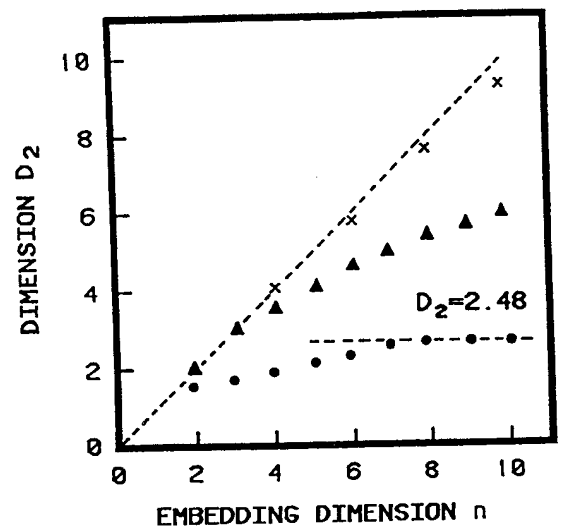

[TR-67]

Acoustic cavitation
Dimension estimation

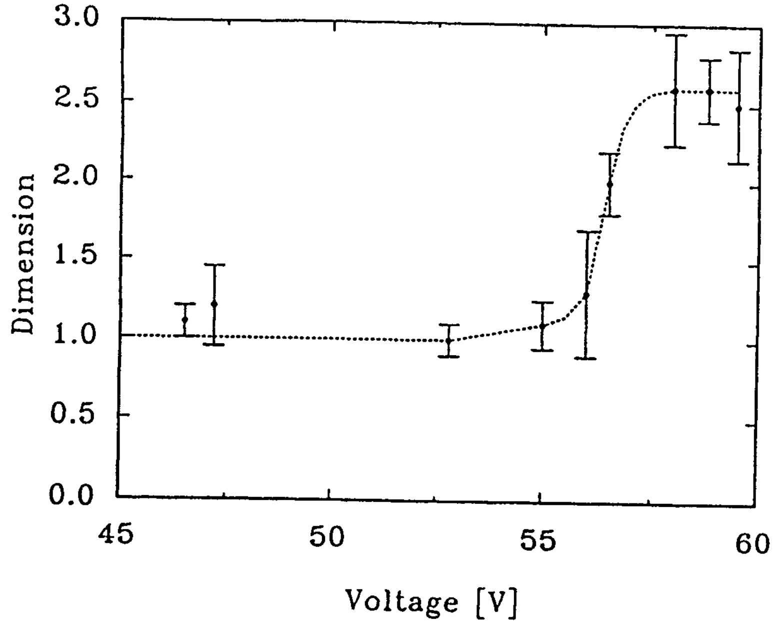

[TR-68]

Acoustic cavitation
Lyapunov spectrum

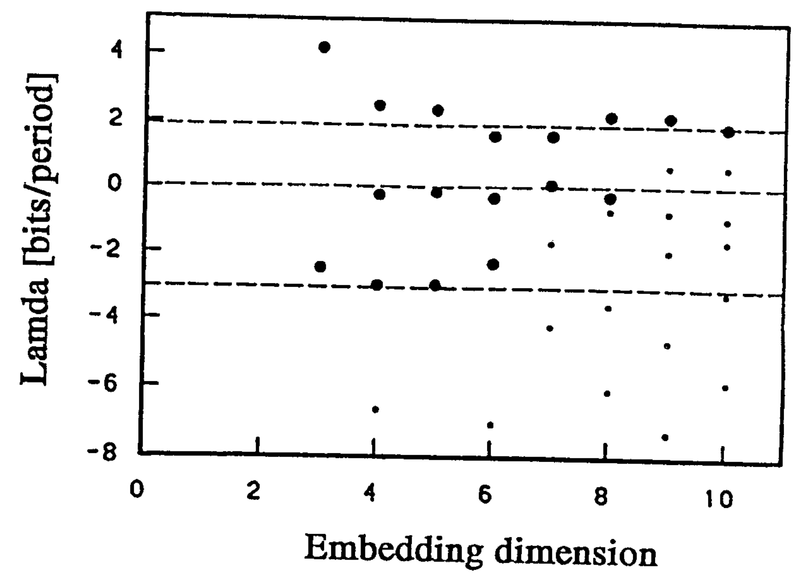

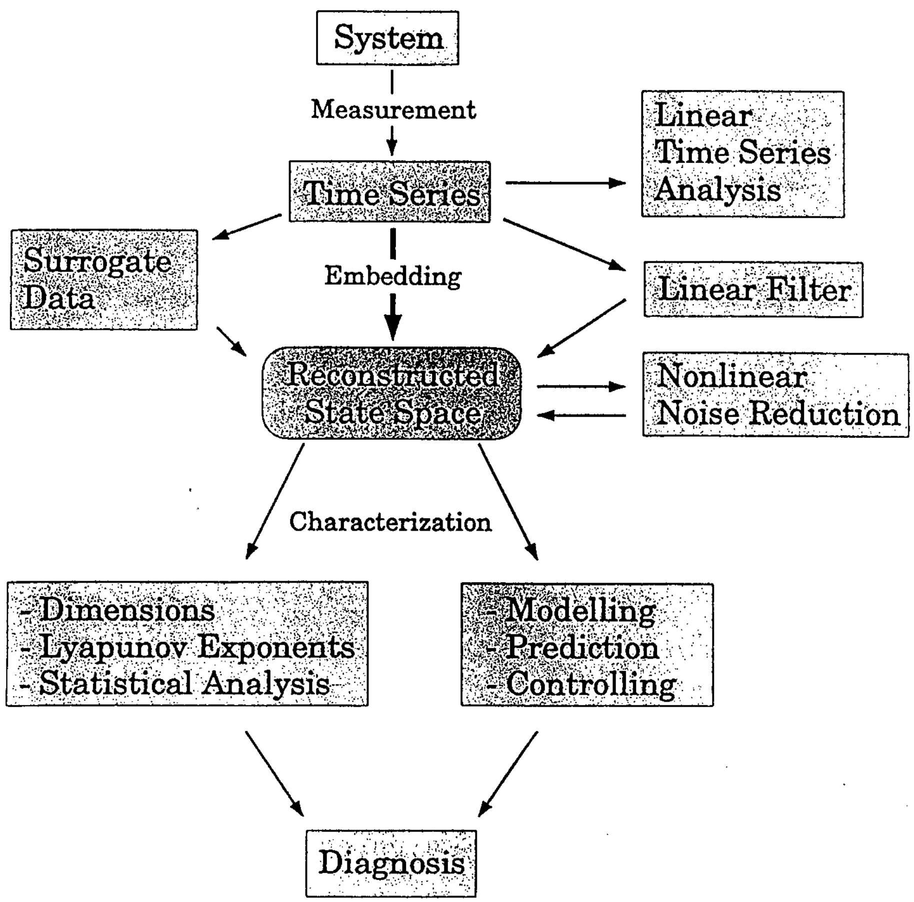
System
Measurement
Time Series
Linear
Time Series
Analysis
Surrogate
Data
Embedding
Linear Filter
Reconstructed
State Space
Nonlinear
Noise Reduction
Characterization
- Dimensions
- Lyapunov Exponents
- Statistical Analysis
- Modelling
- Prediction
- Controlling
Diagnosis

1

Quantum Mechanics Tutorial

J. D. Maynard
The Pennsylvania State University

Purpose

How are Quantum Mechanics and Acoustics related?

- Both involve the same wave phenomena (Wave Mechanics)
- The attenuation of sound involves molecular collisions which must be treated with quantum mechanics
- Solid crystals have quantized sound waves (Phonons)
- Interaction between phonons and electrons, effects of pressure, magnetic fields, light (Raman, Brillouin scattering), etc.
- Acoustics in Macroscopic Quantum Systems (Superfluids)

2

History Events which led to Quantum Mechanics

- **Plank's theory of Blackbody Radiation** (1901)
  - Due to quantized modes of a solid (phonons)
  - Not due light behaving as particles (many textbooks imply this; Plank did it right)
  - Energy of mode is quantized as Plank's constant ($h = 6.625 \times 10^{-34}$ J-s) times frequency of mode

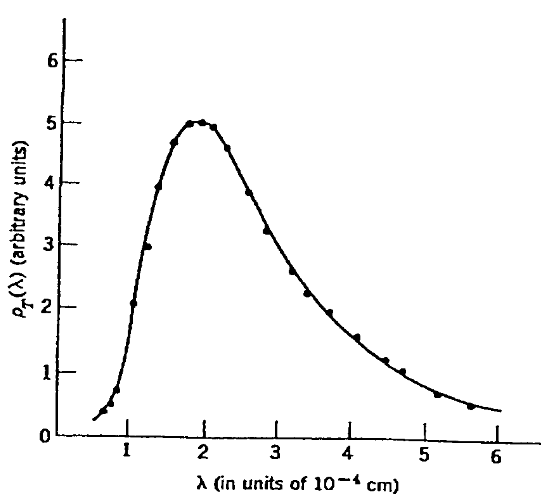

3

Events which led to Quantum Mechanics, continued

- The **Photoelectric Effect** (1905): Light causes electrons to be emitted from a metal
  - Emssion begins almost immediately, even for light intensity of only $10^{-10}W/m^2$
  - The energy of the electron is proportional to the light frequency ν
  - Einstein: Light waves act like particles (photons) with energy $h\nu$
  - Many textbooks say photoelectric effect shows that light must act like particles; absolutely incorrect [Scully, Phys. Today, Mar 1972]
  - Although wrong, light waves acting like particles historically suggested that particles might act like waves

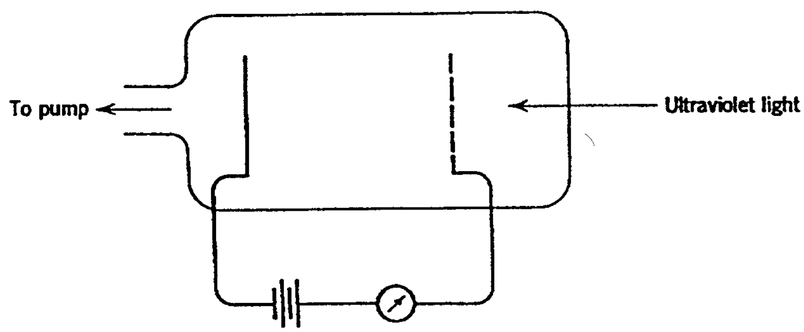

4

Events which led to Quantum Mechanics, continued

- **Rutherford Scattering** (1911): Electrons orbit heavy nucleus
- **Bohr's Theory of Atomic Spectra** (1913): atoms emit light at discrete frequencies
  - Electrons orbit nucleus classically, except only at certain radii
  - The allowed radii are such that the electron's angular momentum is an integer multiple of Plank's constant, divided by 2π.

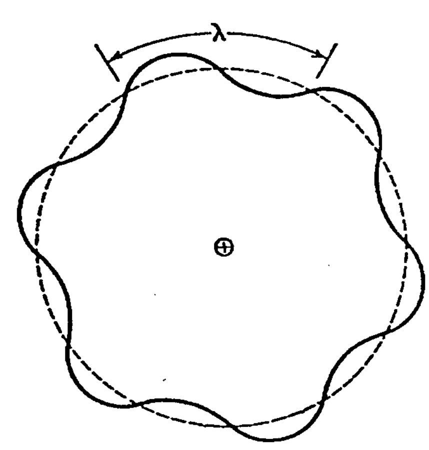

$2\pi r = 6\lambda$

5

Events which led to Quantum Mechanics, continued

- **Compton Scattering** (1923): wavelength of light is shifted when scattered from an electron
  - Historically, gave further evidence for particle nature of light
  - Like photoelectric effect, conclusion is absolutely incorrect
- **De Broglie Waves** (Ph.D. Thesis, 1924): Electron (momentum p, energy E) is a wave with wavelength $\lambda = h/p$ and frequency $\nu = E/h$. Explains all preceding experiments, and predicts that electrons diffract like waves
- **Schrodinger's Wave Equation** for particles (1925) [more later]
- **Heisenberg's Uncertainty Principle** (1927) [more later]
- **Davisson and Germer** (1927): Electrons in a crystal lattice diffract

6

Myths and the Mystique of Quantum Mechanics

- **Wave-Particle Duality** : Electrons may behave either as waves or particles
  - The Law of Physics is the Schrodinger Wave Equation; everything must be explained in terms of waves
  - The Classical Particle picture is only an approximation (e.g. ray tracing in optics)
  - For some reason, people are reluctant to give up the notion of particles
- **Paradoxes** arise from Quantum Mechanics: There are no paradoxes; they only arise if
  - One insists on giving objects particle-like attributes
  - One uses "detectors" which do not obey the laws of physics
- The **Uncertainty Principle** : This has significance only if one refuses to give up the notions of particles
- **Quantum Chaos** : The Schrodinger equation is linear; there is no chaos

7

A Valid Picture of Quantum Mechanics

1. Solve a **Boundary Value Problem** which is mathematical, rigorous, and has a unique solution

NOTE: After step 1) absolutely nothing happens!

2. Make a **Measurement**

- A measurement involves a very large number of complicated elements
- The minimum, simplest element is a graduate student with lab notebook
- A system with many elements is sensitive to small perturbations
- No system is totally isolated (no shield for gravity waves); there are always small perturbations
- The best one can do is use the results of 1) to calculate the probable outcome of a measurement (**John von Neumann**)
- Reference: Zurek, Phys. Today, Oct. 1991, "Decoherence and the Transition from Quantum to Classical"

8

Setup for Quantum Mechanics

Classical Mechanics

Newton's Law	$\vec{F} = m\vec{a} = d\vec{p}/dt$
Linear Momentum	$\vec{p} = m\vec{v}$
Angular Momentum	$\vec{L} = \vec{r} \times \vec{p}$
Kinetic Energy	$T = \frac{1}{2}mv^2$
Potential Energy	$V = \int \vec{F} \cdot d\vec{r}$
Conservation of Energy	$T + V = \text{Constant}$

9

Classical Mechanics, continued

Electrodynamics
$$\vec{F} = q\left[\vec{E} + \frac{1}{c}\left(\vec{v}\times\vec{B}\right)\right]$$

Scalar and Vector Potential
$$\vec{E} = -\vec{\nabla}\phi - \frac{1}{c}\frac{\partial\vec{A}}{\partial t}$$
$$\vec{B} = \vec{\nabla}\times\vec{A}$$

E&M Force Potential
$$U = q\phi - \frac{q}{c}\vec{A}\cdot\vec{v}$$
$$F_x = -\frac{\partial U}{\partial x} + \frac{d}{dt}\frac{\partial U}{\partial v_x}$$

10

Classical Mechanics, continued

Generalized Coordinates
$$\vec{r}_1 = \vec{r}_1\left(q_1\cdots q_N, t\right)$$
$$\vec{r}_M = \vec{r}_M\left(q_1\cdots q_N, t\right)$$

Because of constraints, N $\leq$ 3M

Velocity Dependent Potentials
$$U\left(q_1\cdots q_N, \dot{q}_1\cdots\dot{q}_N\right)$$

Lagrangian
$$L = T - U = L\left(q_i, \dot{q}_i, t\right)$$

Lagrange's Equations
$$\frac{d}{dt}\left(\frac{\partial L}{\partial\dot{q}_i}\right) - \frac{\partial L}{\partial q_i} = 0$$

Note that the first term is second order.

11

Classical Mechanics, continued

Generalized Momenta $$p_j = \frac{\partial L}{\partial \dot{q}_j}$$

Example: Charge in magnetic field $$p_x = m\dot{x} + \frac{q}{c}A_x$$

The **Hamiltonian** $$H\left(q_i, p_i, t\right) = \sum_j \dot{q}_j p_j - L$$

Example: Charge in magnetic field $$H = \frac{1}{2m}\left(\vec{p} - \frac{q}{c}\vec{A}\right)^2 + q\phi$$

Hamilton's Equations
$$\dot{q}_i = \frac{\partial H}{\partial p_i}$$
$$\dot{p}_i = -\frac{\partial H}{\partial q_i}$$

NOTE: There are twice as many equations, but they are first order.

12

Classical Mechanics, continued

Conservation Laws: Suppose, perhaps because of some symmetry, the Hamiltonian does not depend on some q_j. Then

$$\dot{p}_j = -\frac{\partial H}{\partial q_j} = 0 \qquad \rightarrow \qquad p_j = \text{constant}$$

In particular, if L dosen't depend explicitly on time, then $H = \text{constant}$.

If the transformtions defining the generalized coordinates do not depend explicitly on time, and the potential energy is velocity independent (conservative forces) then

$$H = T + V = \text{Total Energy}$$

13

Vector Spaces and Function Spaces

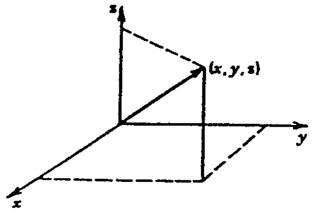

$\vec{A} = \Sigma_i A_i \hat{x}_i$, Inner Product: $\vec{A} \cdot \vec{B} = \Sigma_i A_i B_i$

Functions	$\psi_A(x) = e^{-\frac{1}{2}x^2}\left(8x^3 - 12x\right)$
Inner Product	$< \psi_A \mid \psi_B >= \int \psi_A^*(x)\, \psi_B(x)\, \rho(x)\, dx$
Orthogonality	$< \psi_A \mid \psi_B >= 0$
Unit Vectors	$< \hat{\psi}_i \mid \hat{\psi}_j >= \delta_{ij}$
Operators	$\mid \psi'_A >= P \mid \psi_A >$ Example: $P = \frac{\partial}{\partial x}$
Matrix Representation	$P_{ij} =< \hat{\psi}_i \mid P \mid \hat{\psi}_j >$
Expectation Value	$< P >=< \psi_A \mid P \mid \psi_A >$
Commutator	$[P, Q] = PQ - QP$

14

Quantum Mechanics

Formal Theory

- At a time t_0, the state (given a label "A") of a quantum mechanical system is given by a point in a linear vector space: $\psi_A(t_0)$.
- The state is normalized at all times: $< \psi_A(t) \mid \psi_A(t) >= 1$.
- There exists a time translation generator (linear operator) $T(t, t_0)$ such that

$$\psi_A(t) = T(t, t_0)\, \psi_A(t_0)$$

- Define an operator $H(t)$ such that $T(t + dt, t) = 1 - iH(t)\, dt/\hbar$.

Since $\psi(t + dt) = \psi(t) + (d\psi/dt)\, dt$, then

$$H(t)\, \psi(t) = i\hbar \frac{d\psi}{dt}$$

15

Formal Theory of Quantum Mechanics, continued

Consider the dynamics of the expectation value of an operator P:

$$\frac{d}{dt} < P >= \frac{d}{dt} < \psi(t) \mid P \mid \psi(t) >=< \psi(t) \mid P\frac{d\psi}{dt} > + < \frac{d\psi}{dt} \mid P\psi(t) >$$

$$=< \psi(t) \mid P\frac{H}{i\hbar}\psi(t) > - < \frac{H}{i\hbar}\psi(t) \mid P\psi(t) >= \frac{1}{i\hbar} < [P, H] >$$

- The **Correspondence Principle**

$\lim_{\hbar \to 0} \frac{1}{i\hbar} < [P, H] >= \frac{dP_c}{dt}$, where P_c is the classical quantity

If $P = q_i$ $\quad \lim_{\hbar \to 0} \frac{1}{i\hbar} < [q_i, H] >= \dot{q}_i = \frac{\partial H_c}{\partial p_i}$

If $P = p_i$ $\quad \lim_{\hbar \to 0} \frac{1}{i\hbar} < [p_i, H] >= \dot{p}_i = -\frac{\partial H_c}{\partial q_i}$

These conditions can be satisfied if we let H be the classical Hamiltonian, but with the q_i and p_i replaced with operators satisfying

$$[q_i, q_j] = 0, \quad [p_i, p_j] = 0, \text{ but } \quad [q_i, p_j] = i\hbar\delta_{ij}$$

16

Formal Theory of Quantum Mechanics, continued

There is more than one way to define the q_i and p_i operators.

Coordinate Representation $\quad q_i \to q_i, \quad p_i \to -i\hbar\frac{\partial}{\partial q_i}$

Momentum Representation $\quad p_i \to p_i, \quad q_i \to i\hbar\frac{\partial}{\partial p_i}$

Heisenberg Representation $\quad q_i,\ p_i \to$ Matrices

Example: $\quad [x, p_x] f(x) = x\left(-i\hbar\frac{\partial}{\partial x}\right) f(x) - \left(-i\hbar\frac{\partial}{\partial x}\right) x f(x)$

$$= -xi\hbar\frac{\partial f}{\partial x} + i\hbar f(x) + i\hbar x\frac{\partial f}{\partial x} = i\hbar f(x)$$

In 3-D coordinate representation: $\quad p^2/2m = -\frac{\hbar^2}{2m}\nabla^2$

17

Formal Theory of Quantum Mechanics, continued

Suppose $H = T + V = \dfrac{p^2}{2m} + V(\vec{r}, t)$

Then we get the **Schrodinger Equation:**

$$H\Psi(\vec{r},t) = -\frac{\hbar^2}{2m}\nabla^2\Psi(\vec{r},t) + V(\vec{r},t)\,\Psi(\vec{r},t) = i\hbar\frac{\partial\Psi}{\partial t}$$

Suppose $V(\vec{r},t) = V(\vec{r})$. Separate variables: $\Psi(\vec{r},t) = \psi(\vec{r})\,e^{-i\omega t}$.

Then we get the **Time-independent Schrodinger Equation:**

$$-\frac{\hbar^2}{2m}\nabla^2\psi(\vec{r}) + V(\vec{r})\,\psi(\vec{r}) = E\psi(\vec{r})$$

where $E = \hbar\omega$. For closed systems E will be a discrete eigenvalue, or **Quantized Energy Level.** The eigenfunction $\psi(\vec{r})$ is called a **Stationary State.** The eigenfunction for the lowest E is called the **Ground State.** Discrete eigenvalues are labeled with integers called **Quantum Numbers.**

18

Examples **One-Dimensional Free Particle**

Free particle: $V = 0$ $\qquad -\dfrac{\hbar^2}{2m}\dfrac{d^2\psi}{dx^2} = E\psi, \quad E = \hbar\omega$

$$\frac{d^2\psi}{dx^2} + k^2\psi = 0, \qquad k = \frac{1}{\hbar}\sqrt{2mE}$$

Note classical momentum $p = \sqrt{2mE} \rightarrow p = \hbar k$.

Solutions $\Psi(x,t) = \tilde{A}e^{i(kx-\omega t)}$

Waves of wavelength $\lambda = 2\pi/k = h/p$ and frequency $\nu = \omega/2\pi = E/h$ (de Broglie!).

Note: $\omega = E/\hbar = (\hbar/2m)\,k^2 = \omega(k) \rightarrow$ **Dispersion**

For a common acoustics wave, $\omega = c_0 k$, **Linear Dispersion**

Dispersion is a fundamental difference between free particle Schrodinger waves and common acoustic waves.

19

Wave Velocities and Dispersion

For $\Psi(x,t) = \tilde{A}e^{i(kx-\omega t)}$, $(kx - \omega t) \equiv \phi$ is called the **phase.**

What is the relationship between x and t such the phase ϕ is constant?

$$\phi = \text{constant} \rightarrow \frac{d\phi}{dt} = 0 = k\frac{dx}{dt} - \omega$$

Solving: $(dx/dt) = \omega/k = v_p$, the **Phase Velocity.**

Suppose $\Psi(x,t) = \cos(kx - \omega t) + \cos[(k + \Delta k)x - (\omega + \Delta\omega)t]$

$$= 2\cos\frac{1}{2}(\Delta kx - \Delta\omega t)\cos(\bar{k}x - \bar{\omega}t) = \text{envelope} \times \text{carrierwave}$$

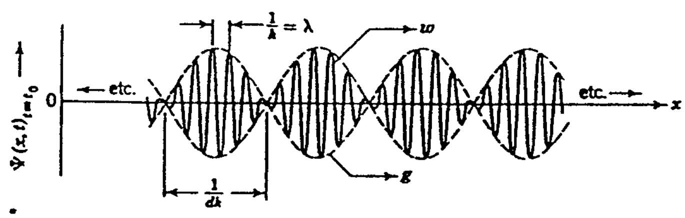

The envelope moves with velocity $\Delta\omega/\Delta k \rightarrow d\omega/dk \equiv v_g$, the **Group Velocity.** For linear dispersion, $v_g = v_p$. Otherwise, $v_g \neq v_p$.

20

Wave Superposition and Wave Packets

The **General Solution** is a linear combination (superposition) of eigenfunctions

$$\Psi(x,t) = \int \tilde{A}(k)\, e^{i[kx-\omega(k)t]}dk$$

Suppose $\tilde{A}(k)$ is peaked around k_0, as shown in the figure:

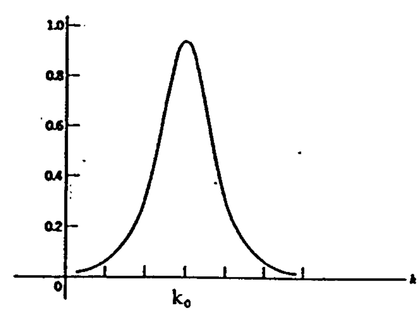

Note that $\Psi(x, t = 0)$ is the Fourier Transform of $\tilde{A}(k)$, which is a wave packet:

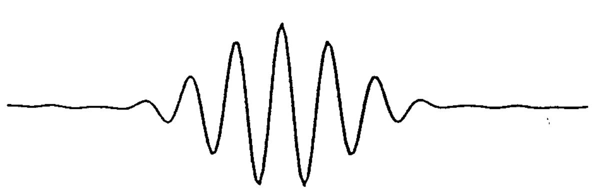

21

Wave Packets, continued

From a theorem for Fourier Transforms, the product of the width of the curve in k -space and the width of the envelope in x -space is a constant. If the curve in k -space is a **Gaussian,** $\exp\left[-(k-k_0)^2/2\right]$, then the envelope in x -space is also a Gaussian, and the product of the widths is minimized.

Recall that $\tilde{A}(k)$ is peaked at k_0. Let $\kappa = k - k_0$. Then

$$\Psi(x,t=0) = \int \tilde{A}(k) e^{ikx} dk = e^{ik_0x} \int \tilde{A}(k_0+\kappa)\, e^{i\kappa x} d\kappa$$

For times $t > 0$, we approximate $\omega(k)$ near k_0 with $\omega(k) \simeq \omega_0 + (d\omega/dk)\,\kappa = \omega_0 + v_g\kappa$. Then

$$\Psi(x,t) = e^{ik_0x} \int \tilde{A}(k_0+\kappa)\, e^{i[\kappa x - \omega(\kappa)t]} d\kappa$$

$$\simeq e^{i(k_0v_g-\omega_0)t} e^{ik_0(x-v_gt)} \int \tilde{A}(k_0+\kappa)\, e^{i\kappa(x-v_gt)} d\kappa$$

$$\simeq e^{i(k_0v_g-\omega_0)t}\, \Psi\left[(x-v_gt),0\right]$$

Taking the modulus eliminates the phase factor, leaving the original envelope of the wave packet evaluated at $(x - v_gt)$, i.e. moving with the group velocity. With non-linear dispersion, the wavenumbers higher and lower than k_0 move with different velocities, causing the wave packet to spread.

22

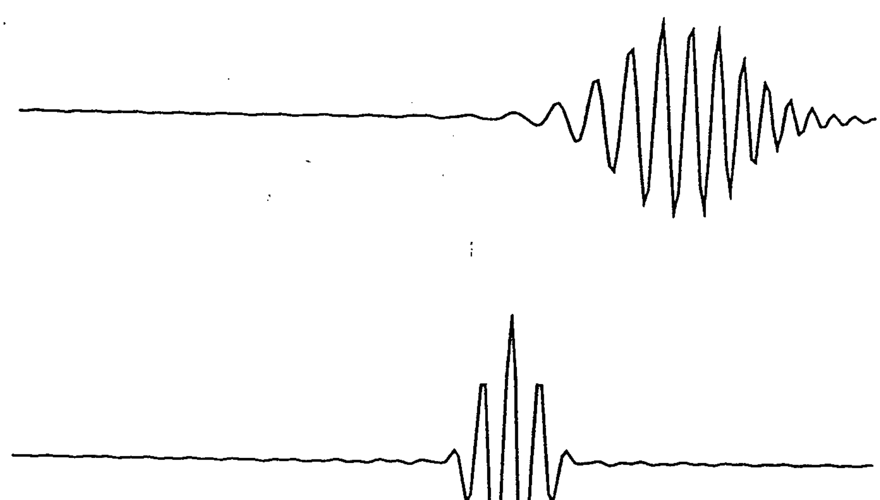

23

Examples — Piecewise Constant Potentials

Piecewise constant potential: $V(x) = V_i =$ constant for $x_i \le x < x_{i+1}$

For $x_i \le x < x_{i+1}$,

$$-\frac{\hbar^2}{2m}\frac{d^2\psi}{dx^2} + V_i\psi = E\psi, \quad E = \hbar\omega$$

$$\frac{d^2\psi}{dx^2} + k_i^2\psi = 0, \qquad k_i = \frac{1}{\hbar}\sqrt{2m(E - V_i)}$$

Solutions:

$$\Psi(x,t) = \tilde{A}_i e^{i(k_i x - \omega t)} + \tilde{B}_i e^{i(-k_i x - \omega t)}$$

Note that in some regions, E may be less than V_i, and k_i will be imaginary. Solutions of the form $\psi(x) \propto e^{-\kappa x}$ are called **Evanescent Waves.**

The coefficients $\tilde{A}_i$ and $\tilde{B}_i$ are found by satisfying the conditions that $\psi(x)$ and its derivative $d\psi/dx$ be continuous at boundaries.

Satisfying all boundary conditions may result in solutions existing only for discrete values E, which are the quantized energy levels.

24

Examples — Step Potential

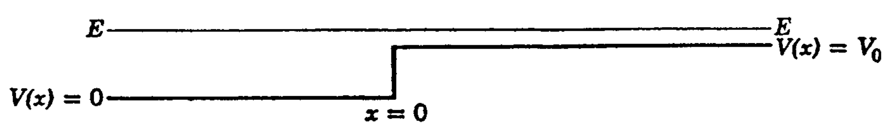

On the left: $\psi(x) = e^{ikx} + \tilde{R}e^{-ikx}, \qquad k = \frac{1}{\hbar}\sqrt{2mE}$

On the right: $\psi(x) = \tilde{T}e^{iqx}, \qquad q = \frac{1}{\hbar}\sqrt{2m(E - V_0)}$

Equating the ψ and the $d\psi/dx$ from the left and right gives two equations, which are solved for the two unknowns $\tilde{R}$ and $\tilde{T}$, the **Complex Reflection and Transmission Coefficients.**

$$\tilde{R} = (k - q)/(k + q) \qquad \tilde{T} = 2k/(k + q)$$

If $E > V_0$, then there are waves on both sides, but with different wavelengths. If a wavepacket were incident, part would be reflected, and part transmitted.

25

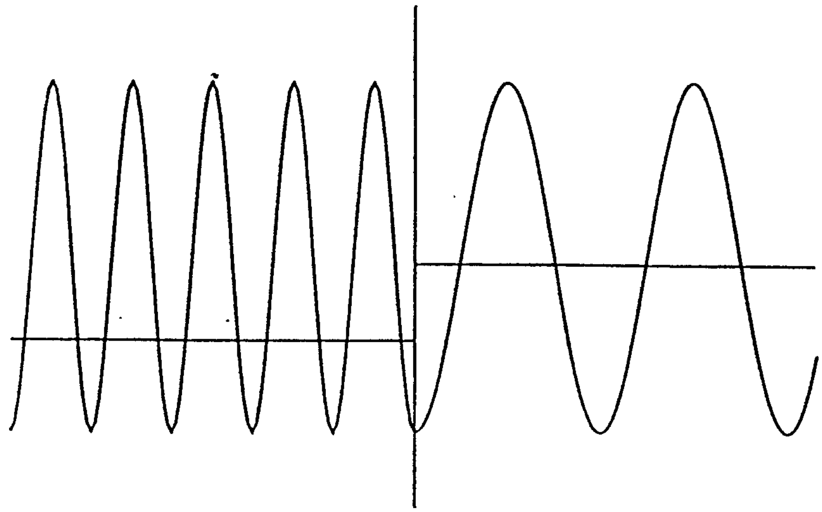

26

Step Potential, continued

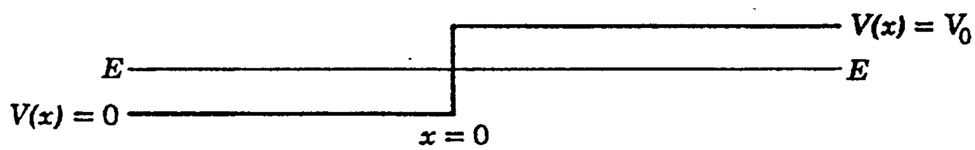

If $E < V_0$, then $q \rightarrow iq$, and the solution on the right becomes an exponentially decreasing evanescent wave.

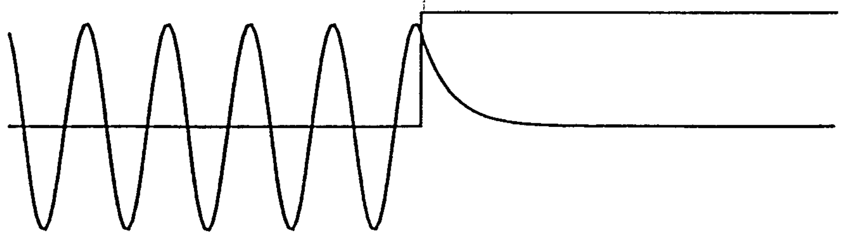

The $\tilde{R}$ and $\tilde{T}$ become more complicated complex numbers, but $|\tilde{R}|^2$, the energy reflection coefficient, would be unity.

If a wavepacket were incident, the superimposed waves with $E > V_0$ would be completely reflected.

27

Examples — Square Barrier Potential

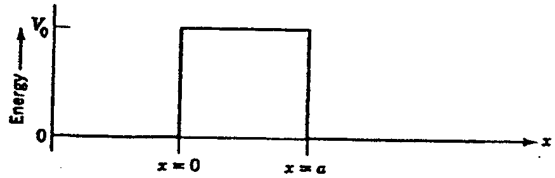

On the left: $\psi(x) = e^{ikx} + \tilde{R}e^{-ikx}, \quad k = \sqrt{2mE}/\hbar$

In the middle: $\psi(x) = \tilde{E}e^{iqx} + \tilde{F}e^{-iqx}, \quad q = \sqrt{2m(E - V_0)}/\hbar$

On the right: $\psi(x) = \tilde{T}e^{ikx}$

If $q = i\kappa$, $\quad \tilde{R} = \dfrac{-i\left(k^2 + \kappa^2\right)\sinh(qa)}{2k\kappa\cosh(qa) - i\left(k^2 - \kappa^2\right)\sinh(qa)}, \quad \tilde{T} =$ etc.

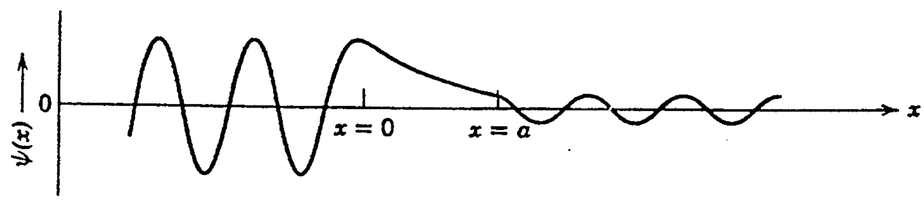

28

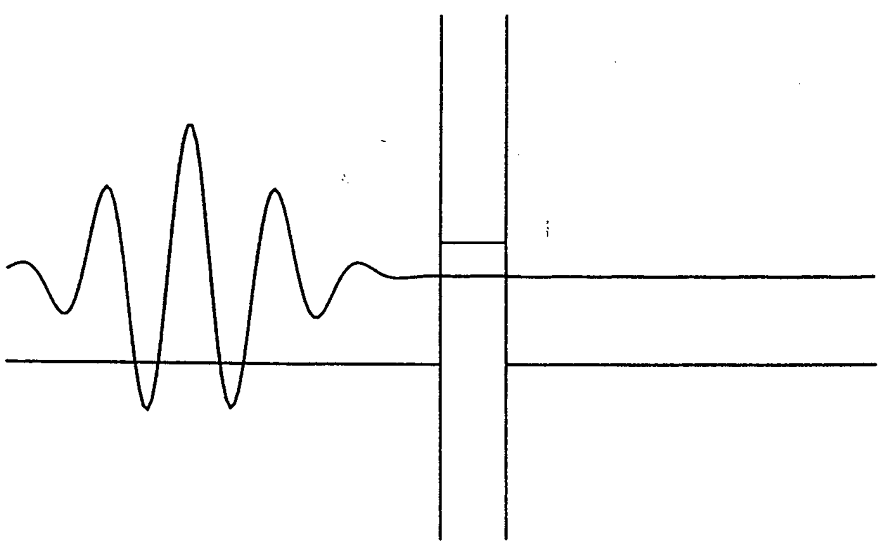

29

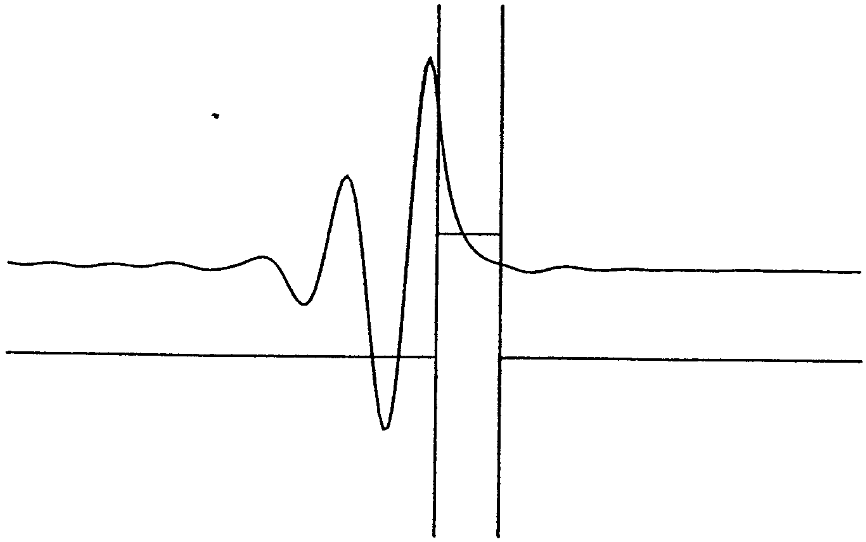

30

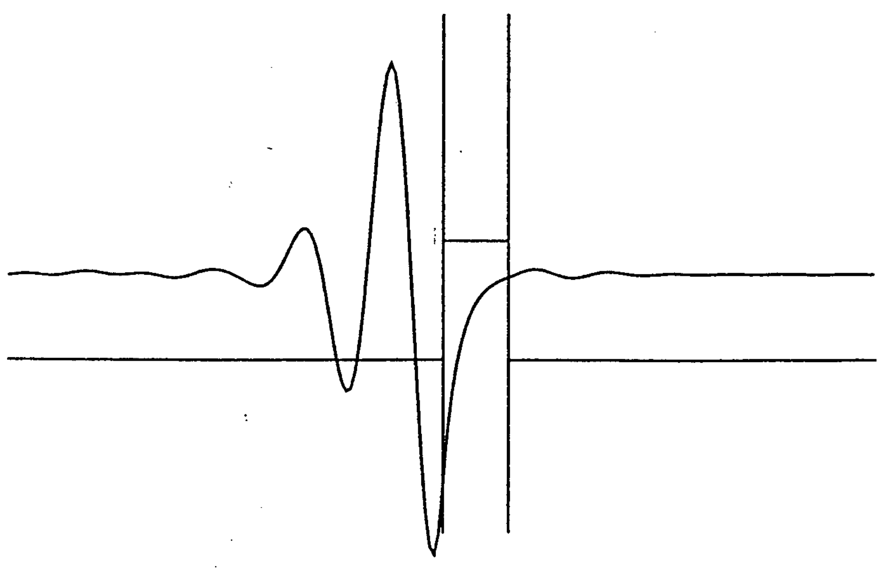

31

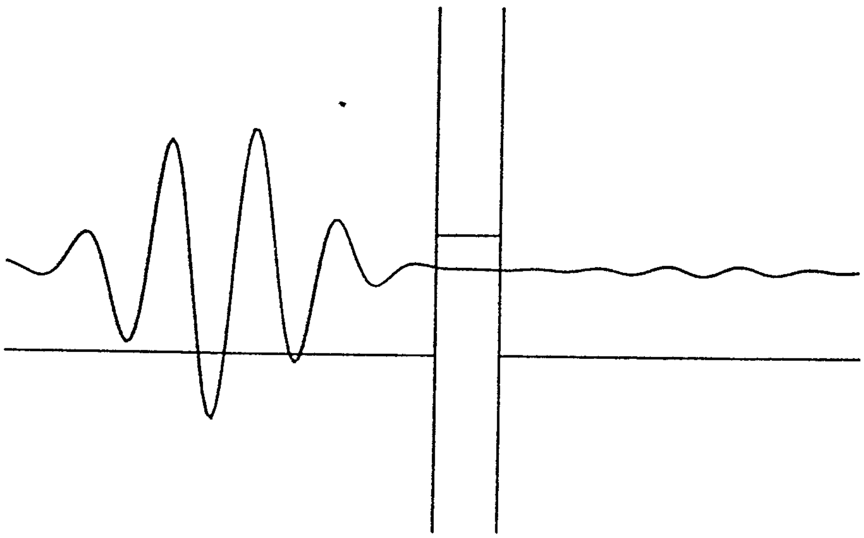

32

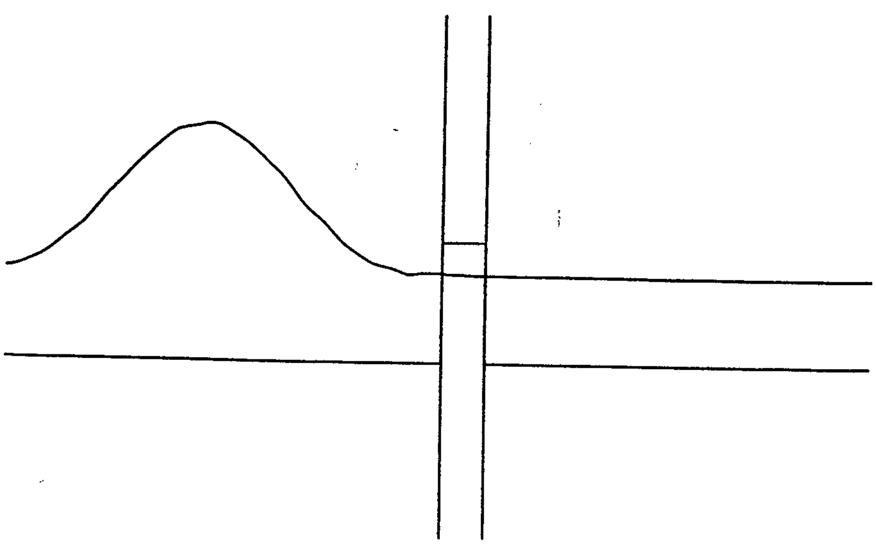

33

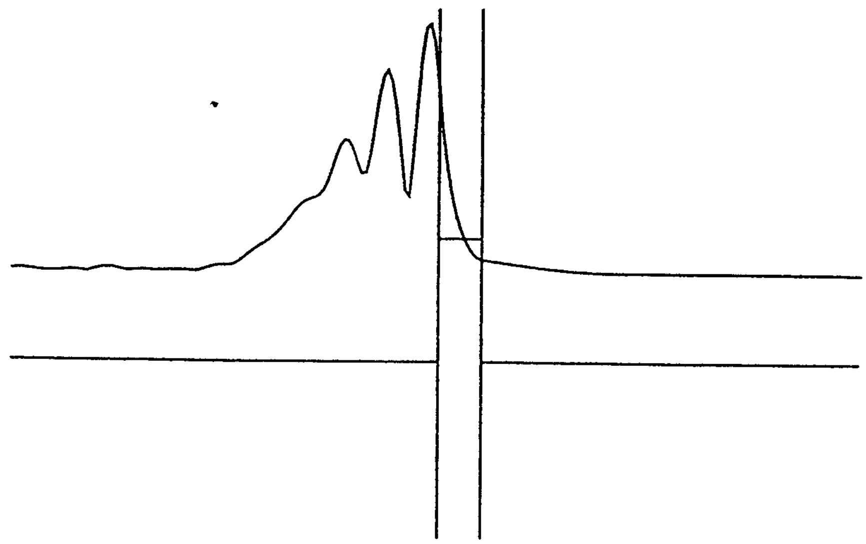

34

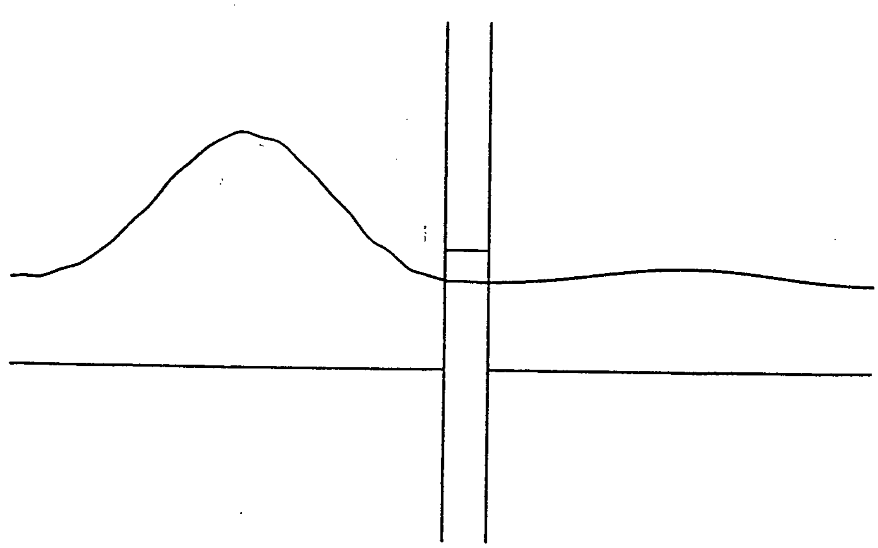

35

Examples **Square Well Potential, $E < V_0$ (Bound States)**

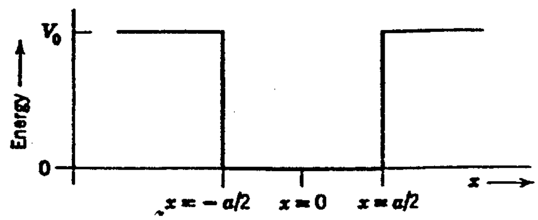

On the left: $\psi(x) = \tilde{A}e^{\kappa x}, \quad \kappa = \sqrt{2m(V_0 - E)}/\hbar$

In the middle: $\psi(x) = \tilde{B}\cos kx + \tilde{C}\sin kx, \quad k = \sqrt{2mE}/\hbar$

On the right: $\psi(x) = \tilde{D}e^{-\kappa x}$

The boundary conditions require either $\tilde{C} = 0$ and $k\tan(ka/2) = \kappa$, or $\tilde{B} = 0$ and $k\cot(ka/2) = -\kappa$. These two possibilities correspond to symmetric and anti-symmetric bound states.

The transcendental equations yield a finite number of discrete values for the energy levels E.

If $V_0 \to \infty$, then the eigenfunction ψ must vanish at $x = \pm a/2$ (the derivative $d\psi/dx$ will be discontinuous). The eigenfunctions are the same as a string clamped at the ends, with $k \propto n$, an integer. However, the string natural frequencies are proportional to n, whereas the quantum energy levels are proportional to n^2.

36

Square Well Potential, $E < V_0$ (Bound States), continued

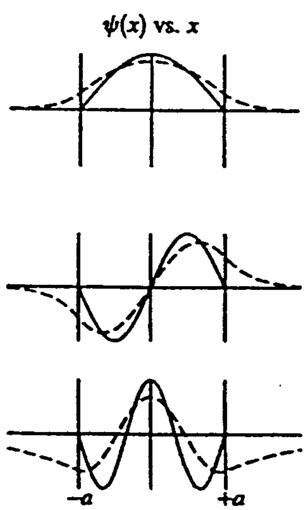

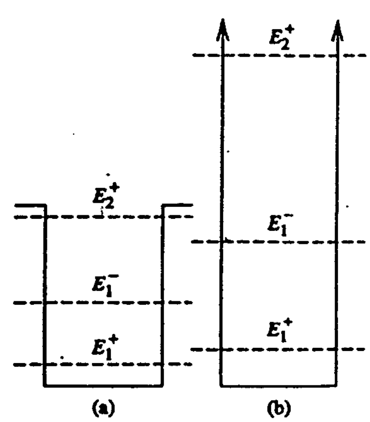

For finite V_0, the eigenfunctions are shown with dashed lines, and the energy levels are shown in (a).

For infinite V_0, the eigenfunctions are shown with solid lines, and the energy levels are shown in (b).

37

Examples **The Simple Harmonic Oscillator Potential**

The Simple Harmonic Oscillator Potential: $V(x) = \frac{1}{2}Kx^2 = \frac{1}{2}m\omega_0^2 x^2$

where K is the spring constant, m is the mass, and ω_0 is the classical oscillator's natural frequency.

The Schrodinger Eq.: $$-\frac{\hbar^2}{2m}\frac{d^2\psi}{dx^2} + \frac{1}{2}m\omega_0^2 x^2\psi = E\psi$$

Let $y = \sqrt{m\omega_0/\hbar}\; x$ and let $\psi(x) = \exp\left(-y^2/2\right) h(y)$. Then

$$\frac{d^2h}{dy^2} - 2y\frac{dh}{dy} + 2\left(\frac{E}{\hbar\omega_0} - \frac{1}{2}\right) h(y) = 0$$

If a series solution for $h(y)$ is tried, then the series diverges unless $(E/\hbar\omega_0 - 1/2) = n$, an integer. Thus the energy levels are quantized with

$$E_n = \left(n + \frac{1}{2}\right)\hbar\omega_0$$

The eigenfunctions $h_n(y)$ are the **Hermite Polynomials.**

38

The Quantum Mechanical Simple Harmonic Oscillator, continued

Normalized Wavefunctions:

$$\Psi_n(x,t) = \left(\frac{\sqrt{m\omega_0/\hbar\pi}}{2^n n!}\right)^{1/2} h_n\left(\sqrt{m\omega_0/\hbar}\; x\right) e^{-(m\omega_0/\hbar)x^2/2}$$

$h_3(y) = 8y^3 - 12y$

$h_2(y) = 4y^2 - 2$

$h_1(y) = 2y$

$h_0(y) = 1$

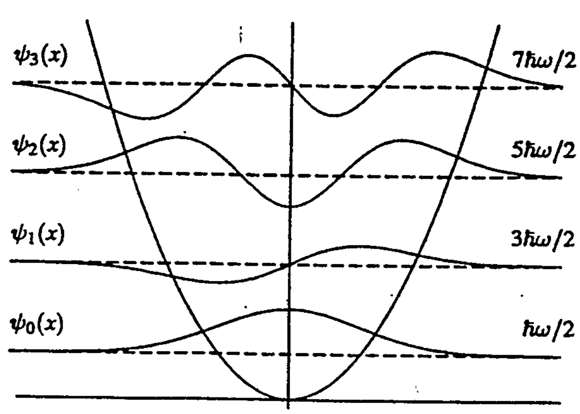

39

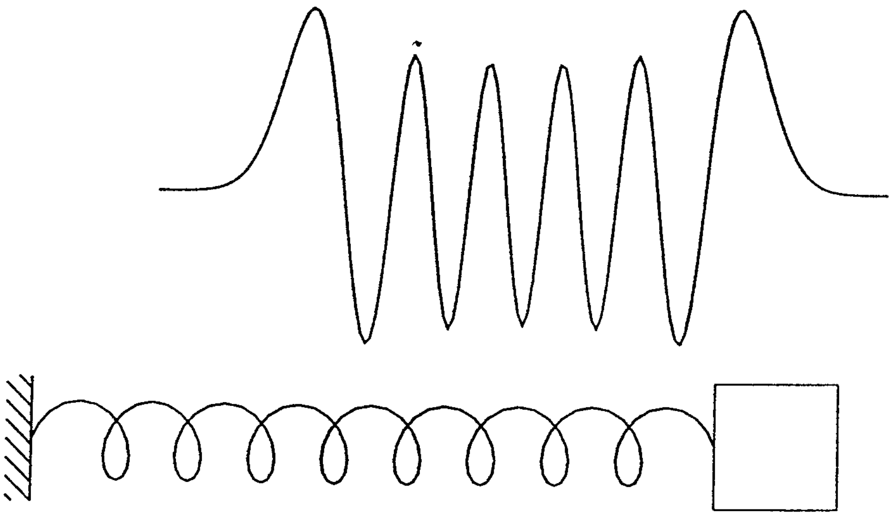

40

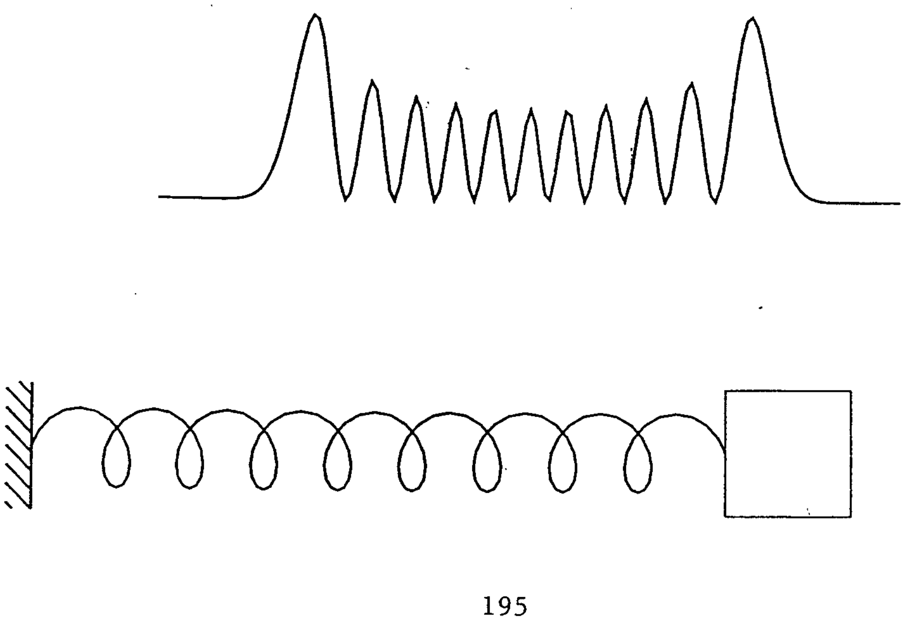

41

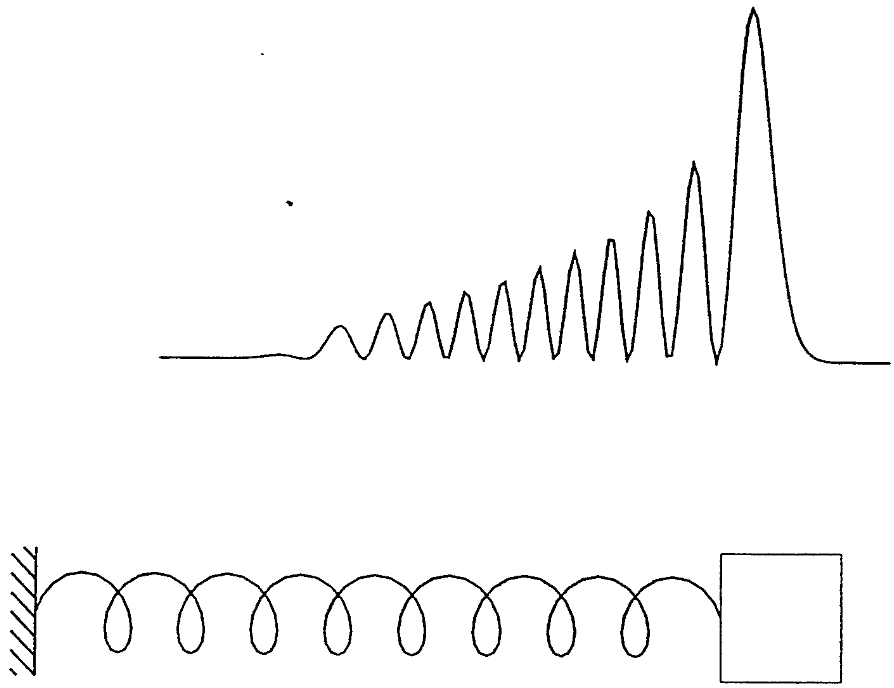

42

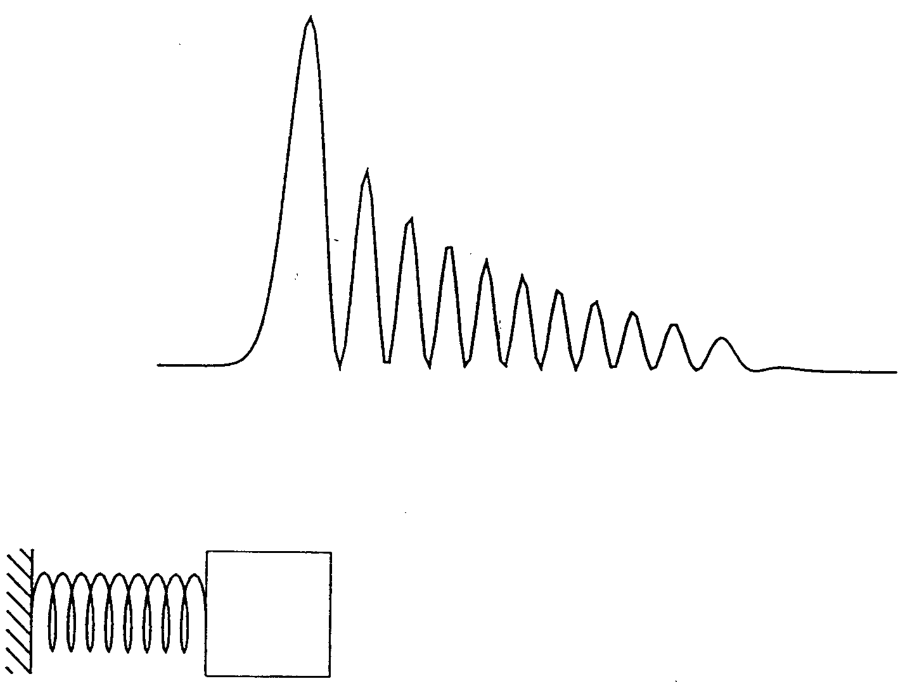

43

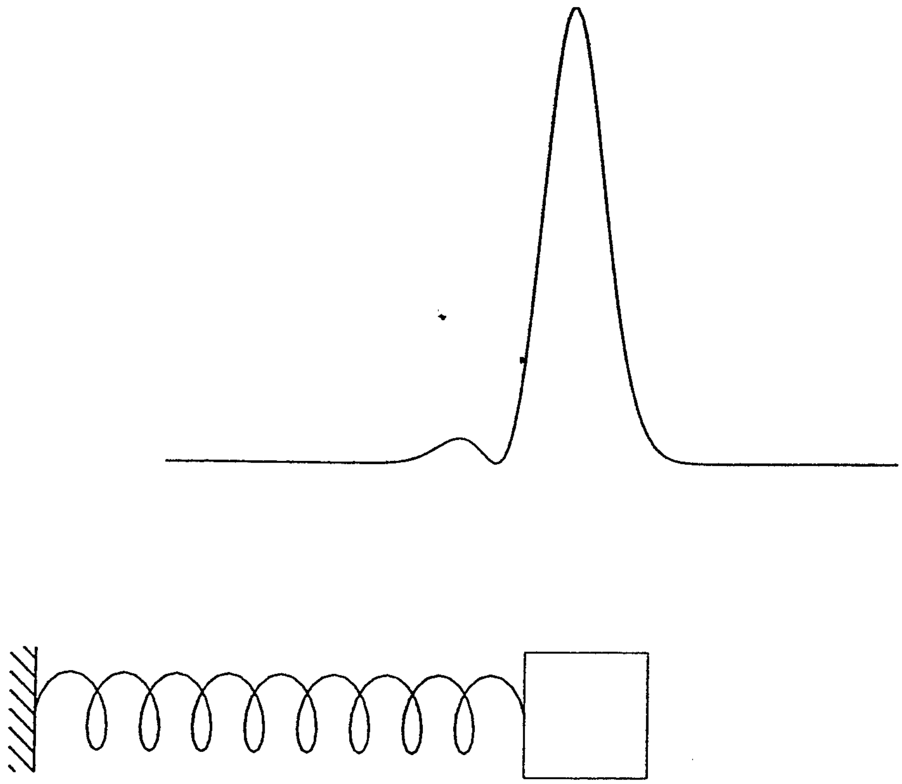

44

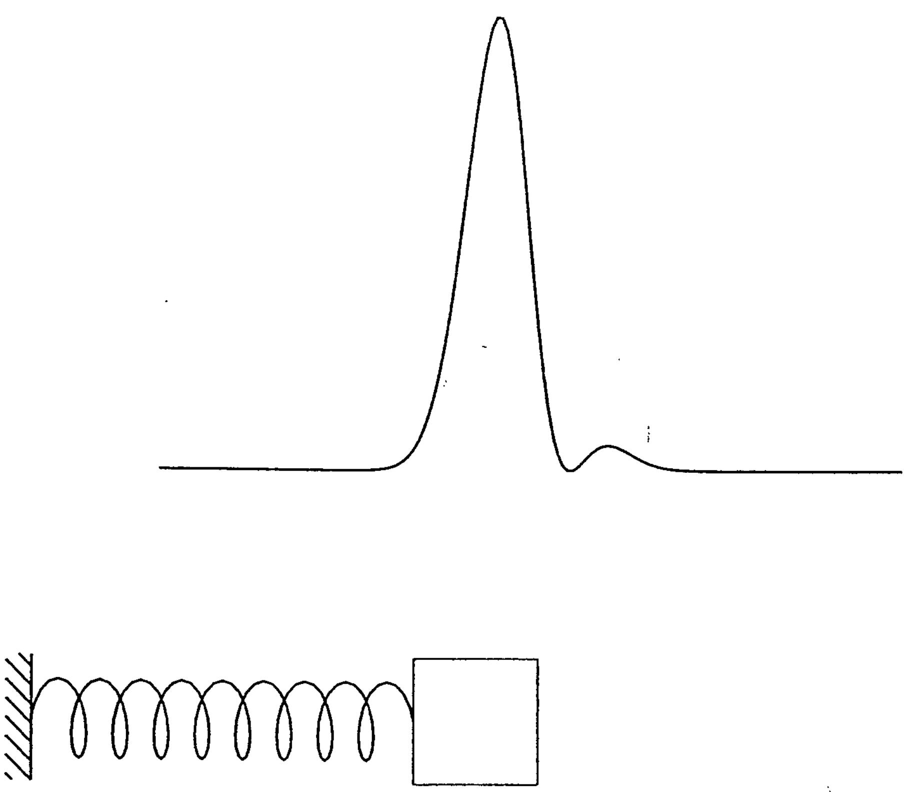

45

The Quantum Mechanical Simple Harmonic Oscillator, continued

For a classical simple harmonic oscillator, $x(t) = A\cos(\omega_0 t)$, and the total energy is $E = (1/2)\, mA^2\omega_0^2$.

Classical result: $x(t) = \sqrt{2E/m\omega_0^2}\cos(\omega_0 t)$

Quantum Expectation Value for state $\Psi_n(x,t)$: $<\Psi_n \mid x \mid \Psi_n> = 0$

Measurement couples states: $\Psi(x,t) = \Psi_n(x,t) + \Psi_{n+1}(x,t)$

Now
$$
\begin{aligned}
<\Psi \mid x \mid \Psi> &= <\Psi_n \mid x \mid \Psi_{n+1}> + <\Psi_{n+1} \mid x \mid \Psi_n> \\
&= 2Re <\Psi_n \mid x \mid \Psi_{n+1}> \\
&= 2Re \int \left(\psi_n(x)\, e^{-i\left(n+\frac{1}{2}\right)\omega_0 t}\right)^* x \left(\psi_{n+1}(x)\, e^{-i\left(n+\frac{3}{2}\right)\omega_0 t}\right) dx \\
&= 2Re \int \psi_n(x)\, x\psi_{n+1}(x)\, dx e^{-i\omega_0 t} \\
&= 2Re\sqrt{n\hbar/2m\omega_0} e^{-i\omega_0 t} \\
&= \sqrt{2n\hbar\omega_0/m\omega_0^2}\cos(\omega_0 t) \simeq \sqrt{2E/m\omega_0^2}\cos(\omega_0 t)
\end{aligned}
$$

46

$\boxed{\text{Example}}$ **Central Forces**

Spherical Coordinates

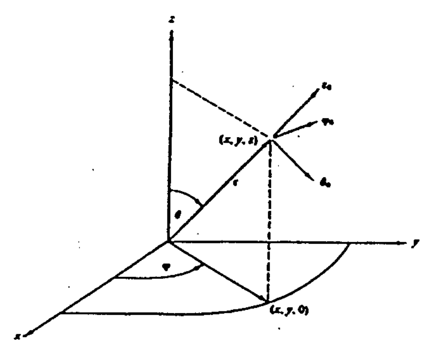

$$
\vec{\nabla} = \hat{r}\frac{\partial}{\partial r} + \hat{\theta}\frac{1}{r}\frac{\partial}{\partial \theta} + \hat{\phi}\frac{1}{r\sin\theta}\frac{\partial}{\partial \phi}
$$

$$
\nabla^2 = \frac{1}{r^2}\frac{\partial}{\partial r}\left(r^2\frac{\partial}{\partial r}\right) + \frac{1}{r^2}\left[\frac{1}{\sin\theta}\frac{\partial}{\partial\theta}\left(\sin\theta\frac{\partial}{\partial\theta}\right) + \frac{1}{\sin^2\theta}\frac{\partial^2}{\partial\phi^2}\right]
$$

Conservative Central Force: $\vec{F} = F\hat{r} \quad \rightarrow \quad V(\vec{r}) = V(r)$

Classical consequences for angular momentum, $\vec{L} = \vec{r} \times \vec{p}$.

$$
\frac{d\vec{L}}{dt} = \vec{\tau} = \vec{r} \times \vec{F} = 0 \quad \rightarrow \quad \vec{L} = \text{constant}
$$

47

Central Force, continued

Quantum Mechanics: $$H\psi = -\frac{\hbar^2}{2m}\nabla^2\psi + V(r)\psi = E\psi$$

$$-\frac{\hbar^2}{2m}\frac{1}{r^2}\frac{\partial}{\partial r}\left(r^2\frac{\partial\psi}{\partial r}\right) + \frac{\hbar^2}{2mr^2}\left[\frac{1}{\sin\theta}\frac{\partial}{\partial\theta}\left(\sin\theta\frac{\partial}{\partial\theta}\right) + \frac{1}{\sin^2\theta}\frac{\partial^2}{\partial\phi^2}\right] + V(r)\psi = E\psi$$

Separate variables: $\psi(r,\theta,\phi) = (1/r)\,R(r)\,\Theta(\theta)\,\Phi(\phi)$. Plug-in and divide:

$$\frac{1}{\Phi}\frac{d^2\Phi}{d\phi^2} = Fn(r,\theta) = \text{constant} = -m^2 \rightarrow \qquad \Phi(\phi) = e^{im\phi}$$

Single valued $\psi(r,\theta,\phi+2\pi) = \psi(r,\theta,\phi) \rightarrow m = 0, \pm 1, \pm 2, \pm 3 \cdots$

$$\frac{1}{\Theta\sin\theta}\frac{d}{d\theta}\left(\sin\theta\frac{d\Theta}{d\theta}\right) - \frac{m^2}{\sin^2\theta} = Fn(r) = \text{constant} = -l(l+1)$$

Solution: Legendre Polynomial, $\Theta(\theta) = P_l^m(\cos\theta)$ and $l =$ integer $\leq |m|$.

$$-\frac{\hbar^2}{2m}\frac{d^2R}{dr^2} + \left[\frac{l(l+1)\hbar^2}{2mr^2} + V(r)\right]R = ER$$

48

Central Force, continued

Combine θ, ϕ: $$Y_l^m(\theta,\phi) = \sqrt{\frac{2l+1}{4\pi}\frac{(l-m)!}{(l+m)!}}(-1)^m e^{im\phi}P_l^m(\cos\theta)$$

Quantum Angular Momentum $\vec{L} = \vec{r}\times\vec{p} = -i\hbar\vec{r}\times\vec{\nabla} = L_x\hat{x} + L_y\hat{y}L_z\hat{z}.$

$$L_x = -i\hbar\left(y\frac{\partial}{\partial z} - z\frac{\partial}{\partial y}\right) = i\hbar\left(\sin\phi\frac{\partial}{\partial\theta} + \cot\theta\cos\phi\frac{\partial}{\partial\phi}\right)$$

$$L_y = -i\hbar\left(z\frac{\partial}{\partial x} - x\frac{\partial}{\partial z}\right) = i\hbar\left(-\cos\phi\frac{\partial}{\partial\theta} + \cot\theta\sin\phi\frac{\partial}{\partial\phi}\right)$$

$$L_z = -i\hbar\left(x\frac{\partial}{\partial y} - y\frac{\partial}{\partial x}\right) = -i\hbar\frac{\partial}{\partial\phi}$$

Note: $$L^2 = -\hbar^2\left[\frac{1}{\sin\theta}\frac{\partial}{\partial\theta}\left(\sin\theta\frac{\partial}{\partial\theta}\right) + \frac{1}{\sin^2\theta}\frac{\partial^2}{\partial\phi^2}\right]$$

$$H = -\frac{\hbar^2}{2m}\frac{1}{r^2}\frac{\partial}{\partial r}\left(r^2\frac{\partial\psi}{\partial r}\right) + \frac{L^2}{2mr^2} + V(r)$$

Note $[H, L^2] = 0$, $[H, L_z] = 0$ $\rightarrow$ $< L^2 > =$ const, and $< L_z > =$ const.

Note $L^2 Y_l^m(\theta,\phi) = l(l+1)\hbar^2 Y_l^m(\theta,\phi)$ and $L_z Y_l^m(\theta,\phi) = m\hbar Y_l^m(\theta,\phi)$

Expected modulus of Angular Momentum: $L = \sqrt{< L^2 >} = \sqrt{l(l+1)}\hbar$

49

$\boxed{\text{Example}}$ **Coulomb Central Force:** $V(r) = (Ze)\,e/r$.

$$-\frac{\hbar^2}{2m}\frac{d^2R}{dr^2} + \left[\frac{l(l+1)\hbar^2}{2mr^2} + V(r)\right] R = -ER$$

$$\frac{1}{r}R(r) = e^{-k_n r}(2k_n r)^l G_n(2k_n r)\,, \text{Laguerre Polynomials}$$

$$k_n = \frac{1}{\hbar}\sqrt{2mE_n}, \qquad E_n = \frac{mZ^2e^4}{2\hbar^2 n^2}, n = 1, 2, 3, \cdots$$

For a given n : $l = 0, 1, 2 \cdots (n-1)$; $m = -l, -l+1, \cdots l-1, l$, [$(2l+1)$ values]

Historical nomenclature: l = 0,1,2,3 are referred to as "s, p, d, f" states.

Energy eigenvalue E_n depends only on n. Eigenfunctions for different l, m are degenerate. Number of degenerate states $= \Sigma_{l=0}^{n-1}(2l+1) = n^2$.

Arbitrary z-direction not a problem, because sum over degenerate states is isotropic.

50

Coulomb Central Force, continued

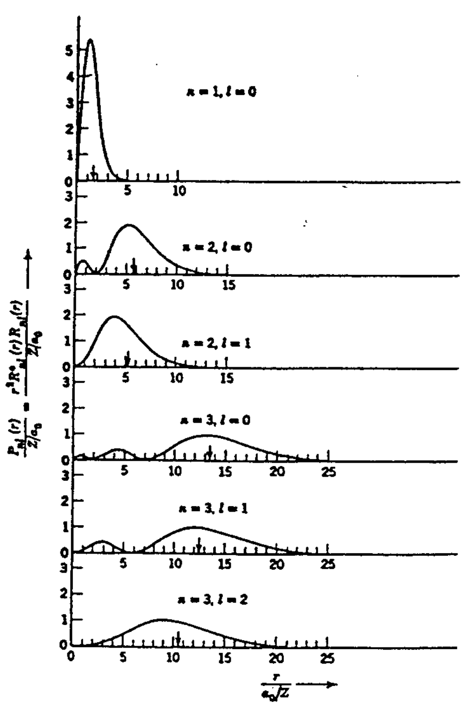

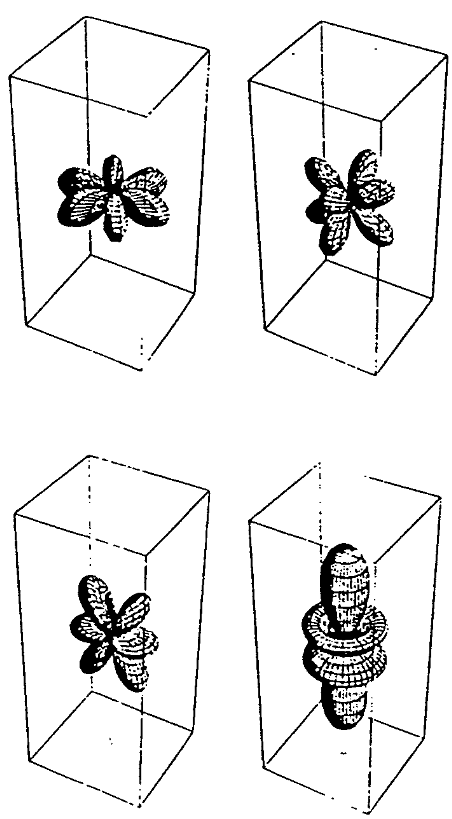

51

Quantum Mechanics — History and Formal Theory, continued

- **Stern-Gerlach Experiment** (1922) Electron in a inhomogeneous magnetic field

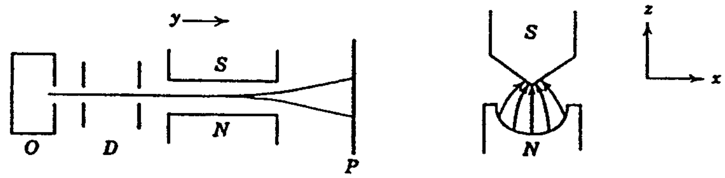

Deflection → magnetic moment → charge with angular momentum. But atoms in ground state had $l = 0$ → electron's orbital angular momentum = 0!

- **Dirac** (1927) Extended formal Hamiltonian theory to include relativistic dynamics → Electron has intrinsic angular momentum, **Spin**

Spin angular momentum: $|\vec{S}| = \sqrt{s(s+1)}\hbar$, with $s = 1/2$. Note $2s + 1 = 2$.

Z-component of electron spin: $S_z = m_s\hbar, \quad m_s = -\frac{1}{2}$ or $+\frac{1}{2}$

Now: Quantum numbers for the single electron atom: n, l, m, m_s

Wave function gets a two-element vector (**Spinor**) attached. Spin operators are 2 x 2 matrices (linear combination of four **Pauli spin matrices**).

52

Quantum Mechanics — Formal Theory, continued

For systems with many particles, there are generalized coordinates (and operators) for each particle.

For classical identical particles, the particles may be distinguished by following their (precise) classical trajectories.

In quantum mechanics, particles are waves, and the Principle of Superposition means that identical quantum particles are **Indistinguishable**

Note: Any complete set of dynamical variables (or quantum numbers) K which describes a single particle can also be employed for n particles of the same kind, even if the particles are interacting.

Consequence: Ψ (Nparticles) involves products $| K_1 > | K_2 > \cdots | K_N >$

Since the particles are indistinguishable, exchanging any pair of $| K >$'s must give the same result (**Exchange Degeneracy**). There are only two forms for Ψ for which $|\Psi|^2$ is invariate under any exchange. Let P indicate one of $N!$ permutations. Then:

$$\Psi_S = \sum_P | K_1 > | K_2 > \cdots | K_N >$$

$$\Psi_A = \sum_P \alpha_P | K_1 > | K_2 > \cdots | K_N >$$

where $\alpha_P = 1$ for even permutations, and = -1 for odd permutations.

53

Formal Theory, Identical Particles, continued

Note: $\Psi_S(\cdots K_i \cdots K_j \cdots) = \Psi_S(\cdots K_j \cdots K_i \cdots)$

and $\Psi_A(\cdots K_i \cdots K_j \cdots) = -\Psi_A(\cdots K_j \cdots K_i \cdots)$.

Note: $\Psi_A = 0$ if any two particles have the same K_i.

- History: **Pauli Exclusion Principle** (1925). [From experimental observations on multi-electron atoms] There can never be one electron in the same quantum state.

Consequence: Electrons must have anti-symmetric wave functions, Ψ_A

Generalization: Particles with half-integral spin quantum numbers must have antisymmetric wave functions; such particles are called **Fermions** . Particles with integral spin quantum numbers must have symmetric wave functions; such particles are called **Bosons** .

Thermodynamic Distribution functions:

Fermi Statistics $\quad f_F(E) = \dfrac{1}{e^{(E-\mu)/kT}+1}$

Bose Statistics $\quad f_B(E) = \dfrac{1}{e^{(E-\mu)/kT}-1}$

54

$\boxed{\text{Perturbation Theory}}$ **Time Independent Potential Fields, $V(r)$**

Suppose one can solve $H_0\psi_n^0 = E_n^0\psi_n^0$

Wish to solve $(H_0 + V)\psi_n = E_n\psi_n$. For small V :

$$E_n \simeq E_n^0 + <\psi_n^0 \mid V \mid \psi_n^0> + \sum_{k\neq n} \frac{|<\psi_k^0 \mid V \mid \psi_n^0>|^2}{E_n^0 - E_k^0} + \cdots$$

$$\psi_n \simeq \psi_n^0 + \sum_{k\neq n} \frac{<\psi_k^0 \mid V \mid \psi_n^0>}{E_n^0 - E_k^0}\psi_k^0 + \cdots$$

If degeneracy $\left(E_n^0 = E_k^0\right)$ then diagonalize matrix.

Variational Method:

$H\psi_0 = E_0\psi_0$ is equivalent to finding the ψ which minimizes

$$\delta H = \frac{<\psi \mid H \mid \psi>}{<\psi \mid \psi>}$$

Write a ψ with parameters, and minimize δH with respect to the parameters.

$\boxed{\text{Perturbation Theory}}$ **Time Evolution** (V may depend on time)

Wish to solve $(H_0 + V)\,\Psi = i\hbar\,(\partial\Psi/\partial t)$

If $\quad H_0\psi_n^0 = \hbar\omega_n\psi_n^0,\quad$ then $\quad \Psi^0\,(t) = \sum_n c_n e^{-i\omega_n t}\psi_n^0$

Assume $$\Psi\,(t) = \sum_n c_n\,(t)\,e^{-i\omega_n t}\psi_n^0$$

Plug in: $$\frac{dc_k}{dt} = \frac{1}{i\hbar}\sum_n <\psi_k^0 \mid V \mid \psi_n^0> c_n e^{-i(\omega_k-\omega_n)t}$$

Assume $c_s\,(t=-\infty) = 1$, and $c_k\,(t=-\infty) = 0$:

$$c_k\,(t) = \frac{1}{i\hbar}\int_{-\infty}^{t} <\psi_k^0 \mid V \mid \psi_n^0> c_s e^{-i(\omega_k-\omega_s)t'}dt'$$

Example: EM Radiation $$\vec{A} = \int_{-\infty}^{\infty}\vec{A}\,(\omega)\,e^{i\left(\vec{k}\cdot\vec{r}-\omega t\right)}d\omega$$

$$H = \frac{1}{2m}\left(\vec{p} - \frac{q}{c}\vec{A}\right)^2 = \frac{p^2}{2m} - \frac{q}{mc}\vec{A}\cdot\vec{p} + \frac{iq\hbar}{2mc}\vec{\nabla}\cdot\vec{A} + \frac{q^2}{2mc^2}A^2$$
$$\simeq \frac{p^2}{2m} - \frac{q}{mc}\vec{A}\cdot\vec{p} = H_0 + V$$

$\omega = \omega_k - \omega_s \rightarrow$ **Resonance** . $<\psi_k^0 \mid V \mid \psi_n^0>= 0 \rightarrow$ **Selection Rules**

PERIODIC, RANDOM AND QUASIPERIODIC MEDIA

Julian D. Maynard
Department of Physics
Pennsylvania State University

[TR-1]

Anderson Localization of Nonlinear Waves

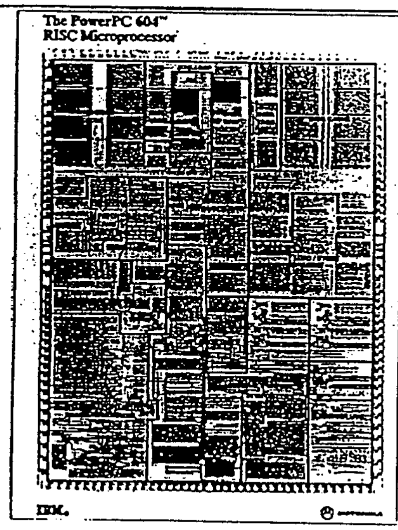

Transistors and connecting wires become small (microns)
Does physics for larger versions still work?
Ohm's Law?

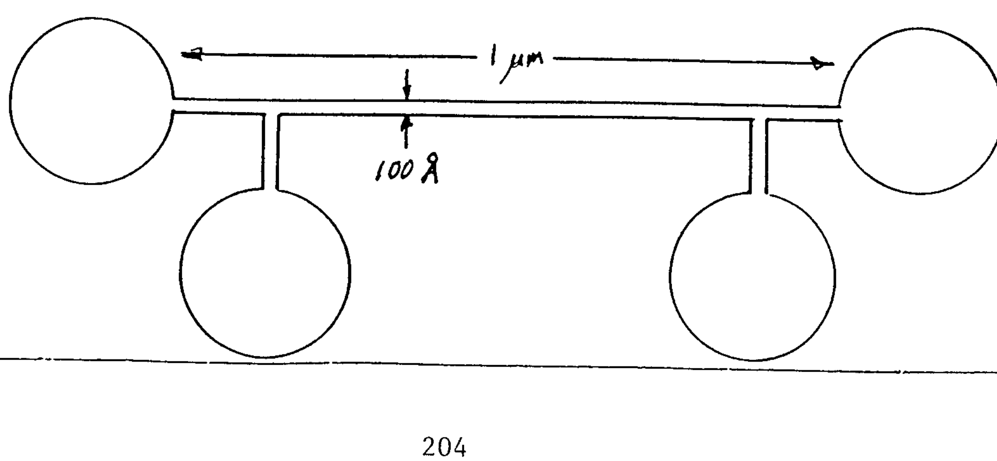

[TR-2]

Tuning-up a Quasicrystal

Problem: Solve Schrodinger Eq. for electron scattering from 10^{23} ions

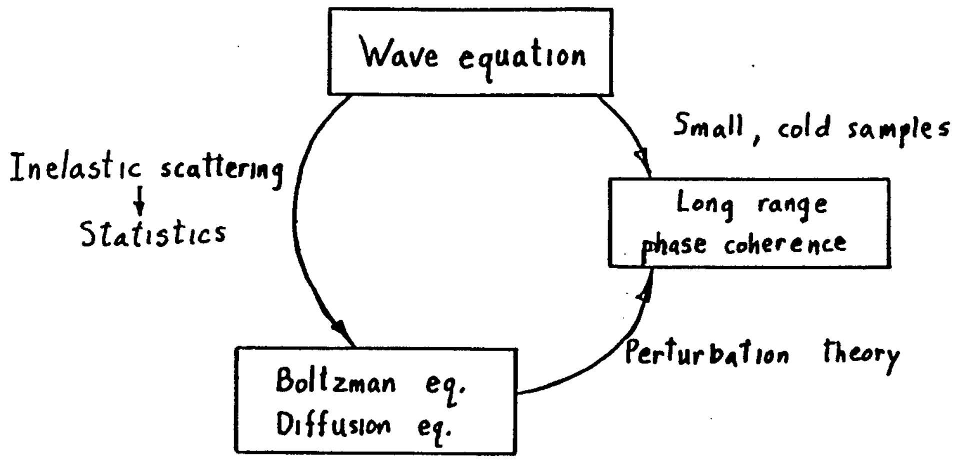

- Anderson localization
- Ahronov-Bohm effect
- Universal conductance fluctuations
- Normal electron persistent currents.

[TR-3]

<u>Mesoscopic</u> – Phase coherence on the scale of microns

<u>Megascopic</u> Phase coherence on the scale of millions of microns

Experiments:
- Phase coherence in a 1-D wire 10 m long
- Density of states in a quasicrystal > 1m in diameter

<u>Classical (acoustic) analog systems</u> ("analog computers")

Advantages
- Precise analogs; $\nabla^2\Psi + [q^2 - V(r)]\Psi = 0$
- All conditions and parameters may be precisely controlled or measured
- Precise measurement of eigenvalues, eigenfunctions, density of states, etc.
- May study time-dependent or non-linear effects exactly

[TRs 4 & 5 Unavailable At Time Of Printing]

[TR-6]

CONTROLLING PLATE RADIATION WITH ANDERSON LOCALIZATION

HYPOTHETICAL PROBLEM IN NOISE REDUCTION

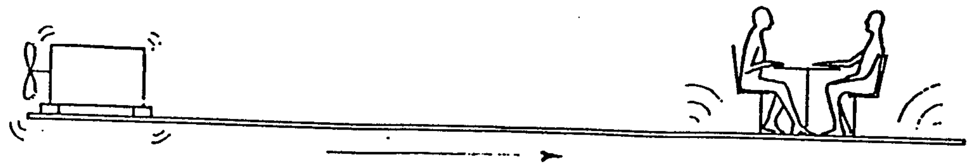

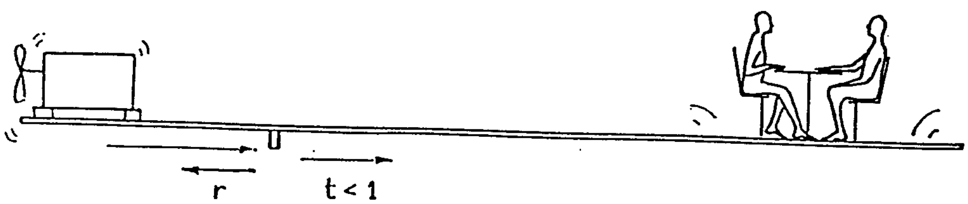

[TR-7]

PERIODIC ARRAY OF IDENTICAL RIBS (Ease of manufacture)

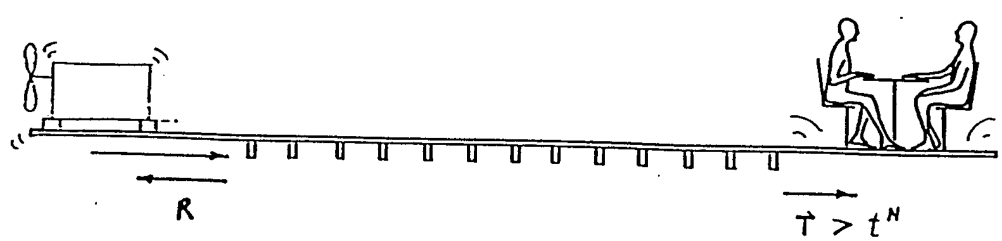

Example: Electron in a metallic crystal

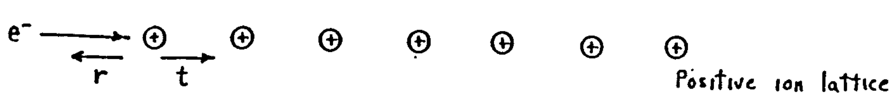

Electrical conductivity $\propto$ distance between scatterers

[TR-8]

DERIVE FROM GROUP THEORY:

Mathematics – FLOQUET'S THEOREM
Solid state – BLOCH'S THEOREM

For a system with a periodic potential or impedance, the eigenfunctions are extended:

$$\Psi_{k,n}(x) = e^{ikx} U_n(x)$$

where $U_n(x+\ell) = U_n(x)$

$|\Psi_{k,n}(x)| \sim$ constant for all x

Solid state: Bloch wave functions →

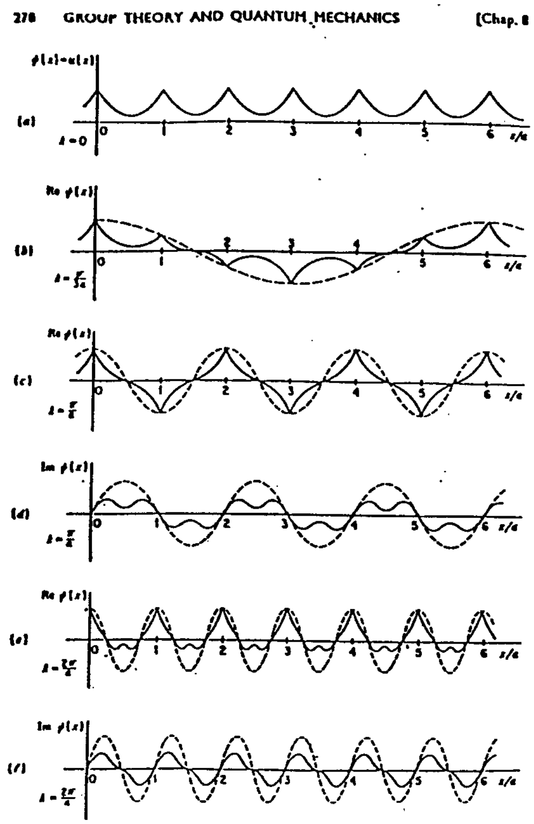

[TR-9]

PERIODIC POTENTIAL $V_0(x+\ell) = V_0(x)$

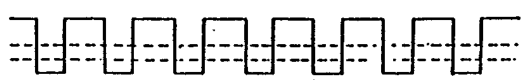

(a)

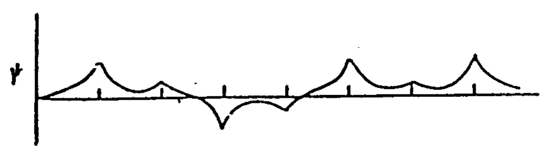

(a)

$V_0(x) + \Delta V$ RANDOM

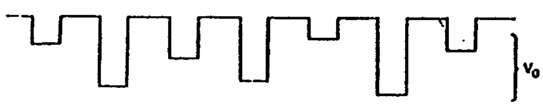

(b)

Random potential energy introduced by Anderson; (a) V_0 (b) $V_0 + \Delta V$

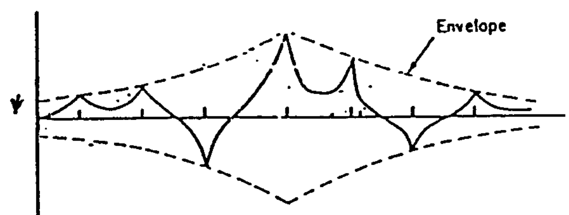

(b)

Wave function ψ of an electron when $L \sim a$. (*a*) Extended states (*b*) localized states.

$\boxed{\text{ANDERSON LOCALIZATION}}$ (1958)

☆ M. Luban + J. Luscombe, Phys. Rev. B35, 9045 (1987)

[TR-10]

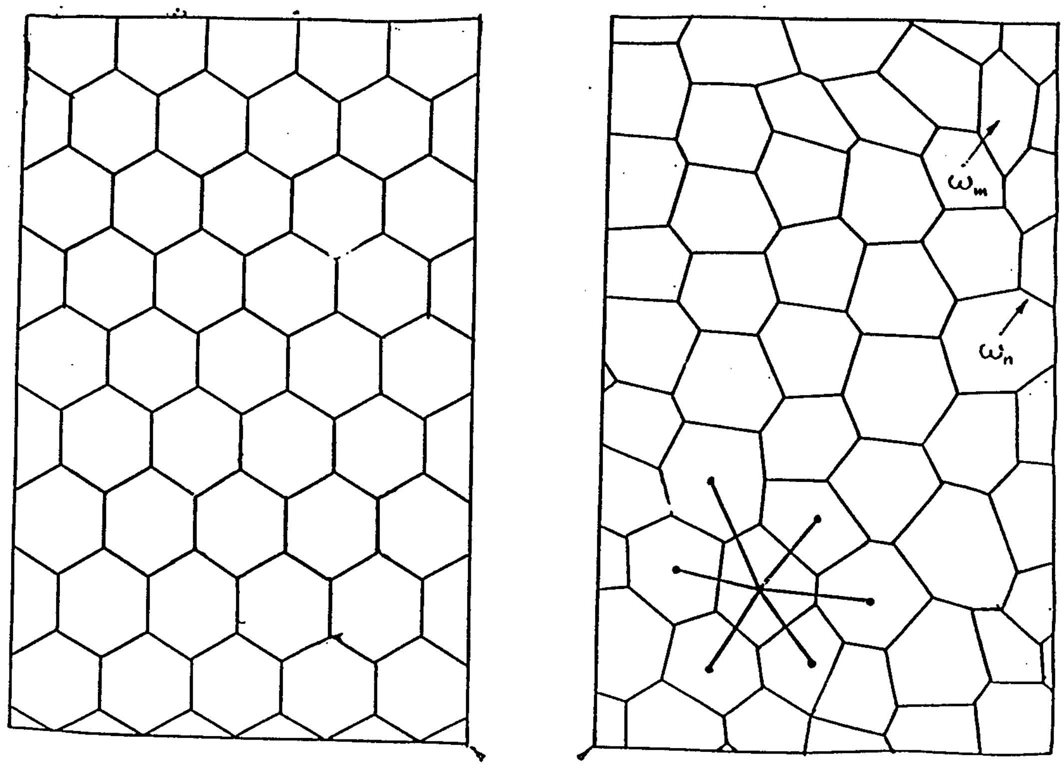
ω_m
ω_n

[TR-11]

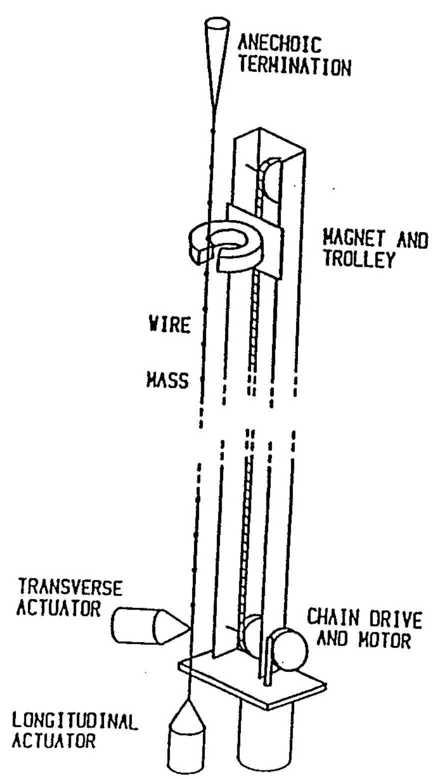
ANECHOIC TERMINATION
MAGNET AND TROLLEY
WIRE
MASS
TRANSVERSE ACTUATOR
CHAIN DRIVE AND MOTOR
LONGITUDINAL ACTUATOR

[TR-12]

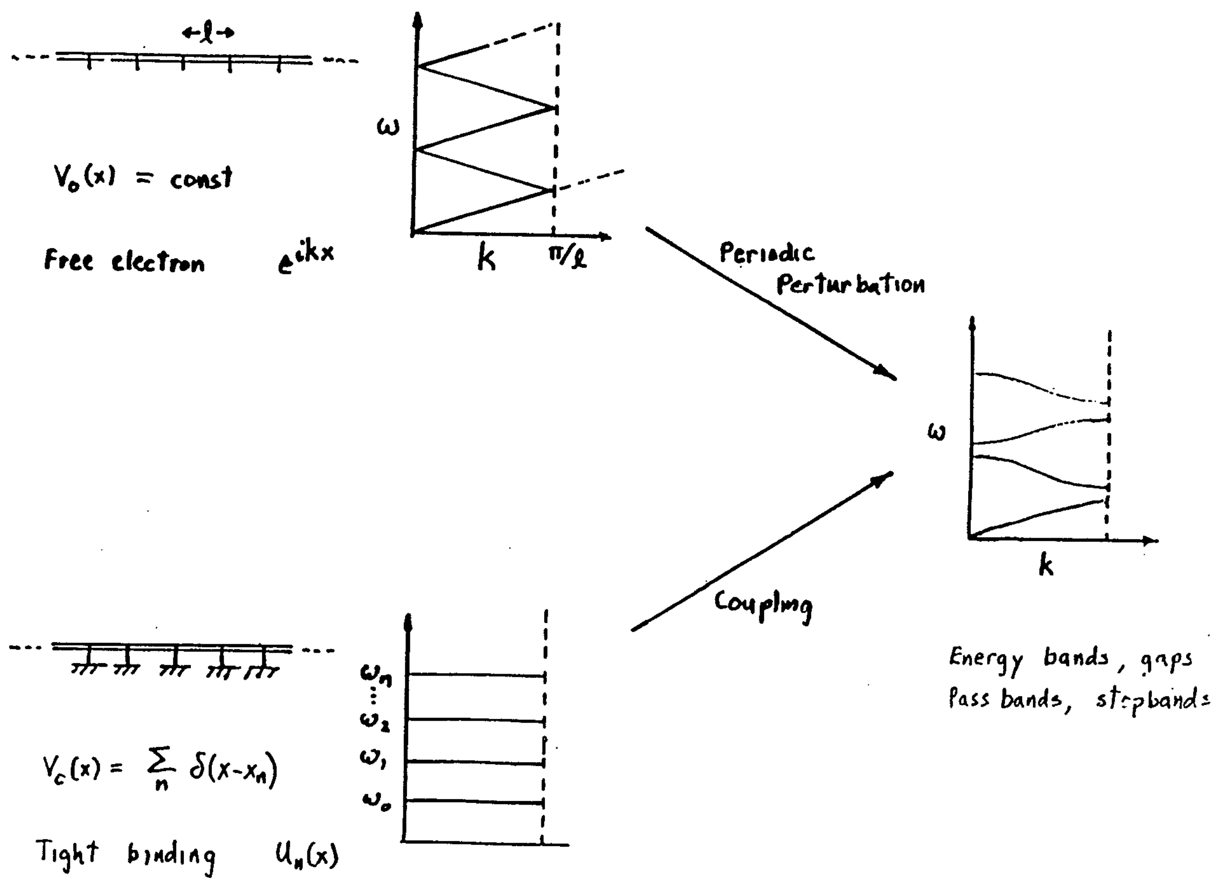

←ℓ→
$V_o(x)$ = const
Free electron e^{ikx}
ω
k
π/ℓ
Periodic Perturbation
ω
k
Coupling
Energy bands, gaps
Pass bands, stopbands
$V_c(x) = \sum_n \delta(x-x_n)$
Tight binding $U_n(x)$
ω_n
ω_2
ω_1
ω_o

[TR-13]

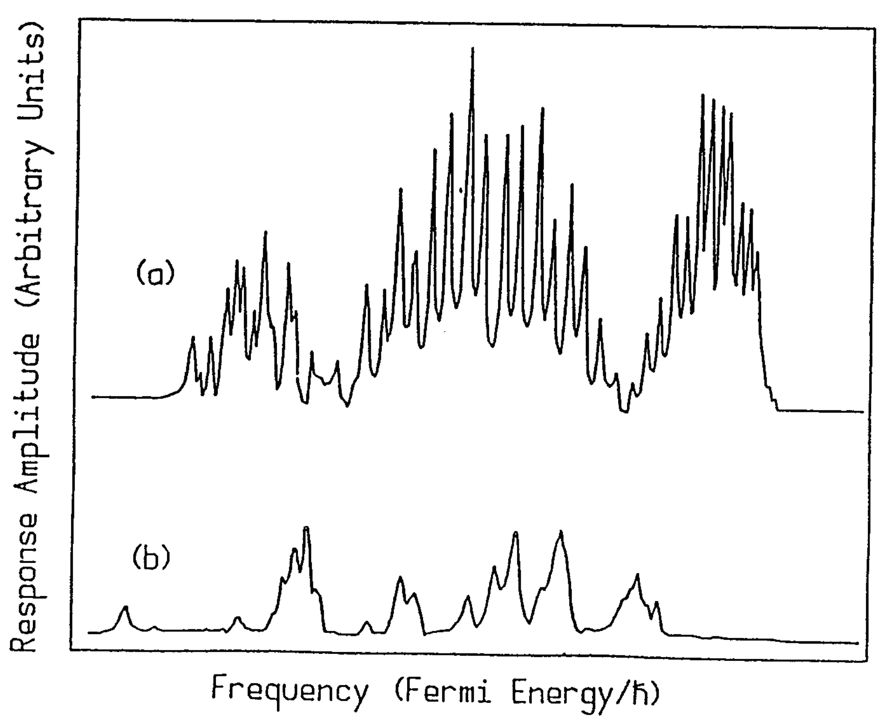

Response Amplitude (Arbitrary Units)
(a)
(b)
Frequency (Fermi Energy/ħ)

[TR-14]

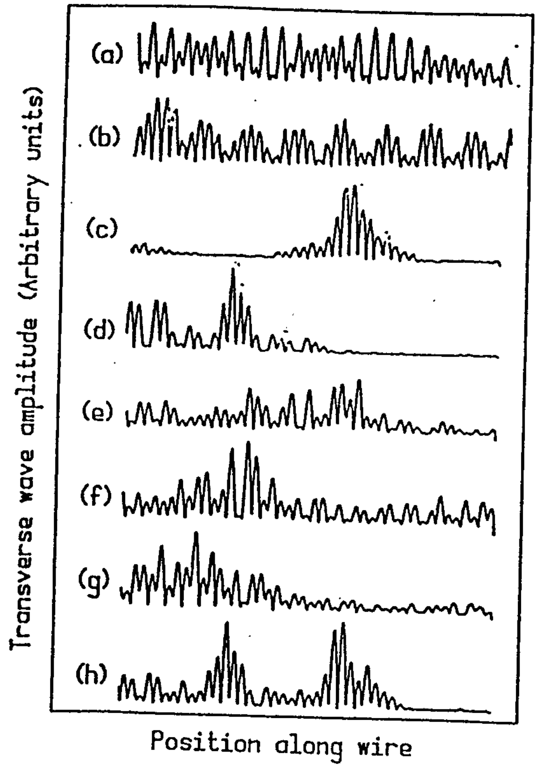

[TRs 15, 16, 17 & 18 Unavailable At Time Of Printing]

[TR-19]

Solid States: Crystalline, Amorphous, Quasicrystalline

Crystal Bravais lattices

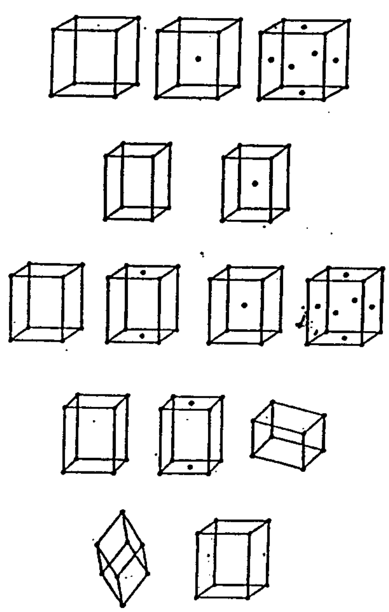

Kittel, page 13:

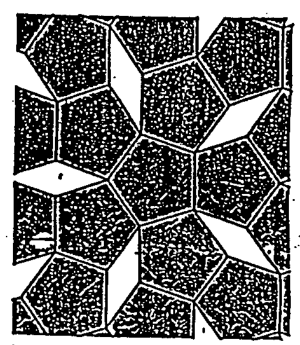

Figure 8a A five-fold axis of symmetry cannot exist in a lattice because it is not possible to fill all space with a connected array of pentagons.

Shechtman NBS, 1982

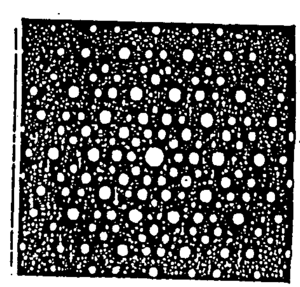

[TR-20]

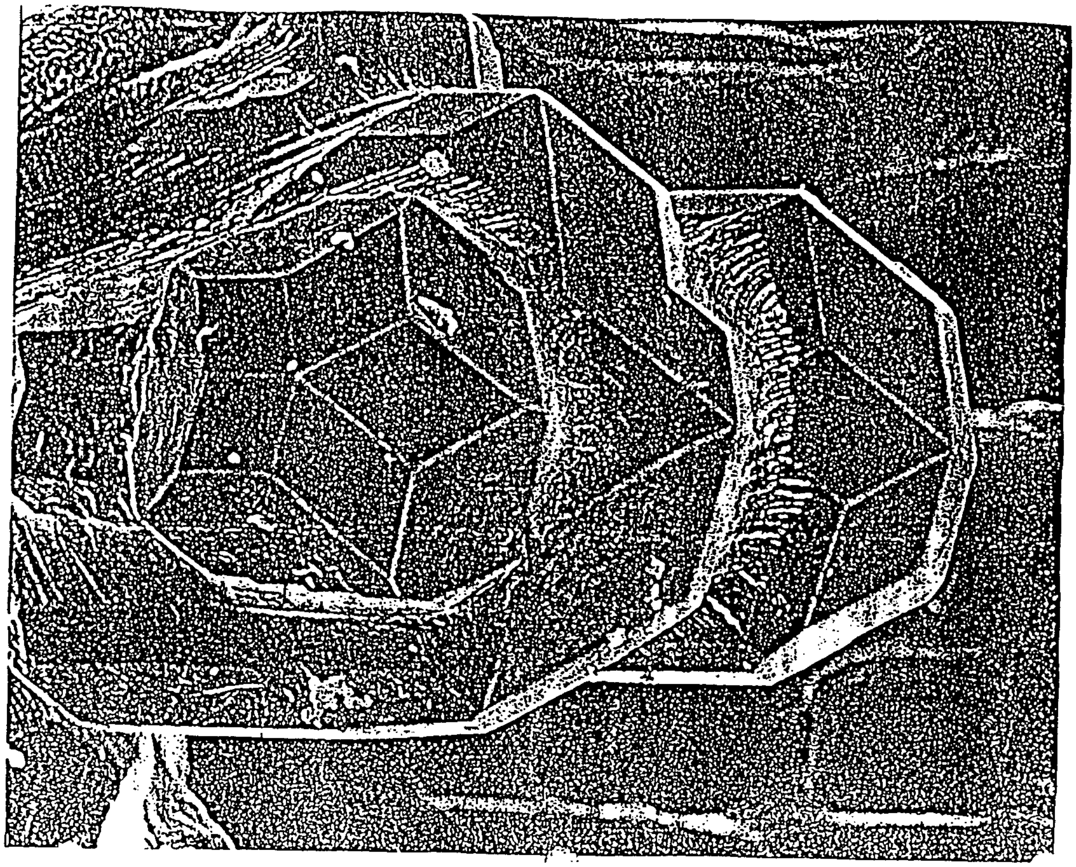

[TR-21]

10 MOSAIC Volume 18 Number 4 Winter 1987/8

[TR-22]

Quasi-periodicity

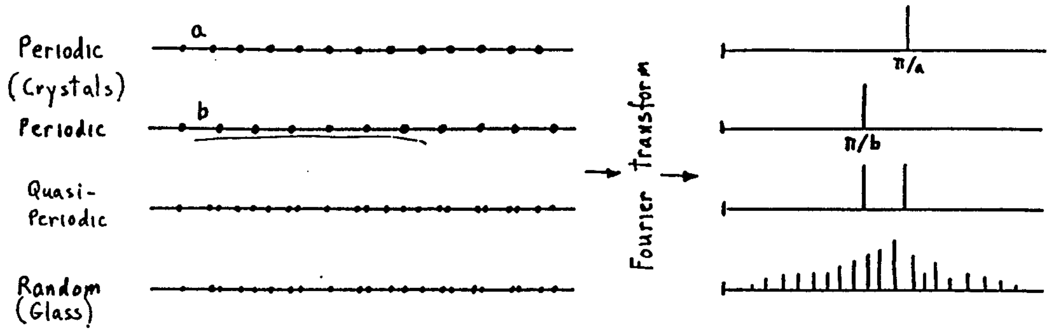

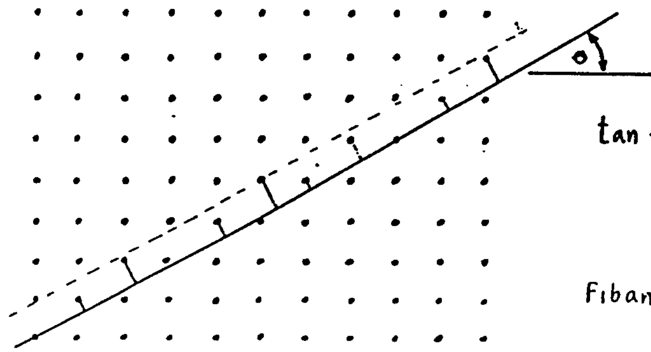

$$\tan\theta = \frac{\sqrt{5}+1}{2}$$

Golden mean

Fibanacci sequence

[TR-23]

Penrose tile

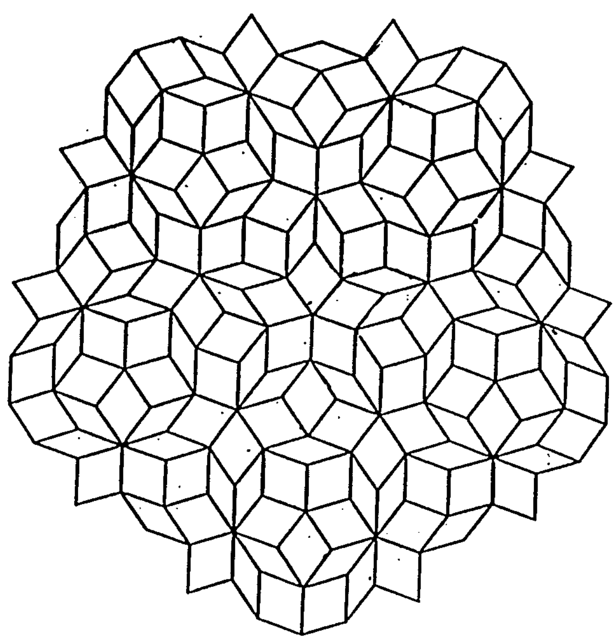

Area of fat rhombus / Area of skinny rhombus $= (\sqrt{5}+1)/2$

[TR-24]

Acoustic Analog Studies of Quasicrystals

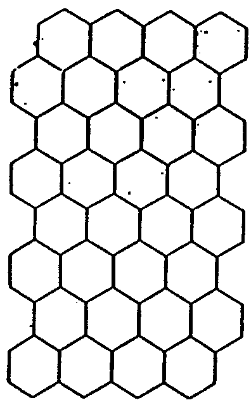

Periodic

Bloch's theorem

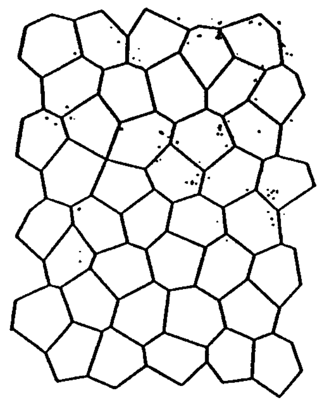

Random

Statistics

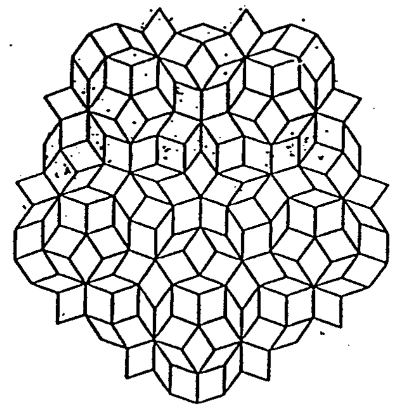

Quasicrystaline

?

[TR-25]

Effects of One-dimensional Quasiperiodicity

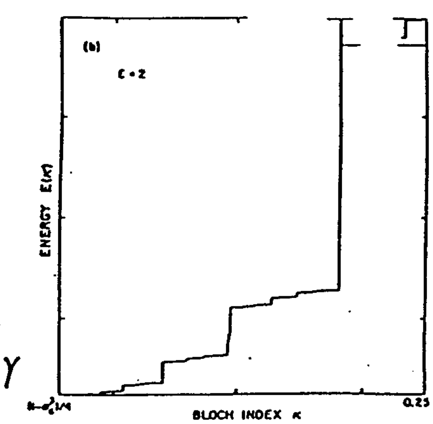

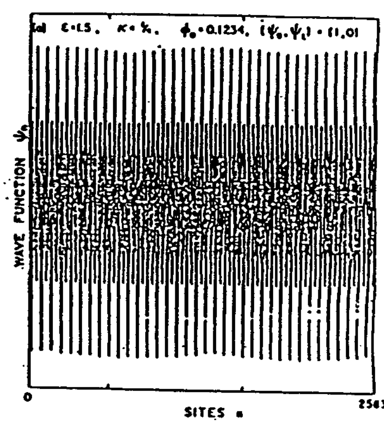

Ostlund + Pandit
Phys Rev B29
1394 (1984)

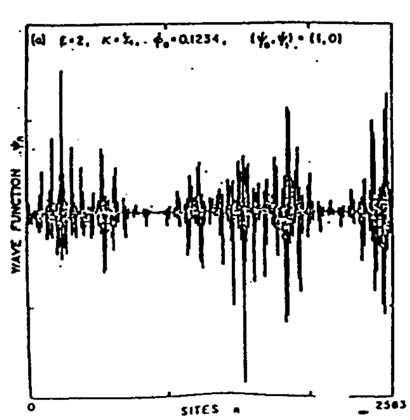

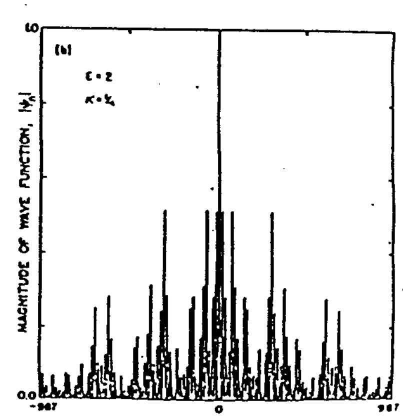

[TR-26 Unavailable At Time Of Printing]

[TR-27]

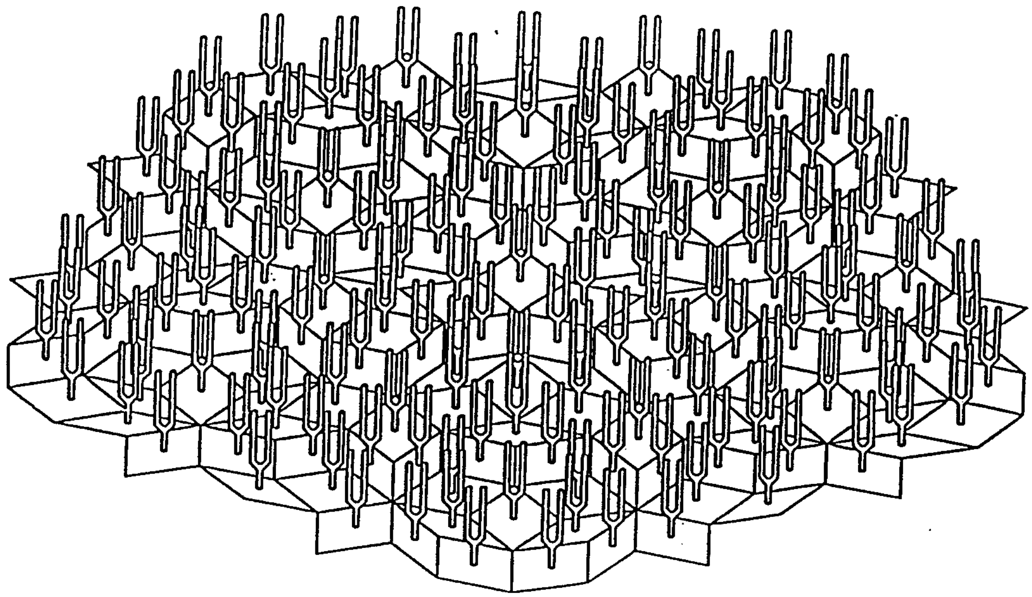

[TR-28]

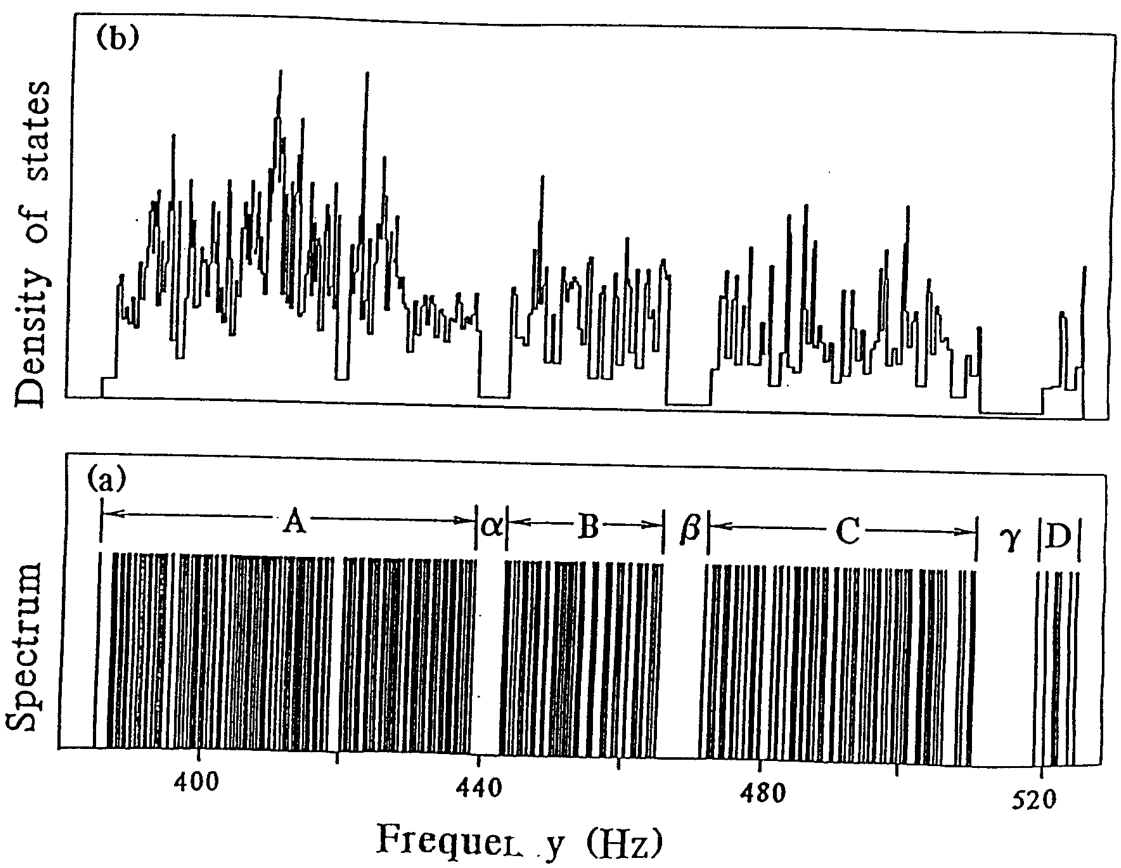

[TR-29]

Measurement of Quasicrystal Eigenfunctions

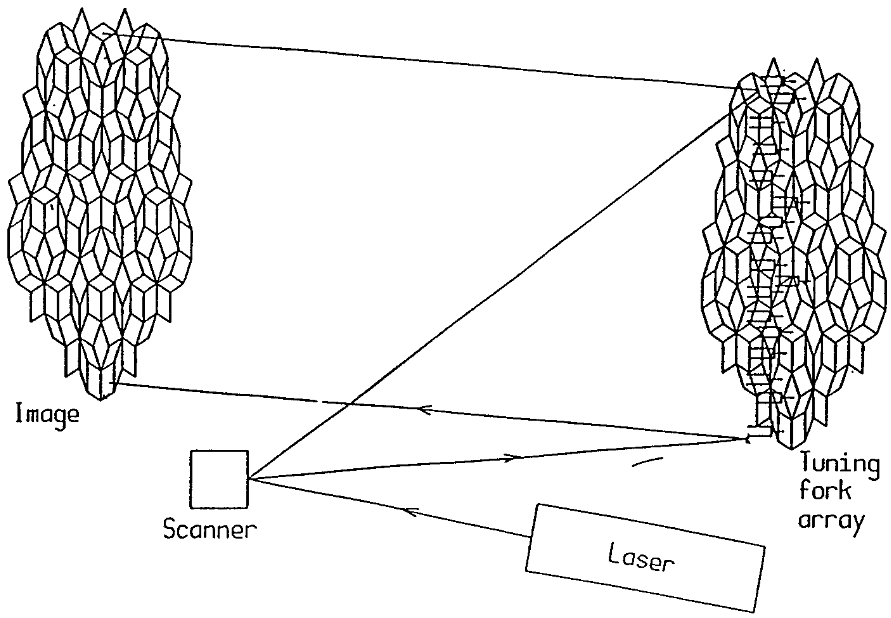

[TR-30]

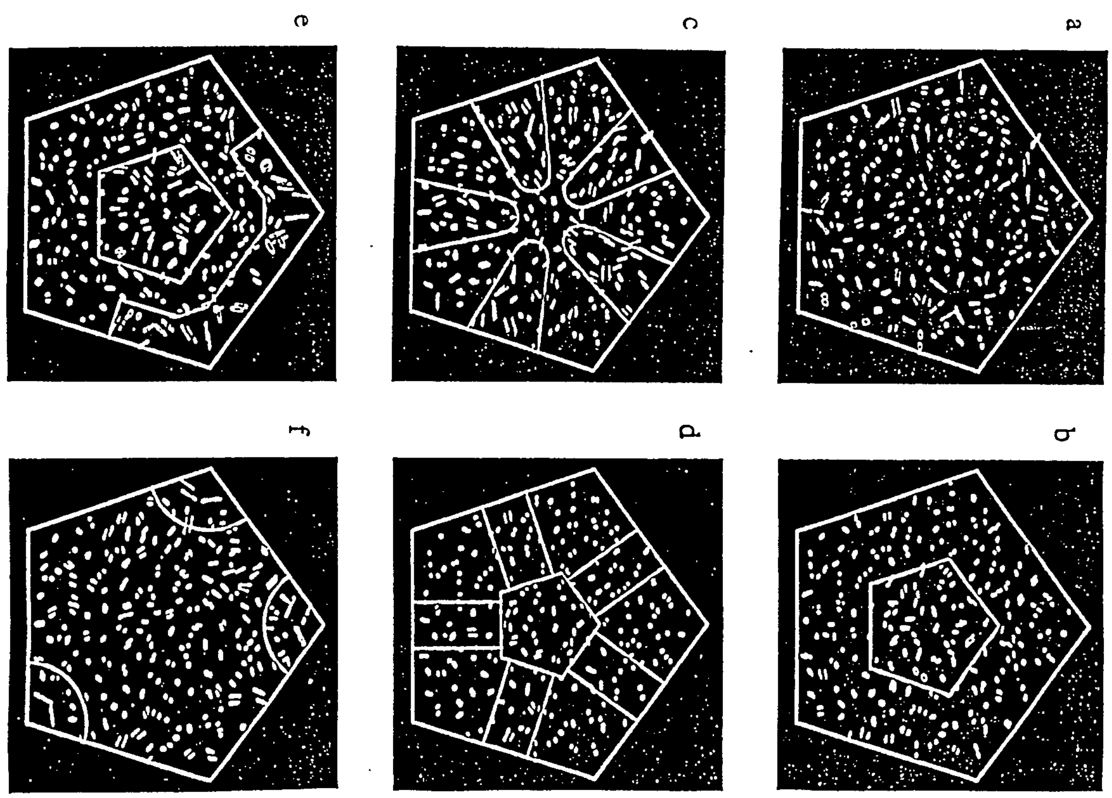

[TR-31]

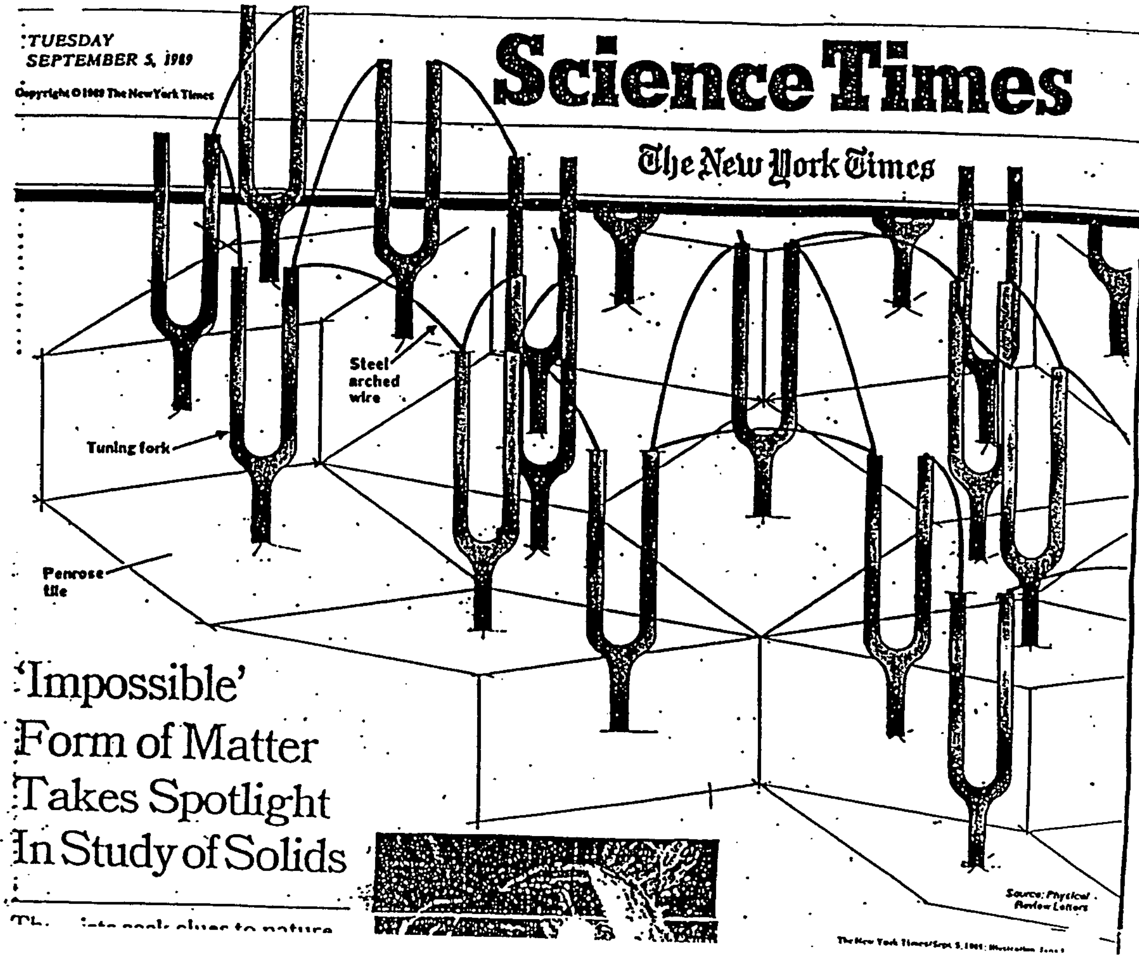
TUESDAY
SEPTEMBER 5, 1989
Copyright © 1989 The New York Times
Science Times
The New York Times
Steel arched wire
Tuning fork
Penrose tile
'Impossible' Form of Matter Takes Spotlight In Study of Solids
Source: Physical Review Letters

[TR-32]

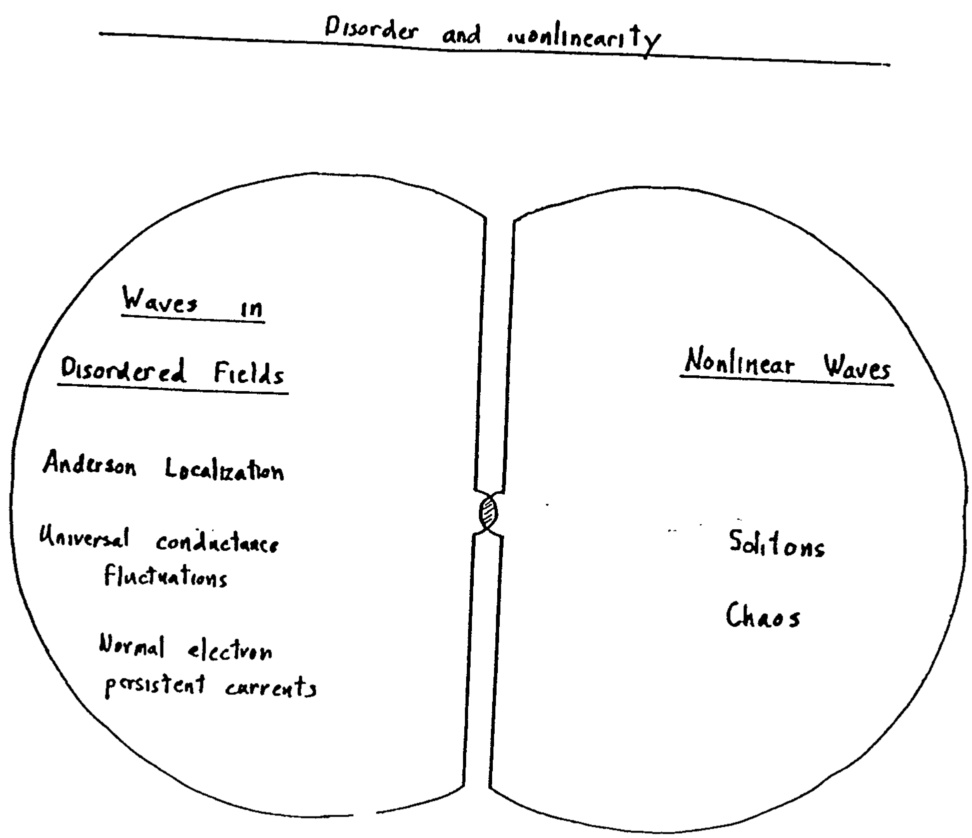
Disorder and nonlinearity
Waves in Disordered Fields
Anderson Localization
Universal conductance fluctuations
Normal electron persistent currents
Nonlinear Waves
Solitons
Chaos

[TR-33]

"What led you to the mathematics of chaos, Dr. Maynard?"

[TR-34]

Does Nonlinearity Weaken ıderson Localization?

Reference:	Yes	No
1. P. Devillard and B. Souillard, J. Stat. Phys. 43, 423 (1986) Fixed output t, find t/r decays as power law for strong nonlinearity	X	
2. B. Doucot and R. Rammal, Europhysics Lett. 3, 969 (1987) Fixed output: power law decay - Fixed input: exponential decay	X	X
3. C. Albanese and J. Frohlich, Commun. Math. Phys. 116, 475 (1988) Rigorous theorem: Eigenstates of NLS eq. remain localized		X
4. Q. Li, C. M. Soukoulis St. Pnevmatikos, and E. N. Economou, Phys. Rev. B 38, 11888 (1988) A soliton can force its way through a binary alloy	X	
5. A. Soffer and M. I. Weinstein, Commun. Math. Phys. Same as 3.		X
6. R. Bourbonnais and R. Maynard, Phys. Rev. Lett. 64, 1397 (1990) Superpositions of localized states spread due to nonlinearity	X	
7. Yu. S. Kivshar, S. A. Gredeskul, A. Sanchez, and L. Vazquez, Phys. Rev. Lett. 64, 1693 (1990) Same as 4, but only for sufficiently strong soliton	X	X
8. R. Scharf and A. R. Bishop, "Nonlinearity with Disorder", ed. F. Abdullaev, A. R. Bishop, and S. Pneuvmatikos (Springer, Berlin, 1992) The nonlinear Schrodinger equation on a disordered chain Numerical results; same as 7	X	X

[TR-35]

Normal mode analysis versus Pulse analysis

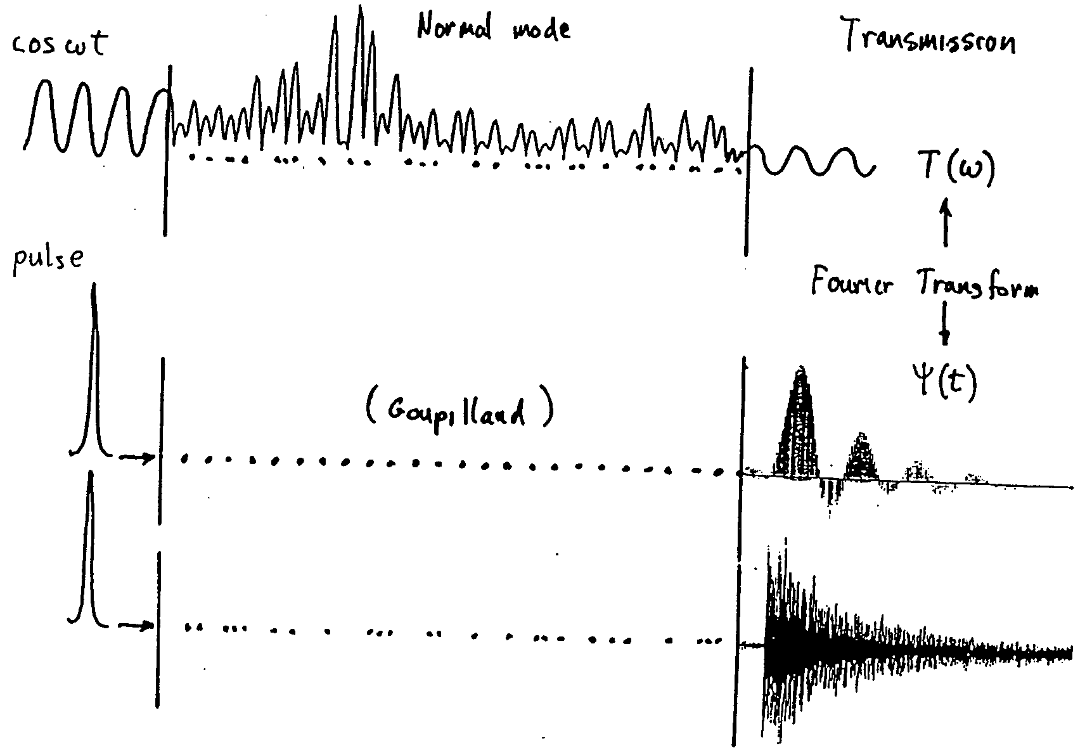

[TR-36]

Nonlinearity in a Stretched String

μ = mass/length

Newton: $\frac{\partial^2\Psi}{\partial x^2} - \frac{\mu}{T}\frac{\partial^2\Psi}{\partial t^2} = 0$ Wave speed $c_0 = \sqrt{T_0/\mu}$

Arc length correction: $T = T_0\left\{1 + \left(\frac{l}{\Delta l}\right)\left[\frac{1}{l}\int_0^l \sqrt{1+\left(\frac{\partial\Psi}{\partial x}\right)^2}\,dx - 1\right]\right\}$

Add masses: $\frac{\partial^2\Psi}{\partial x^2} + q^2\Psi - V(x)\Psi - \left[\frac{1}{2}\left(\frac{l}{\Delta l}\right)\int_0^l\left(\frac{\partial\Psi}{\partial x}\right)^2 dx\right]\Psi = 0$

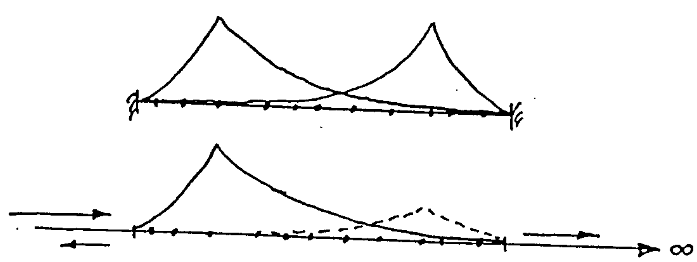

[TR-37]

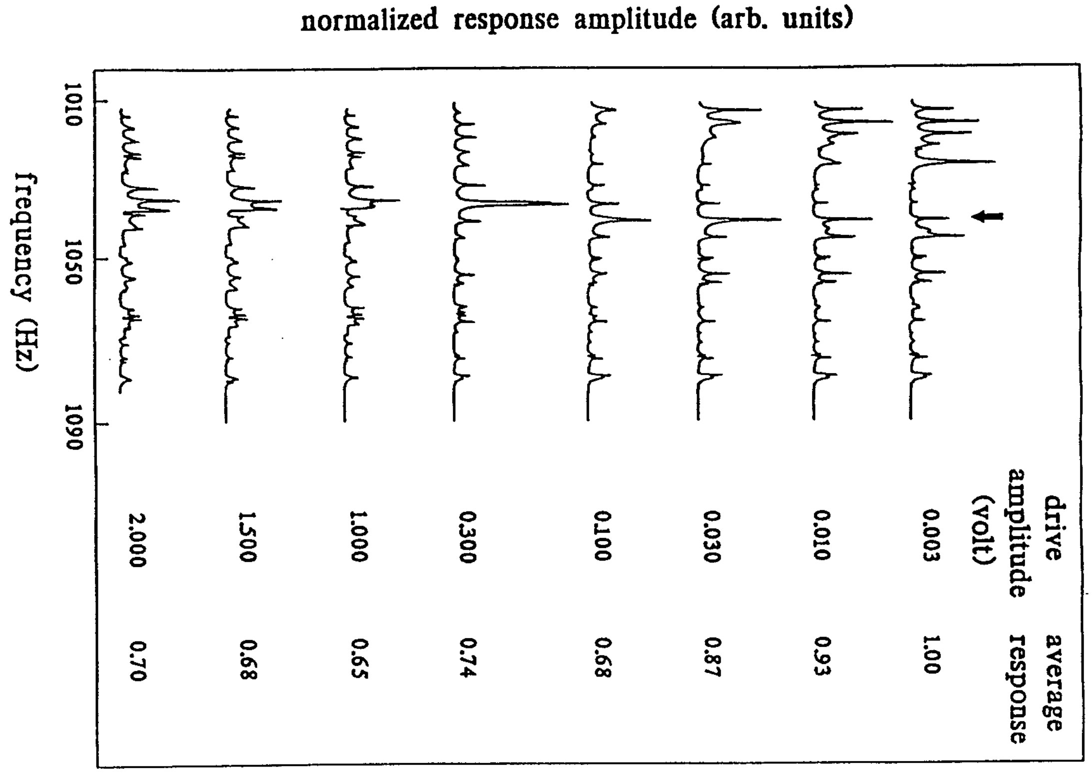
normalized response amplitude (arb. units)
frequency (Hz)
1010
1050
1090
drive amplitude (volt)
average response
0.003 1.00
0.010 0.93
0.030 0.87
0.100 0.68
0.300 0.74
1.000 0.65
1.500 0.68
2.000 0.70

[TR-38]

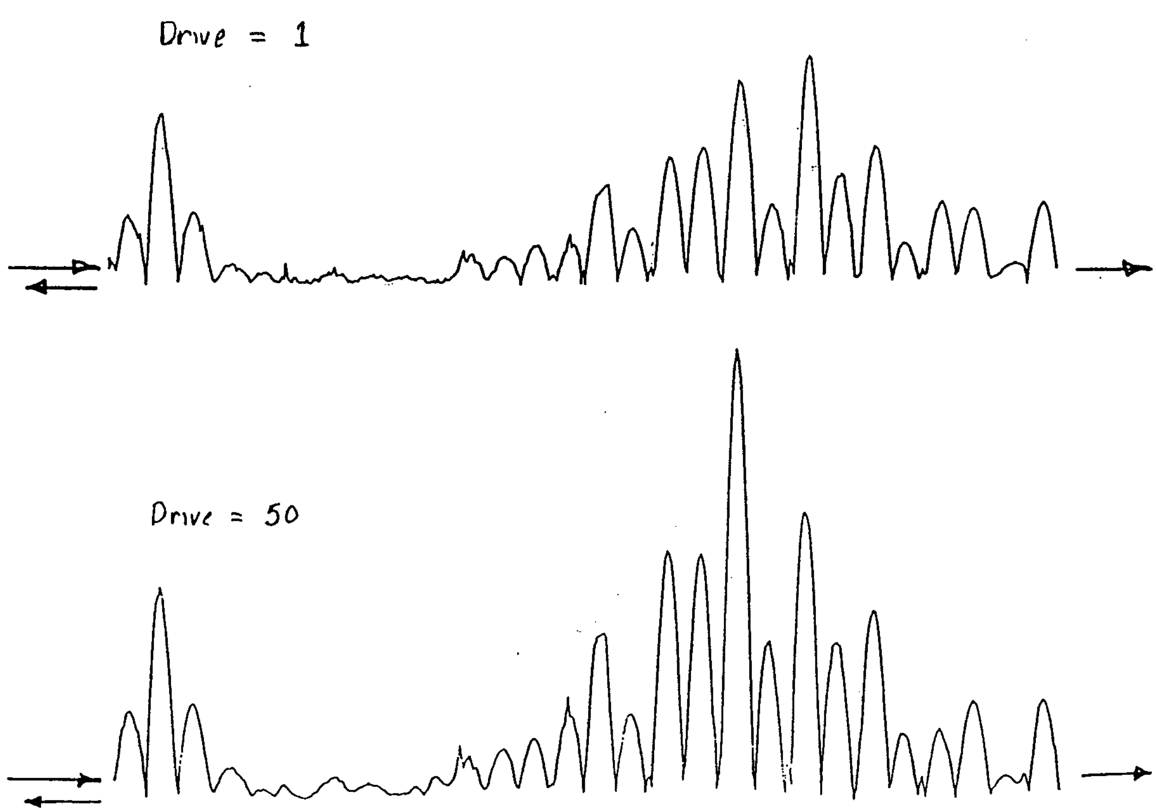
Drive = 1
Drive = 50

[TR-39]

Theoretical Predictions for Nonlinear Pulse in Disordered Medium

Linear system 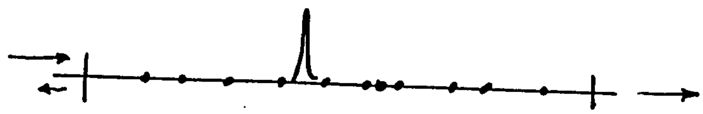

Product of Random Matrices $\begin{pmatrix}\alpha & \beta_1\\ \cdot & \cdot\end{pmatrix}\begin{pmatrix}\alpha_2 & \beta_2\\ \cdot & \cdot\end{pmatrix}\cdots\cdots \begin{pmatrix}\alpha_N & \beta_N\\ \cdot & \cdot\end{pmatrix} \Rightarrow T(\omega)$

Nonlinear pulse has extra degree of freedom

$\Rightarrow$ satisfy conditions locally, within (second) length L_{NL}

Result:

Strong soliton, $L_{NL} \ll L_A$

Intermediate, $L_{NL} \sim L_A$

Weak soliton $L_{NL} \gg L_A$

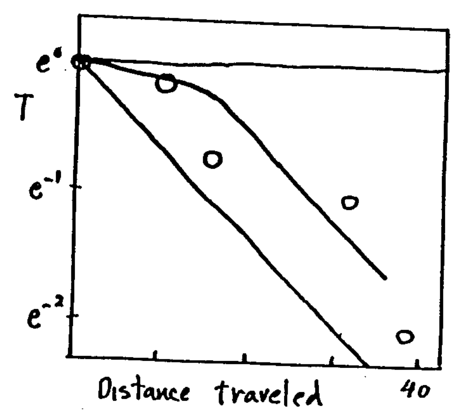

[TR-40]

Nonlinear Waves and Pulses. Surface Waves

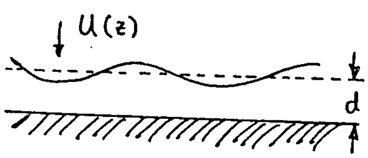

Speed of wave $= \sqrt{d\frac{dU}{dz}} = \sqrt{gd}$

$c(d)$

Finite amplitude: $C(d+\Psi) \longrightarrow$ Nonlinear Wave Eq.

Low attenuation: Superfluid Helium Third Sound $U(z)$ = Van der Waals $\frac{\alpha}{z^3}$

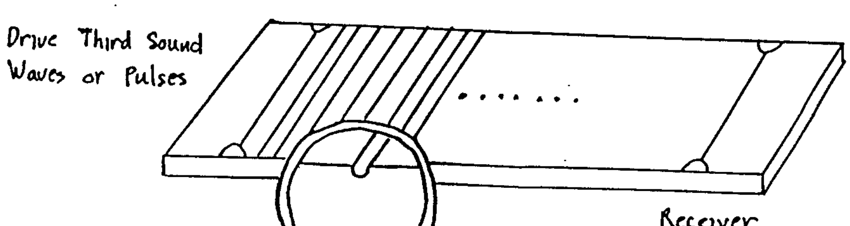

Doug Meegan

[TR-41]

No scatterers (bare substrate)

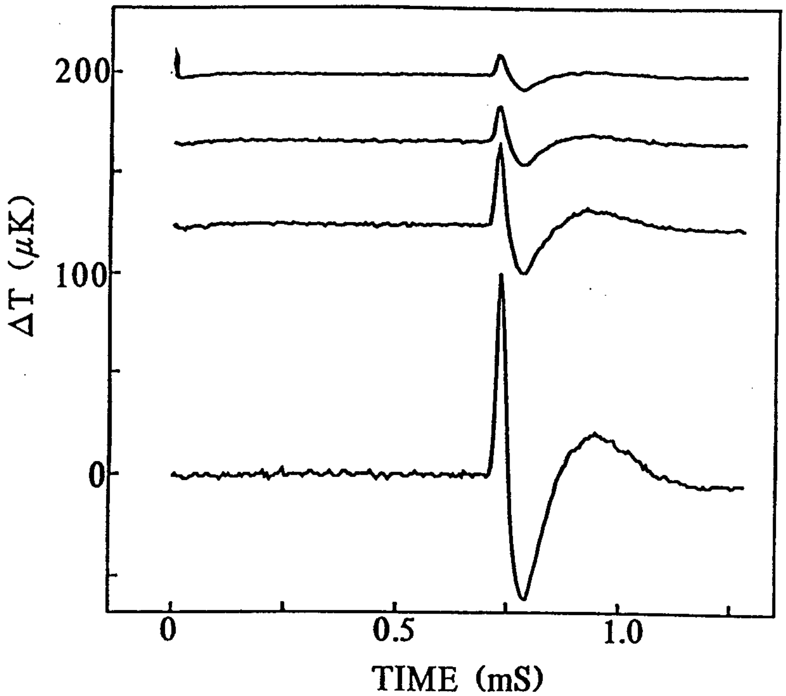

[TR-42]

No scatterers ; Appearance of nonlinear pulse

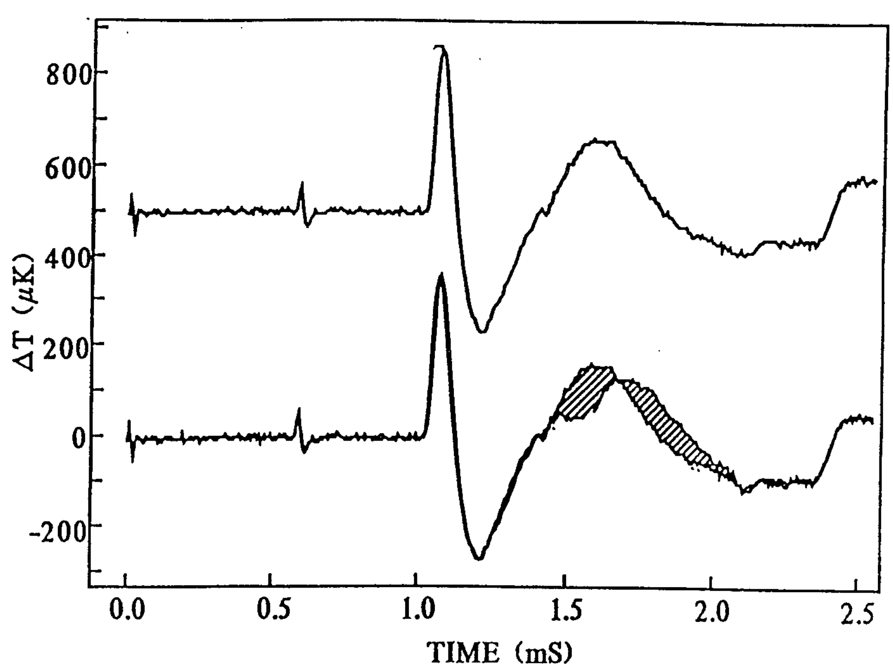

[TR-43]

No scatterers; Nonlinear Pulse: C depends on amplitude

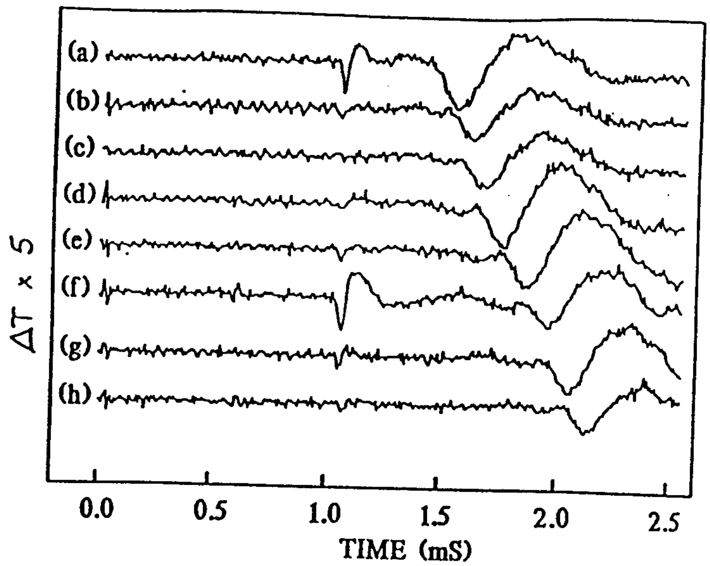

[TR-44]

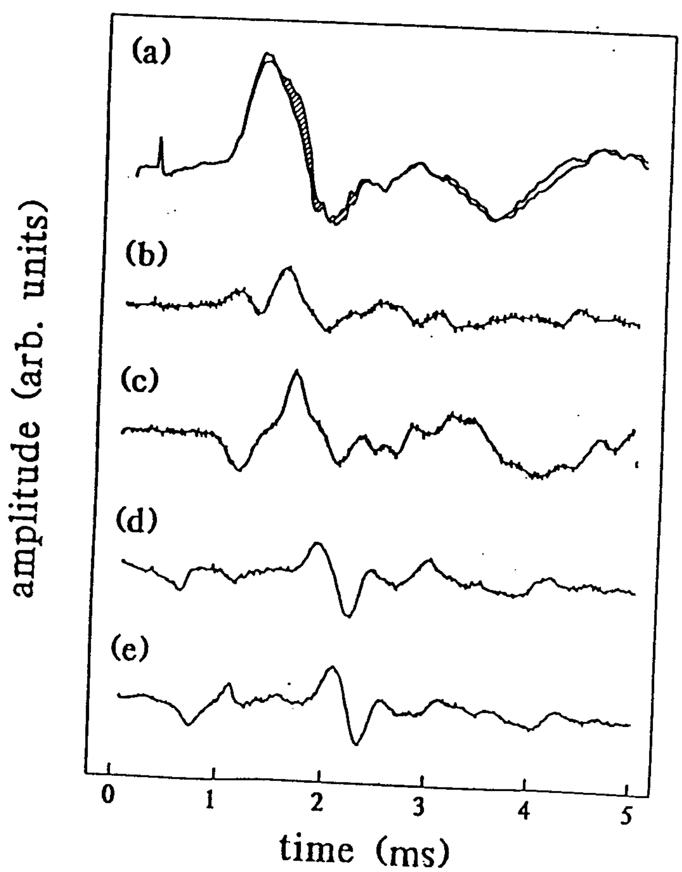

[TR-45]

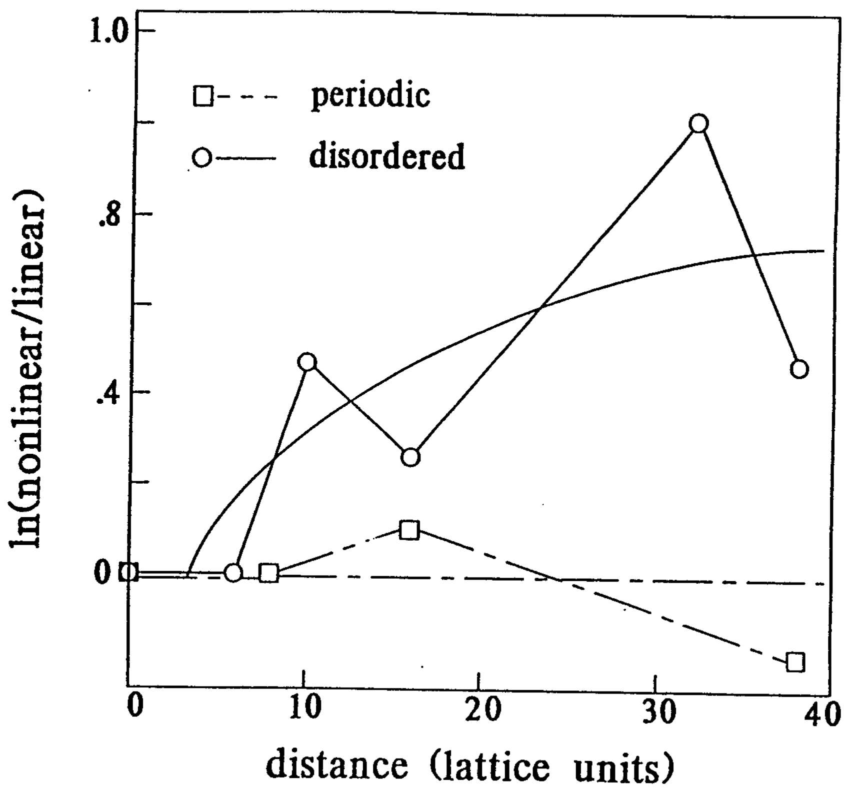
periodic
disordered
ln(nonlinear/linear)
1.0
.8
.4
0
0
10
20
30
40
distance (lattice units)

[TR-46]

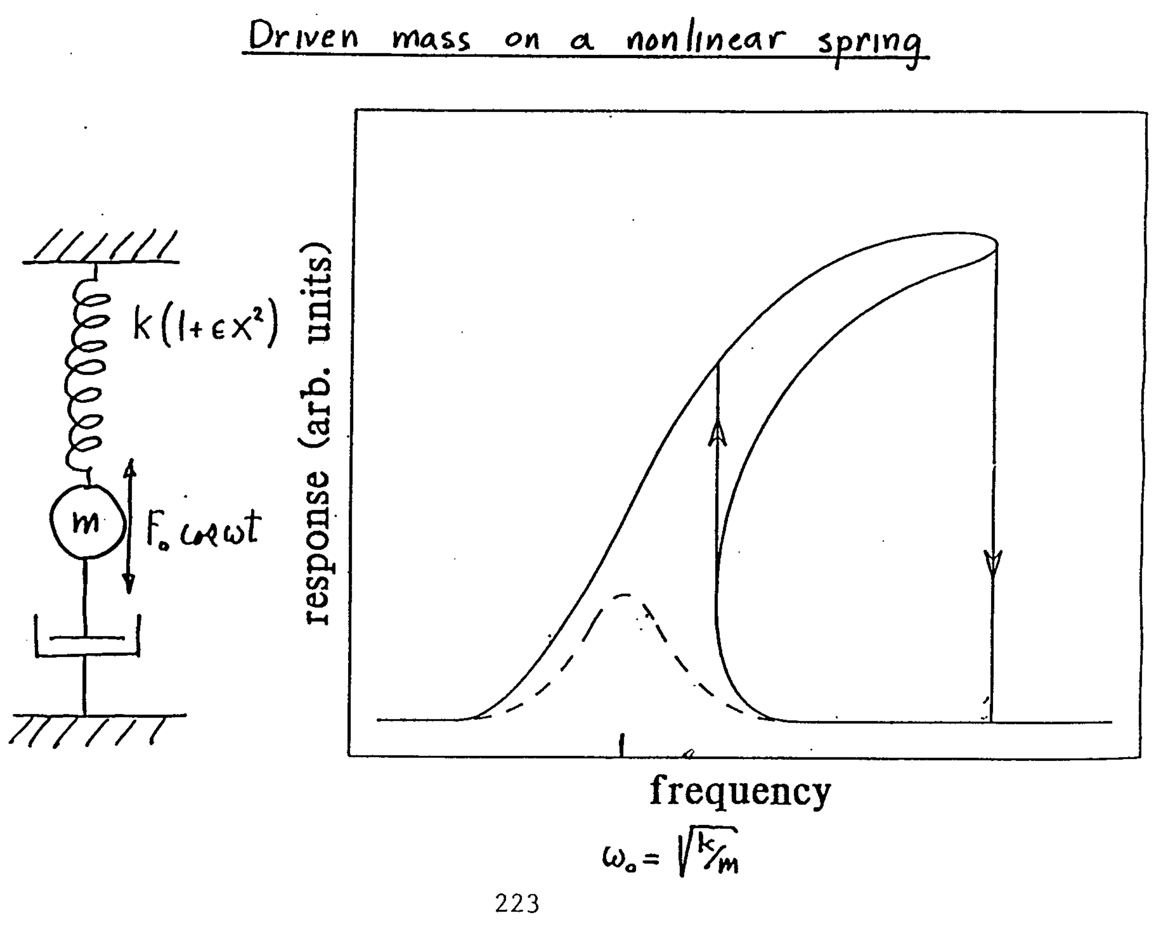
Driven mass on a nonlinear spring
$k(1+\epsilon x^2)$
m
$F_0 \cos \omega t$
response (arb. units)
frequency
$\omega_0 = \sqrt{k/m}$

[TR-47]

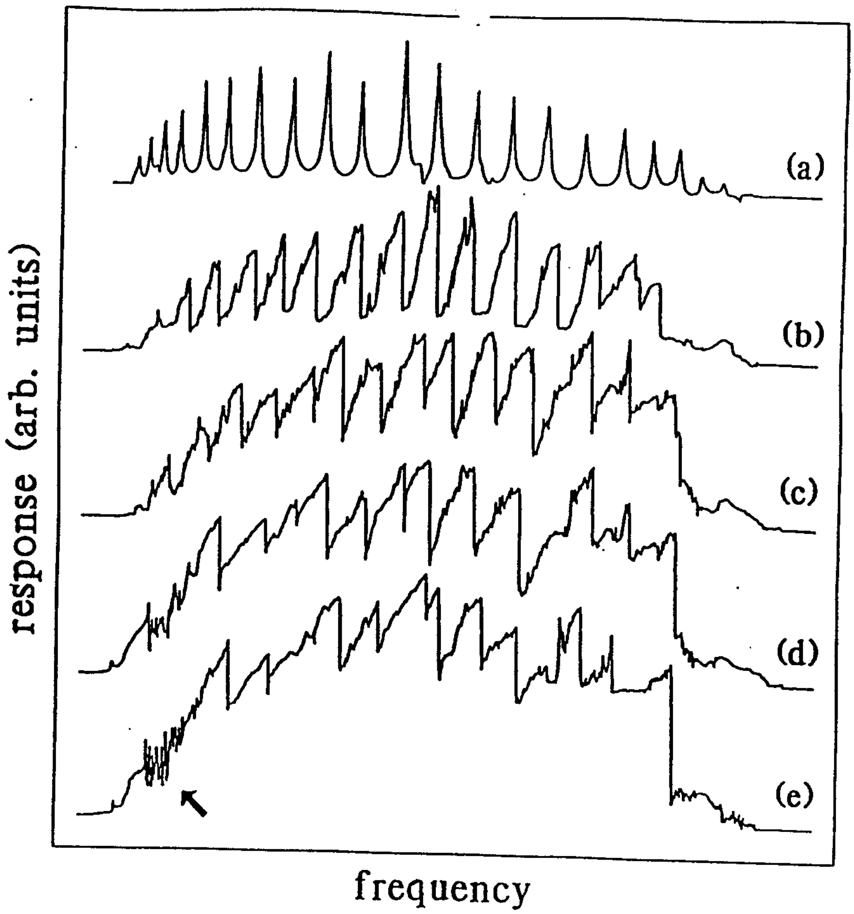
(a)
(b)
(c)
(d)
(e)
response (arb. units)
frequency

[TR-48]

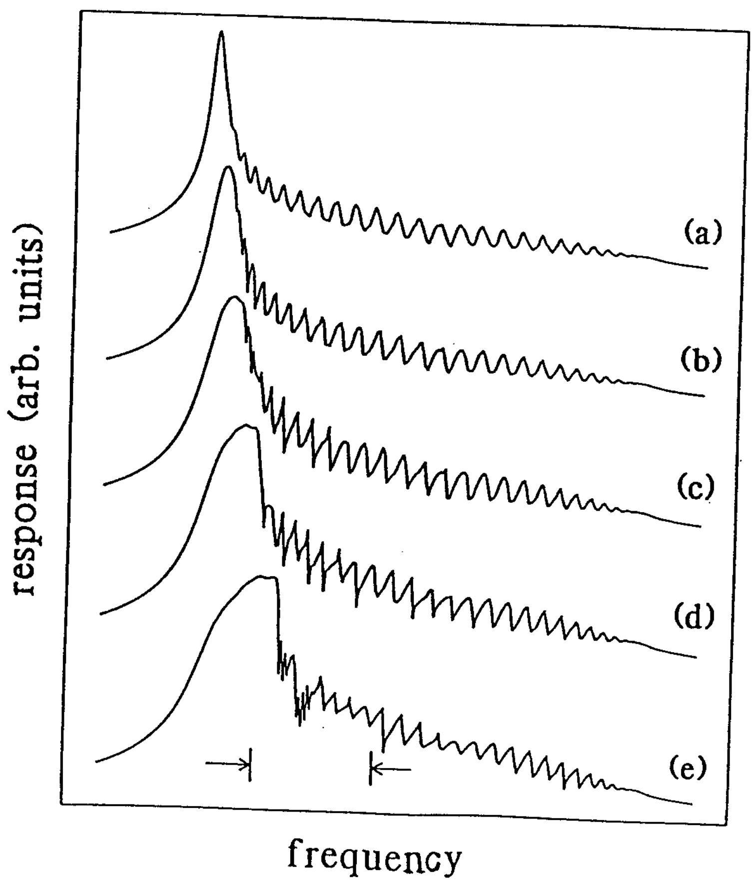
(a)
(b)
(c)
(d)
(e)
response (arb. units)
frequency

[TR-49]

Analytic Solution for a Linear Periodic System

Bloch:

$$\Psi(x) = e^{ikx} u_k(x)$$

$$
\begin{aligned}
&\frac{1}{\rho c}\mathrm{Re}[\tilde{Z}(qa)] = -\{[2(\tfrac{1}{\eta}\sqrt{\sin qa} - \tfrac{1}{\eta}\sqrt{2\eta\cos qa + (\eta^2-1)\sin qa})\cos qa \; + \\
&[(\tfrac{1}{\eta}\sqrt{\sin qa} - \tfrac{1}{\eta}\sqrt{2\eta\cos qa + (\eta^2-1)\sin qa})^2 - \sin qa]\sqrt{\sin qa}\} \; \{\tfrac{1}{\eta}\sqrt{\sin qa} \\
&- \tfrac{1}{\eta}\sqrt{2\eta\cos qa + (\eta^2-1)\sin qa})^2 + \sin qa\}^{-1} \; \{\cosh(N+1)\sinh^{-1}[-\tfrac{1}{4}(1-(\eta^2+1)\cos^2 \\
&(qa+\tan^{-1}\eta) - (\eta^2+1)\sinh^2\tfrac{qa}{2Q}) + (1-(\eta^2+1)^2\cos^2(qa+\tan^{-1}\eta) + \eta^2)\sinh^2\tfrac{qa}{2Q}]^{1/2} \\
&- \tfrac{1}{2}(1-(\eta^2+1)^2\cos^2(qa+\tan^{-1}\eta) - (\eta^2+1)\sinh^2\tfrac{qa}{2Q}]^{\frac{1}{2}} \; \sinh(N+1)\sinh^{-1}[-\tfrac{1}{4} \\
&(1-(\eta^2+1)^2\cos^2(qa+\tan^{-1}\eta) - (\eta^2+1)\sinh^2\tfrac{qa}{2Q} + (1-(\eta^2+1)^2\cos^2(qa+\tan^{-1}\eta) \\
&+\eta^2)\sinh^2\tfrac{qa}{2a}]^{\frac{1}{2}} - \tfrac{1}{2}(1-(\eta^2+1)^2\cos^2(qa+\tan^{-1}\eta) - (\eta^2+1)\sinh^2\tfrac{qa}{2Q}]^{1/2} \\
&\sqrt{\sqrt{\sin^2 qa + \sinh^2\tfrac{qa}{2Q}} + \sin qa\cosh\tfrac{qa}{2Q}} \; + \cos(N+1)\cos^{-1}[(\eta^2+1)\sin(qa+\tan^{-1}\eta) \\
&\cosh\tfrac{qa}{2Q} / \cosh(\sinh^{-1}[-\tfrac{1}{4}(1-(\eta^2+1)\cos^2(qa+\tan^{-1}\eta) - (\eta^2+1)\sinh^2\tfrac{qa}{2Q}) + \cdots
\end{aligned}
$$

[TR-50]

Nonlinearity $\epsilon = 0.005$

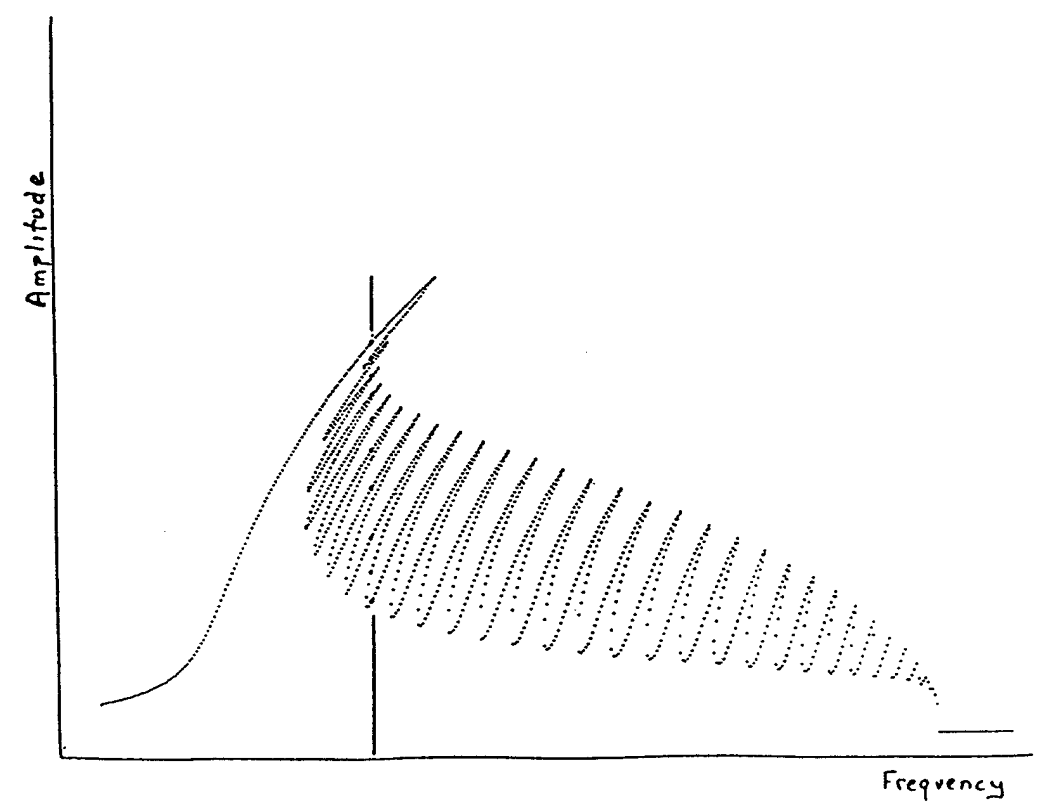

Basin Crowding and Noise

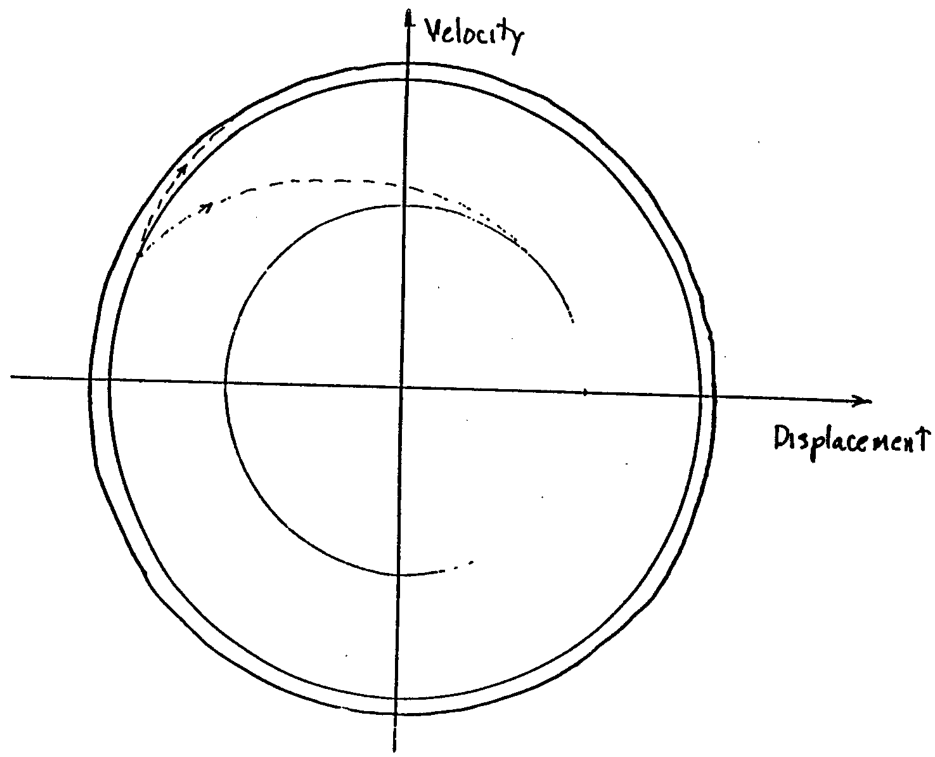

[TR-1]

Resonant Ultrasound Spectroscopy for materials studies and non-destructive testing

Los Alamos

Los Alamos National Laboratory
Los Alamos, New Mexico 87545

Albert Migliori
Timothy W. Darling
John L. Sarrao
Stuart Trugman
Franz J. Friebert
Hans-Rudi Ott — ETH-Zurich
William M. Visscher
Orson Anderson — UCLA
Ray Dixon
U.F. Kocks
R.B. Shwartz
Paul Johnson
Bob Leisure — Colorado State University

Hundreds of administrators, the IPC, the STC, Domenici, Bingamen, KOB, dozens of lawyers, the DOE, the New Mexico Highway and Transportation Dept., DRS Corp., George Rhodes, and many others but I ran out of space!

Resonances

Instruments, Transducers, Computations

Phase transition studies

Electronic structure studies

Non-destructive testing

[TR-2]

WHY STUDY ELASTIC CONSTANTS ?

- $dF = -S\,dT + \sigma_{ik}\,du_{ik}$

FREE ENERGY — STRESS (LIKE PRESSURE) — STRAIN (LIKE VOLUME)

+ HOOKE'S LAW : STRESS "PROPORTIONAL" TO STRAIN
+ SYMMETRIES OF REAL OBJECTS
+ WEIRD COLLAPSE OF INDICES

FOR ORTHORHOMBIC SYMMETRY

$$\underbrace{\begin{pmatrix} T_1 \\ T_2 \\ T_3 \\ T_4 \\ T_5 \\ T_6 \end{pmatrix}}_{\text{STRESS}} = \begin{pmatrix} C_{11} & C_{12} & C_{13} & 0 & 0 & 0 \\ C_{12} & C_{22} & C_{23} & 0 & 0 & 0 \\ C_{13} & C_{23} & C_{33} & 0 & 0 & 0 \\ 0 & 0 & 0 & C_{44} & 0 & 0 \\ 0 & 0 & 0 & 0 & C_{55} & 0 \\ 0 & 0 & 0 & 0 & 0 & C_{66} \end{pmatrix} \underbrace{\begin{pmatrix} e_1 \\ e_2 \\ e_3 \\ e_4 \\ e_5 \\ e_6 \end{pmatrix}}_{\text{STRAIN}} \begin{matrix} \left.\begin{matrix} \\ \\ \\ \end{matrix}\right\} \text{COMPRESSION} \\ \left.\begin{matrix} \\ \\ \\ \end{matrix}\right\} \text{SHEAR} \end{matrix}$$

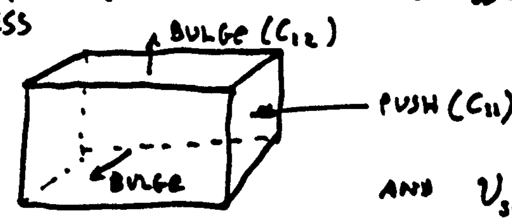

AND $v_{sound} = \sqrt{\frac{C_{11}}{\rho}}$ etc.

[TR-3]

HOW TO USE THIS MESS

ONLY e_1, e_2, e_3 CHANGE VOLUME, THUS IF WE APPLY A HYDROSTATIC PRESSURE P WE CAN FIND THE VOLUME CHANGE AS FOLLOWS

$$\begin{pmatrix} -p \\ -p \\ -p \\ 0 \\ 0 \\ 0 \end{pmatrix} = \begin{pmatrix} c_{11} & c_{12} & c_{13} & & & \\ c_{12} & c_{22} & c_{23} & & 0 & \\ c_{13} & c_{23} & c_{33} & & & \\ & & & c_{44} & & \\ & 0 & & & c_{55} & \\ & & & & & c_{66} \end{pmatrix} \begin{pmatrix} e_1 \\ e_2 \\ e_3 \\ 0 \\ 0 \\ 0 \end{pmatrix} \left.\begin{matrix} \\ \\ \\ \end{matrix}\right\} \text{IGNORE}$$

WHERE $\frac{\Delta V}{V} = e_1 + e_2 + e_3$

FOR AN ISOTROPIC BODY

$c_{12} = c_{13} = c_{23} = \lambda$

$c_{44} = c_{55} = c_{66} = \mu$

$c_{11} = c_{22} = c_{33} = \lambda + 2\mu$

$B = V \frac{\Delta P}{\Delta V} = \lambda + \frac{2}{3}\mu$ I.E. SHEAR IS INCLUDED

SOUND VELOCITIES

ISOTROPIC

$v_l = \sqrt{\frac{\lambda + 2\mu}{\rho}}$ ← SHEAR AGAIN!

$v_t = \sqrt{\frac{\mu}{\rho}}$

ORTHORHOMBIC

$v_{l1} = \sqrt{\frac{c_{11}}{\rho}}$ $v_{l2} = \sqrt{\frac{c_{22}}{\rho}}$ ...

$v_{t1} = \sqrt{\frac{c_{44}}{\rho}}$ ETC.

[TR-4]

Connections to thermodynamics:

Volume, entropy, pressure and the Gibbs free energy G
$dG = -SdT + PdV$ for hydrostatic pressure.

For stress σ_{ik} and strain u_{ik},
$dG = -SdT - u_{ik}d\sigma_{ik}$

Therefore:

$$\left(\frac{\partial G}{\partial T}\right)_P = -S \text{ and } \left(\frac{\partial G}{\partial \sigma_{ij}}\right)_T = -u_{ij} \quad (\partial l/l \text{ if } i=j)$$

One more set of derivatives yields:

$$C_v = T\left(\frac{\partial S}{\partial T}\right)_V \quad \text{(specific heat) and}$$

$$\alpha_{ii} = \left(\frac{\partial u_{ii}}{\partial T}\right)_P \quad \text{(thermal expansion) and}$$

$$\left[c_{ijkl}\right]^{-1} = \left(\frac{\partial u_{ij}}{\partial \sigma_{kl}}\right)_T \quad \text{(elastic constants) ---we measure this!}$$

[TR-5]

A LITTLE THERMO – SLIGHTLY WRONG

$$\Delta G(H_c, T) = G_n - G_s = \frac{V_s H_c^2}{8\pi} \qquad H_c = H_c(T_c)$$

IF TRANSITION IS SECOND ORDER, $H_c(T_c) = 0$!

ENTROPY, SPECIFIC HEAT

$$\Delta S = -\frac{\partial}{\partial T}\Delta G\Big|_{P,H} = -\frac{V_s H_c}{4\pi}\frac{\partial H_c}{\partial T}\Big|_{P,H}$$

$$T\frac{\partial}{\partial T}\Delta S\Big|_{P,H} = \Delta C_p$$

SPECIFIC HEAT

$$\Delta C_p = -\frac{V_s T}{4\pi}\left[H_c\frac{\partial^2 H_c}{\partial T^2} + \left(\frac{\partial H_c}{\partial T}\right)^2\right]$$

SPECIFIC HEAT DISCONTINUITY

VOLUME, BULK MODULUS

$$\Delta V = \frac{\partial}{\partial P}\Delta G\Big|_{T,H} = \frac{V_s H_c}{4\pi}\frac{\partial H_c}{\partial P}\Big|_{T,H}$$

$$-V\frac{\partial P}{\partial V}\Big|_{T,H} = \Delta K$$

BULK MODULUS

$$\Delta K = \frac{K_n^2 V_s}{4\pi}\left[H_c\frac{\partial^2 H_c}{\partial P^2} + \left(\frac{\partial H_c}{\partial P}\right)^2\right]$$

BULK MODULUS DISCONTINUITY

ALSO: α = EXP. COEF. $= \frac{1}{V}\frac{\partial V}{\partial T}\Big)_{P,H} \Rightarrow \Delta\alpha = \frac{1}{4\pi}\left(H_c\frac{\partial^2 H_c}{\partial T\partial P} + \frac{\partial H_c}{\partial T}\frac{\partial H_c}{\partial P}\right)$.

$$\left.\begin{array}{l} P \longrightarrow \text{STRESS} \\ V \longrightarrow \text{STRAIN} \end{array}\right\}$$

ELASTIC CONSTANTS PROBE FULL ANISOTROPIC QUALITIES OF THE FREE ENERGY AT A PHASE TRANSITION

[TR-6]

CHAPTER 1

SIMPLE RESONANCES

1.1 Introduction

The descriptor "resonant ultrasound spectroscopy" (RUS), first used in 1987[1.1], is a reflection of the richness of information revealed by the natural modes of vibration, or resonances, of solids. RUS, much like other high-precision modulus measurement methods, is sensitive to both microscopic and macroscopic properties of an object. Using it, elastic moduli, ultrasonic attenuation, and geometry can all be probed. To extract this information requires an elegant collection of theoretical, computational, and experimental tools. In attempting to decide whether these are the right tools, it will be important to compare RUS to other acoustic techniques. For the comparison to be useful, it is important to explore the general qualities of resonances. We begin this chapter with a discussion of simple resonances and end it with an exploration of the complications that arise when a resonator is subject to forces that use up the energy stored in oscilliatory motion. As expected, the resonator runs down, but what is a little surprising are the intrinsic uncertainties inherent in even the most simple, classical oscillating system.

1.2 Simple resonances

This is a book about the mechanical resonances of solids. More precisely, it is about mechanical resonances of free bodies or bodies not constrained, clamped, or otherwise affected by the outside world. In the overall scheme of things, free resonators are really the only ones that exist. A simple argument

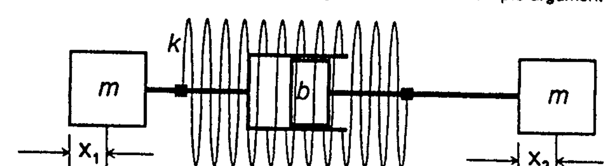

Figure 1.1 A simple mass/spring resonator with free boundary conditions (i.e. it is floating freely in space) and a simple dashpot damping mechanism providing a damping force proportional to velocity.

which has as a solution dy/dt =constant. If we subtract 1.5b from 1.5a, we obtain the more interesting result,

$$-m\frac{d^2x}{dt^2}-2b\frac{dx}{dt}-2kx=0. \qquad 1.7$$

This equation is solved by assuming simple harmonic motion at angular frequency $\omega=2\pi f$ where f is the frequency of oscillation. Then

$$x(t)=x_0e^{-i\omega t},\ \text{and}\frac{d}{dt}\rightarrow -i\omega \qquad 1.8$$

and we are instructed to take the real part of quantities linear in displacement, force etc. to obtain measurable quantities.
Using 1.8, 1.7 becomes

$$\left(\omega^2m+2i\omega b-2k\right)x_0e^{-i\omega t}=0 \qquad 1.9$$

which must be true for any x_0 and t. Thus the quantity in parentheses must always be zero, true only if

$$\omega=\pm\sqrt{\frac{2k}{m}-\left(\frac{b}{m}\right)^2}-\frac{ib}{m}. \qquad 1.10a$$

Defining

$$\omega_0=\sqrt{\frac{2k}{m}} \quad \text{and} \quad \tau=\frac{m}{b} \qquad 1.10b$$

we write $x(t)$ explicitly, choosing (arbitrarily maybe) the lower sign in 1.10a to find that

$$x(t)=x_0e^{i\omega_0t\left(1-1/(\omega_0\tau)^2\right)^{1/2}}e^{-t/\tau}. \qquad 1.11$$

Note that the dissipative effects that cause decay of the initial amplitude of

motion x_0 with time constant τ also shift the frequency to second order in the dimensionless quantity $\omega_0\tau$.

1.3 The driven resonator

The simple example presented in 1.2 is illustrative of what would happen if a mechanical resonator is, for example, hit (gently!) with a hammer. That is, it rings for a while (of order time τ), completing of order

$$Q=\omega_0\tau/2 \qquad 1.12$$

oscillations during that time. Because the decay is exponential, although we say Q cycles are completed, this is not a precise statement. It is correct to a factor of order a few in the sense that after several time constants, the amplitude drops below the noise floor of our measuring system. But we could also drive the resonator with a force F varying harmonically at angular frequency ω and acting only between the two masses (i.e. the center-of mass force is zero) so that 1.7 becomes

$$-m\frac{d^2x}{dt^2}-2b\frac{dx}{dt}-2kx=Fe^{-i\omega t} \qquad 1.13$$

which has as a solution a transient piece from 1.1 at a frequency near ω_0 with amplitude dependent on just how the force is initially applied and that dies away with characteristic time τ plus a steady-state part $x_0(\omega)$ using 1.10b and 1.12 that is

$$x_0(\omega)=\frac{F/m}{\omega^2-\omega_0^2+i\omega\omega_0/Q}. \qquad 1.14$$

The transient piece must not be overlooked in any attempt to measure resonances because before it has decayed away, it beats with the steady-state solution, potentially causing somewhat strange results. This will be discussed in more detail later.

Before we look at some of the properties of 1.14, we shall rewrite it in two other forms below. Noting that the power P dissipated by the resonator is the time average of the force times the velocity (and is **not** linear in force, displacement or the like so that we cannot simple multiply the right side of 1.14

by $x(\omega,t)$), it is easy to show that

$$P = \mathrm{Re}\left[\omega / 2\pi \int_0^{2\pi/\omega} F^{\dagger} e^{i\omega t} \frac{dx}{dt} dt\right] = -1/2\,\mathrm{Re}\left(i\omega F^{\dagger} x_0\right) \tag{1.15}$$

where a † denotes the complex conjugate. We will eventually be forced to deal with the real and imaginary parts of 1.14. We might as well get it over with now to obtain

$$x_0 = \frac{F}{M} \frac{\omega^2 - \omega_0^2 - i\omega\omega_0 / Q}{\left[\left(\omega^2 - \omega_0^2\right)^2 + \left(\omega\omega_0 / Q\right)^2\right]}. \tag{1.16}$$

If we define θ as follows

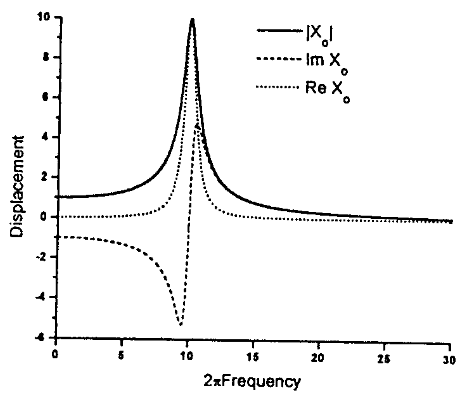

Figure 1.2 The magnitude, real, and imaginary components of the displacement of the simple driven resonator with a Q of 10 and a resonant frequency of 10/2π.

$$\tan\theta = -\frac{\omega\omega_0}{Q\left(\omega^2 - \omega_0^2\right)} \tag{1.17}$$

and note that

$$\left|x_0\right| = \frac{F / M}{\left[\left(\omega^2 - \omega_0^2\right)^2 + \left(\omega\omega_0 / Q\right)^2\right]^{1/2}} \tag{1.18}$$

then θ is the phase between force and displacement and

$$x(\omega,t) = \left|x_0(\omega)\right|\left[\cos\theta(\omega) + i\sin\theta(\omega)\right]e^{-i\omega t}. \tag{1.19}$$

1.4 Dissipation, frequency and Q

We will now look in detail at the three not-quite-equivalent representations 1.9, 1.16, and 1.18. The displacement $|x_0|$ is a maximum when the denominator of 1.18 is a minimum which occurs at

$$\omega = \omega_0\left(1 - \frac{1}{2Q^2}\right)^{1/2}, \tag{1.20}$$

not quite the frequency of oscillation

$$\omega = \omega_0\left(1 - \frac{1}{4Q^2}\right)^{1/2} \tag{1.21}$$

given by 1.9. The motion is exactly out of phase with the force in 1.16 at θ=π/2 where

$$\omega = \omega_0 \tag{1.22}$$

at which point the resonator is purely dissipative, i.e. the load produced by the resonator has no inertial or spring-like component; the resonator exhibits a purely frictional response where the velocity of the masses is in phase with the

Features of RUS

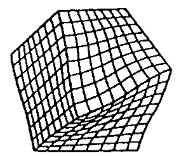

✪Provides the highest absolute accuracy of any routine elastic modulus measurement technique.

✪Determines the full ANISOTROPIC elastic tensor in a single measurement.

✪Can handle the smallest samples of any technique-this minimizes sample prep problems as well as errors introduced by radioactive heating.

✪LANL is the lead laboratory in the world in the development and use of RUS.

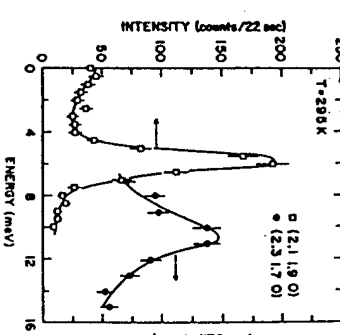

FIG. 4. Spectra of transverse TA_2 phonons measured along [110]. The polarization vector is along [1$\bar{1}$0], i.e., the scattering plane is (hh0) (sample MIT-1).

soft but sharpens significantly. We confirmed by means of additional measurements in other Brillouin zones that this mode has Σ_4 symmetry (in Weber's notation).

Although we expect that the $n=2$ degeneracy is lifted below T_c, we did not observe the expected splitting of the modes, either because the energy resolution of the spectrometer was too coarse or one of the modes renormalizes only weakly and remains buried under the superlattice peak. Further neutron scattering studies are necessary to elucidate this point further.

After identifying the lattice dynamics, which leads to the tetragonal-orthorhombic phase transition, we performed a detailed study of the low-lying phonon branches in order to find evidence for the predicted breathing-mode instability[4] of the LA mode near the zone boundary. The LA phonons were measured in crystals MIT-1 and MIT-2 using very fine steps in momentum in order to find the instability (see Fig. 3 for some representative scans). The phonons remain sharp and the dispersion has a conventional form, i.e., the LA phonon energy increases monotonically with increasing q. This result is in contrast to an observation in isostructural La_2NiO_4 where the phonon energy decreases near the zone boundary. Moreover,

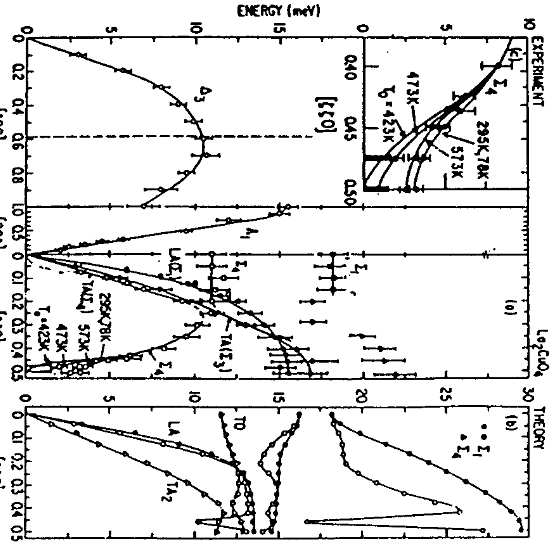

FIG. 5. (a) Summary of the low-lying phonon branches in $La_{2-x}Sr_xCuO_4$ (samples MIT-1 and MIT-2). The lines are guides to the eye. The modes have been labeled according to Ref. 4. The dispersion curves are only weakly temperature dependent, with the exception of the TO phonon near the X point [see inset (c)]. (b) Calculated dispersion curves. Filled symbols show the nonrenormalized energies (bar phonons) and the open circles indicate the phonons with Σ_1 symmetry, which are renormalized by interactions with the conduction electrons. The phonons with Σ_4 symmetry do not renormalize [after Weber (Ref. 4)].

[TR-13]

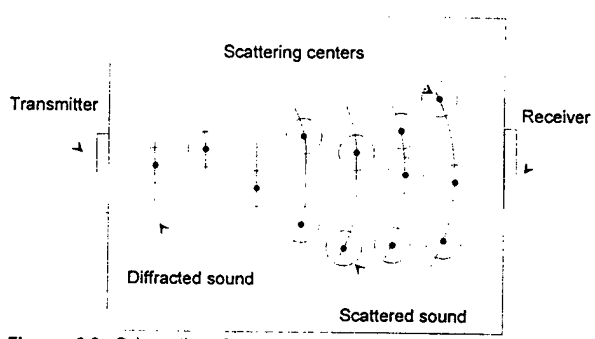

Figure 6.6 Schematic of a pulse-echo measurement with elastic (nondissipative) scattering sources present.

of a laser beam). If the sample has small sound-scattering defects in it such as grain boundaries in a polycrystalline metal, then they too reduce the intensity of the received pulse in ways not reflecting true dissipation. Thus, much care is required for a pulse-echo measurement to return a true measure of attenuation.

This is not the case with a resonance measurement. A resonance measurement uses the Q of a measured mode to determine the losses. Nonparallel sample faces simply shift the resonance frequency. Scattering centers also simply shift the resonance frequency. To see why this very important point must be so, remember that we assume the scatterers to be linear. Let's also assume both the sample and the scatterers to have zero attenuation (elastic or nondissipative). If we had the computational skills, we could simply generate a model in which the sample is now a slightly different one in which we know the position, size, and shape of every scattering center. Because no attenuation mechanism is included in the model, there can be no dissipation of the vibrational energy. But the scatterers still scatter, and the resonances that come from a solution of this rather difficult model shift somewhat from those of the defect-free solid. The result is like a more complex, three-dimensional version of the resonance calculation for the composite resonator of Chapter 2.

A resonance measurement is not, however, perfect, either. A key difference between a pulse-echo setup and a resonance setup is that for pulse-echo the transducers can be made to contact only the sample. The electrical leads can be made negligibly small so as not to conduct any vibrational energy out of the sample-transducer system, and if the sample is

[TR-14]

Signal/noise comaparison of pulsed and resonant measurements

parameter	Impulse	Swept Sine
drive power per unit bandwidth	peak power/full bandwidth $10^6/10^9$=.001	peak power/sweep rate 1/100=0.01
noise bandwidth for complete measurement using optimum receiver	10^9	number of modes x width of each mode x $10=10^4$Hz
drive duty cycle (typical)	10^{-3}	1
detect duty cycle	1	1
square root of all factors, which is a measure of S/N	$3x10^{-7}$	10^{-3}

Table I. Signal-to-noise comparison between impulse (pulse-echo) and swept-sine (RUS) resonance measurement methods for a measurement of a 1 cm sample with resonances having a $Q=10^4$, using 10 modes over 0.5 MHz-1.5MHz=10^6 Hz bandwidth to obtain an elastic modulus. Note that the pulse-echo measurement provides about 0.1% absolute accuracy at best, compared with about 0.01% for the best RUS measurements.

[TR-15]

Elastic constants of copper. B represents bulk modulus.

	Single crystal		Polycrystal (wire-drawn)	
c_{ij} (GPa)	Literature average	Measured[a]	RP	Cylinder
c_{11}	168.75	170.88	193.61	194.25
c_{33}			205.88	203.98
c_{12}	122.14	124.63	105.65	106.84
c_{13}			95.00	95.93
c_{44}	75.48	74.01	39.35	39.46
c_{66}			43.98	43.71
B	137.68	140.05	131.65	132.84

[a]Crystal rotated 45.4° about [100].

[TR-16]

Elastic constants of tantalum at room temperature.

T (K)	ρ (g/cm^3)	c_{11} (GPa)	c_{12} (GPa)	c_{44} (GPa)
300[1]	16.678	266.7	160.8	82.5
300[1]	16.678	266.8	161.4	82.5
300[2]	16.633	260.9	157.4	81.8
298[3]	16.626	260.2	154.5	82.6
295[4]	16.641	266.3	160.5	82.8

[1]D.I. Bolef, J. Appl. Phys. **33**, 2311 (1962).

[2]F.H. Featherstone and J.R. Neighbours, Phys. Rev. **130**, 1324 (1963).

[3]N. Soga, J. Appl. Phys. **37**, 3416 (1966).

[4]Euler angles (defined in Roe's convention) were determined to be $\alpha = 138.3°$, $\beta = 29.7°$, and $\gamma = 155.1°$ by RUS and $\alpha = 135°$, $\beta = 33°$, and $\gamma = 158°$ by X-ray.

[TR-17]

RUS sees, simultaneously, the collapse of one shear modulus and no effect on the other in a 2mm single crystal of $La_{2-x}Sr_xCuO_4$ at the structural phase transition near 223K.

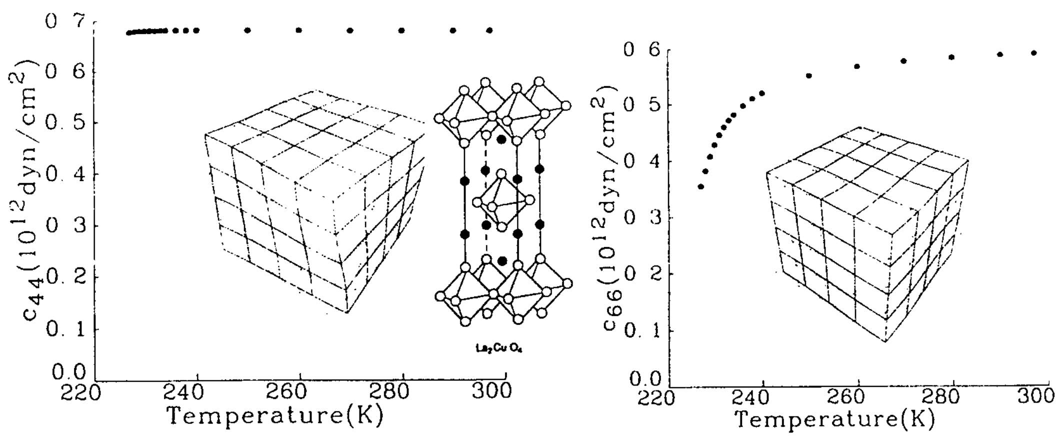

[TR-18]

Rus is a mature, fully commercialized technique, now in its second hardware generation-which includes full phase sensitivity to enhance sharpness

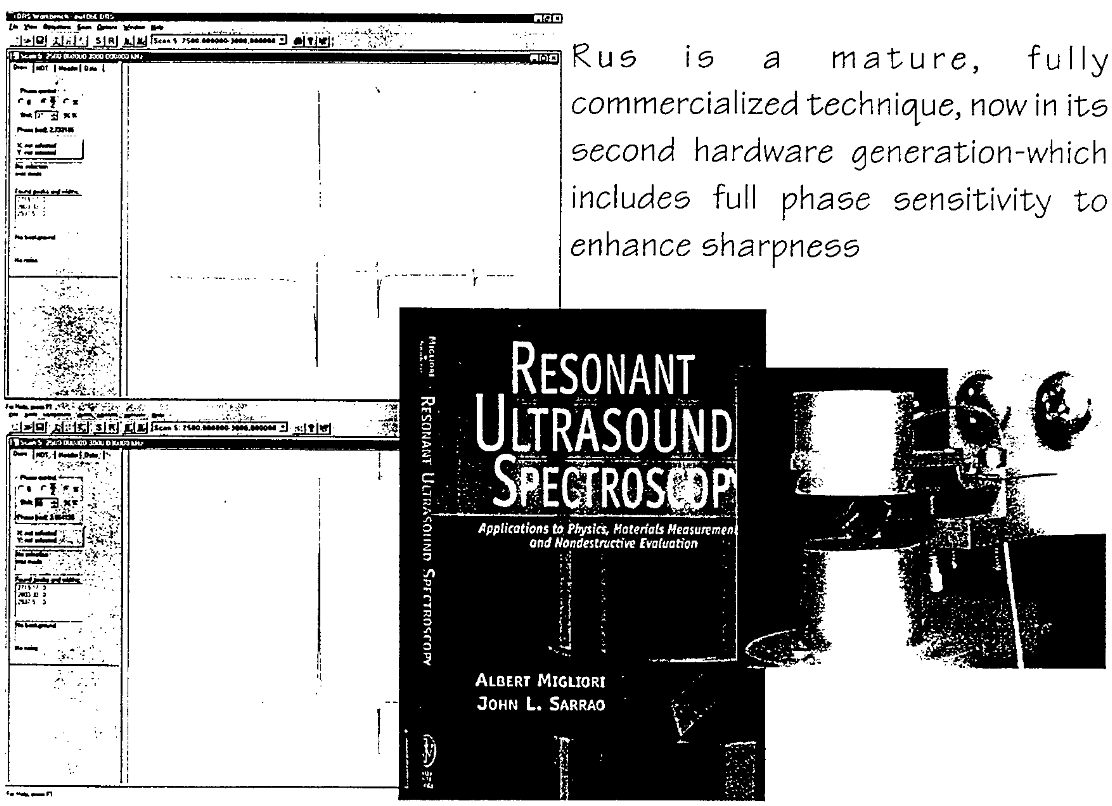

[TR-19]

Reprinted from
26 June 1970, volume 168, pages 1579-1580

SCIENCE

Properties and Composition of Lunar Materials: Earth Analogies

Abstract. *The sound velocity data for the lunar rocks were compared to numerous terrestrial rock types and were found to deviate widely from them. A group of terrestrial materials were found which have velocities comparable to those of the lunar rocks, but they do obey velocity-density relations proposed for earth rocks.*

Certain data from Apollo 11 and Apollo 12 missions present some difficulties in that they require explanations for the signals received by the lunar seismograph as a result of the impact of the lunar module (LEM) on the lunar surface (*1*). In particular, the observed signal does not resemble one due to an impulsive source, but exhibits a generally slow build-up of energy with time. In spite of the appearance of the returned lunar samples, the lunar seismic signal continued to ring for a remarkably long time—a characteristic of very high Q material. The lunar rocks, when studied in the laboratory, exhibited a low Q (*2*). Perhaps most startling of all, however, was the very low sound velocity indicated for the outer lunar layer deduced from the LEM impact signal. The data obtained on the lunar rocks and fines agree well with the results of the Apollo 12 seismic experiment (*2, 3*). These rock velocities are startlingly low. The measured velocities on a vesicular medium grained, igneous rock (10017) having a bulk density of 3.2 g/cm³ were v_p = 1.84, and v_s = 1.05 km/sec. The results for a microbreccia (10046) with a bulk density of 2.2 g/cm³ were v_p = 1.25 and v_s = 0.74 km/sec for the compressional (v_p) and shear (v_s) velocities.

It was of some interest to consider the behavior of these lunar rocks in terms of the expected behavior based on measurements of earth materials. Birch (*4*) first proposed a simple linear relation between compressional velocity and density for rocks. This relation was examined further by Anderson (*5*) who showed that this was a first approximation to a more general relation, derivable from a dependence of the elastic moduli with the density through a power function. Comparison of the results obtained from the returned lunar rocks with the predictions of these relationships expresses graphically the manner they deviate from the behavior of rocks found on earth. The velocities are remarkably lower than what would be predicted from either the Birch or Anderson relationships.

To account for this very low velocity, we decided to consider materials other than those listed initially by Birch (*4*) or more detailed compilation of Anderson and Liebermann (*6*). The search was aided by considerations of much earlier speculations concerning the na-

Table 1. Comparison of compressional velocities of lunar rocks and various earth materials.

Lunar rocks and cheeses	v_p (km/sec)	Sedimentary rocks	v_p (km/sec)	Metamorphic rocks	v_p (km/sec)	Igneous rocks	v_p (km/sec)	Minerals	v_p (km/sec)
Sapsego (Swiss)	2.12	Dolomite	5.6	Schist	5.1	Granite	5.9	Corundum	10.8
Lunar Rock 10017	1.84	Dolomite	4.69	Slate	5.39	Syenite	5.7	Periclase	9.69
Gjetost (Norway)	1.83	Limestone	5.06	Charnockite	6.15	Diorite	5.78	Spinel	9.91
Provolone (Italy)	1.75	Limestone	5.97	Gneiss	4.9	Oligoclase	6.40	Garnet	8.53
Romano (Italy)	1.75	Greywacke	5.4	Marble	6.02	Andesite	5.23	Quartz	6.05
Cheddar (Vermont)	1.72	Greywacke	6.06	Quartzite	5.6	Gabbro	5.8	Hematite	7.90
Emmenthal (Swiss)	1.65	Sandstone	4.90	Amphibolite	6.70	Gabbro	6.8	Olivine	8.42
Muenster (Wisconsin)	1.57			Eclogite	6.89	Norite	6.50	Trevorite	7.23
Lunar Rock 10046	1.25					Diabase	6.33	Lime	7.95

[TR-20]

Seasons Greetings

It brightens the spirits
In times like these,
To know the Moon
Is made of cheese.

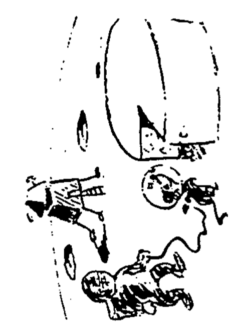

Lunar rocks and cheeses	Sound Velocity, V_p (Kilometers/second)
Lunar Rock 10017	1.84
Gjetost (Norway)	1.83
Provolone (Italy)	1.75
Romano (Italy)	1.75
Cheddar (Vermont)	1.72
Emmenthal (Swiss)	1.65
Muenster (Wisconsin)	1.57
Lunar Rock 10046	1.25

(Science, 168, 1579, 1970)

MINERAL PHYSICS LABORATORY
LAMONT-DOHERTY GEOLOGICAL OBSERVATORY
OF COLUMBIA UNIVERSITY

[TR-21]

John William Strutt, the Baron Rayleigh tried to do this computation. Without a 90MHz Pentium, he found that

In the case of a short rod and of a particle situated near the cylindrical boundary, this lateral motion would be comparable in magnitude with the longitudinal motion, and could not be overlooked without risk of considerable error.

226. The problem of a rectangular plate, whose edges are free, is one of great difficulty, and has for the most part resisted attack[1].

Even with a Pentium, if you try this using finite element methods, the computation time goes like the cube of the numerical accuracy and you can't compute as well as you can measure in a reasonable time on a reasonable computer. However, if you are careful, and smart, as were Orson Anderson and his postdoc Harold Demarest at Bell labs 30 years ago, then.....

[TR-22]

The resonances of a solid, when properly analyzed provide full anisotropic elastic information at very high accuracy

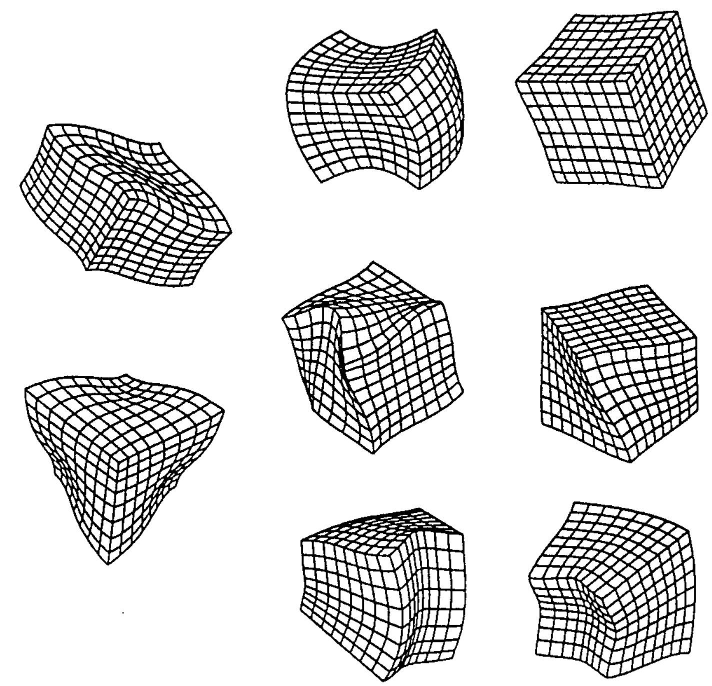

Computation of resonances

from Migliori et.al. Physica B **183**,1,1993

The procedure for solving the direct problem for an arbitrarily shaped elastic solid with volume V, elastic tensor c_{ijkl}, density ρ, and with a free surface S begins with the Lagrangian

$$L = \int_V (\mathrm{KE} - \mathrm{PE})\, \mathrm{d}V \tag{4}$$

where the kinetic energy, KE, is given by

$$\mathrm{KE} = \tfrac{1}{2}\rho\omega^2 u_i^2 , \tag{5}$$

and the potential energy, PE, by

$$\mathrm{PE} = \tfrac{1}{2} c_{ijkl} u_{i,j} u_{k,l} . \tag{6}$$

Following Hamilton, we allow u_i to vary arbitrarily in the volume V and on the surface S ($u_i \rightarrow u_i + \delta u_i$) and calculate the variation δL in L. The result is

$$\delta L = \int_V (\text{left side of eq. (8)})_i \delta u_i \, \mathrm{d}V + \int_S (\text{left side of eq. (9)})_i \delta u_i \, \mathrm{d}S \tag{7}$$

The immediate results are two equations, the elastic wave equation and the vanishing of surface traction

$$\rho\omega^2 u_i + c_{ijkl} u_{k,lj} = 0 , \tag{8}$$

$$n_j c_{ijkl} u_{k,l} = 0 \tag{9}$$

where $\{n_i\}$ is the unit outer normal to S.

Because of the arbitrariness of δu_i in V and on S, the u_i's which correspond to stationary points of L (i.e. $\delta L = 0$) must satisfy eq. (8) in V and eq. (9) on S. There are no such u_i's, of course, unless ω^2 is one of a discrete set of eigenvalues, the normal mode frequencies of free vibration of the system.

Following the Rayleigh–Ritz prescription, we expand the displacement vector in a complete set of functions $\{\Phi_\lambda\}$,

$$u_i = a_{\lambda i}\Phi_\lambda \,, \tag{10}$$

and choose as our basis functions powers of cartesian coordinates:

$$\Phi_\lambda = x^l y^m z^n \,, \tag{11}$$

where $\lambda = (l, m, n)$ is the function label, a set of three nonnegative integers. After substituting eq. (10) into eq. (4), we obtain ($\boldsymbol{a}$ becomes a column vector)

$$L = \tfrac{1}{2}\omega^2 \boldsymbol{a}^{\mathrm{T}}\boldsymbol{E}\boldsymbol{a} - \tfrac{1}{2}\boldsymbol{a}^{\mathrm{T}}\boldsymbol{\Gamma}\boldsymbol{a} \tag{12}$$

The "Calvin and Hobbes" model of the vibrations of a rectangular parallelepiped

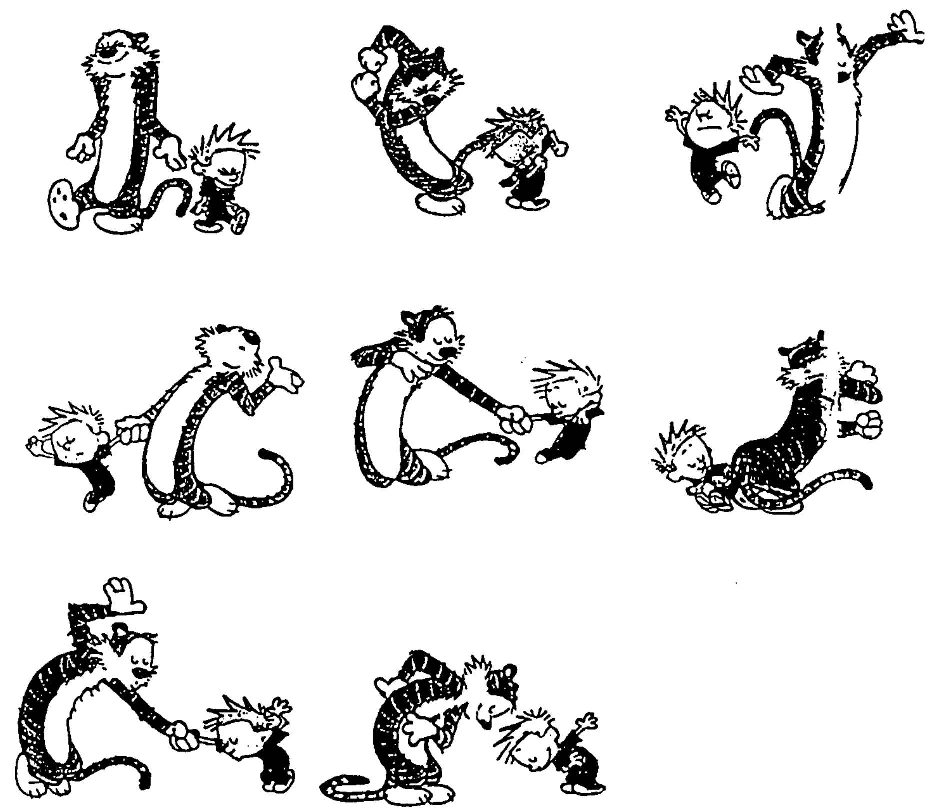

[TR-27]

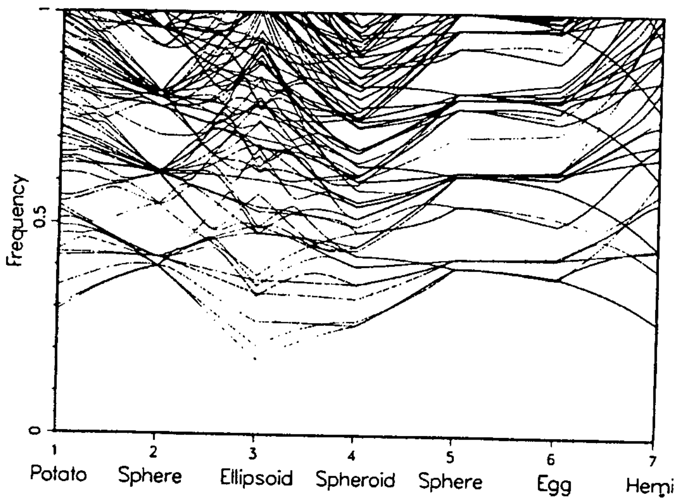

FIG. 8. Frequency spectra of a number of objects in the potato family. The seven stations correspond to shapes as labeled, with semiaxes as given in Table II. The sphere frequencies agree well with those in the literature for these material parameters (Poisson's ratio = 1/4).[20] The dimensional parameters $d_{1+},d_{1-},...,d_{3-}$ are interpolated linearly between the seven stations here. Several interesting features invite comment. First, the potato has no degenerate lines, because of its low symmetry, and the sphere, conversely, has few lines that are nondegenerate. The ellipsoid has no degeneracies, and the spheroid, the egg, and the hemisphere (all being rotationally symmetric) do, but never more than doubly degenerate lines. Small deviations from the sphere in the egg direction do not change any of the frequencies to first order, because d_{3+} increases as much as d_{3-} decreases, compensating one another as far as affecting resonant frequencies is concerned. As in several other figures, apparent avoided crossings on this plot should be viewed with suspicion because the plotting program does not interchange line identities when physically the modes do, in fact, cross. Spectra are computed for 241 abscissa values here and elsewhere, which sets the scale on which avoided crossings may be spurious.

[TR-28]

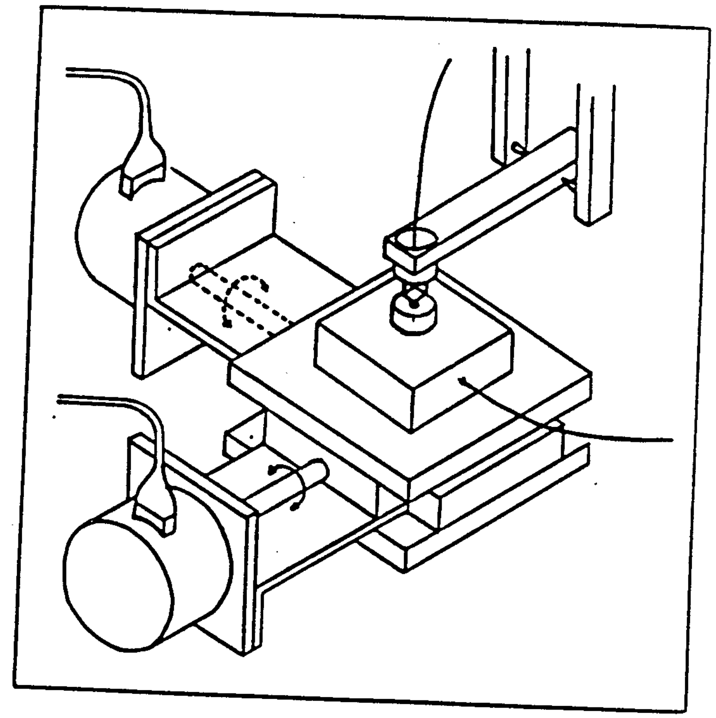

Fig.3 Outline sketch of the stepping-motor driven system used to rock the sample to enable detection of all the modes.

[TR-29]

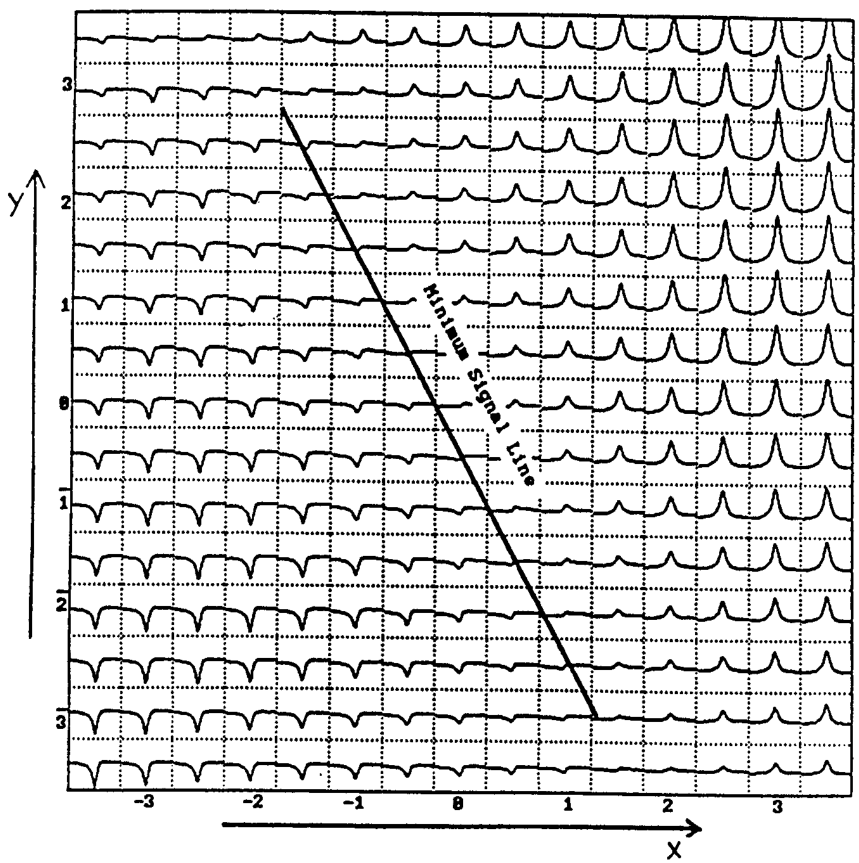

Fig.6 (a)

[TR-30]

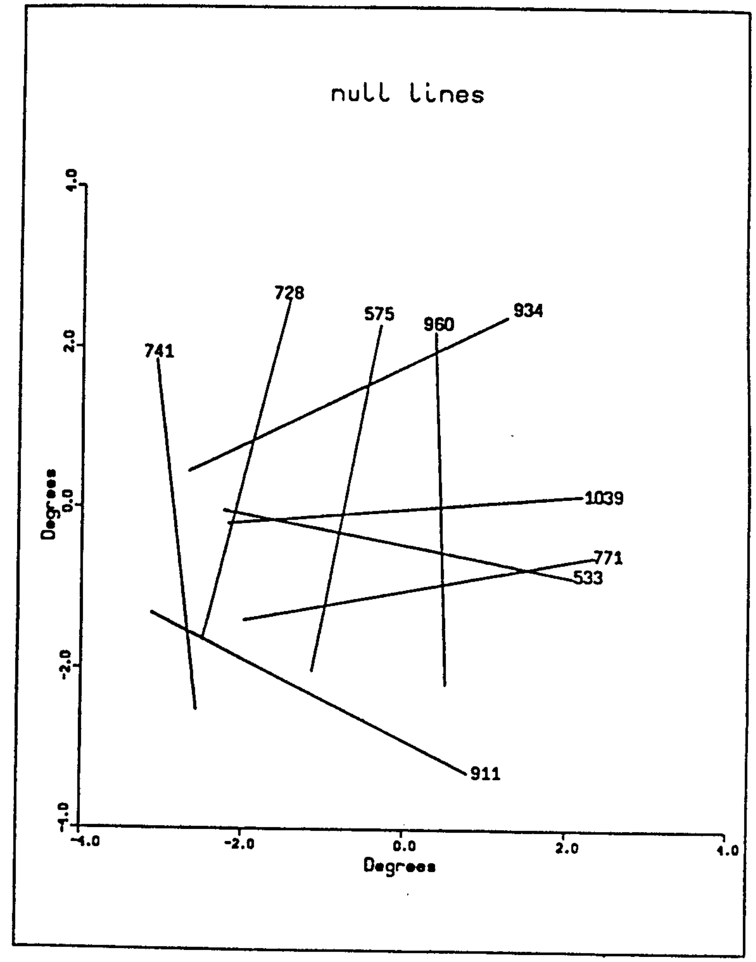

Fig. 5

How well does RUS do?

f in MHz

mode	f(measured)	f(fit)	%err	wt	k	i	df/dc_{ij}	
1	0.340010	0.339508	-0.15	0.00	4	1	0.00	1.00
2	0.447200	0.447009	-0.04	1.00	6	2	0.13	0.87
3	0.490240	0.490304	0.01	1.00	7	2	0.16	0.84
4	0.541860	0.541385	-0.09	1.00	3	2	0.02	0.98
5	0.557460	0.556670	-0.14	1.00	4	2	0.00	1.00
6	0.591740	0.592201	0.08	1.00	5	1	0.05	0.95
7	0.608670	0.608409	-0.04	1.00	6	3	0.30	0.70
8	0.615590	0.615232	-0.06	1.00	2	2	0.02	0.98
9	0.623100	0.622549	-0.09	1.00	8	2	0.07	0.93
10	0.642700	0.642863	0.03	1.00	1	2	0.12	0.88
11	0.675510	0.676327	0.12	1.00	5	2	0.10	0.90
12	0.683560	0.683290	-0.04	1.00	8	3	0.05	0.95
13	0.690650	0.690379	-0.04	1.00	2	3	0.16	0.84
14	0.746720	0.747308	0.08	1.00	5	3	0.10	0.90
15	0.753860	0.754061	0.03	1.00	8	4	0.05	0.95
16	0.827430	0.827516	0.01	1.00	7	3	0.06	0.94
17	0.848300	0.849020	0.08	1.00	1	3	0.03	0.97
18	0.855320	0.854900	-0.05	1.00	4	3	0.08	0.92
19	0.870540	0.870830	0.03	1.00	6	4	0.12	0.88
20	0.878390	0.878949	0.06	1.00	3	3	0.11	0.89
21	0.882080	0.881934	-0.02	1.00	5	4	0.33	0.67
22	0.884870	0.884495	-0.04	1.00	1	4	0.21	0.79
23	0.887380	0.887736	0.04	1.00	7	4	0.20	0.80
24	0.891190	0.891837	0.07	1.00	2	4	0.04	0.96

rms error= 0.0653 %

5120 Steel

Fine grained martensitic steel

free moduli are c11, c44

units: 10^{12}dyn/cm^2

mass=0.2875 gm

0.412 x 0.340 x 0.264 cm

ρ= 7.785 gm/cc

c11=2.7187 ± .19%

c44=0.8148 ±.02%

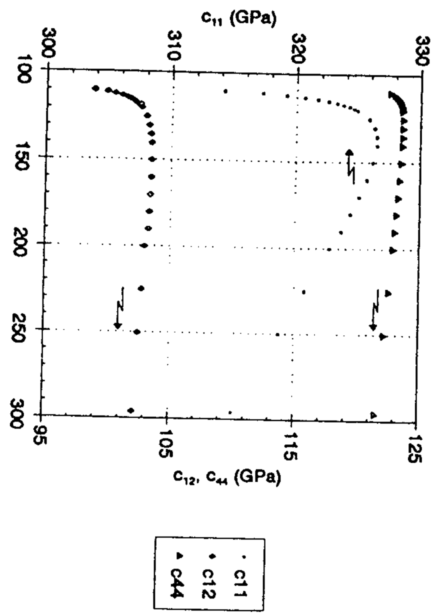

Fig. 10. The three elastic moduli of a single crystal of $SrTiO_3$ near the structural phase transition are shown as a function of temperature. These data were obtained using RUS.

[TR-33]

Ultimate accuracy determined by geometry-for a Si_3N_4 ball bearing, geometry errors are less that 1 part in 10^5. So are the modulus errors!

Table 1
Resonant ultrasound measurement of a 0.63500 cm diameter Si_3N_4 ceramic sphere with a density of 3.2325 g/cm^3. f_m are measured frequencies, f_r are fitted, n is the mode number, k is our designator (to be discussed below) for the symmetry of the mode and i is in essence the harmonic number of each symmetry type. Multiple entries indicate the mode degeneracy. The fit for $\mu = 1.2374 \times 10^{12}$ dyne/cm^2 and $\sigma = 0.2703$ has a χ^2 (%) = 0.0124. This is sufficient to determine μ to about 0.01% and σ to about 0.05%. There are no corrections so these values are absolute.

n	f_r (MHz)	f_m (MHz)	% error	(k, i)
1	0.775706	0.775707	−0.000138	(6, 1), (1, 1), (4, 1), (4, 2), (7, 1)
6	0.819567	0.819983	−0.050778	(5, 1), (3, 1), (5, 2), (8, 1), (2, 1)
11	1.075664	1.075399	0.024614	(1, 2), (7, 2), (6, 2)
14	1.198616	1.198505	0.009239	(5, 3), (2, 2), (3, 2), (8, 2), (3, 3), (8, 3), (2, 3)
21	1.217375	1.217850	−0.039042	(1, 3), (6, 3), (7, 3), (1, 4), (6, 4), (7, 4), (4, 3)
28	1.440760	1.440750	0.000712	(5, 4)
29	1.527060	1.526474	0.039695	(5, 5), (8, 4), (3, 4), (5, 6), (2, 4)
34	1.558358	1.558848	−0.031448	(5, 7), (5, 8), (5, 9), (3, 5), (8, 5), (2, 5), (3, 6), (8, 6), (2, 6)
43	1.580067	1.579871	0.012426	(6, 5), (7, 5), (7, 6), (1, 5), (4, 4), (1, 6), (6, 6), (4, 5), (4, 6)

[TR-34]

RUS Block Diagram

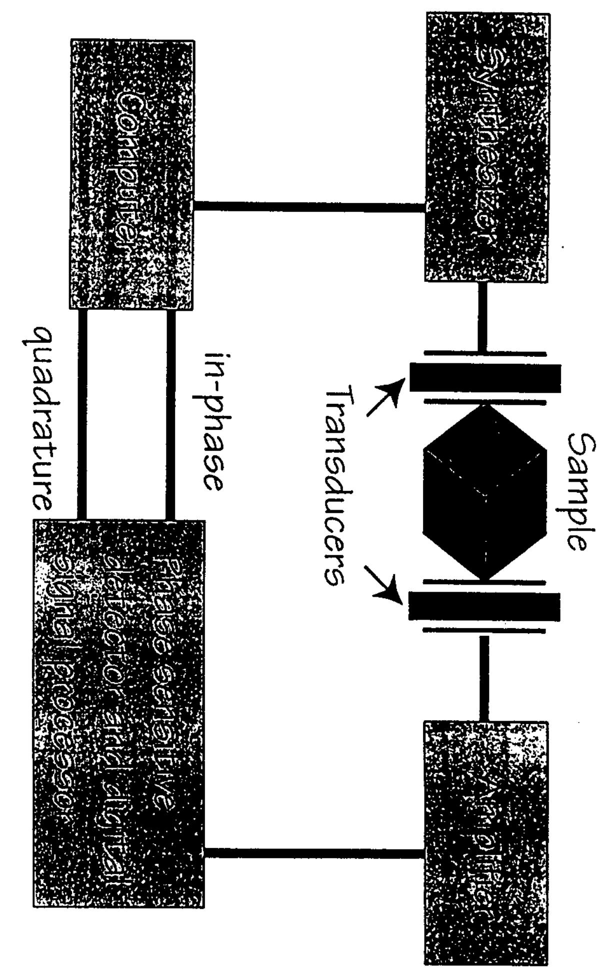

[TR-35]

Transducer construction

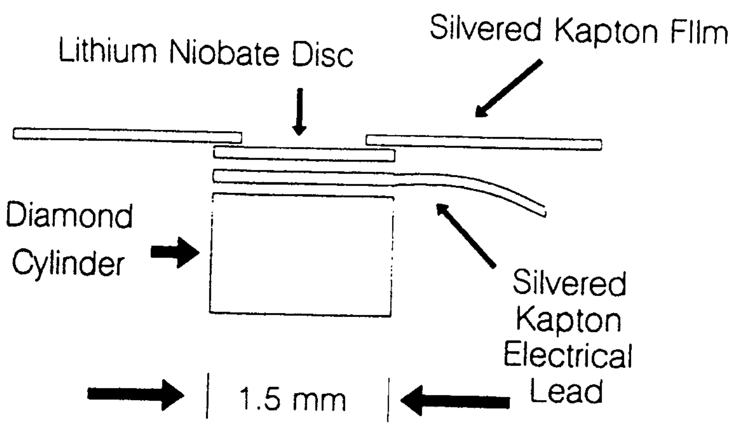

Fig. 3. Shown is a schematic of the diamond/polyimide/ $LiNbO_3$ composite transducer used for all the measurements.

[TR-36 Unavailable at Time of Printing]

[TR-37]

Silver diffusion bonded 0.375"Φ PZT-5A Transducer with Alumina wear plate and alumina backload

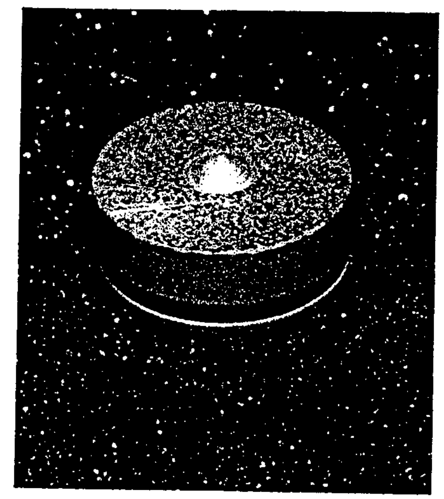

The bare transducer has a 2MHz fundamental compressional mode
This technology won a 1993 RD100 award

[TR-38]

RUS can be used at temperatures as high as 1800 C (O. Anderson et. al.). For more moderate temperatures (700 C), both frequency and attenuation data can be acquired using all-metal diffusion bonded $LiNbO_3$/diamond transducers

HighTemperature RUS System

Piezoelectric material : LiNbO3 : Tc~1197, Tm~1260

Transducers

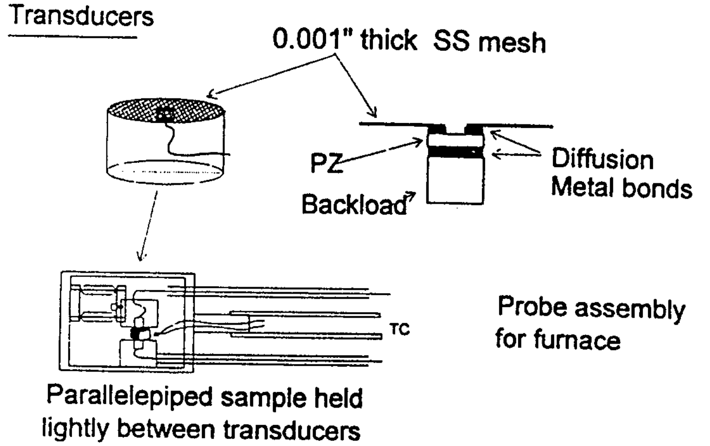

[TR-39]

Resonances of a 5120 steel RPR at 38C and 378C measure using metal diffusion bonded $LiNbO_3$/Alumina transducers

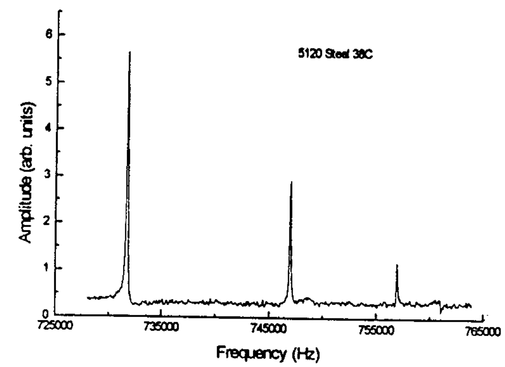

38C

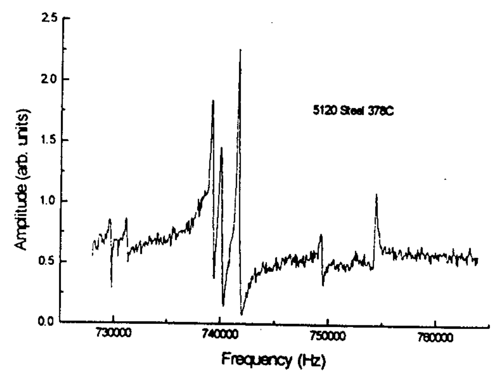

378C

[TR-40]

Cell.wpd

RUS Cell with Silver diffusion bonded transducers, using $LiNbO_3$ and an alumina cylinder backload. This cell can reach 500C

The transducers are mounted beneath the 0.500"Φ 304SS screens that the sample touches. Only the bottom one is visible.

[TR-41]

background, displayed on a digitally addressed computer screen, may be less than 1 pixel. If this is the case, one could not see the resonance by eye and so it might not be searched for with software because the experimenter does not know to tell the software where to look.

7.4 Sample preparation

The samples to be measured must be rectangular parallelepipeds (RPs) of order a millimeter or two on a side and with the faces aligned crystallographically with the microstructure of the sample if there is one, and with parallelism and perpendicularity errors not worse than 1 part in 10^3. Obviously, the surface finish of the sample must be consistent with the wavelengths and precision involved, greatly easing this restriction over the requirements of a pulse-echo sample where optical polishing is required. Unlike the pulse-echo system, the entire sample must be carefully finished, with sharp edges and corners. The tolerances here are difficult to quantify, but it is clear that if, as we shall see, the resonances are to be fit to a part in 10^3, then all the geometric errors combined must be of this order.

If the sample is not isotropic, then the first step is to determine the orientation using some sort of microprobe; x-rays are the most common. The sample is then cut to nearly the final shape using a wire saw, metallurgical

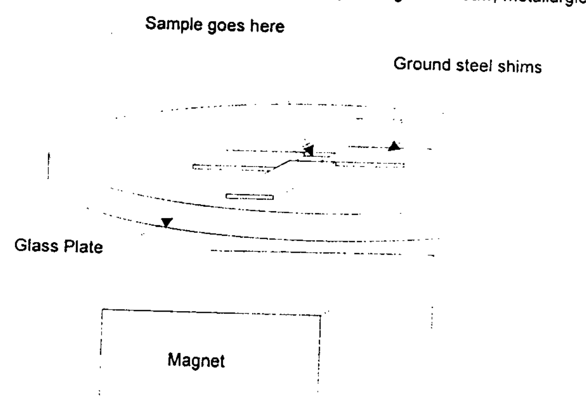

Figure 7.8 An arrangement for high-precision shaping of RP samples. The magnet holds the shims down while molten wax, or other hard cement that can be melted, cools.

[TR-42]

Temperature-dependant studies of elastic properties of Pu are expected to show a rich and complex behavior, and will enable a better understanding of aging, stabilization and fabrication at engineering temperatures

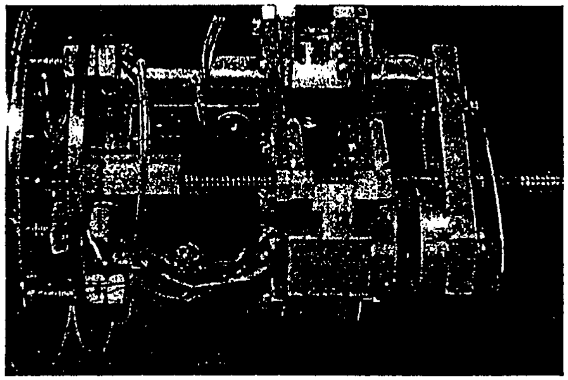

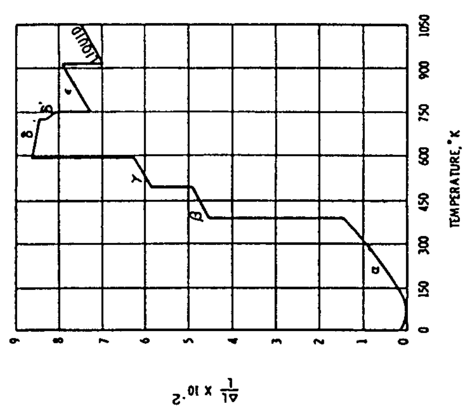

Fig. 3.1—The idealized expansion behavior of plutonium.

[TR-43]

epoxy. When carefully constructed, the capacitance between the groundplane on the 0.5-inch Kapton disk and the Kapton flying lead is about 10 pF. Because the size of these transducers is determined by the need to measure millimeter-sized samples, we are stuck with this small capacitance, and it is a problem. The reason it is a problem is that the capacitance of 2 m of RG 220u coaxial cable, typical of most coax, is about 180 pF. The result is a circuit shown in Figure 7.2. The effective impedance Z_{eff} of the combination of cable and transducer is

$$Z_{eff} = \left(j\omega\left[C_{cable} + C_{transducer}\right]\right)^{-1}, \tag{7.1}$$

where in this chapter, following the convention of electrical engineers j is $\sqrt{-1}$ and ω is $2\pi f$, where f is the frequency. For the capacitances given, and a frequency of 1 MHz, this is an impedance of $-j800\ \Omega$—it looks like a pure capacitive reactance of 800 ohms (Ω). This is not so bad, meaning that it is a reasonably low impedance for work at 1 MHz. What is a problem is that the voltage developed on the bare transducer is produced by strain occurring as the result of the vibrations of the sample. This strain produces a charge q on the bare transducer, and a voltage $V_{bare} = q/C_{transducer}$. But when the cable is connected in parallel to the transducer, the charge is shared between the two capacitances. The result is a reduction of the transducer voltage V_L such that

$$V_L = \frac{C_{transducer}}{C_{cable} + C_{transducer}} V_{bare}, \tag{7.2}$$

which is a factor of 19 for the example given. Although this would not affect signal/noise ratio if the electronics were perfectly matched to it, in practice it

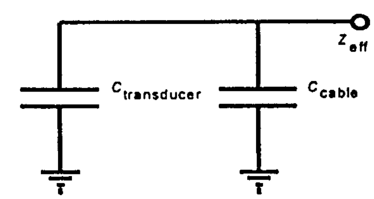

Figure 7.2 Equivalent circuit of the transducer and its cable.

[TR-44]

and doesn't belong here.

In practice, approaches that minimize the attenuation of signal voltage are adequate to prevent degradation of the desired signal by voltage noise. One approach is to "guard" the input; the other is to use what is called a "charge amplifier". The "guard" method involves triaxial cable. Triaxial cable, starting from the inside out, consists of a center wire-like conductor, a cylindrical insulator, a cylindrical conductor, another cylindrical insulator and finally a third cylindrical conductor. The outermost conductor is used as a shield or ground. The inner cylindrical conductor (the driven shield) is connected to the output of a unity-gain amplifier such as the voltage follower described above. The inner conducting wire is connected to the transducer. The effect of this is as follows, the description to be in a somewhat iterative form, remembering that the process is really continuous. The voltage developed at the bare transducer is at first reduced by the capacitance between the innermost conductor and the first (driven) cylindrical conductor because before the amplifier begins to work, the driven shield is connected to ground through the low output impedance of the voltage follower. Almost immediately, the follower applies this same reduced voltage to that shield, reducing the voltage difference between driven shield and transducer lead to nearly zero. With nearly zero voltage difference between driven shield and transducer, the transducer does not have to waste much of its precious charge

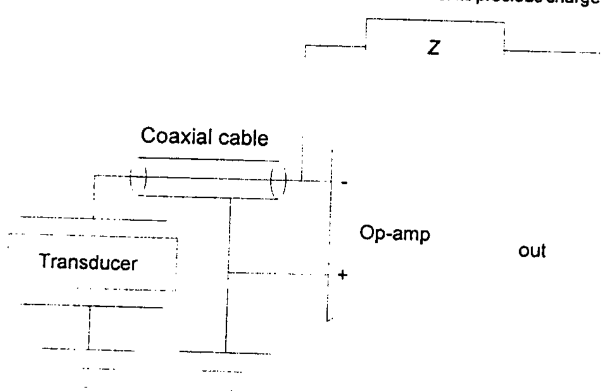

Figure 7.4 This is a simple Op-Amp preamplifier circuit with transducer as input and feedback element Z to be discussed in the text.

[TR-45]

$$V_{out} = -j\omega C_s\left(\frac{1}{1/R + j\omega C}\right)V_s, \tag{7.7}$$

which has two interesting limits. The first is at high frequencies, when $j\omega C$ is much less than R and the gain becomes simply C_s/C, independent of frequency. This is the most desirable of properties for our purposes as C can easily be made about equal to the transducer capacitance, enabling us to get the bare transducer voltage into the rest of an RUS receiver almost without penalty. This works up to about 7 MHz for the MAX410. The low-frequency limit is where the limitations come in. When $\omega=1/RC$, the circuit starts to behave as if only R were present. At this point, the op-amp noise current is pushed mostly through R [which itself generates a noise voltage per $\sqrt{\text{Hz}}$ of $(4Rk_bT)^{1/2}$], and the noise goes way up (10-MHz bandwidth, 1 pA/$\sqrt{\text{Hz}}$ into 10 MΩ yields 300 mV RMS noise!) while at the same time the gain starts to drop rapidly. For R=10 MΩ and C=10 pF, the frequency where this occurs is about 1.6 kHz, well below any frequency we are interested in. Of course, this is the circuit of choice for RUS preamplifiers.

The charge amplifier described above has an additional crucial quality, which was really what we were after all along. Its output impedance is of order 1 Ω or less. This means that the signal at its output, determined by Equation 7.7, can drive almost any load we care to use without changing the output voltage. A typical load would be another, simpler amplifier. Such a circuit is shown in Figure 7.5. As before, the feedback impedance Z_2 holds the inverting terminal at ground, subject to the imperfections in the op-amp,

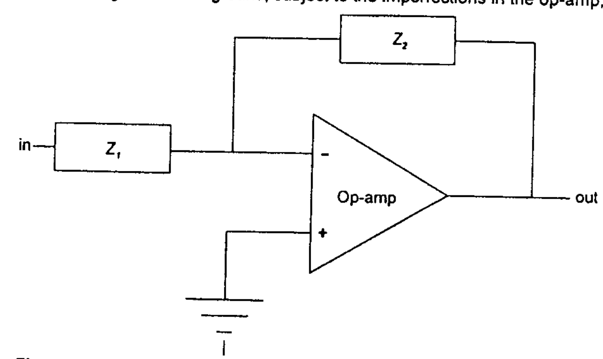

Figure 7.5 A simple inverting amplifier.

and the synthesizer is tuned to a typical weak resonance, the signal will be completely invisible on the scope, buried in the noise. This is because the system has a bandwidth of about 8 MHz, producing about 6 mV RMS of noise at the output above a few kHz and because the 10-MΩ resistor in the charge amplifier generates enormous amounts of noise below a few kHz. Nevertheless, the signal we are after is very well preserved. To find it, we need to get rid of almost all the noise seen on the scope. This is surprisingly easy.

Recalling the discussion of receivers, resonators, Q, and noise bandwidth of Chapter 6, it is clear that all we need do is reduce the bandwidth of the system with some sort of filter as we observe the resonances at many different frequencies. The way to do this for a non-phase-sensitive system (the simpler choice for proceeding with an explanation) is with a mixer and active filter. A mixer is an electronic multiplier with a response described by Equation 7.9. Such devices are readily available as a single integrated circuit. The only reason to use a mixer is that it is hard to design good variable-frequency filters. A filter is a chunk of electronics that passes only some frequencies. It is, as described in Chapter 6, just like a resonator—so much so that all the filters used in most radio receivers (but not ours) are fixed piezoelectric mechanical resonators. Even the electronic ones require several passive components to set the center frequency and Q of the filter. This makes it necessary to change several components to retune the filter as frequency is swept, something at best difficult to do, and essentially impossible if the intent is to tune through resonances electronically as fast as physics allows. The way out is to set the filter at one frequency and do something else to tune. What is done is to generate two frequencies, one at the frequency ω desired for excitation of the driven transducer, the other slightly higher at $\omega+\Delta\omega$. When the RUS signal from the amplifier chain having complex amplitude A at frequency ω reaches the mixer, it is multiplied by a signal of constant amplitude B at frequency $\omega+\Delta\omega$, producing a signal S where

$$S = A\sin(\omega t)B\sin\left[(\omega + \Delta\omega)t\right] = \frac{AB}{2}\left\{\cos\left[(2\omega + \Delta\omega)t\right] - \cos(\Delta\omega\, t)\right\}, \tag{7.9}$$

which now contains two frequencies. Both have amplitudes proportional to the amplitude A that we are after, but one frequency, $\Delta\omega$, is independent of the frequency of the resonance being measured. It is this frequency that the filter is tuned to. A very convenient frequency for $\Delta\omega$ is 1 kHz. This is primarily chosen to roughly match the Q of RUS samples in the following sense. If a sample has a resonance at 1 MHz and a Q of 10,000, then it takes roughly 10 ms for the sample to "ring up" as discussed in Chapter 1. This is a factor of 20 longer than the half-period of $\Delta\omega$. Because it is a signal at $\Delta\omega$ whose amplitude is to be measured, it is good practice to use several cycles of that signal to obtain a measurement, but it would be unnecessarily costly to wait much

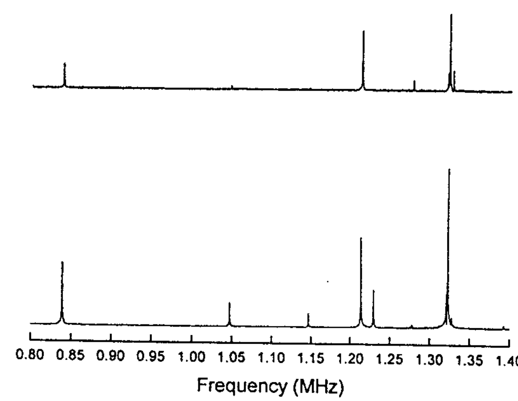

Figure 7.9 Shown are two spectra of an approximately 3 mm alumina RP. The only difference is the mounting position of the sample on the transducers. Note how some modes are absent in the upper scan.

of the sample so that it touches the transducers at the edge of the region of the transducer exposed through the 1-mm hole in the Kapton, substantial lateral drive can be had, while the raised edge of Kapton film securely holds the sample from slipping. This is, however, not good enough. One must mount the sample several times, each time scanning for resonances not present before. In addition, once the sample is mounted, rotating it small amounts about the body diagonal with tweezers will often produce large-amplitude changes in the resonances as well as revealing missed ones. This is all a lot easier than it sounds, and very rewarding, as Figure 7.9 illustrates.

But be sure to find every mode possible, as the lengthy fitting procedures will go much more smoothly. One can still miss modes because an accidental degeneracy may result from a particularly unlucky combination of moduli and sample shape, or because the corner is at a node, but by following the above suggestions, no others will be lost. If no fit can be obtained, sample quality is beyond reproach, the symmetry of the crystal lattice certain, and hours have been spent searching for missing modes, then

[TR-48]

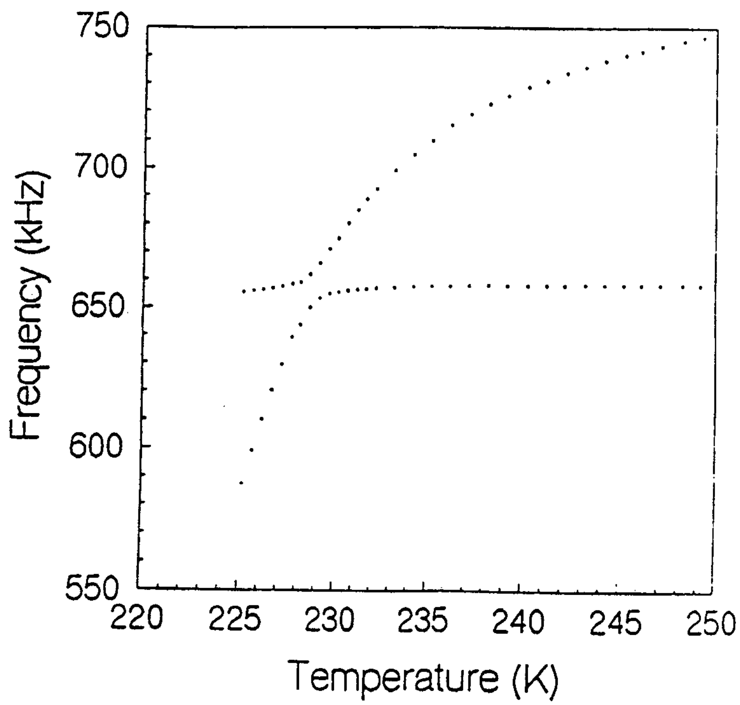

Figure 6

[TR-49]

basis of all the usual sorts of scientific and nonscientific constraints and boundary conditions, decide just how much trouble to take with the data. Fortunately, RUS will provide very valuable results with minimal effort.

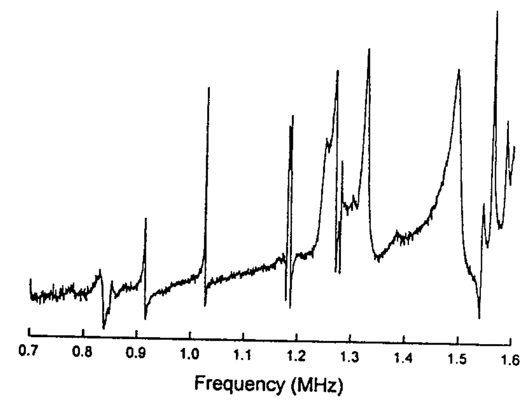

Figure 7.10 The resonance spectrum of $La_{0.83}Sr_{0.17}MnO_3$ taken on a high quality single crystal just above the magnetic transition. This noisy spectrum with considerable background was adequate to determine for the first time, the three cubic moduli of this material to within a few percent.

7.7 Fitting RUS data to determine moduli

The spectrum shown in Figure 7.11 is typical of that obtained on a high-*Q* specimen. As we shall see, there is a missed mode near 0.875 MHz and some modes are split but easily separable as can be seen in Figure 7.12. In order to determine elastic moduli, the mass and dimensions must be measured and then a computer program based on the procedures described in Chapter 4 and [7.8] used. The code (`rpr.exe`) developed by the authors, and the workhorse code in their laboratory, available from the author [7.1], is a good example to use here in expounding upon the nuances of obtaining a satisfactory fit and, hence, moduli. From the spectrum of Figure 7.11 we

generate the following text file called `rprin.dat`, which serves as input to the code.

```
5120 Steel
 2 3 10  0  0.167200  1.00 1
 2.74346 0.82139
  0.3045  0.2665 0.2645
  0.488260  0.486970 0.00
  0.578550  0.577454 0.00
  0.662500  0.662692 1.00
  0.664360  0.664805 1.00
  0.711500  0.711540 1.00
  0.714380  0.714246 1.00
  0.758640  0.758487 1.00
  0.766650  0.767904 1.00
  0.785160  0.786240 1.00
  0.825220  0.826347 1.00
  0.836490  0.836457 1.00
  0.844280  0.844243 1.00
  0.845020  0.844656 1.00
  0.906710  0.906418 1.00
  0.908130  0.908173 1.00
  0.913660  0.913771 1.00
  0.952560  0.952736 1.00
```

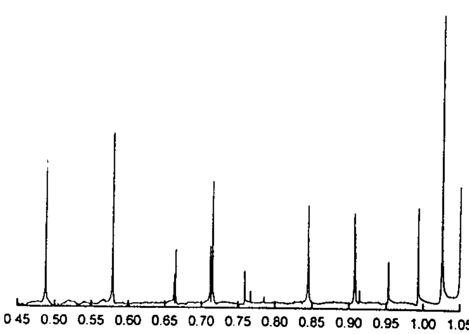

Figure 7.11 The RUS spectrum of an RP of 5120 steel, a fine grained polycrystalline material in the normalized condition.

The first line is simply a comment to remind the user of what is being worked on. The second line of the code contains in order:

a. The number of moduli to be fitted(2, 3, 5, 6, or 9).
b. The number of dimensions to be fitted (0 or 3).
c. The order of polynomials to be used (10 unless a very slow computer is used in which case start with 8 or 9, get close to a fit, and then switch to 10)
d. A control number. If it is 0, then a fit is executed in which the code iteratively adjusts moduli to produce resonances that fit as well as possible the measured ones. If it is any positive integer *n*, the codes simply computes the first n resonances based on the dimensions, mass, and guessed moduli.
e. The mass of the sample in grams.

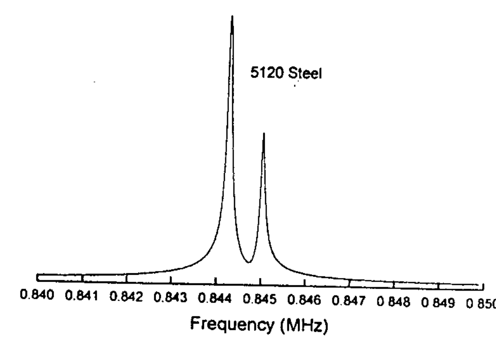

Figure 7.12 An accidental near-degeneracy causing a split mode for the RP of Figure 7.11. Because the splitting is greater than the line width and the *Q* is high (Q=5000), no special pains need be taken to find the frequencies of these two modes.

f. An adjustable convergence parameter normally left at 1.00. Other values control the mix between steepest descent and minimization as is typical in a Levenberg-Marquardt algorithm.
g. A control parameter that blocks screen output so that the code can be called as a C-language subroutine.

The second line contains the initial guesses of elastic moduli in units of 10^{12} dyn/cm^2. There must be the same number of guesses as the moduli to be fit. It is essential to use every possible source to obtain a good starting guess, or else the code may wander around near local minima, never finding anything useful. Note that:

For 2 moduli, the numbers are c_{11} and c_{44}.
For 3 moduli, the numbers are c_{11}, c_{12} and c_{44}.
For 5 moduli, the numbers are c_{33}, c_{23}, c_{12}, c_{44}, c_{66}.
For 6 moduli, the numbers are c_{11}, c_{33}, c_{23}, c_{12}, c_{44}, c_{66}.
For 9 moduli, the numbers are c_{11}, c_{22}, c_{33}, c_{23}, c_{13}, c_{12}, c_{44}, c_{55}, c_{66}.

The third line contains the dimensions of the sample in cm, the first number corresponding to the 1 axis, the second to the 2 axis, the third to the 3 axis. The remaining lines contain first the measured frequency in MHz; the second a number that is not read by the code so it can be anything, but we shall see soon why it is there; and the third number is a weight determining how strongly that mode is included in the fitting procedure. That is, a weight of 1.0 uses the resonance; a weight of 0.0 does not. Values in between reduce the dependence of the fit on that mode and can be used if the experimenter has some good reason to use them.

Running the code for these inputs yields a very poor fit. It is clear that we missed a resonance between the 13th and 14th modes. The output is written to a file called `rprout.dat`. It looks like

```
5120 Steel
free moduli are  c11, c44
using 10 order polynomials    mass=  0.1672 gm  rho= 7.790 gm/cc
 n     fex       fr      %err wt k I df/d(moduli)
 1 0.488260 0.489423  0.24 1. 4 1 0.00 1.00
 2 0.578550 0.581709  0.55 1. 4 2 0.00 1.00
 3 0.662500 0.665424  0.44 1. 6 1 0.10 0.90
 4 0.664360 0.667556  0.48 1. 7 1 0.10 0.90
 5 0.711500 0.715707  0.59 1. 3 1 0.02 0.98
 6 0.714380 0.718480  0.57 1. 2 1 0.01 0.99
 7 0.758640 0.763605  0.65 1. 8 1 0.01 0.99
 8 0.766650 0.773214  0.86 1. 1 1 0.04 0.96
 9 0.785160 0.790428  0.67 1. 5 1 0.02 0.98
10 0.825220 0.831537  0.77 1. 5 2 0.01 0.99
11 0.836490 0.839861  0.40 1. 6 2 0.32 0.68
12 0.844280 0.847863  0.42 1. 7 2 0.32 0.68
13 0.845020 0.848405  0.40 1. 8 2 0.17 0.83
```



```
14 0.906710 0.870343 -4.01 1. 5 3 0.00 1.00
15 0.908130 0.910573  0.27 1. 1 2 0.36 0.64
16 0.913660 0.912945 -0.08 1. 2 2 0.17 0.83
17 0.952560 0.918683 -3.56 1. 3 2 0.17 0.83
  c11    c22    c33    c23    c13    c12    c44    c55    c66
2.7372 2.7372 2.7372 1.0735 1.0735 1.0735 0.8319 0.8319 0.8319
     d1       d2       d3
 0.30450  0.26650  0.26450
loop# 6      rms error= 1.3927 %, changed by 0.000000 %
length of gradient vector=  0.000000  lambda= 1.000
eigenvalues              eigenvectors
    0.02021     1.00 0.03
    9.99788    -0.03 1.00
chisquare  increased  2%  by  the  following  %  changes  in  independent
parameters
  2.95 -0.29
  0.00  0.44
```

The code also produces a file called `rprio.dat`. It looks like

```
5120 Steel
 2 0 10  0   0.167200   1.00 1
 2.73724 0.83188
  0.304500   0.266500   0.264500
  0.488260   0.489423 1.00
  0.578550   0.581709 1.00
  0.662500   0.665424 1.00
  0.664360   0.667556 1.00
  0.711500   0.715707 1.00
  0.714380   0.718480 1.00
  0.758640   0.763605 1.00
  0.766650   0.773214 1.00
  0.785160   0.790428 1.00
  0.825220   0.831537 1.00
  0.836490   0.839861 1.00
  0.844280   0.847863 1.00
  0.845020   0.848405 1.00
  0.906710   0.870343 1.00
  0.908130   0.910573 1.00
  0.913660   0.912945 1.00
  0.952560   0.918683 1.00
```

which is exactly like the file `rprin.dat` except that the fitted frequencies are put in the second (unused) column for convenience in figuring out what to change. We can now insert a missing mode by simply adding a line 0. 0. 0. after the resonance at 0.84502 MHz, rename the file `rprin.dat`, and proceed. At this point, we shall also float the dimensions because we know that sufficient data exists to obtain a fit. Normally this should be left until the best fit is obtained with dimensions fixed. The result of this pass is the following output

```
5120 Steel
free moduli are  c11, c44
free dimensions are   d1, d2, d3
using 10 order polynomials    mass=  0.1672 gm  rho= 7.785 gm/cc

 n     fex       fr      %err wt  ki  df/d(moduli)
 1 0.488260 0.486970 -0.26 1. 4 1 0.00 1.00
```

```
 2 0.578550 0.577454 -0.19 1. 4 2 0.00 1.00
 3 0.662500 0.662692  0.03 1. 6 1 0.09 0.91
 4 0.664360 0.664805  0.07 1. 7 1 0.09 0.91
 5 0.711500 0.711540  0.01 1. 3 1 0.01 0.99
 6 0.714380 0.714246 -0.02 1. 2 1 0.01 0.99
 7 0.758640 0.758487 -0.02 1. 8 1 0.01 0.99
 8 0.766650 0.767904  0.16 1. 1 1 0.04 0.96
 9 0.785160 0.786240  0.14 1. 5 1 0.02 0.98
10 0.825220 0.826347  0.14 1. 5 2 0.01 0.99
11 0.836490 0.836457  0.00 1. 6 2 0.31 0.69
12 0.844280 0.844243  0.00 1. 7 2 0.31 0.69
13 0.845020 0.844656 -0.04 1. 8 2 0.17 0.83
14 0.000000 0.864396  0.00 0. 5 3 0.00 1.00
15 0.906710 0.906418 -0.03 1. 1 2 0.34 0.66
16 0.908130 0.908173  0.00 1. 2 2 0.16 0.84
17 0.913660 0.913771  0.01 1. 3 2 0.16 0.84
18 0.952560 0.952736  0.02 1. 8 3 0.01 0.99

   c11    c22    c33    c23    c13    c12    c44    c55    c66
2.7435 2.7435 2.7435 1.1007 1.1007 1.1007 0.8214 0.8214 0.8214
      d1       d2       d3
 0.30419  0.26670  0.26474
loop# 5     rms error= 0.1028 %, changed by 0.000000 %
length of gradient vector=  0.000002  lambda= 1.000
eigenvalues            eigenvectors
     0.01693    1.00-0.03-0.01 0.00 0.00
     4.83067   -0.03-0.99-0.12-0.01 0.06
   258.19474    0.00 0.07-0.85 0.01-0.53
   306.53173    0.00 0.08-0.35-0.75 0.56
   504.31018    0.00 0.08-0.38 0.66 0.64
chisquare  increased  2%  by  the  following  %  changes  in  independent
parameters
  0.24 -0.02 -0.01  0.00  0.00
  0.00 -0.05  0.02  0.02  0.02
  0.00  0.00 -0.03 -0.01 -0.02
```

yielding a fit good to about 0.1% RMS. A curious property of RUS data that seems independent of the apparatus, sample type, transducers and the like is that the first one or two modes never fit well. If we exclude them by setting the weight to 0. in the file `rprin.dat`, then the code ignores them. Noting that we have 18 modes to determine two elastic moduli and two dimensions (we fit three dimensions, but the sample volume is internally constrained, so effectively only two free dimensional parameters are varied), in this case the elimination of two resonances cannot be a large effect. However, the fit improves greatly as shown in the next pass.

```
5120 Steel
free moduli are   c11, c44
free dimensions are    d1, d2, d3
using 10 order polynomials    mass=  0.1672 gm  rho= 7.785 gm/cc

 n     fex        fr     %err wt k i    df/d(moduli)
 1 0.488260 0.486723 -0.31 0. 4 1 0.00 1.00
 2 0.578550 0.577014 -0.27 0. 4 2 0.00 1.00
 3 0.662500 0.662538  0.01 1. 6 1 0.09 0.91
 4 0.664360 0.664657  0.04 1. 7 1 0.09 0.91
 5 0.711500 0.711131 -0.05 1. 3 2 0.01 0.99
```



```
 6 0.714380 0.713837 -0.08 1. 2 1 0.01 0.99
 7 0.758640 0.757971 -0.09 1. 8 1 0.01 0.99
 8 0.766650 0.767414  0.10 1. 1 1 0.04 0.96
 9 0.785160 0.785842  0.09 1. 5 1 0.02 0.98
10 0.825220 0.825823  0.07 1. 5 2 0.01 0.99
11 0.836490 0.836622  0.02 1. 6 2 0.31 0.69
12 0.844280 0.844401  0.01 1. 7 2 0.30 0.70
13 0.845020 0.844556 -0.05 1. 8 2 0.16 0.84
14 0.000000 0.863782  0.00 0. 5 3 0.00 1.00
15 0.906710 0.906612 -0.01 1. 1 2 0.34 0.66
16 0.908130 0.907974 -0.02 1. 2 2 0.16 0.84
17 0.913660 0.913573 -0.01 1. 3 3 0.16 0.84
18 0.952560 0.952253 -0.03 1. 8 3 0.01 0.99

   c11    c22    c33    c23    c13    c12    c44    c55    c66
2.7554 2.7554 2.7554 1.1147 1.1147 1.1147 0.8203 0.8203 0.8203
      d1       d2       d3
 0.30414  0.26672  0.26475

loop# 9     rms error= 0.0554 %, changed by 0.000000 %

length of gradient vector=  0.000002  lambda= 1.000

eigenvalues            eigenvectors
     0.01437    1.00-0.03-0.01 0.00 0.00
     4.38180   -0.03-0.99-0.10 0.00 0.08
   228.29772    0.00 0.06-0.92 0.02-0.39
   305.96434    0.00 0.08-0.27-0.74 0.61
   403.67989    0.00 0.08-0.27 0.67 0.68

chisquare increased 2% by the following % changes in independent
parameters
  0.13 -0.01 -0.01  0.00  0.00
  0.00 -0.02  0.01  0.01  0.01
  0.00  0.00 -0.02 -0.01 -0.01
```

Finally, the sample was remounted and a careful fine scan performed near 0.863 MHz. The result is that the missing line was found as a very weak resonance at 0.8624 MHz. Using it, the fit is slightly worse, but more modes are used so the confidence level is improved.

```
5120 Steel
free moduli are   c11, c44
free dimensions are    d1, d2, d3
using 10 order polynomials    mass=  0.1672 gm  rho= 7.790 gm/cc

 n     fex        fr     %err wt k i    df/d(moduli)
 1 0.488260 0.486713 -0.32 0. 4 1 0.00 1.00
 2 0.578550 0.576759 -0.31 0. 4 2 0.00 1.00
 3 0.662500 0.662615  0.02 1. 6 1 0.09 0.91
 4 0.664360 0.664738  0.06 1. 7 1 0.09 0.91
 5 0.711500 0.711005 -0.07 1. 3 1 0.01 0.99
 6 0.714380 0.713709 -0.09 1. 2 2 0.01 0.99
 7 0.758640 0.757720 -0.12 1. 8 2 0.01 0.99
 8 0.766650 0.767130  0.06 1. 1 1 0.04 0.96
 9 0.785160 0.785781  0.08 1. 5 1 0.02 0.98
10 0.825220 0.825620  0.05 1. 5 2 0.01 0.99
11 0.836490 0.836681  0.02 1. 6 2 0.31 0.69
```

```
12 0.844280 0.844449  0.02 1. 7 2 0.30 0.70
13 0.845020 0.844597 -0.05 1. 8 3 0.16 0.84
14 0.862400 0.863477  0.12 1. 5 3 0.00 1.00
15 0.906710 0.906592 -0.01 1. 1 2 0.34 0.66
16 0.908130 0.907877 -0.03 1. 2 3 0.16 0.84
17 0.913660 0.913469 -0.02 1. 3 2 0.16 0.84
18 0.952560 0.952217 -0.04 1. 8 4 0.01 0.99

  c11    c22    c33    c23    c13    c12    c44    c55    c66
2.7610 2.7610 2.7610 1.1208 1.1208 1.1208 0.8201 0.8201 0.8201

    d1       d2       d3
 0.30401  0.26670  0.26473

loop# 7      rms error= 0.0643 %, changed by 0.000001 %

length of gradient vector=  0.000002  lambda= 1.000

eigenvalues           eigenvectors
     0.01558    1.00-0.03-0.01 0.00 0.00
     4.69254   -0.03-0.99-0.11 0.00 0.07
   246.97128    0.00 0.07-0.90 0.03-0.43
   305.69754    0.00 0.08-0.31-0.74 0.60
   406.76410    0.00 0.08-0.30 0.67 0.67

chisquare  increased  2%  by  the  following  %  changes  in  independent
parameters
  0.15 -0.01 -0.01  0.00  0.00
  0.00 -0.03  0.01  0.01  0.01
  0.00  0.00 -0.02 -0.01 -0.01
```

At this point we have done as well as the data permit. The output of the code contains several items of interest, and that have been found to be useful. In the header where the moduli (and dimensions if so chosen) to be fit are listed, the order in which they appear defines the order in which some of the following data is associated with them. For example, for the first mode (n=1), the numbers under *df/d*(moduli) are the sensitivities of the first fitted mode *fr* to the elastic moduli (normalized to unity, which means that the numbers listed are the actual derivatives multiplied by a factor the factor of two that appears in the relation between frequency and stiffness). Thus

$$\frac{2c_{11}\partial f_{r1}}{f_{r1}\partial c_{11}} = 0.0 \text{ and } \frac{2c_{44}\partial f_{r1}}{f_{r1}\partial c_{44}} = 1.00, \tag{7.11}$$

where f_{r1} is the first fitted frequency. What this tells us, and which is a general property of RUS measurements, is that one of the modes, in this case the first, depends only on c_{44}. This can be a very useful piece of information because it enables one to use just the frequency of such a mode to track the particular modulus with temperature or some other variable without introducing the scatter associated with a fit. This can boost the precision of RUS to better than 1 ppm when advantage is taken of this effect in a high-*Q* sample. Of course, it was crucial to obtain a fit in order to identify the mode type and its

dependence on the moduli. In this same line are listed the mode number *n*, *fex* the measured frequency; %err, the error in fitting that mode, *k* and *i*, the mode symmetry and order as described in Chapter 4; and the weight used for fitting. Further down in the output we find the fitted moduli, dimensions, the number of iterations required for convergence, the RMS error between fitted and measured frequencies, and the change in that error between the present and previous iteration. Next come the eigenvalues and vectors for reference and debugging if the code crashes, and finally the all-important error matrix. This was discussed in Chapter 5, but we remind the reader that the biggest entry in the first column is the approximate error bar for c_{11}. The biggest entry in the second column is for c_{44}, the third column for d_1, etc. Note that for the last two fits we did, we obtained values of c_{11} of 2.744, 2.755. The half-spread was about 0.2%, roughly consistent with an error bar of 0.15%, and very definitely worse than the RMS error. Note also that the shear moduli always seem to fit better and have tighter error bars—presumably because most of the lower modes are shear-like.

We end this chapter with a fit of the data shown in Figure 7.10. The reader should examine very carefully the modes fitted below with the data in the figure. Note how distorted many line shapes are, and also note that the peaks were not fitted to find the frequencies; they were chosen by eye using a simple plotting program. The fit looks like this:

```
LaSrMno3 285.50 0.0T
free moduli are  c11, c12, c44
using 10 order polynomials    mass=  0.0179 gm  rho= 6.364 gm/cc

 n     fex       fr     %err wt k i    df/d(moduli)
  1 0.835100 0.832982 -0.25 1. 4 1 0.06-0.04 0.98
  2 0.849000 0.849199  0.02 1. 6 1 2.77-1.88 0.11
  3 0.912100 0.911084 -0.11 1. 7 1 2.75-1.86 0.11
  4 1.025500 1.028140  0.26 1. 5 1 3.18-2.18 0.00
  5 1.178600 1.177794 -0.07 1. 5 2 3.15-2.15 0.01
  6 1.184900 1.182407 -0.21 1. 1 1 2.91-1.99 0.07
  7 1.242000 1.247010  0.40 1. 4 2 0.30-0.21 0.91
  8 0.000000 1.265354  0.00 0. 6 2 2.28-1.47 0.19
  9 1.268200 1.268338  0.01 1. 3 1 0.62-0.42 0.80
 10 1.278100 1.280845  0.21 1. 5 3 3.18-2.18 0.00
 11 1.299200 1.297507 -0.13 1. 2 1 1.69-1.15 0.47
 12 1.323600 1.317075 -0.49 1. 8 1 1.41-0.96 0.55
 13 1.491900 1.493765  0.13 1. 2 2 0.77-0.49 0.72
 14 1.541500 1.542163  0.04 1. 1 2 2.71-1.86 0.15
 15 1.561300 1.562077  0.05 1. 7 2 2.47-1.63 0.16
 16 1.586500 1.588603  0.13 1. 8 2 0.17-0.09 0.93
  c11    c22    c33    c23    c13    c12    c44    c55    c66
2.2006 2.2006 2.2006 1.5142 1.5142 1.5142 0.6683 0.6683 0.6683
    d1       d2       d3
 0.17201  0.13944  0.11727
loop# 2      rms error= 0.2159 %, changed by -.000001 %
length of gradient vector=  0.000000  lambda= 1.000
eigenvalues           eigenvectors
     0.00055   0.70 0.15 0.70
     4.44590   0.71-0.15-0.69
    15.44957   0.00-0.98 0.21
```

```
chisquare increased 2% by the following % changes in independent
parameters
  2.28  3.35 -0.04
  0.01 -0.01 -0.12
  0.01 -0.02  0.01
```

Of particular interest is the data for mode n=4. This mode has no dependence on c_{44} and the ratio of the normalized dependence of the mode on c_{11} (3.18) to the dependence of the mode on c_{12} (-2.18), which is -1.46, is nearly exactly the same as the ratio of $-c_{11}/c_{12}$ (-1.45). This is just the condition that the mode frequency be unchanged if both c_{11} and c_{12} are increased by the same amount. The modulus referred to as $c^* = (c_{11}-c_{12})/2$ in a cubic system is the modulus describing the shear stiffness in the (110) direction and is also unchanged by such a change in individual moduli. It determines the sound speed of a pure shear wave, and so c^* is also a pure shear modulus. The code naturally finds resonances that are pure c^* as well as pure c_{44}.

References

7.1 To obtain a PC version optimized for Pentium processors, send $20.00 U.S. and a stamped, self-addressed floppy-disk mailer (do not send a disk) to Albert Migliori, 13 Alamo Creek Drive, Santa Fe, NM 87501.
7.2 M. Schwartz, *Information Transmission, Modulation, and Noise* (McGraw-Hill, New York, 1980).
7.3 MAXIM Integrated Products, 120 San Gabriel Drive, Sunnyvale, CA 94086.
7.4 DDS-1 available from SCITEQ Electronics, 8401 Aero Drive, San Diego, CA 92123.
7.5 LSDAS-16 available from Analogic Corporation, 360 Audubon Rd., Wakefield, MA 01880.
7.6 Y. Sumino, I. Ohno, T. Goto, and M. Kumazawa, *J. Phys. Earth* **24** (1976), 263.
7.7 Stycast 1266 epoxy, Emerson & Cuming Inc., 77 Dragon Ct., Woburn, MA 01888.
7.8 A. Migliori, J.L. Sarrao, William M. Visscher, T.M. Bell, Ming Lei, Z. Fisk, and R.G. Leisure, *Physica B* **1** (1993), 183.
7.9 A. Stekel, J.L. Sarrao, T.M. Bell, Ming Lei, R.G. Leisure, W.M. Visscher, and A. Migliori, *J. Acoust. Soc. Am.* **92** (1992), 663.

Ginzburg-Landau description of second order phase transitions

Linear coupling between strain e_4 and order parameter q

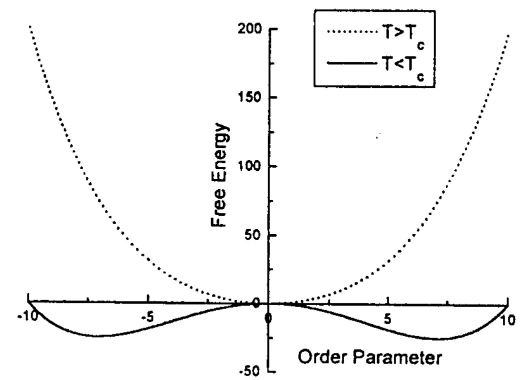

$$F = \frac{1}{2}\alpha(T - T_c)q^2 + \frac{1}{4}\beta q^4 + \frac{1}{2}c_{44}e_4^2 + \gamma e_4 q$$

1. Minimize F with respect to q.

$$\frac{\partial F}{\partial q} = \alpha(T - T_c)q + \beta q^3 + \gamma e_4 = 0 \cdot$$

Note that at zero strain, $T>T_c$, q=0, while for $T<T_c$ q#0.

This is the constraint that we use when computing the elastic response.

2. Compute the elastic response under the constraint.

[TR-60]

$$c_{44}(T) = \frac{d^2F}{de_4^2}\Big|_{e_4=0}$$

Here's how! Use the constraint that F be a minimum and compute:

$$\frac{\partial}{\partial e_4}\left[\alpha(T-T_c)q + \beta q^3 + \gamma e_4\right] = 0$$

$$\frac{\partial q}{\partial e_4} = \frac{-\gamma}{\alpha(T-T_c) + 3\beta q^2}$$

$$\frac{\partial^2 q}{\partial e_4^2} = \frac{3\beta\gamma q}{\left(\alpha(T-T_c) + 3\beta q^2\right)^2}\frac{\partial q}{\partial e_4} = \frac{-3\beta q}{\gamma}\left(\frac{\partial q}{\partial e_4}\right)^3$$

Now compute $c_{44}(T)$

$$\frac{\partial^2 F}{\partial e_4^2} = \left(\alpha(T-T_c) + 3\beta q^2\right)\left(\frac{\partial q}{\partial e_4}\right)^2 + \left(\alpha(T-T_c)q + \beta q^3\right)\frac{\partial^2 q}{\partial e_4^2} + c_{44} + 2\gamma\frac{\partial q}{\partial e_4} + \gamma e_4\frac{\partial^2 q}{\partial e_4^2}$$

Noting that if $T>T_c$ then q=0 and that we are evaluating at e_4=0 we get:

$$\frac{\partial q}{\partial e_4} = \frac{-\gamma}{\alpha(T-T_c)}$$

giving

$$c_{44}(T) = c_{44} - \frac{\gamma^2}{\alpha(T-T_c)} \quad \text{if } T>T_c$$

while for $T<T_c$ we find that

$c_{44}(T) = c_{44} + \dfrac{\gamma^2}{2\alpha(T-T_c)}$ and $q^2 = \dfrac{-\alpha(T-T_c)}{\beta}$, producing a so-called Curie-Weiss behavior on either side of the transition.

[TR-61]

Let's now look at quadratic coupling between strain and order parameter

$$F = \frac{1}{2}\alpha(T-T_c)q^2 + \frac{1}{4}\beta q^4 + \frac{1}{2}c_{44}e_4^2 + \gamma e_4 q^2$$

Minimizing F with respect to the order parameter q yields

$$\frac{dF}{dq} = \left(\alpha(T-T_c) + 2\gamma e_4\right)q + \beta q^3 = 0$$

which has as solutions

q=0 above T_c, ***independent*** of e_4

and

$q^2 = -\dfrac{\alpha(T-T_c) + 2\gamma e_6}{\beta}$ for $T<T_c$ as ling as the strain is small.

The effect of this is that for

$T > T_c \qquad c_{44}(T) = c_{44}$

and for

$T < T_c \qquad c_{44}(T) = c_{44} - \dfrac{\gamma^2}{2\beta}.$

Thus a step discontinuity occurs!

[TR-62]

What happens when coupling is turned on;

$$F = \frac{1}{2}\alpha(T - T_c)q^2 + \frac{1}{4}\beta q^4 + \frac{1}{2}c_{44}e_4^2 + \gamma e_4 q^n$$

$$\frac{\partial F}{\partial e_6} = 0 = c_{44}e_4 + \gamma q^n$$

$$e_4 = \frac{\gamma q^n}{c_{44}}$$

$$T_c' = T_c + \frac{\gamma^2}{\alpha c_{44}} \quad \text{if} \quad n = 1$$

$$\beta' = \beta - \frac{2\gamma^2}{c_{44}} \quad \text{if } n = 2$$

Thus the effect is to either renormalize Tc if n=1, or if n=2, the transition can become first order. Thus elastic coupling can have either weak or strong effects on the underlying physics. Note that a really careful treatment will always produce a first order transition, albeit weak, if n=2.

[TR-63]

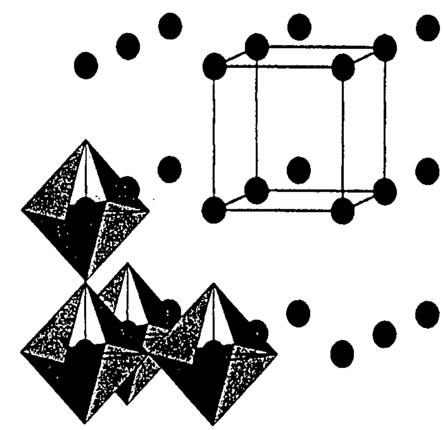

Figure 4. Shown are the Mn ions, a few of the oxygen octahedra and the simple cubic parent unit cell.

RUS sees, simultaneously, the collapse of one shear modulus and no effect on the other in a 2mm single crystal of $La_{2-x}Sr_xCuO_4$ at the structural phase transition near 223K. [TR-64]

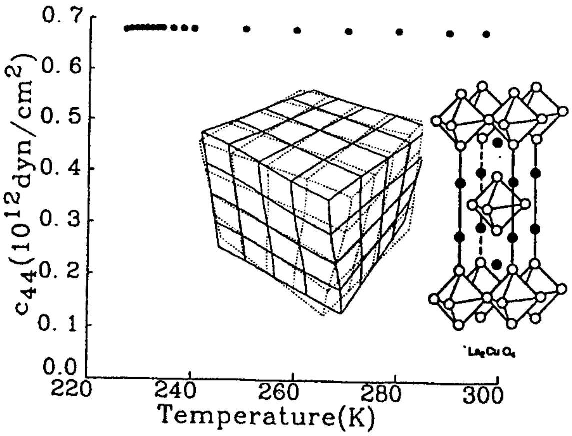

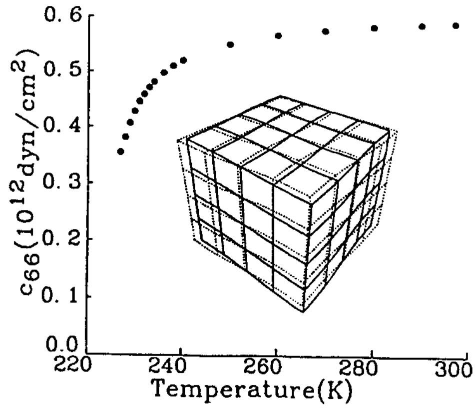

[TR-65]

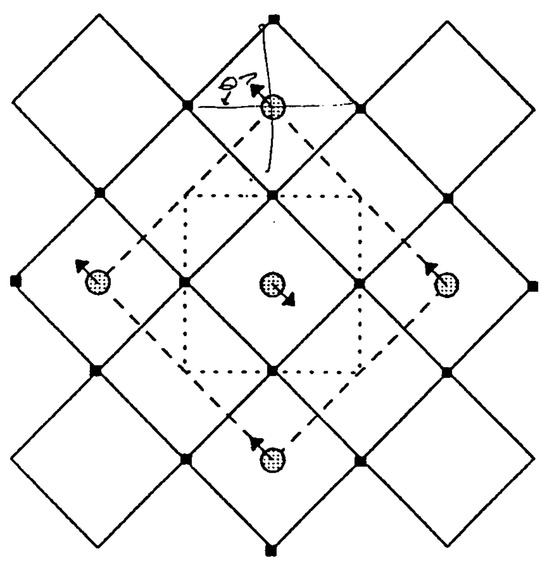

Fig 12 (in plane)

[TR-66]

OCTAHEDRA TILT ⇒ TETRAGONAL TO ORTHORHOMBIC

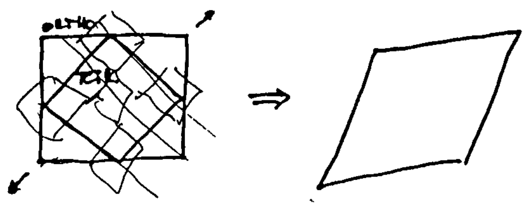

LOOKS JUST LIKE C_{66} SHEAR

QUADRATIC COUPLING OF ORDER PARAM. TO SHEAR (C_{66}) ⇒ $\Gamma = .5$ BUT!

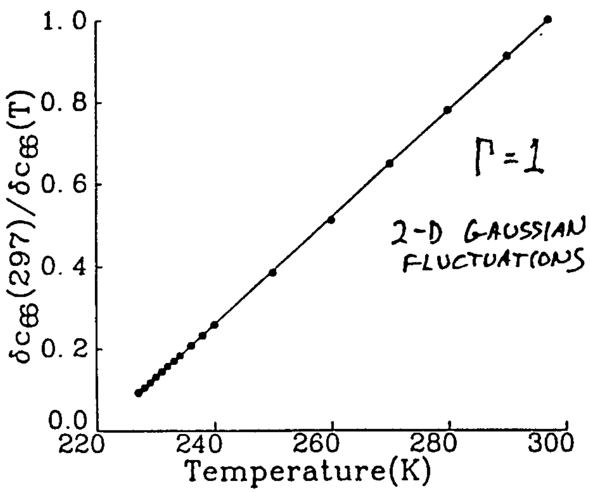

[TR-67]

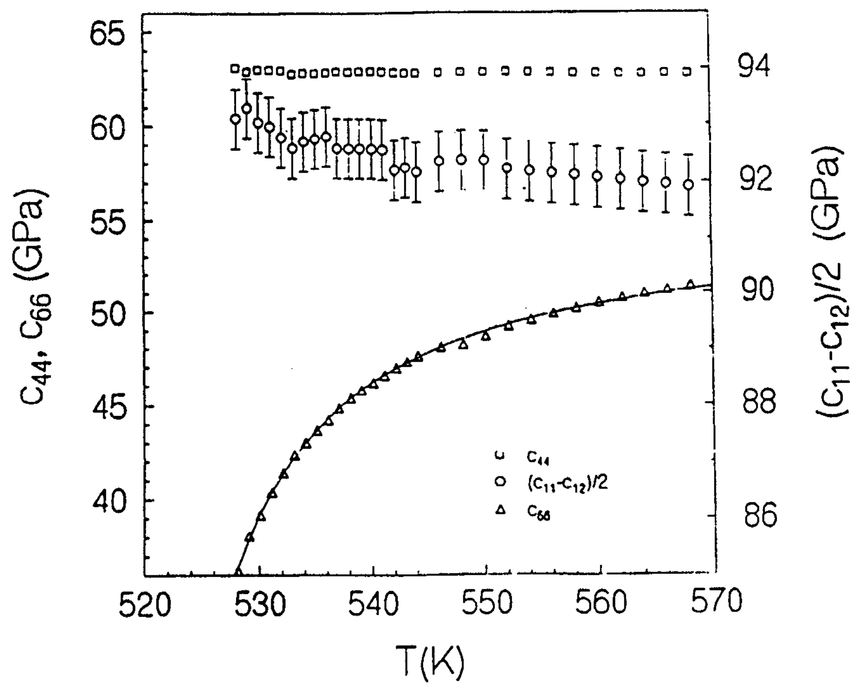

Figure 7
REVISED
Sarao et al.

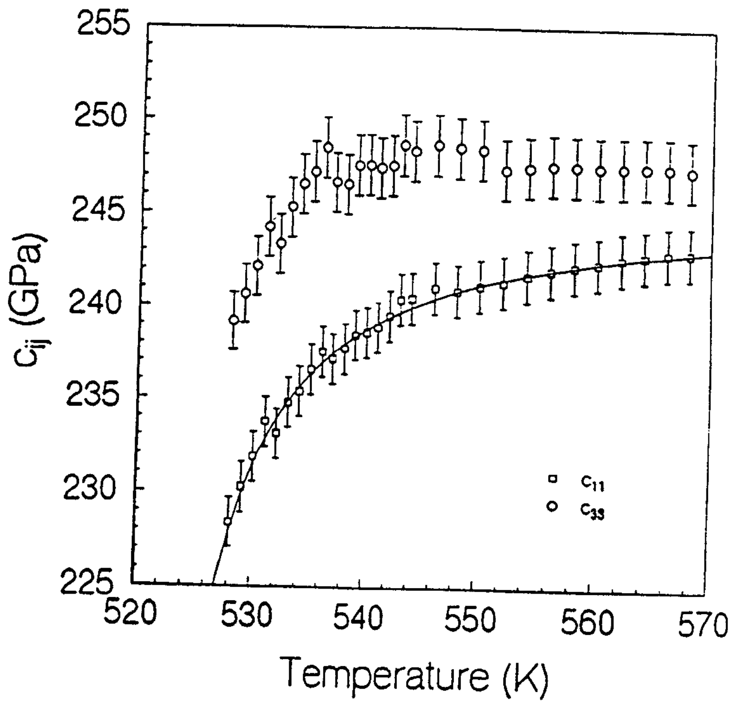

Figure 8
Salce et al.

Electronic Structure of the Narrow-Gap Semiconductor FeSi using RUS

In order to fit the data better, we consider a deformation potential coupling which explicitly includes the contribution of conduction electrons to the elastic moduli through a rigid two-band model ($E(k) = E^0(k) + d_\Gamma(k)\varepsilon_\Gamma$, where $d_\Gamma(k)$ is defined as $\partial E(k)/\partial\varepsilon_\Gamma$, and ε_Γ is a symmetry strain)

Consider the free energy for conduction electrons with band index i and energy $E^i(k)$:

$$F_{el} = -k_B T \sum_{i,k} \ln\left[1 + \exp\left(\frac{\mu - E^i(k)}{k_B T}\right)\right], \tag{2}$$

where μ is the chemical potential. Explicitly calculating the symmetry elastic moduli, $c_\Gamma = \partial^2 F/\partial\varepsilon_\Gamma^2$, and assuming conservation of the total number of quasiparticles [5] yields

$$c_\Gamma = c_\Gamma^0 - \frac{1}{k_B T}\sum_k d_\Gamma^2(k) f_k(1-f_k) + \frac{1}{k_B T}\frac{(\sum_k d_\Gamma(k) f_k(1-f_k))^2}{\sum_k f_k(1-f_k)}, \tag{3}$$

Elastic Constants of FeSi

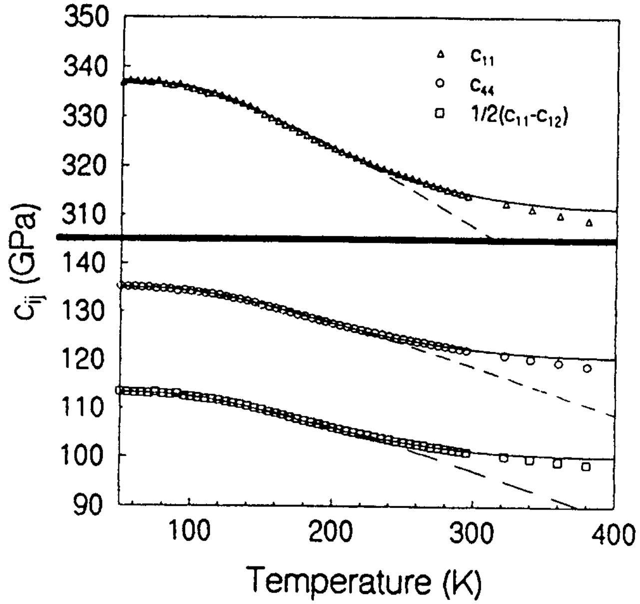

Fig. 1. Elastic moduli of FeSi as a function of temperature. The dashed curves are fits to the Varshni function (Eq. (1); for c_{11}, $s = 70.7$ GPa, $\tau = 365$ K; c_{44}, $s = 39.5$ GPa, $\tau = 366$ K; and for $1/2(c_{11} - c_{12})$, $s = 40.0$ GPa, $\tau = 374$ K). The solid curves are fits using a deformation potential coupling model. The parameters for these fits are given in Table 1.

Physica B **478**,199 (1994)

Simple model for the unusual band-edge density of electronic states in FeSi

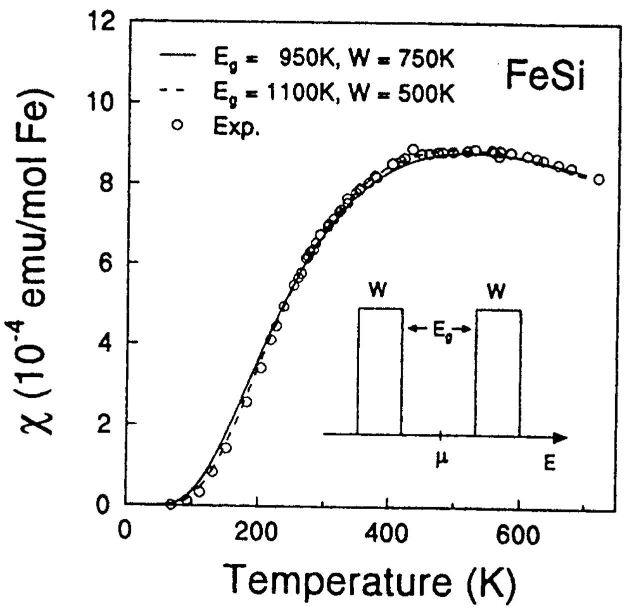

FIG. 1. Magnetic susceptibility of FeSi. Open circles: experimental points after Jaccarino *et al.* (Ref. 5). A low-temperature Curie tail was subtracted from the data as described in Ref. 5. Solid line: calculation using the model density of states shown in the inset with parameters $E_g = 950$ K, $W = 750$ K, and $g = 4.40$ states/cell. Dashed line: calculation using parameters $E_g = 1100$ K, $W = 500$ K, and $g = 4.20$ states/cell.

[TR-72]

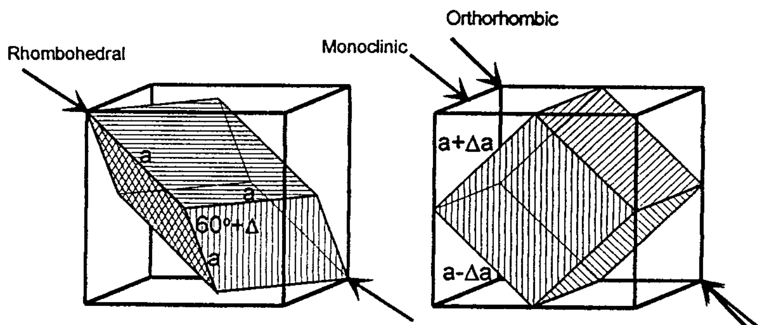

Figure 1. Shown are the parent FCC-like unit cell and the rhombohedral and orthorhombic derivative structures and their orientation with respect to cubic axes. The arrows on the left cube indicate the direction of the distortion that develops to take the cubic structure to rhombohedral. The two sets of arrows on the right cube show the distortion directions that can take a rhombohedral structure and deform it to monoclinic or to orthorhombic. Mn ions are at the corners, the center of the faces, the center of the edges and the body center of the large cube.

[TR-73]

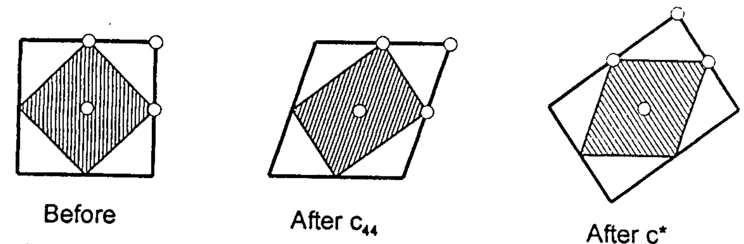

Figure 1Figure 5. Shown are the cubic face with the embedded square array of Mn ions (open circles) that will become the face of the orthorhombic unit cell (left), the orthorhombic distortion caused by a c_{44} shear (middle) and the different orthorhombic distortion caused by a c* shear (right).

[TR-74]

LaSrMno3 290.45 0.0A
free moduli are c11, c12, c44
using 10 order polynomials   mass= 0.0179 gm rho= 6.330 gm/cc

n	fex	fr	%err	wt k i	df/d(moduli)
1	0.835000	0.834413	-0.07	1.00 4 1	0.06-0.04 0.98
2	0.849000	0.850328	0.16	1.00 6 1	2.82-1.93 0.11
3	0.912100	0.910562	-0.17	1.00 7 1	2.79-1.90 0.11
4	1.025500	1.028172	0.26	1.00 5 1	3.23-2.23 0.00
5	1.178600	1.177661	-0.08	1.00 5 2	3.20-2.21 0.01
6	1.184900	1.183404	-0.13	1.00 1 1	2.96-2.04 0.07
7	1.242000	1.245276	0.26	1.00 4 2	0.30-0.21 0.91
8	0.000000	1.269433	0.00	0.00 3 1	0.64-0.44 0.80
9	1.268200	1.269981	0.14	1.00 6 2	2.32-1.51 0.19
10	1.278100	1.279989	0.15	1.00 5 3	3.24-2.24 0.00
11	1.299200	1.297904	-0.10	1.00 2 2	1.70-1.17 0.47
12	1.323600	1.318047	-0.42	1.00 8 2	1.44-0.98 0.54
13	1.491900	1.494187	0.15	1.00 2 3	0.80-0.51 0.71
14	1.541500	1.541511	0.00	1.00 1 2	2.75-1.90 0.15
15	1.561300	1.558194	-0.20	1.00 7 2	2.51-1.67 0.16
16	1.586500	1.587057	0.04	1.00 3 2	2.14-1.46 0.31

Bulk Modulus= 1.772

c11	c22	c33	c23	c13	c12	c44	c55	c66
2.2282	2.2282	2.2282	1.5440	1.5440	1.5440	0.6670	0.6670	0.6670

d1	d2	d3
0.17225	0.13938	0.11778

loop# 4   rms error= 0.1843 %, changed by -.000003 %

length of gradient vector= 0.000001 lambda= 0.000

eigenvalues	eigenvectors
0.00120	0.70 0.12 0.70
2.96322	0.71-0.13-0.69
17.36970	0.00-0.98 0.17

chisquare increased 2% by the following % changes in independent parameters
1.30 1.90 -0.03
0.00 -0.01 -0.12
0.01 -0.02 0.01

[TR-75]

Moduli of La Sr MnO (Darling et al.)
Error bars are ~1% for C* and C_{44} and for the other moduli at T>285K.
For T< 285K the large uncertainty (~25%) in C_{11}, C_{12} and B is due to poor cubic fits

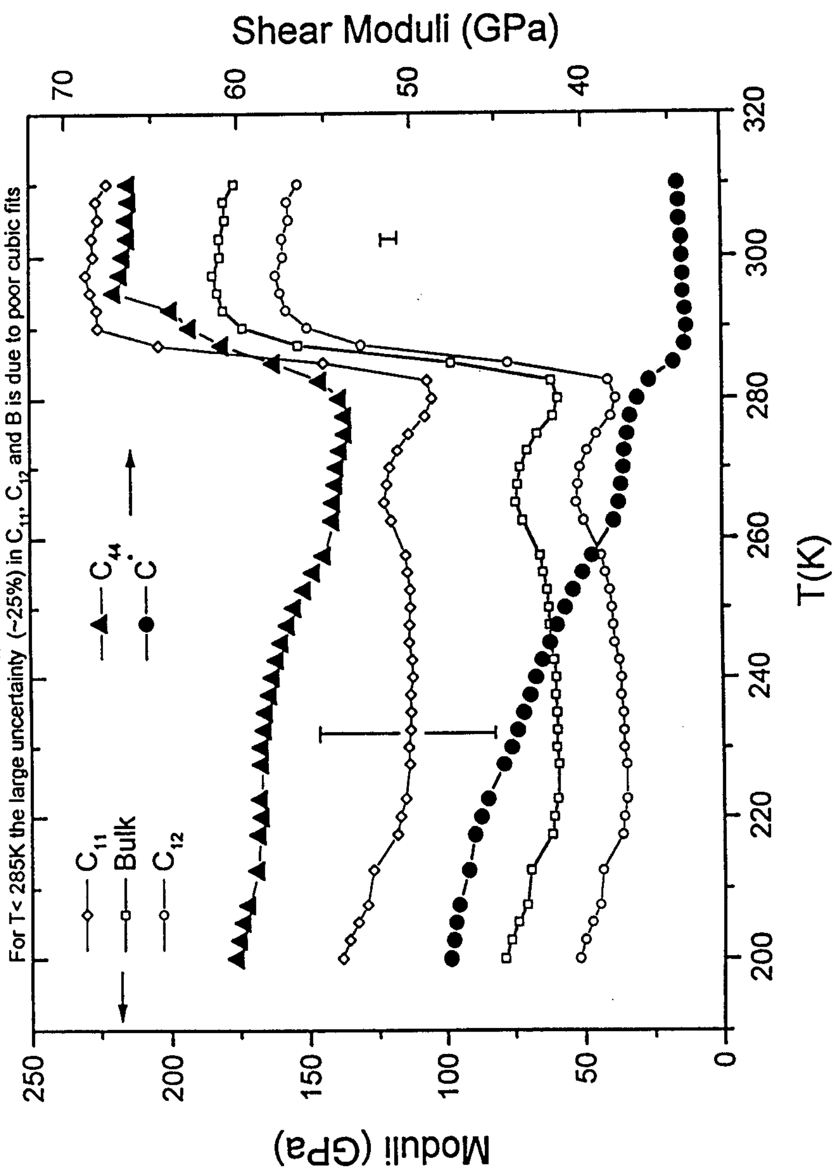

[TR-76]

Table 3.1–CRYSTAL STRUCTURE DATA FOR PLUTONIUM*

Phase	Stability Range, °C	Space Lattice and Space Group	Unit Cell Dimensions, A	Atoms per Unit Cell	X-ray Density, g/cm³	Reference
α	Below ~ 115	Simple monoclinic $P2_1/m$	@ 21°C: a = 6.183 ± 0.001 b = 4.822 ± 0.001 c = 10.963 ± 0.001 β = 101.79° ± 0.01°	16	19.86	6
β	~115 - ~200	Body-centered monoclinic $I2/m$†	@190°C: a = 9.284 ± 0.003 b = 10.463 ± 0.004 c = 7.859 ± 0.003 β = 92.13° ± 0.03°	34	17.70	8
γ	~200 - 310	Face-centered orthohombic $Fddd$	@235°C: a = 3.159 ± 0.001 b = 5.768 ± 0.001 c = 10.162 ± 0.002	8	17.14	9
δ	310 - 452	Face-centered cubic $Fm3m$	@320°C: a = 4.6371 ± 0.0004	4	15.92	10
δ'	452 - 480	Body-centered tetragonal $I4/mmm$	@465°C: a = 3.34 ± 0.01 c = 4.44 ± 0.04	2	16.00	‡
ϵ	480 - 640	Body-centered cubic $Im3m$	@490°C: a = 3.6361 ± 0.0004	2	16.51	10

* From W. H. Zachariasen and F. H. Ellinger, Acta Cryst., 16: 780 (1963), W. H. Zachariasen and F. H. Ellinger, Acta Cryst., 16: 369 (1963), W. H. Zachariasen and F. H. Ellinger, Acta Cryst., 8: 431 (1955), ~~and from F.~~ H. Ellinger, AIME Transactions, 206: 1256 (1956).

† Although space group I2/m is not one of the "standard" space groups tabulated in the International Union of Crystallography, International Tables for X-ray Crystallography, Vol. 1, Kynock Press, Birmingham, England, 1952, its notation is retained to obtain a β-angle of approximately 90°.

‡ See Chapter 5.

[TR-77]

Pu has the largest shear-wave anisotropy of any FCC metal. This can produce distortions, warping and aging effects stronger than expected for other metals–

ELASTIC PROPERTIES OF FACE-CENTERED-CUBIC PLUTONIUM*

H. M. LEDBETTER
Cryogenics Division, Institute for Basic Standards, National Bureau of Standards, Boulder, CO 80302, U.S.A.
and
R. L. MOMENT
Rockwell International, Rocky Flats Plant, Golden, CO 80401, U.S.A.

(Received 22 December 1975)

Table 1. Experimental sound velocities and elastic constants for a Pu-1 wt. % Ga single crystal (velocities refer to a direction 4° from ⟨110⟩ in a {001} plane).

Mass density:	$\rho = 15.75 \pm 0.01$ g/cm³
Longitudinal velocity:	$v_l = 2.0284 \pm 0.0032 \times 10^5$ cm/s
Transverse velocities:	$v_{t_1} = 1.4604 \pm 0.0023 \times 10^5$ cm/s $v_{t_2} = 0.5674 \pm 0.0009 \times 10^5$ cm/s
Elastic stiffnesses:	$C_L = \frac{1}{2}(C_{11} + C_{12} + 2C_{44}) = 6.510 \pm 0.038 \times 10^{10}$ N/m² $C_{44} = 3.359 \pm 0.011 \times 10^{10}$ N/m² $C' = \frac{1}{2}(C_{11} - C_{12}) = 0.478 \pm 0.032 \times 10^{10}$ N/m² $C_{11} = 3.628 \pm 0.036 \times 10^{10}$ N/m² $C_{12} = 2.673 \pm 0.027 \times 10^{10}$ N/m² $B = \frac{1}{3}(C_{11} + 2C_{12}) = 2.991 \pm 0.030 \times 10^{10}$ N/m²
Elastic anisotropies:	$A = C_{44}/C' = 7.03$ (after Zener) $A^* = 3(A-1)^2/[3(A-1)^2 + 25A] = 38.3\%$ (after Chung, Buessem)

The shear anisotropy in δ-stabilized Pu at room temperature is 7:1, and only one measurement of it has ever been made

[TR-79]

Pu structure-alternate view

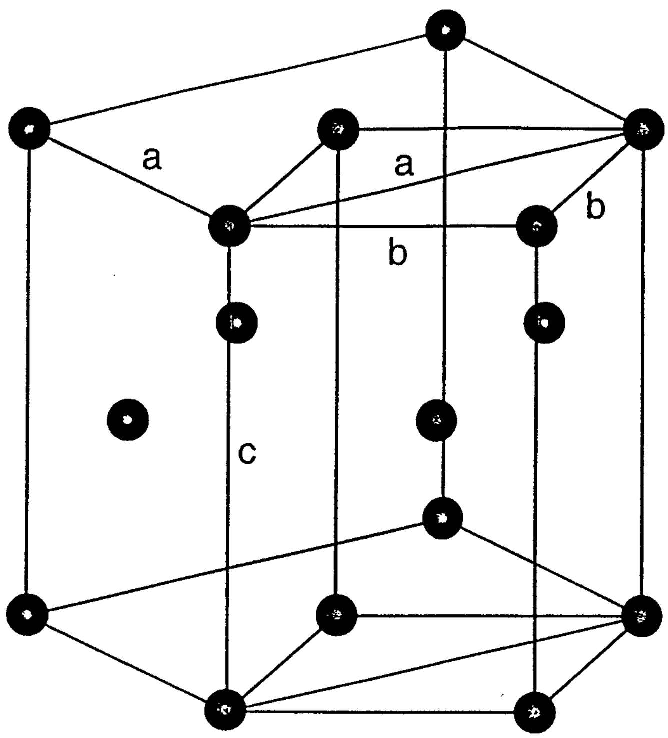

Unit cell dimensions (Å)

	fct a	fct c	bct b	bct c
δ	4.64	4.64	3.28	4.64
δ'	4.72	4.44	3.34	4.44
ε	5.13	3.63	3.63	3.63

[TR-78]

The region near the ε–δ transition in Pu provides a good route for strain-anneal single crystal growth via Bain-like transformations.

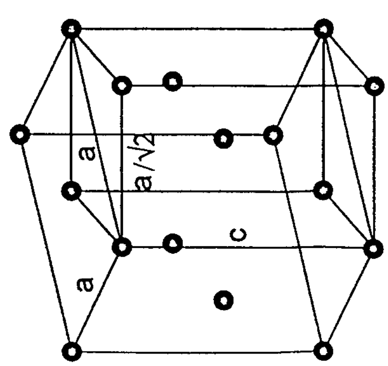

fct and bct representation

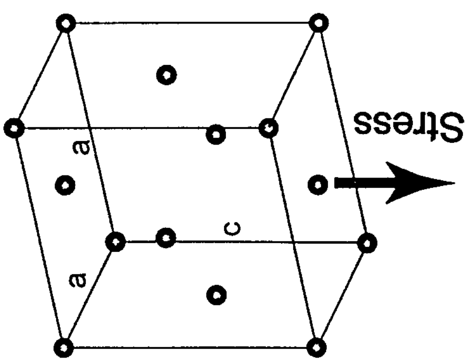

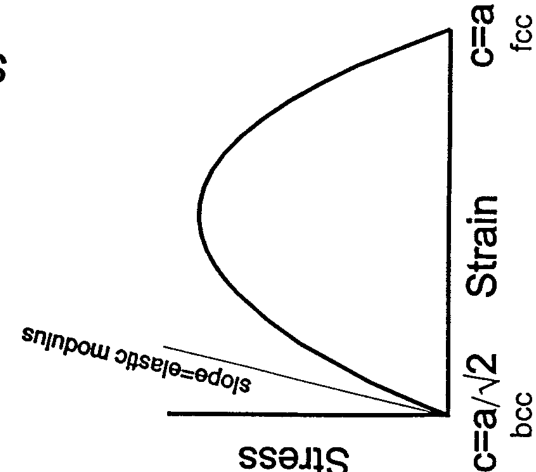

[TR-80]

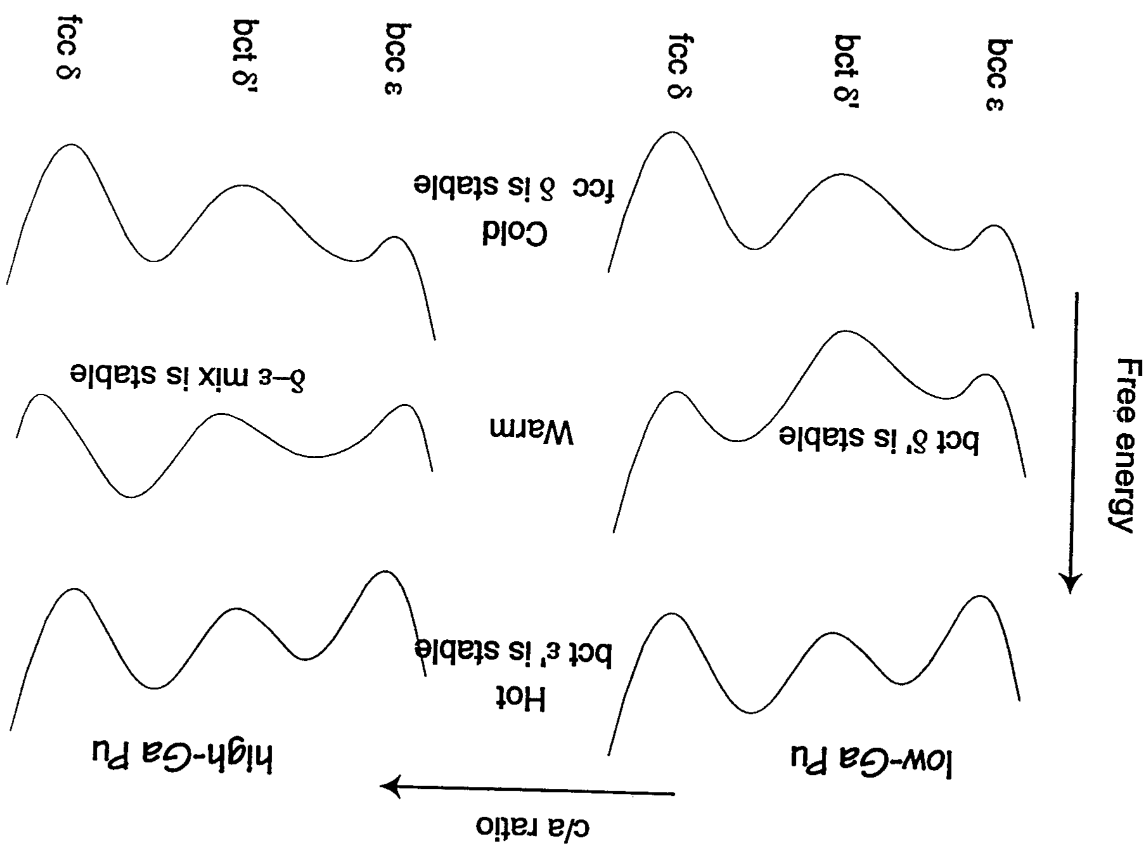

Free energy
fcc δ
bct δ'
bcc ε
Cold
fcc δ is stable
Warm
bct δ' is stable
δ–ε mix is stable
Hot
bct ε' is stable
low-Ga Pu
high-Ga Pu
c/a ratio

[TR-81]

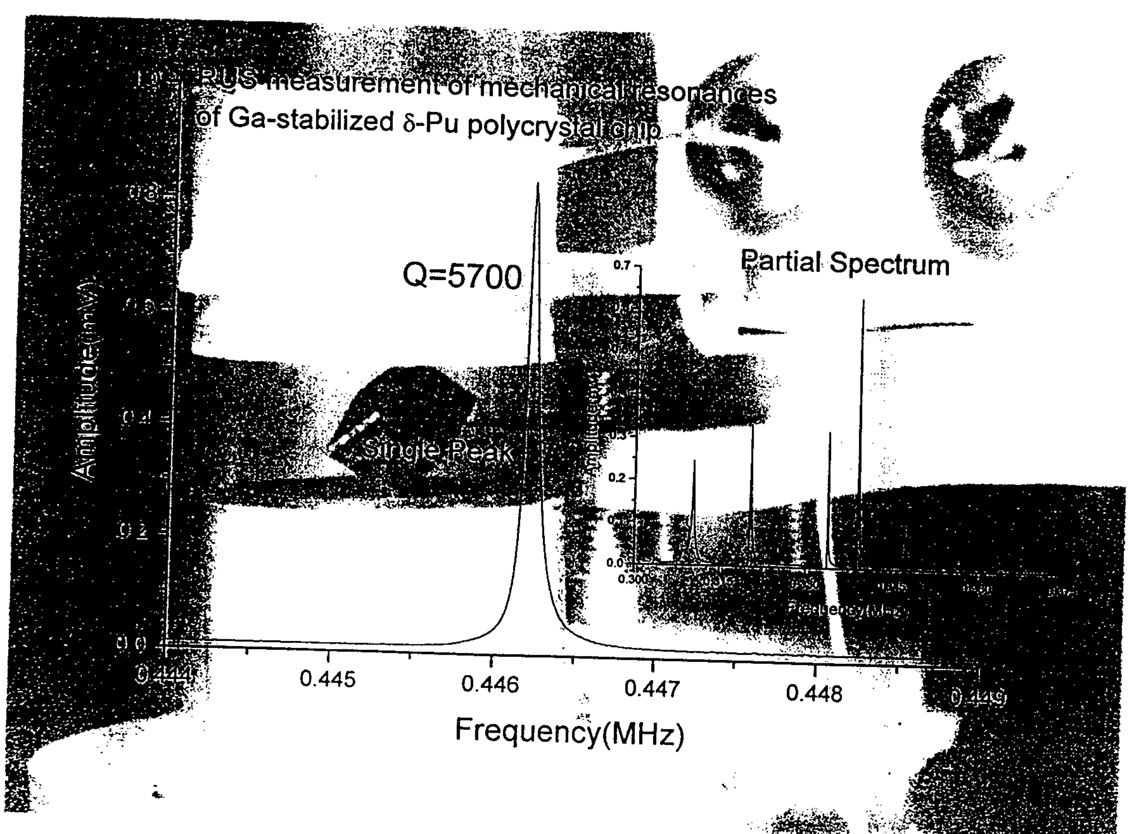

RUS measurement of mechanical resonances
of Ga-stabilized δ-Pu polycrystal chip
Q=5700
Single Peak
Partial Spectrum
Amplitude
0.445
0.446
0.447
0.448
Frequency(MHz)

[TR-83]

We have not succeeded in answering all of our questions. Indeed, we sometimes feel that we have not completely answered any of them. The answers we have found only served to raise a whole new set of questions. In some ways we feel that we are as confused as ever, but we think we are now confused on a higher level, and about more important things.

-Author unknown

RUS has important applications to nondestructive testing for quality control in industry and government.

First launch of the Trident II SLBM

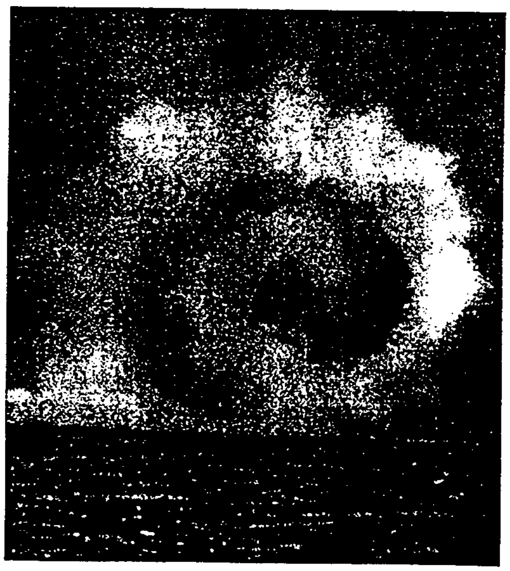

NOT LIKE THIS
(from The Economist)

Resonances can be used to determine manufacturing flaws. Below is shown a spectrum taken from a Si_3N_4 ball bearing used in the space shuttle. The error in roundness causes two degenerate resonances to split. The splitting determines the error in roundness.

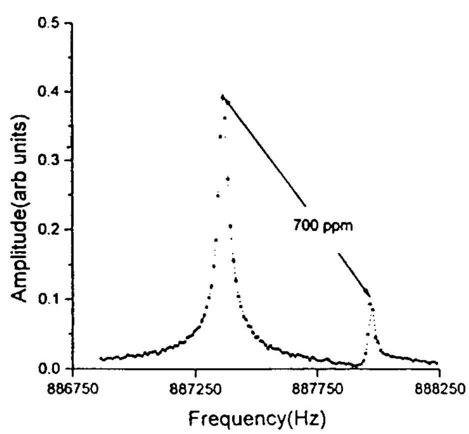

[TR-82]

ACOUSTIC RESONATORS AND THE PROPERTIES OF GASES

Michael Moldover
National Institute of Standards and Technology
Gaithersburg

Why Thermodynamic Temperatures?

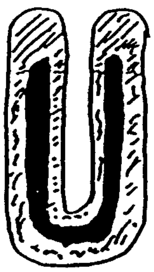

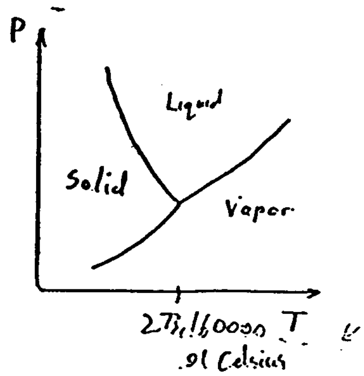

$\frac{\Delta T}{T} \sim 10^{-7}$ (30 μK near room temp)

instrumentation for 3 μK available

crystal size - strain

isotopic composition . . .

Latent Heat: $L = T \frac{dP}{dT}(V_{gas} - V_{liquid})$

Heat of Electrochemical Reaction Q ; EMF $\mathcal{E}$

$$Q = \Delta z \left(\mathcal{E} - T \frac{d\mathcal{E}}{dT}\right)$$

Carnot Efficiency $\eta = 1 - \frac{T_{COLD}}{T_{HOT}}$

Examples of Primary Thermometers

Dilute Gas (equation of state)	$PV = nRT(1 + \frac{B}{V} + \ldots$
Dilute Gas (speed of sound)	$Mc^2 = \frac{C_P^0}{C_V^0} RT(1 + A_1 P + \ldots$
Black Body Radiation (power / area)	$\frac{P}{A} = \sigma T^4 = \frac{\pi^2}{60\hbar^3 c^3}(k_B T)^4$
Johnson Noise (power) ---	$P = \frac{\langle V^2 \rangle}{r} = 4 k_B T \Delta f$
Dipole in Field (energy)	$E = -\bar{\mu} \cdot \bar{B} = -\mu B \left[\operatorname{ctnh}\left(\frac{\mu B}{k_B T}\right) - \left(\frac{\mu B}{k_B T}\right)\right]$

Acoustic Gas Thermometry

dilute monatomic gas

$$\frac{1}{2} m \overline{V^2} = \frac{3}{2} k_B T = \frac{1}{2} m \left(\frac{9}{5} c^2\right) \qquad k_B = \frac{3}{5} \frac{mc^2}{T}$$

$$R = N_A k_B = \frac{3}{5} \frac{Mc^2}{T}$$

$$\frac{T}{T_w} = \frac{T}{273.16\,\mathrm{K}} = \frac{c^2(T)}{c^2(T_w)}$$

Resonance Method

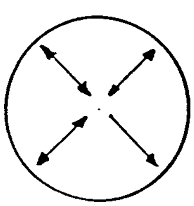

$$c = \frac{length}{time}$$

$$= V^{1/3} \times f \times eigenvalue$$

$$\frac{T}{T_w} = \left(\frac{V^{1/3} \times f}{V_w^{1/3} \times f_w}\right)^2 = \left(1 + \frac{\Delta V(T)}{V_w}\right)^{2/3} \times \left(\frac{f(T)}{f_w}\right)^2$$

dilute monatomic gas $\quad T_w \equiv 273.16$ exact

$\frac{1}{2} m \langle v^2 \rangle = \frac{3}{2} k_B T_w$ defines k_B

$\frac{1}{2} M \langle v^2 \rangle = \frac{3}{2} R T_w$ defines R

$\langle v^2 \rangle = \frac{9}{5} c^2 \qquad c$ = speed of sound

$$R = \frac{Mc^2}{\frac{5}{3} T_w} = \frac{M (Volume)^{2/3}}{\frac{5}{3} 273.16000} \left(\frac{f_n}{\Lambda_n}\right)^2$$

① f_n at T_w in limit $P \to 0$
② Volume at T_w in limit $P \to 0$
③ M
④ T_w

RADIAL RESONANCES IN A SPHERE

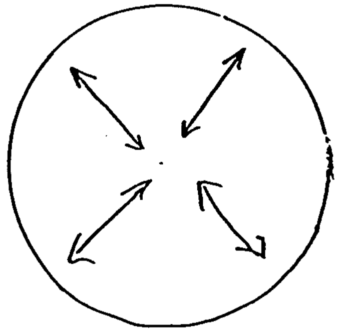

HIGHEST POSSIBLE Q AT LOW DENSITY (NO VISCOUS DAMPING.

NOT SENSITIVE TO SMALL ERRORS IN CONSTRUCTION — NON-DEGENERATE MODES

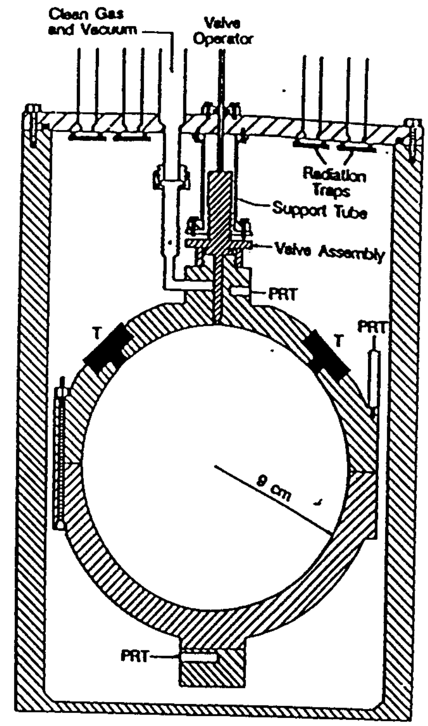

Figure 5. Cross-section of resonator and pressure vessel. Tl transducer assemblies are indicated by "T," and the locations the capsule thermometers are indicated by "PRT."

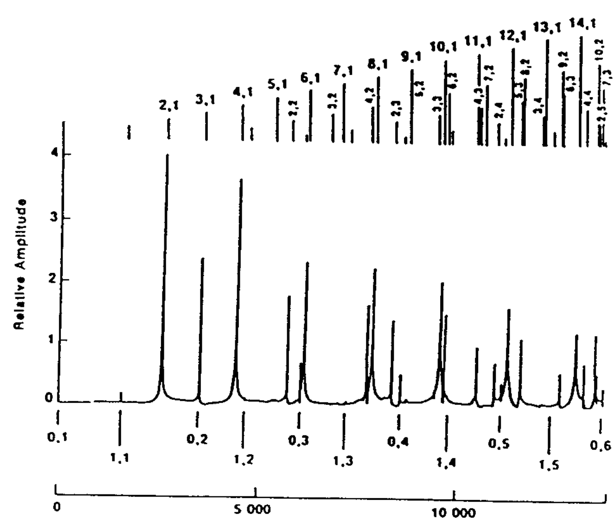

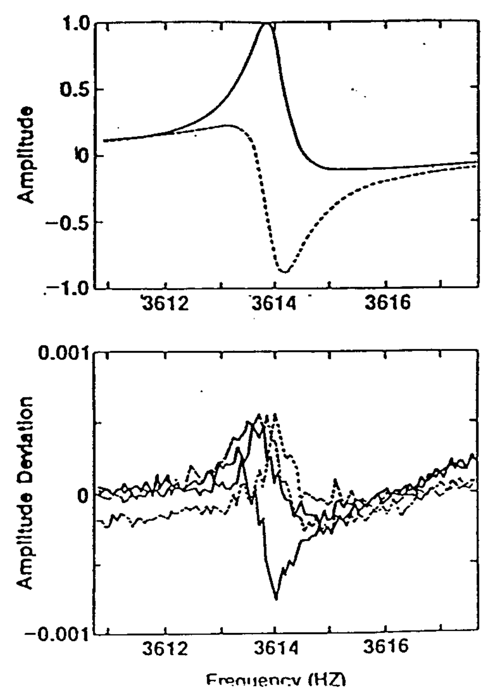

$Q \sim 5000 \qquad \frac{\Delta f}{f} \sim 2 \times 10^{-7}$

$$u + iv = \frac{i f \bar{A}}{f^2 - (f_n + i g_n)^2} + \bar{B} + \bar{C}(f - f_n)$$

Simplest Theory

Rigid spherical shell, ignore temperature

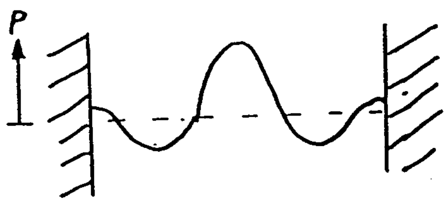

j_n = nth spherical Bessel function

$$\frac{dj_n(\beta a)}{da} = 0\ ; \qquad \beta = \frac{2\pi f}{c}$$

$\rightarrow f(n,l)$ (Rayleigh)

l = # of root; $l = 0, 1, 2, \ldots$

n = # of Bessel fuction; $n = 0, 1, 2, \ldots$

Heat Flow Between Gas and Shell

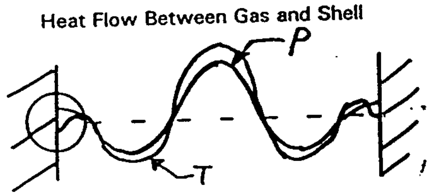

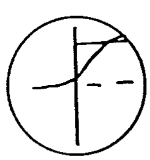

$$\left(\frac{\Delta f + ig}{f}\right)_{heat\ flow} = (-1+i)\left(\frac{\gamma-1}{2a}\right)\sqrt{\frac{D_T}{\pi f}}$$

$$= (-1+i)\left(210\times 10^{-6}\right)\sqrt{\frac{f_{0,1}}{f}\frac{1\ \mathrm{atm}}{P}}$$

Note: $D_T = \dfrac{\lambda}{\rho C_p}$

Perturbation Theory

From Morse and Ingard, Eq. (9.4.14); (Ψ is the velocity potential)

$$\Delta f - ig = -\frac{ic}{4\pi}\,\frac{\int_S \Psi_n^2(r_s)\beta(r_s,f)\,dS}{\int_V \Psi_n^2(r)\,dV}$$

For the thermal boundary layer

$$\beta_t = (1+i)\frac{\pi f}{c}(\gamma-1)\delta_t$$

Upon integrating the bessel functions, you get the "right" answer:

$$\frac{g}{f} = \frac{(\gamma-1)\delta_t}{2a}\,\frac{1}{1-n(n+1)/z_{ns}^2}$$

Note: β_t has equal real and imaginary parts; *therefore* frequency decrease $-\Delta f = g$

One may write down β's for viscous boundary layer, ducts, elastic response of shell, etc. (for radial and for non-radial modes)

$$\frac{f}{2g} = Q = \frac{2\pi\ \text{energy stored}}{\text{energy dissipated in period}}$$

$$\sim \frac{2\pi\ \text{volume}}{(\gamma-1)\delta_t\ \text{area}} = \frac{2\pi\ \frac{4}{3}\pi a^3}{(\gamma-1)\delta_t\ 4\pi a^2}$$

$$\frac{g}{f} \sim \frac{(\gamma-1)\delta_t}{2a}\,\frac{1}{\left(\frac{2\pi}{3}\right)}$$

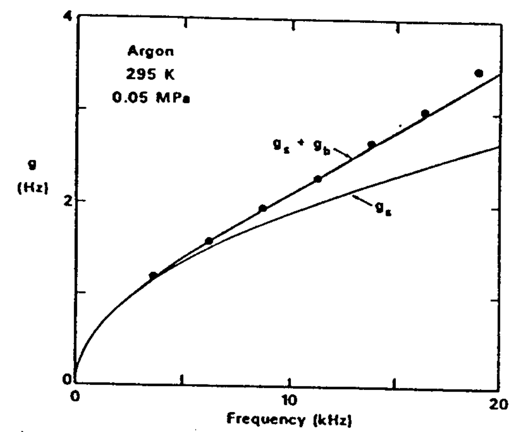

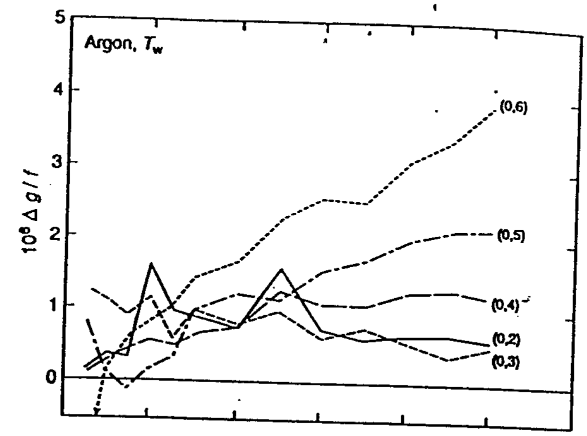

THE SHELL BREATHES

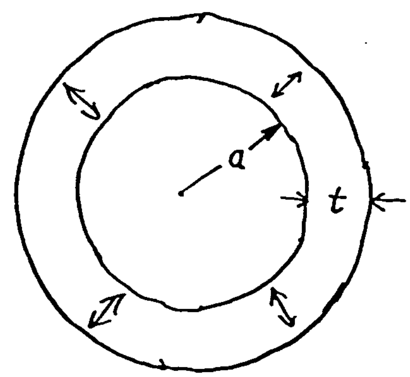

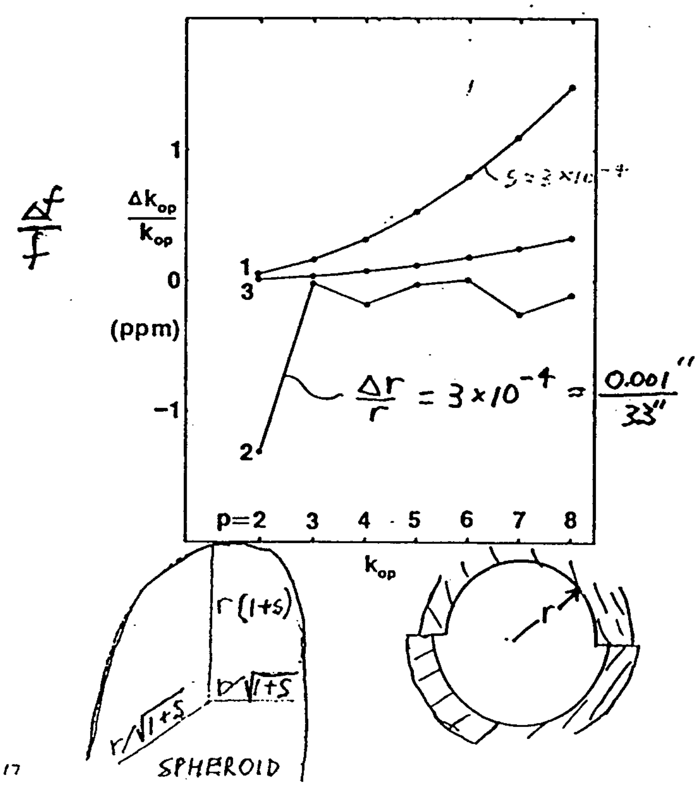

$$\frac{\Delta f}{f} = -\frac{(\rho c^2)_g}{(\rho c^2)_w}\left(\frac{a}{t}\right)\frac{1}{2-(U_p c_g/c_w)^2}$$

$U_p = 4.493,\ 7.725,\ 10.904,\ \cdots$

Argon, 295 K, 0.1 MPa, $p = 1$

$\frac{\Delta f}{f} = -5 \times 10^{-6}$

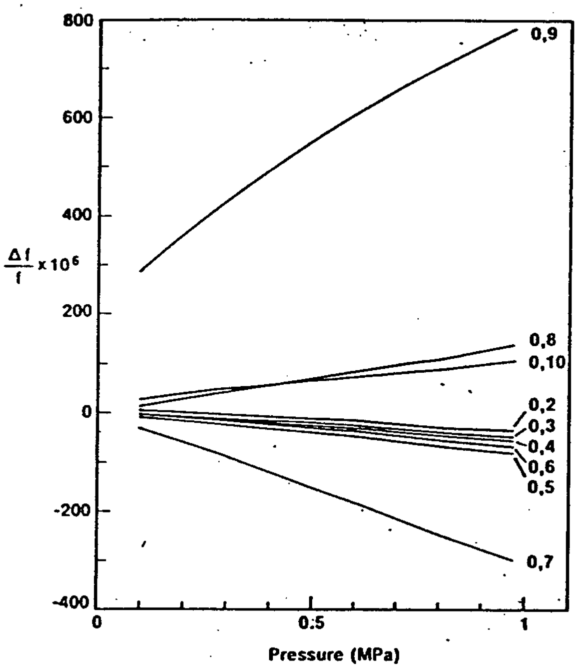

FIG. 9. Measured resonance frequencies minus calculated frequencies (scaled by 10^6/frequency) for (0,s) modes. Here, the calculation includes the effect of the thermal boundary layer and holes in the resonator; however, the calculation omits the effect of shell motion. The linear dependence of $\Delta f/f$ on pressure is a result of shell motion. The slopes depend upon the proximity of the gas resonances to the shell breathing resonance near 20.2 kHz.

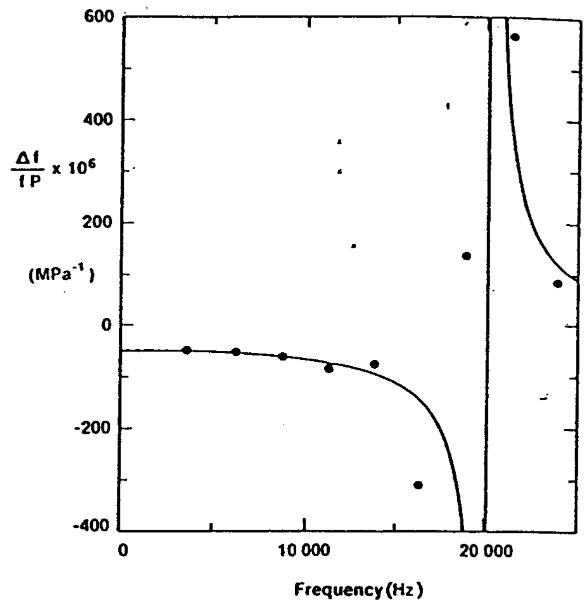

FIG. 11. Response of the shell to radially symmetric excitation as a function of frequency. The points are the average slopes of the curves in Fig. 9. The curve is calculated for an isotropic seamless shell using the theory of elasticity and the elastic constants tabulated for aluminum (see Table V). The idealized shell has a breathing resonance near 20.2 kHz.

Aluminum, 1 liter

Steel
3 liters

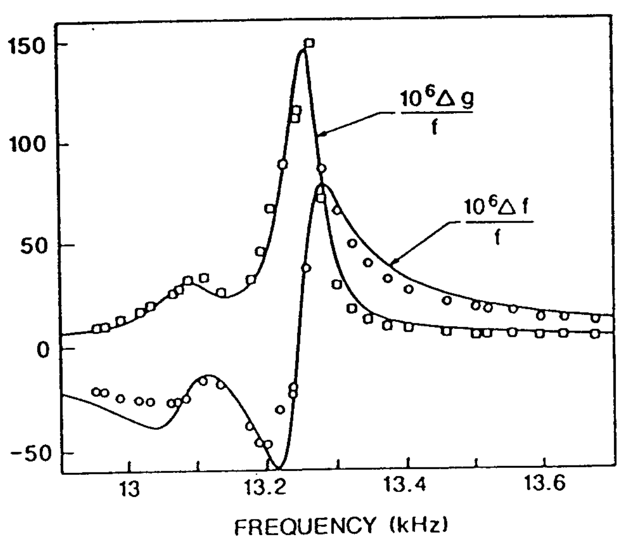

Figure 7. Perturbations to the frequency and half-width of (0,8) mode as a function of frequency, with argon in the resonator at 100 kPa. The frequency was swept by changing the temperature of the resonator, which changes the speed of sound.

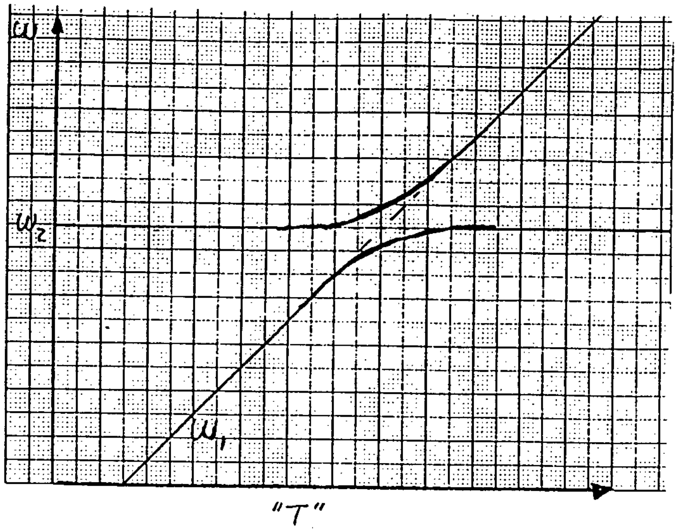

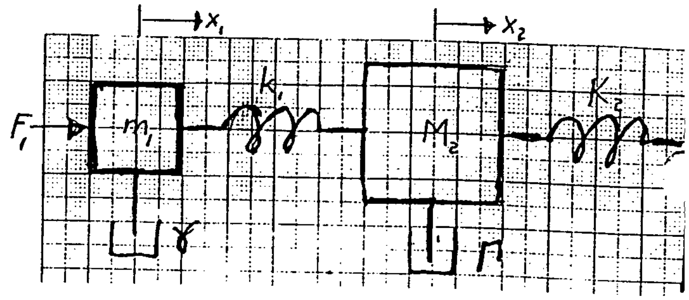

$$\frac{Am_1}{F_1} = \frac{1}{\omega^2 - (\omega_1^2 + i\omega\omega_1/Q_1) - \dfrac{\omega_1^4(m_1/M_2)}{\omega^2 - (\omega_2^2 + i\omega_2/Q_2 + \omega_1^2(m_1/M_2))}}$$

$\frac{m_1}{M_2} = 0.0002$ $Q_1 = 500$

$Q_2 = 100$

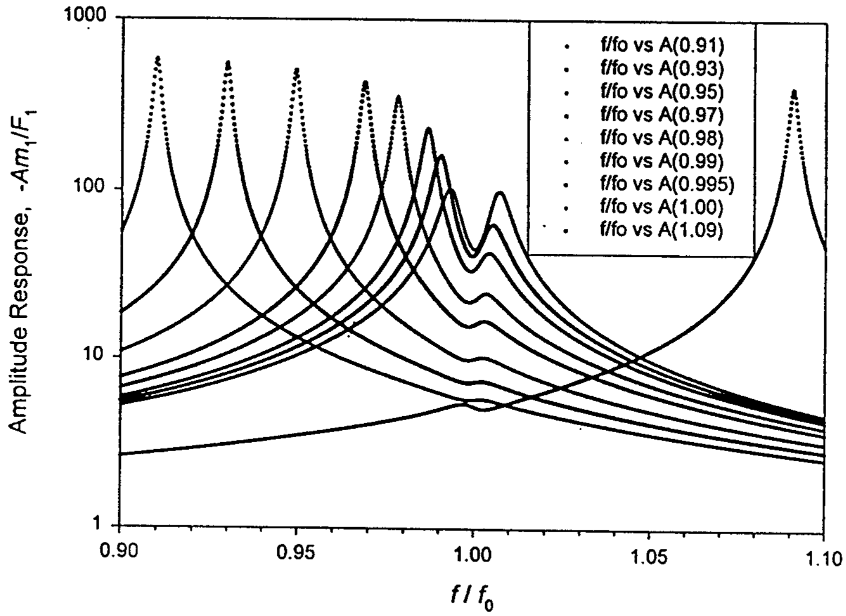

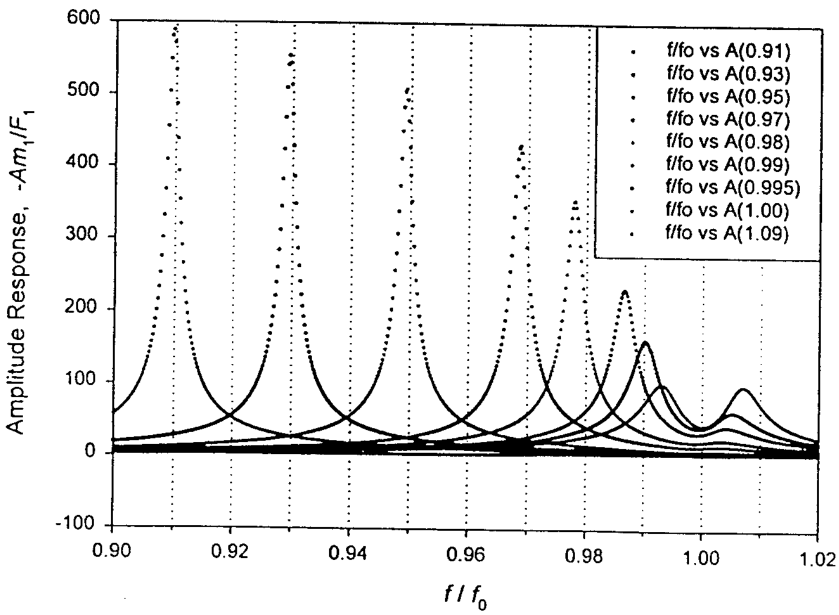

Volume Measurements

Cook 1955 – 1961

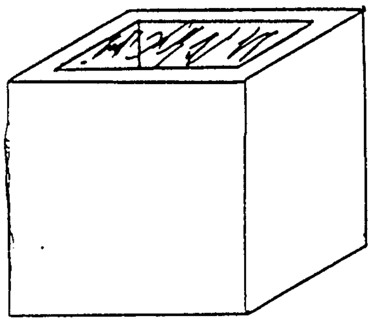

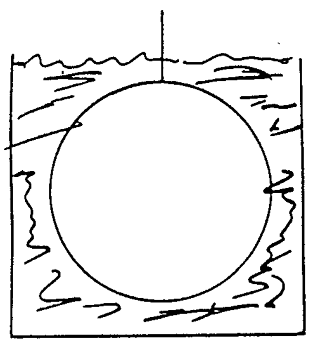

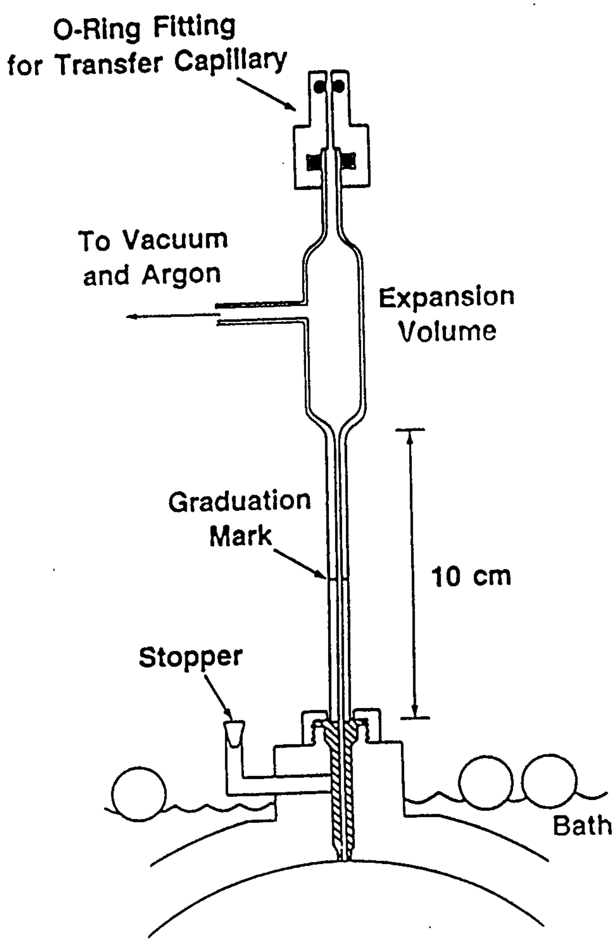

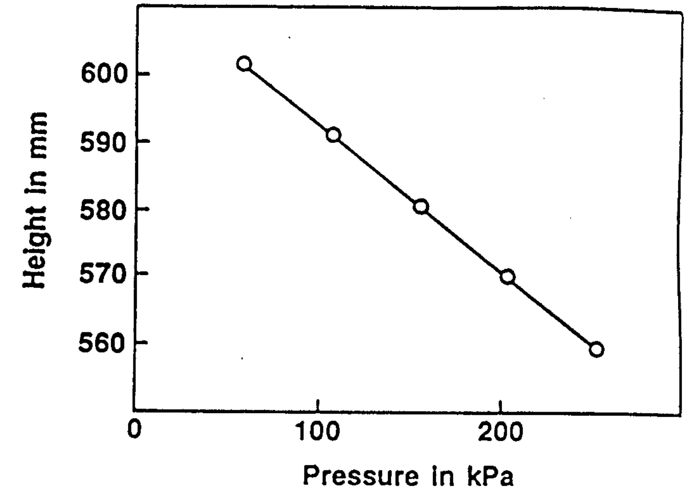

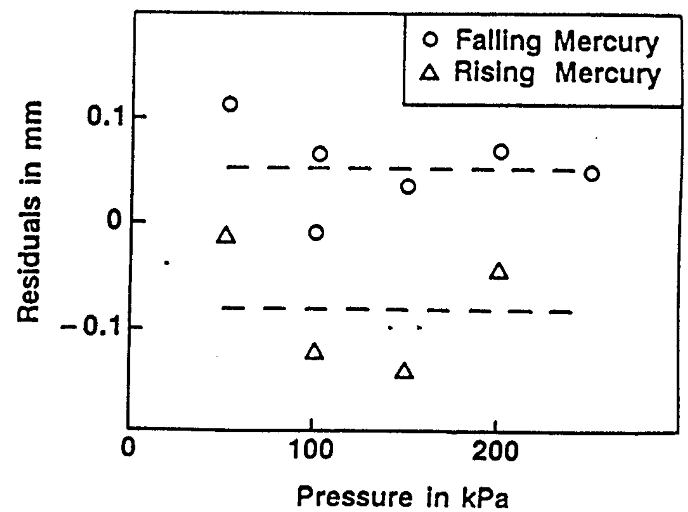

$$C^2_{mix} = \frac{\gamma_{mix} RT}{M_{mix}} = \frac{C_{p1}(1-x) + xC_{p2}}{C_{v1}(1-x) + xC_{v2}} \frac{RT}{M_1(1-x) + M_2 x}$$

where x is mole fraction of component 2.

Table 9. Sensitivity of c_0^2 to impurities

Impurity	M (g/mol)	γ_0	$\frac{1}{c_0^2}\frac{d(c_0^2)}{dx}$ in He	in Ar
H_2	2	1.4	0.23	0.68
He	4	5/3		0.9
H_2O	18	1.32	−3.93	0.12
Ne	20	5/3	−4.0	0.5
N_2	28	1.4	−6.27	0.03
O_2	32	1.4	−7.3	−0.07
Ar	40	5/3	−9.0	
CO_2	44	1.4	−10.3	−0.37
Kr	84	5/3	−20.0	−1.1
Xe	131	5/3	−31.8	−2.3
Hg	201	5/3	−49.0	−4.0

Table 10. Speed of sound ratio determinations

Gas	Comment	$10^6\left(\frac{c(\text{gas})}{c(\text{Ar-M})}-1\right)$	Pressure (kPa)	Date
Ar-A		0.22	115	May 1, 1987
Ar-A		0.27	151	May 2, 1987
Ar-A		0.35	117	May 21, 1987
Ar-40	unprocessed	−191.5[a]	105	May 5, 1987
Ar-40	purified 26 h	−184.63	105	May 4, 1987
Ar-40	purified 120 h	−183.92	131	May 14, 1987
Ar-40	purified 240 h	−184.35	117	May 20, 1987
Ar-40	purified 240 h	−184.00	104	May 22, 1987

[a] The value listed is the mean determined from the (0,2)–(0,6) modes. The rms deviation from the mean for a single ratio was 1.0 ppm for the unprocessed Ar-40 and about 0.1 ppm for all other cases.

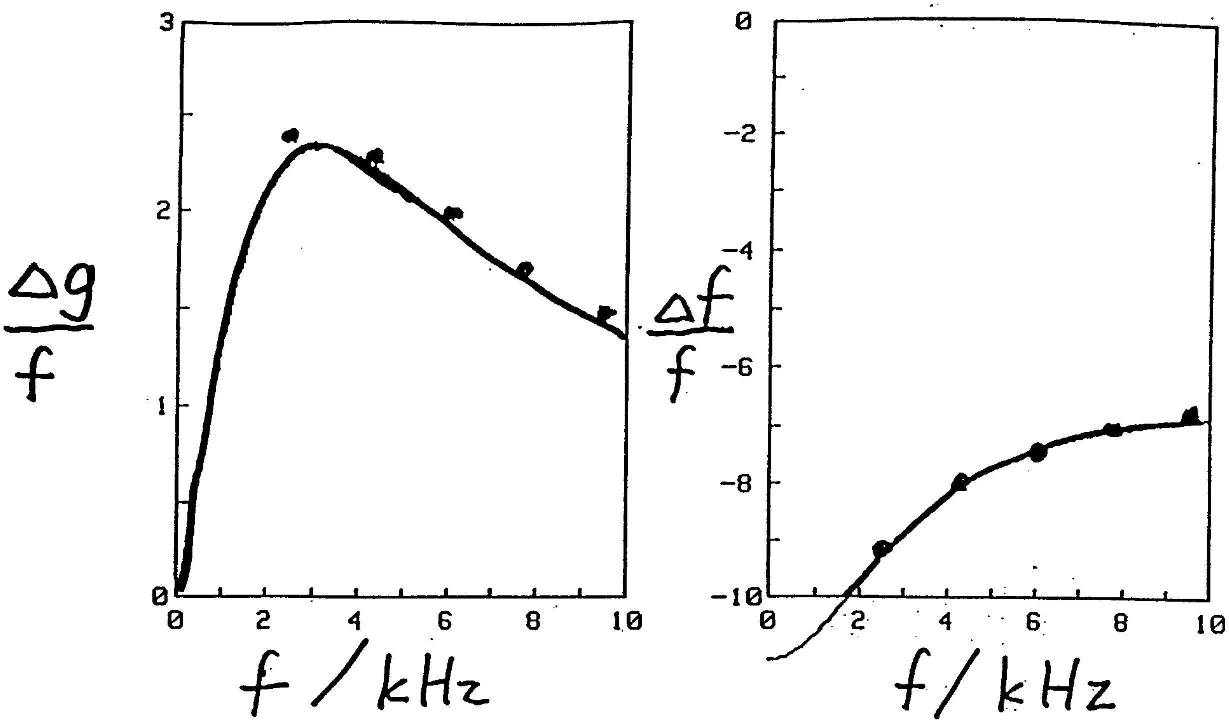

$$\frac{\Delta g}{f} = \frac{2X}{15} \frac{\omega\tau}{1+(\omega\tau)^2}$$

$$\frac{\Delta f}{f} = -\frac{2X}{15}\left[1+\frac{1}{1+(\omega\tau)^2}\right] - \frac{X}{20}$$

$$X = 35 \text{ ppm}$$

$$\frac{1}{\tau_m} = \underset{\substack{\uparrow \\ 50\,\mu s}}{\frac{1-X}{\tau_{Ar}}} + \underset{\substack{\uparrow \\ 8\,\mu s}}{\frac{X}{\tau_{CO_2}}}$$

Table 1. One-sigma uncertainties (in parts per million) from various sources in the redetermination of R

I	$(\text{Volume})^{2/3}$		
	density of mercury at 20 °C	0.81	0.28
	storage and handling of mercury		0.20
	thermal expansion of mercury (0-20 °C)		0.67
	random error of volume measurements		0.20
	corrections from weighing configuration to acoustics configuration		0.10
	mass of counterweights		0.14
II	Temperature		
	random error of calibrations	0.89	0.8
	temperature gradient		0.4
III	M/γ_0		
	Ar-40 standard	0.81	0.7
	comparison of working gas to Ar-40		0.4
IV	Zero-pressure limit of $(f_{0n}/v_{0n})^2$		
	s.d. of c_0^2 from 70 observations at 14 pressures	0.92	0.68
	thermal boundary layer correction (0.3% of thermal conductivity)		0.30
	possible error in location of transducers		0.55
	Square root of the sum of the squares		1.7

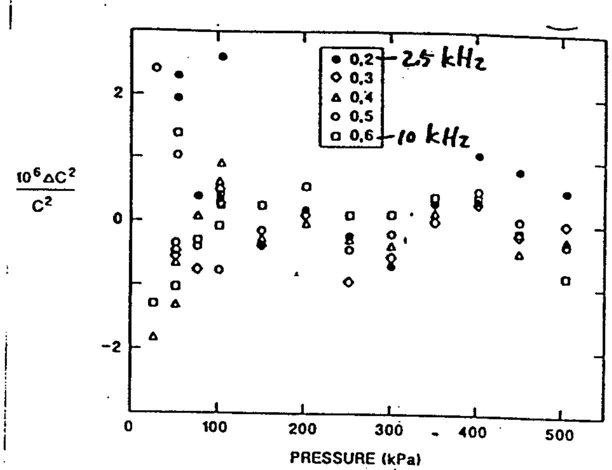

$$\frac{c^2}{a^2} - A_3 p^3 = A_0 + A_1 p + A_2 p^2 + A_{-1} p^{-1}$$

2 ppm — 1 — 10 ppm — 10 ppm — 2 ppm

Goodwin, UCL

$5.40 \pm 0.01 \frac{cm^3}{mol}$

5.5 ± 0.5 Theory

5.24 ± 0.06 Data

accommodation coef

$h = 0.9 \pm 0.1$

Asahi June 13, 1988

気体定数Rの精度
実験で一ケタ向上

一モルの気体定数Rの精度がこれまでよりもほぼ一ケタ向上し、八・三一四四七プラスマイナス〇・〇〇〇一四（誤差百万分の一・七）と実験で求められたことが、筑波研究学園都市で開かれた国際科学技術研究会議で明らかにされた。

発表したのは米国立標準局のマイケル・R・モールドーバー博士。三次の球形の容器に満い アルゴンガスを満たし、共鳴周波数を測定する。ガス圧をゼロに近づけた極限での共鳴周波数を出し、正確な体積などとともにRを求めたという。一モル当たりのジュール単位でとの数値が得られた。

現在使われているRの値は八・三一四五一〇プラスマイナス〇・〇〇〇七〇（誤差百万分の八・四）で、二年前に開かれた国際学術連合の科学技術データ委員会で承認され、八八年版の理科年表にも載っている。モールドーバー博士の求めたRの値は、従来の値の五倍以上の精度を持つ。

工業技術院計量研究所の桜井部長を一昨年招いた森村正直さんは「基礎定数の精度を一ケタ上げる、科学の立場からは画期的な研究だ。ただし、前の基礎定数との調整が必要。そのための科学技術委員会が開かれるのは十年近く先になろう。理科年表の数値が改められるのも、その後になると思う」と話している。

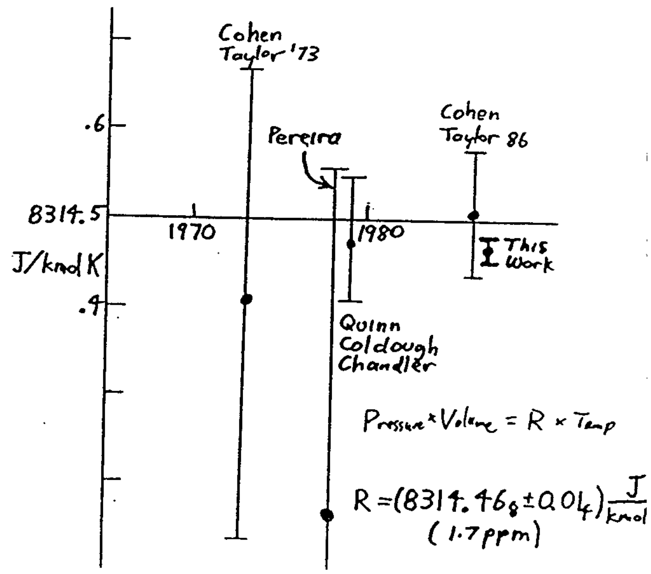

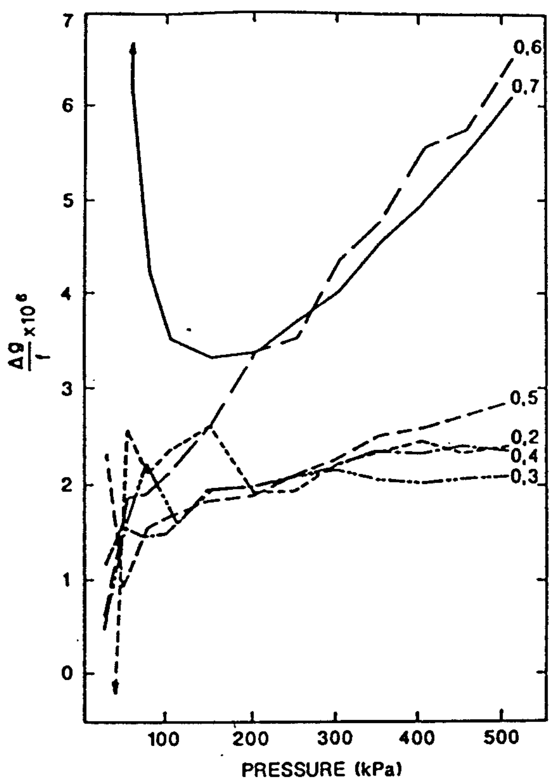

Figure 20. Excess half-widths of (0,*n*) resonances with argon in the resonator scaled by 10^6/frequency. Δg = measured g minus calculated g.

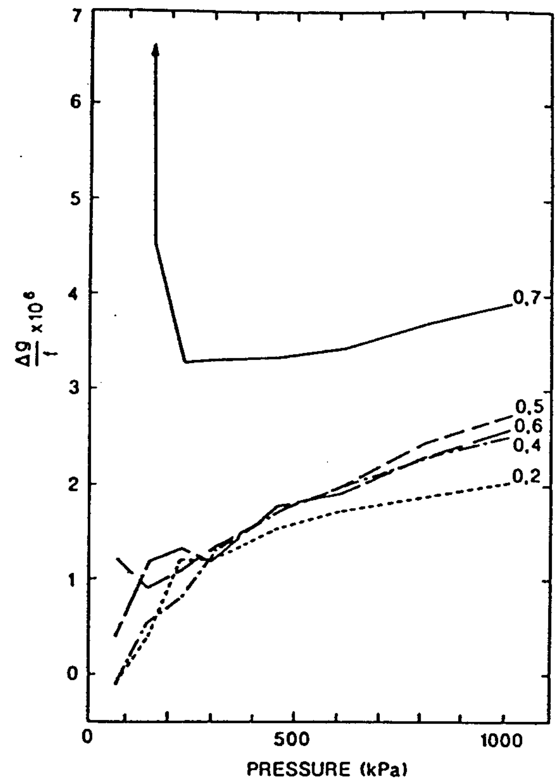

Figure 21. Excess half-widths of (0,*n*) resonances with helium in the resonator scaled by 10^6/frequency. Δg = measured g minus calculated g.

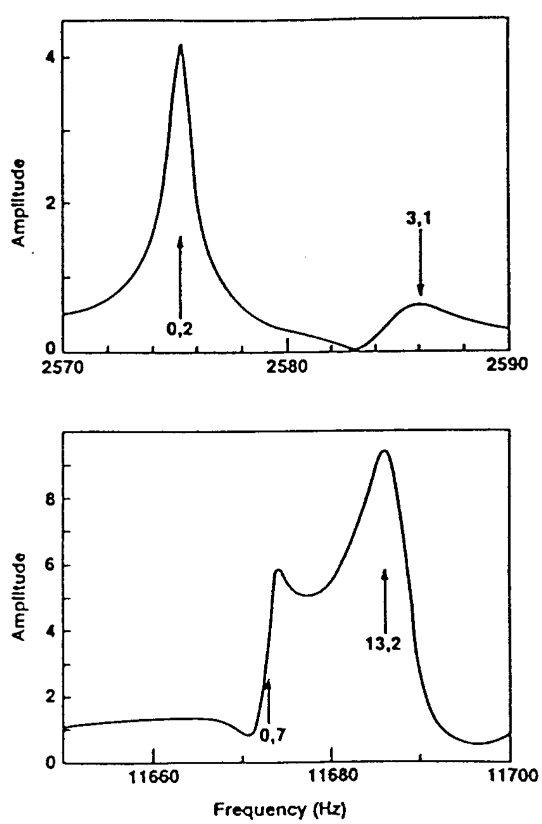

Figure 8. Relative amplitude of the acoustic pressure as a function of frequency in the vicinity of the (0,2) and (0,7) modes.

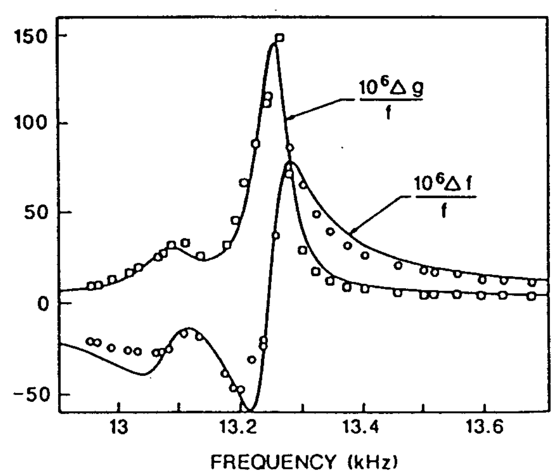

Figure 7. Perturbations to the frequency and half-width of (0,8) mode as a function of frequency, with argon in the resonator at 100 kPa. The frequency was swept by changing the temperature of the resonator, which changes the speed of sound.

Non-radial modes

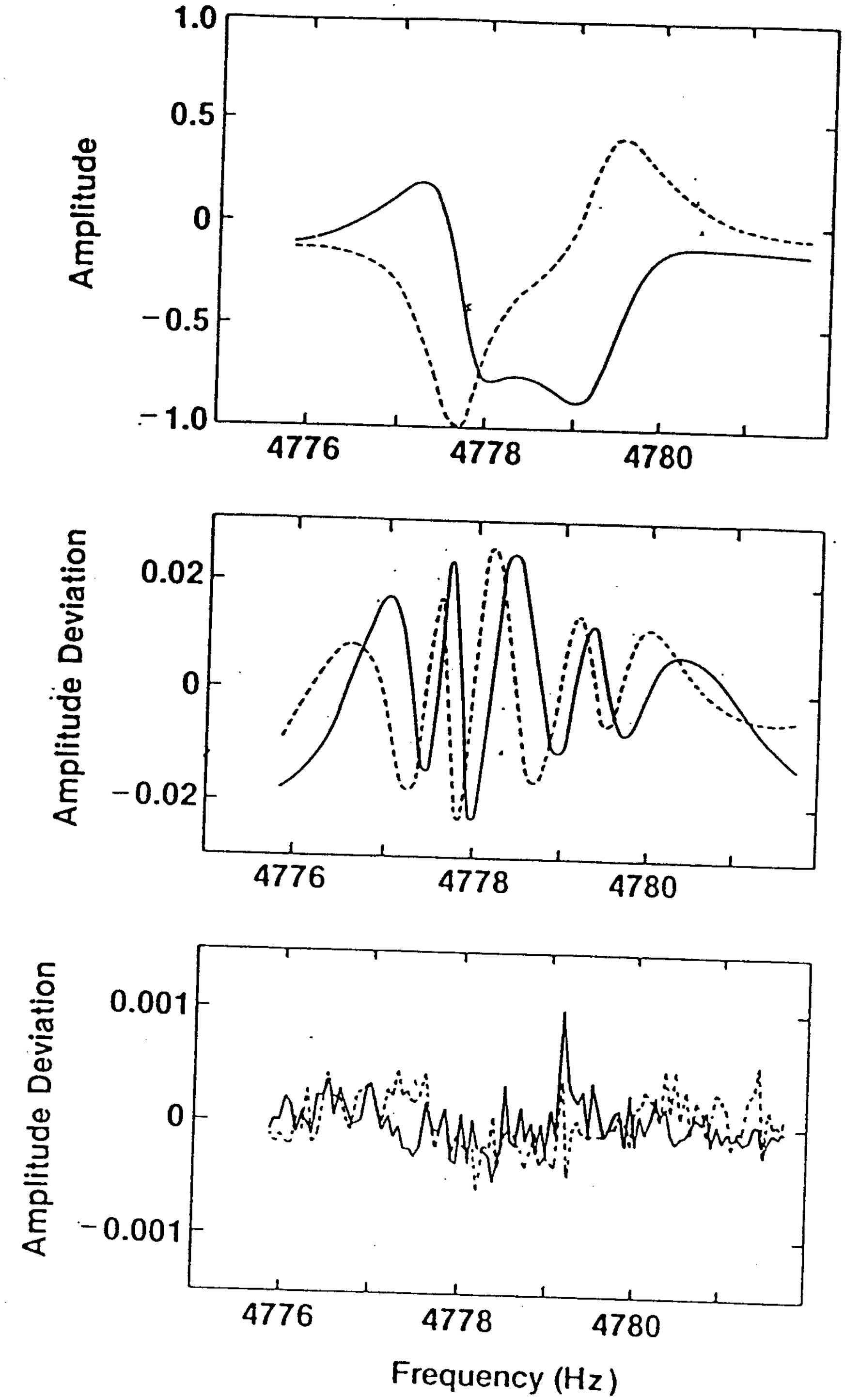

FIG. 5. Top: In-phase (solid curve) and quadrature (dashed curve) voltages from the detector as a function of frequency near the (1,2) resonance in argon at 0.4032 MPa and 296.309 K. Middle: Measured voltages minus two-resonance trial function. Note that the deviations are systematic although the trial function has twelve parameters [eight parameters specify resonances at 4777.63 and 4779.38 Hz, and four specify the constant and linear background terms in Eq. (75)]. Bottom: Measured voltages minus fitted function. The fitted function has sixteen parameters [twelve parameters specify resonances at 4777.693, 4777.903, and 4779.351 Hz with half-widths of 0.550, 0.546, and 0.555 Hz. The remaining four parameters specify B and C in Eq. (75)].

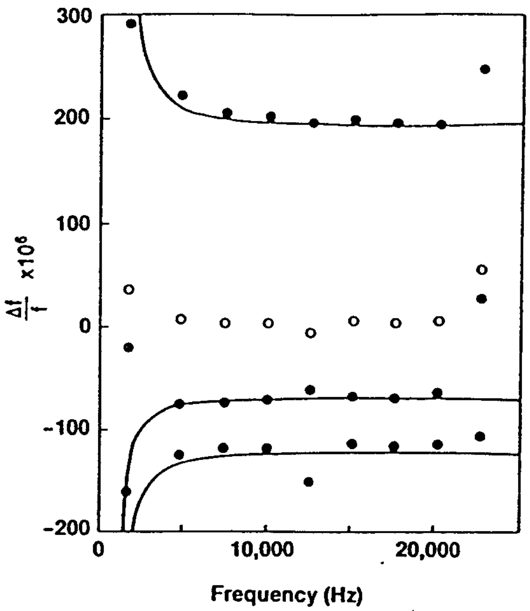

FIG. 16. Measured zero-pressure frequencies minus calculated frequencies for the $(1,s)$ modes. The solid symbols represent the zero pressure intercepts of straight lines fitted to data such as those displayed in Fig. 10. The curves are obtained from Eqs. (68) and (69) with the parameters $\epsilon_0 = 3.5 \times 10^{-4}$ and $\epsilon_1 = 3.1 \times 10^{-4}$. The open symbols are averages of the three zero-pressure frequencies for each $(1,s)$ set of modes. These averages are also plotted in Fig. 15.

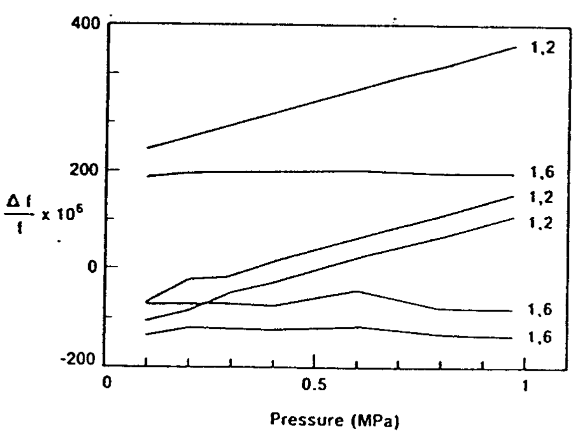

FIG. 10. Measured resonance frequencies minus calculated frequencies (scaled by 10^6/frequency) for the three components of the (1,2) and (1,6) resonances. Here, the calculation includes the effect of the viscous and thermal boundary layers; however, neither the effects of shell motion nor the effects of the holes are included.

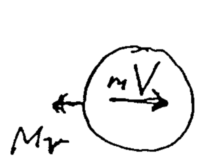

$$\frac{\Delta f}{f} = \frac{m_g}{M_s} \frac{3}{2(\lambda^2-2)}$$

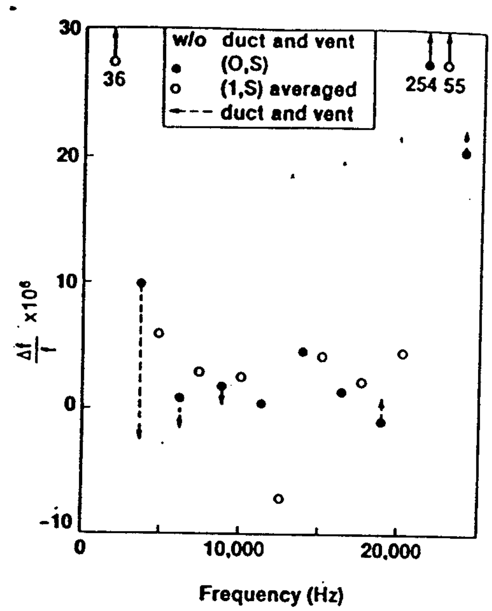

FIG. 15. Measured zero-pressure frequencies minus calculated frequencies for the $(0,s)$ (solid symbols) and $(1,s)$ (open symbols) modes. The symbols represent the zero pressure intercepts of straight lines fitted to data such as those in Figs. 9 and 10. The intercept for the (0,9) mode at 21.4 kHz is 254 parts in 10^6 above the predicted value. The (0,9) mode is close to the resonances in the vent hole and coupling duct.

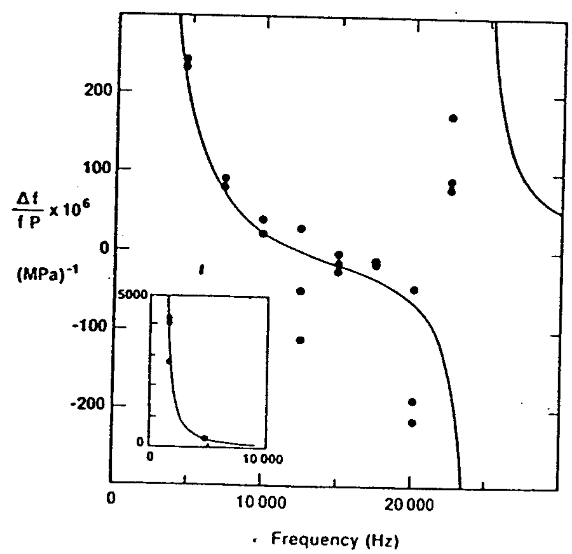

FIG. 12. Elastic response of the shell to excitation with symmetry of $Y_{1m}(\theta,\phi)$ as a function of frequency. The points are the average slopes of curves such as those shown in Fig. 10. The curve is calculated for an isotropic, seamless shell using the theory of elasticity and the elastic constants tabulated for aluminum. The idealized shell has Y_{1m} resonances at 0 and 24.5 kHz.

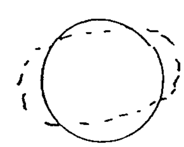

Measurement of the ratio of the speed of sound to the speed of light

James B. Mehl
Physics Department, University of Delaware, Newark, Delaware 19716

Michael R. Moldover
Thermophysics Division, National Bureau of Standards, Gaithersburg, Maryland 20899
(Received 2 June 1986)

Measurements of the resonance frequencies of the acoustic modes and of the microwave modes of a single cavity can determine u/c, the ratio of the speed of sound of a gas to the speed of light. Such measurements with a monatomic gas would determine the thermodynamic temperature T with unprecedented accuracy. By judicious choices of cavity geometry and resonance modes, u/c can be measured to part-per-million accuracy using cavities whose geometry is known only to parts per thousand. These techniques can also be applied to measurements of the universal gas constant R. A measurement of R would also require an accurate determination of the average atomic mass of the monatomic gas.

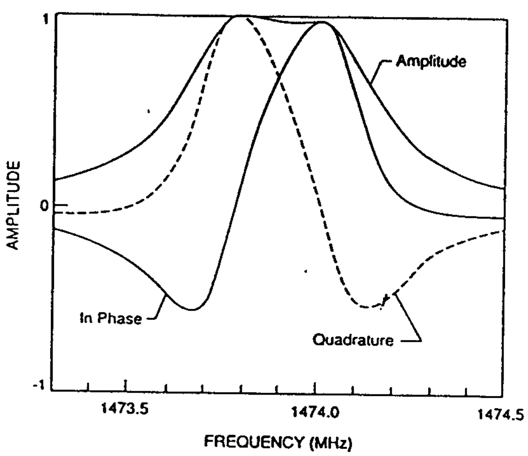

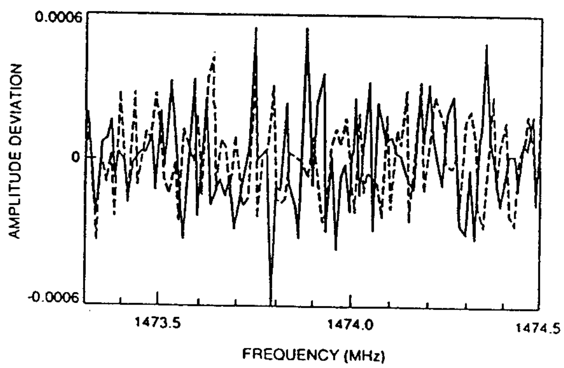

MODE	$10^6 \frac{V(T_g)-V(T_t)}{V(T_t)}$	HALF -WIDTH	# param
TM11	1418.1 ± 0.7	fitted	8
	1418.5 ± 1.0	calc	8
	1419.0 ± 0.4	calc	1
TM12	1416.5 ± 0.8	fitted	9
	1418.1 ± 0.6	calc	9
	1418.2 ± 1.4	calc	1
MERCURY DILATOMETRY	1416.6 ± 1.5		

	Microwave	acoustic
$\frac{\Delta g}{f}$	6-10 ppm	0-2 ppm

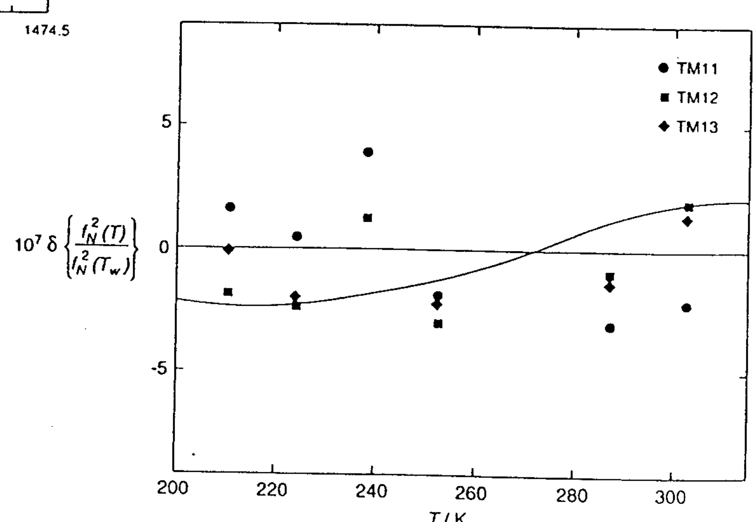

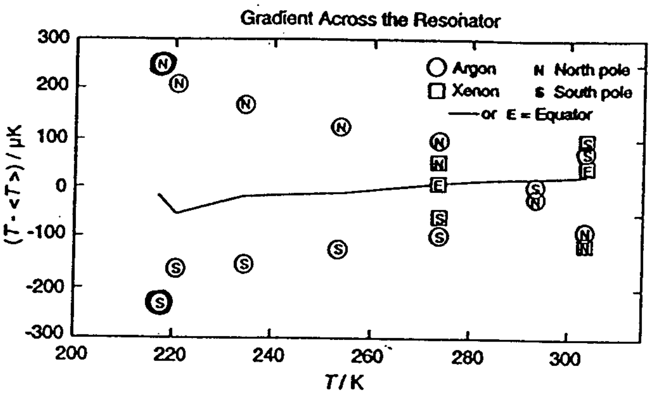

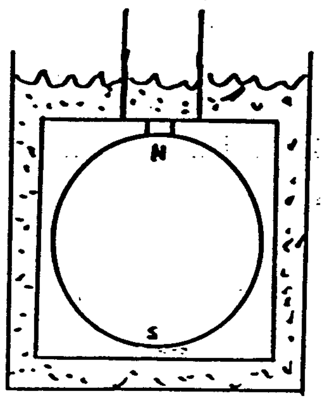

At Present

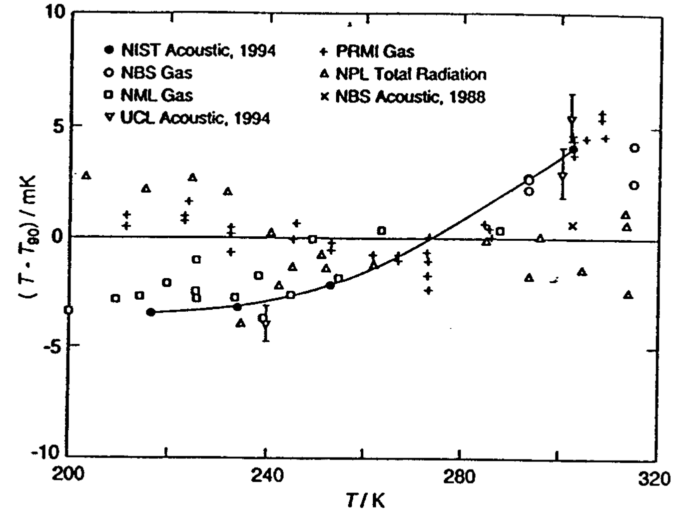

Determination of Thermodynamic Temperatures above 400 K

NBS/NIST results for Constant Volume Gas Thermometry by Guildner and Edsinger (CVGT1) and Edsinger and Schooley (CVGT2) are the most accurate up to approximately 700 K.

Above 700 K, spectral radiometry is used to measure the ratio of radiances from a reference blackbody and from a blackbody at unknown thermodynamic temperature.

Problem: There is an unknown cause of error in the CVGT measurements, and this error grows as $(T_{unknown}/T_{reference})^2$ when radiometry is used to determine thermodynamic temperatures at higher temperatures.

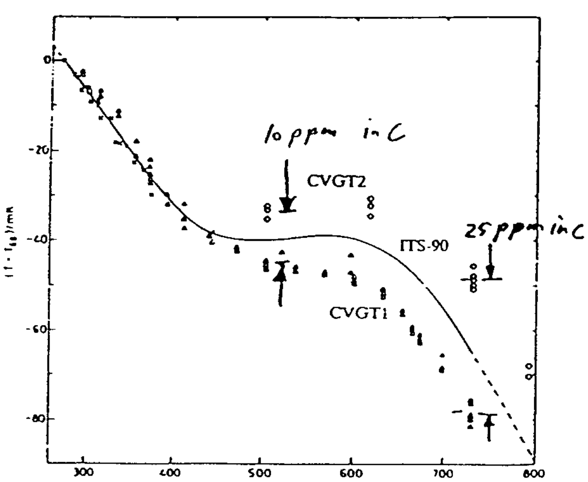

The Future

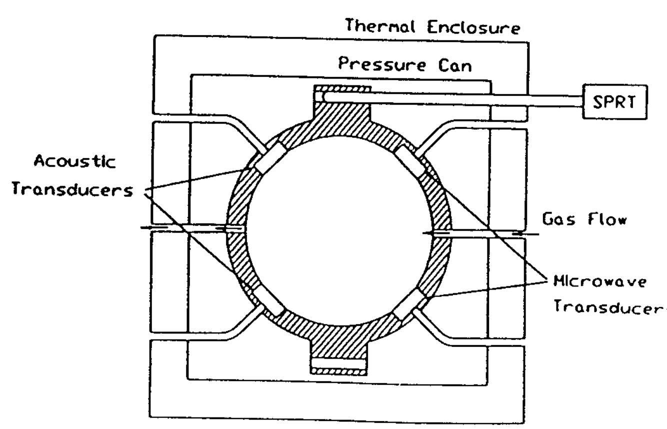

THERMODYNAMIC PROPERTIES

1. Ideal-gas heat-capacity: $C_p^0(T)$

2. Virial equation of state:

$$pV = RT\left(1 + B(T)\rho + C(T)\rho^2 + D(T)\rho^3 + \ldots\right)$$

Note: Resonance techniques are not recommended for liquids because oscillations of container cannot cannot be separated from oscillations of fluid

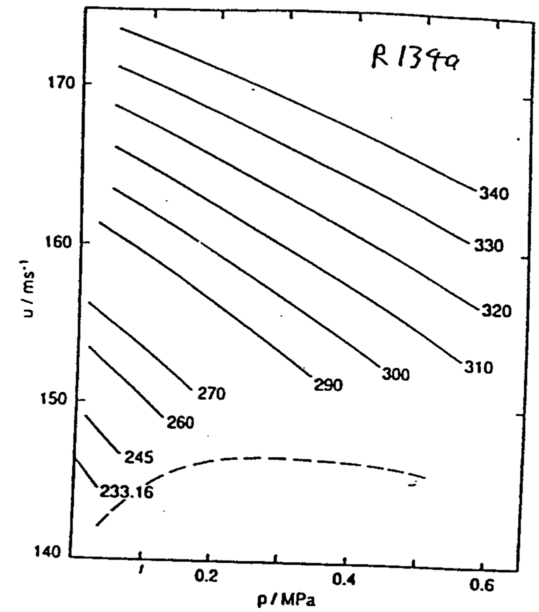

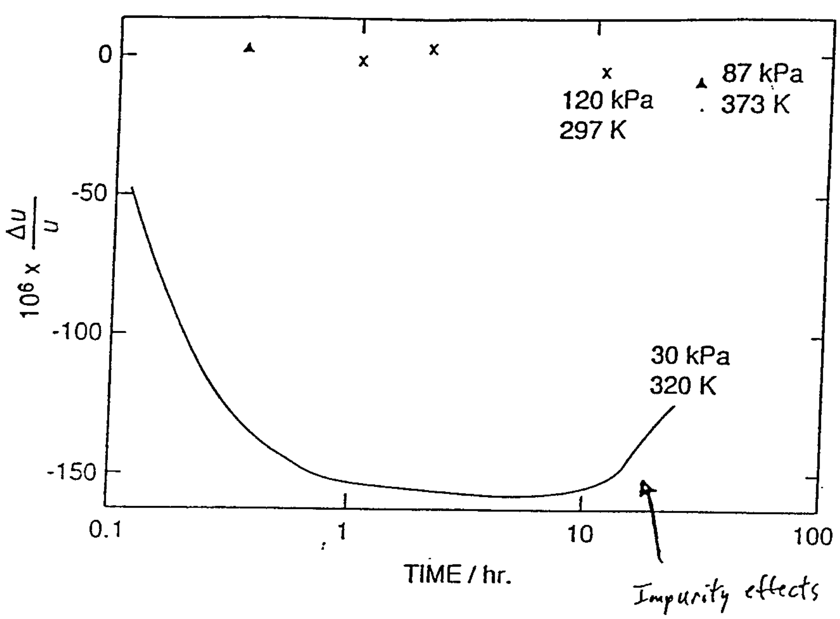

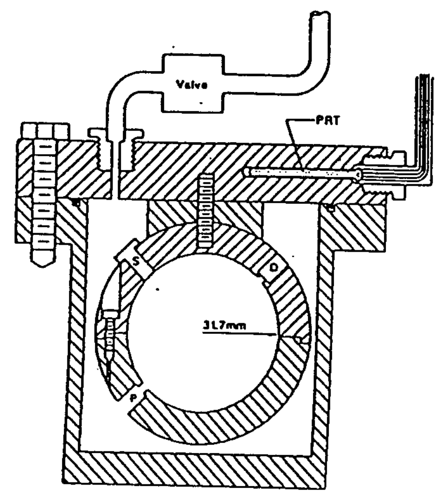

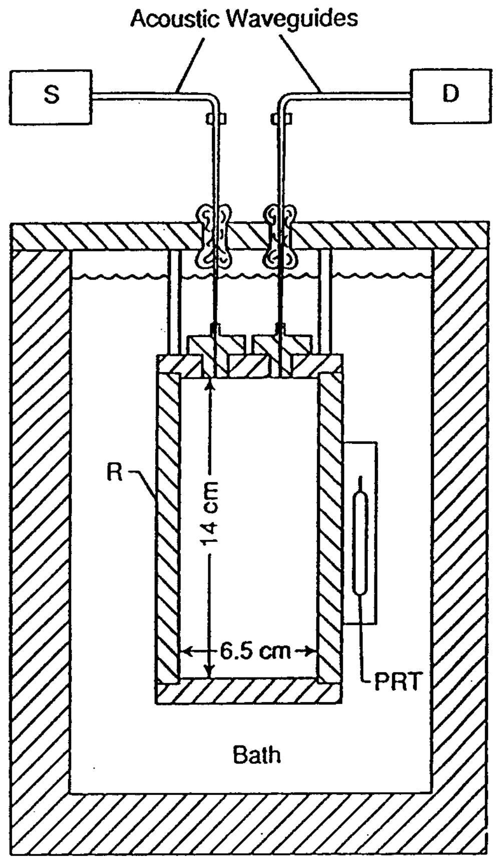
Acoustic Waveguides
S
D
R
14 cm
6.5 cm
PRT
Bath

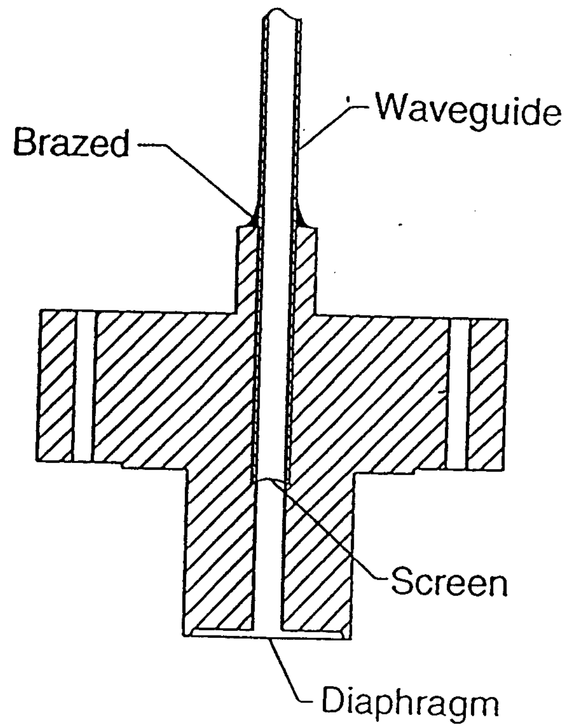
Waveguide
Brazed
Screen
Diaphragm

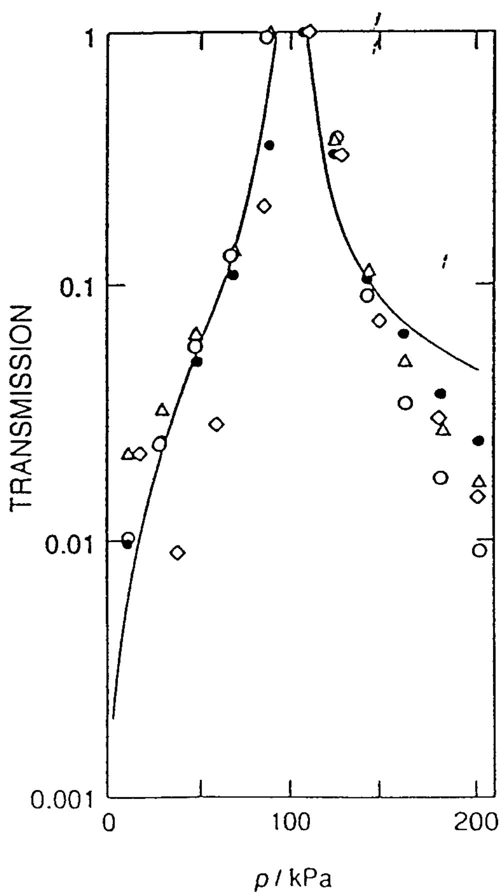
TRANSMISSION
1
0.1
0.01
0.001
0
100
200
p / kPa

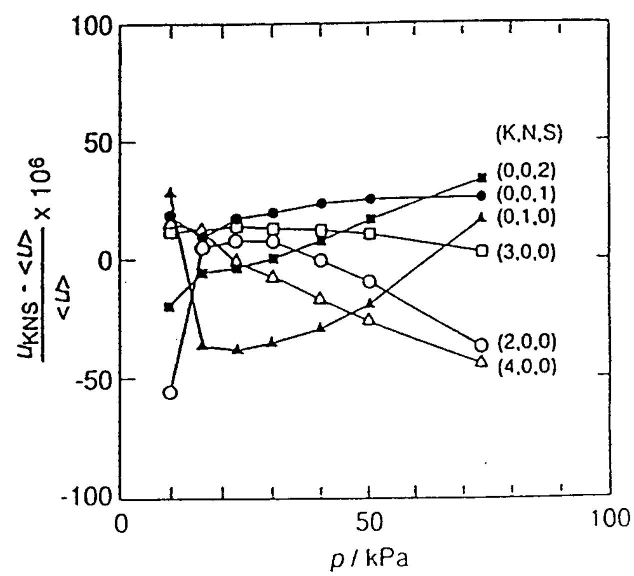
100
50
0
-50
-100
0
50
100
p / kPa
(K,N,S)
(0,0,2)
(0,0,1)
(0,1,0)
(3,0,0)
(2,0,0)
(4,0,0)
x 10^6

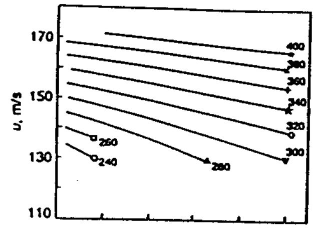

Speed of sound data for CHF_2-CF_3. Pentafluoroethane = refrigerant R125

Temperature range $0.71 \le T/T_c \le 1.18$

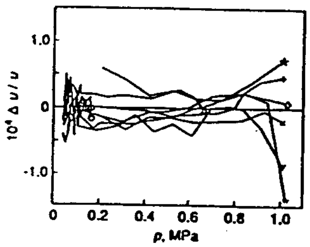

Deviations of data from $u(P,T)$ surface. RMS deviations are $2 \times 10^{-4} \times u$. Impurities cause larger systematic errors. The surface uses 3 parameters for $C_p^o(T)$, (ideal-gas heat-capacity), 3 parameters for each of the virial coefficients $B(T)$ and $C(T)$ and 2 parameters for $D(T)$.

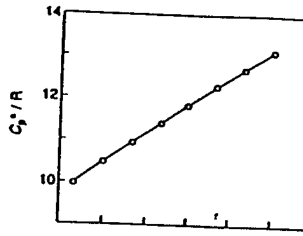

Ideal gas heat capacity of R125, deduced from the speed of sound data through the relation:

$C_p^o(T)/R = Mu_o^2/(Mu_o^2 - RT)$.

R is the universal gas constant; M is the molecular weight and u_o^2 is the zero-pressure limit of $u^2(P,T)$

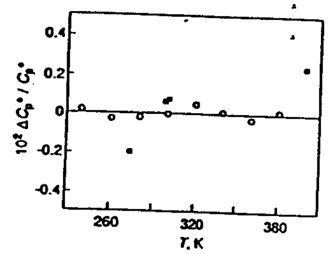

Deviations of $C_p^o(T)/R$ from a polynomial.
- o present data
- ■ independent spectroscopic information (estimated)

compound		temperature range K	maximum pressure kPa	number of isotherms
	Candidate refrigerants for vapor compression cycles			
CF_3-CHF_2	R134a	233 - 340	600	10
$CFCl_2$-CH_3	R141b	260 - 315	.70	5
$CHCl_2$-CF_3	R123	260 - 335	80	6
$CHFCl$-CF_2-Cl	R123a	265 - 300	50	2
CHF_2-O-CHF_2	E134	255 - 327	170	6
CHF_2-O-CHF_2	E134	255 - 374	90	8
CF_3-O-CH_2-CF_3	E245	278 - 384	50	5
CF_3-HF-CHF_2	R236ea	267 - 380	600	8
$CHFCl$-CF_3	R124	250 - 400	900	17
CHF_2-CF_3	R125	240 - 400	1,000	9
CHF_2-CH_3	R152a	240 - 400	1,000	9
CF_3-CH_3	R143a	240 - 400	1,000	9
CF_3-CH_2-CF_3	R236fa	276 - 400	1,000	7
CHF_2-CF_2-CH_2F	R245ca	311 - 400	900	5
CF_3-O-CF_2H	E125	260 - 400	1,000	13
1 composition	R134a/R32/R125	260 - 400	1,000	12
CF_3-CF_2-CF_2-CH_2F	R338mccq	300 - 400	400	6
	Thermoacoustic Refrigeration			
5 compositions	He/Xe	210 - 400	1,500	42
	Semiconductor Processing			
SF_6		230 - 460	1,500	16
CF_4		300 - 475	1,500	9
C_2F_6		210 - 475	1,500	14
Cl_2		~~planned~~ done		
HBr		planned headaches (in progress)		
BCl_3		~~planned~~ done		
WF_6		planned		

Calibration with argon; we measure $f_{argon}/f_{test\ gas}$

method requires stable resonator, frequency standard, and thermometer; however, many errors in calibration can be tolerated.

tolerant of temperature gradients in bath

example: propane, temperature range 210 K - 460 K

$u^2_{propane}$ changes 105%

$(u_{argon}/u_{propane})^2 = (f_a/f_p)^2$ changes 16%

$$\frac{C_p^0(T)}{R} = \frac{Mu^2}{Mu^2 - RT} = \frac{1}{1 - \frac{3}{5}\frac{M_a}{M_p}\left(\frac{f_a}{f_p}\right)^2}$$

to obtain $C_p^0(T)$ to 0.1% requires T to 0.23 K

M_a/M_p to 0.0001

<u>intolerant of impurities</u>, vexing problem with mixtures

inconsistencies among modes < 0.0025%

correlation of $u(p,T)$ < 0.002% r.m.s

excess half-widths: $\Delta g/f$ depending upon mode ~ 0.004% - 0.02%,

$$u^2 = \frac{\gamma^o RT}{M}\left(1 + \frac{\beta_a p}{RT} + \frac{\gamma_a p^2}{RT} + \frac{\delta_a p^3}{RT} + \frac{\epsilon_a p^4}{RT} + \ldots\right)$$

$$\beta_a = 2B + 2(\gamma_0 - 1)T\frac{dB}{dT} + \frac{(\gamma_0 - 1)^2}{\gamma_0}T^2\frac{d^2B}{dT^2}$$

$$\rho = \frac{p}{RT}\,\frac{1}{1 + B\rho + \cdots}$$

Problem: No initial conditions

Ansatz: $B(T)' = b_0[1 + (r^3 - 1)(e^{\frac{\epsilon}{k_B T}} - 1)]$

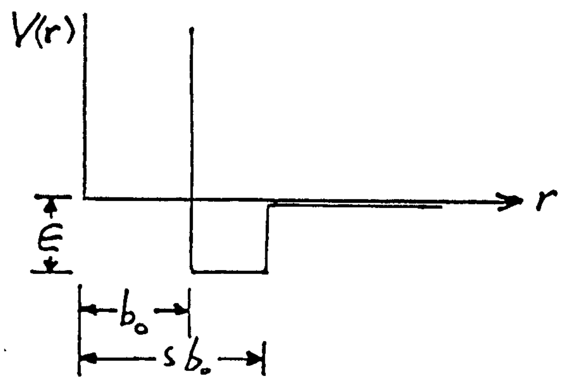

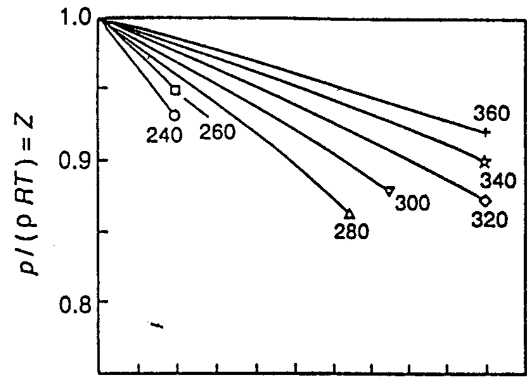

Compression factor of R125 deduced from $u(P,T)$ data using the virial equation. The virial coefficients were assumed to have the temperature dependencies of a hard-core square-well intermolecular potential and the parameters in the potentials were fitted to the $u(P,T)$ data.

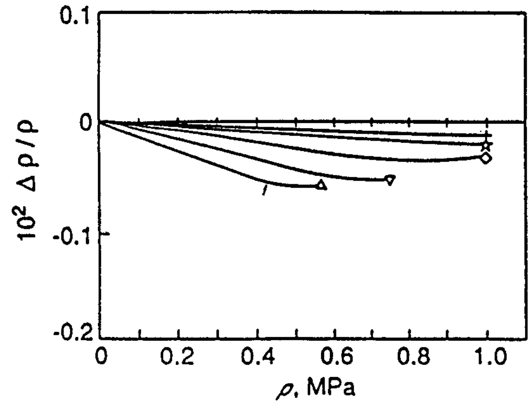

Fractional deviations of the density of R125 deduced from $u(P,T)$ data from independent density measurements by Boyes and Weber.

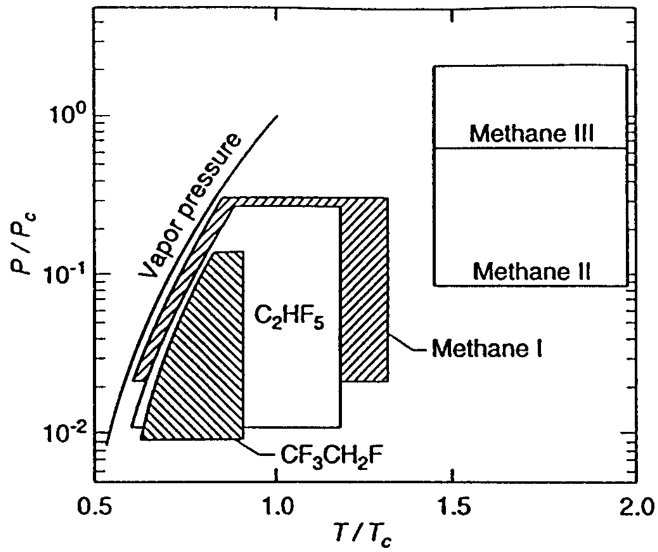

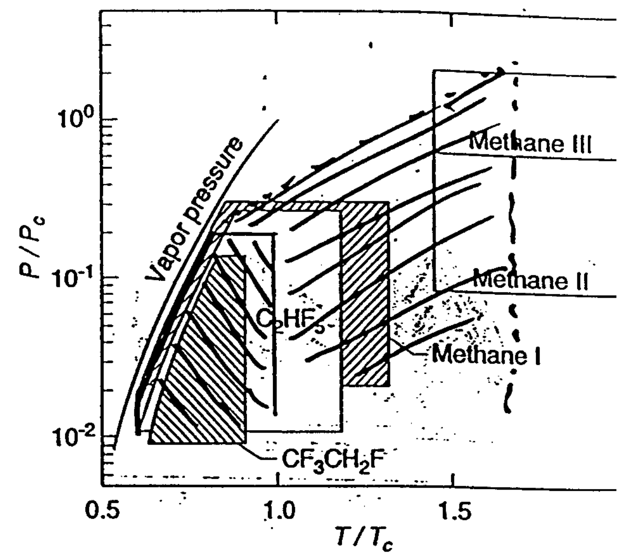

Estrada-Alexander, Trusler.
4-parameter potential
+ 3 body parameter

(11)

TRANSPORT PROPERTIES

1. Greenspan acoustic viscometer for η:

   hard sphere of diameter σ

$$\eta = \frac{(mk_B T)^{1/2}}{\pi^{3/2}\sigma^2}$$

2. Prandtl number machine

$$Pr = \frac{C_p \eta}{\lambda} = \frac{\text{viscous diffusivity}}{\text{thermal diffusivity}}$$

$$= \frac{2}{3} \text{ for hard sphere}$$

3. If time permits, electromagnetic equivalent of Greenspan viscometer: reentrant resonator

Helium

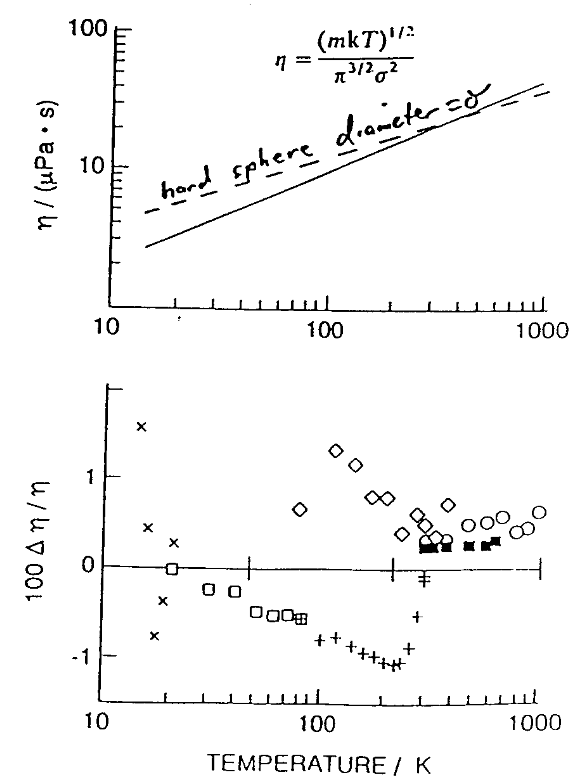

(14)

Loss mechanisms spatially separated in standing waves.

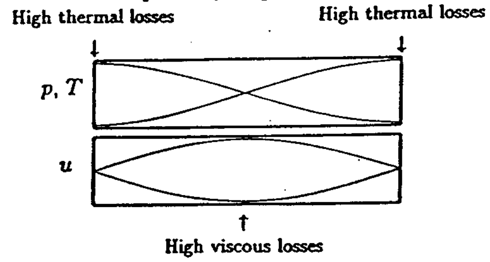

Greenspan viscometer: $\lambda \gg$ length

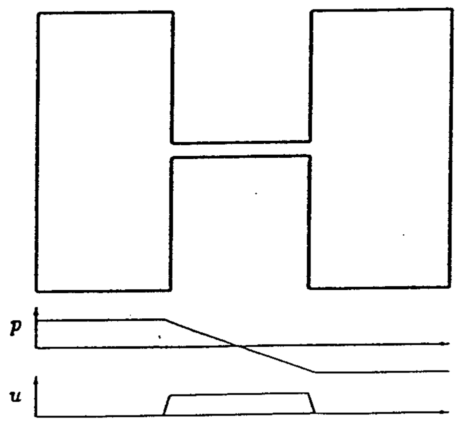

Double Helmholtz Resonator

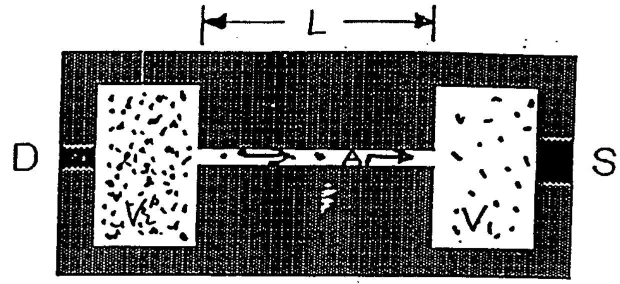

$$\omega_0^2 = \frac{c^2 A}{L}\left[\frac{1}{V_1} + \frac{1}{V_2}\right]$$

$$\omega_1^2 = \frac{\omega_0^2\left(1-(1-i)\frac{\delta_v}{2a}\right)}{1+(1-i)(\gamma-1)\frac{\delta_c S}{2V}}\left\{1+\cdots\right.$$

Acoustic pressure contours near duct end

Calculated from solutions of

$$(\nabla^2 + k^2)p(\mathbf{r}) = 0$$

$$\frac{\partial p}{\partial n} = 0 \quad \text{on boundary}$$

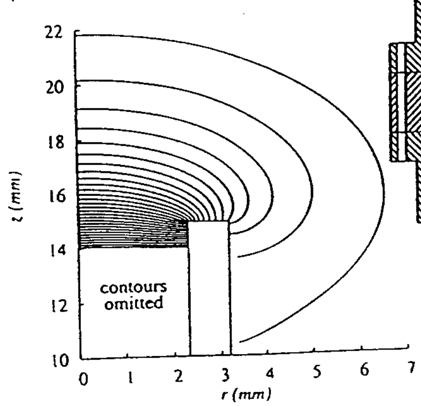

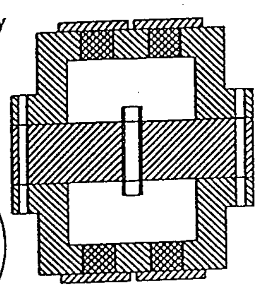

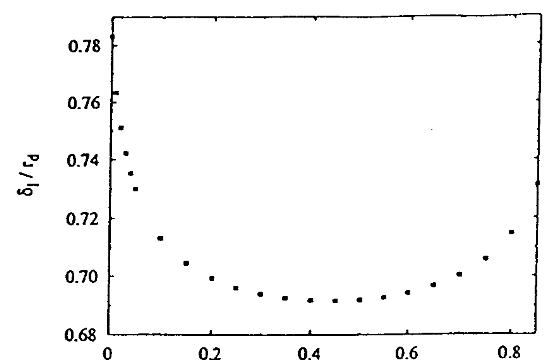

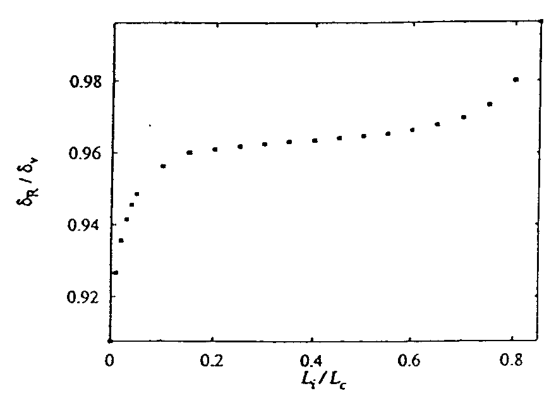

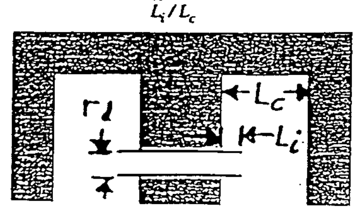

Orifice cross-sections

Sharp corners Rounded corners

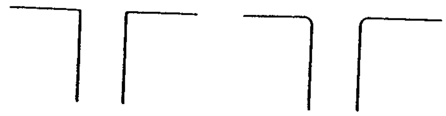

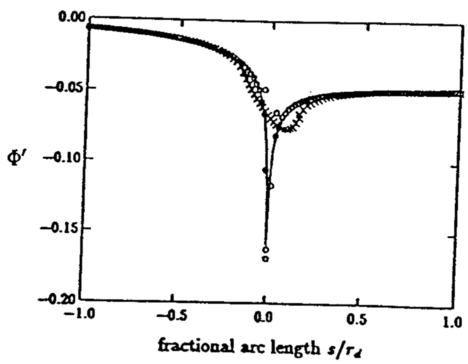

$$\frac{R(r_{ch})}{R(0)} = 1 - \frac{1}{3}\left(\frac{r_{ch}}{r_d}\right)^{(1/3)}$$

$R(0) = 0.9\delta_V$ $R(r_d) \approx 0.6\delta_V$

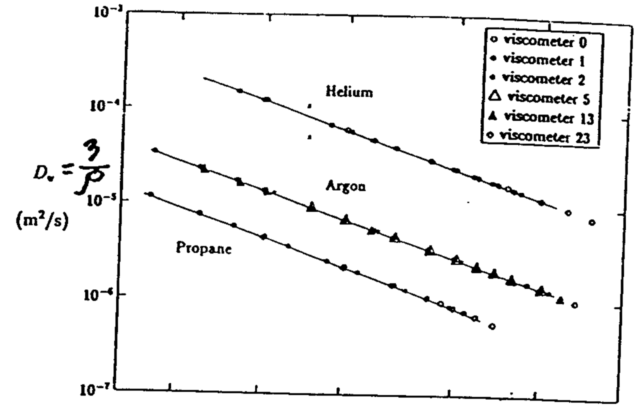

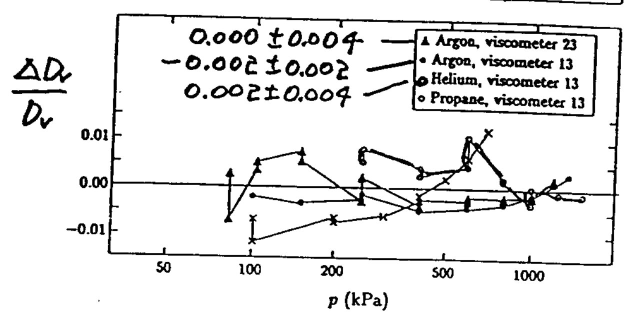

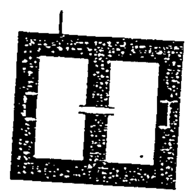

Viscometer 12 0.001 ± 0.006

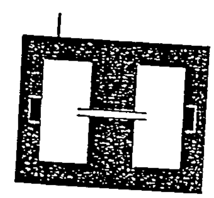

Viscometer 13 −0.002 ± 0.003

Greenspan viscometer as an absolute instrument
(no calibration)— Coordinate measuring machine.
Argon in 4 viscometers
Experimental η compared with reference values

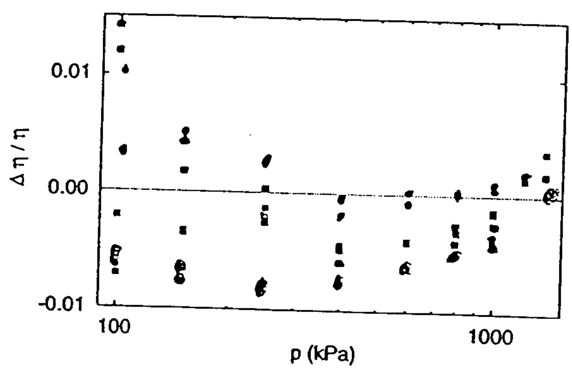

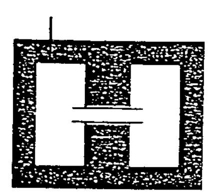

Viscometer 23 0.002 ± 0.003

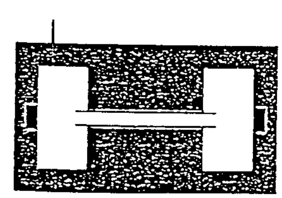

Viscometer 24 −0.005 ± 0.003

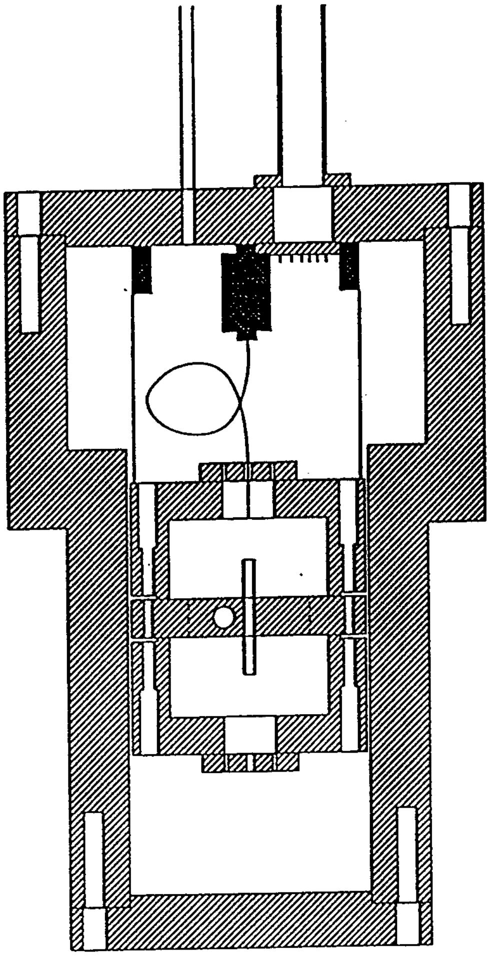

Greenspan Viscometer

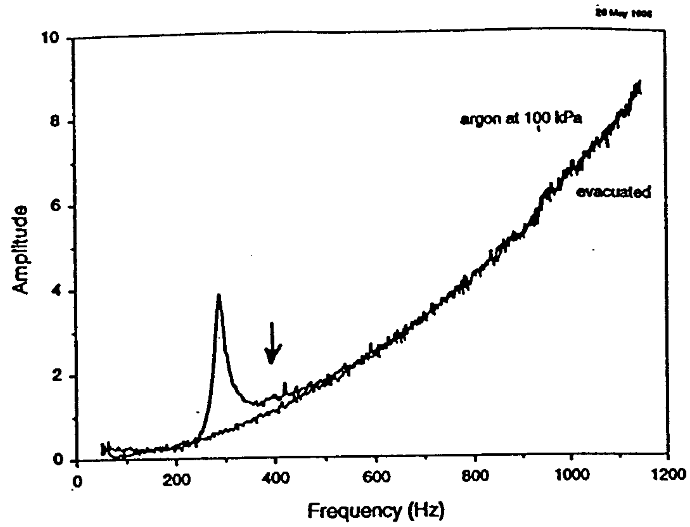

Argon (280 K; 977 kPa)

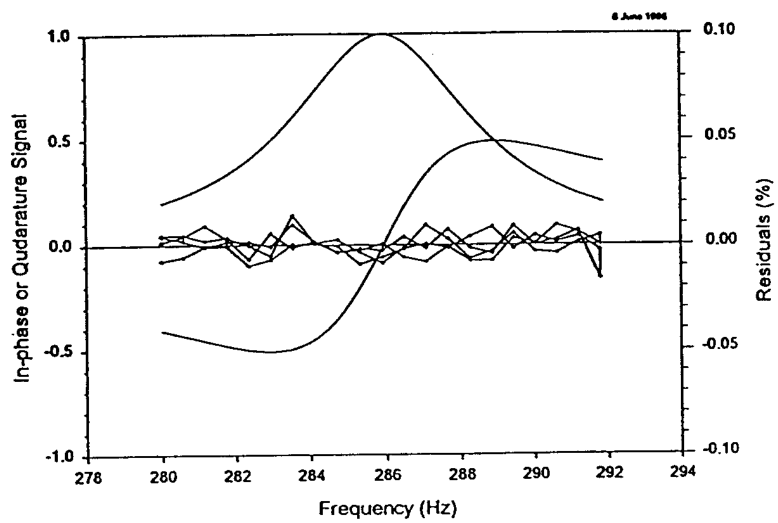

Helium 1.8 MPa (Argon in pressure vessel)

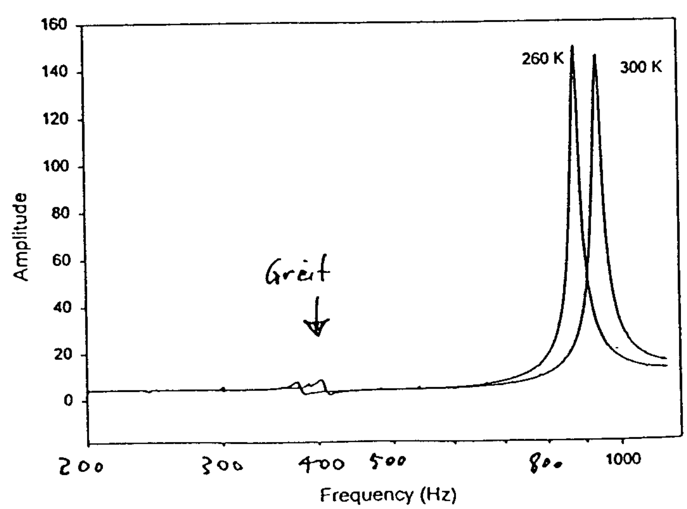

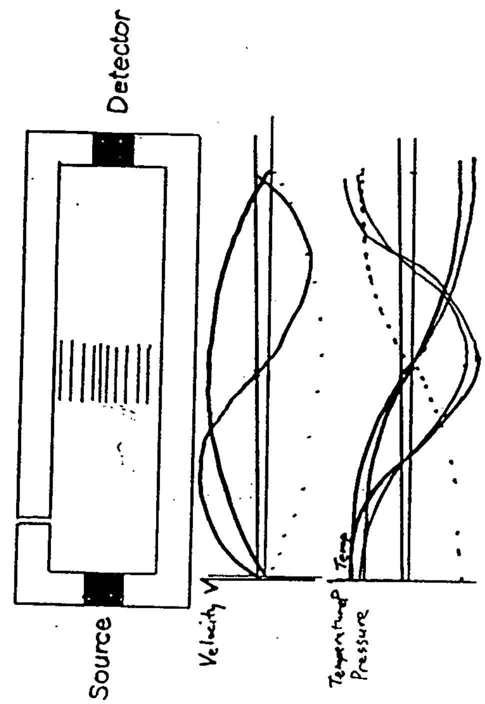
Source
Detector
Velocity V
Temperature
Pressure
Temp

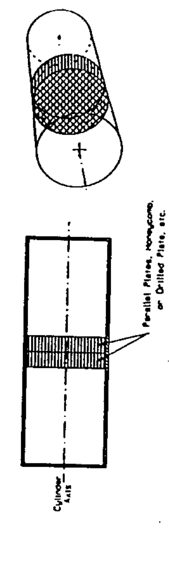
Cylinder Axis
Parallel Plates, Honeycomb, or Drilled Plate, etc.

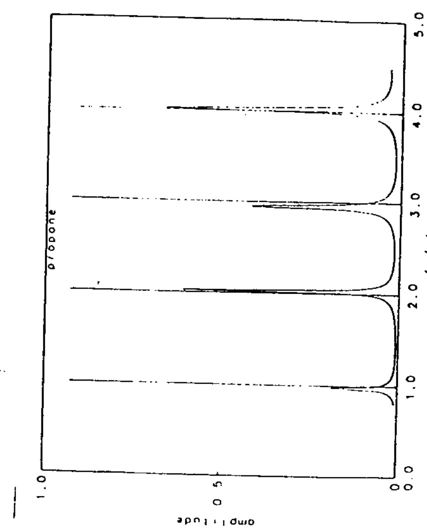
propane
amplitude

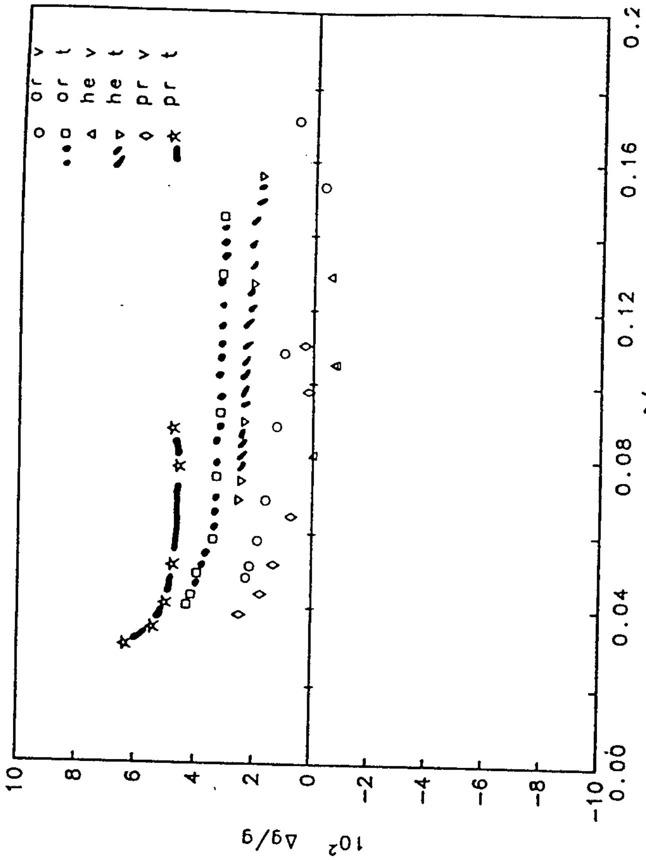
ar v
ar t
he v
he t
pr v
pr t
$10^2\ \Delta g/g$
δ/r_h

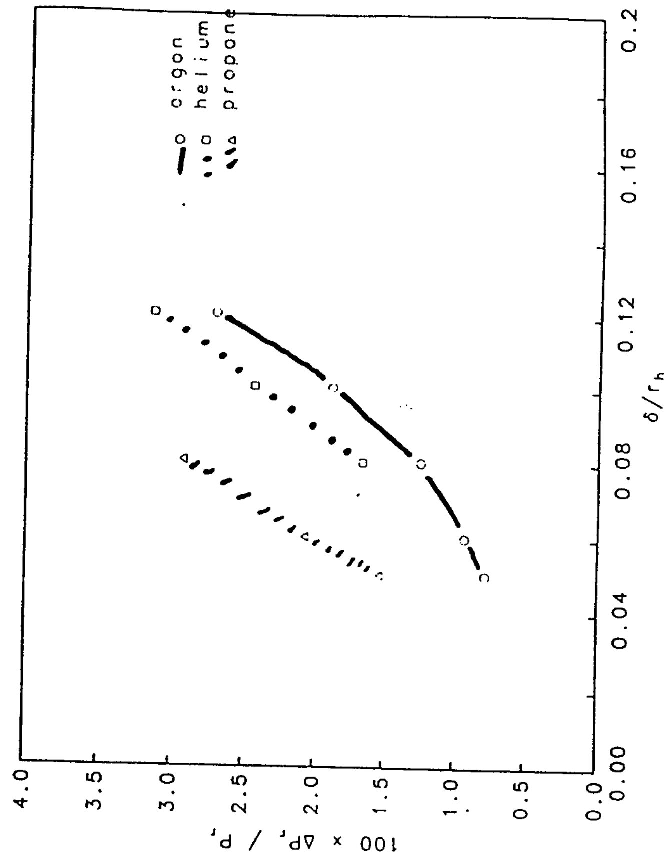
argon
helium
propane
$100 \times \Delta P_r\ /\ P_r$
δ/r_h

A winner in the annual Bulwer-Lytton contest for the best bad writing:

"As a scientist, Throckmorton knew that if he were ever to break wind in the sound chamber, he would never hear the end of it."

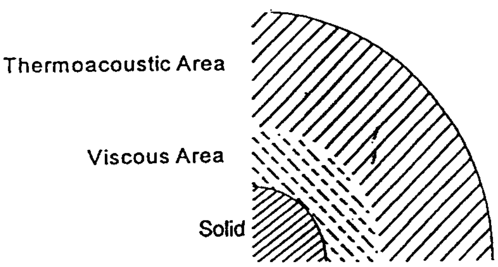

$$\frac{\text{Viscous Area}}{\text{Thermoacoustic Area}} = \left(\frac{\delta_v}{\delta_T}\right)^2 = \text{Prandtl Number} = \frac{\eta C_p}{\lambda}$$

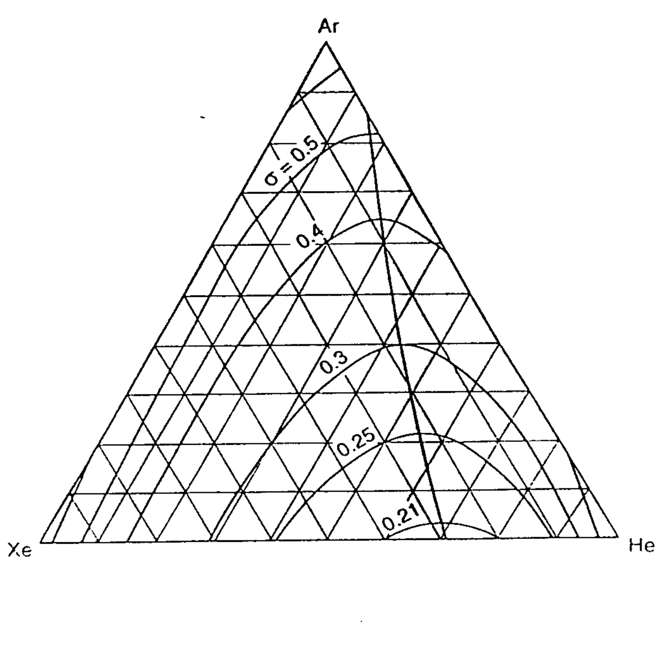

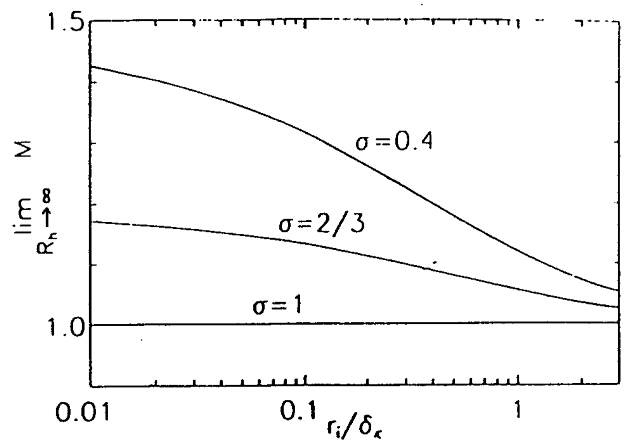

FIG. 3. A figure of merit giving the ratio of inviscid thermoacoustic heat transport to viscous power dissipation, as a function of pin size, in the large-pore-size limit. Results for three Prandtl numbers are shown: $\sigma=1$; $\sigma=0.67$, such as for pure monatomic gases; and $\sigma=0.4$, such as for dilute mixtures of argon or xenon in helium. For small enough pin radius, and for small enough Prandtl number, the pin stack is significantly superior to parallel plates or circular pores, for which $\lim_{R_h\to\infty} M = 1$ for all σ.

$$M=\sqrt{\sigma}\,\mathrm{Im}[\,f_\kappa]\,|1-f_\nu|^2/\mathrm{Im}[\,f_\nu] \tag{8}$$

of these two quantities as a tentative figure of merit for comparison of different stack geometries. We include the factor $\sqrt{\sigma}$ (where $\sigma=\mu c_p/K$ is the gas's Prandtl number) in M so that when $R_h\to\infty$ for circular pores and parallel plates, $M\to 1$ independent of σ.

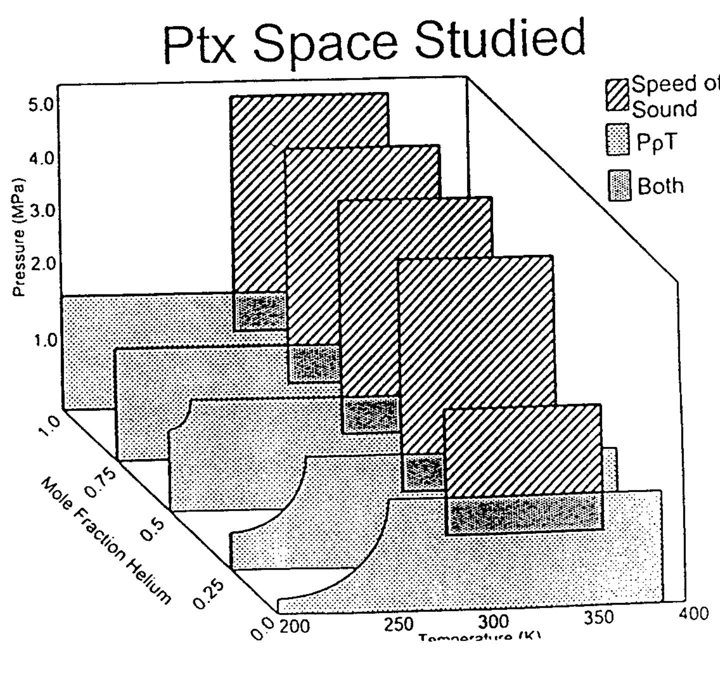

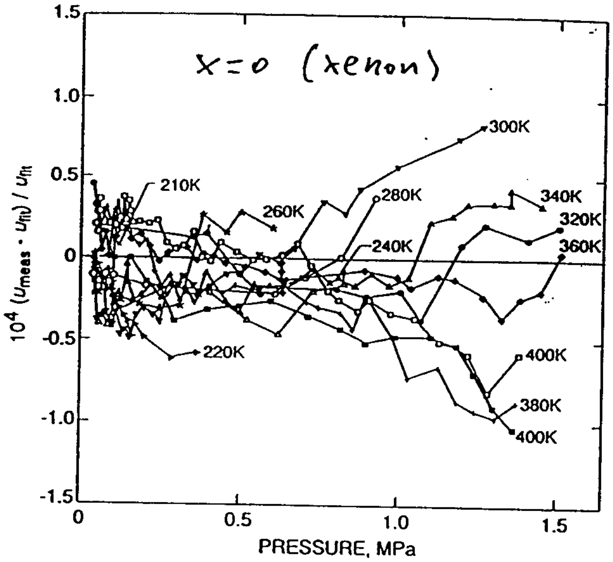
x=0 (xenon)
1.5
1.0
0.5
0
-0.5
-1.0
-1.5
0
0.5
1.0
1.5
PRESSURE, MPa
10^4 (u_meas - u_fit) / u_fit
210K
220K
240K
260K
280K
300K
320K
340K
360K
380K
400K
400K

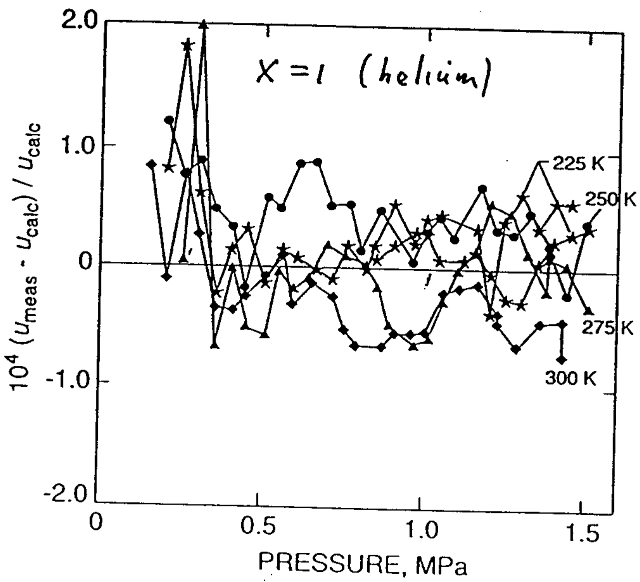
X=1 (helium)
2.0
1.0
0
-1.0
-2.0
0
0.5
1.0
1.5
PRESSURE, MPa
10^4 (u_meas - u_calc) / u_calc
225 K
250 K
275 K
300 K

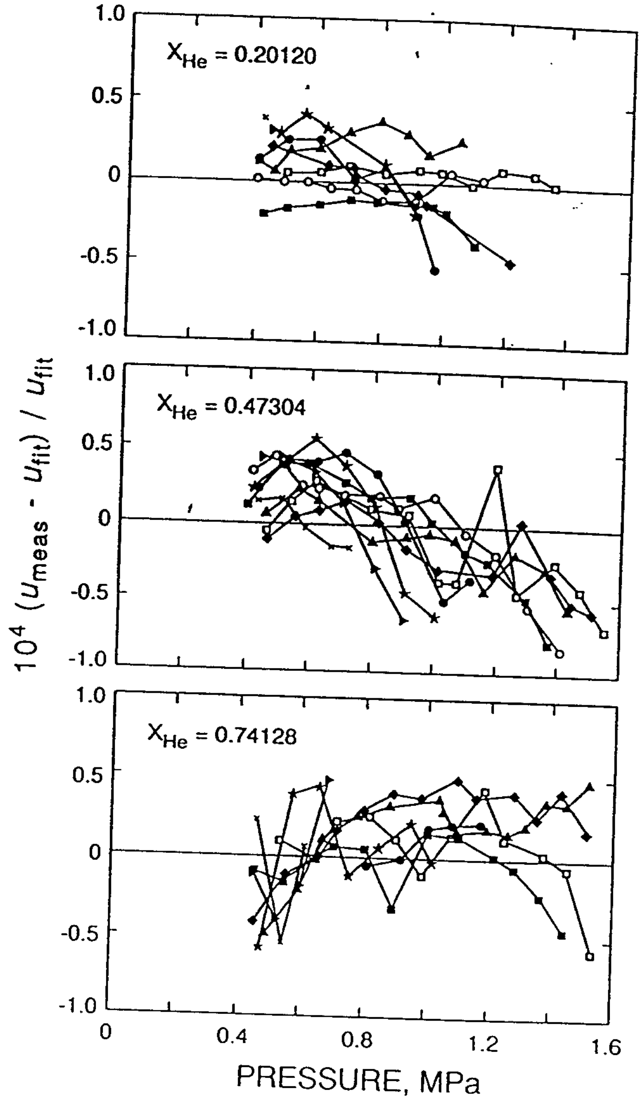
X_He = 0.20120
X_He = 0.47304
X_He = 0.74128
1.0
0.5
0
-0.5
-1.0
0
0.4
0.8
1.2
1.6
PRESSURE, MPa
10^4 (u_meas - u_fit) / u_fit

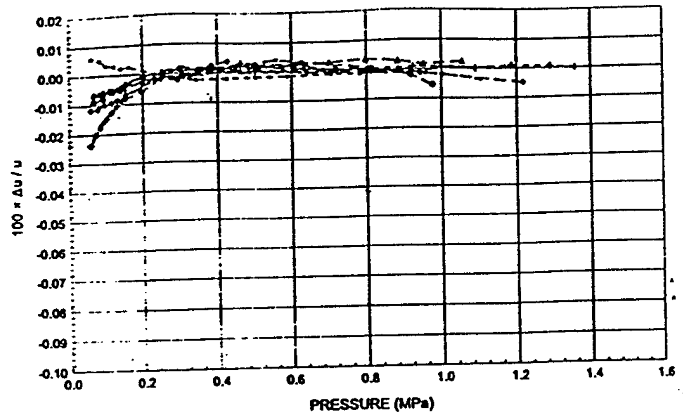

Deviation plot for Helium-Xenon, X_{He} = 0.2014, mixture with the base line as the surface fit. Where ■ -400K; ✚ -375 K; ◆ - 350 K; ▲ - 325 K; ✳ - 300 K; ● - 275 K; ★ -250 K; - 225 K; ✖ -210 K

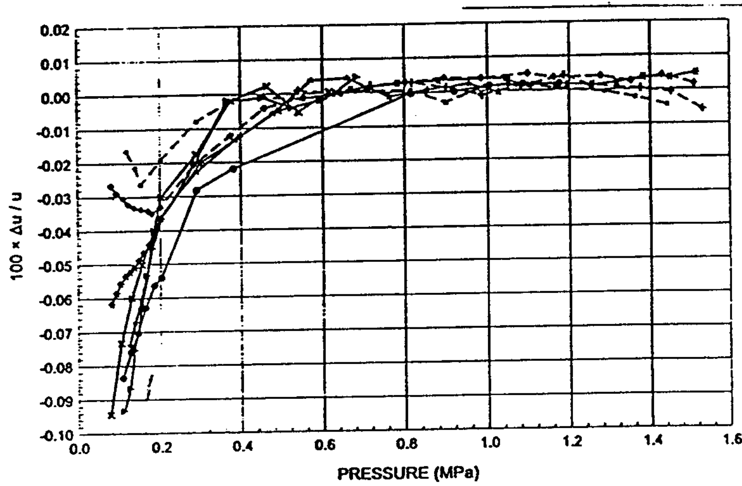

Deviation plot for Helium-Xenon, X_{He} = 0.7413, mixture with the base line as the surface fit. Where ■ - 400K; ✚ - 375 K; ◆ - 350 K; ▲ - 325 K; ✳ - 300 K; ● - 275 K; ★ - 250 K; - 225 K; ✖ - 210 K

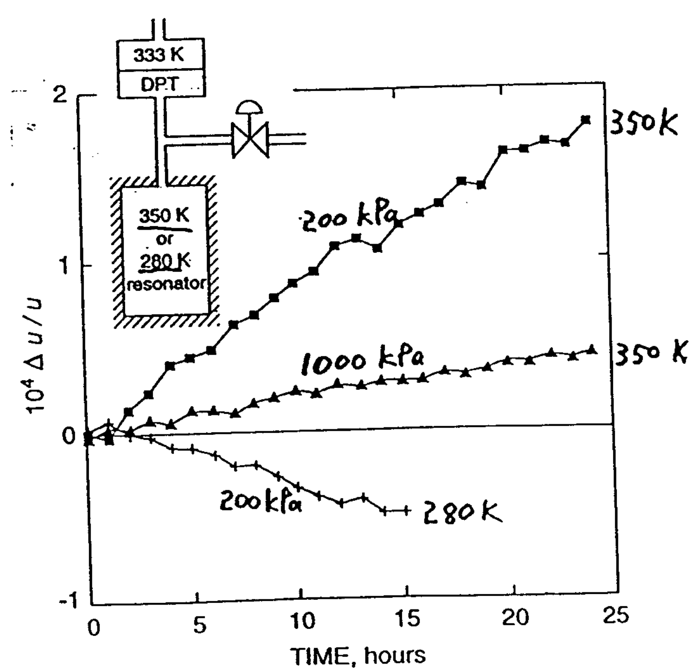

Bulk Losses In a Mixture

$$\frac{\alpha p}{f^2} = \frac{8\pi^2\eta}{3u\gamma} + \frac{2\pi^2(\gamma-1)\lambda}{u\gamma c_p} + \frac{2\pi^2\gamma x_1 x_2 p D_{12}}{u^3}\left\{\frac{M_2 - M_1}{M} + \frac{\gamma - 1}{\gamma}\,\frac{\kappa_T}{x_1 x_2}\right.$$

- Viscous
- Thermal
- Diffusive
- Boundry losses for diffusive ?

$$f = f + \Delta f_{\text{thermal}} + \Delta f_{\text{viscous}} + \Delta f_{\text{diffusive}}$$

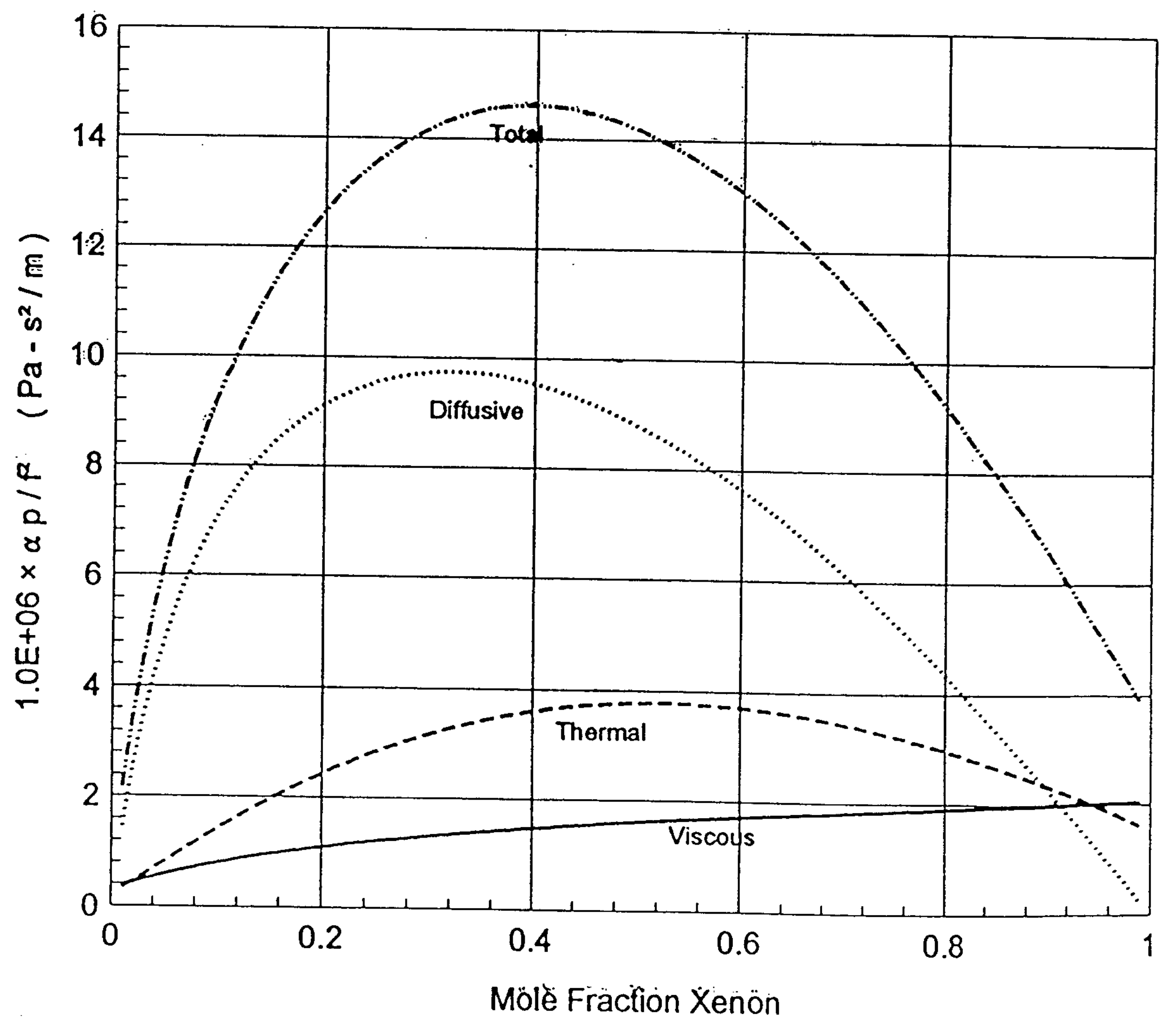

[TR-1]

SCANNING ACOUSTIC MICROSCOPY: LENSES, TIPS & SONOELECTRONICS

Calvin F. Quate
Ginzton Laboratory
Stanford University

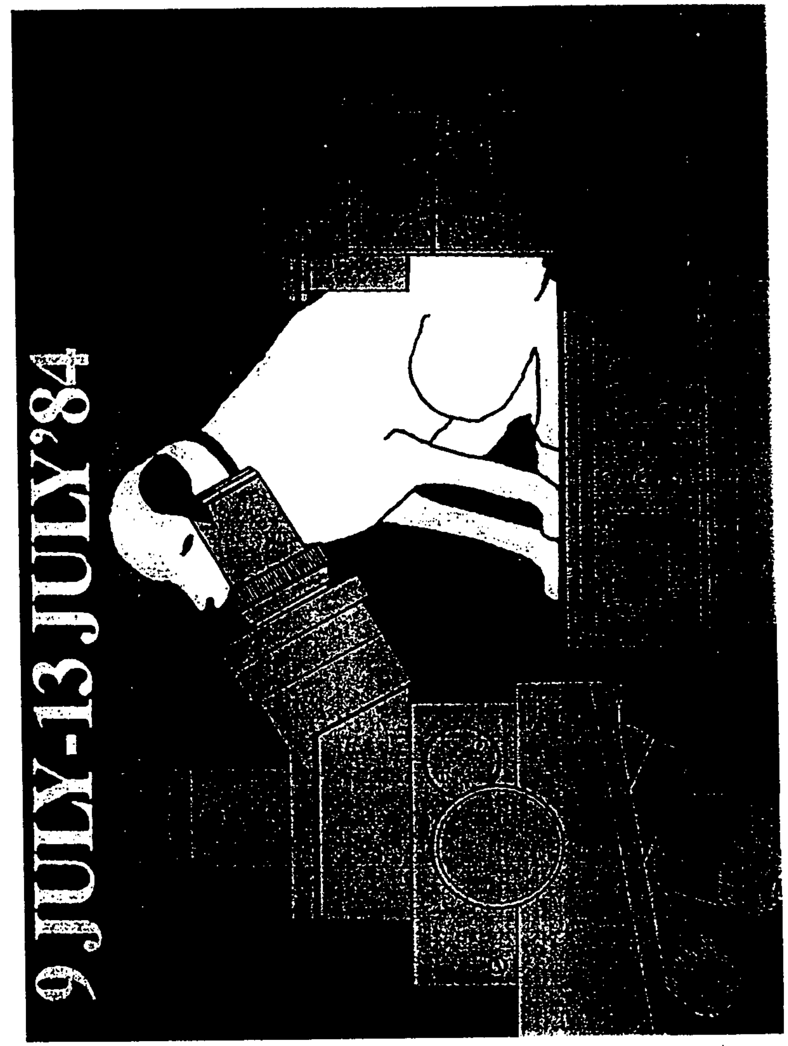

[TR-2]

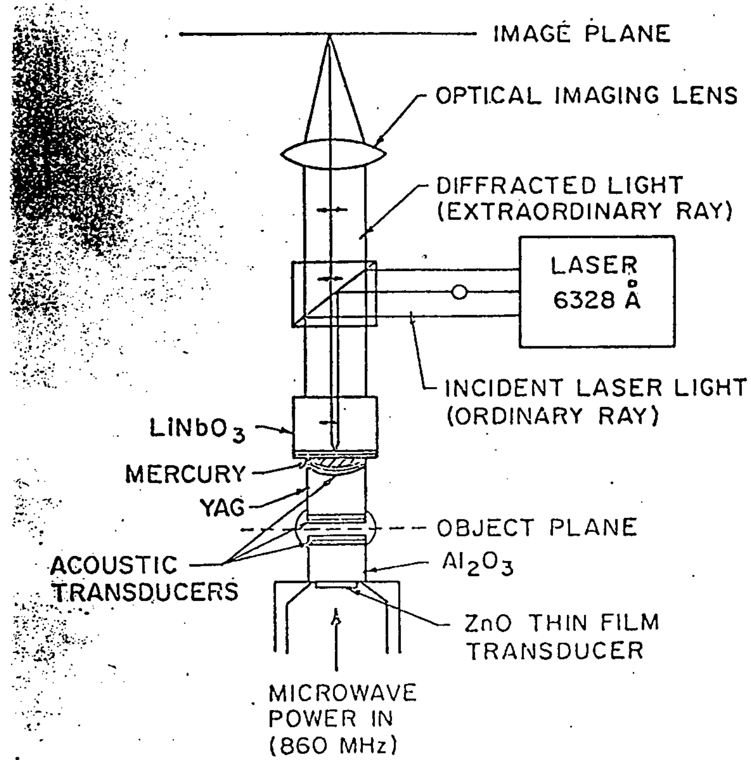

FIG. 1--Experimental setup

[TR-3]

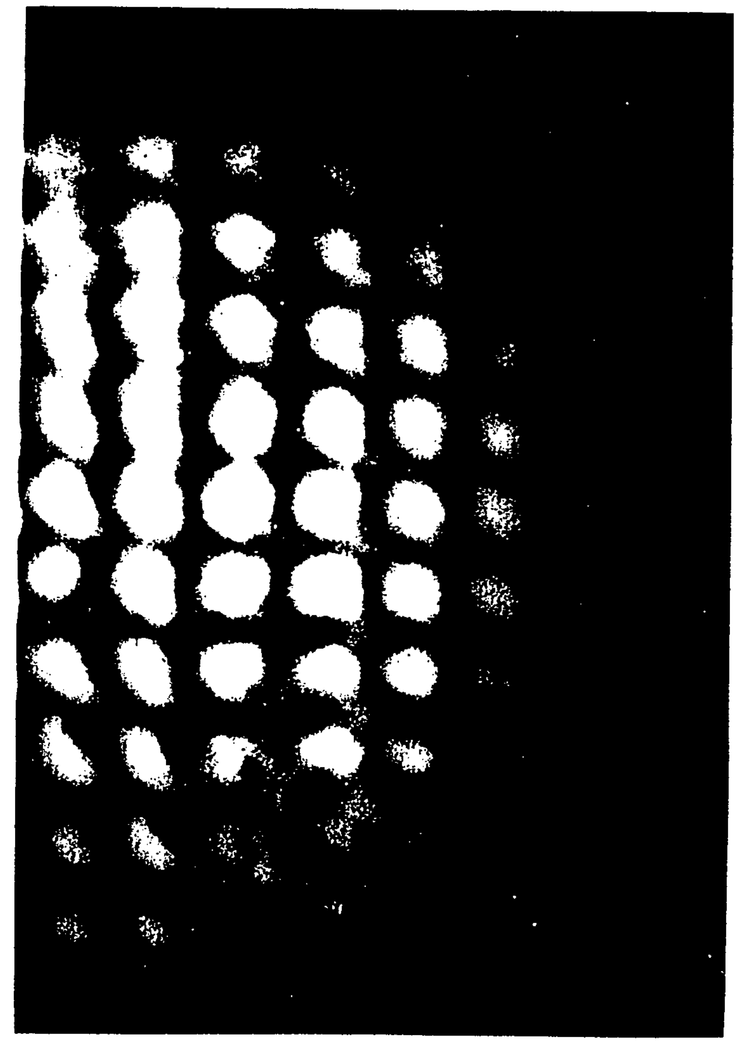

Image of 50 μ periodic mesh. in focus region

[TR-4]

2596-5

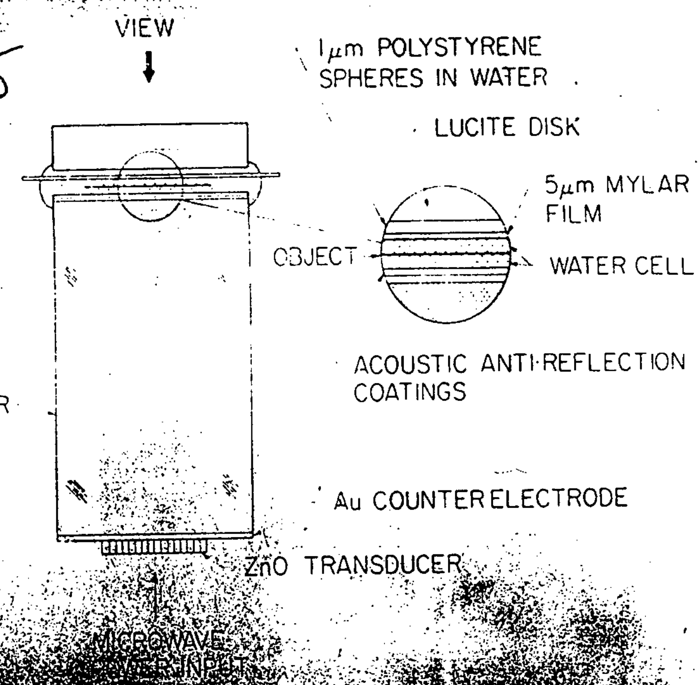

Fig. 5. Experimental arrangement for single-beam imaging.

[TR-5]

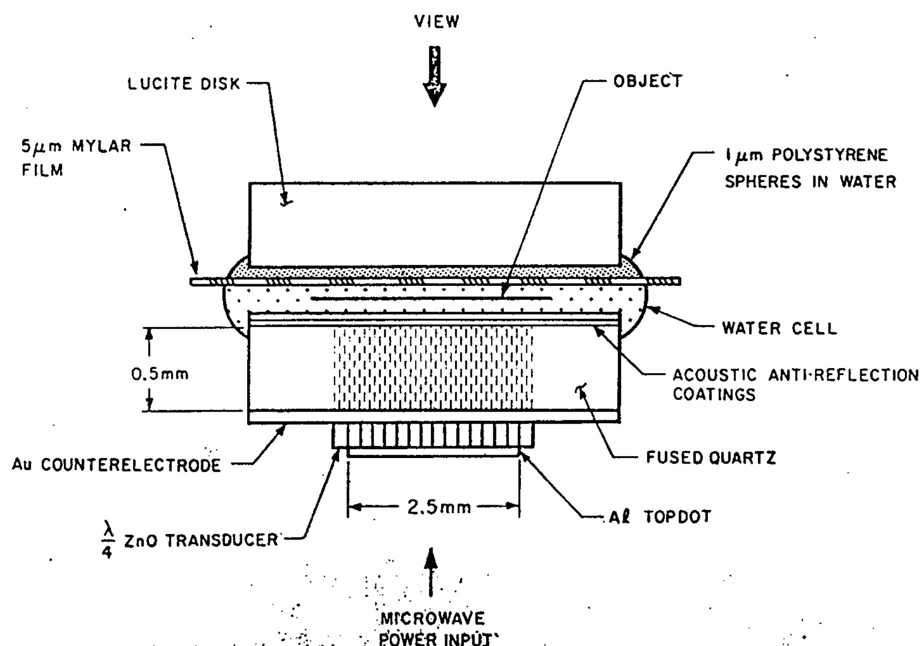

FIG. 3 Experimental [illegible] ect in the extremely near field

[TR-6]

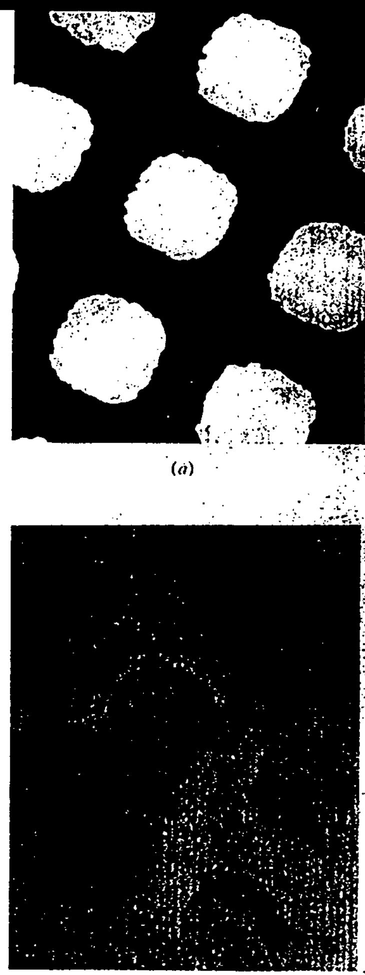

(a) (b)

3536-20

FIG. 3. Circular nickel mesh (300 μm holes on 420 μm centers).

(a) Optical image ; (b) Acoustical image.

[TR-7]

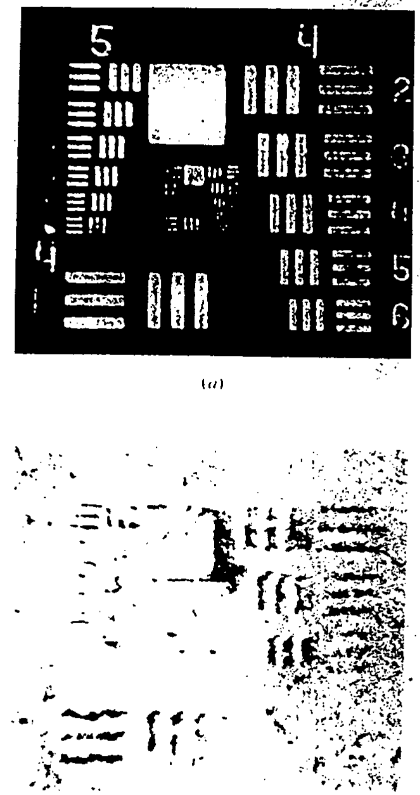

(a) (b)

FIG. 6. [illegible] USAF Resolution Test Chart ; Groups + 4 and 5

(a) Group 4	(b) Group 5
[illegible].00 l/mm	(1) 32.00 l/mm
(2) 17.96	(2) 35.92
(3) 20.[illegible]	(3) 40.64
(4) 22.80	(4) 45.60
(5) [illegible]	(5) 51.12
(6) [illegible]	(6) 57.02

[TR-8]


100 μm
(a)
100 μm
human lung tissue
Optical image
Acoustical image.

[TR-9]

[TR-10]

[TR-11]

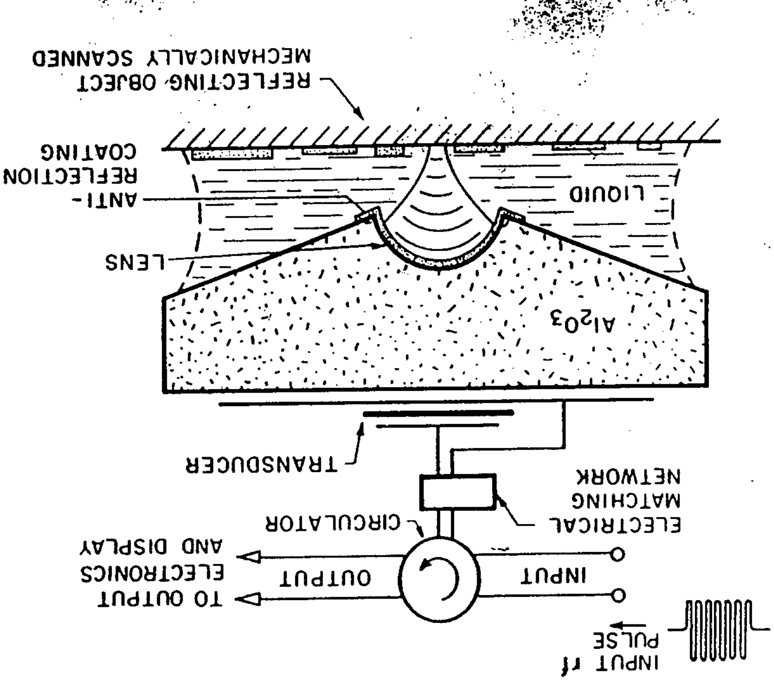

FIGURE 1. Configuration of the reflection acoustic microscope.

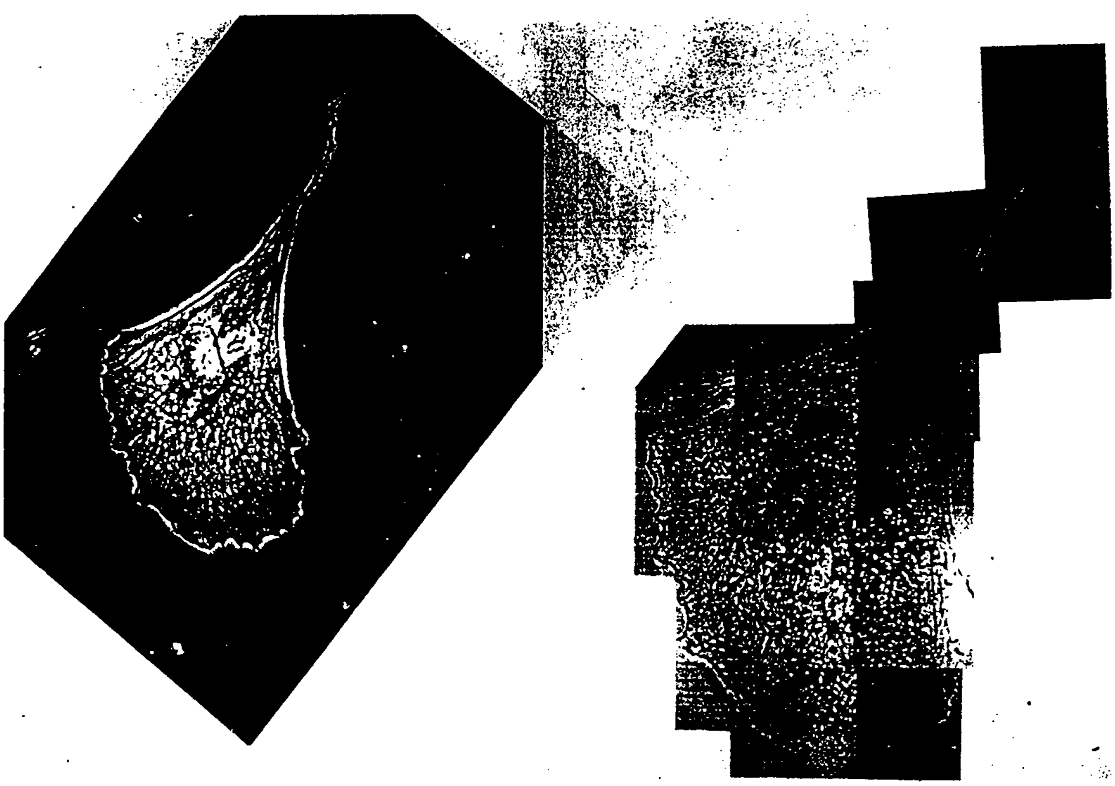

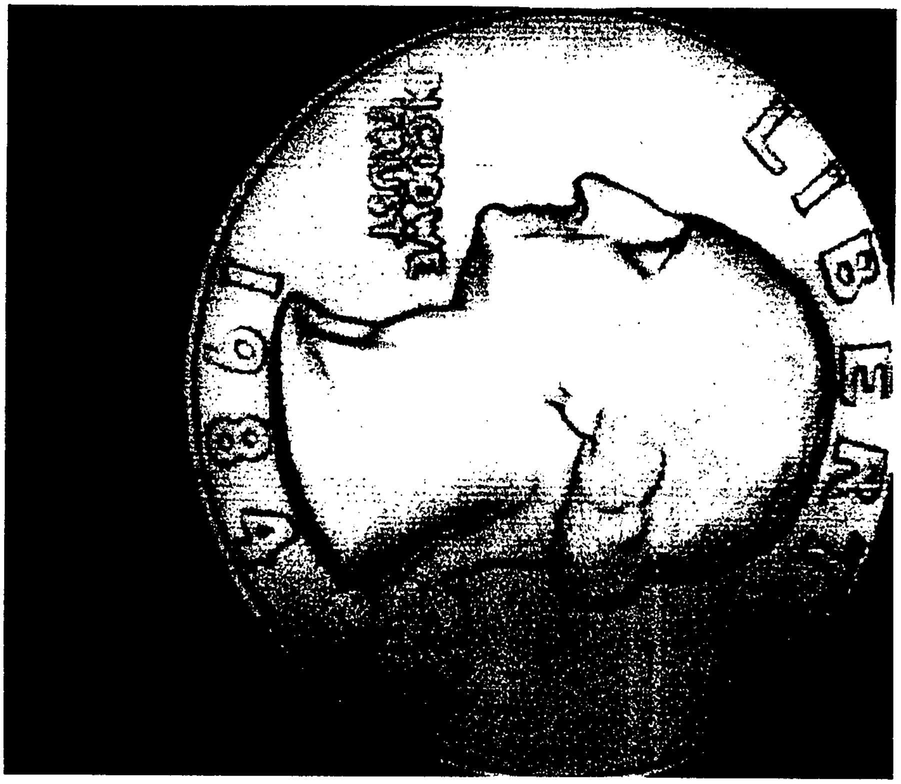

[TR-14]

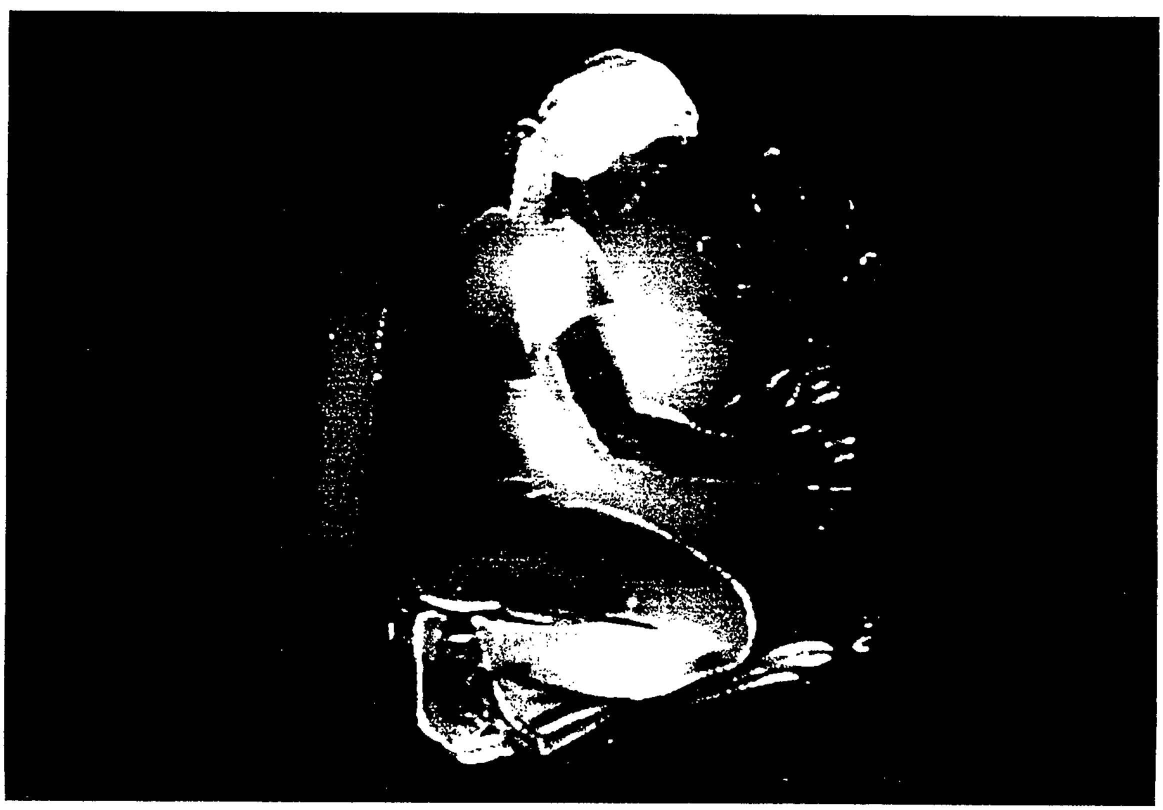

[TR-15]

[TR-16]

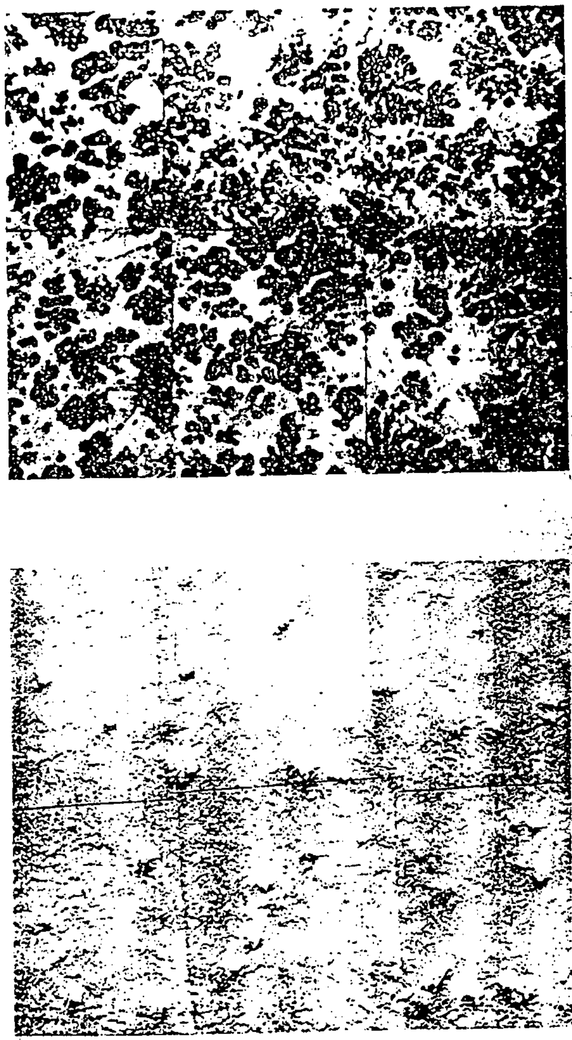

(a) OPTICAL DIC

(b) ACOUSTIC (1100 MHz)

100 μm

Co-Ti ALLOY SHOWING 2 PHASES. OVERALL COMPOSITION 59 % Co 41 % Ti

[TR-17]

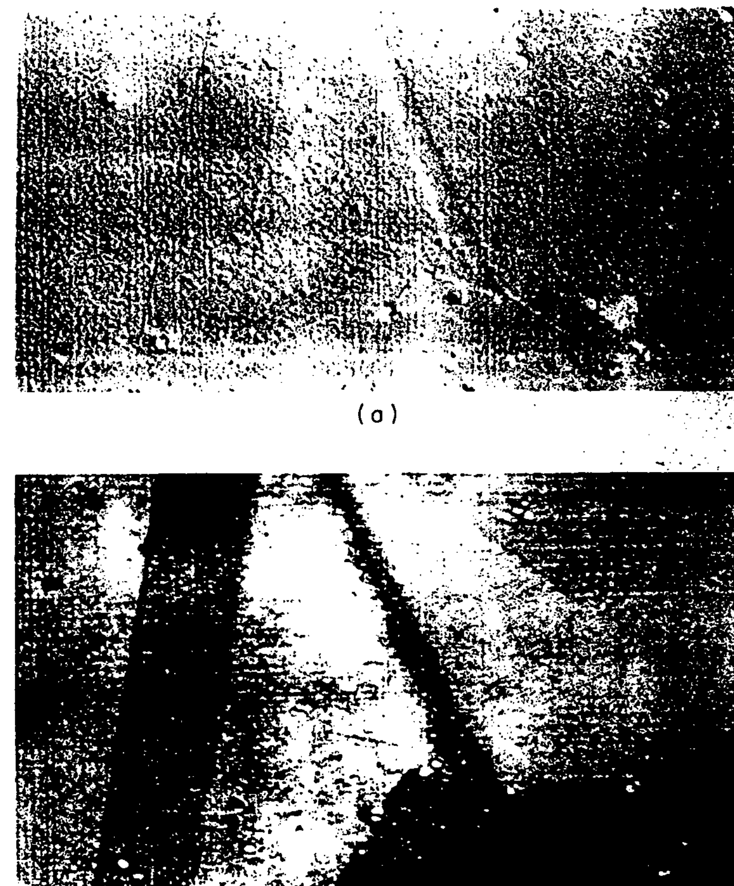

(a)

(b)

FIG. 4.6---Optical (a) and acoustic (b) comparison of polished brass surface. Field of view is 55 × 90 μm

[TR-18]

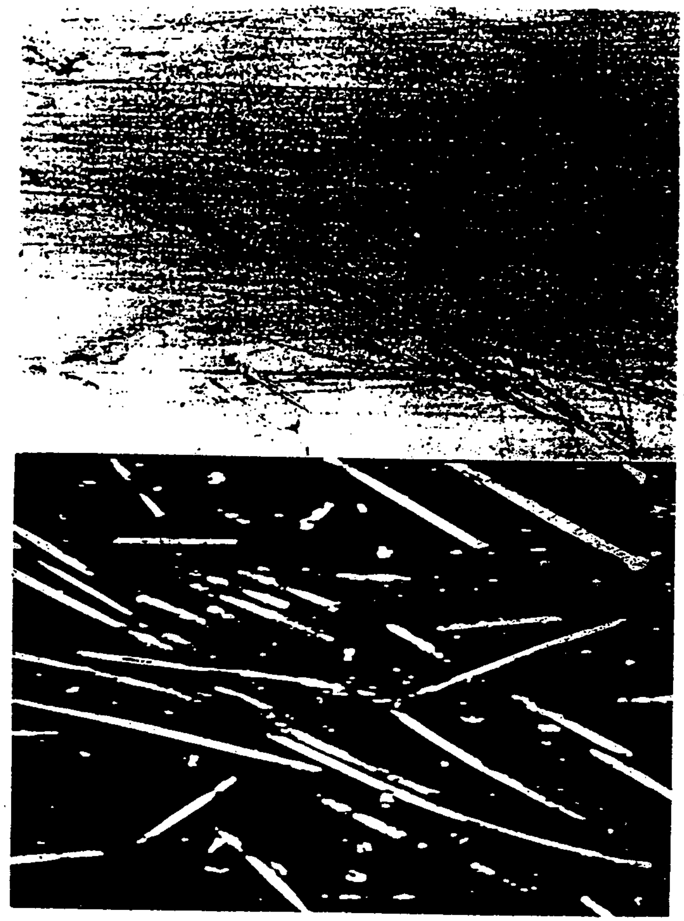

(a)

(b)

[TR-19]

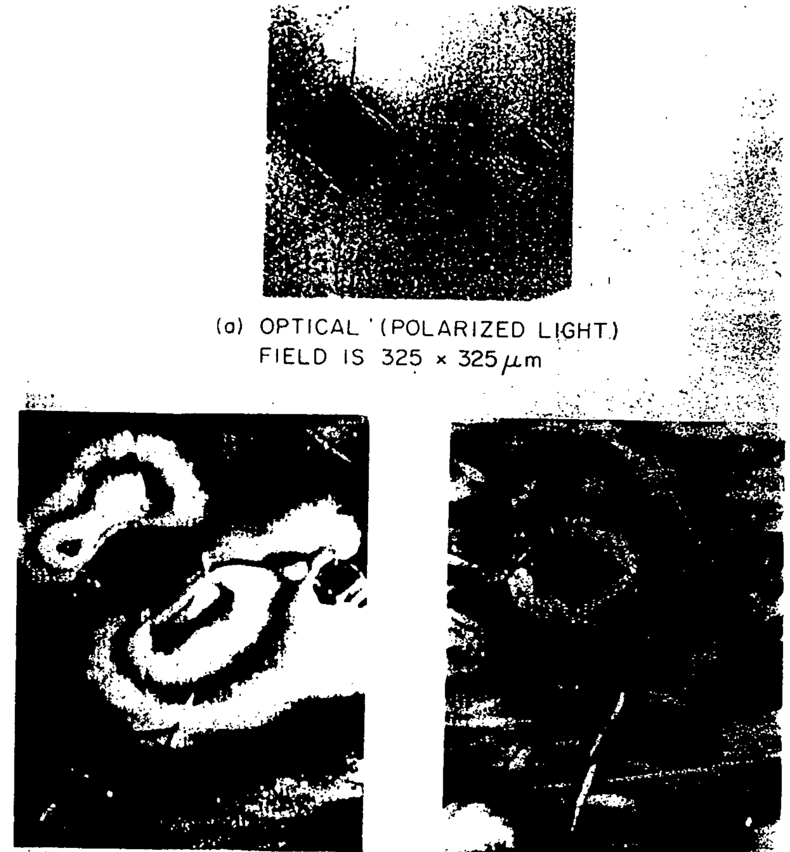

(a) OPTICAL (POLARIZED LIGHT) FIELD IS 325 × 325 μm

(b) ACOUSTIC FOCUS #1

(c) ACOUSTIC FOCUS #2

COMPARISON IMAGES FOR AN ALUMINUM SAMPLE WITH AN OXIDE LAYER

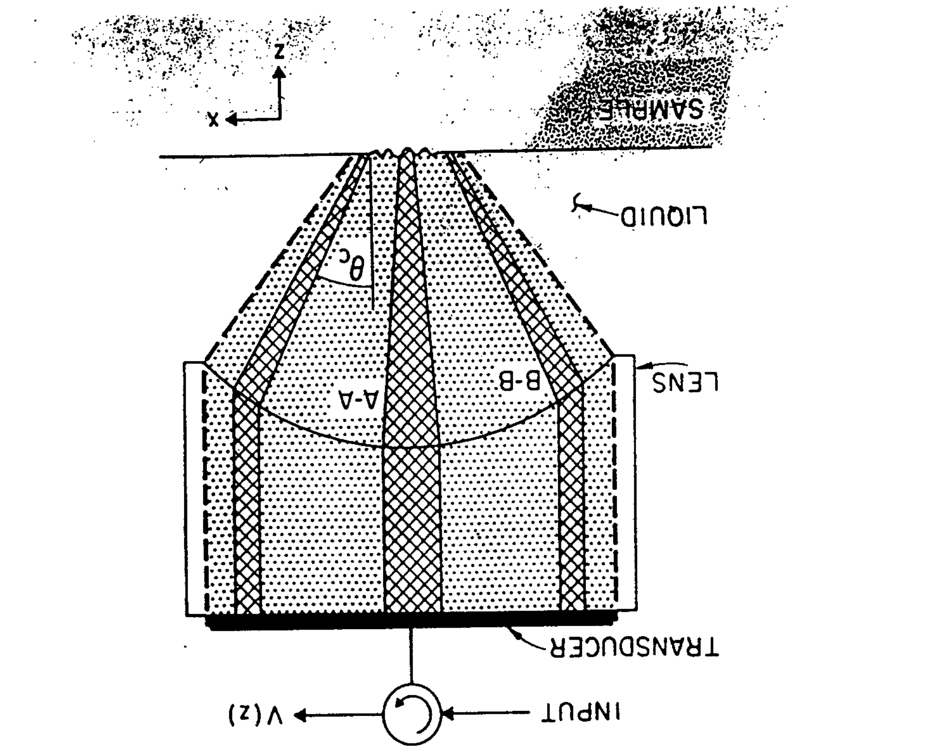
SAMPLE
z
x
LIQUID
θ_c
A-A
B-B
LENS
TRANSDUCER
INPUT
V(z)

[TR-21]

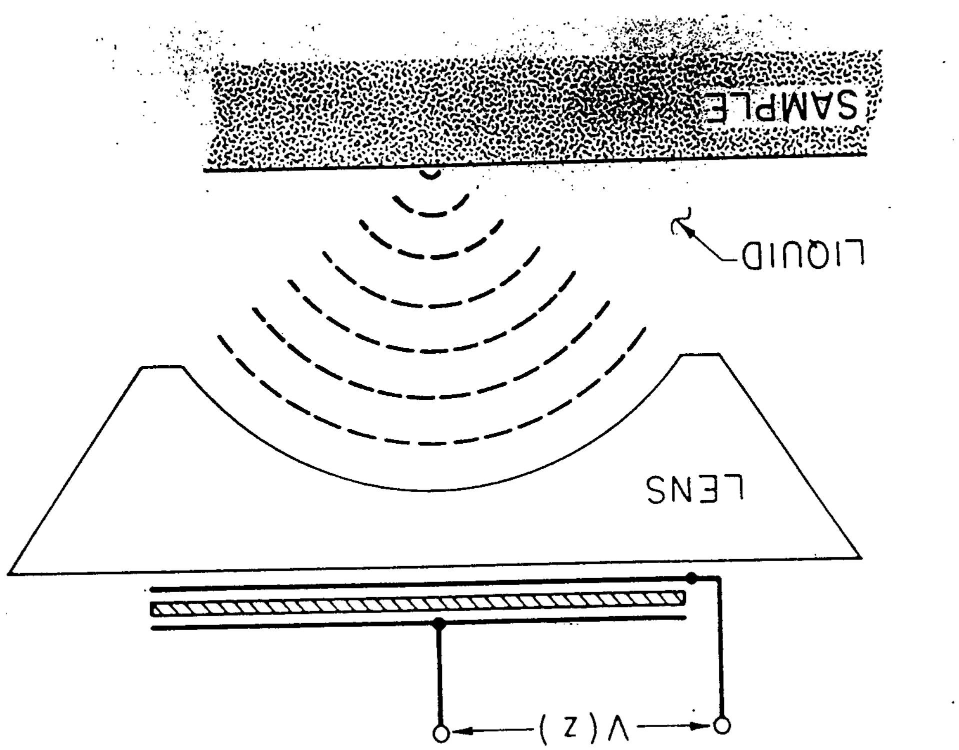
SAMPLE
LIQUID
LENS
V (z)

[TR-20]

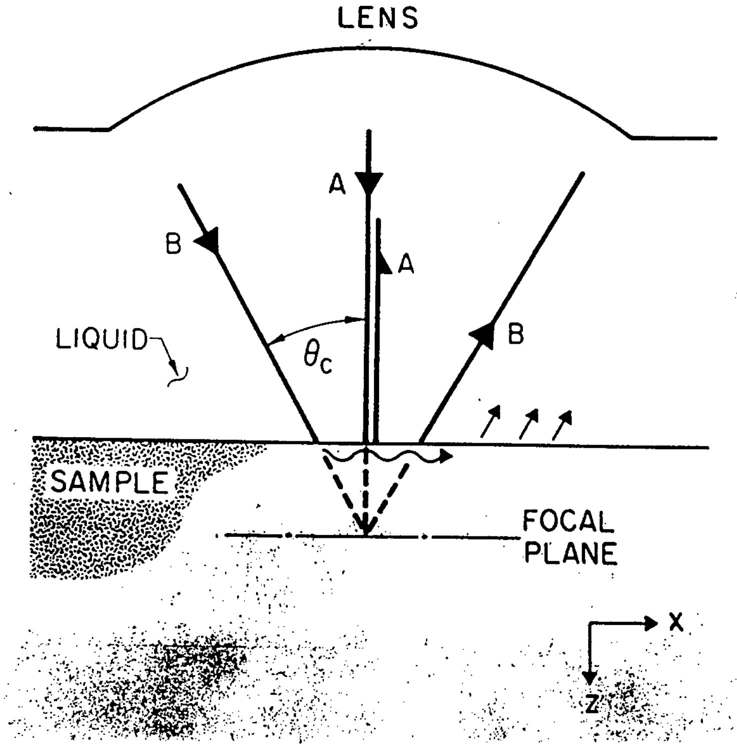

LENS
A
B
A
B
LIQUID
θ_c
SAMPLE
FOCAL
PLANE
X
Z

[TR-22]

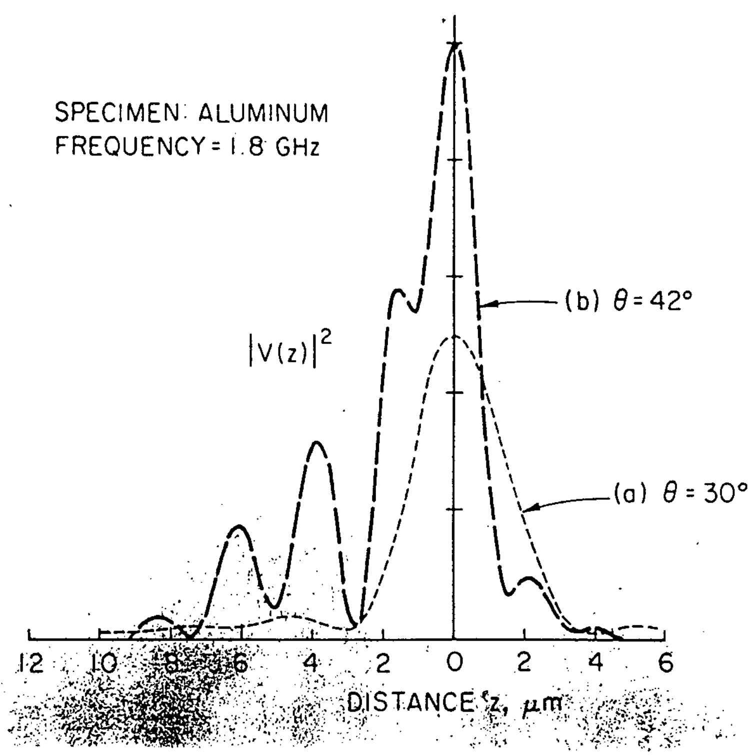

SPECIMEN: ALUMINUM
FREQUENCY = 1.8 GHz
$|V(z)|^2$
(b) $\theta = 42°$
(a) $\theta = 30°$
12
10
8
6
4
2
0
2
4
6
DISTANCE z, μm

[TR-23]

[TR-24]

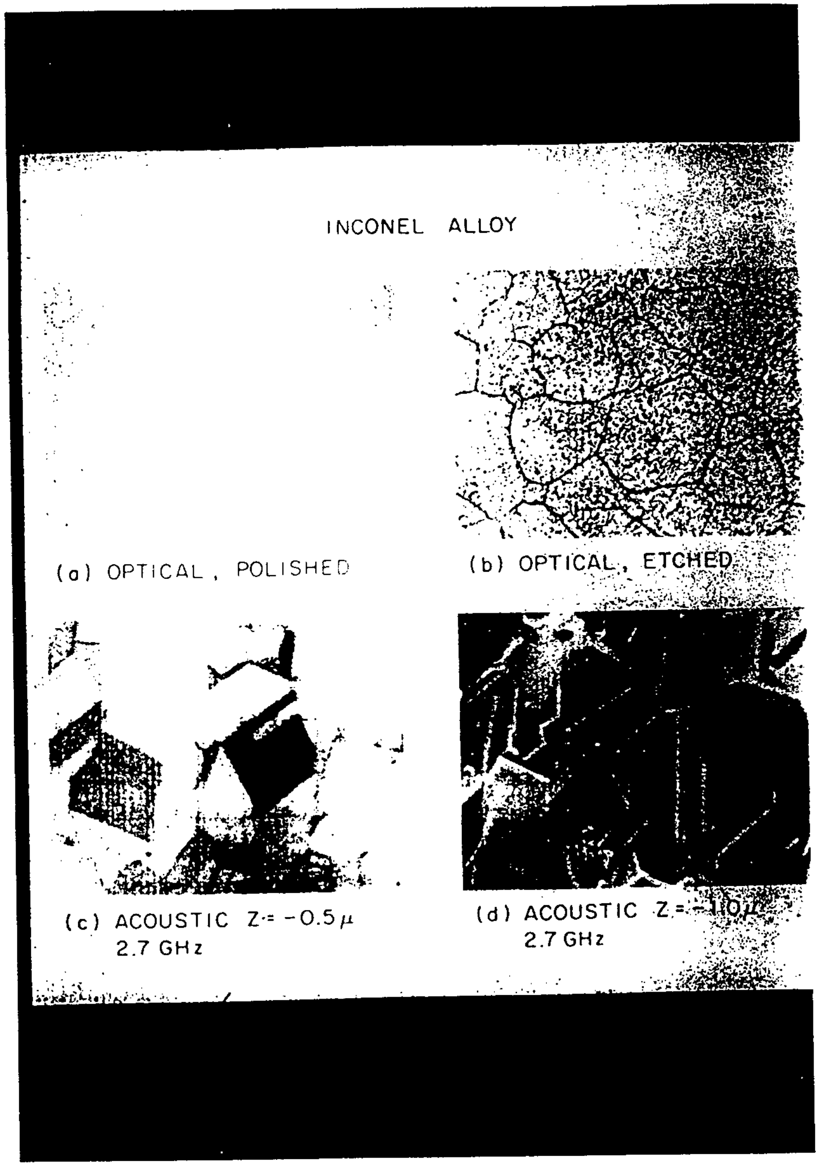
INCONEL ALLOY
(a) OPTICAL, POLISHED
(b) OPTICAL, ETCHED
(c) ACOUSTIC Z = −0.5μ
2.7 GHz
(d) ACOUSTIC Z = −1.0μ
2.7 GHz

[TR-25]


20μm
Z = 0
Z = −1
Z = −1.5
INCONEL

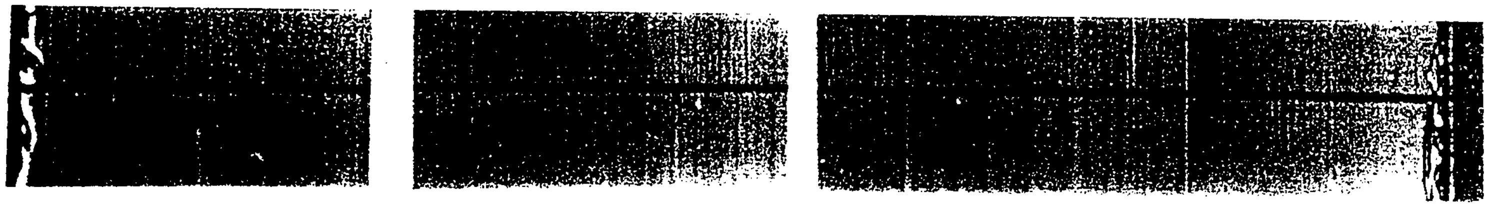

(a) OPTICAL

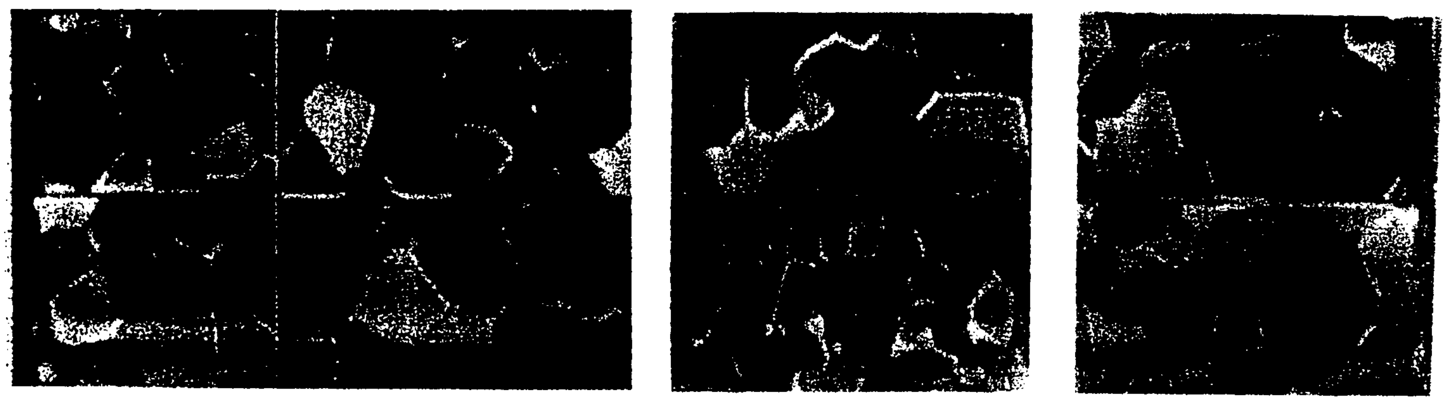

(b) ACOUSTIC

MAGNETIC RECORDING HEAD
TRACK # 2 OF SAMPLE 40241

Fig. 3A.9 A full color acoustic image composed from the three images of three primary colors in Fig. 3A.7.

[TR-28 Unavailable At Time Of Printing]

[TR-29]

[TR-30]

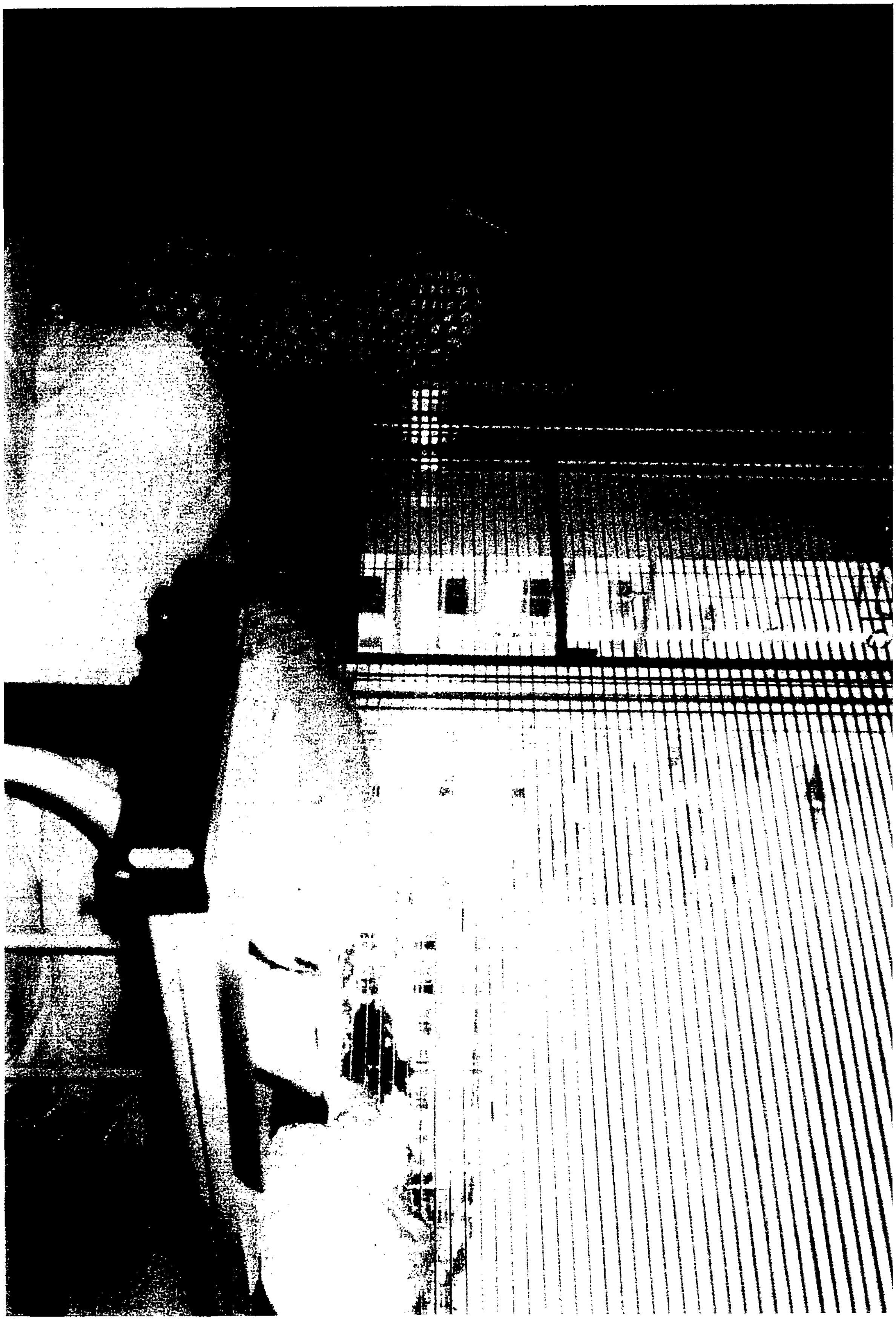

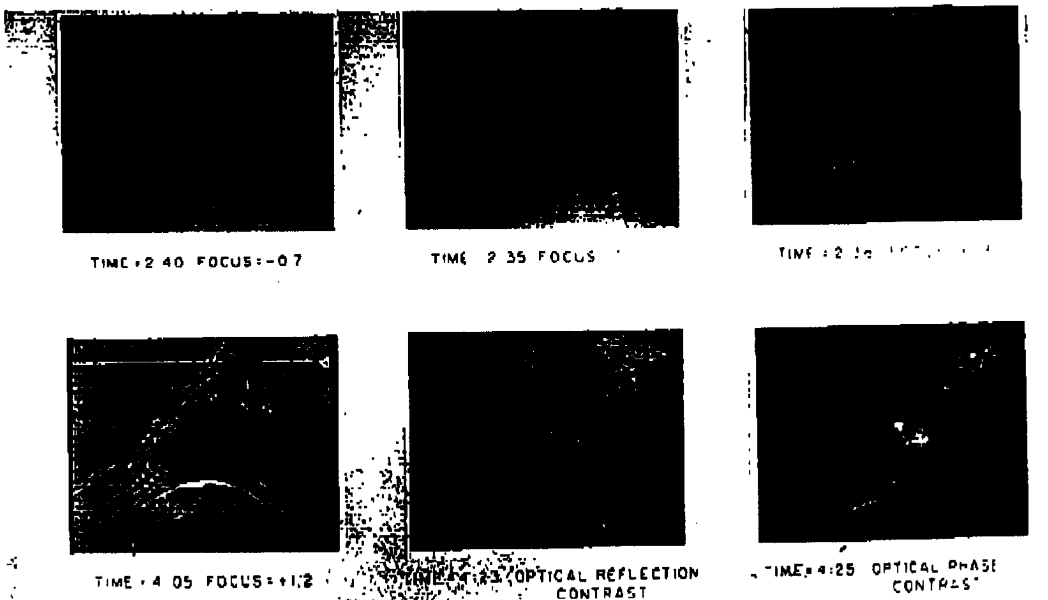

COMPARISON OF [illegible] OPTICAL MICROGRAPHS OF LIVING CHICK HEART [illegible] ON A GLASS SUBSTRATE

(700 MHz) [illegible] APRIL 26, 1980

[TR-32]

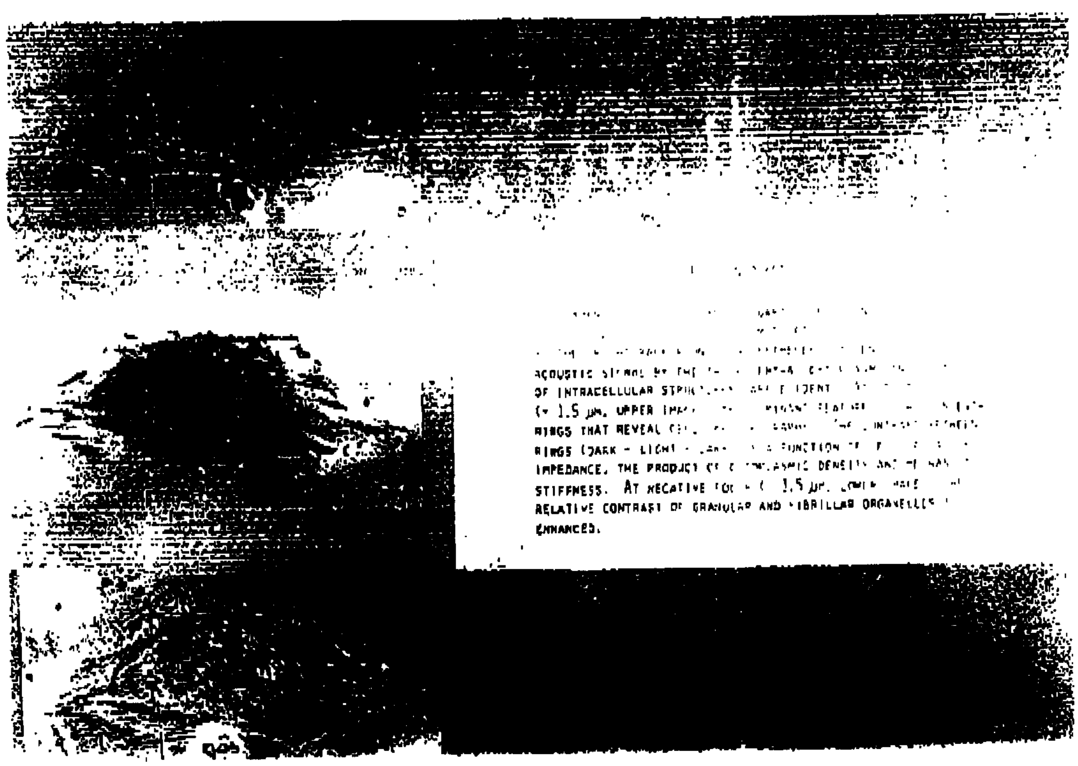

ACOUSTIC SIGNAL BY THE [illegible] OF INTRACELLULAR STRUCTURES [illegible] (+ 1.5 μm, UPPER IMAGE [illegible] RINGS THAT REVEAL [illegible] RINGS (DARK – LIGHT – [illegible] FUNCTION [illegible] IMPEDANCE, THE PRODUCT OF [illegible] DENSITY AND [illegible] STIFFNESS. AT NEGATIVE FOCUS (– 1.5 μm, LOWER IMAGE [illegible] RELATIVE CONTRAST OF GRANULAR AND FIBRILLAR ORGANELLES [illegible] ENHANCED.

[TR-31]

[TR-33]

[TR-34]

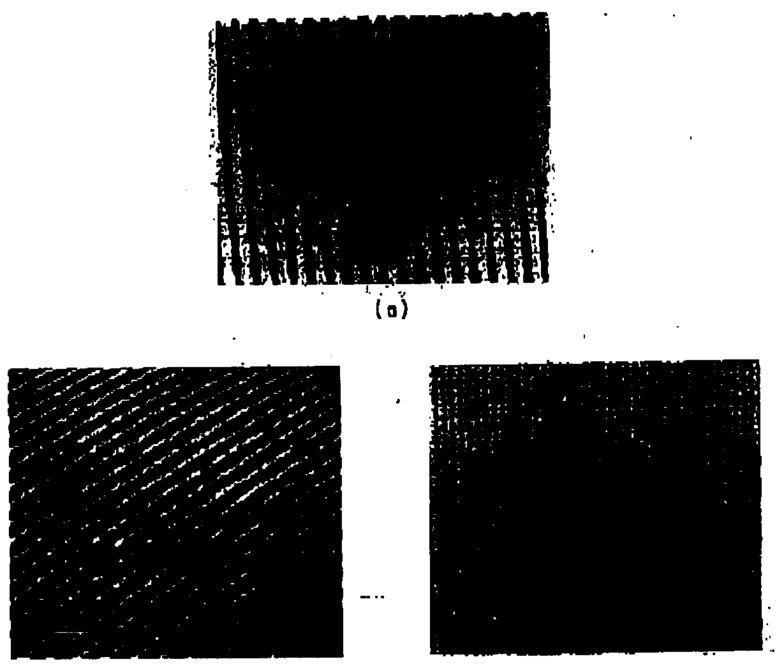

(a)

(b) (c)

FIG. 4-3. Images of grating with 4000 Å period. The acoustic image (a) was taken in liquid argon at 2.0 GHz. Images (b) and (c) are by scanning electron and optical microscopy, respectively.

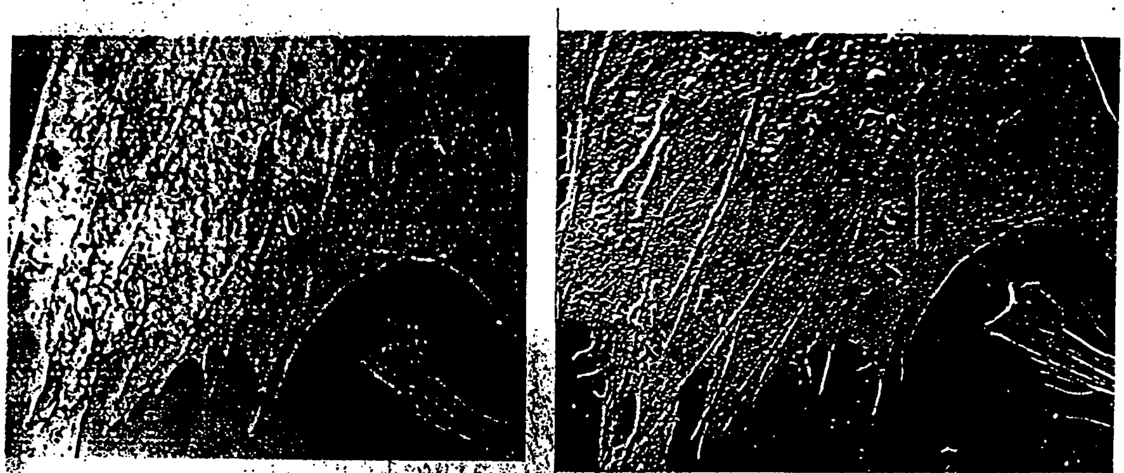

(a) ACOUSTIC (b) SEM

[TR-36]

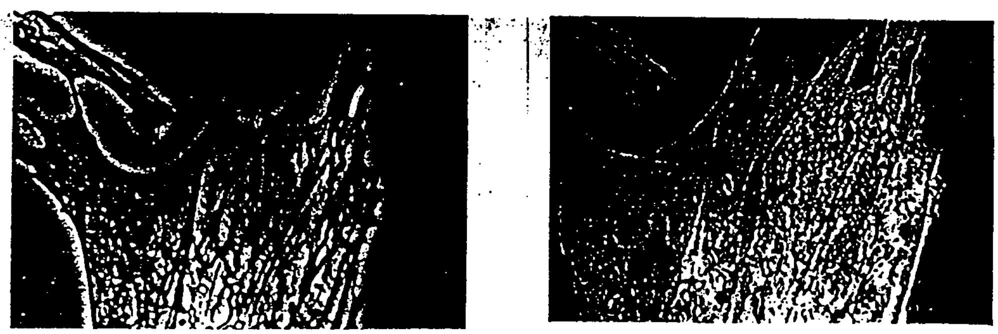

(a) OPTICAL (b) ACOUSTIC

(c) SEM

[TR-35]

[TR-37]

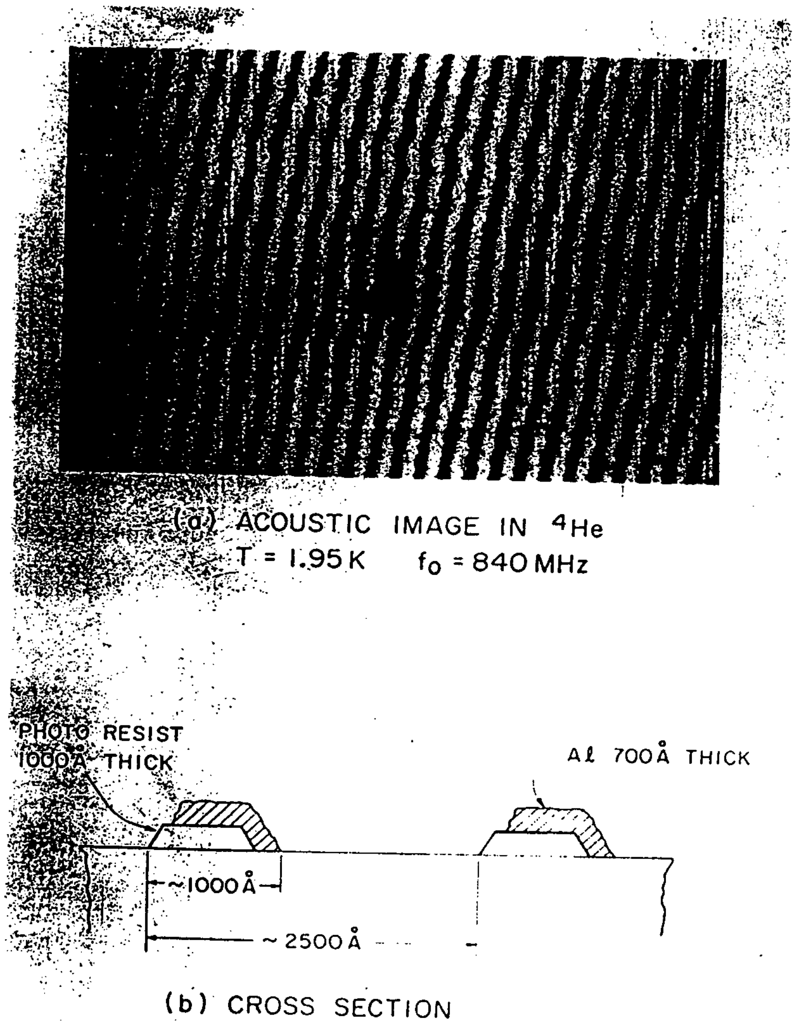

FIG. 3-25. Acoustic image of grating with [illegible] period.

[TR-38]

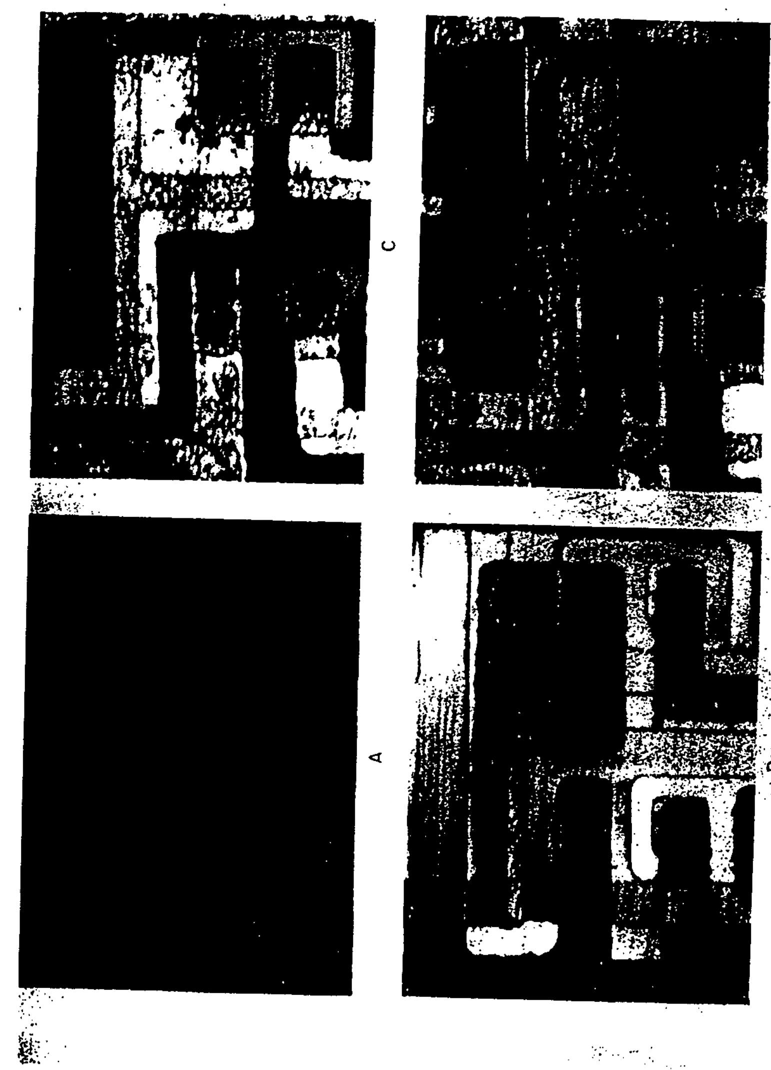

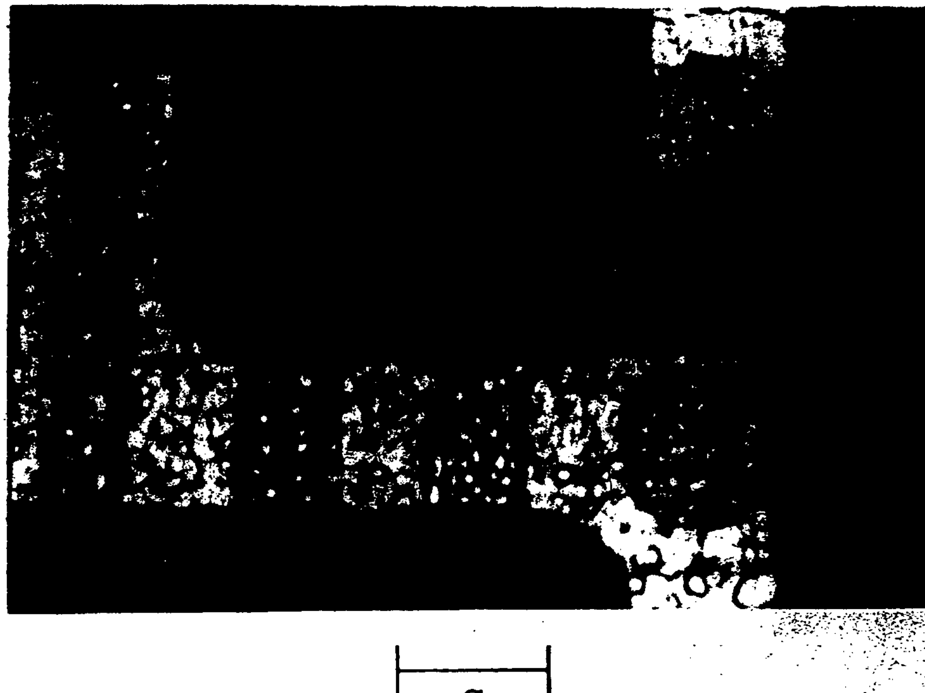

a

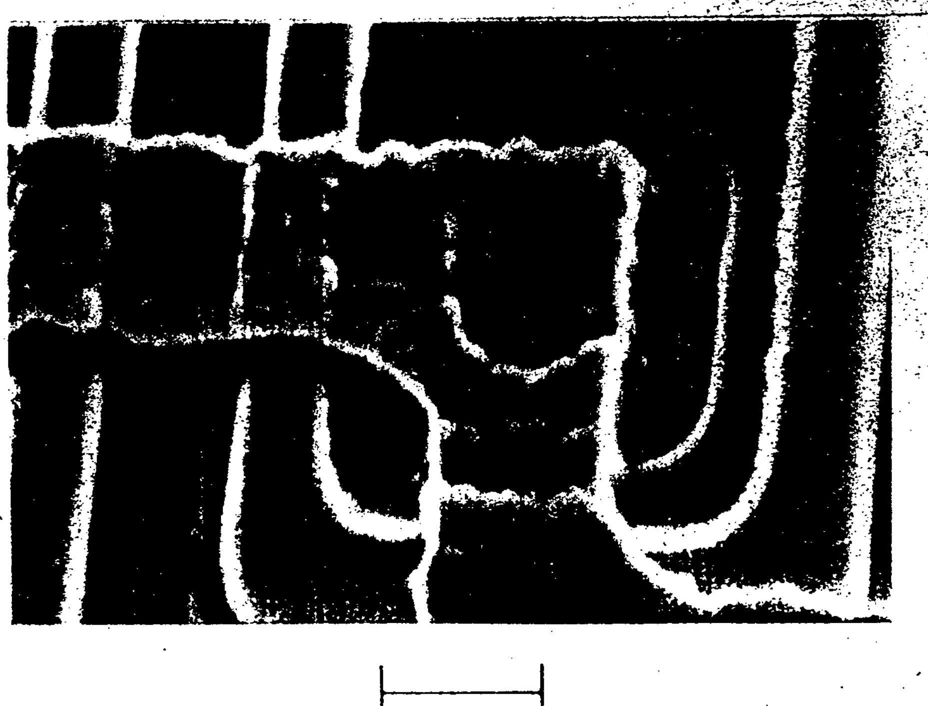

b

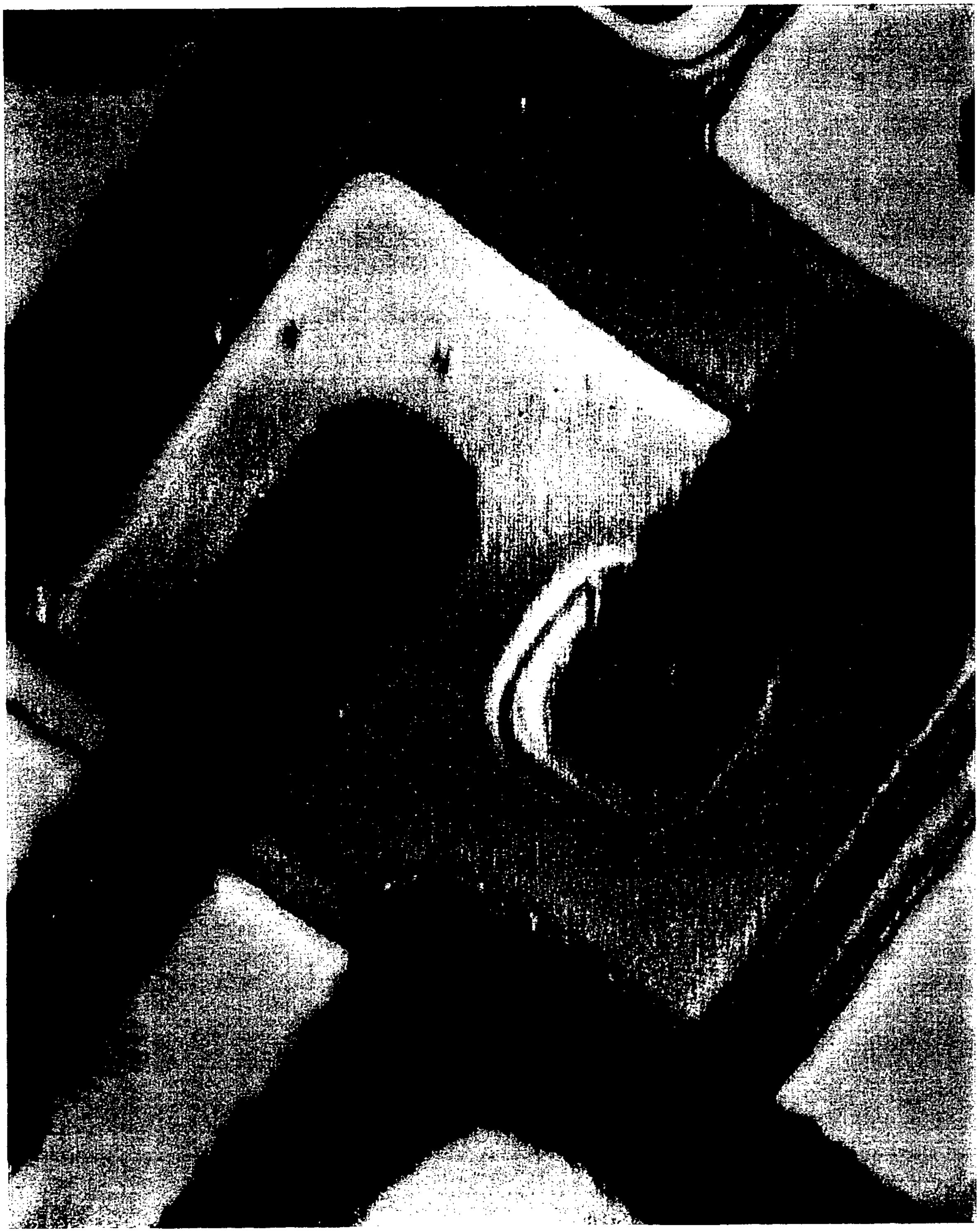

[TR-41]

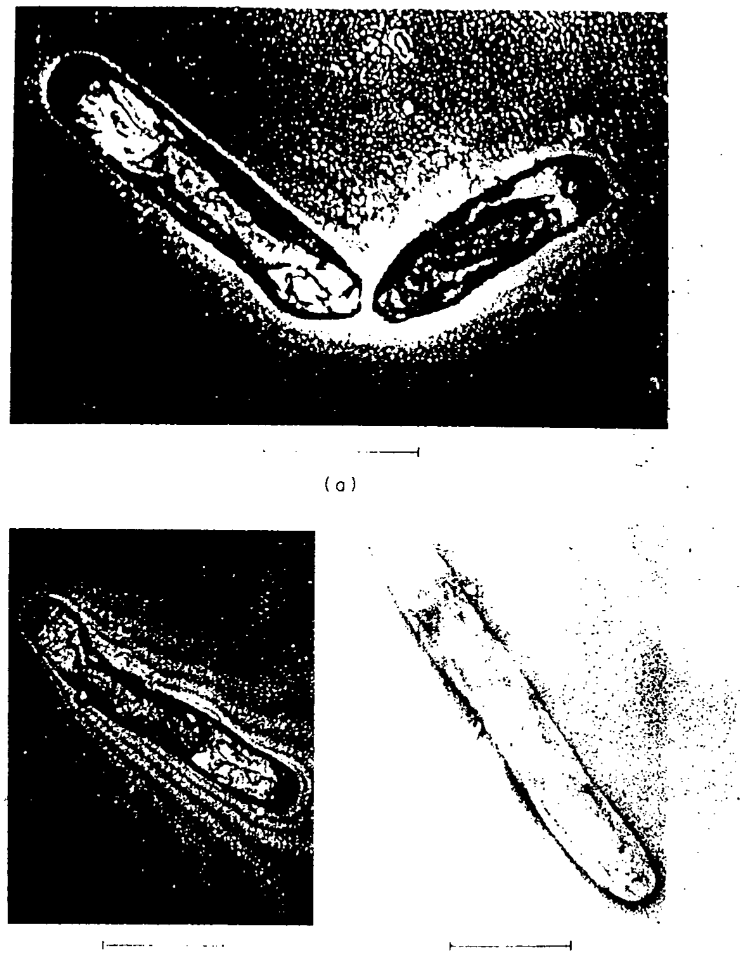

(a)

(b)

(c)

FIGURE 4.6 - (a), (b) Acoustic, and (c) TEM images of similar myxo bacteria. Scale bars are 1 μm.

[TR-42]

[TR-43]

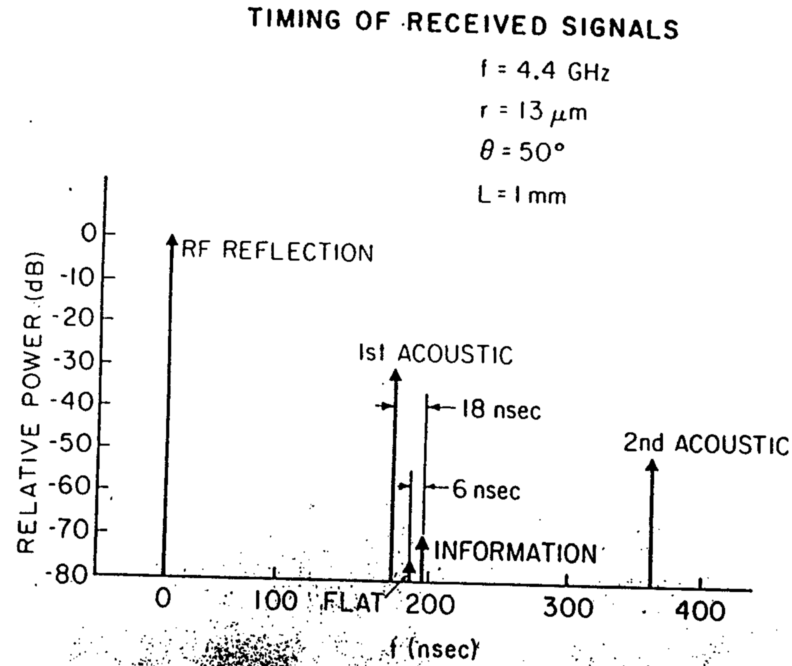

FIGURE 3.1--Typical timing and relative amplitudes of signals received from the transducer.

[TR-44]

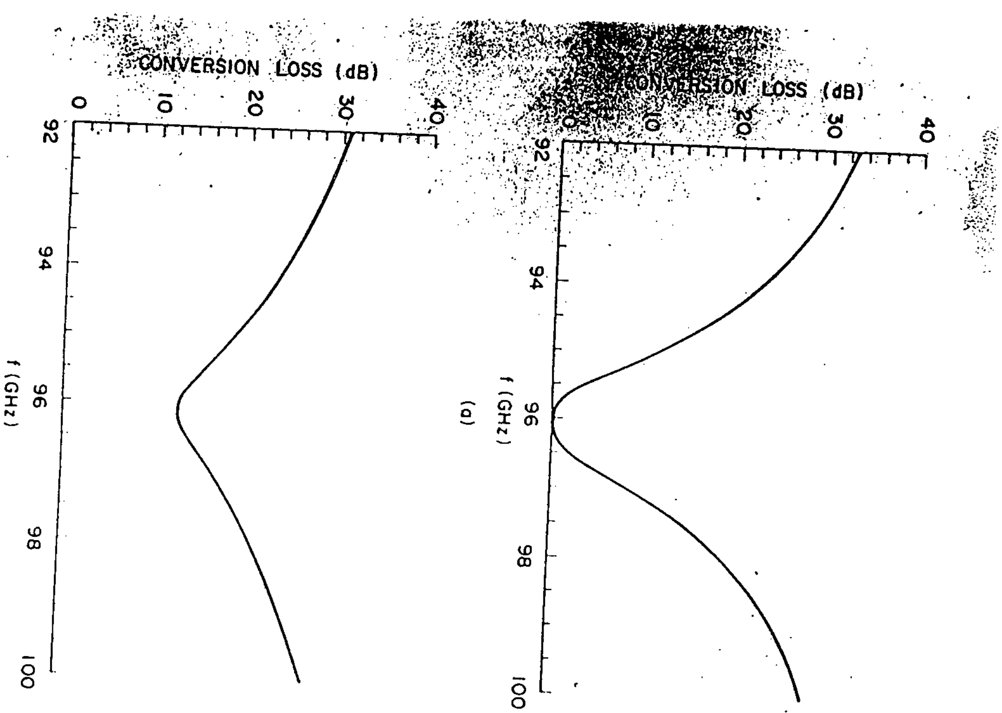

FIGURE 5.2--Conversion loss (theoretical) vs. frequency for 96 GHz transducers. (a) All losses are neglected. (b) Conductor losses are included.

[TR-45]

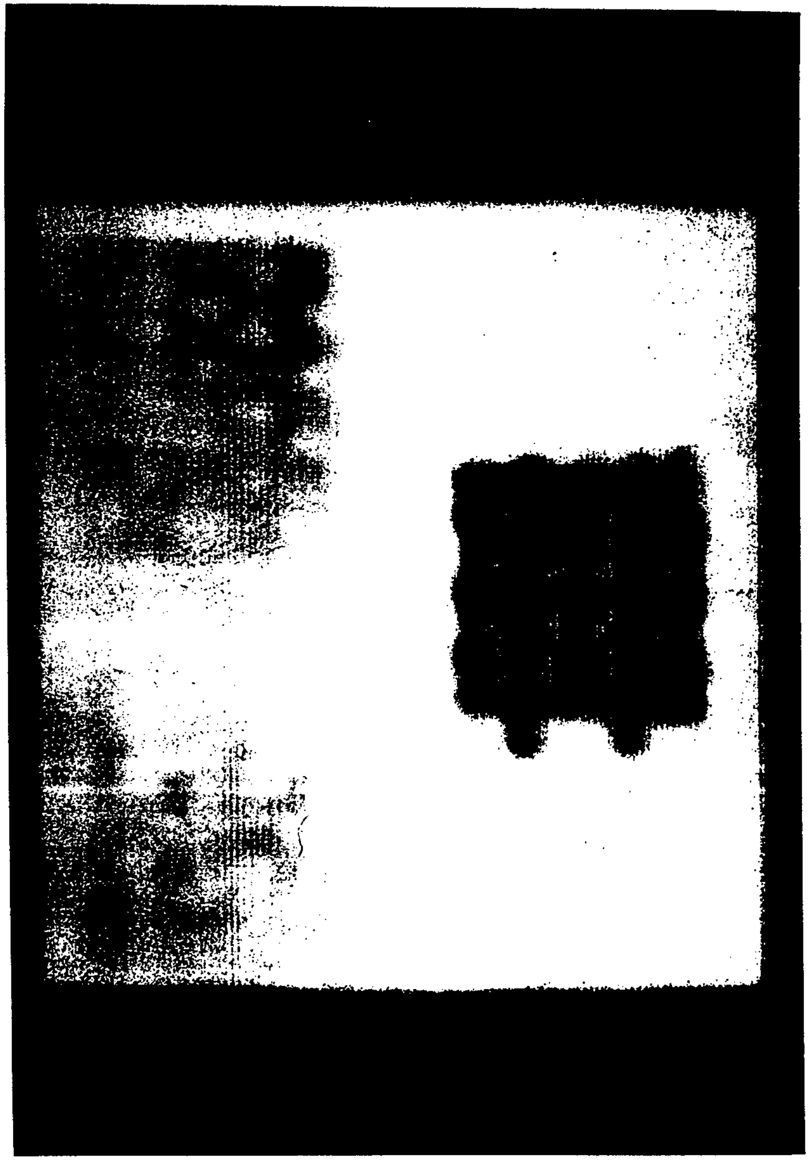

[TR-46]

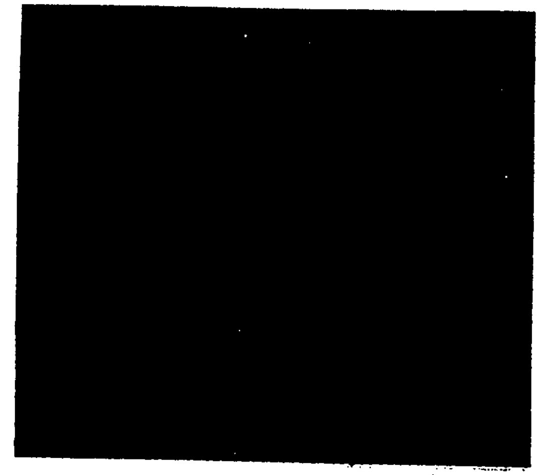

(a)

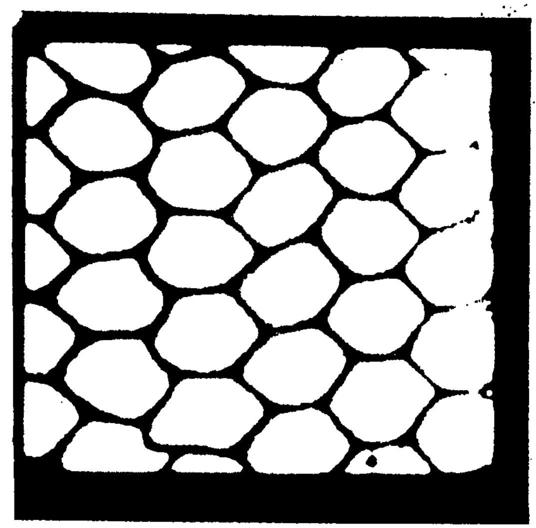

(b)

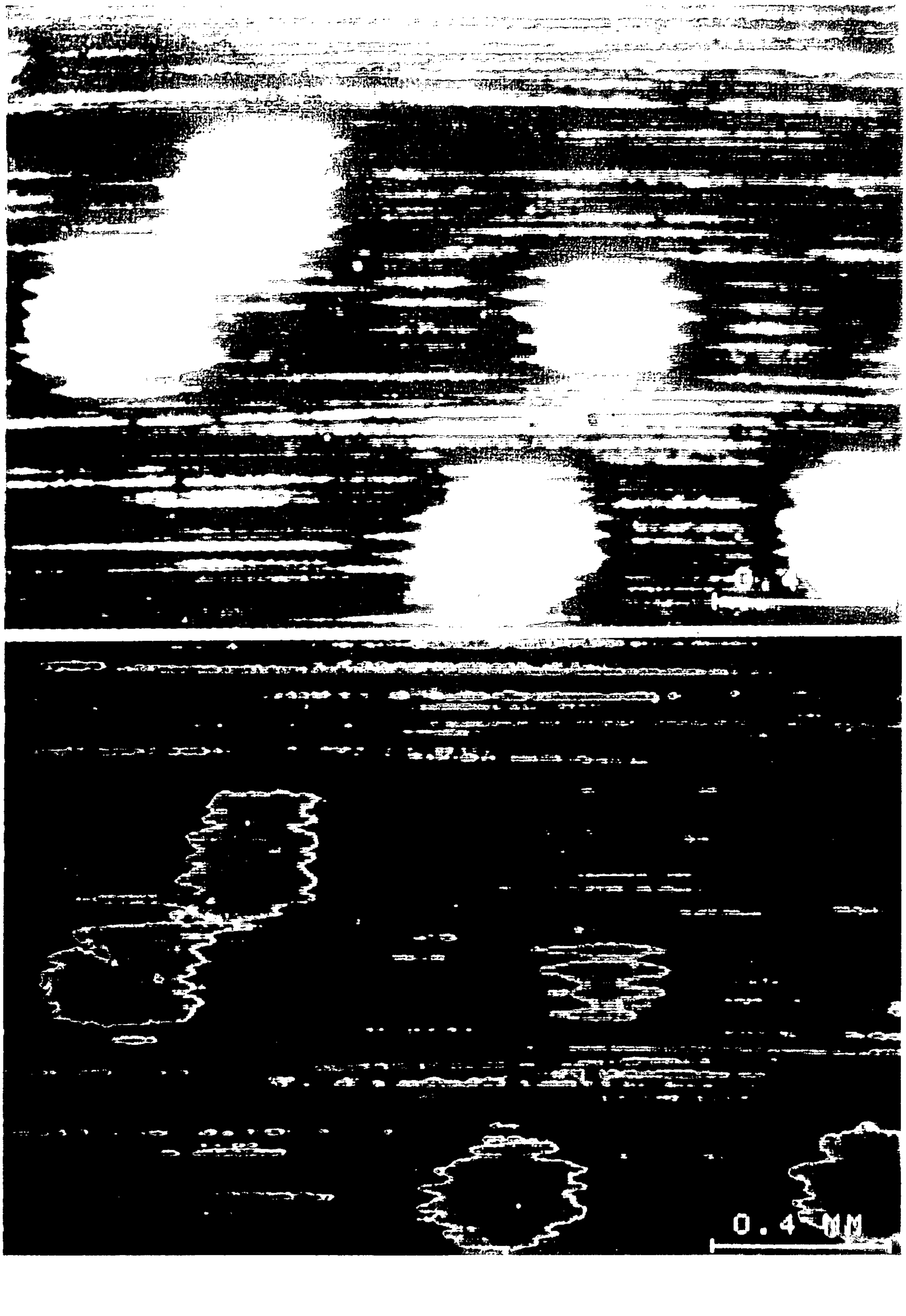
0.4 MM

[TR-48]

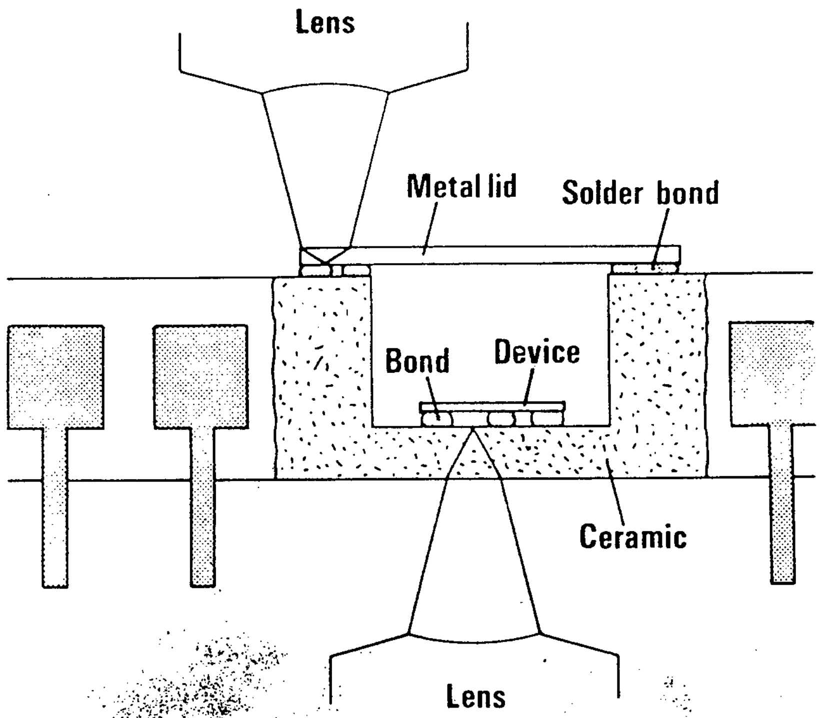

[TR-49]

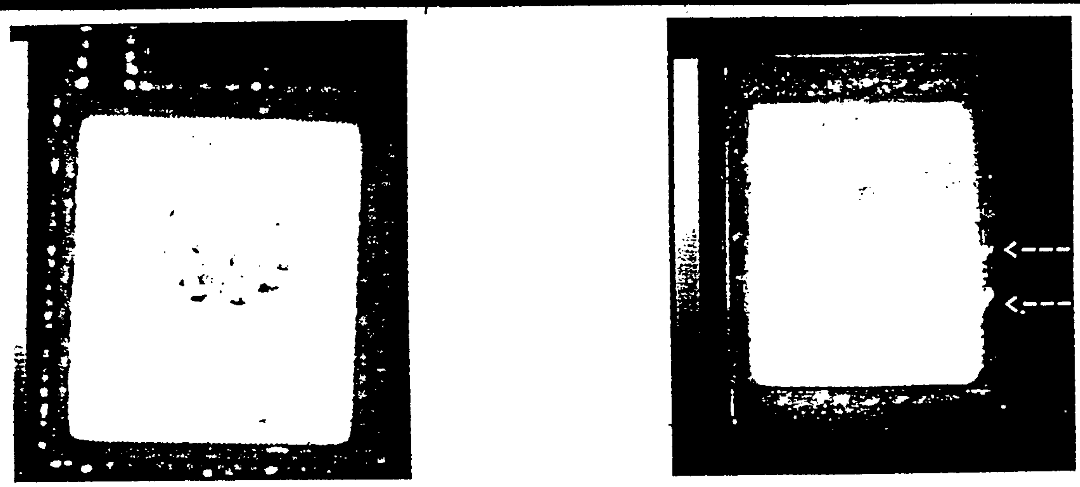

(a) (b)

Fig. 18. (a) Image of solder bond fixing the package lid, revealing two voids that nearly break the hermetic seal. (b) Image through the ceramic of the device-ceramic bond with suprisingly few points of contact. Field of view is 12 × 12 mm

[TR-50]

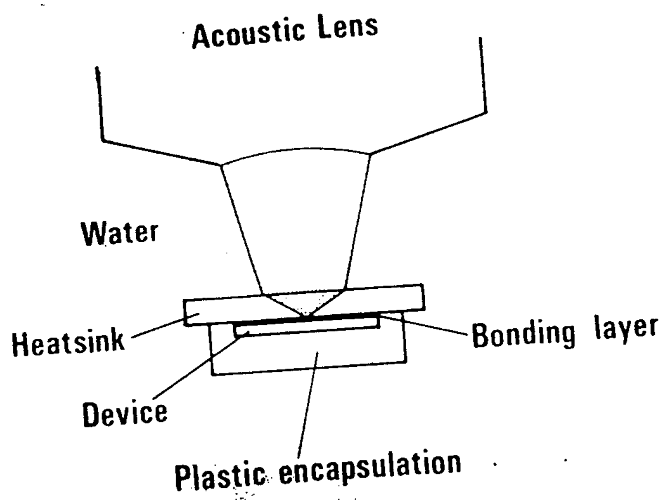

(a)

Fig. 15. (a) Geometry for examining device-heatsink bonding in packaged transistor devices. The acoustic beam is focused onto the bond layer through the heatsink.

[TR-51]

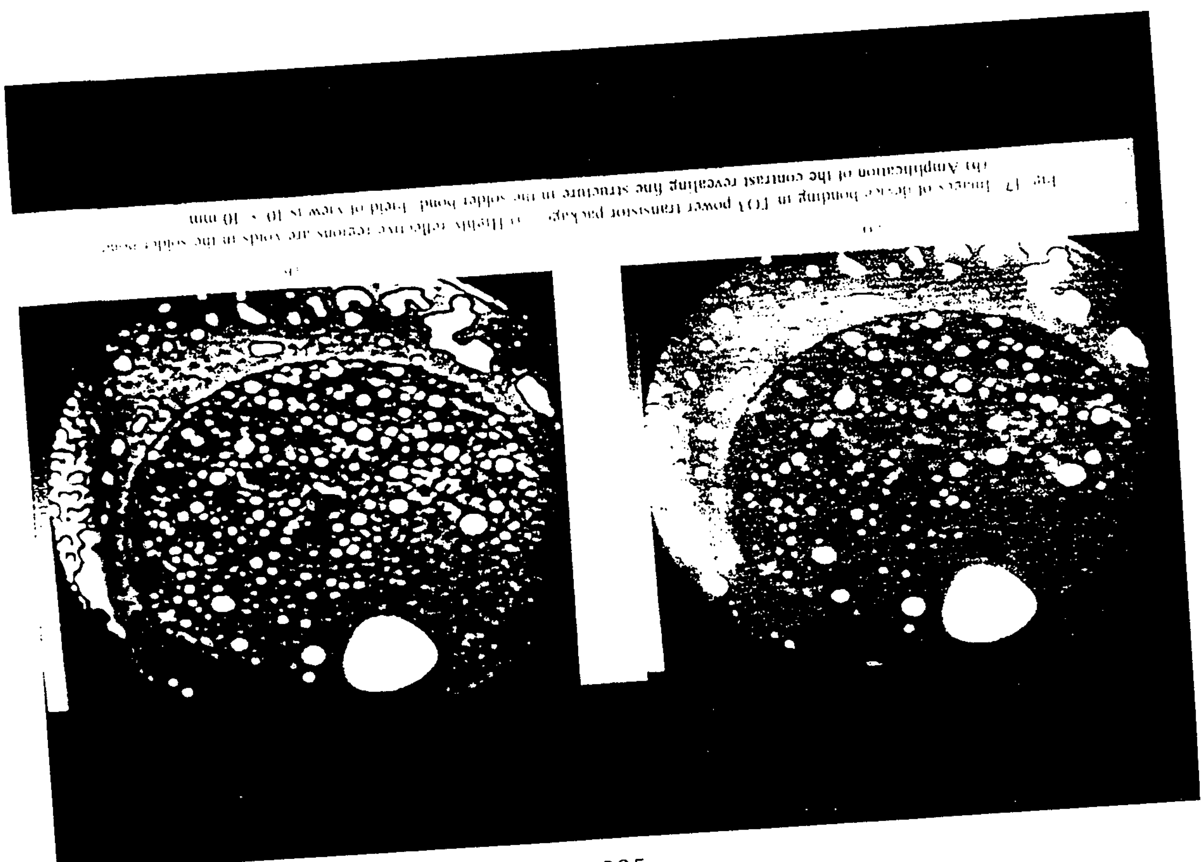

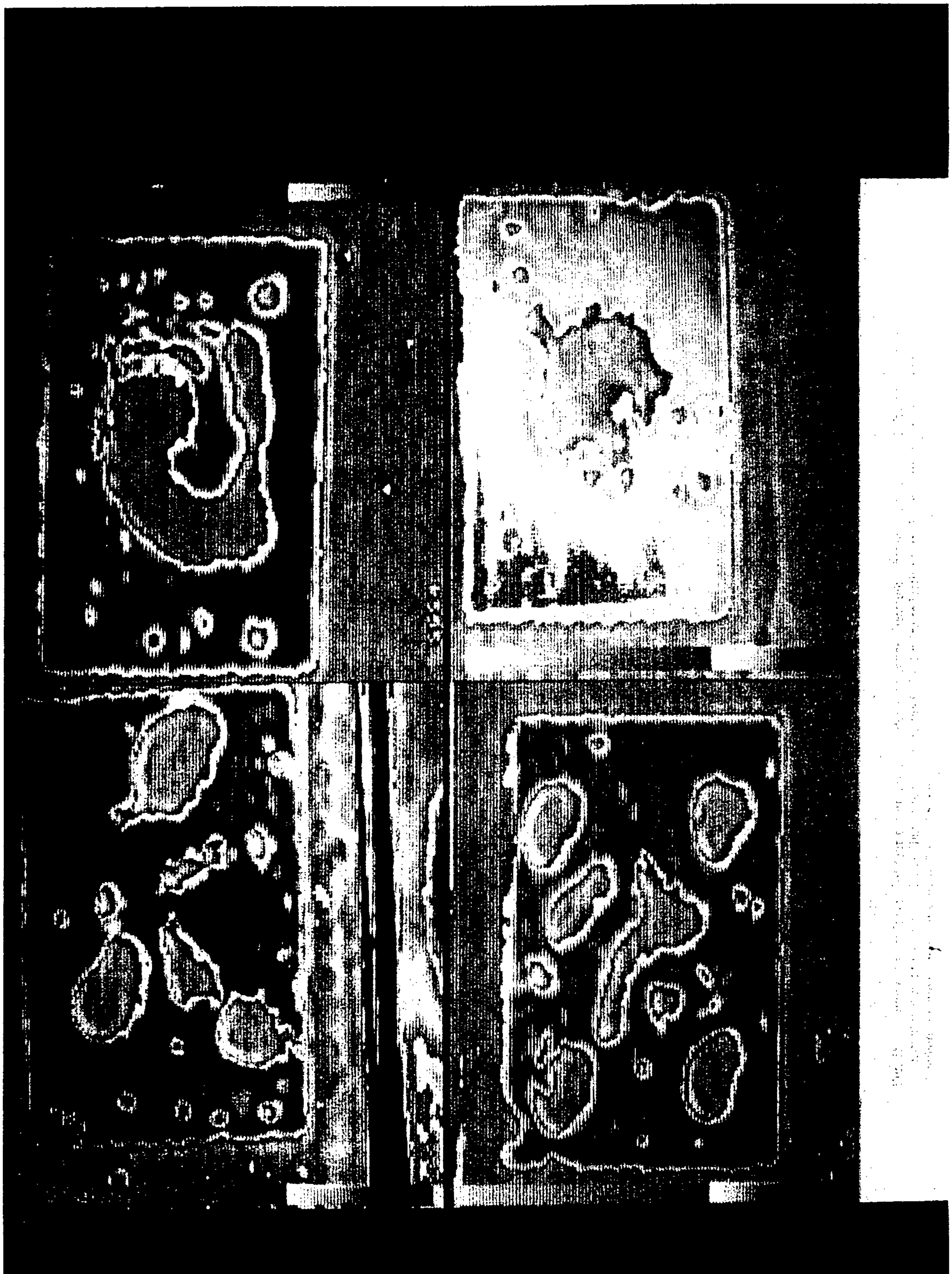

[TR-52]

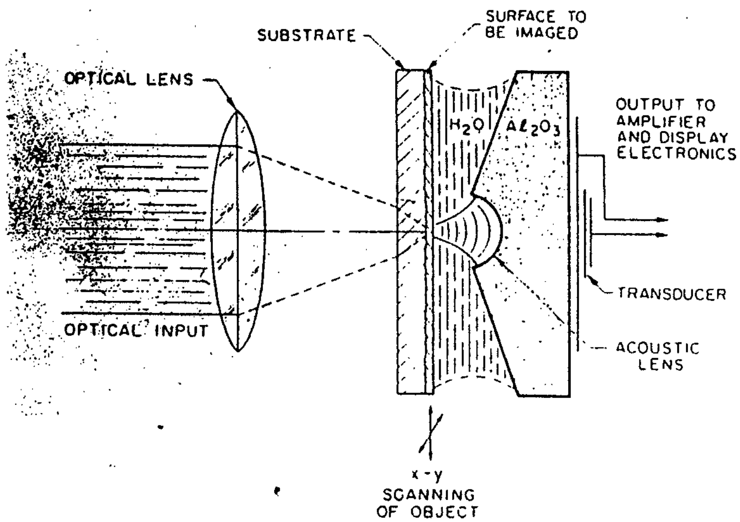

Figure 4-1. The experimental arrangement for photoacoustic imaging of thin films on optically transparent substrates using an acoustic lens to collect the sound generated by the modulated optical power

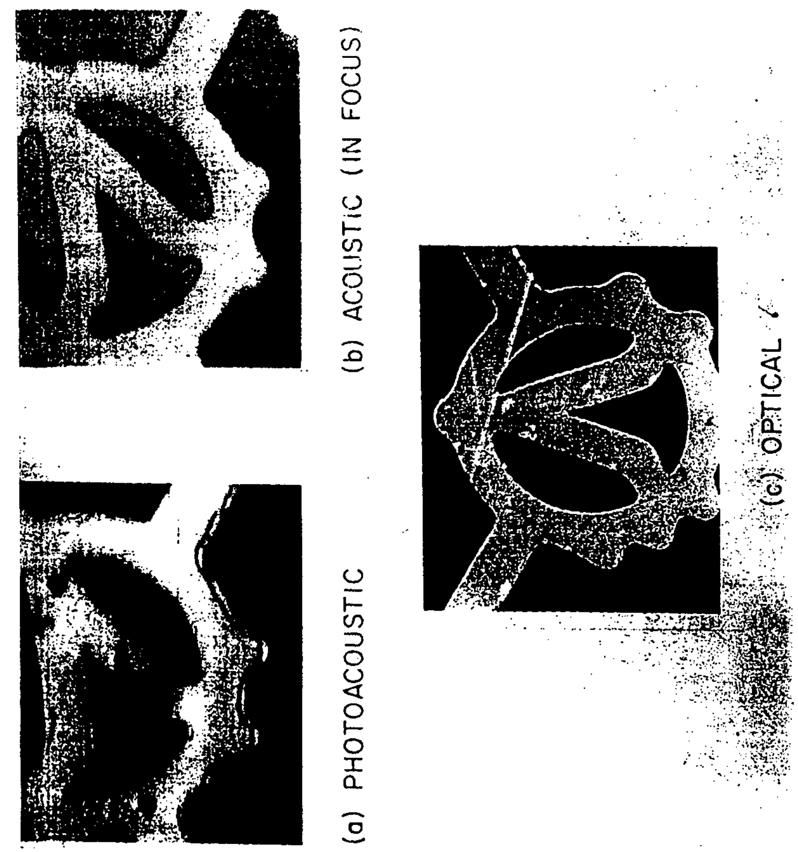

(b) ACOUSTIC (IN FOCUS)

(a) PHOTOACOUSTIC

(c) OPTICAL

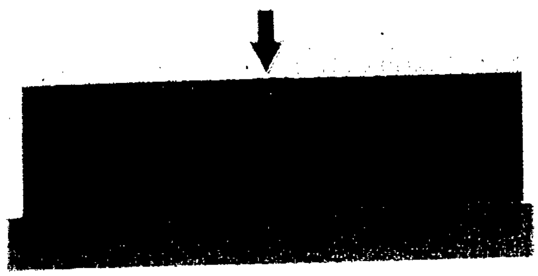

Figure 1a. Illustration of the generation of an ultrahigh frequency sound pulse used in picosecond ultrasonics. The thick arrow indicates the generating laser pulse arriving at the surface of a sample consisting of a film (blue) deposited on a substrate (orange). The absorbed light causes a sudden temperature rise thermal expansion within the region shown in red.

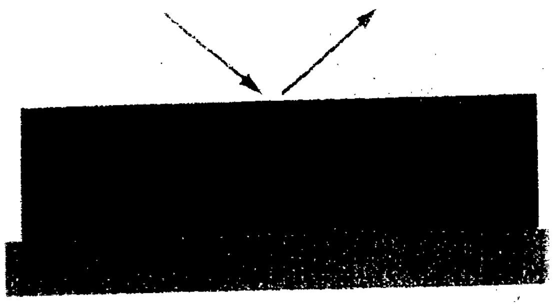

Figure 1b. Illustration of the sound pulse generated in the heated region of Fig. 1a as it propagates away from the surface at the velocity of sound in the film (blue). The presence of the sound pulse in the film gives rise to a small change in its reflectivity which is greatest when the sound is close to the surface. The reflectivity change is measured continuously by means of a laser beam (shown in red) as the sound propagates in the film.

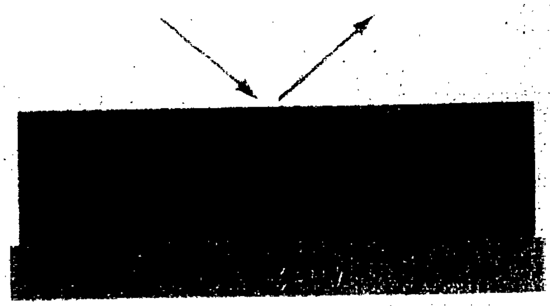

Figure 1c. Illustration of the sound pulse after reflection from the interface between the film (blue) and substrate (orange). Part of the sound escapes into the substrate, and the remainder travels back to the surface of the film. The fraction of the incident sound reflected at the interface is a function of the acoustic mismatch of the film and substrate materials, and also of the film to substrate adhesion.

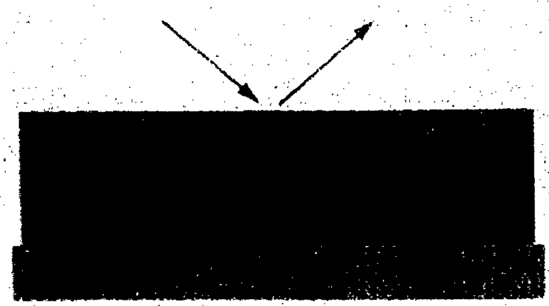

Figure 1d. Illustration of the sound pulse at a later time returning to the surface of the film where it causes a sudden change in the reflectivity DR(t). This reflectivity change (an echo) measured using the laser beam shown in red.

[TR-56 Unavailable At Time Of Printing]

[TR-57]

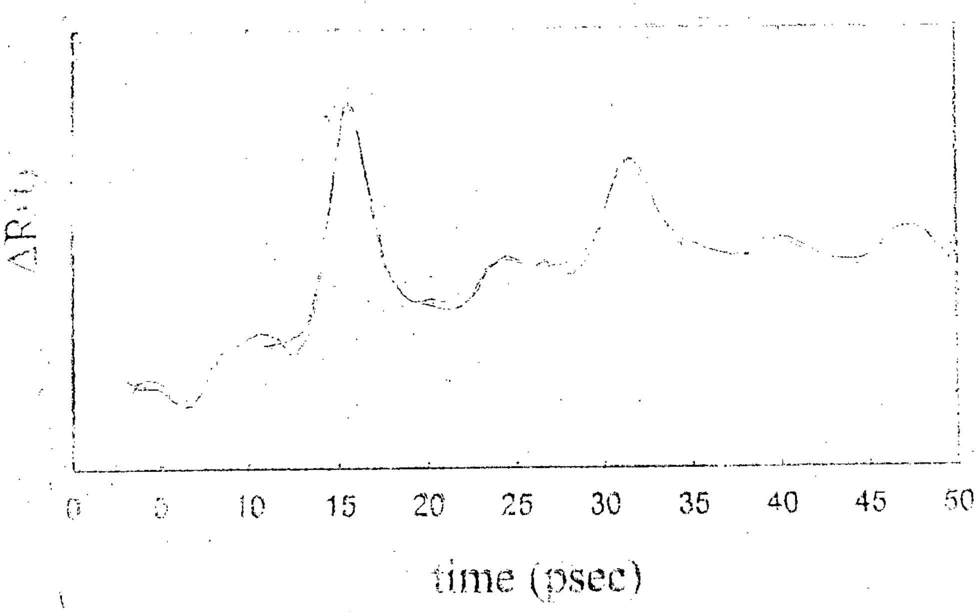

Figure 5a. Acoustic vibrations of a bilayer consisting of 393Å TiN deposited on 230A PVD Ti on thick ILD. Blue line is data, and red line is a theoretical fit.

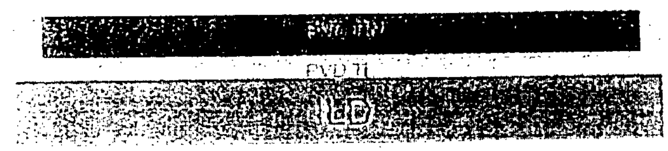

Figure 5b. Sample structure for measurement shown in Figure 5a. (393Å PVD TiN/ 230Å deposited on thick ILD).

[TR-58 Unavailable At Time Of Printing]

[TR-59]

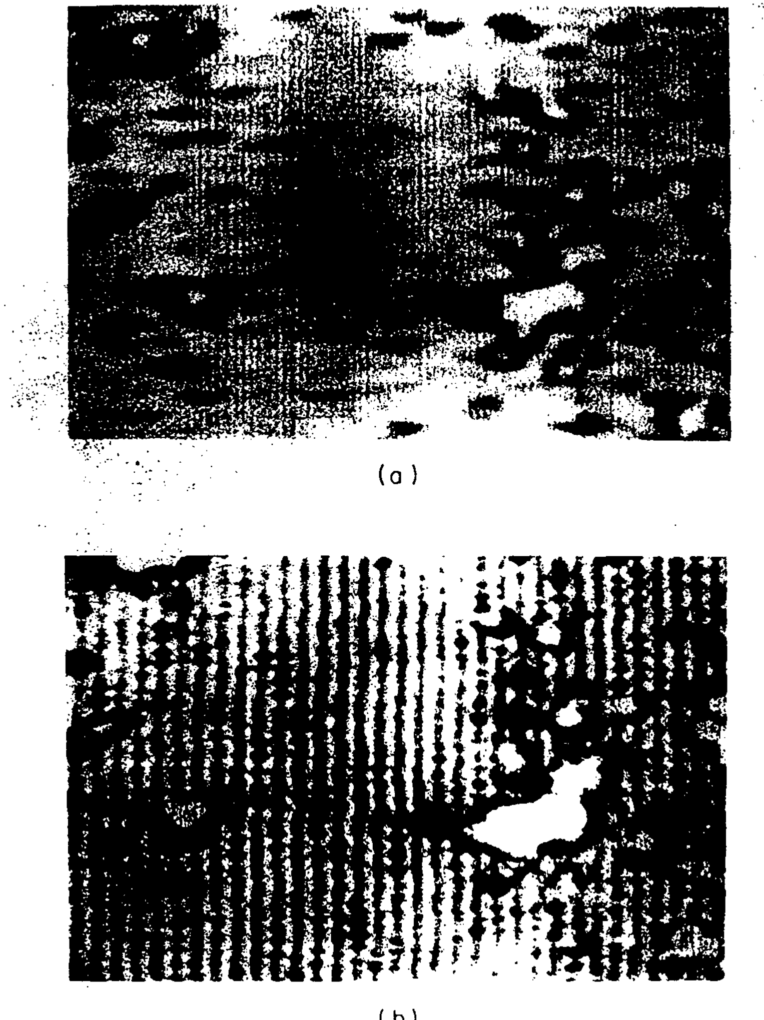

FIG. 5-1. Nonlinear resolution of 2000 Å grating in liquid argon. Image (a) was taken at low input power, while (b) was taken at higher power.

[TR-60]

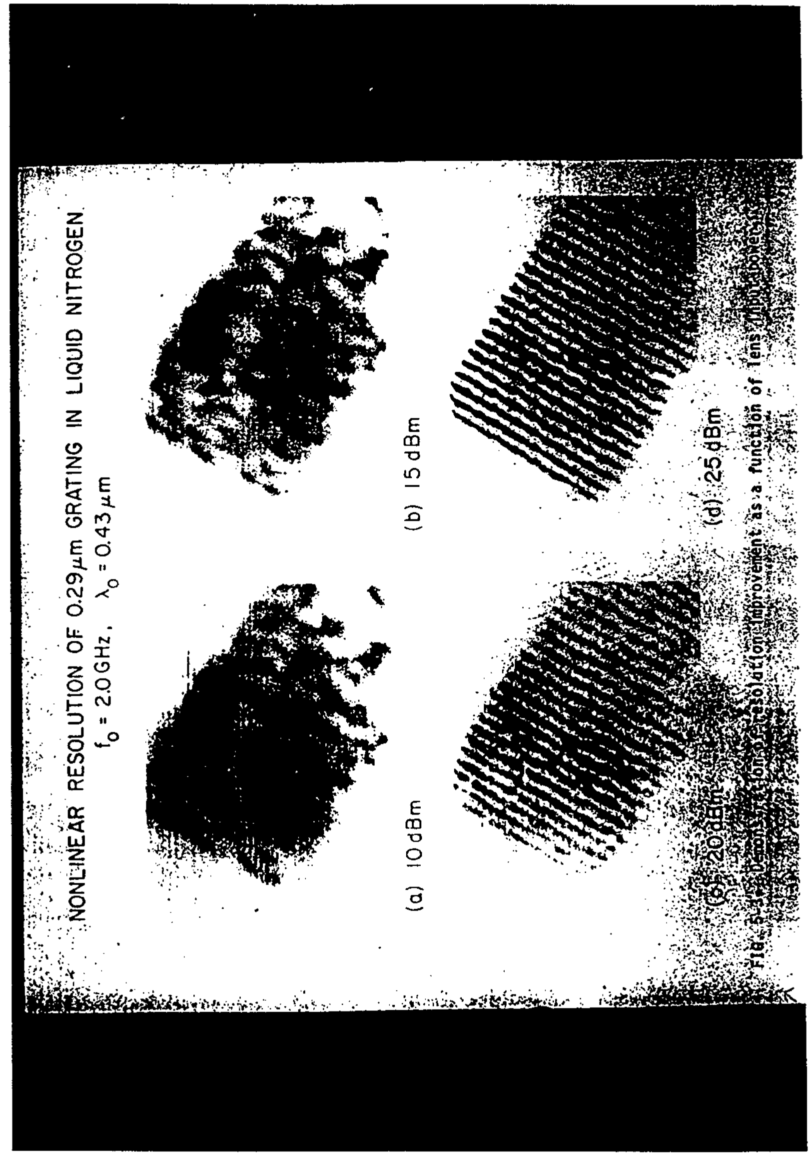

[TR-61]

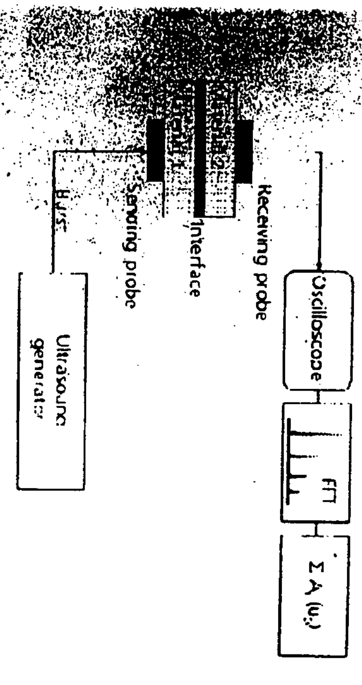

Experimental apparatus in order to test the adhesion of a bond

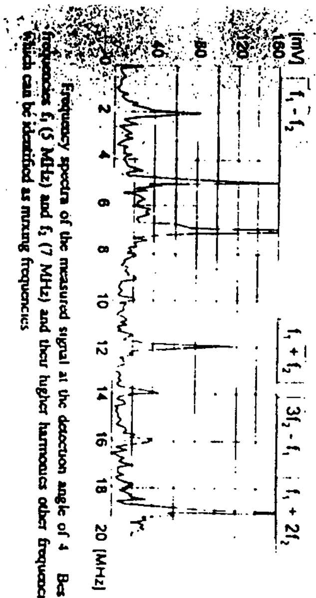

Frequency spectra of the measured signal at the detection angle of 4. Besides the fundamental frequencies f_1 (5 MHz) and f_2 (7 MHz) and their higher harmonics other frequencies could be detected which can be identified as mixing frequencies

[TR-62]

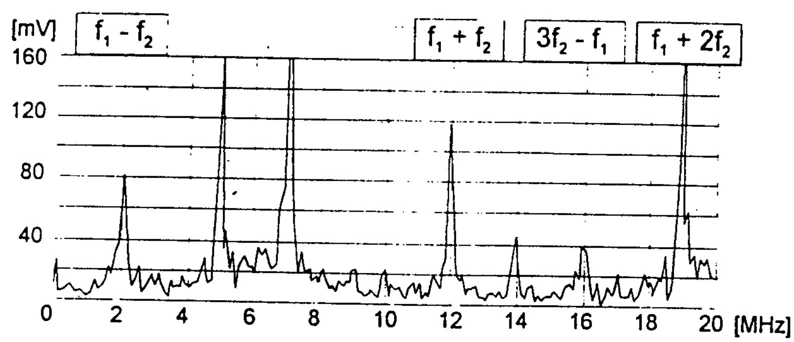

Frequency spectra of the measured signal at the detection angle of 4°. Besides the fundamental frequencies f_1 (5 MHz) and f_2 (7 MHz) and their higher harmonics other frequencies could be detected which can be identified as mixing frequencies.

[TR-63]

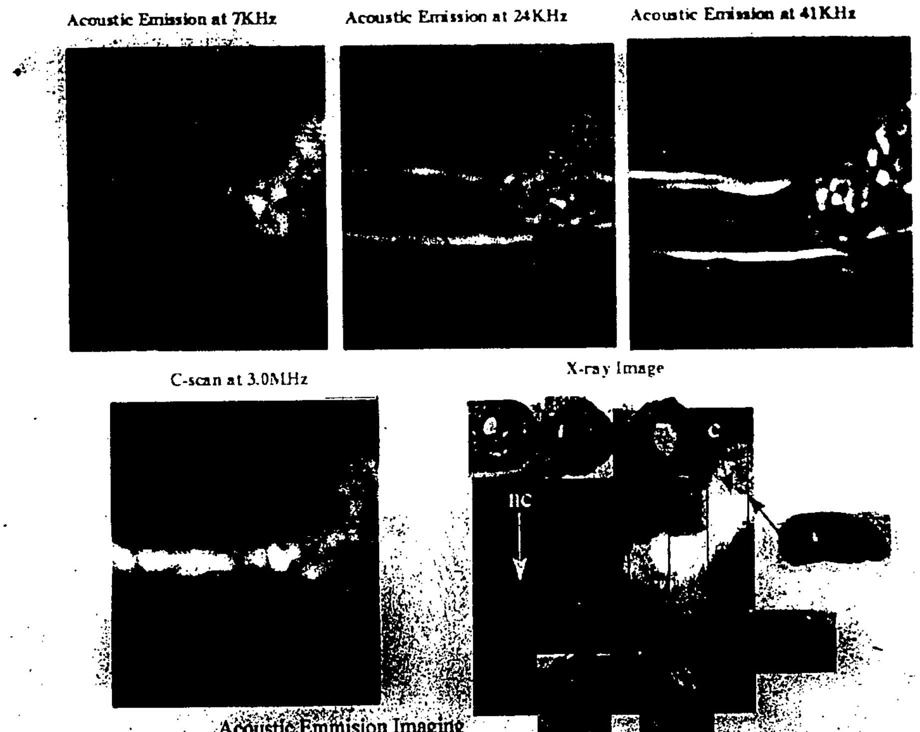

Acoustic Emmision Imaging
Jim Greenleaf, Mayo Foundation

[TR-64]

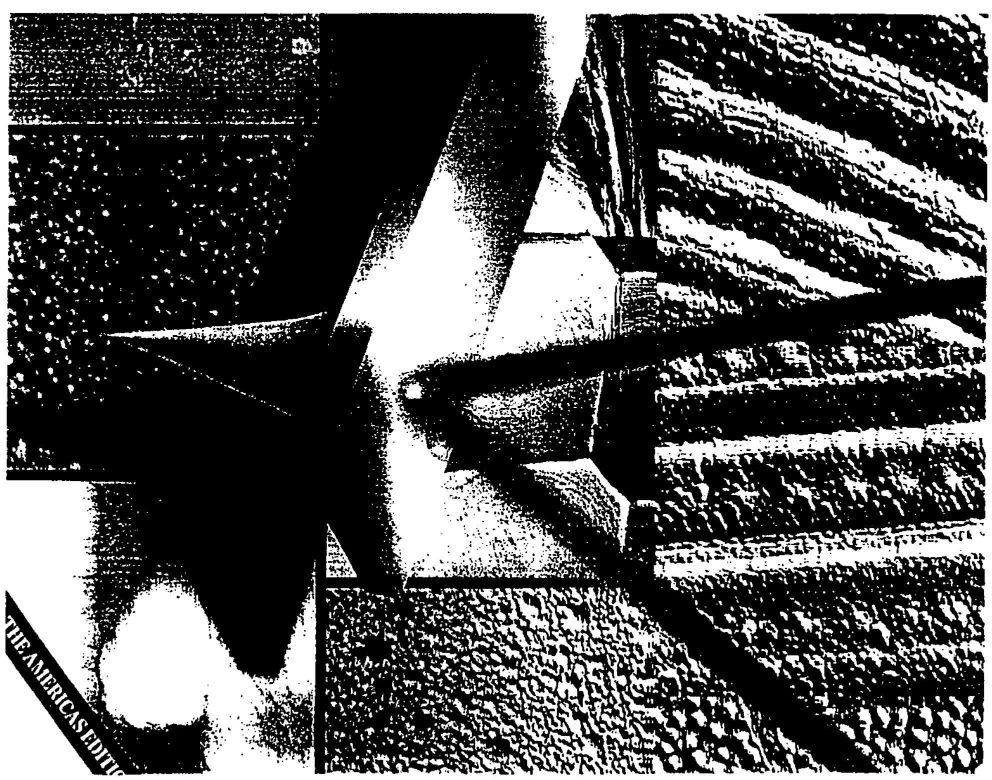

[TR-65]

Principles of Ultrasonic Force Microscopy
Kolosov and Yamanaka, 1993

Atomic Force Microscope (AFM) vs Ultrasonic Force Microscope (UFM)

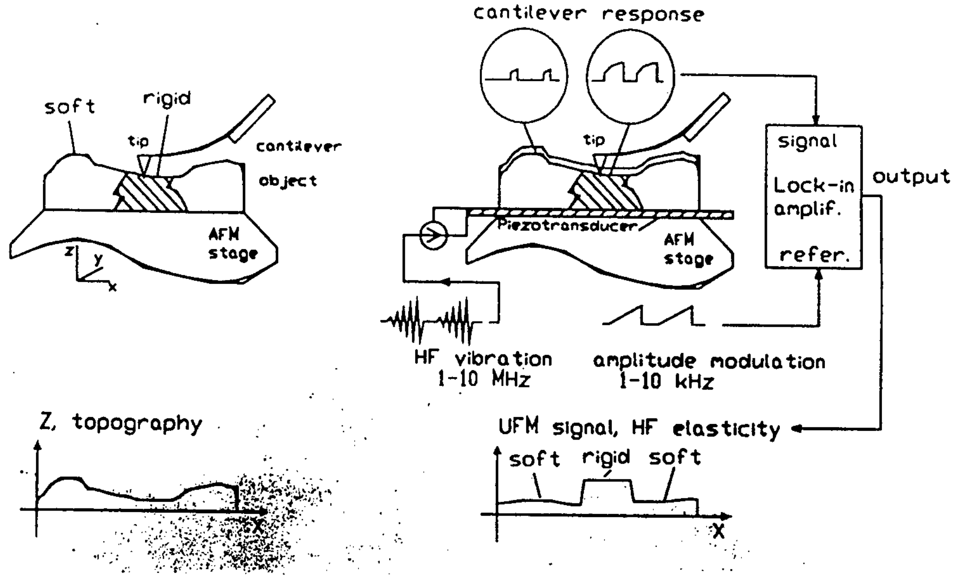

[TR-66]

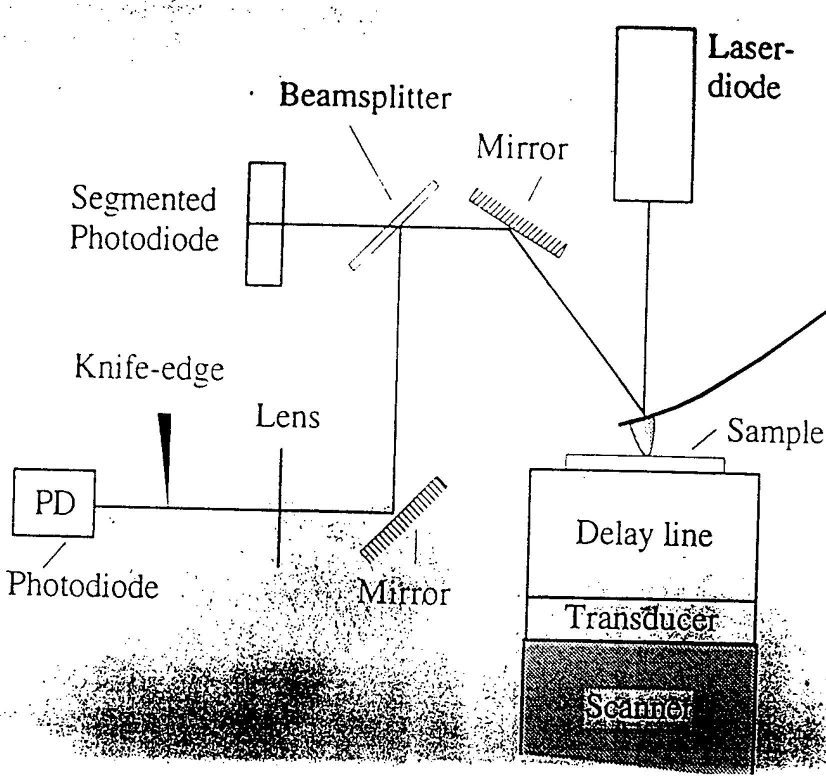

Atomic Force Acoustic Microscope

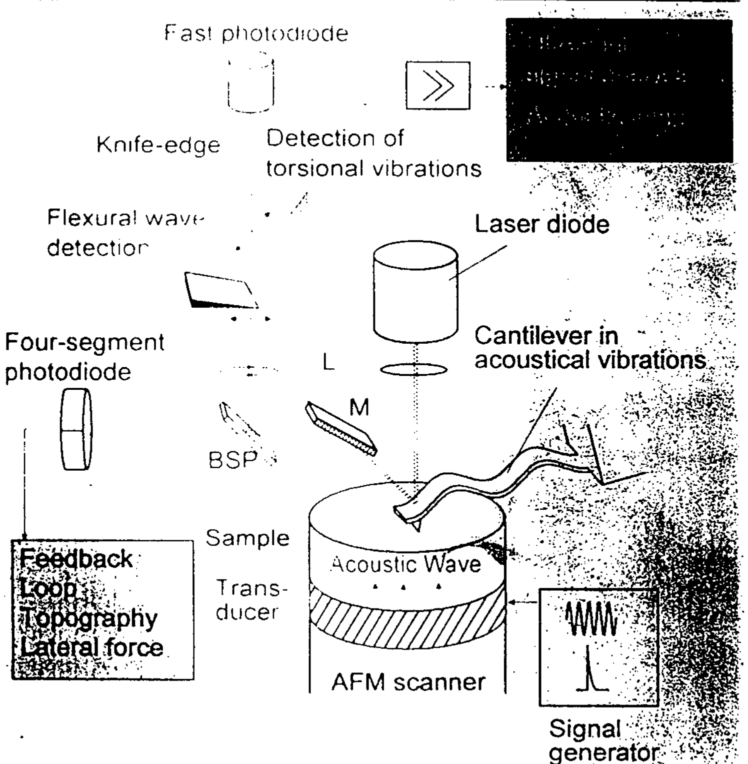

Fraunhofer IZFP

Acoustical images of a polymer sample

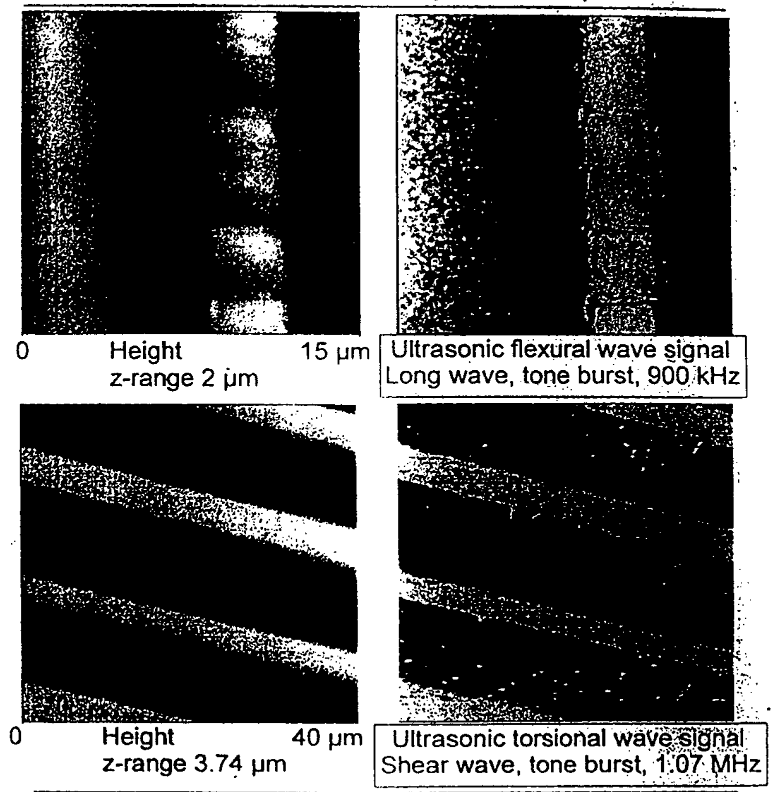

Fraunhofer IZFP

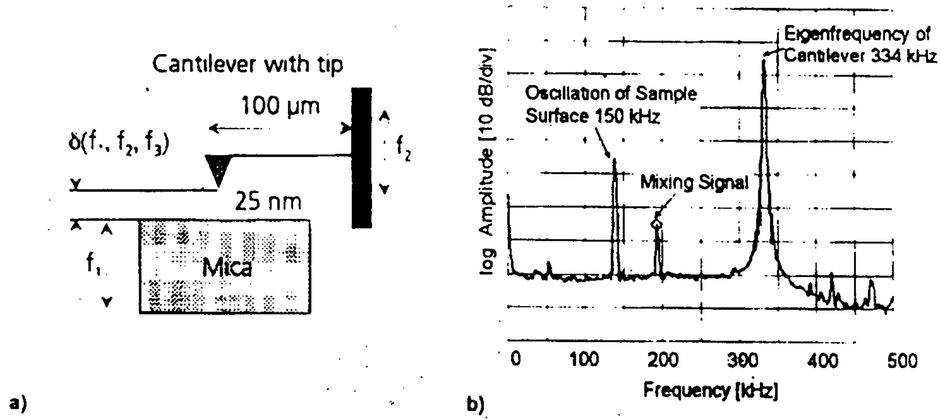

a) Experimental set-up to probe a single contact. b) Measured frequency spectrum of the cantilever oscillations. Besides the two exciting frequencies, the difference frequency can be observed clearly.

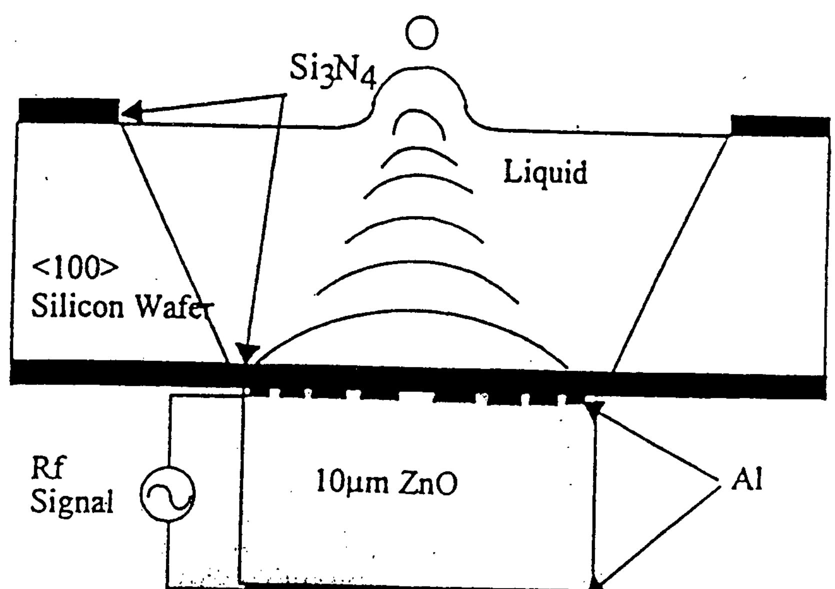

Lensless liquid ejector using a constructive interference of acoustic waves.

[TR-1]

POROUS MATERIALS

JAMES M. SABATIER
NATIONAL CENTER FOR PHYSICAL ACOUSTICS
UNIVERSITY OF MISSISSIPPI

1. A FEW ACOUSTIC MEASUREMENTS ON THE BEACH
2. POROUS MEDIUM PHYSICAL PROPERTIES
3. SOUND PROPAGATION IN RIGID POROUS MEDIA
4. SOUND PROPAGATION IN PORO-ELASTIC MEDIUM

[TR-2]

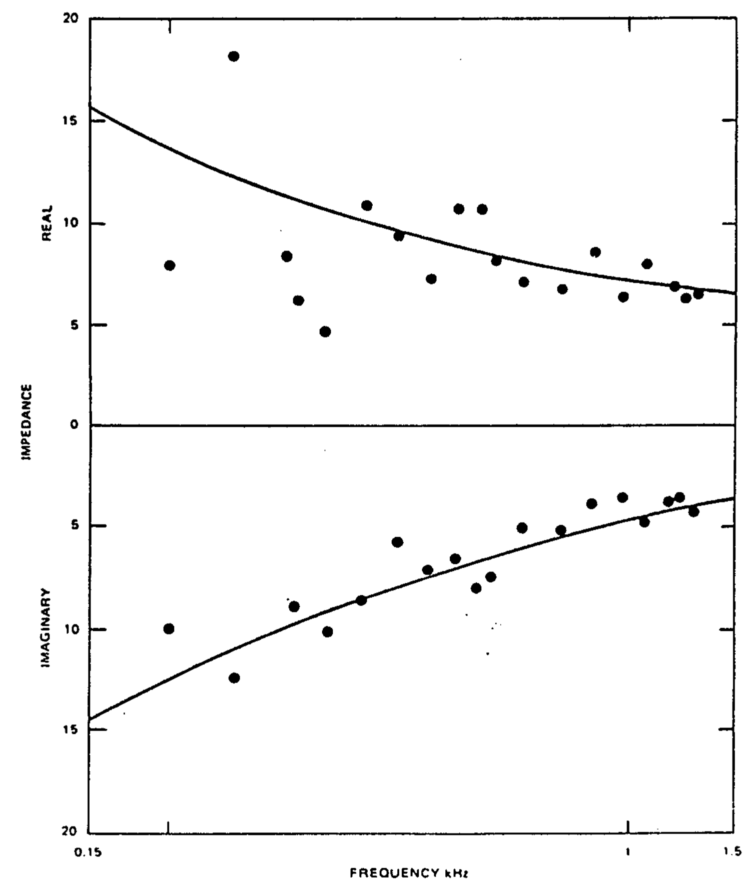

Figure A2. Comparison between the impedance of a sandy soil surface measured (dots) at oblique incidence and theoretical predictions at normal incidence (solid lines) for each of the three models discussed.

[TR-3]

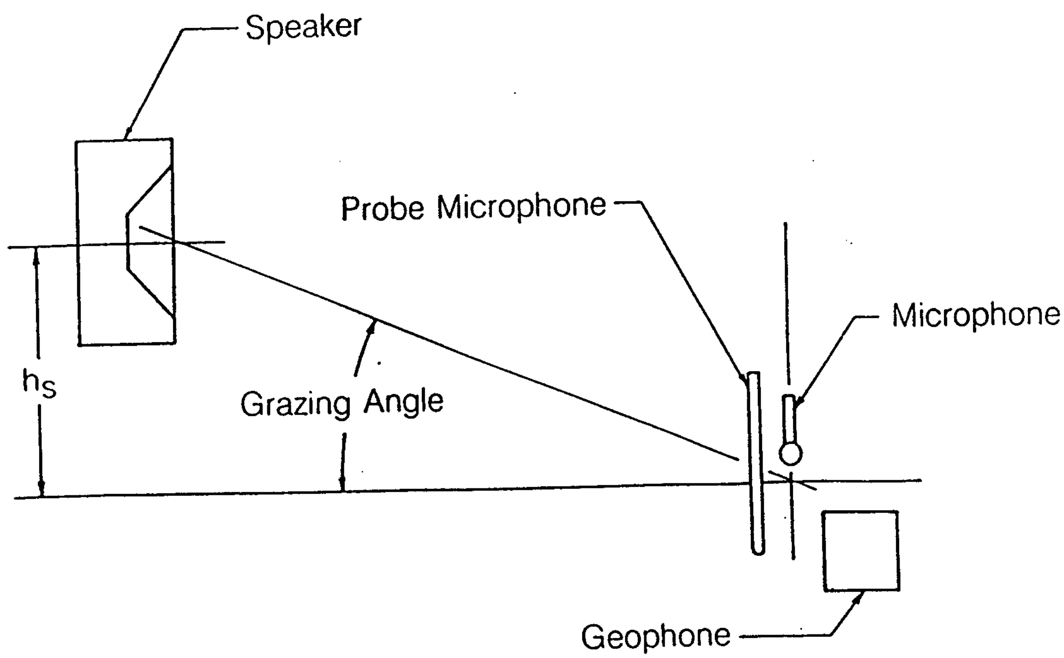

Figure C2. Relative positions of source and sensors used for seismic transfer measurements.

[TR-4]

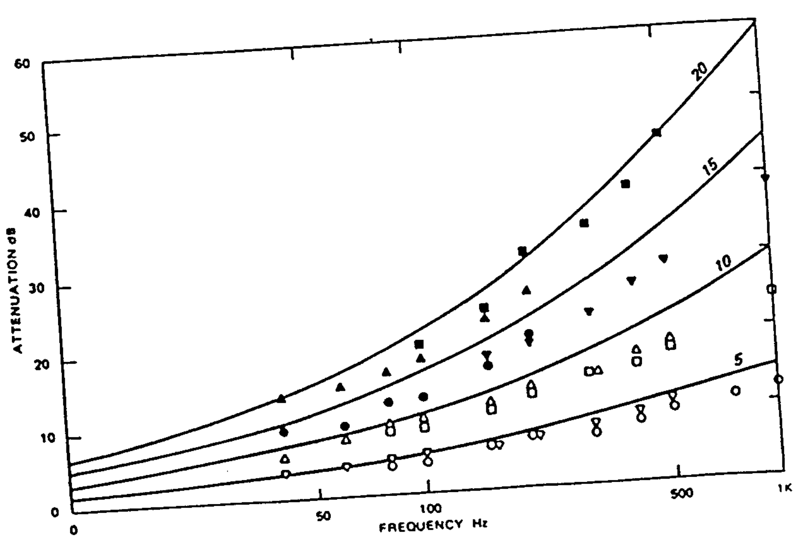

Figure B4. Attenuation versus depth in a sand quarry. Measurements were made with probe at 5 cm (△○), 10 cm (△□), 15 cm (●▲), and 20 cm (▲■).

Attenborough, Bass, Bolen

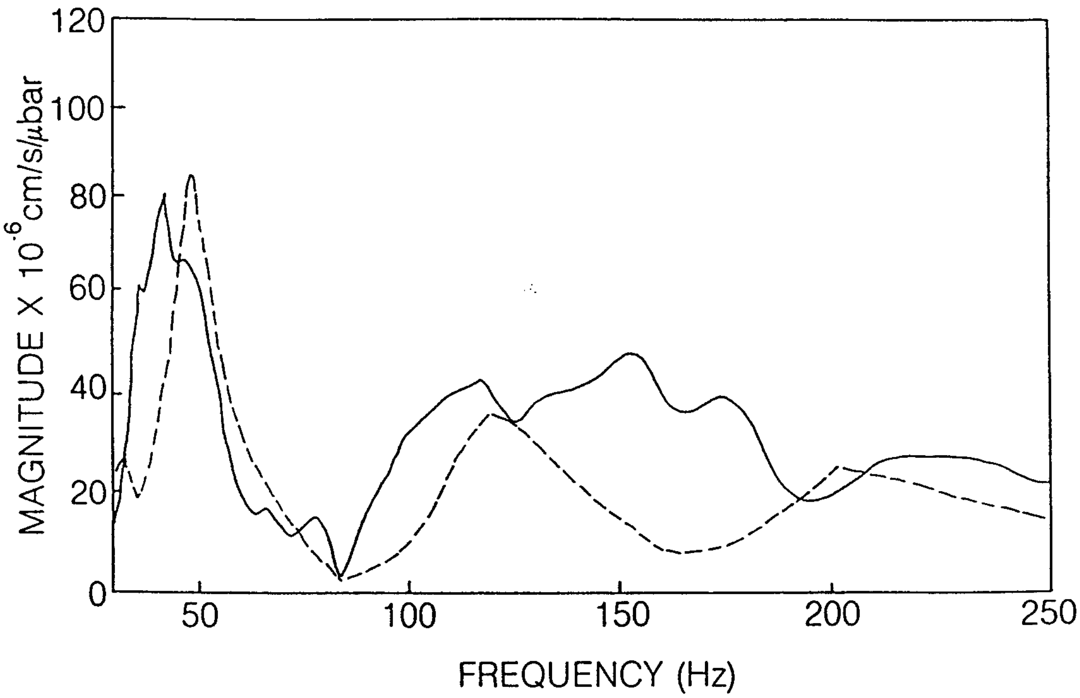

Figure C3. Measured (solid line) and predicted (dashed line) vertical seismic transfer function for Loess.

[TR-6]

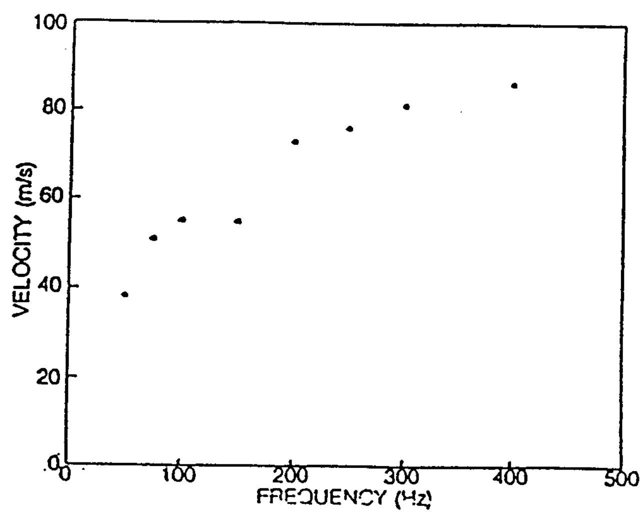

Figure 3.4. Acoustic phase velocity measured with the probe microphone in a sand with a flow resistivity of 85 rayls/cm.

[TR-5]

[TR-7]

PHYSICAL PROPERTIES OF POROUS MATERIALS

The sample material consists of a frame or matrix saturated with a fluid

$\rho_s \equiv$ density of solid component
$\rho_f \equiv$ density of saturating fluid

Porosity $(\Omega) \equiv \dfrac{\text{volume of fluid}}{\text{volume of bulk}}$

$$\Omega = \frac{v_f}{v_b}$$

$$V_b = v_f + v_s$$

Bulk density of porous material

$$\rho_b = (1 - \Omega)\rho_s + \Omega\rho_f$$

There are no isolated voids

[TR-8]

FLOW RESISTIVITY

Porous sample in a pipe of cross-sectional area A. Apply a differential pressure to cease steady flow.

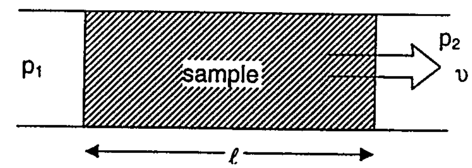

Flow resistance

$$S = \frac{\Delta p}{\upsilon} \qquad \Delta p = p_1 - p_2 \qquad \upsilon \equiv \text{average flow velocity/area}$$

Flow resistivity

$$\sigma = \frac{S}{\ell}$$

$$\sigma = \frac{\Delta p}{\upsilon \cdot \ell} \qquad \text{(units } Nsm^{-4}\text{)}$$

Measurement Techniques

Leonard's – Simplified Flow Resistance, JASA **17** (1946)
Rudnick – Boundary Modification – JASA

[TR-9]

LEONARD'S APPARATUS WITH RUDNICK'S MODIFICATION

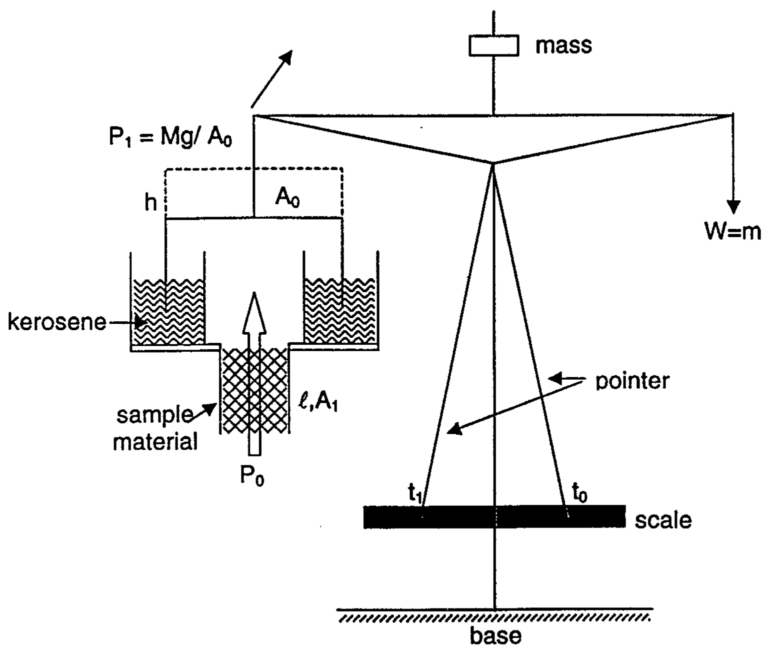

[TR-10]

TORTUOSITY MEASUREMENT

Dielectric frame or matrix saturated with a conducting fluid

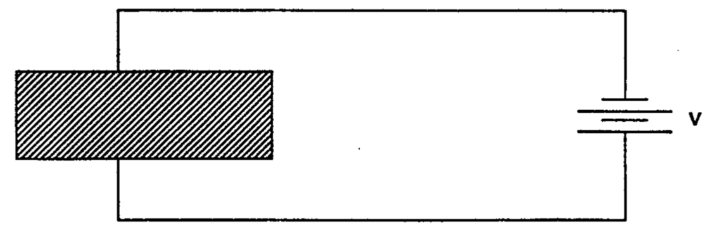

Resistivity of fluid alone = r_f

Resistivity of saturated material = r_c

$$q_2 = \Omega \frac{r_c}{r_f}$$

[TR-11]

SIMPLE POROUS MEDIA MODEL

1. "Soda Straw"

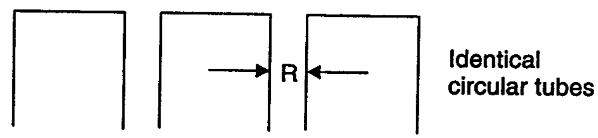

$n \equiv$ number of pores of radius R per unit area of cross-section

$\Omega = n\pi R^2 \equiv$ porosity

2. Geometrical Packing of Spheres

simple cubic, bcc, etc.

3. More Relevant – Random Packing of Spheres

soils, sediments, sands

[TR-12]

A BRIEF REVIEW OF LINEAR IDEAL ACOUSTCS

The linearized equations of state, continuity, and motion are:

$$p(s) = Bs = B\frac{\rho - \rho_0}{\rho_0} \qquad \text{"State"}$$

$$\rho_0 \nabla \bullet \bar{u} + \frac{\partial p}{\partial t} = 0 \qquad \text{"Continuity"}$$

$$-\nabla p = \rho_0 \frac{\partial \bar{u}}{\partial t} \qquad \text{"Motion"}$$

Acoustic variables: p, ρ, u are pressure, density and velocity, respectively

Combine these to yield a wave equation

[TR-13]

WAVE EQUATIONS FOR FLUIDS (IDEAL)

$$\boxed{\nabla^2 p = \frac{1}{c^2}\frac{\partial^2 \rho}{\partial t^2}}$$

$c^2 = \sqrt{\frac{\beta}{\rho_0}}$ $\beta \equiv$ adiabatic bulk modulus

$\beta = \gamma p_0$

p = acoustic pressure

ρ_0 = air density

$r \equiv$ ratio of specific heats C_p/C_v

GENERAL SOLUTION

$$P = Ae^{i(\omega t - kx)}$$

$$K = \frac{\omega}{c} = \omega\sqrt{\frac{\rho_0}{\beta}}$$

[TR-14]

FLUIDS WITHOUT ABSORPTION

Write Wave Number

$$\tilde{k} = (k_r - i\alpha)$$

Solution now is

$$P = e^{-\alpha x} e^{-i(k_r x - \square t)}$$

Rewrite Wave Equation as

$$\nabla^2 p = \frac{1}{\tau^2}\frac{\partial^2 p}{\partial t^2}$$

$$\tilde{k} = \frac{\omega}{\tau} = \omega\sqrt{\frac{\tilde{\rho}'}{\tilde{\beta}'}}$$

Our goal becomes to determine the effects of viscous friction and thermal conduction and write these effects down in terms of $\tilde{\rho}'$ and $\tilde{\beta}'$.

[TR-15]

VISCOUS FRICTION FORCE (SHEAR VISCOSITY)

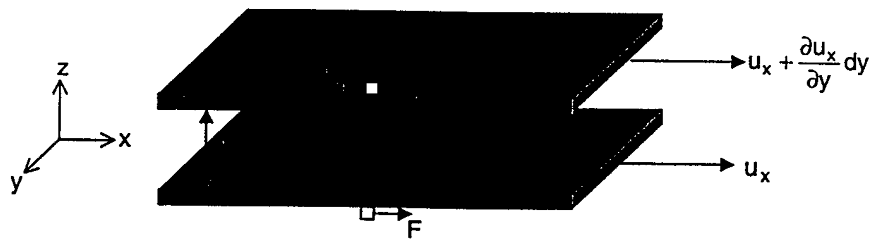

Two fluid layers moving at different speeds

$F \sim [\Delta u_x, \text{Area}, dy]$

$$F \propto \left[u_x + \frac{\partial u_x}{\partial y} dy - u_x\right] dxdz \frac{1}{dy}$$

$$\text{Stress} = \frac{F}{A} \approx \frac{\partial u_x}{\partial y} \Rightarrow \text{Strain rate} = \frac{\Delta L}{L} \cdot \frac{1}{t} = \frac{\Delta V}{L}$$

$$P_{xy} = \eta \frac{\partial u_x}{\partial y}$$

For a volume element:

$$P_{xy} = \eta \left(\frac{\partial u_x}{\partial y} + \frac{\partial u_y}{\partial x} \right)$$ $\eta \equiv$ coefficient of viscosity

[TR-16]

VISCOUS PENETRATION DEPTH

$\frac{1}{e}$ drop-off of velocity from the wall

$$\delta_\eta = \sqrt{\frac{2\eta}{\omega\rho}}$$ δ_η is the viscous penetration depth

In air at 10 kHz,

$\delta_\eta = 20\ \mu$

[TR-17]

SOUND PROPAGATION IN A SINGLE CYLINDRICAL TUBE WITH VISCOUS DRAG AND THERMAL CONDUCTION

Zwicker and Kosten, *Sound Absorbing Materials*

Tube:

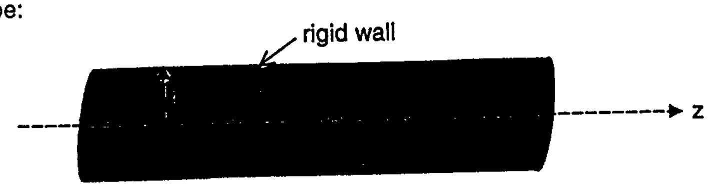

Z. & K. assume: pressure is independent of r; frequency is below first non-planar mode

Others: Tijdeman, Arnott, Stinson

Show that $p = p(z)$ is valid.

[TR-18]

APPLY TO A CYLINDRICAL TUBE

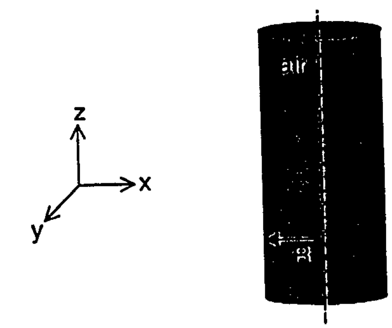

Assume

$u = u(z)$
$u_x = u_y = 0$
$u_z = 0$
$r = R$

$F = ma$

$$i\omega\rho_0 u_z = \frac{\partial p}{\partial z} + \eta\left(\frac{\partial^2 u_z}{\partial x^2} + \frac{\partial^2 u_z}{\partial y^2}\right)$$

In cylindrical coordinates

$$i\omega\rho_0 u_z = -\frac{\partial p}{\partial z} + \frac{\eta}{r}\frac{\partial}{\partial r}\left(r\frac{\partial u_z}{\partial r}\right)$$

Bessel's equation and solution for velocity

$$u_z = -\frac{1}{i\omega\rho_0}\frac{\partial p}{\partial z}\left(1 - \frac{J_0(2r)}{J_0(\ell R)}\right)$$

$$\ell = \sqrt{\frac{-i\omega\rho_0}{\eta}}$$

[TR-19]

AVERAGE VELOCITY ACROSS TUBE

$$\bar{u}_z = \frac{\int_0^R u_z 2\pi r dr}{\pi R^2}$$

$$\bar{u}_z = -\frac{1}{i\omega\rho_0}\frac{\partial p}{\partial z}\left[1 - \frac{2}{s\sqrt{-i}}\frac{J_1(s\sqrt{-i})}{J_0(s\sqrt{-i})}\right]$$

with

$$s = \sqrt{\frac{\omega\rho_0 R^2}{\eta}} = \frac{R\sqrt{2}}{\delta_\eta} \equiv \text{shear wave number}$$

In terms of "effective" or "complex density," F = ma can be written as

$$-\frac{\partial p}{\partial z} = i\omega\rho\bar{u}_z$$

where

$$\rho = \rho_0\left[1 - \frac{2}{s\sqrt{-i}}\frac{J_1(s\sqrt{-i})}{J_0(s\sqrt{-i})}\right]^{-1} \Rightarrow \text{effective density}.$$

Effective density for semi-infinite slit of width 2a is

$$\rho = \rho_0\left[1 - \frac{\tanh(s'\sqrt{i})}{s'\sqrt{i}}\right]^{-1}$$

with

$$s' = \sqrt{\frac{\omega\rho_0 a^2}{\eta}}$$

[TR-20]

J. F. Allard
Propagation of Sound in Porous Media
Elsevier, 1993

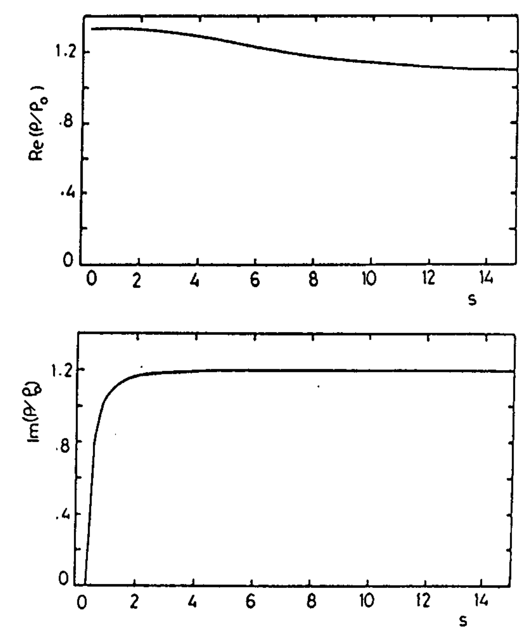

FIG. 4.4. The ratio ρ/ρ_0, where ρ is the effective density of a fluid of density ρ_0 in a cylindrical tube having a circular cross-section, as a function of s.

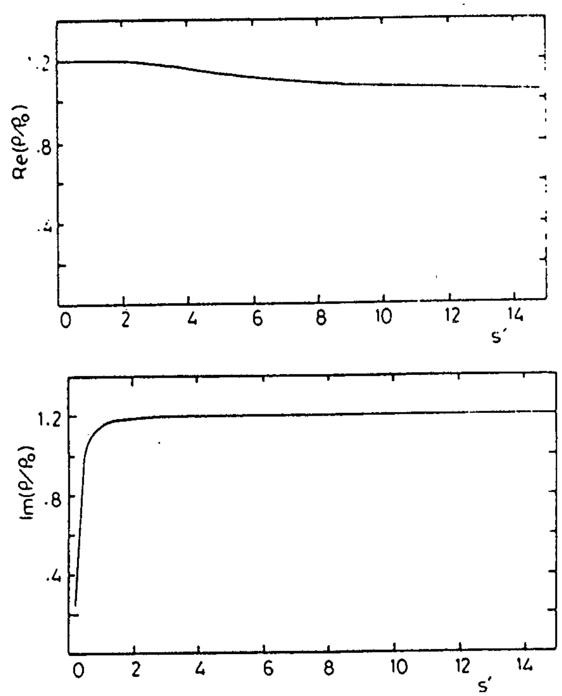

FIG. 4.5. The ratio ρ/ρ_0, where ρ is the effective density of a fluid of density ρ_0, in a slit, as a function of s'.

ref:
Allard

EFFECTIVE BULK MODULUS
(Incorporate Thermal Conductivity)

References:

Attenborough, "Acoustical Characteristics of Porous Materials," Phys. Rep. **82** (3), 1982.

David Craig, "Acoustic Propagation in Fractal Porous Media," Ph.D. Dissertation, University of Mississippi, 1995.

Stinson, JASA **89**, 1991.

Considering heat conduction and compression of the fluid, arrive at effective bulk modulus.

Circular tube:

$$k = \gamma p_0 \left[1 + (\gamma - 1) \frac{2}{N_{Pr} s\sqrt{-i}} \frac{J_1(N_{Pr} s\sqrt{-i})}{J_0(N_{Pr} s\sqrt{-i})} \right]^{-1}$$

$\gamma = \dfrac{c_p}{c_v}$; N_{pr} is the Prandtl #

Slit, width 2a

$$k = \gamma p_0 \left[1 + (\gamma - 1) \frac{\tanh(N_{Pr} s'\sqrt{i})}{N_{Pr} s'\sqrt{i}} \right]^{-1}$$

[TR-23]

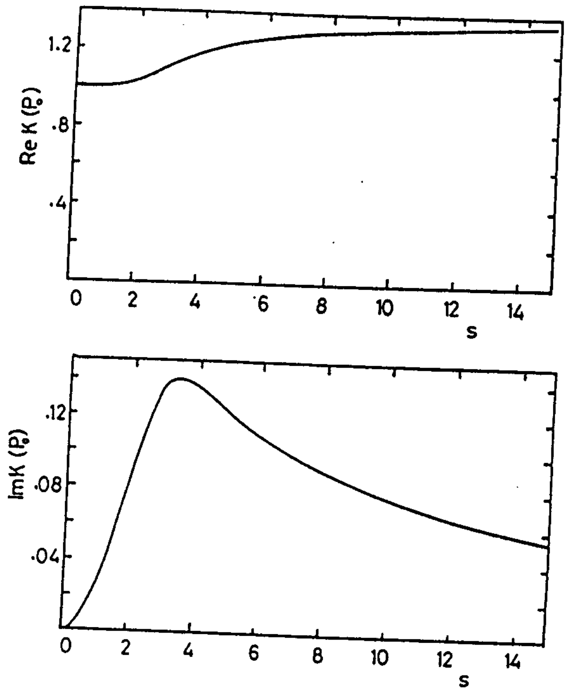

ɔ. 4.6. The bulk modulus K of air in a cylindrical tube having a circular cross-section as a function of s. The unit is the atmospheric pressure P_0.

ref.
Allard

[TR-24]

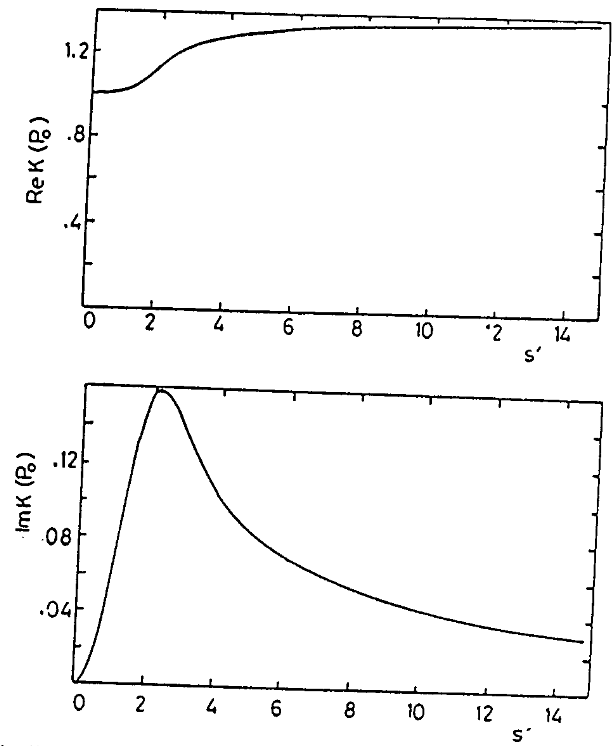

FIG. 4.7. The bulk modulus K of air in a slit as a function of s'. The unit is the atmospheric pressure P_0.

ref: Allard

[TR-25]

HIGH AND LOW FREQUENCY APPROXIMATIONS

For small/large s, use asymptotic expression for $J_1()/J_0()$. In k, since $N_{pr} \sim 1$, use same results.

Recall $s = \sqrt{\dfrac{\omega\rho_0 R^2}{\eta}}$.

High Frequency

$$s \text{ large} \Rightarrow \frac{\eta}{\omega\rho_0} << R^2 \Rightarrow \delta_\eta \text{ is small compared to tube size}$$

R  velocity is "flat"

$J_1()/J_0() = i$

$$F = ma \Rightarrow -\frac{\partial p}{\partial x} = i\omega\rho_0\bar{u}_z + (1+i)\bar{u}_z \cdot \left(\frac{2\eta}{R^2}\rho_0\omega\right)^{1/2}$$

Effective bulk modulus: $k = \gamma p_0 \dfrac{1+\sqrt{2}(-1+i)(\gamma-1)}{N_{pr}s}$

Low Frequency

$$s \text{ small} \Rightarrow \sqrt{\frac{\eta}{\omega\rho_0}} >> R \Rightarrow \delta_\eta \text{ fills significant fraction of tube diameter}$$

Rewrite 2^{nd} law as: $-\dfrac{\partial p}{\partial x} = \underbrace{\dfrac{4}{3}i\omega\rho_0\bar{u}_z}_{\text{small}} + \underbrace{\dfrac{8\eta}{R^2}\bar{u}_z}_{\text{large}}$

[TR-26]

i.e., $\dfrac{\eta}{R^2} >> \rho_0\omega \Rightarrow -\dfrac{\partial p}{\partial x} = \dfrac{8\eta}{R^2}\bar{u}_z$

Effective bulk modulus: $k = p_0\left[1+\dfrac{i}{8}\left(\dfrac{\gamma-1}{\gamma}\right)\left(N_{Pr}^2\delta^2\right)\right]$

One can continue this for slits.

See Attenborough, Phys. Rep. **82**(3) and Allard, *Sound Propagation in Porous Media,* Elsevier 1993.

FLOW RESISTIVITY IN BULK MATERIAL WITH CAPILLARY TUBES

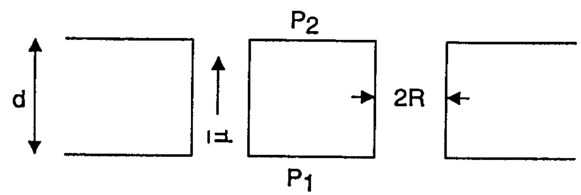

n # of pores of radius R per unit

$$\sigma \equiv \frac{\Delta p}{u \cdot d} = \frac{\Delta p}{\bar{u}(n\pi R^2)d}$$

For D.C. flow (ω=0), $\bar{u}_z = \frac{R^2}{8\eta}\left(-\frac{\partial p}{\partial z}\right)$

Substitute for $\sigma \equiv \frac{\Delta p}{u \cdot d} = \frac{\Delta p}{\bar{u}(n\pi R^2)d}$

$$\sigma = \frac{8\eta}{\left(n\pi R^2\right)R^2} = \frac{8\eta}{\Omega R^2}$$

Recall $s = \sqrt{\frac{\omega\rho_0 R^2}{\eta}}$,and eliminate $\frac{R}{\eta}$

$$s = \sqrt{\frac{8\omega\rho_0}{\sigma\Omega}}$$ shear wave number without measurables

Rewriting shear wave number for tubes

$$s= \sqrt{\frac{8\omega\rho_0}{\sigma\Omega}} \quad \text{Tubes}$$

For slits, a similar analysis yields

$$\sigma = \frac{3\eta}{\Omega a^2}.$$

Recall $s' = \sqrt{\frac{\omega\rho_0 a^2}{\eta}}$ $\qquad \frac{a^2}{\eta} = \frac{3}{\sigma}$

And in terms of σ, Ω

$$s' = \sqrt{\frac{3\omega\rho_0}{\sigma\Omega}}.$$

Compare effective density and bulk modulus for bulk material composed of cylinders and slits.

PORE TORTUOSITY

Carman, *Flow of Gases through Porous Materials*

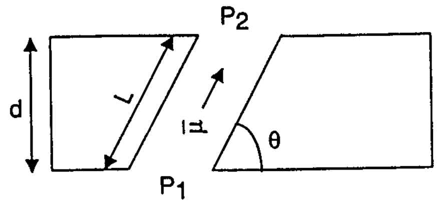

Porosity: $\Omega = \frac{n\pi R^2}{\cos\theta}$

Flow Resistivity: $\frac{\Delta p}{V \cdot d}$ $\quad V \equiv \frac{\text{volume velocity}}{\text{area}}$

Pressure Gradient in pores: $\frac{P_2 - P_1}{L} = \frac{P_2 - P_1}{d}\cos\theta$

$$\sigma = \frac{P_2 P_1}{n\left(\bar{u}\pi R^2\right)d} \qquad n \equiv \frac{\text{number of pores}}{\text{area}}$$

For D.C. Flow, $\omega = 0$,

$$\bar{u}_z = \frac{R^2}{8\eta}\left(-\frac{\partial P}{\partial z}\right) \qquad \frac{\Delta P}{\bar{u}\Delta z} \to \frac{8\eta}{R^2}$$

$$\sigma = \frac{8\eta}{R^2 n\pi R^2}\frac{1}{\cos\theta} = \frac{8\eta}{n\pi R^4 \cos\theta}$$

Substitute for $\Omega = \frac{n\pi R^2}{\cos\theta}$

$$\sigma = \frac{8\eta}{\Omega R^2 \cos^2\theta}$$

Recall $\sqrt{\frac{\omega\rho_0 R^2}{\eta}}$

Substitute for $\frac{\eta}{R^2} \Rightarrow \boxed{s = \sqrt{\frac{8\omega\rho_0 q^2}{\sigma\Omega}}}$ in terms of measurable quantities

with $q^2 = \frac{1}{\cos^2\theta}$

[TR-31]

ATTENBOROUGH / BIOT

SCALING BETWEEN CYLINDERS AND SLITS

Attenborough – scaled ρ and k

$$\rho_c(s) \approx \rho_s(5/3\, s)$$

Biot – scaled "viscous correction function"

$$G_c(s) = -\frac{s}{4}\sqrt{-i}\,\frac{T_1}{T_0}\left[1 - \frac{2}{s\sqrt{-i}}\frac{T_1}{T_0}\right]^{-1}$$

$$T_1 = J_1\left(s\sqrt{-i}\right)$$

$$T_0 = J_0\left(s\sqrt{-i}\right)$$

$$s = \sqrt{\frac{\omega \rho_0 R^2}{\eta}}$$

$$G_s(s') = \frac{1}{3}\sqrt{i}\,\frac{\tan\left(s'\sqrt{i}\right)}{\left[1 - \frac{\tan\left(s'\sqrt{i}\right)}{s'\sqrt{i}}\right]}$$

$$G_c(s) = G_s(s')$$

$$s' = \sqrt{\frac{\omega \rho_0 a^2}{\eta}} \qquad s = \frac{4}{3}s'$$

[TR-32]

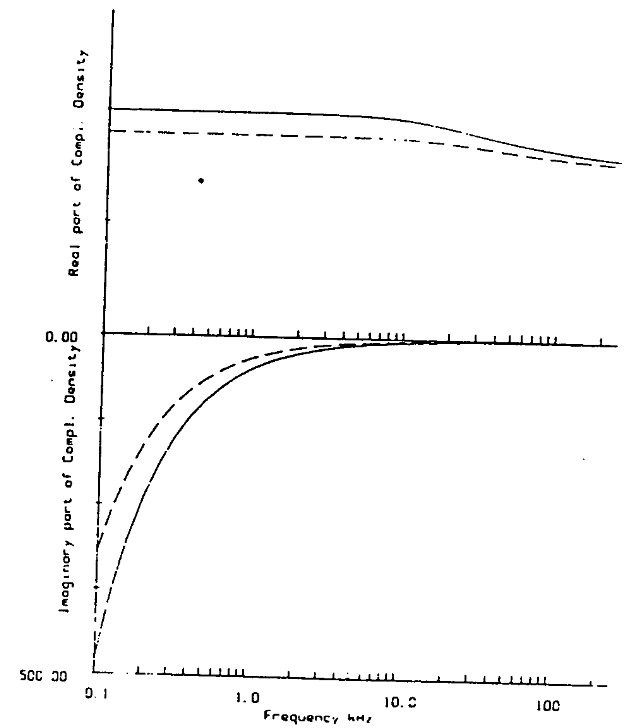

FIG. 3. Plot of real and imaginary parts of $\rho_c(\lambda_c)$ and $\rho_s(\lambda_s)$ against frequency [Eqs. (14) and (15)], where the frequency range $100 < f < 25\,760$ Hz corresponds to $0.119 < \lambda_s < 3.5$.

Attenborough, JASA 81(1) Jan 1987

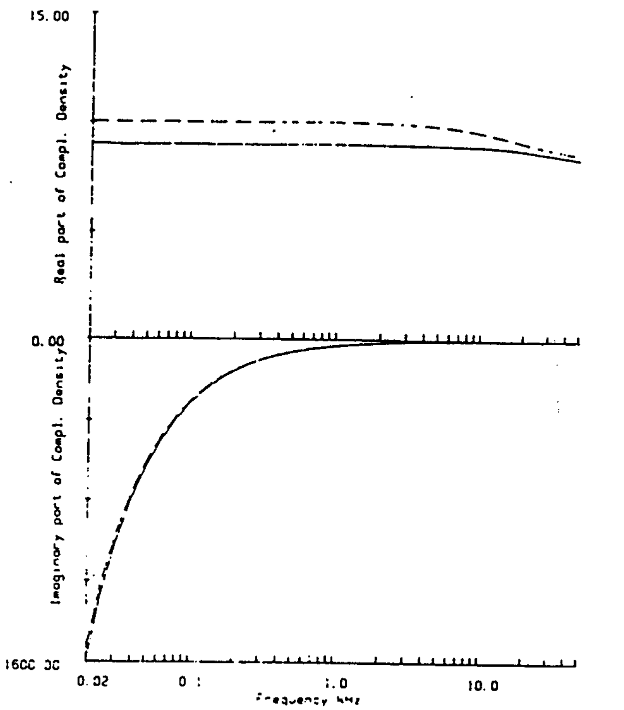

FIG. 4. Test of pore shape scaling for $\rho(\lambda)$. Plot of $\rho_s(\lambda_s)$ (continuous lines) against $\rho_c(5/3\ \lambda_s)$ (broken lines) in the range $0.119 < \lambda_s < 6$.

A Attenborough

Propagation of Sound in Porous Media

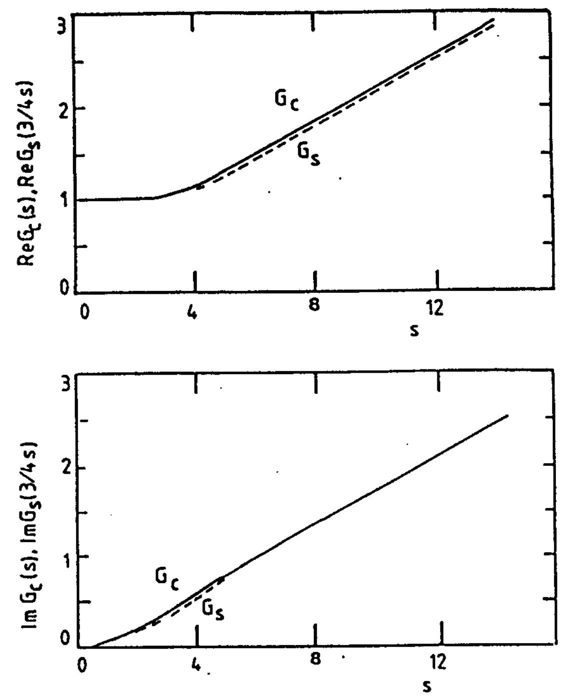

FIG. 4.9. The form factors $G_c(s)$ and $G_s(s')$ for $s' = \frac{3}{4}s$.

Allard

[TR-35]

RESULTS OF SCALING

Pore Shape: S_p

$$s = \frac{1}{S_p}\sqrt{\frac{8\omega\rho_0 q^2}{\sigma\Omega}}$$

Cylinders without $S_p = 1.0$.

[TR-36]

SUMMARY – ACOUSTIC WAVE NUMBER

(low frequency approximation)
(Ω, q^2, σ, S_p)

Bulk wave number

$$K_b = \omega\sqrt{\frac{\rho}{k}}$$

$$K_b = k_0\sqrt{\gamma}\left[aq^2 + \frac{i\sigma\Omega}{S_p\rho_0\omega}\right]^{1/2}$$

$$a = \left(\frac{4}{3} - \frac{\gamma-1}{\gamma}\right)N_{pr}$$

$$k_0 = \frac{\omega}{c_0}$$

[TR-37]

SUMMARY – ACOUSTIC IMPEDANCE

Low Frequency

$$z = \frac{1}{\rho_0 c_0}\,\omega\sqrt{\frac{\rho}{k_b}}$$

$$z_{low} \cong (1+i)\sqrt{\frac{\sigma}{\Omega}}$$

$$z_{high} \cong \sqrt{\frac{q^2}{\Omega^2}}$$

Only ratios of $\frac{\sigma}{\Omega}$ or $\frac{q^2}{\Omega^2}$ can be determined.

Consider low frequency approximation for k_b

$$k_b \cong k_0\sqrt{r}\left[aq^2 + i\frac{\sigma\Omega}{\rho_0\omega}\right]^{1/2}$$

$$a = \left(\frac{4}{3} - \frac{\gamma-1}{\gamma}\right)N_{Pr}$$

$$\mathrm{Real}\left[k_b^2\right] = k_r^2 - k_i^2 \approx aq^2$$

$$\mathrm{Im}\left[k_b^2\right] \cong \gamma\left(\frac{\omega}{c_0}\right)^2 \frac{\sigma\Omega}{\rho_0\omega}$$

[TR-38]

ACOUSTIC PROBE

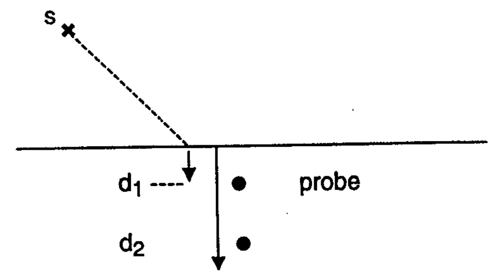

$$\tilde{T}_{d_2 d_1} \approx \frac{e^{ik_b d_2}}{e^{ik_b d_1}}$$

Phase: $\phi = \tan^{-1}\left(\frac{T_i}{T_k}\right) = k_r\Delta d$

$$\text{Magnitude (dB)} = 10.0\log_{10}|T|^2$$
$$= 20\log_{10} e^{-k_i\Delta d}$$
$$= -20\,k_i\Delta d\log_{10} e$$

or $k_r = \frac{\phi}{\Delta d}$, $k_i = -\frac{\mathrm{mag(dB)}\ln 10.0}{20.0\Delta d}$

[TR-39]

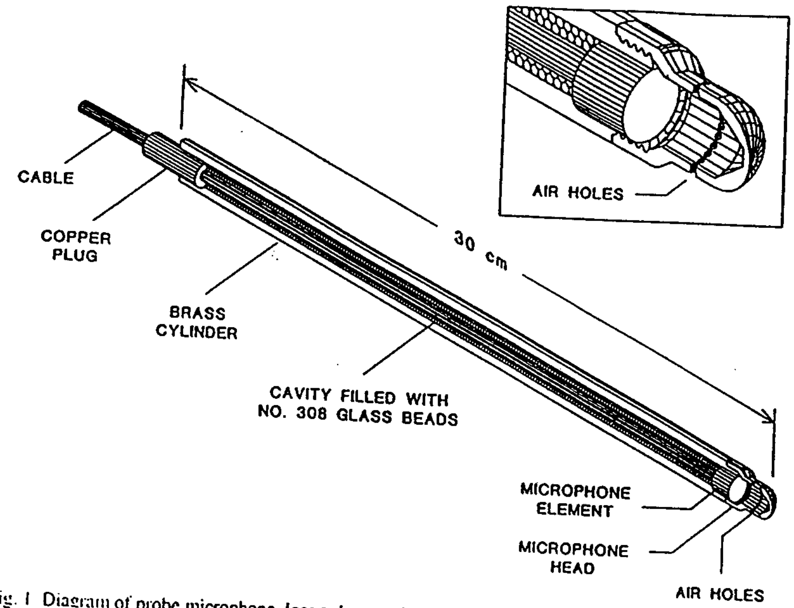

Fig. 1 Diagram of probe microphone. Insert shows enlarged view of the nose cone and microphone element

[TR-40]

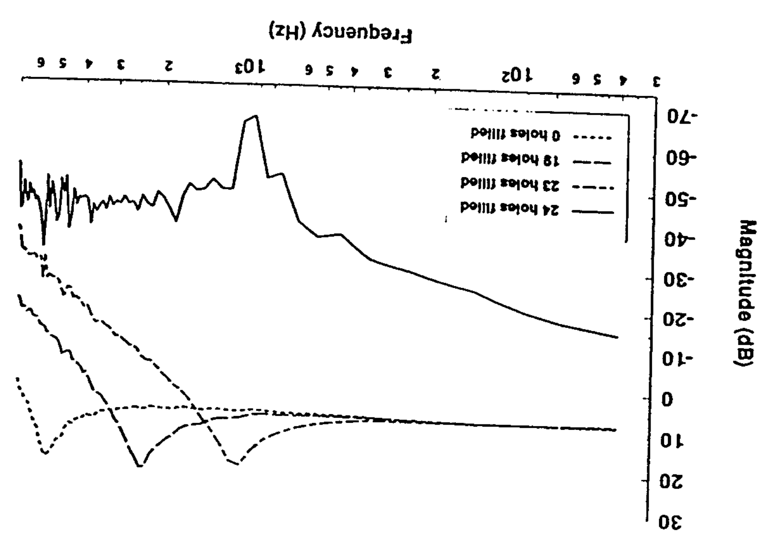

[TR-41]

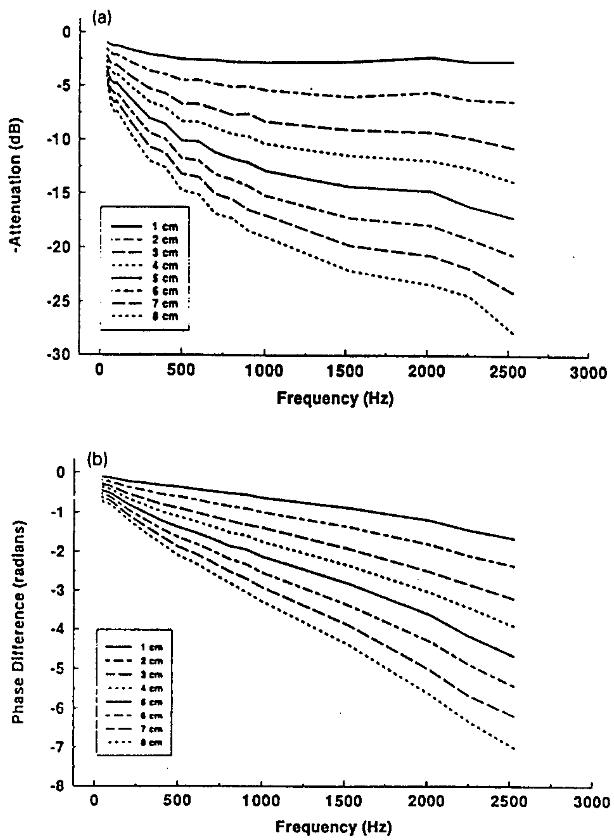

Fig 4. Magnitude (a) and phase (b) in 500 μm spherical glass beads for depths between 1 and 8 cm.

[TR-42]

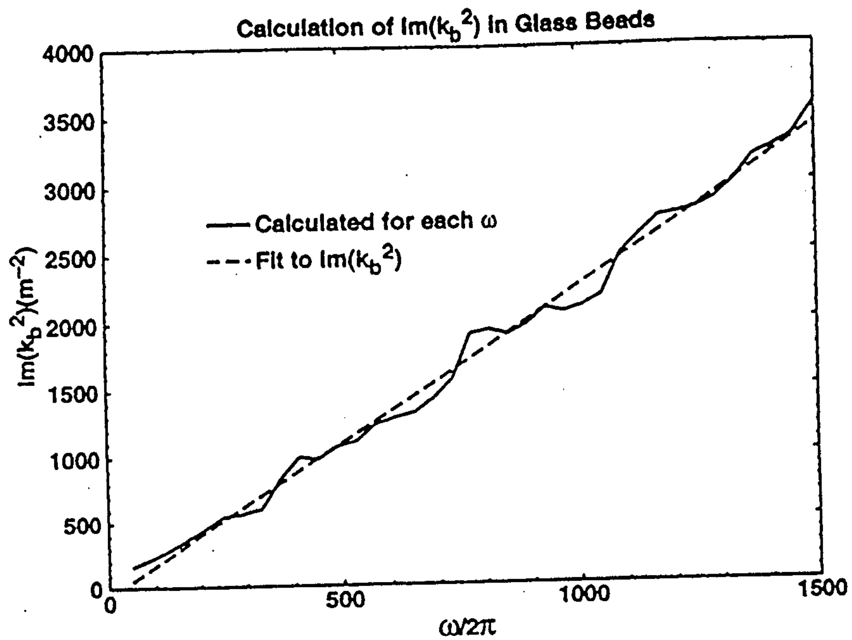

FIG. 6. The imaginary part of k_b^2 from the glass bead probe data is shown (solid line) along with a linear fit $a_1+b_1\omega$ (dashed). Using Eq. (9) the coefficient of ω can be used to calculate the product $\sigma_b\Omega$ shown in Table III.

i.e. Frederickson JASA 99 (3) 1996

[TR-43]

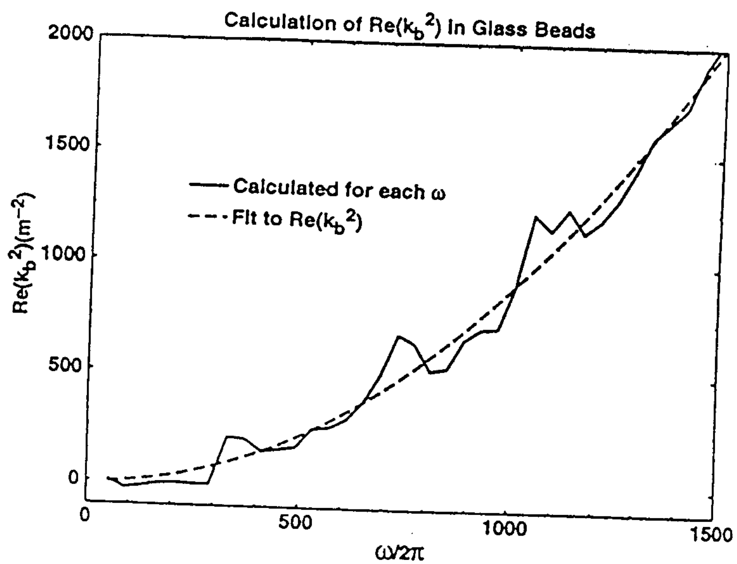

FIG. 5. The value of Re (k_b^2) calculated from the probe data taken in glass beads is shown (solid line) along with a fit of the form $a_1 + c_1\omega^2$ (dashed). Equation (8) is used to relate c_1 to q^2. The value of q^2 calculated from c_1 is the dashed line in Fig. 4 and is given in Table III.

Frederickson

[TR-44]

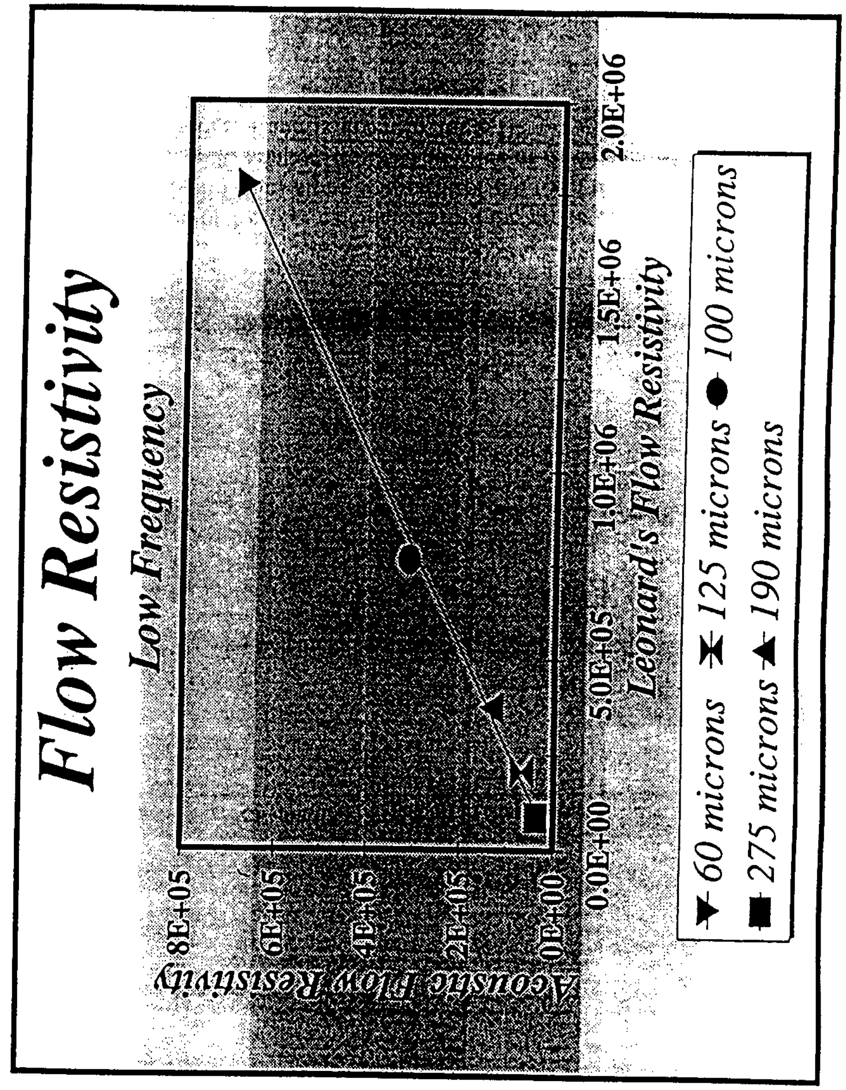

ACOUSTIC INVERSION FOR PORE PROPERTIES

Lloyd's Mirror

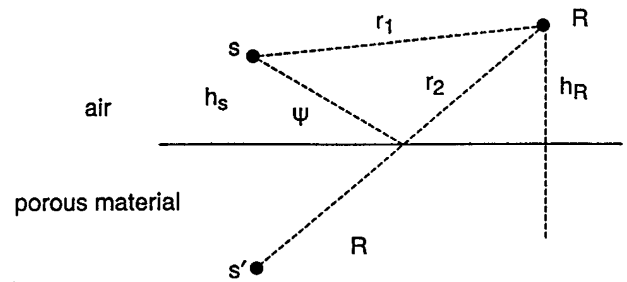

$$P_{TOT} = \frac{e^{ik_0 r_1}}{r_1} + \frac{Qe^{ik_0 r_2}}{r_2}$$

$$Q = R + (1 - R)F(f, \psi, z)$$

$$z = z(\Omega, \sigma, q^2)$$

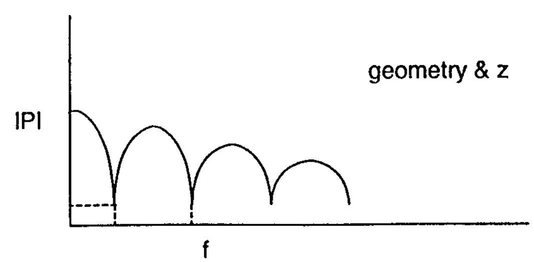

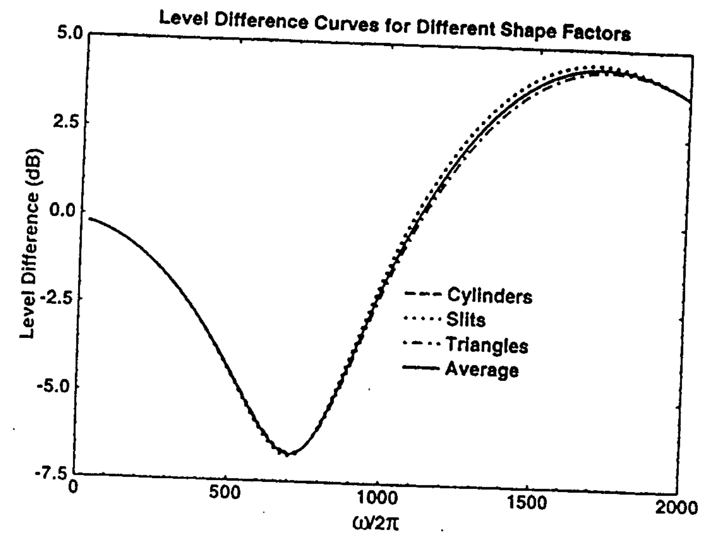

FIG. 2. This figure shows the effect of varying the shape parameter a_z in calculated level difference spectra. The percent range of variation about the average value is from 92% (for slits) to 107% (for equilateral triangles). There is very little effect on either the location or depth of the primary dip. The geometry used is source height =40 cm, range =1.63 m, top microphone at 40 cm, bottom microphone at 10 cm. The rigid-frame porous parameters are $\sigma_b = 75\,000$ (N s/m^4), $q^2 = 1.90$, and $\Omega = 0.37$.

Fredrickson

[TR-47]

COUPLING OF SOUND INTO PORO-ELASTIC SOIL

- Airborne Source
- Pore Pressure Sensor – Probe Microphone
- Frame Velocity Sensor – Geophone

Rigid frame no longer appropriate

Consider Biot Model for poro-elasticity used in rock physics community

[TR-48]

BIOT WAVE EQUATIONS

$$\nabla^2(He - C\xi) = \frac{\partial^2}{\partial t^2}(\rho e - \rho_f \xi)$$

$$\nabla^2(Ce - M\xi) = \frac{\partial^2}{\partial t^2}(\rho_f e - m\xi) - \sigma F(s)\frac{\partial \xi}{\partial t}$$

H, C, M: elastic constants

ρ, ρ_f: frame and fluid density

$$m = \frac{q^2 \rho_f}{\Omega}$$

σ: bulk flow resistivity

Dynamic Flow Resistivity

$$F(s) = -\frac{1}{4}\frac{\sqrt{-i}T\left[\sqrt{-i}s\right]}{1 - \frac{2}{\sqrt{-i}sT\left[\sqrt{-i}s\right]}}$$

$$T(\sqrt{-i}s) = \frac{J_1(\sqrt{-i}s)}{J_0(\sqrt{-i}s)}$$

$$s = \sqrt{\frac{8\omega\rho_0}{\sigma\Omega}}$$

Idealized volume element attached to the frame; frame and fluid dilatations are:

$e = \nabla \cdot \vec{u}$,

$u \equiv$ frame displacement
$e \equiv$ strain of volume element

$\xi = \Omega(\overline{u} - \overline{U}) = \nabla \cdot \vec{w}$

$U \equiv$ fluid displacement
$w \equiv$ relative fluid displacement
$\xi \equiv$ fluid volume moving in/out of volume element

Rectangular coordinates: $e = e_x + e_y + e_z$; $e_x = \frac{\partial u_x}{\partial x}$, etc.

Elastic constants: H, C, M

$$H = \frac{(k_r - k_b)^2}{(D - k_b)^2} + k_b + \frac{4}{3}\mu$$

k_r: grain bulk modulus

k_f: fluid bulk modulus

k_b: frame bulk modulus

$$D = k_r\left(1 + \Omega\left(\frac{k_r}{k_f} - 1\right)\right)$$

$$C = k_r \frac{k_r - k_b}{D - k_b}$$

$$M = \frac{k_r^2}{D - k_b}$$

STRESS / STRAIN RELATIONS

Components of stress / strain tensor

$$\tau_{xx} = He - 2\mu(e_x + e_z) - C\xi$$

$$\tau_{xx} = He - 2\mu(e_z + e_x) - C\xi$$

$$\tau_{zz}$$

$$\tau_{xy} = \mu\gamma_z \qquad \gamma_z = \frac{1}{2}\left(\frac{\partial u_x}{\partial y} + \frac{\partial u_y}{\partial x}\right)$$

$$\tau_{yz} = \mu\gamma_x \qquad \gamma_x = \frac{1}{2}\left(\frac{\partial u_y}{\partial z} + \frac{\partial u_z}{\partial y}\right)$$

$$\tau_{zx}$$

$$P_f = M\xi - Ce$$

Suppose medium is a fluid

$$\Omega \to 1$$

$$P_f = M\xi = k_f \cdot \xi$$

For an elastic solid

$$\Omega \to 0$$

$$\tau_{zz} = He - 2\mu(e_x + e_y)$$

$$H = k_r + \frac{4}{3}\mu$$

[TR-51]

CONSIDER SOLUTIONS FOR WAVE EQUATIONS

Choose

$E = Ae^{i(\ell x - \omega t)}$

$\xi = Be^{i(\ell x - wt)}$

Substituting into wave equation yields

$(H\ell^2 - \rho\omega^2)A + (\rho_f\omega^2 - C\ell^2)B = 0$

$(C\ell^2 - \rho_f\omega^2)A + (m\omega^2 - M\ell^2 - i\sigma\omega F(s))B = 0$

Det () = 0

$$\begin{vmatrix} H\ell^2 - \rho\omega^2 & \rho_f\omega^2 - C\ell^2 \\ C\ell^2 - \rho_f\omega^2 & m\omega^2 - M\ell^2 - i\sigma\omega F(s) \end{vmatrix} = 0$$

Solution is quadratic in $\ell^2 \Rightarrow$ two roots or wave types

Biot Type I, II Waves

Ratio of amplitudes of fluid and frame motion

$$M_i = \frac{B}{A} = -\frac{\left(H\ell^2 - \rho\omega^2\right)}{\left(\rho_f\omega^2 - C\ell^2\right)}$$

Numerical results for "standard input" for soils

II Wave Highly dispersive

I Wave Seismic "p-wave"

Plona Results

[TR-52]

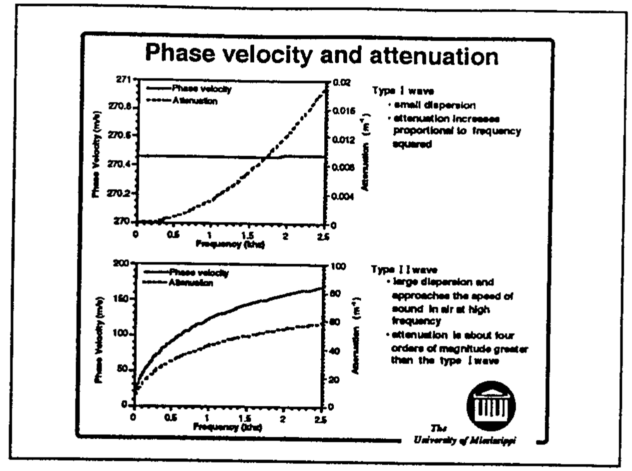

- Biot (1956) theory.
- Vector decomposition to separate the dilatation and rotational deformations.
- Plane wave approximation.
- Dispersion relations are solved for the, usually complex valued, propagation vectors.
  - Real part -> phase velocity.
  - Imaginary part -> intrinsic attenuation per meter.
- Intrinsic attenuation as considered here is associated with the conversion of "wave energy" to heat as a consequence of the fluid viscosity. It does not include energy which is scattered due to heterogeneities.

Type I P-wave (seismic or fast wave):

- little dispersion in velocity and small attenuation predicted.
- larger of the two compressional wave velocities.

Type II P-wave (slow or acoustic wave):

- dispersive phase velocity and highly attenuated.
- both velocity and attenuation increase with increasing frequency.

[TR-53]

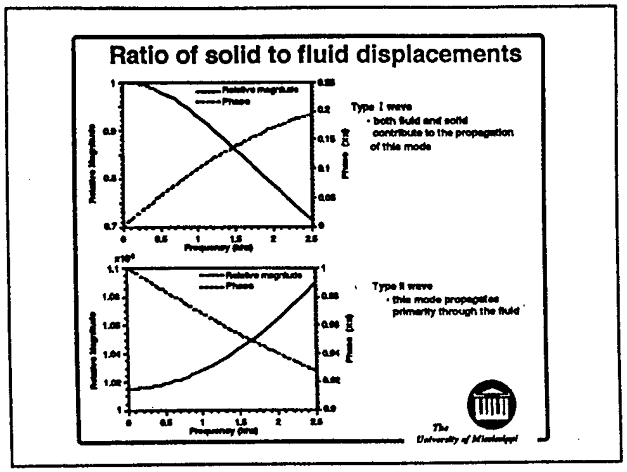

Type I P-wave

- a relative magnitude of ~ 1 indicates that the solid and fluid both undergo deformation during the passage of a type I P wave.
- the fluid and solid displacement are shown to be approximately in phase.
- the components start decoupling as the frequency increases.
- strongly dependent on the porosity, frame shear modulus, frame bulk modulus.

Type II P-wave

- very small (10^{-3}) ratio of solid to fluid displacements indicates that the type I I wave propagates primarily as a fluid deformation.
- the fluid and solid displacement are shown to be 180 degrees out of phase.
- due to large fluid deformation, associated with this mode, it has a large influence on the pore-pressure.
- strongly dependent on porosity, tortuosity, and flow resistivity (permeability).

[TR-54]

GENERAL BOUNDARY CONDITIONS
POROUS MATERIALS

Continuity of:

1. $\sigma_{nn}, \dot{u}_n$ — $\perp$ component of stress, matrix velocity
2. $\sigma_{ns}, \dot{u}_s$ — $\parallel$ components of stress, velocity
3. $s, \dot{u}_n$ — $\perp$ component of fluid velocity pressure, $s = -\Omega p$

Porous-Solid over solid interface

1. $\sigma_{nn} + s = \overline{\sigma}_{nn}$
2. $\dot{u}_n = \overline{\dot{u}}_n$
3. $\sigma_{ns} = \overline{\sigma}_{ns}$
4. $\dot{u}_s = \overline{\dot{u}}_s$
5. $\dot{U}_n - \dot{u}_n = 0$

Fluid over porous surface

1. $\sigma_{nn} + s = -\overline{p}$
2. $(1-\beta)\dot{u}_n + \beta\dot{U}_n = \overline{\dot{U}}_n$
3. $\sigma_{ns} = 0$
4. $p = \overline{p}$

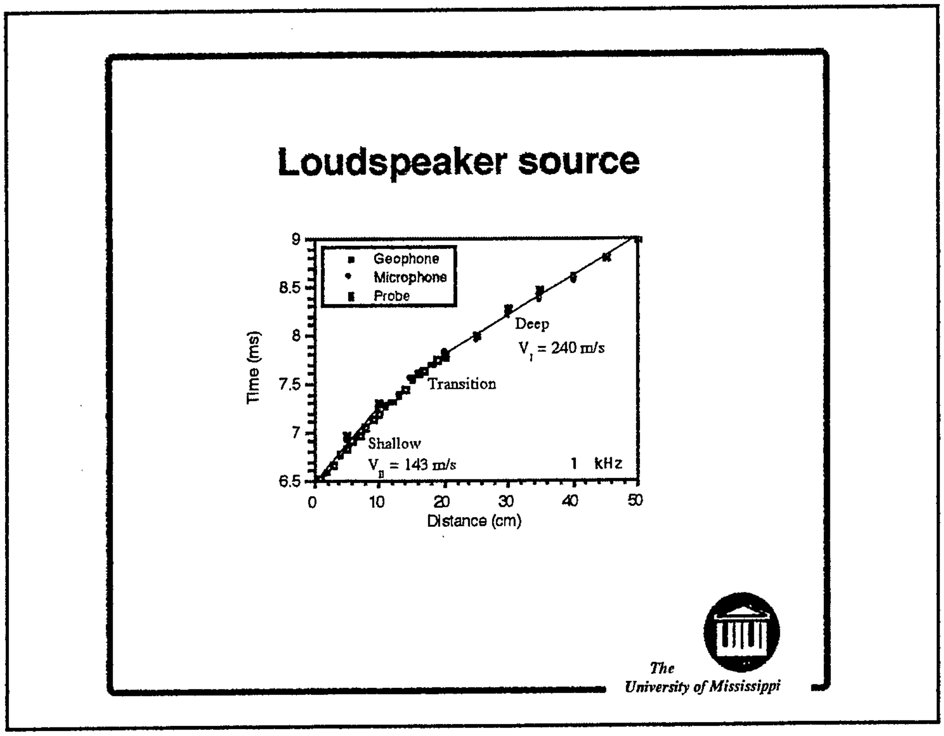

- Loudspeaker source.
- Travel time curve using a 1 kHz tone burst.
- Porous medium is composed of commericially available sandblasting sand
- The signal on probe microphone, in-situ microphones and geophones are dominated by the type II P-wave at depths less than about 15 cm.
- The type I P-wave dominates at depths greater than 20 cm.

Hickey, JASA

Shaker source

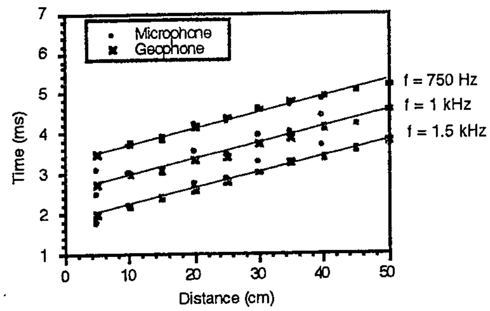

The University of Mississippi

- Mechanical shaker source.
- Travel time curves using 3 different tone bursts.
- No measurements with the probe microphone.
- The in-situ microphones and geophones are responding to the same wave.
- The single slope indicates the presence of only one wave type, i.e. Type I P-wave.
- No dispersion in velocity over this frequency range.
- The measure velocity is the same as measured at depths greater than 20 cm using the loudspeaker source.

Hickey, JASA

[TR-57 Unavailable At Time Of Printing]

[TR-58]

DEFINE QUANTITITES THAT ARE MEASURABLE

Acoustic Surface Impedance

$P_{surface} = -ik_f\ell_i(B_I + B_R), \qquad i = 1, 2$

$Vel_{surface} = -i\omega\cos\theta_i(B_I - B_R), \qquad i = 1, 2$

Impedance

$$z = \frac{P}{V} = \frac{k_f \ell_i}{\omega\cos\theta_i}\frac{B_R + B_I}{B_R - B_I}$$

Pressure below surface in porous material

$P_{below} = P_i + P_i', \qquad i = 1,2$

For down- and up-going waves

Velocity

V_n – sum of ⊥ components of type 1 and 2 going up and down + shear

[TR-59]

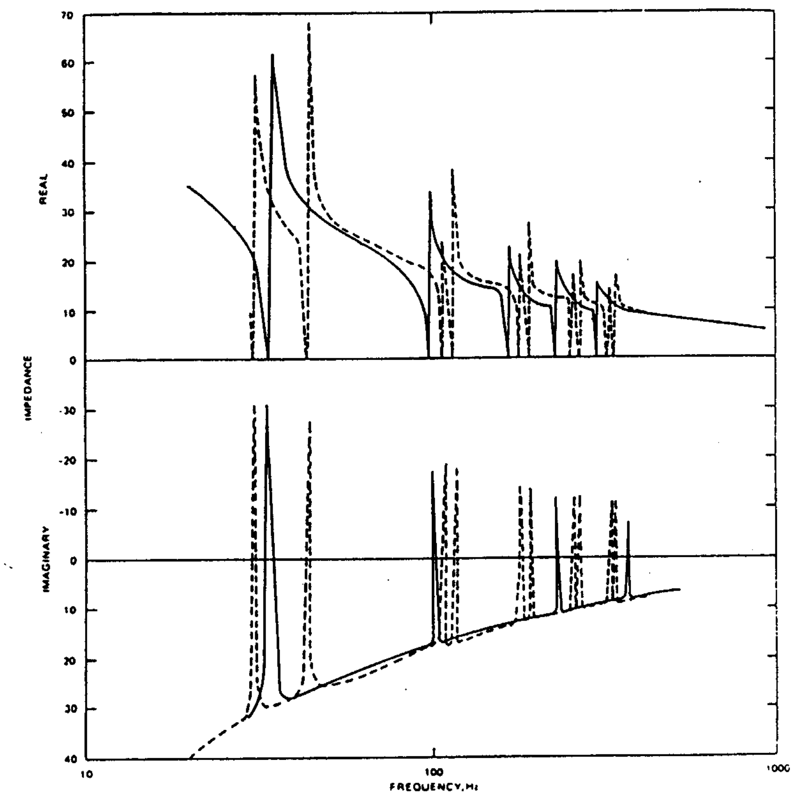

Figure A4. The influence of increasing the wave-speeds in the substrate by a factor of 10^2 on the predicted normal surface impedance of the poro-elastic layer at normal incidence (solid line) and 80° (dashed line) incidence.

[TR-60]

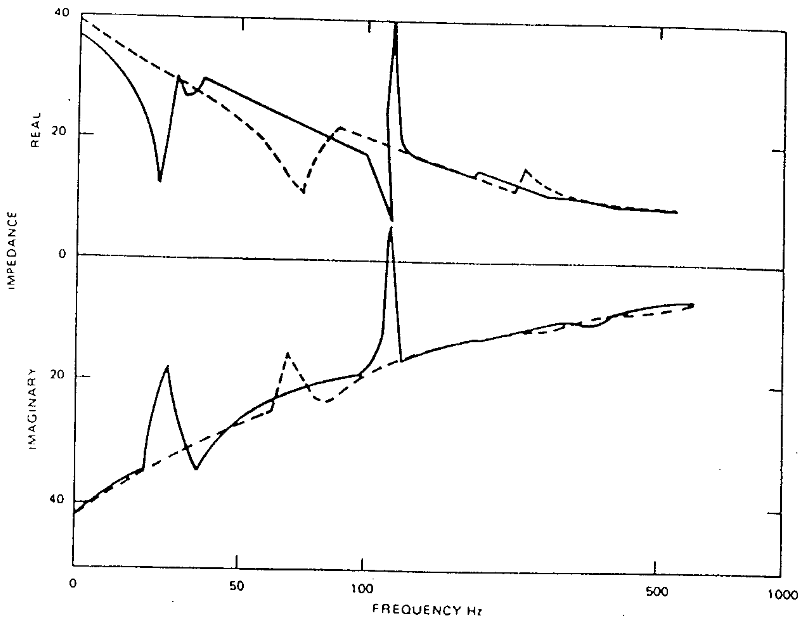

Figure A5. Influence of layer depth (1 m, dashed line; 2 m, solid line) on poro-elastic layer impedance at 80° incidence assuming the same properties as in Fig. A2.

[TR-61]

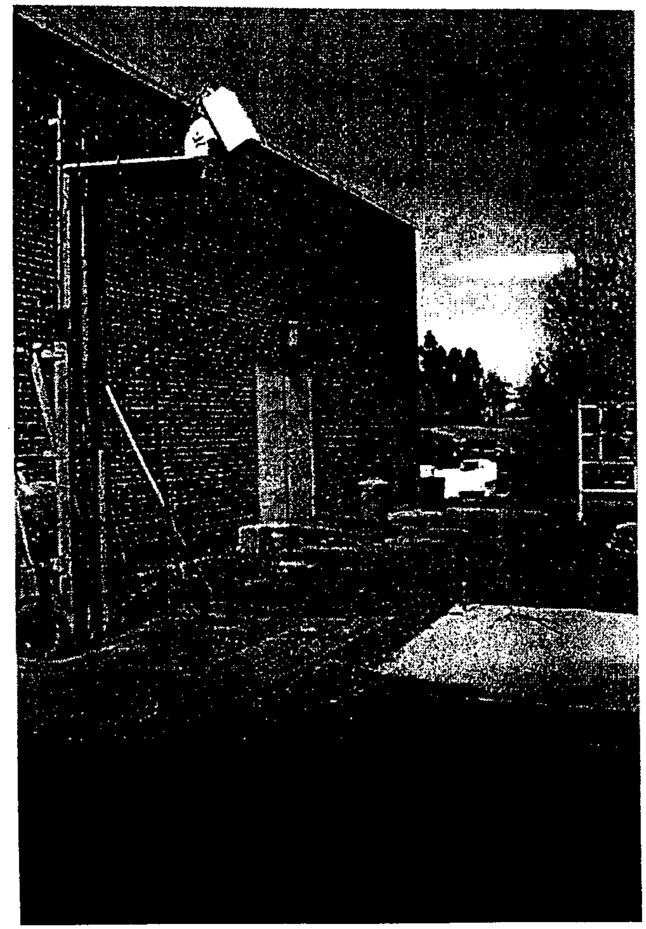

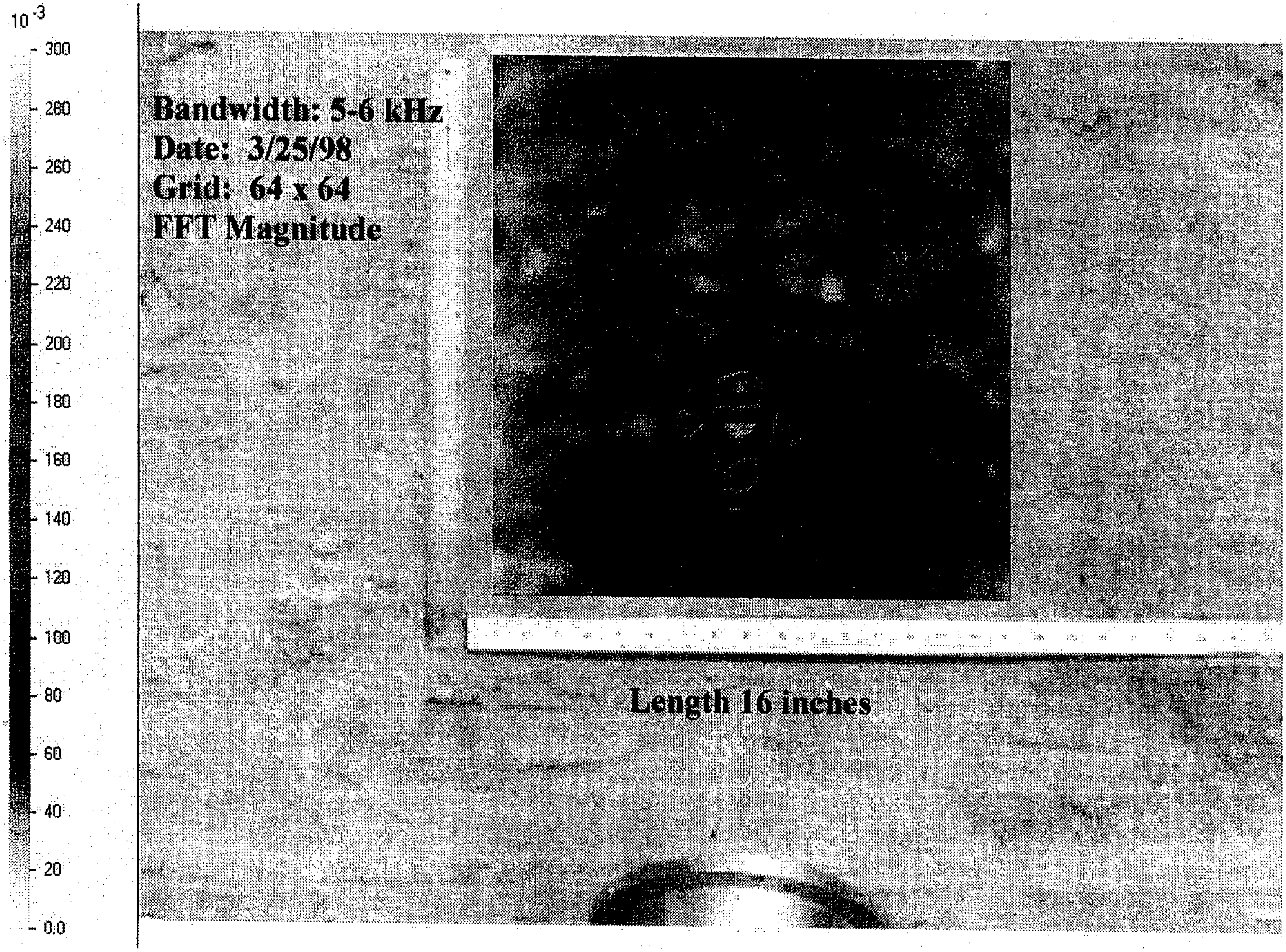

10 -3
300
280
260
240
220
200
180
160
140
120
100
80
60
40
20
0.0
Bandwidth: 5-6 kHz
Date: 3/25/98
Grid: 64 x 64
FFT Magnitude
Length 16 inches

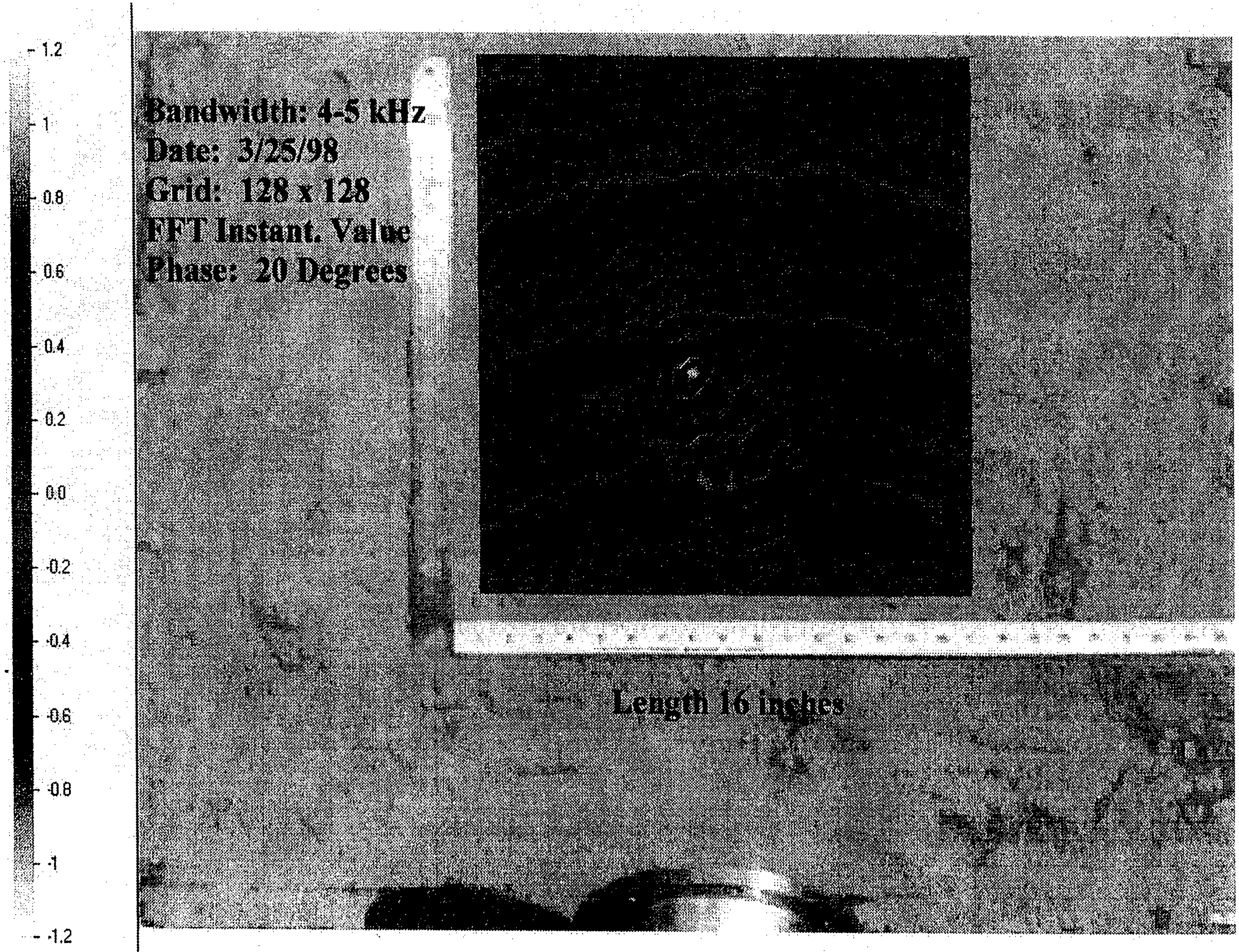

1.2
1
0.8
0.6
0.4
0.2
0.0
-0.2
-0.4
-0.6
-0.8
-1
-1.2
Bandwidth: 4-5 kHz
Date: 3/25/98
Grid: 128 x 128
FFT Instant. Value
Phase: 20 Degrees
Length 16 inches

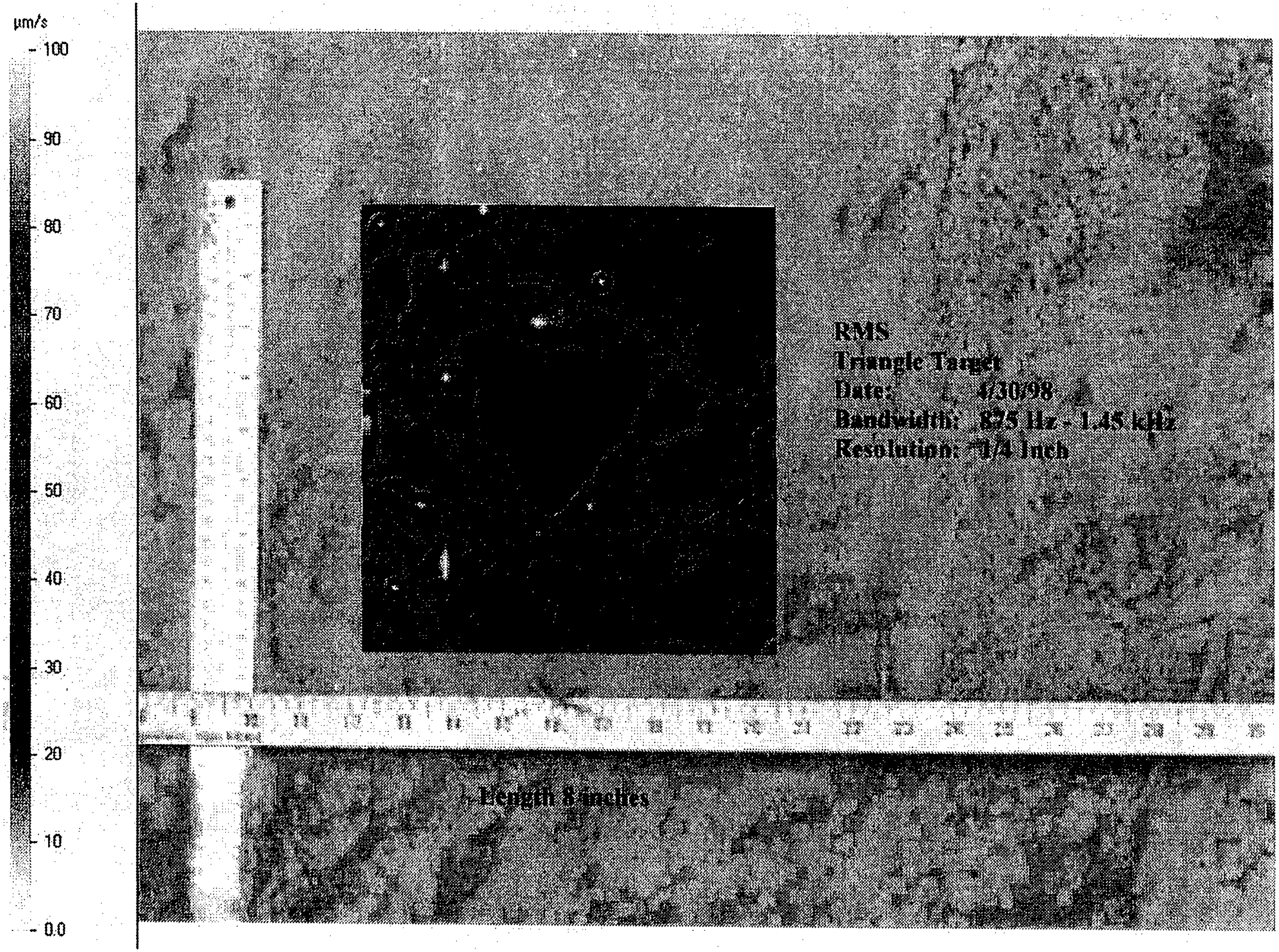
µm/s
100
90
80
70
60
50
40
30
20
10
0.0
RMS
Triangle Target
Date: 4/30/98
Bandwidth: 875 Hz - 1.45 kHz
Resolution: 1/4 Inch
Length 8 inches

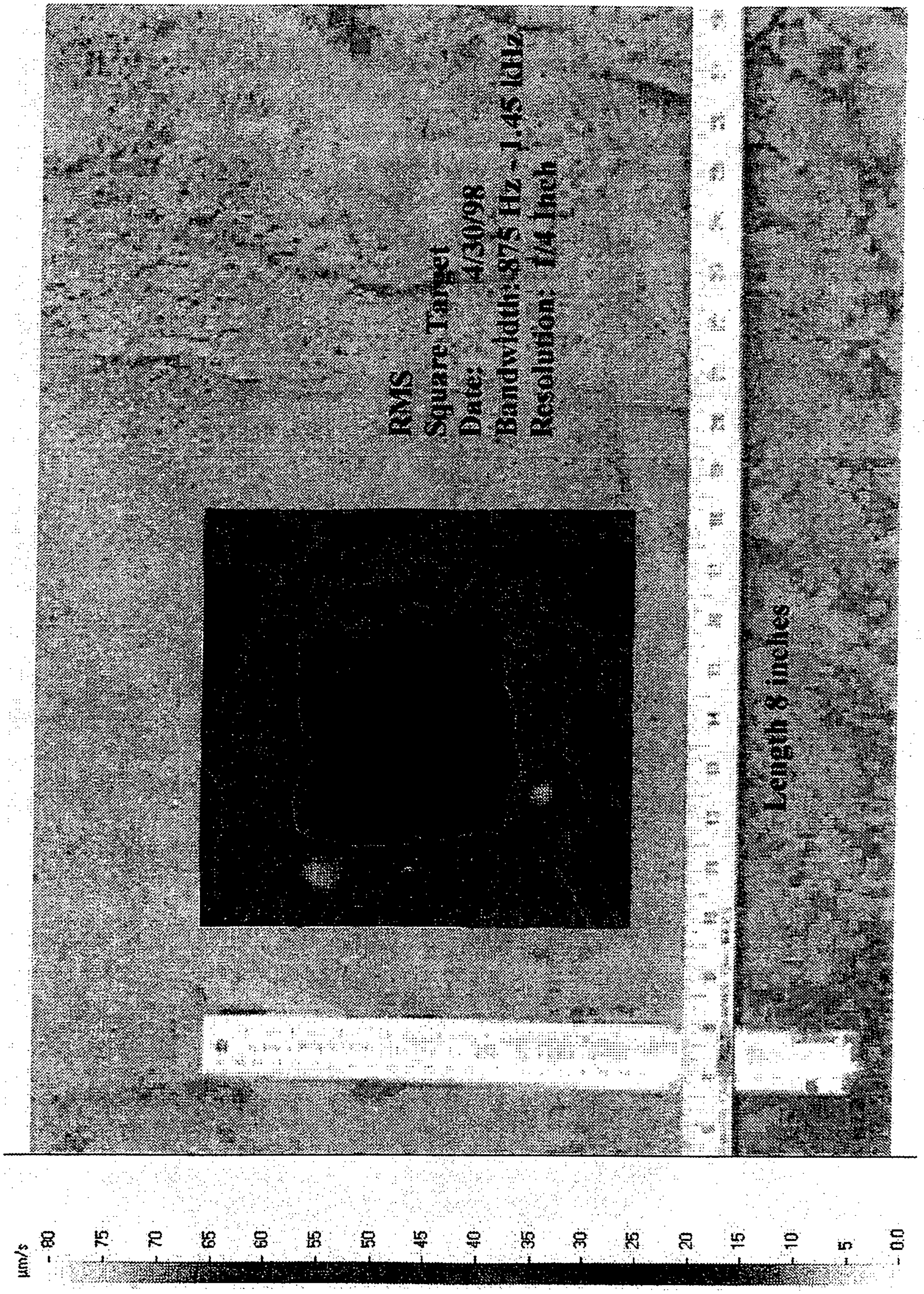
RMS
Square Target
Date: 4/30/98
Bandwidth: 875 Hz - 1.45 kHz
Resolution: 1/4 Inch
Length 8 inches
µm/s
80
75
70
65
60
55
50
45
40
35
30
25
20
15
10
5
0.0

[TR-65]

REPORT DOCUMENTATION PAGE

Form Approved
OMB No. 0704-0188

1. AGENCY USE ONLY *(Leave Blank)*	2. REPORT DATE 15 Dec 99	3. REPORT DYPE AND DATES COVERED Final 01 Feb 97 - 21 June 98

4. TITLE AND SUBTITLE
Proceedings of the 1998 Physical Acoustics Summer School: Volume II. Transparencies

5. FUNDING NUMBERS
PE 61153N
G N00014-98-1-0044

6. AUTHOR(S)
Henry E. Bass

7. PERFORMING ORGANIZATION NAME(S) AND ADDRESS(ES)
Jamie L. Whitten National Center for Physical Acoustics
The University of Mississippi
University, MS 38677

8. PERFORMING ORGANIZATION REPORT NUMBER

9. SPONSORING / MONITORING AGENCY NAME(S) AND ADDRESS(ES)
Office of Naval Research
ONR 331
800 North Quincy Street
Arlington, VA 22217-5660

10. SPONSORING / MONITORING AGENCY REPORT NUMBER

11. SUPPLEMENTARY NOTES

12a. DISTRIBUTION / AVAILABILITY STATEMENT
Approved for public release; Distribution unlimited

12b. DISTRIBUTION CODE

13. ABSTRACT *(Maximum 200 words)*
Volume II of the Proceedings of the 1998 Physical Acoustics Summer School contains copies of the transparencies used during the lectures. Volume I contains verbatim transcriptions of the lectures and Volume III contains copies of the background materials sent to student participants prior to the summer school.

14. SUBJECT TERMS Physical Acoustics, Acoustic Resonators, Chaos, Nonlinear Bubble Dynamics, Nonlinear Acoustics, Periodic, Random, and Quasiperiodic Media, Porous Media, Quantum Mechanics, Resonant Ultrasound Spectroscopy, Scanning Acoustic Microscopy, Sensor Physics, Sonoluminescence, Thermoacoustics

15. NUMBER OF PAGES
373

16. PRICE CODE

17. SECURITY CLASSIFICATION OF REPORT	18. SECURITY CLASSIFICATION OF THIS PAGE	19. SECURITY CLASSIFICATION OF ABSTRACT	20. LIMITATION OF ABSTRACT
UNCLASSIFIED	UNCLASSIFIED	UNCLASSIFIED	

NSN 7540-01-280-5500

Standard Form 298 (Rev. 2-89)
Prescribed by ANSI Std. Z39-1
298-102